NASA/TM–2014-218176

Buckling Analysis for Stiffened Anisotropic Circular Cylinders Based on Sanders' Nonlinear Shell Theory

Michael P. Nemeth
Langley Research Center, Hampton, Virginia

March 2014

NASA STI Program . . . in Profile

Since its founding, NASA has been dedicated to the advancement of aeronautics and space science. The NASA scientific and technical information (STI) program plays a key part in helping NASA maintain this important role.

The NASA STI program operates under the auspices of the Agency Chief Information Officer. It collects, organizes, provides for archiving, and disseminates NASA's STI. The NASA STI program provides access to the NASA Aeronautics and Space Database and its public interface, the NASA Technical Report Server, thus providing one of the largest collections of aeronautical and space science STI in the world. Results are published in both non-NASA channels and by NASA in the NASA STI Report Series, which includes the following report types:

- TECHNICAL PUBLICATION. Reports of completed research or a major significant phase of research that present the results of NASA Programs and include extensive data or theoretical analysis. Includes compilations of significant scientific and technical data and information deemed to be of continuing reference value. NASA counterpart of peer-reviewed formal professional papers, but having less stringent limitations on manuscript length and extent of graphic presentations.

- TECHNICAL MEMORANDUM. Scientific and technical findings that are preliminary or of specialized interest, e.g., quick release reports, working papers, and bibliographies that contain minimal annotation. Does not contain extensive analysis.

- CONTRACTOR REPORT. Scientific and technical findings by NASA-sponsored contractors and grantees.

- CONFERENCE PUBLICATION. Collected papers from scientific and technical conferences, symposia, seminars, or other meetings sponsored or co-sponsored by NASA.

- SPECIAL PUBLICATION. Scientific, technical, or historical information from NASA programs, projects, and missions, often concerned with subjects having substantial public interest.

- TECHNICAL TRANSLATION. English-language translations of foreign scientific and technical material pertinent to NASA's mission.

Specialized services also include organizing and publishing research results, distributing specialized research announcements and feeds, providing information desk and personal search support, and enabling data exchange services.

For more information about the NASA STI program, see the following:

- Access the NASA STI program home page at *http://www.sti.nasa.gov*

- E-mail your question to help@sti.nasa.gov

- Fax your question to the NASA STI Information Desk at 443-757-5803

- Phone the NASA STI Information Desk at 443-757-5802

- Write to:
  STI Information Desk
  NASA Center for AeroSpace Information
  7115 Standard Drive
  Hanover, MD 21076-1320

NASA/TM–2014-218176

Buckling Analysis for Stiffened Anisotropic Circular Cylinders Based on Sanders' Nonlinear Shell Theory

Michael P. Nemeth
Langley Research Center, Hampton, Virginia

National Aeronautics and
Space Administration

Langley Research Center
Hampton, Virginia 23681-2199

March 2014

Available from:

NASA Center for AeroSpace Information
7115 Standard Drive
Hanover, MD 21076-1320
443-757-5802

Contents

Summary

Nonlinear and linear-bifurcation buckling equations for elastic, geometrically perfect, right-circular cylindrical shells subjected to combined loads is presented. The loads include compression, shear, and uniform external and hydrostatic pressure. The analysis includes constitutive equations that are applicable to stiffened or unstiffened cylinders made from isotropic or laminated-composite materials. Complete sets of equations are presented for the nonlinear boundary-value problem of shell buckling and the corresponding prebuckling and linear-bifurcation buckling problems that are based on Sanders' shell theory for "small" strains and "moderately small" rotations.

Based on these equations, a three-parameter approximate Rayleigh-Ritz solution and a classical solution to the buckling problem are presented for cylinders with simply supported edges. Extensive comparisons of results obtained from these solutions with published results are also presented for a wide range of cylinder constructions. These comparisons include laminated-composite cylinders with a wide variety of shell-wall orthotropies and anisotropies. Numerous results are also given that show the discepancies between the results obtained by using Donnell's equations and variants of Sanders' equations. For some cases, nondimensional parameters are identified and "master" curves are presented that facilitate the concise representation of results.

Major Symbols

The major symbols used in the present study are given as follows.

A	principal membrane stiffness of an isotropic cylinder, lb/in.
A_r, A_s	cross-sectional area of the ring and stringers, respectively (see equations (12)), in^2
A_{11}, A_{12}, A_{16}, A_{22}, A_{26}, A_{66}, [A]	homogenized shell membrane stiffnesses (see equation (12a) and (19)), lb/in.
B_{11}, B_{12}, B_{16}, B_{22}, B_{26}, B_{66}, [B]	homogenized shell coupling stiffnesses (see equation (12b) and (19)), lb
$\mathcal{G}_{1i}(x, y)$, $\mathcal{G}_{2i}(x, y)$, $\mathcal{G}_{3i}(x, y)$	basis functions used in Rayleigh-Ritz analysis and defined by equations (53)
$[\mathcal{G}]$	matrix of Rayleigh-Ritz basis functions defined by equation (55)
$\mathcal{B}_{11}(\ )$ through $\mathcal{B}_{43}(\ )$	Differential operators given in equations (30) and defined in Appendix A

$\bar{\mathcal{E}}_{21}(\ )$ through $\bar{\mathcal{E}}_{33}(\ )$	Differential operators given in equations (30) and defined in Appendix A
c_1, c_2, c_4	tracers used to identify various shell theories (see equations (1), (2), and (8))
$\bar{C}_{ij}$	transformed shear stiffnesses appearing in equation (85b), psi
$[\mathbf{C}_{ij}]$	constitutive matrices defined by equations (87)
{d}	vector of constants used in Rayleigh-Ritz analysis and defined by equations (56)
d_r, d_s	spacing of the ring and stringers, respectively (see equations (12)), in.
D	principal bending stiffness of an isotropic cylinder, in.-lb
D_{11}, D_{12}, D_{16}, D_{22}, D_{26}, D_{66}, [D]	homogenized shell bending and twisting stiffnesses (see equations (12c) and (19)), in.-lb
$[D_{\mathcal{P}}]$, $\left[D^*_{\mathcal{P}}\right]$	matrices defined by equations (59d) and (59e), respectively
$[D_{\varepsilon}]$, $[D_{\varphi}]$, $[D_{\kappa}]$	matrices defined by equations (59a)-(59c), respectively
e_r, e_s	eccentricity of the ring and stringers, respectively (see equations (12)), in.
E	Young's moduli of an isotropic material, psi
E_r, E_s	Young's moduli of the ring and stringers, respectively (see equations (12)), psi
E_1, E_2	principal Young's moduli of a lamina, psi
G_{ij}	geometric stiffness coefficients defined by equations (78) and (79)
G_r, G_s	shear moduli of the ring and stringers, respectively (see equations (12)), psi
G_{12}	principal shear modulus of a lamina, psi

$[G], [G^*]$	geometric stiffness matrics defined by equation (62b) and (62c), respectively
$\mathcal{G}_{11}(\ )$ through $\mathcal{G}_{33}(\ )$	Differential operators given in equation (29) and defined in Appendix A
h	shell-wall thickness, in.
h/R	maximum shell thickness divided by the minimum principal radius of curvature
I_r^c, I_s^c	centroidal moments of inertia of the rings and stringers, (see equations (12)), in^4
J_r, J_s	torsion constants for the ring and stringers, respectively (see equations (12)), in^4
K_{ij}	stiffness coefficients defined by equations (78) and (79)
$[K]$	stiffness matrix defined by equation (62a)
$[K^T]$	stiffness matrix defined by equation (64b)
$\mathcal{K}\left(\{{}^{(1)}u\}, \{\delta^{(1)}u\}\right)$	bilinear stiffness functional defined by equation (45a), in.-lb
$\mathcal{K}_g\left(\{{}^{(1)}u\}, \{\delta^{(1)}u\}\right)$	bilinear geometric stiffness functional defined by equation (45a), in.-lb
$\mathcal{K}_g^*\left({}^{(1)}u, \delta^{(1)}u\right)$	bilinear geometric stiffness functional associated with the passive prebuckling loads and defined by equation (52a), in.-lb
ℓ_1 through ℓ_{11}	load factors appearing in equation (8a)
ℓ_1^* through ℓ_{11}^*	load factors associated with the passive prebuckling loads and defined by equations (47)
L	length of the cylinder midsurface (see figure 1), in.

L_1, L_2, L_3	load factors defined by equations (28)
L_1^*, L_2^*, L_3^*	load factors associated with the passive prebuckling loads and defined by equations (48)
$\mathcal{L}_{11}(\ )$ through $\mathcal{L}_{33}(\ )$	Differential operators given in equation (29) and defined in Appendix A
m	number of axial half-waves appearing in the buckle patterns defined by equations (77) and (108)
m_{cr}	value of m corresponding to the critical loading parameter
$M_{xx}^T, M_{yy}^T, M_{xy}^T, \{M^T\}$	membrane thermal stress resultants (see equation (11) and (19)), in-lb/in.
$\mathcal{M}_{xx}, \mathcal{M}_{yy}, \mathcal{M}_{xy}, \{\mathcal{M}\}$	effective bending stress resultants (see equation (4) and (19)), in-lb/in.
$\overset{(0)}{\mathcal{M}}_{xx}, \overset{(0)}{\mathcal{M}}_{yy}, \overset{(0)}{\mathcal{M}}_{xy}, \{\overset{(0)}{\mathcal{M}}\}$	effective bending stress resultants of the prebuckling state defined by equations (20) and (21), in-lb/in.
$\overset{(1)}{\mathcal{M}}_{xx}, \overset{(1)}{\mathcal{M}}_{yy}, \overset{(1)}{\mathcal{M}}_{xy}, \{\overset{(1)}{\mathcal{M}}\}$	effective bending stress resultants of adjacent equilibrium states defined by equations (20) and (21), in-lb/in.
$M_0(y), M_L(y)$	applied bending stress resultants at x = 0 and x = L, respectively, (see equation (8a)), lb/in.
n	number of full circumferential waves appearing in the buckle patterns (see figure 4) defined by equations (77) and (108)
n_{cr}	value of n corresponding to the critical loading parameter
$N_0(y), N_L(y)$	applied axial stress resultants at x = 0 and x = L, respectively, (see equation (8a)), lb/in.
N_x	uniform compressive stress resultant applied at x = 0 and x = L, lb/in.
N_{xy}	uniform shearing stress resultant applied at x = 0 and x = L, lb/in.

N_x^{cr}, N_{xy}^{cr}	values of N_x and N_{xy} at buckling, respectively, lb/in.
$N_{xx}^T, N_{yy}^T, N_{xy}^T, \{N^T\}$	membrane thermal stress resultants (see equation (11) and (19)), lb/in.
$\mathcal{N}_{xx}, \mathcal{N}_{yy}, \mathcal{N}_{xy}, \{\mathcal{N}\}$	effective membrane stress resultants (see equations (4) and (19)), lb/in.
$\overset{(0)}{\mathcal{n}}_{xx}, \overset{(0)}{\mathcal{n}}_{yy}, \overset{(0)}{\mathcal{n}}_{xy}$	functions defining the prebuckling stress-resultants in equations (28), lb/in.
$\overset{(0)^*}{\mathcal{n}}_{xx}, \overset{(0)^*}{\mathcal{n}}_{yy}, \overset{(0)^*}{\mathcal{n}}_{xy}$	functions defining the passive prebuckling stress-resultants in equations (48), lb/in.
$\overset{(0)}{\mathcal{N}}_{xx}, \overset{(0)}{\mathcal{N}}_{yy}, \overset{(0)}{\mathcal{N}}_{xy}, \left\{\overset{(0)}{\mathcal{N}}\right\}$	effective membrane stress resultants of the prebuckling state defined by equations (20) and (21), lb/in.
$\overset{(1)}{\mathcal{N}}_{xx}, \overset{(1)}{\mathcal{N}}_{yy}, \overset{(1)}{\mathcal{N}}_{xy}, \left\{\overset{(1)}{\mathcal{N}}\right\}$	effective membrane stress resultants of adjacent equilibrium states defined by equations (20) and (21), lb/in.
$\left[\overset{(0)}{\mathcal{n}}\right], \left[\overset{(0)}{\mathcal{N}}\right]$	matrices associated with the prebuckling stress state, defined by equation (43), lb/in.
p^{cr}	value of the applied external pressure at buckling, psi
$\tilde{p}$	loading parameter (see equation 8a))
$\tilde{p}_{cr}$	value of the loading parameter at buckling
$\left\{\overset{(1)}{\mathcal{P}}\right\}$	vector defined by equation (39b), psi
$q_{ext} = p$	applied external pressure acting inward, psi
q_{int}	internal pressure applied and held fixed prior to buckling, psi
q_x, q_y, q_ζ	applied surface tractions (see equations (8)), psi

Q_x, Q_y	transverse-shear stress resultants defined by equations (9d) and (9e)), lb/in.
$\overset{(0)}{Q}_x$, $\overset{(0)}{Q}_y$	transverse-shear stress resultants of the prebuckling state defined by equations (22c) and (22d)), lb/in.
$\overset{(0)}{Q}_x$, $\overset{(0)}{Q}_y$	transverse-shear stress resultants of adjacent equilibrium states defined by equations (23c) and (23d)), lb/in.
$\overline{Q}_{ij}$	transformed, reduced (plane stress) stiffnesses of classical laminated-shell and laminated-plate theories (see equation (85a)), psi
R	radius of curvature of the cylinder midsurface (see figure 1), in.
$S_0(y)$, $S_L(y)$	applied circumferential stress resultant at $x = 0$ and $x = L$, respectively, (see equation (8a)), lb/in.
u_x, u_y, w	axial, circumferential, and radial midsurface displacement fields, in.
$\overset{(0)}{u}_x$, $\overset{(0)}{u}_y$, $\overset{(0)}{w}$	prebuckling midsurface displacement fields, in.
$\overset{(1)}{u}_x$, $\overset{(1)}{u}_y$, $\overset{(1)}{w}$	midsurface displacement fields of adjacent equilibrium states, in.
U_i, V_i, W_i	constants used in Rayleigh-Ritz analysis and defined by equations (53)
$V_0(y)$, $V_L(y)$	applied radial stress resultants at $x = 0$ and $x = L$, respectively, (see equation (8a)), lb/in.
x, y, ζ	coordinates of the cylinder, as depicted in figure 1
Z	Batdorf's parameter, $\frac{L^2}{Rh}\sqrt{1-\nu^2}$
$\{\delta d\}$	vector of constants used in Rayleigh-Ritz analysis and defined by equations (58)
$\delta\varepsilon_{xx}$, $\delta\varepsilon_{yy}$, $\delta\varepsilon_{\zeta\zeta}$, $\delta\gamma_{y\zeta}$, $\delta\gamma_{x\zeta}$, $\delta\gamma_{xy}$	virtual strains appearing in equation (5)
$\delta\varepsilon^{o}_{xx}$, $\delta\varepsilon^{o}_{yy}$, $\delta\gamma^{o}_{xy}$	midsurface virtual membrane strains (see equation (4))

$\delta\varepsilon^{(1)}_{xx}$, $\delta\varepsilon^{(1)}_{yy}$, $\delta\gamma^{(1)}_{xy}$, $\left\{\delta\varepsilon^{(1)}\right\}$	midsurface virtual membrane strains of adjacent equilibrium states appearing in equations (37) and (38)
$\delta\varphi_x$, $\delta\varphi_y$	virtual rotations of the shell midsurface (see equations (8), radians
$\delta\bar{\varphi}^{(1)}_x$, $\delta\bar{\varphi}^{(1)}_y$, $\delta\bar{\varphi}^{(1)}_n$, $\left\{\delta\bar{\varphi}^{(1)}\right\}$	midsurface virtual linear rotation parameters of adjacent states appearing in equations (37) and (38), radians
$\delta\kappa^{o}_{xx}$, $\delta\kappa^{o}_{yy}$, $\delta\kappa^{o}_{xy}$	midsurface virtual bending strains (see equation (4)), in^{-1}
$\delta\kappa^{(1)}_{xx}$, $\delta\kappa^{(1)}_{yy}$, $\delta\kappa^{(1)}_{xy}$, $\left\{\delta\kappa^{(1)}\right\}$	midsurface virtual bending strains of adjacent equilibrium states appearing in equations (37) and (38), in^{-1}
$\left\{\delta\mathcal{P}^{(1)}\right\}$	vector defined by equation (39c), psi
δW_{ext}	external virtual work per unit area of shell midsurface defined by equations (8), in.-lb
δW_{int}	internal virtual work per unit area of shell midsurface defined by equation (5), in.-lb
$\delta W^{(1)}$	virtual work associated with linear bifurcation (see equation (31)), in.-lb
$\delta\mathcal{W}^{(1)}$	virtual work per unit area associated with linear bifurcation (see equation (31)), lb/in.
$\delta\mathcal{W}^{(1)\,B}$	virtual work per unit length associated with linear bifurcation (see equation (31)), lb
δu_x, δu_y, δw	virtual displacements of the shell midsurface along the x-, y-, and ζ-axes, respectively, in. (see equations (8))
$\Delta^0_x(y)$, $\Delta^0_y(y)$, $\Delta^0_\zeta(y)$	applied axial, circumferential, and radial displacements at x = 0, respectively, (see equations (10)), in.
$\Delta^L_x(y)$, $\Delta^L_y(y)$, $\Delta^L_\zeta(y)$	applied axial, circumferential, and radial displacements at x = L, respectively, (see equations (10)), in.

$\varepsilon_{xx}, \varepsilon_{yy}, \varepsilon_{\zeta\zeta}, \gamma_{y\zeta}, \gamma_{x\zeta}, \gamma_{xy}$	shell strains defined by equations (7)
$\varepsilon^{o}_{xx}, \varepsilon^{o}_{yy}, \gamma^{o}_{xy}, \{\varepsilon^{o}\}$	midsurface normal and shearing strains defined by equations (2) and (15)
$\varepsilon^{o}_{xxL}, \varepsilon^{o}_{yyL}$	linear part of membrane strains defined by equations (2a) and (2b)
$\overset{(0)}{\varepsilon}_{xx}, \overset{(0)}{\varepsilon}_{yy}, \overset{(0)}{\gamma}_{xy}, \{\overset{(0)}{\varepsilon}\}$	midsurface membrane strains of the prebuckling state defined by equations (17) and (18)
$\overset{(1)}{\varepsilon}_{xx}, \overset{(1)}{\varepsilon}_{yy}, \overset{(1)}{\gamma}_{xy}, \{\overset{(1)}{\varepsilon}\}$	midsurface membrane strains of adjacent equilibrium states defined by equations (17) and (18)
$\kappa^{o}_{xx}, \kappa^{o}_{yy}, \kappa^{o}_{xy}, \{\kappa^{o}\}$	changes in midsurface curvature and torsion defined by equations (3) and (16), in^{-1}
$\overset{(0)}{\kappa}_{xx}, \overset{(0)}{\kappa}_{yy}, \overset{(0)}{\kappa}_{xy}, \{\overset{(0)}{\kappa}\}$	midsurface bending strains of the prebuckling state defined by equations (17) and (18), in^{-1}
$\overset{(1)}{\kappa}_{xx}, \overset{(1)}{\kappa}_{yy}, \overset{(1)}{\kappa}_{xy}, \{\overset{(1)}{\kappa}\}$	midsurface bending strains of adjacent equilibrium states defined by equations (17) and (18), in^{-1}
$\tilde{\lambda}$	passive loading parameter associated with a fixed, stable prebuckling stress state (see equations (46)-(51))
$\sigma_{xx}, \sigma_{yy}, \sigma_{\zeta\zeta}, \sigma_{y\zeta}, \sigma_{x\zeta}, \sigma_{xy}$	shell stresses, psi
θ	fiber orientation angle of a lamina measured from the cylinder generators, degrees
τ	parameter used to define skewedness of the buckle pattern defined by equations (108)
τ_{cr}	value of τ at buckling
$\varphi_{x}, \varphi_{y}, \varphi_{n}, \{\varphi\}$	linear rotation parameters for the cylinder midsurface defined by equations (1), radians (see also equation (14b))
$\overset{(0)}{\varphi}_{x}, \overset{(0)}{\varphi}_{y}, \overset{(0)}{\varphi}_{n}, \{\overset{(0)}{\varphi}\}$	midsurface linear rotation parameters of the prebuckling state defined by equation (14c), radians

$\overset{(1)}{\varphi}_x, \overset{(1)}{\varphi}_y, \overset{(1)}{\varphi}_n, \left\{\overset{(1)}{\varphi}\right\}$	midsurface linear rotation parameters of adjacent states defined by equation (14d), radians
$\phi_0(y), \phi_L(y)$	applied rotations at x = 0 and x = L, respectively (see equations (10)), radians
ν	Poisson's ratio of an isotropic material
ν_{12}	major Poisson's ratio of a lamina
$[\partial_p], [\partial_p^*]$	matrix of differential operators defined by equations (41d) and (52c), respectively, lb/in^3
$[\partial_q], [\partial_q^*]$	matrix of live-pressure derivatives defined by equations (39d) and (52d), respectively, lb/in^3
$[\partial_\varphi]$	matrix of differential operators defined by equation (41c), in^{-1}
$[\partial_\varepsilon]$	matrix of differential operators defined by equation (41a), in^{-1}
$[\partial_\kappa]$	matrix of differential operators defined by equation (41b), in^{-2}
ξ	parameter defining the "distance" between adjacent equlibrium states (see equations (13))

Introduction

Shell buckling is a highly nonlinear phenomenon that still remains as an obstacle to the development of efficient structural designs. This design obstacle is manifested primarily by the high degree of sensitivity to "small" initial geometric imperfections exhibited by thin-walled curved members subjected to compression-dominated stress states.[1] This sensitivity generally corresponds to a significant reduction in buckling resistance, compared to that of the corresponding idealized geometrically perfect structure, that is difficult to quantify in the preliminary design stage with the fidelity needed to reduce structural mass. In addition, the general effects of boundary conditions and load introduction, material orthotropies and anisotropies, cutouts and other structural details, and combined-load interactions on imperfection sensitivity are still not known well enough to reduce structural mass in the preliminary structural design stage.[1-4] For example, experiments and analyses conducted on compression-loaded curved panels have shown extreme sensitivity of the buckling resistance to small deviations from idealized support conditions (reference 2). Other types of imperfections that can cause significant reductions in buckling resistance are described in reference 1.

Shell buckling is also an important consideration in the design modification of thin-walled structures, particularly in weight-critical aerospace applications. For example, significant reductions in the wall thicknesses of the Space Shuttle external tank were implemented to reduce structural mass in order to reach the high-inclination orbit of the International Space Station without substantially reducing the payload capacity of the Orbiter. The corresponding redesign of the external tank required in-depth, sophisticated nonlinear shell buckling analyses.[5-10] In these analyses, measured initial geometric imperfections were not available for most of the external tank. As a result, the imperfection sensitivity was assessed by using artificial imperfection shapes that are known to yield very conservative predictions of buckling resistance.

Technology advancements have been made over the past 30 years that combine high-fidelity analysis tools, measurement systems, and experimental methods to yield very accurate predictions of shell buckling resistance. These advancements were made possible by long-term investments in fundamental research. Most of these advancements have focused on the right-circular cylindrical shell-a very common structural form found in aerospace applications that is highly sensitive to initial geometric imperfections when subjected to compression-dominated stress states. In particular, the results presented in references 11-16 show extremely good correlation between high-fidelity nonlinear finite-element analyses and high-fidelty experiments conducted at the NASA Langley Research Center. Moreover, these results illustrate the fact that the "best" prediction of buckling resistance is obtained from a high-fidelity nonlinear analysis that uses actual measured imperfection data. However, when designing a new shell, measured imperfection data do not exist. Thus, an alternate approach must be used to account for the reduced buckling resistance caused by initial geometric, and other, imperfections in the early stages of design (e.g., see reference 1).

The analyses of the Space Shuttle external tank (references 5-10) illustrate that perhaps the "next best" method for accounting for inital geometric imperfections is to include an imperfection shape in the form of one or more of the buckling modes obtained from a linear bifurcation

(eigenvalue) analysis of the geometrically perfect structure. Usually, the single mode that corresponds to the smallest eigenvalue is sufficient for shells that are not highly symmetric around the circumference. Here, the term "symmetry" means symmetric with respect to geometry, wall construction, boundary conditions, and loads. For cylinders that are "highly symmetric," the eigenvalues obtained from a linear bifurcation analysis will be closely spaced or, at worst, several modes will correspond to the smallest eigenvalue. For this case, an imperfection shape in the form of a combination of these modes may produce the smallest buckling load because of modal interaction. Then, a series of nonlinear analyses are conducted in which the imperfection amplitude is varied over a predetermined range that is expected to be within manufacturing tolerances. Typically, the imperfection amplitude is less than one or two "nominal" wall thicknesses. A comparison of the buckling load obtained from a nonlinear analysis with a zero-valued imperfection amplitude and the corresponding linear eigenvalue provides a measure of the "integral" effect of nonlinear prebuckling deformations on the response of the baseline, geometrically perfect structure. The overall smallest buckling load in the range of imperfection amplitudes is taken as the buckling load. Use of a "buckling-mode imperfection" in the nonlinear analysis represents a very strong bias toward buckling at the lowest possible load. Combined with an additional factor of safety, it is expected that the corresponding design will be overly, and perhaps ultra-, conservative. In any case, this approach is relatively time consuming, as compared to the common practice used in preliminary design that uses a linear bifurcation analysis in conjunction with a knockdown factor.[1]

In developing a shell design, a large number of configurations are often examined to determine sensitivies to a wide range of parameters. As a result, a trade-off between analysis speed and accuracy is used to obtain a "coarse" global view of the design space. Presently, using nonlinear finite element analyses to obtain the buckling resistance of shells is not feasible, especially when large design spaces must be navigated. In contrast, less accurate special-purpose linear bifurcation analyses can be conducted rapidly. When the design matures, the corresponding design space becomes smaller and refinements to the buckling-resistance predictions can be obtained with high-fidelity analysis tools.

Prior to the development of reliable nonlinear finite element analysis capabilities, linear bifurcation analyses were used for idealized, representative problems, and imperfection sensitivities were accounted for by using empirical "knockdown" factors.[1] These knockdown factors represent lower bounds to experimental data and may yield overly conservative designs and added weight. In particular, the pedigree of some of the older test data used is unknown and boundary conditions are generally manifested as a random effect. In addition, a compilation of knockdown factors for laminated-composite shells does not presently exist and knockdown factors for isotropic shells are used without a physical basis. Even with all these flaws, the use of a simplified linear analysis that captures the "baseline" buckling resistance and a reasonable estimate of a knockdown factor is still a viable approach to the preliminary design of buckling-critical shells. With the recent advancements in desk-top computing capabilities that are well-suited for special purpose analysis tools and future refinements in empirical knockdown factors, this basic design approach is likely to see continued use. The present study builds on this basic design approach.

Numerous linear bifurcation buckling analyses for cylinders have appeared in the literature

over the past 50 years. Most of these analyses are based on Donnell's simplified, approximate equations for shallow shells (e. g., see reference 17) and most of the others are based on the more robust equations given by Flügge.[18] Even fewer analyses have been presented that are based on Sanders' nonlinear equations.[19] Sanders' nonlinear equations are based on "small" strains and "moderately small" rotations and are considered to be among the best first-approximation theory for general thin shells. For each of these three sets of equations, the details of the corresponding buckling analyses are generally presented in an abbreviated form and spread across numerous publications. Thus, a major objective of the present study is to present a detailed, complete exposition of the linear-bifurcation buckling equations for right-circular cylindrical shells subjected to combined loads. The buckling equations are based on Sanders' nonlinear equations for the practical case of shell deformations with "small" strains and "moderately small" rotations, and negligible transverse shearing deformations. The detail and completeness of the presentation are designed to make confident-use of the equations accessable to design engineers with a less specialized background, and to provide a "stand-alone" reference document. The shells are presumed to be made generally of laminated-composite materials and possess a regular arrangement of stiffeners. In addition, the equations have a broad range of applicability and contain Donnell's shallow shell equations as a special case.[19] A second objective is to present a comprehensive set of comparisons with previously published results that will add confidence to their usage. The comparisons include isotropic, orthotropic, and anisotropic wall constructions with and without rings and stringers. The loads include compression, shear, and "live" uniform external and hydrostatic pressure in which the pressure remains normal to the shell surface during deformation.

To accomplish the objectives of the present study, Sanders' nonlinear equations for thin, elastic shells are presented first, with the constitutive equations modified to include laminated-composite walls with a homogenized regular arrangement of rings and stringers. Then, a detailed bifurcation analysis is presented and the linear boundary-value problem and corresponding variational equations governing buckling are given. Next, the buckling analysis is extended to include two distinct loading systems, which greatly expands the range of applications. One loading system is a fixed set of passive loads that are applied at an intensity that does not result in buckling. The other set of loads are proportional to a single loading parameter that is increased monotonically in magnitude until buckling occurs. Next, a Rayleigh-Ritz formulation of the buckling equations is presented that makes solutions obtainable for a broad class of problems that do not possess closed-form solutions to the partial differential equations governing buckling. Then, a classical solution is presented for specially orthotropic cylinders with simply supported edges and subjected to compression and uniform pressure loads. This classical solution is particularly important in that a simplified variant based on Donnell's equations has seen extensive used in design for nearly 50 years. Next, a simple approximate Rayleigh-Ritz solution is presented that includes full shell wall anisotropy and the full range of combined loads considered in the present study. Finally, an extensive set of results and comparisons with prevoius studies are presented for a broad range of shell configurations and loads. Most of the results are based on the classical solution presented herein and are relevant to current design practices. Altogether, the results presented herein appear to be the most comprehensive set assembled into one document. The results are intended to show clearly the consequences of neglecting various terms in the analyses for a wide range of shell constructions. Moreover, the results and comparisons are also intended to give an indication of the range of validity of the simple, approximate Rayleigh-Ritz

solution. This entire collection of analysis details, results, and comparisons with published studies should be very useful to future developments in shell-buckling research.

Sanders' Nonlinear Equations

The equations presented subsequently are based on the nonlinear equations given by Sanders[19] for the special case of right-circular cylindrical shells. The geometry and coordinate system used herein for a geometrically perfect right-circular cylinder are shown in figure 1. Points of the shell in its unloaded and undeformed reference state are given by the coordinates (x, y, ζ), where x is an axial coordinate, y is a circumferential arc-length coordinate, and ζ is an outward radial coordinate with its origin at the middle surface. The middle surface has a length L and a radius R, and the shell wall has a uniform thickness h.

The primary kinematic variables in Sanders' equations for right-circular cylinders are the axial, circumferential, and radial middle-surface displacement fields denoted by $u_x(x, y)$, $u_y(x, y)$, and $w(x, y)$, respectively. The linear rotation parameters that correspond to rotations of differential material line elements coincident with the surface normal vector at a generic point $(x, y, 0)$ of the middle surface are given by

$$\varphi_x = -\frac{\partial w}{\partial x} \tag{1a}$$

and

$$\varphi_y = c_2 \frac{u_y}{R} - \frac{\partial w}{\partial y} \tag{1b}$$

Rotation of differential line elements in the tangent plane, about the normal vector at $(x, y, 0)$, is given by

$$\varphi_n = \frac{c_2}{2}\left[\frac{\partial u_y}{\partial x} - \frac{\partial u_x}{\partial y}\right] \tag{1c}$$

In these equations, and the equations that follow, two parameters, c_1 and c_2, appear that are used to trace the contributions of various terms to the equations governing the nonlinear and buckling response. As a result, these parameters are referred to herein as *tracers*. These tracers are equal to either unity or zero unless noted otherwise. For example, specifying $c_1 = 0$ eliminates terms associated with nonlinear rotations about the normal vector at $(x, y, 0)$, φ_n^2, and specifying $c_1 = c_2 = 0$ reduces Sanders' equations to Donnell's equations.

The nonlinear membrane-strain fields of the shell middle surface given in reference 19 are expressed as

$$\varepsilon_{xx}^{o} = \frac{\partial u_x}{\partial x} + \frac{1}{2}\left(\varphi_x^2 + c_1\varphi_n^2\right) \tag{2a}$$

$$\varepsilon^{o}_{yy} = \frac{\partial u_y}{\partial y} + \frac{w}{R} + \frac{1}{2}\left(\varphi_y^2 + c_1\varphi_n^2\right) \tag{2b}$$

$$\gamma^{o}_{xy} = 2\varepsilon^{o}_{xy} = \frac{\partial u_x}{\partial y} + \frac{\partial u_y}{\partial x} + \varphi_x\varphi_y \tag{2c}$$

when specialized to a surface in the form of a right-circular cylinder. Likewise, the bending-strain fields of the middle surface, associated with changes in surface curvature and torsion caused by deformation are given by

$$\kappa^{o}_{xx} = \frac{\partial \varphi_x}{\partial x} \tag{3a}$$

$$\kappa^{o}_{yy} = \frac{\partial \varphi_y}{\partial y} \tag{3b}$$

$$\kappa^{o}_{xy} = \frac{\partial \varphi_y}{\partial x} + \frac{\partial \varphi_x}{\partial y} + \frac{c_2}{R}\varphi_n \tag{3c}$$

Relationships between these middle-surface strains and the strains at any point (x, y, ζ) of the shell are obtained by comparing the virtual work given by equations (26)-(30) in reference 20 with the internal virtual work of the corresponding three-dimensional elastic cylinder undergoing small strains and moderately small rotations. In addition, use is made of the definitions for the generally unsymmetric stress results of classical shell theory that are encountered prior to neglecting ζ/R in the definitions (see reference 21, pp. 33). The internal virtual work of the shell, given by equations (26)-(30) in reference 20 and expressed in terms of the virtual strains associated with equations (2) and (3), is given by

$$\delta W_{int} = \int_0^L \int_0^{2\pi R} \left(\mathcal{N}_{xx}\delta\varepsilon^{o}_{xx} + \mathcal{N}_{yy}\delta\varepsilon^{o}_{yy} + \mathcal{N}_{xy}\delta\gamma^{o}_{xy} + \mathcal{M}_{xx}\delta\kappa^{o}_{xx} + \mathcal{M}_{yy}\delta\kappa^{o}_{yy} + \mathcal{M}_{xy}\delta\kappa^{o}_{xy} \right) dydx \tag{4}$$

where $\mathcal{N}_{xx}$, $\mathcal{N}_{yy}$, $\mathcal{N}_{xy}$, $\mathcal{M}_{xx}$, $\mathcal{M}_{yy}$, and $\mathcal{M}_{xy}$ are the effective stress resultants used by Sanders. The corresponding three-dimensional expression for the internal virtual work is given by

$$\delta W_{int} = \int_0^L \int_0^{2\pi R} \int_{-\frac{h}{2}}^{-\frac{h}{2}} \left(\sigma_{xx}\delta\varepsilon_{xx} + \sigma_{yy}\delta\varepsilon_{yy} + \sigma_{\zeta\zeta}\delta\varepsilon_{\zeta\zeta} + \sigma_{y\zeta}\delta\gamma_{y\zeta} + \sigma_{x\zeta}\delta\gamma_{x\zeta} + \sigma_{xy}\delta\gamma_{xy} \right) \left[1 + \frac{\zeta}{R} \right] d\zeta dydx \tag{5}$$

where σ_{xx}, σ_{yy}, $\sigma_{\zeta\zeta}$, $\sigma_{y\zeta}$, $\sigma_{x\zeta}$, and σ_{xy} are the stresses, and $\delta\varepsilon_{xx}$, $\delta\varepsilon_{yy}$, $\delta\varepsilon_{\zeta\zeta}$, $\delta\gamma_{y\zeta}$, $\delta\gamma_{x\zeta}$, and $\delta\gamma_{xy}$ are the

variations of the strains at the point (x, y, ζ). By applying the definitions for the generally unsymmetric stress resultants for shells to equations (26)-(30) in reference 20, the effective stress resultants of the cylindrical shell are identified as follows

$$\mathcal{N}_{xx} \equiv \int_{-\frac{h}{2}}^{-\frac{h}{2}} \sigma_{xx}\left[1 + \frac{\zeta}{R}\right] d\zeta \tag{6a}$$

$$\mathcal{N}_{yy} \equiv \int_{-\frac{h}{2}}^{-\frac{h}{2}} \sigma_{yy}\, d\zeta \tag{6b}$$

$$\mathcal{N}_{xy} \equiv \frac{1}{2}\left(\int_{-\frac{h}{2}}^{-\frac{h}{2}} \sigma_{xy}\, d\zeta + \int_{-\frac{h}{2}}^{-\frac{h}{2}} \sigma_{xy}\left[1 + \frac{\zeta}{R}\right] d\zeta \right) + \frac{1}{4R}\left(\int_{-\frac{h}{2}}^{-\frac{h}{2}} \sigma_{xy}\left[1 + \frac{\zeta}{R}\right] \zeta\, d\zeta - \int_{-\frac{h}{2}}^{-\frac{h}{2}} \sigma_{xy}\zeta\, d\zeta \right) \tag{6c}$$

$$\mathcal{M}_{xx} \equiv \int_{-\frac{h}{2}}^{-\frac{h}{2}} \sigma_{xx}\left[1 + \frac{\zeta}{R}\right] \zeta\, d\zeta \tag{6d}$$

$$\mathcal{M}_{yy} \equiv \int_{-\frac{h}{2}}^{-\frac{h}{2}} \sigma_{yy}\zeta\, d\zeta \tag{6e}$$

$$\mathcal{M}_{xy} \equiv \frac{1}{2}\left(\int_{-\frac{h}{2}}^{-\frac{h}{2}} \sigma_{xy}\zeta\, d\zeta + \int_{-\frac{h}{2}}^{-\frac{h}{2}} \sigma_{xy}\left[1 + \frac{\zeta}{R}\right] \zeta\, d\zeta \right) \tag{6f}$$

Finally, substituting equations (6) into (4) and comparing the result with equation (5) reveals that the corresponding three-dimensional strain field is given by

$$\varepsilon_{xx}(x, y, \zeta) = \varepsilon^{o}_{xx}(x, y) + \zeta\, \kappa^{o}_{xx}(x, y) \tag{7a}$$

$$\varepsilon_{yy}(x, y, \zeta) = \left[\varepsilon^{o}_{yy}(x, y) + \zeta\, \kappa^{o}_{yy}(x, y)\right]\left[1 + \frac{\zeta}{R}\right]^{-1} \tag{7b}$$

$$\varepsilon_{\zeta\zeta}(x, y, \zeta) = 0 \tag{7c}$$

$$\gamma_{xy}(x, y, \zeta) = \frac{1}{2}\left[\gamma^{o}_{xy}(x, y) + \zeta\, \kappa^{o}_{xy}(x, y)\right]\left(1 + \left[1 + \frac{\zeta}{R}\right]^{-1}\right) + \frac{1}{4}\gamma^{o}_{xy}(x, y)\left(\frac{\zeta}{R}\right)^{2}\left[1 + \frac{\zeta}{R}\right]^{-1} \tag{7d}$$

$$\gamma_{x\zeta}(x, y, \zeta) = 0 \tag{7e}$$

$$\gamma_{y\zeta}(x, y, \zeta) = 0 \tag{7f}$$

In a first-approximation shell theory, the external loads applied to a shell are, in general, composed of surface tractions and edge traction resultants that are applied to the middle surface and its boundary, respectively. For the problems considered herein, all applied loads and applied displacements leading to buckling vary proportionally with respect to a loading parameter, $\tilde{p}$, and the relative proportions of the loads and applied displacements are defined by a set of load factors. The loading parameter is presumed to increase monotonically from a value of zero, which is presumed to correspond to a stress- and strain- free state. The corresponding external virtual work of the shell is expressed as (e.g., see references 22 and 23)

$$\begin{aligned}
\delta W_{ext} = \tilde{p}\int_0^L\int_0^{2\pi R} & \left[\left(\ell_1 q_x + c_4\ell_3 q_\zeta \varphi_x\right)\delta u_x + \left(\ell_2 q_y + c_4\ell_3 q_\zeta \varphi_y\right)\delta u_y \right. \\
& \left. + \ell_3 q_\zeta + c_4\ell_3\left(q_\zeta\left[\varepsilon^{o}_{xxL} + \varepsilon^{o}_{yyL}\right] + \frac{\partial q_\zeta}{\partial x}\,u_x + \frac{\partial q_\zeta}{\partial y}\,u_y + \frac{\partial q_\zeta}{\partial \zeta}\,w\right)\delta w\right] dy dx \\
& + \tilde{p}\int_0^{2\pi R}\left[\ell_4 N_0(y)\delta u_x + \ell_5 S_0(y)\delta u_y + \ell_6 V_0(y)\delta w + \ell_7 M_0(y)\delta\varphi_x\right]_{x=0} dy \\
& + \tilde{p}\int_0^{2\pi R}\left[\ell_8 N_L(y)\delta u_x + \ell_9 S_L(y)\delta u_y + \ell_{10} V_L(y)\delta w + \ell_{11} M_L(y)\delta\varphi_x\right]_{x=L} dy
\end{aligned} \tag{8a}$$

where $q_x(x, y)$, $q_y(x, y)$, and $q_\zeta(x, y, \zeta)$ are functions defining the spatial distribution of the surface tractions that are applied to the middle surface in the axial, circumferential, and radial directions, respectively. In addition, q_ζ is presumed to be a nonconservative, "live" pressure loading that remains normal to the middle surface during deformation; hence the functional dependence of q_ζ on the radial coordinate ζ. The symbols $N_0(y)$, $S_0(y)$, $V_0(y)$, and $M_0(y)$ represent the spatial distribution of the stress resultants of tractions that are applied to the end of the cylinder at $x = 0$. Likewise, $N_L(y)$, $S_L(y)$, $V_L(y)$, and $M_L(y)$ represent the applied loads at $x = L$. The symbols ℓ_1 through ℓ_{11} are the load factors mentioned previously. The symbols ε^{o}_{xxL} and ε^{o}_{yyL} denote the linear part of the strains given by equations (2a) and (2b), respectively, and all terms multiplied by c_4

are terms associated with a nonconservative, "live" pressure loading. These "live" pressure terms are obtained from Cohen,[21] and are consistent with the potential energy terms given by Koiter[22] for uniform pressure (see equation (3.5) in reference 24) for the "small" strain and "moderate" rotation theory of Sanders.[19] For "dead" pressure loading, $c_4 = 0$ and for "live" pressure loading $c_4 = 1$. In addition, whenever Donnell's equations are used ($c_1 = c_2 = 0$), $c_4 = 0$ is typically used herein. Integrating the live pressure terms by parts gives

$$\int_0^L \int_0^{2\pi R} \left(q_\zeta \left[\varphi_x \, \delta u_x + \varphi_y \, \delta u_y \right] + \left[q_\zeta \left(\varepsilon^o_{xxL} + \varepsilon^o_{yyL} \right) + \frac{\partial q_\zeta}{\partial x} u_x + \frac{\partial q_\zeta}{\partial y} u_y + \frac{\partial q_\zeta}{\partial \zeta} w \right] \delta w \right) dy dx =$$

$$\frac{1}{2}\delta \int_0^L \int_0^{2\pi R} \left[q_\zeta \left(\varphi_x u_x + \varphi_y u_y + \left(\varepsilon^o_{xxL} + \varepsilon^o_{yyL} \right) w \right) + \frac{\partial q_\zeta}{\partial x} \left(w u_x \right) + \frac{\partial q_\zeta}{\partial y} \left(w u_y \right) + \frac{\partial q_\zeta}{\partial \zeta} w^2 \right] dy dx +$$

$$\frac{1}{2} \int_0^{2\pi R} \left[q_\zeta \left(u_x \, \delta w - w \, \delta u_x \right) \right]_0^L dy \tag{8b}$$

Substituting equation (8b) into (8a) yields the external virtual work

$$\delta W_{ext} = \int_0^L \int_0^{2\pi R} \left[\ell_1 q_x \, \delta u_x + \ell_2 q_y \, \delta u_y + \ell_3 q_\zeta \, \delta w \right] dy dx +$$

$$\frac{\tilde{p}}{2}\delta \int_0^L \int_0^{2\pi R} c_4 \ell_3 \left(q_\zeta \left[\varphi_x u_x + \varphi_y u_y + \left(\varepsilon^o_{xxL} + \varepsilon^o_{yyL} \right) w \right] + \frac{\partial q_\zeta}{\partial x} \left(w u_x \right) + \frac{\partial q_\zeta}{\partial y} \left(w u_y \right) + \frac{\partial q_\zeta}{\partial \zeta} w^2 \right) dy dx +$$

$$\frac{1}{2}\tilde{p} \int_0^{2\pi R} \left[c_4 \ell_3 q_\zeta \left(u_x \, \delta w - w \, \delta u_x \right) \right]_0^L dy + \tag{8c}$$

$$+ \tilde{p} \int_0^{2\pi R} \left[\ell_4 N_0(y) \delta u_x + \ell_5 S_0(y) \delta u_y + \ell_6 V_0(y) \delta w + \ell_7 M_0(y) \delta \varphi_x \right]_{x=0} dy$$

$$+ \tilde{p} \int_0^{2\pi R} \left[\ell_8 N_L(y) \delta u_x + \ell_9 S_L(y) \delta u_y + \ell_{10} V_L(y) \delta w + \ell_{11} M_L(y) \delta \varphi_x \right]_{x=L} dy$$

Inspection of this equation reveals that the external virtual work can be represented as the variation of a potential function when the boundary integral involving c_4 vanishes. This equation is slightly different from that given by Cohen,[23] but is consistent with that given by Budiansky[22] and by Sheinman and Tene.[25]

Next equations (1)-(3) are used to obtain expressions for the virtual strains appearing in equation (4) in terms of the primary virtual-displacement fields δu_x, δu_y, and δw. Enforcing $\delta W_{int} = \delta W_{ext}$, integrating by parts to reduce derivatives of δu_x, δu_y, and δw to independent variations, and enforcing the fundamental theorem of the Calculus of Variations yields the equilibrium equations and boundary conditions. The three equilibrium equations corresponding to the primary virtual displacements are

$$\frac{\partial \mathcal{N}_{xx}}{\partial x} + \frac{\partial \mathcal{N}_{xy}}{\partial y} - \frac{c_2}{2}\frac{\partial}{\partial y}\left(\frac{\mathcal{M}_{xy}}{R} + c_1\left(\mathcal{N}_{xx} + \mathcal{N}_{yy}\right)\varphi_n \right) + \tilde{p}\left(\ell_1 q_x + c_4 \ell_3 q_\zeta \varphi_x\right) = 0 \tag{9a}$$

$$\frac{\partial \mathcal{N}_{xy}}{\partial x} + \frac{\partial \mathcal{N}_{yy}}{\partial y} + \frac{c_2}{R}\left(Q_y + \frac{1}{2}\frac{\partial \mathcal{M}_{xy}}{\partial x} - \varphi_x \mathcal{N}_{xy} - \varphi_y \mathcal{N}_{yy} \right) + \tilde{p}\left(\ell_2 q_y + c_4 \ell_3 q_\zeta \varphi_y\right) + \frac{c_1}{2}\frac{\partial}{\partial x}\left[\left(\mathcal{N}_{xx} + \mathcal{N}_{yy}\right)\varphi_n\right] = 0 \tag{9b}$$

$$\frac{\partial Q_x}{\partial x} + \frac{\partial Q_y}{\partial y} - \frac{\mathcal{N}_{yy}}{R} + \tilde{p}\ell_3\left(q_\zeta + c_4 q_\zeta\left[\varepsilon^{o}_{xxL} + \varepsilon^{o}_{yyL}\right] + c_4\left[\frac{\partial q_\zeta}{\partial x}u_x + \frac{\partial q_\zeta}{\partial y}u_y + \frac{\partial q_\zeta}{\partial \zeta}w\right]\right) - \frac{\partial}{\partial x}\left[\varphi_x \mathcal{N}_{xx} + \varphi_y \mathcal{N}_{xy}\right] - \frac{\partial}{\partial y}\left[\varphi_x \mathcal{N}_{xy} + \varphi_y \mathcal{N}_{yy}\right] = 0 \tag{9c}$$

where

$$Q_x = \frac{\partial \mathcal{M}_{xx}}{\partial x} + \frac{\partial \mathcal{M}_{xy}}{\partial y} \tag{9d}$$

and

$$Q_y = \frac{\partial \mathcal{M}_{xy}}{\partial x} + \frac{\partial \mathcal{M}_{yy}}{\partial y} \tag{9e}$$

The live pressure terms in equations (9) are those multiplied by the tracer c_4 and are consistent with those given in reference 26. The boundary conditions for the edge $x = 0$ that are obtained from the variational process are given by

$$\mathcal{N}_{xx} = \tilde{p}\ell_4 N_0(y) \quad \text{or} \quad u_x = \tilde{p}\ell_4 \Delta^{0}_{x}(y) \tag{10a}$$

$$\mathcal{N}_{xy} + \frac{3c_2\mathcal{M}_{xy}}{2R} + \frac{c_1}{2}\left(\mathcal{N}_{xx} + \mathcal{N}_{yy}\right)\varphi_n = \tilde{p}\ell_5 S_0(y) \quad \text{or} \quad u_y = \tilde{p}\ell_5 \Delta_y^0(y) \tag{10b}$$

$$Q_x + \frac{\partial \mathcal{M}_{xy}}{\partial y} - \varphi_x \mathcal{N}_{xx} - \varphi_y \mathcal{N}_{xy} = \tilde{p}\ell_6 V_0(y) \quad \text{or} \quad w = \tilde{p}\ell_6 \Delta_\zeta^0(y) \tag{10c}$$

$$\mathcal{M}_{xx} = \tilde{p}\ell_7 M_0(y) \quad \text{or} \quad \varphi_x = -\frac{\partial w}{\partial x} = \tilde{p}\ell_7 \phi_0(y) \tag{10d}$$

and for the edge $x = L$ are given by

$$\mathcal{N}_{xx} = \tilde{p}\ell_8 N_L(y) \quad \text{or} \quad u_x = \tilde{p}\ell_8 \Delta_x^L(y) \tag{10e}$$

$$\mathcal{N}_{xy} + \frac{3c_2\mathcal{M}_{xy}}{2R} + \frac{c_1}{2}\left(\mathcal{N}_{xx} + \mathcal{N}_{yy}\right)\varphi_n = \tilde{p}\ell_9 S_L(y) \quad \text{or} \quad u_y = \tilde{p}\ell_9 \Delta_y^L(y) \tag{10f}$$

$$Q_x + \frac{\partial \mathcal{M}_{xy}}{\partial y} - \varphi_x \mathcal{N}_{xx} - \varphi_y \mathcal{N}_{xy} = \tilde{p}\ell_{10} V_L(y) \quad \text{or} \quad w = \tilde{p}\ell_{10} \Delta_\zeta^L(y) \tag{10g}$$

$$\mathcal{M}_{xx} = \tilde{p}\ell_{11} M_L(y) \quad \text{or} \quad \varphi_x = -\frac{\partial w}{\partial x} = \tilde{p}\ell_{11} \phi_L(y) \tag{10h}$$

The constitutive equations are approximate by definition because the relationships between stresses and strains are determined experimentally. In Sanders' theory, simplified constitutive equations are derived on the basis of neglecting ζ/R in equations (6) and (7). This simplification yields the same constitutive equations of Love's first approximation, classical shell theory that are given by

$$\left\{\begin{array}{c} \mathcal{N}_{xx} \\ \mathcal{N}_{yy} \\ \mathcal{N}_{xy} \\ \hline \mathcal{M}_{xx} \\ \mathcal{M}_{yy} \\ \mathcal{M}_{xy} \end{array}\right\} = \left[\begin{array}{ccc|ccc} A_{11} & A_{12} & A_{16} & B_{11} & B_{12} & B_{16} \\ A_{12} & A_{22} & A_{26} & B_{12} & B_{22} & B_{26} \\ A_{16} & A_{26} & A_{66} & B_{16} & B_{26} & B_{66} \\ \hline B_{11} & B_{12} & B_{16} & D_{11} & D_{12} & D_{16} \\ B_{12} & B_{22} & B_{26} & D_{12} & D_{22} & D_{26} \\ B_{16} & B_{26} & B_{66} & D_{16} & D_{26} & D_{66} \end{array}\right] \left\{\begin{array}{c} \varepsilon_{xx}^o \\ \varepsilon_{yy}^o \\ \gamma_{xy}^o \\ \hline \kappa_{xx}^o \\ \kappa_{yy}^o \\ \kappa_{xy}^o \end{array}\right\} - \left\{\begin{array}{c} N_{xx}^T \\ N_{yy}^T \\ N_{xy}^T \\ \hline M_{xx}^T \\ M_{yy}^T \\ M_{xy}^T \end{array}\right\} \tag{11}$$

where the terms appearing in the matrix are the shell-wall stiffnesses and the rightmost vector contains the ficticious thermal stress resultants associated with changes in the temperature field

acting on a shell from that of the stress- and strain-free reference state. For a thin laminated-composite shell with a regular array of rings and stringers, such as that shown in figure 2, a homogenized first-approximation representation of the stiffnesses in equation (11) are given by

$$\begin{bmatrix} A_{11} & A_{12} & A_{16} \\ A_{12} & A_{22} & A_{26} \\ A_{16} & A_{26} & A_{66} \end{bmatrix} = \begin{bmatrix} A_{11}^{shell} & A_{12}^{shell} & A_{16}^{shell} \\ A_{12}^{shell} & A_{22}^{shell} & A_{26}^{shell} \\ A_{16}^{shell} & A_{26}^{shell} & A_{66}^{shell} \end{bmatrix} + \begin{bmatrix} \frac{E_s A_s}{d_s} & 0 & 0 \\ 0 & \frac{E_r A_r}{d_r} & 0 \\ 0 & 0 & 0 \end{bmatrix} \tag{12a}$$

$$\begin{bmatrix} B_{11} & B_{12} & B_{16} \\ B_{12} & B_{22} & B_{26} \\ B_{16} & B_{26} & B_{66} \end{bmatrix} = \begin{bmatrix} B_{11}^{shell} & B_{12}^{shell} & B_{16}^{shell} \\ B_{12}^{shell} & B_{22}^{shell} & B_{26}^{shell} \\ B_{16}^{shell} & B_{26}^{shell} & B_{66}^{shell} \end{bmatrix} + \begin{bmatrix} \frac{E_s A_s}{d_s} e_s & 0 & 0 \\ 0 & \frac{E_r A_r}{d_r} e_r & 0 \\ 0 & 0 & 0 \end{bmatrix} \tag{12b}$$

$$\begin{bmatrix} D_{11} & D_{12} & D_{16} \\ D_{12} & D_{22} & D_{26} \\ D_{16} & D_{26} & D_{66} \end{bmatrix} = \begin{bmatrix} D_{11}^{shell} & D_{12}^{shell} & D_{16}^{shell} \\ D_{12}^{shell} & D_{22}^{shell} & D_{26}^{shell} \\ D_{16}^{shell} & D_{26}^{shell} & D_{66}^{shell} \end{bmatrix} + \begin{bmatrix} \frac{E_s}{d_s}\left(I_s^c + e_s^2 A_s\right) & 0 & 0 \\ 0 & \frac{E_r}{d_r}\left(I_r^c + e_r^2 A_r\right) & 0 \\ 0 & 0 & \frac{1}{4}\left(\frac{G_s J_s}{d_s} + \frac{G_r J_r}{d_r}\right) \end{bmatrix} \tag{12c}$$

In equations (12), E_s and E_r are the elastic moduli of the stringers and rings, respectively. Likewise, G_s and G_r are the corresponding shear moduli, A_s and A_r are the cross-sectional areas, I_s^c and I_r^c are the centroidal moments of inertia, J_s and J_r are the torsion constants, e_s and e_r are the eccentricies of the cross-sectional centroids with respect to the middle surface, and d_s and d_r define the spacing of the stringers and rings, respectively. The constitutive terms with the superscript "shell" are the usual definitions given for laminated-composite plates (e.g., see reference 27). Expressions for other stiffener configurations are found in reference 28.

Bifurcation Analysis

The buckling equations of the present study are obtained by following the procedure of classical linear-bifurcation analysis, as presented by Brush and Almroth.[17] As such, the shell is presumed to be geometrically perfect and elastic, and a continuously connected family of linear prebuckling states given by $\overset{(0)}{u}_x(x, y)$, $\overset{(0)}{u}_y(x, y)$, and $\overset{(0)}{w}(x, y)$ is presumed to exist as a loading parameter $\tilde{p}$ is monotinically increased, in a continuous manner, from an inital value of zero. This set of prebuckling states is referred to herein as the primary or prebuckling equilibrium path. The stresses and deformations in the prebuckling states are presumed to vary proportionally with an

increase in the loading parameter. When the loading parameter is equal to zero, the shell is presumed to be in a stress-free and strain-free state or to be in a stress and strain state associated with passive loading condition that is not related to the loading parameter and that does not lead to an instability.

The goal of the bifurcation analysis is to determine the critical value of the loading parameter for which an equilibrium state exists, other than the corresponding prebuckling equilibrium state for a given geometrically perfect shell. Geometrically, this critical value of the loading parameter represents the intersection of the primary equlibrium path with one or more adjacent equilibrium paths, that are associated with a deformed configuration of the shell, in the solution space. Mathematically, this critical value corresponds to the existence of two or more solutions to the nonlinear boundary-value problem. This point of intersection is obtained by expressing the displacement fields of the idealized shell as an infinitesimal perturbation about an arbitrary primary equilibrium state; that is,

$$u_x(x, y) = \overset{(0)}{u}_x(x, y) + \xi \overset{(1)}{u}_x(x, y) \tag{13a}$$

$$u_y(x, y) = \overset{(0)}{u}_y(x, y) + \xi \overset{(1)}{u}_y(x, y) \tag{13b}$$

$$w(x, y) = \overset{(0)}{w}(x, y) + \xi \overset{(1)}{w}(x, y) \tag{13c}$$

The parameter ξ defines the "distance" between adjacent equlibrium states and can be made as small as required so that terms involving its products are negligible. Substituting these expansions into equations (1), which defines the linear rotation parameters, yields

$$\{\varphi\} = \{\overset{(0)}{\varphi}\} + \xi \{\overset{(1)}{\varphi}\} \tag{14a}$$

where

$$\{\varphi\} = \begin{Bmatrix} \varphi_x \\ \varphi_y \\ \varphi_n \end{Bmatrix} \tag{14b}$$

$$\{\overset{(0)}{\varphi}\} = \begin{Bmatrix} \overset{(0)}{\varphi}_x(x, y) \\ \overset{(0)}{\varphi}_y(x, y) \\ \overset{(0)}{\varphi}_n(x, y) \end{Bmatrix} = \begin{Bmatrix} -\dfrac{\partial \overset{(0)}{w}}{\partial x} \\ \dfrac{c_2}{R} \overset{(0)}{u}_y \\ \dfrac{c_2}{2} \left[\dfrac{\partial \overset{(0)}{u}_y}{\partial x} - \dfrac{\partial \overset{(0)}{u}_x}{\partial y} \right] \end{Bmatrix} \tag{14c}$$

and

$$\left\{\overset{(1)}{\varphi}\right\} = \begin{Bmatrix} \overset{(1)}{\varphi}_x(x, y) \\ \overset{(1)}{\varphi}_y(x, y) \\ \overset{(1)}{\varphi}_n(x, y) \end{Bmatrix} = \begin{Bmatrix} -\dfrac{\partial \overset{(1)}{w}}{\partial x} \\ \dfrac{c_2}{R}\overset{(1)}{u}_y - \dfrac{\partial \overset{(1)}{w}}{\partial y} \\ \dfrac{c_2}{2}\left[\dfrac{\partial \overset{(1)}{u}_y}{\partial x} - \dfrac{\partial \overset{(1)}{u}_x}{\partial y}\right] \end{Bmatrix} \tag{14d}$$

Next, the middle-surface strains are expressed in column vector form as

$$\left\{\varepsilon^o\right\} = \begin{Bmatrix} \varepsilon^o_{xx} \\ \varepsilon^o_{yy} \\ \gamma^o_{xy} \end{Bmatrix} = \begin{Bmatrix} \dfrac{\partial u_x}{\partial x} + \dfrac{1}{2}\left(\varphi_x^2 + c_1\varphi_n^2\right) \\ \dfrac{\partial u_y}{\partial y} + \dfrac{w}{R} + \dfrac{1}{2}\left(\varphi_y^2 + c_1\varphi_n^2\right) \\ \dfrac{\partial u_x}{\partial y} + \dfrac{\partial u_y}{\partial x} + \varphi_x\varphi_y \end{Bmatrix} \tag{15}$$

and

$$\left\{\kappa^o\right\} = \begin{Bmatrix} \kappa^o_{xx} \\ \kappa^o_{yy} \\ \kappa^o_{xy} \end{Bmatrix} = \begin{Bmatrix} \dfrac{\partial \varphi_x}{\partial x} \\ \dfrac{\partial \varphi_y}{\partial y} \\ \dfrac{\partial \varphi_y}{\partial x} + \dfrac{\partial \varphi_x}{\partial y} + \dfrac{c_2}{R}\varphi_n \end{Bmatrix} \tag{16}$$

Substituting equations (13) into equations (15) and (16) gives

$$\left\{\varepsilon^o\right\} = \left\{\overset{(0)}{\varepsilon}\right\} + \xi\left\{\overset{(1)}{\varepsilon}\right\} + \mathcal{O}\left(\xi^2\right) \tag{17a}$$

$$\left\{\kappa^o\right\} = \left\{\overset{(0)}{\kappa}\right\} + \xi\left\{\overset{(1)}{\kappa}\right\} \tag{17b}$$

where

$$\left\{\overset{(0)}{\varepsilon}\right\} = \begin{Bmatrix} \overset{(0)}{\varepsilon}_{xx} \\ \overset{(0)}{\varepsilon}_{yy} \\ \overset{(0)}{\gamma}_{xy} \end{Bmatrix} = \begin{Bmatrix} \dfrac{\partial \overset{(0)}{u}_x}{\partial x} \\ \dfrac{\partial \overset{(0)}{u}_y}{\partial y} + \dfrac{\overset{(0)}{w}}{R} \\ \dfrac{\partial \overset{(0)}{u}_x}{\partial y} + \dfrac{\partial \overset{(0)}{u}_y}{\partial x} \end{Bmatrix} \tag{18a}$$

and

$$\left\{\overset{(1)}{\varepsilon}\right\} = \begin{Bmatrix} \overset{(1)}{\varepsilon}_{xx} \\ \overset{(1)}{\varepsilon}_{yy} \\ \overset{(1)}{\gamma}_{xy} \end{Bmatrix} = \begin{Bmatrix} \dfrac{\partial \overset{(1)}{u}_x}{\partial x} \\ \dfrac{\partial \overset{(1)}{u}_y}{\partial y} + \dfrac{\overset{(1)}{w}}{R} \\ \dfrac{\partial \overset{(1)}{u}_x}{\partial y} + \dfrac{\partial \overset{(1)}{u}_y}{\partial x} \end{Bmatrix} \tag{18b}$$

$$\left\{\overset{(0)}{\kappa}\right\} = \begin{Bmatrix} \overset{(0)}{\kappa}_{xx} \\ \overset{(0)}{\kappa}_{yy} \\ \overset{(0)}{\kappa}_{xy} \end{Bmatrix} = \begin{Bmatrix} \dfrac{\partial \overset{(0)}{\varphi}_x}{\partial x} \\ \dfrac{\partial \overset{(0)}{\varphi}_y}{\partial y} \\ \dfrac{\partial \overset{(0)}{\varphi}_y}{\partial x} + \dfrac{\partial \overset{(0)}{\varphi}_x}{\partial y} + \dfrac{c_2}{R}\overset{(0)}{\varphi}_n \end{Bmatrix} = \begin{Bmatrix} -\dfrac{\partial^2 \overset{(0)}{w}}{\partial x^2} \\ \dfrac{c_2}{R}\dfrac{\partial \overset{(0)}{u}_y}{\partial y} - \dfrac{\partial^2 \overset{(0)}{w}}{\partial y^2} \\ \dfrac{c_2}{2R}\left(3\dfrac{\partial \overset{(0)}{u}_y}{\partial x} - \dfrac{\partial \overset{(0)}{u}_x}{\partial y}\right) - 2\dfrac{\partial^2 \overset{(0)}{w}}{\partial x \partial y} \end{Bmatrix} \tag{18c}$$

and

$$\left\{\overset{(1)}{\kappa}\right\} = \begin{Bmatrix} \overset{(1)}{\kappa}_{xx} \\ \overset{(1)}{\kappa}_{yy} \\ \overset{(1)}{\kappa}_{xy} \end{Bmatrix} = \begin{Bmatrix} \dfrac{\partial \overset{(1)}{\varphi}_x}{\partial x} \\ \dfrac{\partial \overset{(1)}{\varphi}_y}{\partial y} \\ \dfrac{\partial \overset{(1)}{\varphi}_y}{\partial x} + \dfrac{\partial \overset{(1)}{\varphi}_x}{\partial y} + \dfrac{c_2}{R}\overset{(1)}{\varphi}_n \end{Bmatrix} = \begin{Bmatrix} -\dfrac{\partial^2 \overset{(1)}{w}}{\partial x^2} \\ \dfrac{c_2}{R}\dfrac{\partial \overset{(1)}{u}_y}{\partial y} - \dfrac{\partial^2 \overset{(1)}{w}}{\partial y^2} \\ \dfrac{c_2}{2R}\left(3\dfrac{\partial \overset{(1)}{u}_y}{\partial x} - \dfrac{\partial \overset{(1)}{u}_x}{\partial y}\right) - 2\dfrac{\partial^2 \overset{(1)}{w}}{\partial x \partial y} \end{Bmatrix} \tag{18d}$$

As part of the linearization process, terms that are nonlinear in the prebuckling rotations $\overset{(0)}{\varphi}_x$, $\overset{(0)}{\varphi}_y$, and $\overset{(0)}{\varphi}_n$ have been neglected in equations (18). In equation (17a), the symbol $\mathcal{O}(\xi^2)$ denotes terms of second order that are neglected.

The constitutive equations, given by equations (11), are expressed in matrix form as

$$\left\{\mathcal{N}\right\} = [A]\left\{\varepsilon^o\right\} + [B]\left\{\kappa^o\right\} \pm \left\{N^T\right\} \tag{19a}$$

and

$$\left\{\mathcal{M}\right\} = [B]\left\{\varepsilon^o\right\} + [D]\left\{\kappa^o\right\} \pm \left\{M^T\right\} \tag{19b}$$

where $\left\{\varepsilon^o\right\}$ and $\left\{\kappa^o\right\}$ are defined by equations (15) and (16), respectively, and

$$\left\{\mathcal{N}\right\}^T = \left\{\mathcal{N}_{xx} \;\; \mathcal{N}_{yy} \;\; \mathcal{N}_{xy}\right\} \tag{19c}$$

$$\{\mathcal{M}\}^{\mathbf{T}} = \{\mathcal{M}_{xx}\ \mathcal{M}_{yy}\ \mathcal{M}_{xy}\} \tag{19d}$$

$$[\mathrm{A}] = \begin{bmatrix} \mathrm{A}_{11}\ \mathrm{A}_{12}\ \mathrm{A}_{16} \\ \mathrm{A}_{12}\ \mathrm{A}_{22}\ \mathrm{A}_{26} \\ \mathrm{A}_{16}\ \mathrm{A}_{26}\ \mathrm{A}_{66} \end{bmatrix} \tag{19e}$$

$$[\mathrm{B}] = \begin{bmatrix} \mathrm{B}_{11}\ \mathrm{B}_{12}\ \mathrm{B}_{16} \\ \mathrm{B}_{12}\ \mathrm{B}_{22}\ \mathrm{B}_{26} \\ \mathrm{B}_{16}\ \mathrm{B}_{26}\ \mathrm{B}_{66} \end{bmatrix} \tag{19f}$$

$$[\mathrm{D}] = \begin{bmatrix} \mathrm{D}_{11}\ \mathrm{D}_{12}\ \mathrm{D}_{16} \\ \mathrm{D}_{12}\ \mathrm{D}_{22}\ \mathrm{D}_{26} \\ \mathrm{D}_{16}\ \mathrm{D}_{26}\ \mathrm{D}_{66} \end{bmatrix} \tag{19g}$$

$$\{\mathrm{N}^{\mathrm{T}}\}^{\mathbf{T}} = \{\mathrm{N}_{xx}^{\mathrm{T}}\ \mathrm{N}_{yy}^{\mathrm{T}}\ \mathrm{N}_{xy}^{\mathrm{T}}\} \tag{19h}$$

$$\{\mathrm{M}^{\mathrm{T}}\}^{\mathbf{T}} = \{\mathrm{M}_{xx}^{\mathrm{T}}\ \mathrm{M}_{yy}^{\mathrm{T}}\ \mathrm{M}_{xy}^{\mathrm{T}}\} \tag{19i}$$

In these equations, the bold superscript "**T**" denotes matrix transposition. Substituting equations (17) into equations (19a) and (19b) yields

$$\{\mathcal{N}\} = \{\overset{(0)}{\mathcal{N}}\} + \xi\{\overset{(1)}{\mathcal{N}}\} + \mathcal{O}(\xi^2) \tag{20a}$$

and

$$\{\mathcal{M}\} = \{\overset{(0)}{\mathcal{M}}\} + \xi\{\overset{(1)}{\mathcal{M}}\} + \mathcal{O}(\xi^2) \tag{20b}$$

where

$$\{\overset{(0)}{\mathcal{N}}\} \equiv \begin{Bmatrix} \overset{(0)}{\mathcal{N}}_{xx} \\ \overset{(0)}{\mathcal{N}}_{yy} \\ \overset{(0)}{\mathcal{N}}_{xy} \end{Bmatrix} = [\mathrm{A}]\{\overset{(0)}{\varepsilon}\} + [\mathrm{B}]\{\overset{(0)}{\kappa}\} - \{\mathrm{N}^{\mathrm{T}}\} \tag{21a}$$

$$\left\{\overset{(0)}{\mathcal{M}}\right\} \equiv \begin{Bmatrix} \overset{(0)}{\mathcal{M}}_{xx} \\ \overset{(0)}{\mathcal{M}}_{yy} \\ \overset{(0)}{\mathcal{M}}_{xy} \end{Bmatrix} = [B]\left\{\overset{(0)}{\varepsilon}\right\} + [D]\left\{\overset{(0)}{\kappa}\right\} - \left\{M^{T}\right\} \tag{21b}$$

$$\left\{\overset{(1)}{\mathcal{N}}\right\} \equiv \begin{Bmatrix} \overset{(1)}{\mathcal{N}}_{xx} \\ \overset{(1)}{\mathcal{N}}_{yy} \\ \overset{(1)}{\mathcal{N}}_{xy} \end{Bmatrix} = [A]\left\{\overset{(1)}{\varepsilon}\right\} + [B]\left\{\overset{(1)}{\kappa}\right\} \tag{21c}$$

$$\left\{\overset{(1)}{\mathcal{M}}\right\} \equiv \begin{Bmatrix} \overset{(1)}{\mathcal{M}}_{xx} \\ \overset{(1)}{\mathcal{M}}_{yy} \\ \overset{(1)}{\mathcal{M}}_{xy} \end{Bmatrix} = [B]\left\{\overset{(1)}{\varepsilon}\right\} + [D]\left\{\overset{(1)}{\kappa}\right\} \tag{21d}$$

with $\left\{\overset{(0)}{\varepsilon}\right\}$, $\left\{\overset{(1)}{\varepsilon}\right\}$, $\left\{\overset{(0)}{\kappa}\right\}$, and $\left\{\overset{(1)}{\kappa}\right\}$ given by equations (18). Similarly, expansion of the equilibrium equations, given by equations (9), results in

$$\frac{\partial \overset{(0)}{\mathcal{N}}_{xx}}{\partial x} + \frac{\partial \overset{(0)}{\mathcal{N}}_{xy}}{\partial y} - \frac{c_2}{2}\frac{\partial}{\partial y}\left(\frac{\overset{(0)}{\mathcal{M}}_{xy}}{R}\right) + \tilde{p}\left(\ell_1 q_x + c_4 \ell_3 q_\zeta \overset{(0)}{\varphi}_x\right) = 0 \tag{22a}$$

$$\frac{\partial \overset{(0)}{\mathcal{N}}_{xy}}{\partial x} + \frac{\partial \overset{(0)}{\mathcal{N}}_{yy}}{\partial y} + \frac{c_2}{R}\left(\overset{(0)}{Q}_y + \frac{1}{2}\frac{\partial \overset{(0)}{\mathcal{M}}_{xy}}{\partial x}\right) + \tilde{p}\left(\ell_2 q_y + c_4 \ell_3 q_\zeta \overset{(0)}{\varphi}_y\right) = 0 \tag{22b}$$

$$\overset{(0)}{Q}_x = \frac{\partial \overset{(0)}{\mathcal{M}}_{xx}}{\partial x} + \frac{\partial \overset{(0)}{\mathcal{M}}_{xy}}{\partial y} \tag{22c}$$

$$\overset{(0)}{Q}_y = \frac{\partial \overset{(0)}{\mathcal{M}}_{xy}}{\partial x} + \frac{\partial \overset{(0)}{\mathcal{M}}_{yy}}{\partial y} \tag{22d}$$

$$\frac{\partial \overset{(0)}{Q}_x}{\partial x} + \frac{\partial \overset{(0)}{Q}_y}{\partial y} - \frac{\overset{(0)}{\mathcal{N}}_{yy}}{R} + \tilde{p}\ell_3\left(q_\zeta + c_4 q_\zeta\left(\overset{(0)}{\varepsilon}_{xx} + \overset{(0)}{\varepsilon}_{yy}\right) + \frac{\partial q_\zeta}{\partial x}\overset{(0)}{u}_x + \frac{\partial q_\zeta}{\partial y}\overset{(0)}{u}_y + \frac{\partial q_\zeta}{\partial \zeta}\overset{(0)}{w}\right) = 0 \tag{22e}$$

for the zeroth-order terms and

$$\frac{\partial \overset{(1)}{\mathcal{N}}_{xx}}{\partial x} + \frac{\partial \overset{(1)}{\mathcal{N}}_{xy}}{\partial y} - \frac{1}{2}\frac{\partial}{\partial y}\left(c_2 \frac{\overset{(1)}{\mathcal{M}}_{xy}}{R} + c_1 \left(\overset{(0)}{\mathcal{N}}_{xx} + \overset{(0)}{\mathcal{N}}_{yy} \right) \overset{(1)}{\varphi}_n \right) + c_4 \ell_3 \tilde{p} q_\zeta \overset{(1)}{\varphi}_x = 0 \tag{23a}$$

$$\frac{\partial \overset{(1)}{\mathcal{N}}_{xy}}{\partial x} + \frac{\partial \overset{(1)}{\mathcal{N}}_{yy}}{\partial y} + \frac{c_2}{R}\left(\overset{(1)}{Q}_y + \frac{1}{2}\frac{\partial \overset{(1)}{\mathcal{M}}_{xy}}{\partial x} - \overset{(1)}{\varphi}_x \overset{(0)}{\mathcal{N}}_{xy} - \overset{(1)}{\varphi}_y \overset{(0)}{\mathcal{N}}_{yy} \right) + \frac{c_1}{2}\frac{\partial}{\partial x}\left[\left(\overset{(0)}{\mathcal{N}}_{xx} + \overset{(0)}{\mathcal{N}}_{yy} \right) \overset{(1)}{\varphi}_n \right] + c_4 \ell_3 \tilde{p} q_\zeta \overset{(1)}{\varphi}_y = 0 \tag{23b}$$

$$\overset{(1)}{Q}_x = \frac{\partial \overset{(1)}{\mathcal{M}}_{xx}}{\partial x} + \frac{\partial \overset{(1)}{\mathcal{M}}_{xy}}{\partial y} \tag{23c}$$

$$\overset{(1)}{Q}_y = \frac{\partial \overset{(1)}{\mathcal{M}}_{xy}}{\partial x} + \frac{\partial \overset{(1)}{\mathcal{M}}_{yy}}{\partial y} \tag{23d}$$

$$\frac{\partial \overset{(1)}{Q}_x}{\partial x} + \frac{\partial \overset{(1)}{Q}_y}{\partial y} - \frac{\overset{(1)}{\mathcal{N}}_{yy}}{R} - \frac{\partial}{\partial x}\left[\overset{(1)}{\varphi}_x \overset{(0)}{\mathcal{N}}_{xx} + \overset{(1)}{\varphi}_y \overset{(0)}{\mathcal{N}}_{xy} \right] - \frac{\partial}{\partial y}\left[\overset{(1)}{\varphi}_x \overset{(0)}{\mathcal{N}}_{xy} + \overset{(1)}{\varphi}_y \overset{(0)}{\mathcal{N}}_{yy} \right] + c_4 \ell_3 \tilde{p}\left[q_\zeta \left(\overset{(1)}{\varepsilon}_{xx} + \overset{(1)}{\varepsilon}_{yy} \right) + \frac{\partial q_\zeta}{\partial x} \overset{(1)}{u}_x + \frac{\partial q_\zeta}{\partial y} \overset{(1)}{u}_y + \frac{\partial q_\zeta}{\partial \zeta} \overset{(1)}{w} \right] = 0 \tag{23e}$$

for the first-order terms. Similarly, expanding the boundary conditions, given by equations (10), yields the nonhomogeneous boundary conditions

$$\overset{(0)}{\mathcal{N}}_{xx} = \tilde{p}\ell_4 N_0(y) \quad \text{or} \quad \overset{(0)}{u}_x = \tilde{p}\ell_4 \Delta_x^0(y) \tag{24a}$$

$$\overset{(0)}{\mathcal{N}}_{xy} + \frac{3c_2 \overset{(0)}{\mathcal{M}}_{xy}}{2R} = \tilde{p}\ell_5 S_0(y) \quad \text{or} \quad \overset{(0)}{u}_y = \tilde{p}\ell_5 \Delta_y^0(y) \tag{24b}$$

$$\overset{(0)}{Q}_x + \frac{\partial \overset{(0)}{\mathcal{M}}_{xy}}{\partial y} = \tilde{p}\ell_6 V_0(y) \quad \text{or} \quad \overset{(0)}{w} = \tilde{p}\ell_6 \Delta_\zeta^0(y) \tag{24c}$$

$$\overset{(0)}{\mathcal{M}}_{xx} = \tilde{p}\ell_7 M_0(y) \quad \text{or} \quad \overset{(0)}{\varphi}_x = -\frac{\partial \overset{(0)}{w}}{\partial x} = \tilde{p}\ell_7 \phi_0(y) \tag{24d}$$

at $x = 0$ and

$$\overset{(0)}{\mathcal{N}}_{xx} = \tilde{p}\ell_8 N_L(y) \quad \text{or} \quad \overset{(0)}{u}_x = \tilde{p}\ell_8 \Delta_x^L(y) \tag{24e}$$

$$\overset{(0)}{\mathcal{N}}_{xy} + \frac{3c_2 \overset{(0)}{\mathcal{M}}_{xy}}{2R} = \tilde{p}\ell_9 S_L(y) \quad \text{or} \quad \overset{(0)}{u}_y = \tilde{p}\ell_9 \Delta_y^L(y) \tag{24f}$$

$$\overset{(0)}{Q}_x + \frac{\partial \overset{(0)}{\mathcal{M}}_{xy}}{\partial y} = \tilde{p}\ell_{10} V_L(y) \quad \text{or} \quad \overset{(0)}{w} = \tilde{p}\ell_{10} \Delta_\zeta^L(y) \tag{24g}$$

$$\overset{(0)}{\mathcal{M}}_{xx} = \tilde{p}\ell_{11} M_L(y) \quad \text{or} \quad \overset{(0)}{\varphi}_x = -\frac{\partial \overset{(0)}{w}}{\partial x} = \tilde{p}\ell_{11} \phi_L(y) \tag{24h}$$

at $x = L$ for the zeroth-order terms, and the homogeneous boundary conditions

$$\overset{(1)}{\mathcal{N}}_{xx} = 0 \quad \text{or} \quad \overset{(1)}{u}_x = 0 \tag{25a}$$

$$\overset{(1)}{\mathcal{N}}_{xy} + \frac{3c_2 \overset{(1)}{\mathcal{M}}_{xy}}{2R} + \frac{c_1}{2}\left(\overset{(0)}{\mathcal{N}}_{xx} + \overset{(0)}{\mathcal{N}}_{yy}\right)\overset{(1)}{\varphi}_n = 0 \quad \text{or} \quad \overset{(1)}{u}_y = 0 \tag{25b}$$

$$\overset{(1)}{Q}_x + \frac{\partial \overset{(1)}{\mathcal{M}}_{xy}}{\partial y} - \overset{(1)}{\varphi}_x \overset{(0)}{\mathcal{N}}_{xx} - \overset{(1)}{\varphi}_y \overset{(0)}{\mathcal{N}}_{xy} = 0 \quad \text{or} \quad \overset{(1)}{w} = 0 \tag{25c}$$

$$\overset{(1)}{\mathcal{M}}_{xx} = 0 \quad \text{or} \quad \overset{(1)}{\varphi}_x = \pm \frac{\partial \overset{(1)}{w}}{\partial x} = 0 \tag{25d}$$

at $x = 0$ and $x = L$ for the first-order terms.

Equations (18a), (18c), (21a), (21b), (22) and (24) define a general linear prebuckling equilibrium state for each value of the loading parameter $\tilde{p}$. The linear boundary-value problem associated with these equations can be obtained directly by neglecting nonlinearities in the original nonlinear boundary-value problem defined by equations (1)-(11). Solution of these equations generally yield membrane stress resultants that are linear functions of the loading parameter. In addition, the prebuckling equilibrium states exhibit zones of bending that are often localized near a relatively stiff boundary in many practical problems. An example of this behavior is shown in figure 3 for a compression-loaded cylinder with ends that are restrained to prohibit radial displacements. A common approximation, that is also used herein, is to presume that the effect of these localized zones on the buckling response is negligible and that a membrane state of stress and a uniform radial-displacement field exist in the shell prior to buckling that is linearly dependent on the loading parameter. Likewise, it is presumed herein that the contribution of the

live pressure terms in equations (22) to the prebuckling stress state are negligible.

Equations (18b), (18d), (21c), (21d), (23) and (25) define equilibrium states that are adjacent to states on the primary equilibrium path and are referred to herein as the buckling equations. Examination of these equations indicates that the loading parameter enters the buckling equations through the prebuckling stress resultants and the "live" applied pressure terms. For a linear membrane prebuckling stress state, the membrane stress resultants are obtained by neglecting the bending stress resultants in equations (22) and (24), which yields

$$\overset{(0)}{\mathcal{N}}_{yy} = \tilde{p}\ell_3 q_\zeta R \tag{26a}$$

$$\frac{\partial \overset{(0)}{\mathcal{N}}_{xy}}{\partial x} = -\frac{\partial \overset{(0)}{\mathcal{N}}_{yy}}{\partial y} - \tilde{p}\ell_2 q_y \tag{26b}$$

$$\frac{\partial \overset{(0)}{\mathcal{N}}_{xx}}{\partial x} = -\frac{\partial \overset{(0)}{\mathcal{N}}_{xy}}{\partial y} - \tilde{p}\ell_1 q_x \tag{26c}$$

These equations can be integrated sequentially, with the functions of integration determined from the boundary conditions

$$\overset{(0)}{\mathcal{N}}_{xx} = \tilde{p}\ell_4 N_0(y) \quad \text{or} \quad \overset{(0)}{u}_x = \tilde{p}\ell_4 \Delta_x^0(y) \tag{27a}$$

$$\overset{(0)}{\mathcal{N}}_{xy} = \tilde{p}\ell_5 S_0(y) \quad \text{or} \quad \overset{(0)}{u}_y = \tilde{p}\ell_5 \Delta_y^0(y) \tag{27b}$$

at $x = 0$ and

$$\overset{(0)}{\mathcal{N}}_{xx} = \tilde{p}\ell_8 N_L(y) \quad \text{or} \quad \overset{(0)}{u}_x = \tilde{p}\ell_8 \Delta_x^L(y) \tag{27c}$$

$$\overset{(0)}{\mathcal{N}}_{xy} = \tilde{p}\ell_9 S_L(y) \quad \text{or} \quad \overset{(0)}{u}_y = \tilde{p}\ell_9 \Delta_y^L(y) \tag{27d}$$

at $x = L$. When stress-resultant boundary conditions are applied to the ends of the cylinder, equations (26) and (27) can be solved directly to give the prebuckling membrane stress resultants in terms of the loading parameter, the applied surface and edge loads, and the load factors. No constitutive terms appear in the expressions. For this case, the prebuckling membrane stress resultants are expressible as

$$\overset{(0)}{\mathcal{N}}_{xx} = -\tilde{p}L_1 \overset{(0)}{\mathcal{N}}_{xx}(x, y) \tag{28a}$$

$$\overset{(0)}{\mathcal{N}}_{yy} = -\tilde{p}L_2 \overset{(0)}{\mathcal{N}}_{yy}(x, y) \tag{28b}$$

$$\overset{(0)}{\mathcal{N}}_{xy} = \tilde{p} L_3 \overset{(0)}{n}_{xy}(x, y) \tag{28c}$$

where L_1, L_2, and L_3 are known in terms of the load factors and $\overset{(0)}{n}_{xx}$, $\overset{(0)}{n}_{yy}$, and $\overset{(0)}{n}_{xy}$ are known functions. The negative signs in equations (21a) and (21b) are used so that compressive stresses correspond to positive values of the loading parameter. When a displacement boundary condition is specified from equations (27), equations (18a) and (21a) are used to express the displacements in terms of the unknown membrane stress resultants, the constitutive terms, and the ficticious thermal membrane stress resultants that arise from restrained thermal expansion and heating that is spatially nonuniform with respect to the (x, y) coordinates. Moreover, the second derivatives of $\overset{(0)}{w}(x, y)$ in equation (18c) are neglected. As a result, the general representation given by equations (28) remain valid for displacement boundary conditions. The expression that results for $\overset{(0)}{w}(x, y)$ is generally inconsistent with the actual displacement boundary conditions, if specified, given by equations (24c), (24d), (24g), and (24h), as presumed.

Examination of equations (18b), (18d), (21c), (21d), (23), (25), and (28) reveals that the differential equations governing buckling and the corresponding boundary conditions are homogeneous. Thus, the buckling equations constitute a boundary-eigenvalue problem for which the loading parameter $\tilde{p}$ is the eigenvalue and $\overset{(1)}{u}_x(x, y)$, $\overset{(1)}{u}_y(x, y)$, and $\overset{(1)}{w}(x, y)$ are the corresponding eigenfunctions. The smallest positive value of $\tilde{p}$ corresponds to the first intersection of one, or more, adjacent equilibrium paths with the primary equilibrium path. Thus, this value of the loading parameter is commonly referred to as the critical value and is denoted herein by $\tilde{p}_{cr}$. The corresponding eigenfunctions yield the deformed shape of the shell. The values of the applied loads are specified by equations (26) and (27), and their values at buckling are obtained by replacing $\tilde{p}$ with $\tilde{p}_{cr}$ in these equations.

In solving Sanders' linear buckling equations, the differential equations and boundary conditions are often expressed in terms of the loading parameter and the displacements $\overset{(1)}{u}_x(x, y)$, $\overset{(1)}{u}_y(x, y)$, and $\overset{(1)}{w}(x, y)$. The resulting displacement formulation of the buckling equations is derived in Appendix A. In particular, the differential equations are expressed in operator form as

$$\begin{bmatrix} \mathcal{L}_{11}(\,) & \mathcal{L}_{12}(\,) & \mathcal{L}_{13}(\,) \\ \mathcal{L}_{12}(\,) & \mathcal{L}_{22}(\,) & \mathcal{L}_{23}(\,) \\ \mathcal{L}_{13}(\,) & \mathcal{L}_{23}(\,) & \mathcal{L}_{33}(\,) \end{bmatrix} \begin{Bmatrix} \overset{(1)}{u}_x \\ \overset{(1)}{u}_y \\ \overset{(1)}{w} \end{Bmatrix} = \tilde{p} \begin{bmatrix} \mathcal{G}_{11}(\,) & \mathcal{G}_{12}(\,) & \mathcal{G}_{13}(\,) \\ \mathcal{G}_{21}(\,) & \mathcal{G}_{22}(\,) & \mathcal{G}_{23}(\,) \\ \mathcal{G}_{31}(\,) & \mathcal{G}_{32}(\,) & \mathcal{G}_{33}(\,) \end{bmatrix} \begin{Bmatrix} \overset{(1)}{u}_x \\ \overset{(1)}{u}_y \\ \overset{(1)}{w} \end{Bmatrix} \tag{29}$$

and the boundary conditions given by equations (25) are expressed as

$$\mathcal{B}_{11}\left(\overset{(1)}{u}_x\right) + \mathcal{B}_{12}\left(\overset{(1)}{u}_y\right) + \mathcal{B}_{13}\left(\overset{(1)}{w}\right) = 0 \quad \text{or} \quad \overset{(1)}{u}_x = 0 \tag{30a}$$

$$\mathcal{B}_{21}\left(\overset{(1)}{u}_x\right) + \mathcal{B}_{22}\left(\overset{(1)}{u}_y\right) + \mathcal{B}_{23}\left(\overset{(1)}{w}\right) = \tilde{p}\left[\overline{\mathcal{B}}_{21}\left(\overset{(1)}{u}_x\right) + \overline{\mathcal{B}}_{22}\left(\overset{(1)}{u}_y\right)\right] \quad \text{or} \quad \overset{(1)}{u}_y = 0 \tag{30b}$$

$$\mathcal{B}_{31}\left(\overset{(1)}{u}_x\right) + \mathcal{B}_{32}\left(\overset{(1)}{u}_y\right) + \mathcal{B}_{33}\left(\overset{(1)}{w}\right) = \tilde{p}\left[\overline{\mathcal{B}}_{32}\left(\overset{(1)}{u}_y\right) + \overline{\mathcal{B}}_{33}\left(\overset{(1)}{w}\right)\right] \quad \text{or} \quad \overset{(1)}{w} = 0 \tag{30c}$$

$$\mathcal{B}_{41}\left(\overset{(1)}{u}_x\right) + \mathcal{B}_{42}\left(\overset{(1)}{u}_y\right) + \mathcal{B}_{43}\left(\overset{(1)}{w}\right) = 0 \quad \text{or} \quad \frac{\partial \overset{(1)}{w}}{\partial x} = 0 \tag{30d}$$

where the operators are linear and are defined in Appendix A.

Variational Formulation of the Buckling Equations

A variational statement for linear bifurcation buckling is obtained by noting that equations (23a), (23b), and (23e) represent summations of forces in the three coordinate directions, for the adjacent equilibrium states. Thus, a statement of the corresponding virtual work is given by

$$\delta \overset{(1)}{W} = -\int_0^L \int_0^{2\pi R} \delta \overset{(1)}{\mathcal{W}}\, dy dx + \int_0^{2\pi R} \delta \overset{(1)}{\mathcal{W}}^{B} \Big]_{x=0}^{x=L} dy = 0 \tag{31}$$

where

$$\delta \overset{(1)}{\mathcal{W}} = \left[\frac{\partial \overset{(1)}{\mathcal{N}}_{xx}}{\partial x} + \frac{\partial \overset{(1)}{\mathcal{N}}_{xy}}{\partial y} - \frac{c_2}{2}\frac{\partial}{\partial y}\left(\frac{\overset{(1)}{\mathcal{M}}_{xy}}{R} + c_1\left(\overset{(0)}{\mathcal{N}}_{xx} + \overset{(0)}{\mathcal{N}}_{yy}\right)\overset{(1)}{\varphi}_n\right) + c_4 \ell_3 \tilde{p} q_\zeta \overset{(1)}{\varphi}_x\right]\delta u +$$

$$\left[\frac{\partial \overset{(1)}{\mathcal{N}}_{xy}}{\partial x} + \frac{\partial \overset{(1)}{\mathcal{N}}_{yy}}{\partial y} + \frac{c_2}{R}\left(\overset{(1)}{Q}_y + \frac{1}{2}\frac{\partial \overset{(1)}{\mathcal{M}}_{xy}}{\partial x}\right) - \frac{1}{R}\left[\overset{(1)}{\varphi}_x \overset{(0)}{\mathcal{N}}_{xy} + \overset{(1)}{\varphi}_y \overset{(0)}{\mathcal{N}}_{yy}\right] +\right.$$

$$\left. \frac{c_1}{2}\frac{\partial}{\partial x}\left[\left(\overset{(0)}{\mathcal{N}}_{xx} + \overset{(0)}{\mathcal{N}}_{yy}\right)\overset{(1)}{\varphi}_n\right] + c_4 \ell_3 \tilde{p} q_\zeta \overset{(1)}{\varphi}_y\right]\delta v +$$

$$\left[\frac{\partial \overset{(1)}{Q}_x}{\partial x} + \frac{\partial \overset{(1)}{Q}_y}{\partial y} - \frac{\overset{(1)}{\mathcal{N}}_{yy}}{R} - \frac{\partial}{\partial x}\left[\overset{(1)}{\varphi}_x \overset{(0)}{\mathcal{N}}_{xx} + \overset{(1)}{\varphi}_y \overset{(0)}{\mathcal{N}}_{xy}\right] - \frac{\partial}{\partial y}\left[\overset{(1)}{\varphi}_x \overset{(0)}{\mathcal{N}}_{xy} + \overset{(1)}{\varphi}_y \overset{(0)}{\mathcal{N}}_{yy}\right] +\right.$$

$$c_4 \ell_3 \tilde{p}\left[q_\zeta \left(\overset{(1)}{\varepsilon}_{xx} + \overset{(1)}{\varepsilon}_{yy} \right) + \frac{\partial q_\zeta}{\partial x} \overset{(1)}{u}_x + \frac{\partial q_\zeta}{\partial y} \overset{(1)}{u}_y + \frac{\partial q_\zeta}{\partial \zeta} \overset{(1)}{w} \right] \Bigg] \delta w \tag{32a}$$

$$\begin{aligned} \delta \overset{(1)}{W}{}^{B} = \overset{(1)}{N}_{xx}\, \delta u + \left[\overset{(1)}{N}_{xy} + \frac{3c_2 \overset{(1)}{M}_{xy}}{2R} + \frac{c_1}{2}\left(\overset{(0)}{N}_{xx} + \overset{(0)}{N}_{yy} \right) \overset{(1)}{\varphi}_n \right] \delta v + \\ \left[\overset{(1)}{Q}_x + \frac{\partial \overset{(1)}{M}_{xy}}{\partial y} + \overset{(1)}{\varphi}_x \overset{(0)}{N}_{xx} + \overset{(1)}{\varphi}_y \overset{(0)}{N}_{xy} \right] \delta w - \overset{(1)}{M}_{xx} \frac{\partial \delta w}{\partial x} \end{aligned} \tag{32b}$$

where δu, δv, and δw are arbitrary virtual displacement fields along the x, y, and ζ directions, respectively. These virtual displacements represent kinematically admissible departures from the primary equilibrium configuration. Integrating the double integral by parts, and enforcing circumferential continuity of the integrands gives

$$\begin{aligned} \int_0^L \int_0^{2\pi R} \Bigg[& \overset{(1)}{N}_{xx} \frac{\partial \delta u}{\partial x} + \overset{(1)}{N}_{xy} \left(\frac{\partial \delta u}{\partial y} + \frac{\partial \delta v}{\partial x} \right) + \overset{(1)}{N}_{yy} \left(\frac{\partial \delta v}{\partial y} + \frac{\delta w}{R} \right) + \\ & \overset{(1)}{M}_{xx} \frac{\partial \delta \psi_x}{\partial x} + \overset{(1)}{M}_{yy} \frac{\partial \delta \psi_y}{\partial y} + \overset{(1)}{M}_{xy} \left(\frac{\partial \delta \psi_y}{\partial x} + \frac{\partial \delta \psi_x}{\partial y} + \frac{\delta \psi_n}{R} \right) + \\ & \overset{(0)}{N}_{xx} \left(c_1 \overset{(1)}{\varphi}_n \delta \psi_n + \overset{(1)}{\varphi}_x \delta \psi_x \right) + \overset{(0)}{N}_{yy} \left(\overset{(1)}{\varphi}_y \delta \psi_y + c_1 \overset{(1)}{\varphi}_n \delta \psi_n \right) + \overset{(0)}{N}_{xy} \left(\overset{(1)}{\varphi}_x \delta \psi_y + \overset{(1)}{\varphi}_y \delta \psi_x \right) + \\ & - c_4 \ell_3 \tilde{p} \left(q_\zeta \overset{(1)}{\varphi}_x \delta u + q_\zeta \overset{(1)}{\varphi}_y \delta v + \left[q_\zeta \left(\overset{(1)}{\varepsilon}_{xx} + \overset{(1)}{\varepsilon}_{yy} \right) + \frac{\partial q_\zeta}{\partial x} \overset{(1)}{u}_x + \frac{\partial q_\zeta}{\partial y} \overset{(1)}{u}_y + \frac{\partial q_\zeta}{\partial \zeta} \overset{(1)}{w} \right] \delta w \right) \Bigg] \, dy dx = 0 \end{aligned} \tag{33}$$

for which

$$\delta \psi_x = - \frac{\partial \delta w}{\partial x} \tag{34a}$$

$$\delta \psi_y = c_2 \frac{\delta v}{R} - \frac{\partial \delta w}{\partial y} \tag{34b}$$

$$\delta \psi_n = \frac{c_2}{2} \left(\frac{\partial \delta v}{\partial x} - \frac{\partial \delta u}{\partial y} \right) \tag{34c}$$

Next, enforcing the conditions that the virtual displacements satisfy the kinematic boundary conditions given by equations (25) and the strain-displacement relations given equations (18b) and (18d) results in the following form for equation (33)

$$\int_0^L \int_0^{2\pi R} \Bigg[\overset{(1)}{\mathcal{N}}_{xx}\delta\overset{(1)}{\varepsilon}_{xx} + \overset{(1)}{\mathcal{N}}_{xy}\delta\overset{(1)}{\gamma}_{xy} + \overset{(1)}{\mathcal{N}}_{yy}\delta\overset{(1)}{\varepsilon}_{yy} + \overset{(1)}{\mathcal{M}}_{xx}\delta\overset{(1)}{\kappa}_{xx} + \overset{(1)}{\mathcal{M}}_{yy}\delta\overset{(1)}{\kappa}_{yy} + \overset{(1)}{\mathcal{M}}_{xy}\delta\overset{(1)}{\kappa}_{xy} +$$

$$\overset{(0)}{\mathcal{N}}_{xx}\left(\overset{(1)}{\varphi}_x\,\delta\overset{(1)}{\varphi}_x + c_1\overset{(1)}{\varphi}_n\delta\overset{(1)}{\varphi}_n\right) + \overset{(0)}{\mathcal{N}}_{xy}\left(\overset{(1)}{\varphi}_x\delta\overset{(1)}{\varphi}_y + \overset{(1)}{\varphi}_y\delta\overset{(1)}{\varphi}_x\right) + \overset{(0)}{\mathcal{N}}_{yy}\left(\overset{(1)}{\varphi}_y\delta\overset{(1)}{\varphi}_y + c_1\overset{(1)}{\varphi}_n\delta\overset{(1)}{\varphi}_n\right) + \tag{35}$$

$$- c_4\ell_3\tilde{p}\left(q_\zeta\overset{(1)}{\varphi}_x\delta\overset{(1)}{u}_x + q_\zeta\overset{(1)}{\varphi}_y\delta\overset{(1)}{u}_y + \left[q_\zeta\left(\overset{(1)}{\varepsilon}_{xx} + \overset{(1)}{\varepsilon}_{yy}\right) + \frac{\partial q_\zeta}{\partial x}\overset{(1)}{u}_x + \frac{\partial q_\zeta}{\partial y}\overset{(1)}{u}_y + \frac{\partial q_\zeta}{\partial \zeta}\overset{(1)}{w}\right]\delta\overset{(1)}{w}\right)\Bigg] dydx = 0$$

which is a subset of the variational principle given by equation (115) in reference 22, except that it contains the additional terms presented by Cohen.[23] An alternate form of equation (35) is obtained by integrating the terms involving q_ζ by parts. This process yields

$$\int_0^L \int_0^{2\pi R} \left(q_\zeta\left[\overset{(1)}{\varphi}_x\delta\overset{(1)}{u}_x + \overset{(1)}{\varphi}_y\delta\overset{(1)}{u}_y\right] + \left[q_\zeta\left(\overset{(1)}{\varepsilon}_{xx} + \overset{(1)}{\varepsilon}_{yy}\right) + \frac{\partial q_\zeta}{\partial x}\overset{(1)}{u}_x + \frac{\partial q_\zeta}{\partial y}\overset{(1)}{u}_y + \frac{\partial q_\zeta}{\partial \zeta}\overset{(1)}{w}\right]\delta\overset{(1)}{w}\right) dydx =$$

$$\frac{1}{2}\int_0^L \int_0^{2\pi R} q_\zeta\left(\overset{(1)}{\varphi}_x\delta\overset{(1)}{u}_x + \overset{(1)}{\varphi}_y\delta\overset{(1)}{u}_y + \left(\overset{(1)}{\varepsilon}_{xx} + \overset{(1)}{\varepsilon}_{yy}\right)\delta\overset{(1)}{w} + \delta\overset{(1)}{\varphi}_x\overset{(1)}{u}_x + \delta\overset{(1)}{\varphi}_y\overset{(1)}{u}_y + \left(\delta\overset{(1)}{\varepsilon}_{xx} + \delta\overset{(1)}{\varepsilon}_{yy}\right)\overset{(1)}{w}\right) dydx$$

$$+ \frac{1}{2}\int_0^L \int_0^{2\pi R} \left(\frac{\partial q_\zeta}{\partial x}\left(\overset{(1)}{w}\delta\overset{(1)}{u}_x + \overset{(1)}{u}_x\delta\overset{(1)}{w}\right) + \frac{\partial q_\zeta}{\partial y}\left(\overset{(1)}{w}\delta\overset{(1)}{u}_y + \overset{(1)}{u}_y\delta\overset{(1)}{w}\right) + 2\frac{\partial q_\zeta}{\partial \zeta}\overset{(1)}{w}\delta\overset{(1)}{w}\right) dydx + \tag{36}$$

$$\frac{1}{2}\int_0^{2\pi R}\left[q_\zeta\left(\overset{(1)}{u}_x\delta\overset{(1)}{w} - \overset{(1)}{w}\delta\overset{(1)}{u}_x\right)\right]_0^L dy$$

This expression is consistent with that given by Budiansky[22] for uniform pressure. Substituting equation (36) into (35) yields the desired form given by

$$\int_0^L \int_0^{2\pi R} \Bigg[\overset{(1)}{\mathcal{N}}_{xx}\delta\overset{(1)}{\varepsilon}_{xx} + \overset{(1)}{\mathcal{N}}_{xy}\delta\overset{(1)}{\gamma}_{xy} + \overset{(1)}{\mathcal{N}}_{yy}\delta\overset{(1)}{\varepsilon}_{yy} + \overset{(1)}{\mathcal{M}}_{xx}\delta\overset{(1)}{\kappa}_{xx} + \overset{(1)}{\mathcal{M}}_{yy}\delta\overset{(1)}{\kappa}_{yy} + \overset{(1)}{\mathcal{M}}_{xy}\delta\overset{(1)}{\kappa}_{xy} +$$

$$\overset{(0)}{\mathcal{N}}_{xx}\left(\overset{(1)}{\varphi}_x\,\delta\overset{(1)}{\varphi}_x + c_1\overset{(1)}{\varphi}_n\delta\overset{(1)}{\varphi}_n\right) + \overset{(0)}{\mathcal{N}}_{xy}\left(\overset{(1)}{\varphi}_x\delta\overset{(1)}{\varphi}_y + \overset{(1)}{\varphi}_y\delta\overset{(1)}{\varphi}_x\right) + \overset{(0)}{\mathcal{N}}_{yy}\left(\overset{(1)}{\varphi}_y\delta\overset{(1)}{\varphi}_y + c_1\overset{(1)}{\varphi}_n\delta\overset{(1)}{\varphi}_n\right)$$

$$-\frac{c_4}{2}\ell_3\tilde{p}q_\zeta\left(\overset{(1)}{\varphi}_x\delta\overset{(1)}{u}_x + \overset{(1)}{\varphi}_y\delta\overset{(1)}{u}_y + \left(\overset{(1)}{\varepsilon}_{xx} + \overset{(1)}{\varepsilon}_{yy}\right)\delta\overset{(1)}{w} + \delta\overset{(1)}{\varphi}_x\overset{(1)}{u}_x + \delta\overset{(1)}{\varphi}_y\overset{(1)}{u}_y + \left(\delta\overset{(1)}{\varepsilon}_{xx} + \delta\overset{(1)}{\varepsilon}_{yy}\right)\overset{(1)}{w}\right) \tag{37}$$

$$-\frac{c_4}{2}\ell_3\tilde{p}\left(\frac{\partial q_\zeta}{\partial x}\left(\overset{(1)}{w}\delta\overset{(1)}{u}_x + \overset{(1)}{u}_x\delta\overset{(1)}{w}\right) + \frac{\partial q_\zeta}{\partial y}\left(\overset{(1)}{w}\delta\overset{(1)}{u}_y + \overset{(1)}{u}_y\delta\overset{(1)}{w}\right) + 2\frac{\partial q_\zeta}{\partial \zeta}\overset{(1)}{w}\delta\overset{(1)}{w}\right)\Bigg]\,dydx$$

$$-\frac{c_4}{2}\ell_3\tilde{p}\int_0^{2\pi R}\left[q_\zeta\left(\overset{(1)}{u}_x\delta\overset{(1)}{w} - \overset{(1)}{w}\delta\overset{(1)}{u}_x\right)\right]_0^L dy = 0$$

The boundary integral term in this equation represents the nonconservative contribution of the live pressure loading to the virtual work. To utilize static methods of stability analysis, the problems considered herein require the boundary conditions to be specified such that loading constitutes a conservative system. A convenient matrix form of equation (37), with the boundary integral neglected, is given by

$$\int_0^L \int_0^{2\pi R} \Bigg[\left\{\overset{(1)}{\mathcal{N}}\right\}^T\left\{\delta\overset{(1)}{\varepsilon}\right\} + \left\{\overset{(1)}{\mathcal{M}}\right\}^T\left\{\delta\overset{(1)}{\kappa}\right\} + \left\{\overset{(1)}{\varphi}\right\}^T\left[\overset{(0)}{\mathcal{N}}\right]\left\{\delta\overset{(1)}{\varphi}\right\}$$

$$-\frac{1}{2}\tilde{p}\left(\left\{\overset{(1)}{\mathcal{P}}\right\}^T\left\{\delta\overset{(1)}{u}\right\} + \left\{\overset{(1)}{u}\right\}^T\left\{\delta\overset{(1)}{\mathcal{P}}\right\}\right) - \frac{1}{2}\tilde{p}\left\{\overset{(1)}{u}\right\}^T\left[\partial_q\right]\left\{\delta\overset{(1)}{u}\right\}\Bigg] dydx = 0 \tag{38}$$

where

$$\left[\overset{(0)}{\mathcal{N}}\right] = \begin{bmatrix} \overset{(0)}{\mathcal{N}}_{xx} & \overset{(0)}{\mathcal{N}}_{xy} & 0 \\ \overset{(0)}{\mathcal{N}}_{xy} & \overset{(0)}{\mathcal{N}}_{yy} & 0 \\ 0 & 0 & c_1\left(\overset{(0)}{\mathcal{N}}_{xx} + \overset{(0)}{\mathcal{N}}_{yy}\right) \end{bmatrix} \tag{39a}$$

$$\left\{\overset{(1)}{\mathcal{P}}\right\} = c_4 \ell_3 q_\zeta \begin{Bmatrix} \overset{(1)}{\varphi}_x \\ \overset{(1)}{\varphi}_y \\ \overset{(1)}{\varepsilon}_{xx} + \overset{(1)}{\varepsilon}_{yy} \end{Bmatrix} \tag{39b}$$

$$\left\{\delta\overset{(1)}{\mathcal{P}}\right\} = c_4 \ell_3 q_\zeta \begin{Bmatrix} \delta\overset{(1)}{\varphi}_x \\ \delta\overset{(1)}{\varphi}_y \\ \delta\overset{(1)}{\varepsilon}_{xx} + \delta\overset{(1)}{\varepsilon}_{yy} \end{Bmatrix} \tag{39c}$$

$$\left[\partial_q\right] \equiv c_4 \ell_3 \begin{bmatrix} 0 & 0 & \dfrac{\partial q_\zeta}{\partial x} \\ 0 & 0 & \dfrac{\partial q_\zeta}{\partial y} \\ \dfrac{\partial q_\zeta}{\partial x} & \dfrac{\partial q_\zeta}{\partial y} & 2\dfrac{\partial q_\zeta}{\partial \zeta} \end{bmatrix} \tag{39d}$$

$\left\{\delta\overset{(1)}{\varepsilon}\right\} = \delta\left\{\overset{(1)}{\varepsilon}\right\}$, $\left\{\delta\overset{(1)}{\kappa}\right\} = \delta\left\{\overset{(1)}{\kappa}\right\}$, and $\left\{\delta\overset{(1)}{\varphi}\right\} = \delta\left\{\overset{(1)}{\varphi}\right\}$. In addition,

$$\left\{\overset{(1)}{u}\right\}^T = \left\{\overset{(1)}{u}_x \;\; \overset{(1)}{u}_y \;\; \overset{(1)}{w}\right\} \tag{40}$$

and $\left\{\delta\overset{(1)}{u}\right\} = \delta\left\{\overset{(1)}{u}\right\}$. Next, using equation (40) and expressing the strains, given by equations (18), the rotations, given by equations (14d), and equations (39b) and (39c) in differential operator form gives

$$\left\{\overset{(1)}{\varepsilon}\right\} = \begin{bmatrix} \dfrac{\partial}{\partial x} & 0 & 0 \\ 0 & \dfrac{\partial}{\partial y} & \dfrac{1}{R} \\ \dfrac{\partial}{\partial y} & \dfrac{\partial}{\partial x} & 0 \end{bmatrix} \begin{Bmatrix} \overset{(1)}{u}_x \\ \overset{(1)}{u}_y \\ \overset{(1)}{w} \end{Bmatrix} \equiv \left[\partial_\varepsilon\right]\left\{\overset{(1)}{u}\right\} \tag{41a}$$

$$\left\{\overset{(1)}{\kappa}\right\} = \begin{bmatrix} 0 & 0 & -\dfrac{\partial^2}{\partial x^2} \\ 0 & \dfrac{c_2}{R}\dfrac{\partial}{\partial y} & -\dfrac{\partial^2}{\partial y^2} \\ \dfrac{c_1 c_2}{2R}\dfrac{\partial}{\partial y} & \dfrac{c_2}{2R}\left(c_1 + 2\right)\dfrac{\partial}{\partial x} & 0 \end{bmatrix} \begin{Bmatrix} \overset{(1)}{u}_x \\ \overset{(1)}{u}_y \\ \overset{(1)}{w} \end{Bmatrix} \equiv \left[\partial_\kappa\right]\left\{\overset{(1)}{u}\right\} \tag{41b}$$

$$\left\{\overset{(1)}{\varphi}\right\} = \begin{bmatrix} 0 & 0 & -\dfrac{\partial}{\partial x} \\ 0 & \dfrac{c_2}{R} & -\dfrac{\partial}{\partial y} \\ -\dfrac{c_2}{2}\dfrac{\partial}{\partial y} & \dfrac{c_2}{2}\dfrac{\partial}{\partial x} & 0 \end{bmatrix} \begin{Bmatrix} \overset{(1)}{u}_x \\ \overset{(1)}{u}_y \\ \overset{(1)}{w} \end{Bmatrix} \equiv \left[\partial_\varphi\right]\left\{\overset{(1)}{u}\right\} \tag{41c}$$

and

$$\left\{\overset{(1)}{\mathcal{P}}\right\} = c_4 \ell_3 q_\zeta \begin{bmatrix} 0 & 0 & -\dfrac{\partial}{\partial x} \\ 0 & \dfrac{1}{R} & -\dfrac{\partial}{\partial y} \\ \dfrac{\partial}{\partial x} & \dfrac{\partial}{\partial y} & \dfrac{1}{R} \end{bmatrix} \begin{Bmatrix} \overset{(1)}{u}_x \\ \overset{(1)}{u}_y \\ \overset{(1)}{w} \end{Bmatrix} \equiv \left[\partial_{\mathcal{P}}\right]\left\{\overset{(1)}{u}\right\} \tag{41d}$$

$$\left\{\delta\overset{(1)}{\mathcal{P}}\right\} = c_4 \ell_3 q_\zeta \begin{bmatrix} 0 & 0 & -\dfrac{\partial}{\partial x} \\ 0 & \dfrac{1}{R} & -\dfrac{\partial}{\partial y} \\ \dfrac{\partial}{\partial x} & \dfrac{\partial}{\partial y} & \dfrac{1}{R} \end{bmatrix} \begin{Bmatrix} \delta\overset{(1)}{u}_x \\ \delta\overset{(1)}{u}_y \\ \delta\overset{(1)}{w} \end{Bmatrix} \equiv \left[\partial_{\mathcal{P}}\right]\left\{\delta\overset{(1)}{u}\right\} \tag{41e}$$

equation (38) is transformed into

$$\int_0^L \int_0^{2\pi R} \Bigg[\left\{\overset{(1)}{\mathcal{N}}\right\}^T \left(\left[\partial_\varepsilon\right]\left\{\delta\overset{(1)}{u}\right\}\right) + \left\{\overset{(1)}{\mathcal{M}}\right\}^T \left(\left[\partial_\kappa\right]\left\{\delta\overset{(1)}{u}\right\}\right) + \left(\left[\partial_\varphi\right]\left\{\overset{(1)}{u}\right\}\right)^T \left[\overset{(0)}{\mathcal{N}}\right] \left(\left[\partial_\varphi\right]\left\{\delta\overset{(1)}{u}\right\}\right) +$$

$$- \frac{1}{2}\tilde{p}\left(\left(\left[\partial_{\mathcal{P}}\right]\left\{\overset{(1)}{u}\right\}\right)^T \left\{\delta\overset{(1)}{u}\right\} + \left\{\overset{(1)}{u}\right\}^T \left(\left[\partial_{\mathcal{P}}\right]\left\{\delta\overset{(1)}{u}\right\}\right)\right) - \frac{1}{2}\tilde{p}\left\{\overset{(1)}{u}\right\}^T \left[\partial_q\right]\left\{\delta\overset{(1)}{u}\right\} \Bigg] dy dx = 0 \tag{42}$$

Next, substituting equations (28) into equation (39a) gives

$$\left[\overset{(0)}{\mathcal{N}}\right] = -\tilde{p}\begin{bmatrix} L_1\overset{(0)}{\varepsilon}_{xx} & -L_3\overset{(0)}{\varepsilon}_{xy} & 0 \\ -L_3\overset{(0)}{\varepsilon}_{xy} & L_2\overset{(0)}{\varepsilon}_{yy} & 0 \\ 0 & 0 & c_1\left(L_1\overset{(0)}{\varepsilon}_{xx} + L_2\overset{(0)}{\varepsilon}_{yy}\right) \end{bmatrix} \equiv -\tilde{p}\left[\overset{(0)}{\varepsilon}\right] \tag{43}$$

Substituting equations (41a) and (41b) into equations (21c) and (21d), and then substituting the resulting equations and equation (43) into equation (42) gives the variational statement as

$$\mathcal{K}\left(\{\overset{(i)}{u}\}, \{\delta\overset{(i)}{u}\}\right) = \tilde{p}\,\mathcal{K}_g\left(\{\overset{(i)}{u}\}, \{\delta\overset{(i)}{u}\}\right) \tag{44}$$

where

$$\mathcal{K}\left(\{\overset{(i)}{u}\}, \{\delta\overset{(i)}{u}\}\right) = \int_0^L \int_0^{2\pi R} \Big[\left([\partial_\varepsilon]\{\overset{(1)}{u}\}\right)^T [A]\left([\partial_\varepsilon]\{\delta\overset{(1)}{u}\}\right) + \left([\partial_\kappa]\{\overset{(1)}{u}\}\right)^T [D]\left([\partial_\kappa]\{\delta\overset{(1)}{u}\}\right) + \left([\partial_\kappa]\{\overset{(1)}{u}\}\right)^T [B]\left([\partial_\varepsilon]\{\delta\overset{(1)}{u}\}\right) + \left([\partial_\varepsilon]\{\overset{(1)}{u}\}\right)^T [B]\left([\partial_\kappa]\{\delta\overset{(1)}{u}\}\right) \Big] dydx \tag{45a}$$

is defined herein as the *bilinear stiffness functional* and

$$\mathcal{K}_g\left(\{\overset{(i)}{u}\}, \{\delta\overset{(i)}{u}\}\right) = \int_0^L \int_0^{2\pi R} \Big[\left([\partial_\varphi]\{\overset{(1)}{u}\}\right)^T [\overset{(0)}{n}]\left([\partial_\varphi]\{\delta\overset{(1)}{u}\}\right) + \frac{1}{2}\left(\left([\partial_p]\{\overset{(1)}{u}\}\right)^T \{\delta\overset{(1)}{u}\} + \{\overset{(1)}{u}\}^T \left([\partial_p]\{\delta\overset{(1)}{u}\}\right)\right) + \frac{1}{2}\{\overset{(1)}{u}\}^T [\partial_q]\{\delta\overset{(1)}{u}\} \Big] dydx \tag{45b}$$

is defined as the *bilinear geometric stiffness* functional. Both of these functionals are symmetric with respect to their column-vector arguments.

Analysis for Two Loading Systems

Sometimes it is desirable to find the buckling load of a cylinder that is subjected to an independent set of loads prior to application of the loading parameter $\tilde{p}$. For example, one might want to investigate the buckling behavior of a cylinder that is first subjected to a fixed internal pressure and then loaded in axial compression until buckling occurs. To distinguish between these two loading systems, it is convenient to define a passive loading parameter $\tilde{\lambda}$ and a set of corresponding load factors that are associated with an initial, stable membrane-prebuckling stress state. The passive loading parameter is scaled to any convenient value that corresponds to a stable prebuckling equilibrium state. Subsequent application of the loading parameter $\tilde{p}$ leads to buckling and, as a result, is referred to herein as the active loading parameter. The loads that

correspond to $\tilde{p}$ are referred to herein as the active loading system.

The membrane-prebuckling boundary-value problem for the active loading system is defined by equations (26) and (27) and constitutes a linear boundary-value problem. Thus, the membrane-prebuckling boundary-value problem for the combined action of both loading systems is obtained directly by applying the replacement rules

$$\tilde{p}\ell_1 q_x \rightarrow \tilde{p}\ell_1 q_x + \tilde{\lambda}\ell_1^* q_x^* \tag{46a}$$

$$\tilde{p}\ell_2 q_y \rightarrow \tilde{p}\ell_2 q_y + \tilde{\lambda}\ell_2^* q_y^* \tag{46b}$$

$$\tilde{p}\ell_3 q_\zeta \rightarrow \tilde{p}\ell_3 q_\zeta + \tilde{\lambda}\ell_3^* q_\zeta^* \tag{46c}$$

to equations (26) and

$$\tilde{p}\ell_4 N_0(y) \rightarrow \tilde{p}\ell_4 N_0(y) + \tilde{\lambda}\ell_4^* N_0^*(y) \quad \text{or} \quad \tilde{p}\ell_4 \Delta_x^0(y) \rightarrow \tilde{p}\ell_4 \Delta_x^0(y) + \tilde{\lambda}\ell_4^* \Delta_x^{0*}(y) \tag{47a}$$

$$\tilde{p}\ell_5 S_0(y) \rightarrow \tilde{p}\ell_5 S_0(y) + \tilde{\lambda}\ell_5^* S_0^*(y) \quad \text{or} \quad \tilde{p}\ell_5 \Delta_y^0(y) \rightarrow \tilde{p}\ell_5 \Delta_y^0(y) + \tilde{\lambda}\ell_5^* \Delta_y^{0*}(y) \tag{47b}$$

$$\tilde{p}\ell_8 N_L(y) \rightarrow \tilde{p}\ell_8 N_L(y) + \tilde{\lambda}\ell_8^* N_L^*(y) \quad \text{or} \quad \tilde{p}\ell_8 \Delta_x^L(y) \rightarrow \tilde{p}\ell_8 \Delta_x^L(y) + \tilde{\lambda}\ell_8^* \Delta_x^{L*}(y) \tag{47c}$$

$$\tilde{p}\ell_9 S_L(y) \rightarrow \tilde{p}\ell_9 S_L(y) + \tilde{\lambda}\ell_9^* S_L^*(y) \quad \text{or} \quad \tilde{p}\ell_9 \Delta_y^L(y) \rightarrow \tilde{p}\ell_9 \Delta_y^L(y) + \tilde{\lambda}\ell_9^* \Delta_y^{L*}(y) \tag{47d}$$

to the boundary conditions given by equations (27). Solution of the prebuckling boundary-value problem leads to prebuckling stress resultants that can be expressed as

$$\overset{(0)}{\mathcal{N}}_{xx} = -\tilde{p}L_1 \overset{(0)}{\mathcal{N}}_{xx}(x, y) - \tilde{\lambda}L_1^* \overset{(0)^*}{\mathcal{N}}_{xx}(x, y) \tag{48a}$$

$$\overset{(0)}{\mathcal{N}}_{yy} = -\tilde{p}L_2 \overset{(0)}{\mathcal{N}}_{yy}(x, y) - \tilde{\lambda}L_2^* \overset{(0)^*}{\mathcal{N}}_{yy}(x, y) \tag{48b}$$

$$\overset{(0)}{\mathcal{N}}_{xy} = \tilde{p}L_3 \overset{(0)}{\mathcal{N}}_{xy}(x, y) + \tilde{\lambda}L_3^* \overset{(0)^*}{\mathcal{N}}_{xy}(x, y) \tag{48c}$$

The only unknown appearing in equations (48) is the active loading parameter $\tilde{p}$.

To include the effects of the passive and active systems in the bifurcation analysis, equations (48) are used in equations (23) and (25). In addition, the replacement rules defined by equations (46) are used in equations (23). Inclusion of the passive loading system in the bifurcation analysis results in the conversion of equations (29) and (30) into

$$\left[\begin{bmatrix} \mathcal{L}_{11}(\,) & \mathcal{L}_{12}(\,) & \mathcal{L}_{13}(\,) \\ \mathcal{L}_{12}(\,) & \mathcal{L}_{22}(\,) & \mathcal{L}_{23}(\,) \\ \mathcal{L}_{13}(\,) & \mathcal{L}_{23}(\,) & \mathcal{L}_{33}(\,) \end{bmatrix} - \tilde{\lambda}\begin{bmatrix} \mathcal{G}^{*}_{11}(\,) & \mathcal{G}^{*}_{12}(\,) & \mathcal{G}^{*}_{13}(\,) \\ \mathcal{G}^{*}_{21}(\,) & \mathcal{G}^{*}_{22}(\,) & \mathcal{G}^{*}_{23}(\,) \\ \mathcal{G}^{*}_{13}(\,) & \mathcal{G}^{*}_{32}(\,) & \mathcal{G}^{*}_{33}(\,) \end{bmatrix}\right]\begin{Bmatrix} \overset{(1)}{u}_x \\ \overset{(1)}{u}_y \\ \overset{(1)}{w} \end{Bmatrix} = \tilde{p}\begin{bmatrix} \mathcal{G}_{11}(\,) & \mathcal{G}_{12}(\,) & \mathcal{G}_{13}(\,) \\ \mathcal{G}_{21}(\,) & \mathcal{G}_{22}(\,) & \mathcal{G}_{23}(\,) \\ \mathcal{G}_{13}(\,) & \mathcal{G}_{32}(\,) & \mathcal{G}_{33}(\,) \end{bmatrix}\begin{Bmatrix} \overset{(1)}{u}_x \\ \overset{(1)}{u}_y \\ \overset{(1)}{w} \end{Bmatrix} \tag{49}$$

and

$$\mathcal{B}_{11}\left(\overset{(1)}{u}_x\right) + \mathcal{B}_{12}\left(\overset{(1)}{u}_y\right) + \mathcal{B}_{13}\left(\overset{(1)}{w}\right) = 0 \quad \text{or} \quad \overset{(1)}{u}_x = 0 \tag{50a}$$

$$\left[\mathcal{B}_{21}(\,) - \tilde{\lambda}\overline{\mathcal{B}}^{*}_{21}(\,)\right]\overset{(1)}{u}_x + \left[\mathcal{B}_{22}(\,) - \tilde{\lambda}\overline{\mathcal{B}}^{*}_{22}(\,)\right]\overset{(1)}{u}_y + \mathcal{B}_{23}\left(\overset{(1)}{w}\right) = \tilde{p}\left[\overline{\mathcal{B}}_{21}\left(\overset{(1)}{u}_x\right) + \overline{\mathcal{B}}_{22}\left(\overset{(1)}{u}_y\right)\right]$$

$$\text{or} \quad \overset{(1)}{u}_y = 0 \tag{50b}$$

$$\mathcal{B}_{31}\left(\overset{(1)}{u}_x\right) + \left[\mathcal{B}_{32}(\,) - \tilde{\lambda}\overline{\mathcal{B}}^{*}_{32}(\,)\right]\overset{(1)}{u}_y + \left[\mathcal{B}_{33}(\,) - \tilde{\lambda}\overline{\mathcal{B}}^{*}_{33}(\,)\right]\overset{(1)}{w} = \tilde{p}\left[\overline{\mathcal{B}}_{32}\left(\overset{(1)}{u}_y\right) + \overline{\mathcal{B}}_{33}\left(\overset{(1)}{w}\right)\right]$$

$$\text{or} \quad \overset{(1)}{w} = 0 \tag{50c}$$

$$\mathcal{B}_{41}\left(\overset{(1)}{u}_x\right) + \mathcal{B}_{42}\left(\overset{(1)}{u}_y\right) + \mathcal{B}_{43}\left(\overset{(1)}{w}\right) = 0 \quad \text{or} \quad \frac{\partial \overset{(1)}{w}}{\partial x} = 0 \tag{50d}$$

where the operators are linear and are defined in Appendix A. In addition, equation (44) becomes

$$\mathcal{K}\left(\overset{(1)}{u},\, \delta\overset{(1)}{u}\right) - \tilde{\lambda}\,\mathcal{K}^{*}_{g}\left(\overset{(1)}{u},\, \delta\overset{(1)}{u}\right) = \tilde{p}\,\mathcal{K}_{g}\left(\overset{(1)}{u},\, \delta\overset{(1)}{u}\right) \tag{51}$$

where

$$\mathcal{K}^{*}_{g}\left(\left\{\overset{(1)}{u}\right\},\, \left\{\delta\overset{(1)}{u}\right\}\right) = \int_0^L \int_0^{2\pi R} \left[\left(\left[\partial_\varphi\right]\left\{\overset{(1)}{u}\right\}\right)^{T}\left[\overset{(0)}{n}{}^{*}\right]\left(\left[\partial_\varphi\right]\left\{\delta\overset{(1)}{u}\right\}\right) + \right.$$

$$\left. \frac{1}{2}\left(\left(\left[\partial^{*}_{p}\right]\left\{\overset{(1)}{u}\right\}\right)^{T}\left\{\delta\overset{(1)}{u}\right\} + \left\{\overset{(1)}{u}\right\}^{T}\left(\left[\partial^{*}_{p}\right]\left\{\delta\overset{(1)}{u}\right\}\right)\right) - \frac{1}{2}\left\{\overset{(1)}{u}\right\}^{T}\left[\partial^{*}_{q}\right]\left\{\delta\overset{(1)}{u}\right\}\right] \mathrm{d}y\mathrm{d}x \tag{52a}$$

$$\left[{}^{(0)}{}^{*}_{\mathcal{N}}{}^{*} \right] = \begin{bmatrix} L_1^{*(0)} {}^{*}_{\mathcal{N}_{xx}} & -L_3^{*(0)} {}^{*}_{\mathcal{N}_{xy}} & 0 \\ -L_3^{*(0)} {}^{*}_{\mathcal{N}_{xy}} & L_2^{*(0)} {}^{*}_{\mathcal{N}_{yy}} & 0 \\ 0 & 0 & c_1 \left(L_1^{*(0)} {}^{*}_{\mathcal{N}_{xx}} + L_2^{*(0)} {}^{*}_{\mathcal{N}_{yy}} \right) \end{bmatrix} \tag{52b}$$

and

$$\left[\partial^{*}_{\mathcal{P}} \right] = c_4 \ell_3^{*} q_\zeta^{*} \begin{bmatrix} 0 & 0 & -\frac{\partial}{\partial x} \\ 0 & \frac{1}{R} & -\frac{\partial}{\partial y} \\ \frac{\partial}{\partial x} & \frac{\partial}{\partial y} & \frac{1}{R} \end{bmatrix} \tag{52c}$$

$$\left[\partial_q^{*} \right] = c_4 \ell_3^{*} \begin{bmatrix} 0 & 0 & \frac{\partial q_\zeta^{*}}{\partial x} \\ 0 & 0 & \frac{\partial q_\zeta^{*}}{\partial y} \\ \frac{\partial q_\zeta^{*}}{\partial x} & \frac{\partial q_\zeta^{*}}{\partial y} & 2\frac{\partial q_\zeta^{*}}{\partial \zeta} \end{bmatrix} \tag{52d}$$

Rayleigh-Ritz Formulation

For many problems of practical interest, closed-form solutions for the boundary-eigenvalue problem governing buckling do not exist. As a result, direct solutions to the corresponding variational problem, such as the Rayleigh-Ritz method, are often used. For this method, the buckling displacements are generally represented by series expansions that satisfy completeness requirements and any kinematic boundary conditions. For example, the displacements may be expressed as

$$u_x^{(1)} = \sum_{i=1}^{N_u} U_i \, \mathcal{G}_{1i}(x, y) \tag{53a}$$

$$u_y^{(1)} = \sum_{i=1}^{N_v} V_i \, \mathcal{G}_{2i}(x, y) \tag{53b}$$

$$\overset{(1)}{w} = \sum_{i=1}^{N_v} W_i \, \mathcal{L}_{3i}(x, y) \tag{53c}$$

where U_i, V_i, and W_i are constants and $\mathcal{L}_{1i}$, $\mathcal{L}_{2i}$, and $\mathcal{L}_{3i}$ are specified basis functions. In matrix form, equations (53) are expressed as

$$\left\{\overset{(1)}{u}\right\} = \begin{Bmatrix} \overset{(1)}{u}_x \\ \overset{(1)}{u}_y \\ \overset{(1)}{w} \end{Bmatrix} = \left[\mathcal{L}\right]\{d\} \tag{54}$$

where

$$\left[\mathcal{L}\right] = \left[\begin{array}{cccc:cccc:cccc} \mathcal{L}_{11} & \mathcal{L}_{12} & \cdots & \mathcal{L}_{1N_u} & 0 & 0 & \cdots & 0 & 0 & 0 & \cdots & 0 \\ 0 & 0 & \cdots & 0 & \mathcal{L}_{21} & \mathcal{L}_{22} & \cdots & \mathcal{L}_{2N_v} & 0 & 0 & \cdots & 0 \\ 0 & 0 & \cdots & 0 & 0 & 0 & \cdots & 0 & \mathcal{L}_{31} & \mathcal{L}_{32} & \cdots & \mathcal{L}_{3N_w} \end{array}\right] \tag{55}$$

and

$$\{d\}^T = \left\{ \begin{array}{cccc:cccc:cccc} U_1 & U_2 & \cdots & U_{N_u} & V_1 & V_2 & \cdots & V_{N_v} & W_1 & W_2 & \cdots & W_{N_w} \end{array}\right\} \tag{56}$$

Upon defining the displacement fields by using equation (54), the virtual displacements are given by

$$\left\{\delta\overset{(1)}{u}\right\} = \begin{Bmatrix} \delta\overset{(1)}{u}_x \\ \delta\overset{(1)}{u}_y \\ \delta\overset{(1)}{w} \end{Bmatrix} = \left[\mathcal{L}\right]\{\delta d\} \tag{57}$$

where

$$\{\delta d\}^T = \left\{ \begin{array}{cccc:cccc:cccc} \delta U_1 & \delta U_2 & \cdots & \delta U_{N_u} & \delta V_1 & \delta V_2 & \cdots & \delta V_{N_v} & \delta W_1 & \delta W_2 & \cdots & \delta W_{N_w} \end{array}\right\} \tag{58}$$

Substituting equation (54) into equations (41) gives

$$\left\{\overset{(1)}{\varphi}\right\} = \left(\left[\partial_\varphi\right]\left[\mathcal{L}\right]\right)\{d\} \equiv \left[D_\varphi\right]\{d\} \tag{59a}$$

$$\left\{\overset{(1)}{\varepsilon}\right\} = \left(\left[\partial_\varepsilon\right]\left[\mathcal{L}\right]\right)\{d\} \equiv \left[D_\varepsilon\right]\{d\} \tag{59b}$$

$$\left\{\overset{(1)}{\kappa}\right\} = \left(\left[\partial_\kappa\right]\left[\mathcal{L}\right]\right)\{d\} \equiv \left[D_\kappa\right]\{d\} \tag{59c}$$

$$\left[\partial_p\right]\left\{\overset{(1)}{u}\right\} = \left(\left[\partial_p\right]\left[\mathcal{L}\right]\right)\{d\} \equiv \left[D_p\right]\{d\} \tag{59d}$$

$$\left[\partial_{\mathcal{P}}^{*}\right]\left\{\overset{(1)}{u}\right\} = \left(\left[\partial_{\mathcal{P}}^{*}\right]\left[\mathcal{N}\right]\right)\{d\} \equiv \left[D_{\mathcal{P}}^{*}\right]\{d\} \tag{59e}$$

Similarly, the variations are given by

$$\left\{\delta\overset{(1)}{\varphi}\right\} = [D_{\varphi}]\{\delta d\} \tag{60a}$$

$$\left\{\delta\overset{(1)}{\varepsilon}\right\} = [D_{\varepsilon}]\{\delta d\} \tag{60b}$$

$$\left\{\delta\overset{(1)}{\kappa}\right\} = [D_{\kappa}]\{\delta d\} \tag{60c}$$

$$\left[\partial_{\mathcal{P}}\right]\left\{\delta\overset{(1)}{u}\right\} = \left(\left[\partial_{\mathcal{P}}\right]\left[\mathcal{N}\right]\right)\{\delta d\} \equiv \left[D_{\mathcal{P}}\right]\{\delta d\} \tag{60d}$$

$$\left[\partial_{\mathcal{P}}^{*}\right]\left\{\delta\overset{(1)}{u}\right\} = \left(\left[\partial_{\mathcal{P}}^{*}\right]\left[\mathcal{N}\right]\right)\{\delta d\} \equiv \left[D_{\mathcal{P}}^{*}\right]\{\delta d\} \tag{60e}$$

By using equations (53) and (54), equations (43) and (50a) become

$$\mathcal{K}\left(\overset{(1)}{u}, \delta\overset{(1)}{u}\right) = \{d\}^{T}\left[K\right]\{\delta d\} \tag{61a}$$

$$\mathcal{K}_{g}\left(\overset{(1)}{u}, \delta\overset{(1)}{u}\right) = \{d\}^{T}\left[G\right]\{\delta d\} \tag{61b}$$

$$\mathcal{K}_{g}^{*}\left(\overset{(1)}{u}, \delta\overset{(1)}{u}\right) = \{d\}^{T}\left[G^{*}\right]\{\delta d\} \tag{61c}$$

where

$$\left[K\right] = \int_{0}^{L}\int_{0}^{2\pi R}\left(\left[D_{\varepsilon}\right]^{T}\left[A\right]\left[D_{\varepsilon}\right] + \left[D_{\kappa}\right]^{T}\left[B\right]\left[D_{\varepsilon}\right] + \left[D_{\varepsilon}\right]^{T}\left[B\right]\left[D_{\kappa}\right] + \left[D_{\kappa}\right]^{T}\left[D\right]\left[D_{\kappa}\right]\right)dydx \tag{62a}$$

$$\left[G\right] = \frac{1}{2}\int_{0}^{L}\int_{0}^{2\pi R}\left(2\left[D_{\varphi}\right]^{T}\left[\overset{(0)}{\mathcal{N}}\right]\left[D_{\varphi}\right] + \left[D_{\mathcal{P}}\right]^{T}\left[\mathcal{N}\right] + \left[\mathcal{N}\right]^{T}\left[D_{\mathcal{P}}\right] + \left[\mathcal{N}\right]^{T}\left[\partial_{q}\right]\left[\mathcal{N}\right]\right)dydx \tag{62b}$$

$$\left[G^*\right] = \frac{1}{2}\int_0^L \int_0^{2\pi R} \left(2\left[D_\varphi\right]^T \left[\overset{(0)}{\mathscr{N}}{}^*\right]\left[D_\varphi\right] + \left[D_{\mathscr{P}}^*\right]^T \left[\mathscr{E}\right] + \left[\mathscr{E}\right]^T \left[D_{\mathscr{P}}^*\right] + \left[\mathscr{E}\right]^T \left[\partial_q^*\right] \left[\mathscr{E}\right] \right) dy\,dx \quad (62c)$$

In these equations, it is noted that $\left[K\right] = \left[K\right]^T$, $\left[G\right] = \left[G\right]^T$ and $\left[G^*\right] = \left[G^*\right]^T$. In addition, equation (42) becomes

$$\{\delta d\}^T \left(\left[K\right]\{d\} - \tilde{\lambda}\left[G^*\right]\{d\} - \tilde{p}\left[G\right]\{d\} \right) = 0 \quad (63)$$

For arbitrary variations, satisfaction of equation (61) requires

$$\left[K^T\right]\{d\} = \tilde{p}\left[G\right]\{d\} \quad (64a)$$

where

$$\left[K^T\right] \equiv \left[K\right] - \tilde{\lambda}\left[G^*\right] \quad (64b)$$

Equation (62) constitutes a *generalized algebraic eigenvalue problem* in which $\tilde{p}$ is an eigenvalue and $\{d\}$ is the corresponding eigenvector. The matrices $\left[K\right]$, $\left[G\right]$, and $\left[K^T\right]$ are referred to herein as the stiffness, geometric stiffness, and total stiffness matrices, respectively.

Classical Solution

Closed-form solutions to the buckling equations can be obtained for some special cases. For example, consider a simply supported cylinder with a ring-and-stringer-stiffened wall construction that satisfies the constitutive equations given by

$$\begin{bmatrix} A_{11} & A_{12} & A_{16} \\ A_{12} & A_{22} & A_{26} \\ A_{16} & A_{26} & A_{66} \end{bmatrix} = \begin{bmatrix} A_{11}^{shell} & A_{12}^{shell} & 0 \\ A_{12}^{shell} & A_{22}^{shell} & 0 \\ 0 & 0 & A_{66}^{shell} \end{bmatrix} + \begin{bmatrix} \frac{E_s A_s}{d_s} & 0 & 0 \\ 0 & \frac{E_r A_r}{d_r} & 0 \\ 0 & 0 & 0 \end{bmatrix} \quad (65a)$$

$$\begin{bmatrix} B_{11} & B_{12} & B_{16} \\ B_{12} & B_{22} & B_{26} \\ B_{16} & B_{26} & B_{66} \end{bmatrix} = \begin{bmatrix} B_{11}^{shell} & B_{12}^{shell} & 0 \\ B_{12}^{shell} & B_{22}^{shell} & 0 \\ 0 & 0 & B_{66}^{shell} \end{bmatrix} + \begin{bmatrix} \frac{E_s A_s}{d_s} e_s & 0 & 0 \\ 0 & \frac{E_r A_r}{d_r} e_r & 0 \\ 0 & 0 & 0 \end{bmatrix} \tag{65b}$$

$$\begin{bmatrix} D_{11} & D_{12} & D_{16} \\ D_{12} & D_{22} & D_{26} \\ D_{16} & D_{26} & D_{66} \end{bmatrix} = \begin{bmatrix} D_{11}^{shell} & D_{12}^{shell} & 0 \\ D_{12}^{shell} & D_{22}^{shell} & 0 \\ 0 & 0 & D_{66}^{shell} \end{bmatrix} + \begin{bmatrix} \frac{E_s}{d_s}\left(I_s^c + e_s^2 A_s\right) & 0 & 0 \\ 0 & \frac{E_r}{d_r}\left(I_r^c + e_r^2 A_r\right) & 0 \\ 0 & 0 & \frac{1}{4}\left(\frac{G_s J_s}{d_s} + \frac{G_r J_r}{d_r}\right) \end{bmatrix} \tag{65c}$$

The cylinder is subjected to uniform axial compressive loads at the ends and uniform external pressure that is applied normal to the middle surface; that is,

$$N_0(y) = - N_x \tag{66a}$$

$$N_L(y) = - N_x \tag{66b}$$

$$q_\zeta = - q_{ext} \tag{66c}$$

$N_0(y)$ and $N_L(y)$ are defined by equations (27a) and (27c), respectively. These loads constitute the only nonzero active loads associated with the loading parameter $\tilde{p}$. For the case of pure uniform axial compression, $q_{ext} = 0$ and N_x is a specified value. For pure external pressure, pressing radially inward, $N_x = 0$ and q_{ext} is a specified positive value. Similarly, for uniform hydrostatic pressure, q_{ext} is a specified value and $N_x = q_{ext} R/2$.

The cylinder is also subjected to a uniform internal pressure given by

$$q_\zeta^* = q_{int} \tag{67a}$$

that is a passive load associated with the loading parameter $\tilde{\lambda}$ and the replacement rule given by equation (46c). In a sealed cylinder, the internal pressure induces a state of uniform axial tension given by

$$N_0^*(y) = N_x^* \tag{67b}$$

$$N_L^*(y) = N_x^* \tag{67c}$$

where the symbols in these equations are identified by the replacement rules defined by equations (47a) and (47c), and where $N_x^* = q_{int}\frac{R}{2}$. The internal pressure is the only nonzero component of the passive loading system and, as a result, it is convenient to set $\tilde{\lambda} = 1,\ \ell_3^* = 1,\ \ell_4^* = 1,$ and $\ell_8^* = 1$ in the replacement rules defined by equations (46) and (47). Inclusion of the internal pressure permits examination of the buckling behavior of pressure-stabilized cylinders.

The boundary conditions for this example, as defined by equations (10) and the replacement rules defined by equations (46) and (47), are given by

$$\mathcal{N}_{xx} = -\tilde{p}\ell_4 N_x + q_{int}\frac{R}{2} \tag{68a}$$

$$u_y = 0 \tag{68b}$$

$$w = 0 \tag{68c}$$

$$M_{xx} = 0 \tag{68d}$$

at $x = 0$ and $x = L$, where N_x is scaled identically at each cylinder end such that $\ell_8 = \ell_4$. Thus, the boundary conditions for the prebuckling state, given by equations (27) and the replacement rules defined by equations (46) and (47), become

$$\overset{(0)}{\mathcal{N}}_{xx} = -\tilde{p}\ell_4 N_x + q_{int}\frac{R}{2} \tag{69a}$$

$$\overset{(0)}{u}_y = 0 \tag{69b}$$

at $x = 0$ and $x = L$. The corresponding homogeneous boundary conditions for the buckling problem, as defined by equations (30), are given by

$$\overset{(1)}{\mathcal{N}}_{xx} = \mathcal{B}_{11}\left(\overset{(1)}{u}_x\right) + \mathcal{B}_{12}\left(\overset{(1)}{u}_y\right) + \mathcal{B}_{13}\left(\overset{(1)}{w}\right) = 0 \tag{70a}$$

$$\overset{(1)}{u}_y = 0 \tag{70b}$$

$$\overset{(1)}{w} = 0 \tag{70c}$$

$$\overset{(1)}{\mathcal{M}}_{xx} = \mathcal{B}_{41}\left(\overset{(1)}{u}_x\right) + \mathcal{B}_{42}\left(\overset{(1)}{u}_y\right) + \mathcal{B}_{43}\left(\overset{(1)}{w}\right) = 0 \tag{70d}$$

at $x = 0$ and $x = L$. The operators appearing in these boundary conditions are given in Appendix A. Using equations (65) and (A11), the buckling-problem boundary conditions reduce to

$$A_{11}\frac{\partial \overset{(1)}{u}_x}{\partial x} + A_{12}\left(\frac{\partial \overset{(1)}{u}_y}{\partial y} + \frac{\overset{(1)}{w}}{R}\right) \pm B_{11}\frac{\partial^2 \overset{(1)}{w}}{\partial x^2} + B_{12}\left(\frac{c_2}{R}\frac{\partial \overset{(1)}{u}_y}{\partial y} \pm \frac{\partial^2 \overset{(1)}{w}}{\partial y^2}\right) = 0 \tag{71a}$$

$$\overset{(1)}{u}_y = 0 \tag{71b}$$

$$\overset{(1)}{w} = 0 \tag{71c}$$

$$B_{11}\frac{\partial \overset{(1)}{u}_x}{\partial x} + \left(B_{12} + D_{12}\frac{c_2}{R}\right)\frac{\partial \overset{(1)}{u}_y}{\partial y} \pm D_{11}\frac{\partial^2 \overset{(1)}{w}}{\partial x^2} \pm D_{12}\frac{\partial^2 \overset{(1)}{w}}{\partial y^2} + B_{12}\frac{\overset{(1)}{w}}{R} = 0 \tag{71d}$$

at $x = 0$ and $x = L$.

The membrane prebuckling stress state is obtained by first substituting equations (66c) and (67a) into equation (46c) and then substituting the result into equation (26a). Then, $\tilde{\lambda} = 1$ and $\ell_3^* = 1$ are used to get

$$\overset{(0)}{\mathcal{N}}_{yy}(x, y) = -\tilde{p}\ell_3 q_{ext} R + q_{int} R \tag{72a}$$

Likewise, equations (26b) and (26c) give

$$\overset{(0)}{\mathcal{N}}_{xy} = \bar{C}(y) \tag{72b}$$

$$\overset{(0)}{\mathcal{N}}_{xx} = -\frac{d\bar{C}(y)}{dy}\, x + C_2(y) \tag{72c}$$

Enforcing boundary conditions at $x = 0$ and $x = L$ given by equation (69a) indicates that $C_2(y) = -\tilde{p}\ell_4 N_x + q_{int}\frac{R}{2}$ and $\bar{C}$ is a constant. Thus,

$$\overset{(0)}{\mathcal{N}}_{xx} = -\tilde{p}\ell_4 N_x + q_{int}\frac{R}{2} \tag{73a}$$

$$\overset{(0)}{\mathcal{N}}_{xy} = \bar{C} \tag{73b}$$

Using equations (72a) and (73) with equations (18a), (18c), and (21a) and neglecting second derivatives of $\overset{(0)}{w}(x, y)$ in equation (18c) gives

$$A_{11}\frac{\partial \overset{(0)}{u}_x}{\partial x} + \left(A_{12} + \frac{c_2}{R}B_{12}\right)\frac{\partial \overset{(0)}{u}_y}{\partial y} + \frac{A_{12}}{R}\overset{(0)}{w} = -\tilde{p}\ell_4 N_x + q_{int}\frac{R}{2} \tag{74a}$$

$$A_{12}\frac{\partial \overset{(0)}{u}_x}{\partial x} + \left(A_{22} + \frac{c_2}{R}B_{22}\right)\frac{\partial \overset{(0)}{u}_y}{\partial y} + \frac{A_{22}}{R}\overset{(0)}{w} = -\tilde{p}\ell_3 q_{ext}R + q_{int}R \tag{74b}$$

$$\left(A_{66} - \frac{c_2}{2R}B_{66}\right)\frac{\partial \overset{(0)}{u}_x}{\partial y} + \left(A_{66} + \frac{3c_2}{2R}B_{66}\right)\frac{\partial \overset{(0)}{u}_y}{\partial x} = \overline{C} \tag{74c}$$

Equation (74c) can only be satisfied if $\overset{(0)}{u}_x = \overset{(0)}{u}_x(x)$ and $\overset{(0)}{u}_y = B_5 x + B_6$, where B_5 and B_6 are constants. The boundary condition given by equation (67b) indicates that $B_5 = B_6 = 0$ and $\overset{(0)}{u}_y(x, y) = 0$. As a result, $\overline{C} = 0$ and

$$\overset{(0)}{\mathcal{N}}_{xy}(x, y) = 0 \tag{75}$$

Equations (74a) and (74b) are then solved to obtain $\overset{(0)}{u}_x(x)$ and $\overset{(0)}{w}(x)$.

By comparing equations (72a), (73a), and (75) with equations (48), and using $\tilde{\lambda} = 1$ and $\ell_3^* = 1$, it follows that

$$L_1 = \ell_4 N_x \tag{76a}$$

$$L_2 = \ell_3 q_{ext} R \tag{76b}$$

$$L_3 = 0 \tag{76c}$$

$$L_1^* = -q_{int}\frac{R}{2} \tag{76d}$$

$$L_2^* = -q_{int}R \tag{76e}$$

$$L_3^* = 0 \tag{76f}$$

In addition, all functions of (x, y) on the right-hand-sides of equations (48) are equal to unity. In equations (76), $\ell_4 N_x$ and $\ell_3 q_{ext}$, and q_{int} are specified quantities. For example, to analyze a compression-loaded cylinder that has a fixed internal pressure, it is convenient to pick $\ell_4 = 1$, and $\ell_3 = 0$ such that $L_1 = N_x$ and $L_2 = 0$. At buckling, the active applied load $\tilde{p}\ell_4 N_x$ becomes

$N_x^{cr} = \tilde{p}_{cr} N_x$. For a cylinder subjected to hydrostatic external pressure, q_{ext}, $\ell_4 N_x = q_{ext}\frac{R}{2}$, $\ell_3 = 1$, and $q_{int} = 0$. At buckling, the active applied load $\tilde{p}\ell_3 q_{ext}$ becomes $q_{ext}^{cr} = \tilde{p}_{cr} q_{ext}$.

The solution of equations (49) is obtained by using trigonometric displacements functions that satisfy all the boundary conditions; that is,

$$\overset{(1)}{u}_x = \bar{u}\cos\left(\frac{m\pi x}{L}\right)\cos\left(\frac{ny}{R}\right) \tag{77a}$$

$$\overset{(1)}{u}_y = \bar{v}\sin\left(\frac{m\pi x}{L}\right)\sin\left(\frac{ny}{R}\right) \tag{77b}$$

$$\overset{(1)}{w} = \bar{w}\sin\left(\frac{m\pi x}{L}\right)\cos\left(\frac{ny}{R}\right) \tag{77c}$$

for values of $m \in \{1, 2, 3, ...\}$ and $n \in \{0, 1, 2, , ...\}$. The circumferential waveforms appearing in equation (77c) are shown in figure 4. Substituting equations (77) into (49), using the expressions for the operators given in Appendix A, noting that all functions of (x, y) on the right-hand-sides of equations (47) are equal to unity, and using equations (76) yields the generalized algebraic eigenvalue problem

$$\begin{bmatrix} K_{11} & K_{12} & K_{13} \\ K_{12} & K_{22} & K_{23} \\ K_{13} & K_{23} & K_{33} \end{bmatrix} \begin{Bmatrix} \bar{u} \\ \bar{v} \\ \frac{m\pi}{L}\bar{w} \end{Bmatrix} = \tilde{p} \begin{bmatrix} G_{11} & G_{12} & G_{13} \\ G_{12} & G_{22} & G_{23} \\ G_{13} & G_{23} & G_{33} \end{bmatrix} \begin{Bmatrix} \bar{u} \\ \bar{v} \\ \frac{m\pi}{L}\bar{w} \end{Bmatrix} \tag{78}$$

where

$$K_{11} = A_{11} + \left(A_{66} - B_{66}\frac{c_2}{R} + D_{66}\frac{c_2}{4R^2} - \frac{c_1}{4}\left(L_1^* + L_2^*\right)\right)\left(\frac{nL}{m\pi R}\right)^2 \tag{79a}$$

$$K_{12} = -\left(\frac{nL}{m\pi R}\right)\left(A_{12} + A_{66} + \left[B_{12} + B_{66}\right]\frac{c_2}{R} - D_{66}\frac{3c_2}{4R^2} + \frac{c_1}{4}\left(L_1^* + L_2^*\right)\right) \tag{79b}$$

$$K_{13} = -\left[\left(\frac{A_{12}}{R} + \frac{c_4 L_2^*}{R}\right)\left(\frac{L}{m\pi}\right)^2 + B_{11} - \left(D_{66}\frac{c_2}{R} - B_{12} - 2B_{66}\right)\left(\frac{nL}{m\pi R}\right)^2\right] \tag{79c}$$

$$\begin{aligned} K_{22} = \left(A_{66} + B_{66}\frac{3c_2}{R} + D_{66}\frac{9c_2}{4R^2}\right) + \left(A_{22} + 2B_{22}\frac{c_2}{R} + D_{22}\frac{c_2}{R^2}\right)\left(\frac{nL}{m\pi R}\right)^2 \\ - \frac{\left(c_2 - c_4\right)L_2^*}{R^2}\left(\frac{L}{m\pi}\right)^2 - \frac{c_1}{4}\left(L_1^* + L_2^*\right) \end{aligned} \tag{79d}$$

$$K_{23} = \left(\frac{nL}{m\pi R}\right)\left[\frac{1}{R}\left(A_{22} + B_{22}\frac{c_2}{R}\right)\left(\frac{L}{m\pi}\right)^2 + \left(B_{12} + 2B_{66} + \left[D_{12} + 3D_{66}\right]\frac{c_2}{R}\right) + \left(B_{22} + D_{22}\frac{c_2}{R}\right)\left(\frac{nL}{m\pi R}\right)^2\right] - \frac{(c_2 - c_4)L_2^*}{R}\left(\frac{L}{m\pi}\right)^2\left(\frac{nL}{m\pi R}\right) \tag{79e}$$

$$K_{33} = \frac{A_{22}}{R^2}\left(\frac{L}{m\pi}\right)^4 + \frac{2}{R}\left(\frac{L}{m\pi}\right)^2\left[B_{12} + B_{22}\left(\frac{nL}{m\pi R}\right)^2\right] + \left[D_{11} + 2\left(D_{12} + 2D_{66}\right)\left(\frac{nL}{m\pi R}\right)^2 + D_{22}\left(\frac{nL}{m\pi R}\right)^4\right] - \left(\frac{L}{m\pi}\right)^2\left[L_1^* + L_2^*\left(\frac{nL}{m\pi R}\right)^2 - \frac{c_4 L_2^*}{R^2}\left(\frac{L}{m\pi}\right)^2\right] \tag{79f}$$

$$G_{11} = \frac{c_1}{4}\left(L_1 + L_2\right)\left(\frac{nL}{m\pi R}\right)^2 \tag{80a}$$

$$G_{12} = \frac{c_1}{4}\left(L_1 + L_2\right)\left(\frac{nL}{m\pi R}\right) \tag{80b}$$

$$G_{13} = \frac{c_4 L_2}{R}\left(\frac{L}{m\pi}\right)^2 \tag{80c}$$

$$G_{22} = \frac{(c_2 - c_4)L_2}{R^2}\left(\frac{L}{m\pi}\right)^2 + \frac{c_1}{4}\left(L_1 + L_2\right) \tag{80d}$$

$$G_{23} = \frac{(c_2 - c_4)L_2}{R}\left(\frac{L}{m\pi}\right)^2\left(\frac{nL}{m\pi R}\right) \tag{80e}$$

$$G_{33} = \left(\frac{L}{m\pi}\right)^2\left[L_1 + L_2\left(\frac{nL}{m\pi R}\right)^2 - \frac{c_4 L_2}{R^2}\left(\frac{L}{m\pi}\right)^2\right] \tag{80e}$$

In these expressions, the nonzero load factors are given by equations (76a), (76b), and (76e). Nontrivial solutions to equation (78) are given by the determinant

$$\left|\begin{bmatrix} K_{11} & K_{12} & K_{13} \\ K_{12} & K_{22} & K_{23} \\ K_{13} & K_{23} & K_{33} \end{bmatrix} - \tilde{p}\begin{bmatrix} G_{11} & G_{12} & G_{13} \\ G_{12} & G_{22} & G_{23} \\ G_{13} & G_{23} & G_{33} \end{bmatrix}\right| = 0 \tag{81}$$

which is expressed as

$$C_3\tilde{p}^3 + C_2\tilde{p}^2 - C_1\tilde{p} + C_0 = 0 \tag{82}$$

where

$$C_0 = K_{33}\left(K_{11}K_{22} - K_{12}^2\right) + \left(K_{12}K_{13} - K_{11}K_{23}\right)K_{23} + \left(K_{12}K_{23} - K_{22}K_{13}\right)K_{13} \tag{83a}$$

$$\begin{aligned} C_1 = {} & G_{11}\left(K_{22}K_{33} - K_{23}^2\right) + G_{22}\left(K_{11}K_{33} - K_{13}^2\right) + G_{33}\left(K_{11}K_{22} - K_{12}^2\right) + \\ & 2G_{12}\left(K_{13}K_{23} - K_{12}K_{33}\right) + 2G_{13}\left(K_{12}K_{23} - K_{13}K_{22}\right) + 2G_{23}\left(K_{12}K_{13} - K_{11}K_{23}\right) \end{aligned} \tag{83b}$$

$$\begin{aligned} C_2 = {} & K_{11}\left(G_{22}G_{33} - G_{23}^2\right) + K_{22}\left(G_{11}G_{33} - G_{13}^2\right) + K_{33}\left(G_{11}G_{22} - G_{12}^2\right) + \\ & 2K_{12}\left(G_{13}G_{23} - G_{12}G_{33}\right) + 2K_{13}\left(G_{12}G_{23} - G_{13}G_{22}\right) + 2K_{23}\left(G_{12}G_{13} - G_{11}G_{23}\right) \end{aligned} \tag{83c}$$

$$C_3 = G_{11}G_{23}^2 + G_{22}G_{13}^2 - G_{33}\left(G_{11}G_{22} - G_{12}^2\right) - 2G_{12}G_{13}G_{23} \tag{83d}$$

The critical value of the loading parameter, $\tilde{p}_{cr}$, is the smallest positive value that satisfies equation (82) for values of $m \in \{1, 2, 3, ...\}$ and $n \in \{0, 1, 2, , ...\}$. The corresponding values of the wave numbers, m and n, are denoted by m_{cr} and n_{cr}, respectively.

For the special case in which nonlinear rotations about the normal are neglected, $c_1 = 0$, which results in $G_{11} = G_{12} = 0$. In addition, for "live" pressure, $c_2 - c_4 = 0$ and, as a result, the coefficient $C_3 = 0$ and equation (82) reduces to

$$C_2\tilde{p}^2 - C_1\tilde{p} + C_0 = 0 \tag{84a}$$

with the simplifications

$$C_2 = K_{11}\left(G_{22}G_{33} - G_{23}^2\right) \tag{84b}$$

$$C_1 = G_{22}\left(K_{11}K_{33} - K_{13}^2\right) + G_{33}\left(K_{11}K_{22} - K_{12}^2\right) + 2G_{23}\left(K_{12}K_{13} - K_{11}K_{23}\right) \tag{84c}$$

$$C_0 = K_{33}\left(K_{11}K_{22} - K_{12}^2\right) + \left(K_{12}K_{13} - K_{11}K_{23}\right)K_{23} + \left(K_{12}K_{23} - K_{22}K_{13}\right)K_{13} \tag{84d}$$

Applying the quadratic equation and taking the smallest postive, real-valued solution gives

$$\tilde{p} = \frac{C_1}{2C_2} - \sqrt{\left(\frac{C_1}{2C_2}\right)^2 - \frac{C_0}{C_2}} \tag{85}$$

When only axial compression loads are present, the load factor $L_2 = 0$, the coefficient $C_2 = 0$, and equation (85) becomes

$$\tilde{p} = \frac{C_0}{C_1} \tag{86}$$

For the special case of reduction to Donnell-type equations, $c_1 = c_2 = c_4 = 0$, which results in $G_{11} = G_{12} = G_{22} = G_{23} = 0$, $C_2 = C_3 = 0$, and

$$\tilde{p} = \frac{K_{33}}{G_{33}} + \frac{\left(K_{12}K_{13} - K_{11}K_{23}\right)K_{23} + \left(K_{12}K_{23} - K_{22}K_{13}\right)K_{13}}{G_{33}\left(K_{11}K_{22} - K_{12}^2\right)} \tag{87}$$

Upon obtaining the critical value of the loading parameter, $\tilde{p}_{cr}$, and the corresponding wave numbers, m_{cr} and n_{cr}, the buckling mode (eigenvector) is obtained by substituting these values into equations (79) and (80). The resulting expressions are then substituted into equations (78), which gives

$$\begin{bmatrix} K_{11}^{cr} & K_{12}^{cr} & K_{13}^{cr} \\ K_{12}^{cr} & K_{22}^{cr} & K_{23}^{cr} \\ K_{13}^{cr} & K_{23}^{cr} & K_{33}^{cr} \end{bmatrix} \begin{Bmatrix} \bar{u} \\ \bar{v} \\ \frac{m_{cr}\pi}{L}\bar{w} \end{Bmatrix} = \tilde{p}_{cr} \begin{bmatrix} G_{11}^{cr} & G_{12}^{cr} & G_{13}^{cr} \\ G_{12}^{cr} & G_{22}^{cr} & G_{23}^{cr} \\ G_{13}^{cr} & G_{23}^{cr} & G_{33}^{cr} \end{bmatrix} \begin{Bmatrix} \bar{u} \\ \bar{v} \\ \frac{m_{cr}\pi}{L}\bar{w} \end{Bmatrix} \tag{88}$$

where the superscript "cr" indicates that the coefficients given by equations (62) and (63) have been evaluated for $m = m_{cr}$ and $n = n_{cr}$. Only two of the three equations given by matrix equation (88) are independent. Using the first and third equations to find $\bar{u}$ and $\bar{v}$ in terms of $\bar{w}$ yields

$$\bar{u} = \frac{m_{cr}\pi}{L} \frac{\left(K_{12}^{cr} - \tilde{p}_{cr}G_{12}^{cr}\right)\left(K_{33}^{cr} - \tilde{p}_{cr}G_{33}^{cr}\right) - \left(K_{13}^{cr} - \tilde{p}_{cr}G_{13}^{cr}\right)\left(K_{23}^{cr} - \tilde{p}_{cr}G_{23}^{cr}\right)}{\left(K_{11}^{cr} - \tilde{p}_{cr}G_{11}^{cr}\right)\left(K_{23}^{cr} - \tilde{p}_{cr}G_{23}^{cr}\right) - \left(K_{13}^{cr} - \tilde{p}_{cr}G_{13}^{cr}\right)\left(K_{12}^{cr} - \tilde{p}_{cr}G_{12}^{cr}\right)} \bar{w} \tag{89a}$$

$$\bar{v} = \frac{m_{cr}\pi}{L} \frac{\left(K_{13}^{cr} - \tilde{p}_{cr}G_{13}^{cr}\right)^2 - \left(K_{11}^{cr} - \tilde{p}_{cr}G_{11}^{cr}\right)\left(K_{33}^{cr} - \tilde{p}_{cr}G_{33}^{cr}\right)}{\left(K_{11}^{cr} - \tilde{p}_{cr}G_{11}^{cr}\right)\left(K_{23}^{cr} - \tilde{p}_{cr}G_{23}^{cr}\right) - \left(K_{13}^{cr} - \tilde{p}_{cr}G_{13}^{cr}\right)\left(K_{12}^{cr} - \tilde{p}_{cr}G_{12}^{cr}\right)} \bar{w} \tag{89b}$$

Substituting these two expressions into equations (77) gives the buckling mode in terms of the unknown normal-direction amplitude, $\bar{w}$; i. e.,

$$u_x^{(1)} = \frac{m_{cr}\pi}{L} \frac{\left(K_{12}^{cr} - \tilde{p}_{cr}G_{12}^{cr}\right)\left(K_{33}^{cr} - \tilde{p}_{cr}G_{33}^{cr}\right) - \left(K_{13}^{cr} - \tilde{p}_{cr}G_{13}^{cr}\right)\left(K_{23}^{cr} - \tilde{p}_{cr}G_{23}^{cr}\right)}{\left(K_{11}^{cr} - \tilde{p}_{cr}G_{11}^{cr}\right)\left(K_{23}^{cr} - \tilde{p}_{cr}G_{23}^{cr}\right) - \left(K_{13}^{cr} - \tilde{p}_{cr}G_{13}^{cr}\right)\left(K_{12}^{cr} - \tilde{p}_{cr}G_{12}^{cr}\right)} \bar{w} \cos\left(\frac{m_{cr}\pi x}{L}\right) \cos\left(\frac{n_{cr}y}{R}\right) \tag{90a}$$

$$u_y^{(1)} = \frac{m_{cr}\pi}{L} \frac{\left(K_{13}^{cr} - \tilde{p}_{cr}G_{13}^{cr}\right)^2 - \left(K_{11}^{cr} - \tilde{p}_{cr}G_{11}^{cr}\right)\left(K_{33}^{cr} - \tilde{p}_{cr}G_{33}^{cr}\right)}{\left(K_{11}^{cr} - \tilde{p}_{cr}G_{11}^{cr}\right)\left(K_{23}^{cr} - \tilde{p}_{cr}G_{23}^{cr}\right) - \left(K_{13}^{cr} - \tilde{p}_{cr}G_{13}^{cr}\right)\left(K_{12}^{cr} - \tilde{p}_{cr}G_{12}^{cr}\right)} \bar{w} \sin\left(\frac{m_{cr}\pi x}{L}\right) \sin\left(\frac{n_{cr}y}{R}\right) \tag{90b}$$

$$\overset{(1)}{w} = \bar{w}\,\sin\left(\frac{m_{cr}\pi x}{L}\right)\cos\left(\frac{n_{cr} y}{R}\right) \tag{90c}$$

A typical buckle pattern given by equations (90) is shown in figure 5 for $m_{cr} = 2$ and $n_{cr} = 4$.

For axisymmetric buckling modes, given by $n_{cr} = 0$, equation (77b) indicates that $\overset{(1)}{u}_y = 0$. In addition; $K_{12}^{cr} = 0$, $K_{23}^{cr} = 0$, $G_{11}^{cr} = 0$, $G_{12}^{cr} = 0$, and $G_{23}^{cr} = 0$. Thus, equation (88) reduces to

$$\begin{bmatrix} K_{11}^{cr} & K_{13}^{cr} \\ K_{13}^{cr} & K_{33}^{cr} \end{bmatrix} \begin{Bmatrix} \bar{u} \\ \frac{m_{cr}\pi}{L}\bar{w} \end{Bmatrix} = \tilde{p}_{cr} \begin{bmatrix} G_{11}^{cr} & G_{13}^{cr} \\ G_{13}^{cr} & G_{33}^{cr} \end{bmatrix} \begin{Bmatrix} \bar{u} \\ \frac{m_{cr}\pi}{L}\bar{w} \end{Bmatrix} \tag{91}$$

Only one of these two equations is independent. Using the first equation to find $\bar{u}$ in terms of $\bar{w}$ yields

$$\bar{u} = -\frac{m_{cr}\pi}{L}\,\frac{K_{13}^{cr} - \tilde{p}_{cr} G_{13}^{cr}}{K_{11}^{cr}}\,\bar{w} \tag{92}$$

Substituting this expression and $n_{cr} = 0$ into equation (77a) gives

$$\overset{(1)}{u}_x = -\frac{m_{cr}\pi}{L}\,\frac{K_{13}^{cr} - \tilde{p}_{cr} G_{13}^{cr}}{K_{11}^{cr}}\,\bar{w}\cos\left(\frac{m_{cr}\pi x}{L}\right) \tag{93}$$

The Cartesian coordinates of the deformed (buckling mode) shell, (x*, y*, z*), are given by

$$x^* = X + \overset{(1)}{u}_x \tag{94a}$$

$$y^* = Y + \overset{(1)}{u}_y \cos\theta + \overset{(1)}{w}\sin\theta \tag{94b}$$

$$z^* = Z - \overset{(1)}{u}_y \sin\theta + \overset{(1)}{w}\cos\theta \tag{94c}$$

where (X, Y, Z) are the corresponding Cartesian coordinates of the undeformed shell and

$$Y = R\sin\theta \tag{95a}$$

$$Z = R\cos\theta \tag{95b}$$

A Rayleigh-Ritz Solution

Consider a fully anisotropic shell that is simply supported at each end, with the boundary conditions, as defined by equations (10), given by

$$\mathcal{N}_{xx} = -\tilde{p}\ell_4 N_x + q_{int}\frac{R}{2} \tag{96a}$$

$$u_y = 0 \tag{96b}$$

$$w = 0 \tag{96c}$$

$$M_{xx} = 0 \tag{96d}$$

at $x = 0$ and

$$\mathcal{N}_{xx} = -\tilde{p}\ell_4 N_x + q_{int}\frac{R}{2} \tag{96e}$$

$$u_y = \tilde{p}\ell_9\Delta_s \tag{96f}$$

$$w = 0 \tag{96g}$$

$$M_{xx} = 0 \tag{96h}$$

at $x = L$, where N_x is an applied uniform compression stress resultant that is scaled identically at each cylinder end such that $\ell_8 = \ell_4$, and Δ_s is a constant twisting displacement. Thus, the boundary conditions for the prebuckling state, given by equations (27), become

$$\overset{(0)}{\mathcal{N}}_{xx} = -\tilde{p}\ell_4 N_x + q_{int}\frac{R}{2} \tag{97a}$$

$$\overset{(0)}{u}_y = 0 \tag{97b}$$

at $x = 0$ and

$$\overset{(0)}{\mathcal{N}}_{xx} = -\tilde{p}\ell_4 N_x + q_{int}\frac{R}{2} \tag{97c}$$

$$\overset{(0)}{u}_y = \tilde{p}\ell_9\Delta_s \tag{97d}$$

at $x = L$. The corresponding homogeneous boundary conditions for the buckling problem, as defined by equations (30), are given by equations (70) and (71).

The membrane prebuckling stress state is obtained by first substituting equations (66c) and (67a) into equation (46c) and then substituting the result into equation (26a). Then, $\tilde{\lambda} = 1$ and $\ell_3^* = 1$ are used to get

$$\overset{(0)}{\mathcal{N}}_{yy}(x, y) = -\tilde{p}\ell_3 q_{ext} R + q_{int} R \tag{98a}$$

Likewise, equations (26b) and (26c) give

$$\overset{(0)}{\mathcal{N}}_{xy} = \bar{C}(y) \tag{98b}$$

$$\overset{(0)}{\mathcal{N}}_{xx} = -\frac{\partial \bar{C}(y)}{\partial y} x + C_2(y) \tag{98c}$$

Enforcing boundary conditions at $x = 0$ and $x = L$ given by equations (97a) and (97c) indicates that $C_2(y) = -\tilde{p}\ell_4 N_x + q_{int}\frac{R}{2}$ and $\bar{C}$ is a constant. Thus,

$$\overset{(0)}{\mathcal{N}}_{xx} = -\tilde{p}\ell_4 N_x + q_{int}\frac{R}{2} \tag{99a}$$

$$\overset{(0)}{\mathcal{N}}_{xy} = \bar{C} \tag{99b}$$

Using equations (98a) and (99) with equations (18a), (18c), and (21a) and neglecting second derivatives of $\overset{(0)}{w}(x, y)$ in equation (18c) gives

$$A_{11}\frac{\partial \overset{(0)}{u}_x}{\partial x} + \left(A_{16} - \frac{c_2}{2R}B_{16}\right)\frac{\partial \overset{(0)}{u}_x}{\partial y} + \left(A_{16} + \frac{3c_2}{2R}B_{16}\right)\frac{\partial \overset{(0)}{u}_y}{\partial x} + \left(A_{12} + \frac{c_2}{R}B_{12}\right)\frac{\partial \overset{(0)}{u}_y}{\partial y} + \frac{A_{12}}{R}\overset{(0)}{w} = -\tilde{p}\ell_4 N_x + q_{int}\frac{R}{2} \tag{100a}$$

$$A_{12}\frac{\partial \overset{(0)}{u}_x}{\partial x} + \left(A_{26} - \frac{c_2}{2R}B_{26}\right)\frac{\partial \overset{(0)}{u}_x}{\partial y} + \left(A_{26} + \frac{3c_2}{2R}B_{26}\right)\frac{\partial \overset{(0)}{u}_y}{\partial x} + \left(A_{22} + \frac{c_2}{R}B_{22}\right)\frac{\partial \overset{(0)}{u}_y}{\partial y} + \frac{A_{22}}{R}\overset{(0)}{w} = -\tilde{p}\ell_3 q_{ext} R + q_{int} R \tag{100b}$$

$$A_{16}\frac{\partial \overset{(0)}{u}_x}{\partial x} + \left(A_{66} - \frac{c_2}{2R}B_{66}\right)\frac{\partial \overset{(0)}{u}_x}{\partial y} + \left(A_{66} + \frac{3c_2}{2R}B_{66}\right)\frac{\partial \overset{(0)}{u}_y}{\partial x} + \left(A_{26} + \frac{c_2}{R}B_{26}\right)\frac{\partial \overset{(0)}{u}_y}{\partial y} + \frac{A_{26}}{R}\overset{(0)}{w} = \bar{C} \tag{100c}$$

Noting that the right-hand sides of these equations are constants, it follows that they are satisfied if $\overset{(0)}{u}_x = B_3 x + B_4$ and $\overset{(0)}{u}_y = B_5 x + B_6$, where B_3, B_4, B_5, and B_6 are constants. The boundary conditions given by equations (97b) and (97d) indicate that $B_5 = \tilde{p}\ell_9 \frac{\Delta_s}{L}$ and $B_6 = 0$. Thus,

$$\overset{(0)}{u}_y = \tilde{p}\ell_9 \frac{\Delta_s}{L} x \tag{101}$$

Substituting $\overset{(0)}{u}_x = B_3 x + B_4$ and equation (101) into equations (100) produces

$$A_{11} B_3 + \frac{A_{12}}{R} \overset{(0)}{w} = -\tilde{p}\ell_4 N_x + q_{int} \frac{R}{2} - \left(A_{16} + \frac{3c_2}{2R} B_{16} \right) \tilde{p}\ell_9 \frac{\Delta_s}{L} \tag{102a}$$

$$A_{12} B_3 + \frac{A_{22}}{R} \overset{(0)}{w} = -\tilde{p}\ell_3 q_{ext} R + q_{int} R - \left(A_{26} + \frac{3c_2}{2R} B_{26} \right) \tilde{p}\ell_9 \frac{\Delta_s}{L} \tag{102b}$$

$$A_{16} B_3 + \left(A_{66} + \frac{3c_2}{2R} B_{66} \right) \tilde{p}\ell_9 \frac{\Delta_s}{L} + \frac{A_{26}}{R} \overset{(0)}{w} = \bar{C} \tag{102c}$$

The first two of these three equations gives

$$B_3 = \frac{\tilde{p}\ell_9 \frac{\Delta_s}{L} \left[A_{12} \left(A_{26} + \frac{3c_2}{2R} B_{26} \right) - A_{22} \left(A_{16} + \frac{3c_2}{2R} B_{16} \right) \right] + \tilde{p} \left[A_{12} \ell_3 q_{ext} R - A_{22} \ell_4 N_x \right] + \frac{q_{int} R}{2} \left[A_{22} - 2A_{12} \right]}{A_{11} A_{22} - A_{12}^2} \tag{103a}$$

$$\frac{\overset{(0)}{w}}{R} = \frac{\tilde{p}\ell_9 \frac{\Delta_s}{L} \left[A_{12} \left(A_{16} + \frac{3c_2}{2R} B_{16} \right) - A_{11} \left(A_{26} + \frac{3c_2}{2R} B_{26} \right) \right] + \tilde{p} \left[A_{12} \ell_4 N_x - A_{11} \ell_3 q_{ext} R \right] + \frac{q_{int} R}{2} \left[2A_{22} - A_{12} \right]}{A_{11} A_{22} - A_{12}^2} \tag{103b}$$

The constant B_4 in $\overset{(0)}{u}_x = B_3 x + B_4$ represents a rigid-body displacement. Thus,

$$\overset{(0)}{u}_x = B_3 x \tag{104}$$

Combining equations (99b) and (102c), and using equations (103), give

$$\overset{(0)}{\mathcal{N}}_{xy} = \tilde{p} \left[B_{10} \ell_9 \frac{\Delta_s}{L} + B_7 \ell_4 N_x + B_8 \ell_3 q_{ext} R \right] + B_9 \frac{q_{int} R}{2} \tag{105a}$$

where

$$B_7 = \frac{A_{12} A_{26} - A_{22} A_{16}}{A_{11} A_{22} - A_{12}^2} \tag{105b}$$

$$B_8 = \frac{A_{12}A_{16} - A_{11}A_{26}}{A_{11}A_{22} - A_{12}^2} \tag{105c}$$

$$B_9 = \frac{A_{22}\left(A_{16} + 2A_{26}\right) - A_{12}\left(A_{26} + 2A_{16}\right)}{A_{11}A_{22} - A_{12}^2} \tag{105d}$$

$$B_{10} = B_8\left(A_{26} + \frac{3c_2}{2R}B_{26}\right) + B_7\left(A_{16} + \frac{3c_2}{2R}B_{16}\right) + \left(A_{66} + \frac{3c_2}{2R}B_{66}\right) \tag{105e}$$

Equations (98a), (99a), and (105a) define the prebuckling membrane stress resultants, and indicate that prebuckling shear stresses are generated by the axial and pressure loads, in addition to the end twist, because of the shell anisotropy. By comparing these equations with equations (48), and using $\tilde{\lambda} = 1$ and $\ell_3^* = 1$, it follows that

$$L_1 = \ell_4 N_x \tag{106a}$$

$$L_2 = \ell_3 q_{ext} R \tag{106b}$$

$$L_3 = B_{10}\ell_9\frac{\Delta_s}{L} + B_7\ell_4 N_x + B_8\ell_3 q_{ext} R = B_{10}\ell_9\frac{\Delta_s}{L} + B_7 L_1 + B_8 L_2 \tag{106c}$$

$$L_1^* = -\frac{q_{int}R}{2} \tag{107a}$$

$$L_2^* = -\, q_{int}R \tag{107b}$$

$$L_3^* = B_9\frac{q_{int}R}{2} \tag{107c}$$

In addition, all functions of (x, y) on the right-hand-sides of equations (48) are equal to unity. In equations (106) and (107), $\ell_4 N_x$ and $\ell_3 q_{ext}$, $\ell_9\Delta_s$, and q_{int} are specified quantities. At buckling, the active applied load $\tilde{p}\ell_4 N_x$ becomes $N_x^{cr} = \tilde{p}_{cr}N_x$, the active applied load $\tilde{p}\ell_3 q_{ext}$ becomes $q_{ext}^{cr} = \tilde{p}_{cr}\ell_3 q_{ext}$, and the active applied twist becomes $\Delta_s^{cr} = \tilde{p}_{cr}\ell_9\Delta_s$.

Relatively simple, approximate representations of the displacement fields that satisfy the kinematic boundary conditions, given by equations (68b) and (68c), are

$$\overset{(1)}{u}_x = \bar{u}\cos\left(\frac{m\pi x}{L}\right)\cos\left(\frac{n}{R}\left(y - \tau x\right)\right) \tag{108a}$$

$$\overset{(1)}{u}_y = \bar{v}\,\sin\left(\frac{m\pi x}{L}\right)\sin\left(\frac{n}{R}\left(y - \tau x\right)\right) \tag{108b}$$

$$\overset{(1)}{w} = \bar{w}\,\sin\left(\frac{m\pi x}{L}\right)\cos\left(\frac{n}{R}\left(y - \tau x\right)\right) \tag{108c}$$

where $m \in \left\{1, 2, 3, ...\right\}$, $n \in \left\{0, 1, 2, , ...\right\}$, and τ is a real number. These displacement functions generally yield skewed buckle patterns such as that shown in figure 6. Along the nodal lines of the contour plot in figure 6b, the radial displacement defined by equation (108c) is equal to zero. Enforcing this condition requires

$$\cos\left(\frac{n}{R}\left(y - \tau x\right)\right) = 0 \quad \text{or} \quad \frac{n}{R}\left(y - \tau x\right) = \pm\left(2p - 1\right)\frac{\pi}{2} \tag{108d}$$

for values of $p \in \left\{1, 2, 3, ...\right\}$. This equation defines the family of straight nodal lines shown in figure 6b. The slope of any nodal line, as defined by the angle ϕ shown in the figure, is given by $\phi = \mathrm{Tan}^{-1}\tau$. It is noteworthy that setting $\tau = 0$ in equations (108) yields the displacement functions used in the classical solution. Thus, this particular Rayleigh-Ritz solution represents a first-approximation enhancement of the classical solution to address shell anisotropy and torsion loads.

The matrix of basis functions and the column vector of displacement amplitudes in equation (54) are expressed as

$$\left[\mathscr{G}\right] = \begin{bmatrix} \mathscr{G}_{11} & 0 & 0 \\ 0 & \mathscr{G}_{22} & 0 \\ 0 & 0 & \mathscr{G}_{33} \end{bmatrix} \tag{109a}$$

and

$$\left\{d\right\}^T = \left\{\bar{u}, \bar{v}, \bar{w}\right\} \tag{109b}$$

where

$$\mathscr{G}_{11} = \cos\left(\frac{m\pi x}{L}\right)\cos\left(\frac{n}{R}\left(y - \tau x\right)\right) \tag{110a}$$

$$\mathscr{G}_{22} = \sin\left(\frac{m\pi x}{L}\right)\sin\left(\frac{n}{R}\left(y - \tau x\right)\right) \tag{110b}$$

$$\mathscr{G}_{33} = \sin\left(\frac{m\pi x}{L}\right)\cos\left(\frac{n}{R}\left(y - \tau x\right)\right) \tag{110c}$$

With these expressions, the operators in equations (59) produce

$$\left[D_{\varphi}\right]=\begin{bmatrix} 0 & 0 & -\frac{\partial \mathscr{b}_{33}}{\partial x} \\ 0 & \frac{c_2 \mathscr{b}_{22}}{R} & -\frac{\partial \mathscr{b}_{33}}{\partial y} \\ -\frac{c_2}{2}\frac{\partial \mathscr{b}_{11}}{\partial y} & \frac{c_2}{2}\frac{\partial \mathscr{b}_{22}}{\partial x} & 0 \end{bmatrix} \tag{111a}$$

$$\left[D_{\varepsilon}\right]=\begin{bmatrix} \frac{\partial \mathscr{b}_{11}}{\partial x} & 0 & 0 \\ 0 & \frac{\partial \mathscr{b}_{22}}{\partial y} & \frac{\mathscr{b}_{33}}{R} \\ \frac{\partial \mathscr{b}_{11}}{\partial y} & \frac{\partial \mathscr{b}_{22}}{\partial x} & 0 \end{bmatrix} \tag{111b}$$

$$\left[D_{\kappa}\right]=\begin{bmatrix} 0 & 0 & -\frac{\partial^2 \mathscr{b}_{33}}{\partial x^2} \\ 0 & \frac{c_2}{R}\frac{\partial \mathscr{b}_{22}}{\partial y} & -\frac{\partial^2 \mathscr{b}_{33}}{\partial y^2} \\ \frac{c_1 c_2}{2R}\frac{\partial \mathscr{b}_{11}}{\partial y} & \frac{c_2}{2R}\left(c_1+2\right)\frac{\partial \mathscr{b}_{22}}{\partial x} & 0 \end{bmatrix} \tag{111c}$$

$$\left[D_{\mathscr{p}}\right]=-c_4 \ell_3 q_{ext}\begin{bmatrix} 0 & 0 & -\frac{\partial \mathscr{b}_{33}}{\partial x} \\ 0 & \frac{\mathscr{b}_{22}}{R} & -\frac{\partial \mathscr{b}_{33}}{\partial y} \\ \frac{\partial \mathscr{b}_{11}}{\partial x} & \frac{\partial \mathscr{b}_{22}}{\partial y} & \frac{\mathscr{b}_{33}}{R} \end{bmatrix} \tag{111d}$$

$$\left[D_{\mathscr{P}}^{*}\right] = c_4 \ell_3^{*} q_{int} \begin{bmatrix} 0 & 0 & -\dfrac{\partial \mathscr{b}_{33}}{\partial x} \\ 0 & \dfrac{\mathscr{b}_{22}}{R} & -\dfrac{\partial \mathscr{b}_{33}}{\partial y} \\ \dfrac{\partial \mathscr{b}_{11}}{\partial x} & \dfrac{\partial \mathscr{b}_{22}}{\partial y} & \dfrac{\mathscr{b}_{33}}{R} \end{bmatrix} \tag{111e}$$

In addition, the matrices given by equations (39d) and (52d) are zero-valued matrices. The eigenvalue problem given by equations (62) and (64) is expressed as

$$\begin{bmatrix} k_{11} & k_{12} & k_{13} \\ k_{12} & k_{22} & k_{23} \\ k_{13} & k_{23} & k_{33} \end{bmatrix} \begin{Bmatrix} \bar{u} \\ \bar{v} \\ \bar{w} \end{Bmatrix} = \tilde{p} \begin{bmatrix} g_{11} & g_{12} & g_{13} \\ g_{12} & g_{22} & g_{23} \\ g_{13} & g_{23} & g_{33} \end{bmatrix} \begin{Bmatrix} \bar{u} \\ \bar{v} \\ \bar{w} \end{Bmatrix} \tag{112}$$

where the stiffness and geometric stiffness coefficients in this equation are given in Appendix B. After simplification, equation (112) is expressed as

$$\begin{bmatrix} K_{11} & K_{12} & K_{13} \\ K_{12} & K_{22} & K_{23} \\ K_{13} & K_{23} & K_{33} \end{bmatrix} \begin{Bmatrix} \bar{u} \\ \bar{v} \\ \dfrac{m\pi}{L}\bar{w} \end{Bmatrix} = \tilde{p} \begin{bmatrix} G_{11} & G_{12} & G_{13} \\ G_{12} & G_{22} & G_{23} \\ G_{13} & G_{23} & G_{33} \end{bmatrix} \begin{Bmatrix} \bar{u} \\ \bar{v} \\ \dfrac{m\pi}{L}\bar{w} \end{Bmatrix} \tag{113}$$

where

$$K_{11} = A_{11}\left[1 + \left(\frac{nL}{m\pi R}\right)^2 \tau^2\right] + \left[A_{66} - \frac{c_2}{R}B_{66} + \frac{c_2}{4R^2}D_{66} - \left(2A_{16} - \frac{c_2}{R}B_{16}\right)\tau - \frac{c_1}{4}\left(L_1^{*} + L_2^{*}\right)\right]\left(\frac{nL}{m\pi R}\right)^2 \tag{114a}$$

$$K_{12} = -\left(\frac{nL}{m\pi R}\right)\left[A_{12} + A_{66} + \frac{c_2}{R}\left[B_{12} + B_{66}\right] - \frac{3c_2}{4R^2}D_{66} - \left(2A_{16} + \frac{3c_2}{R}B_{16}\right)\tau + \frac{c_1}{4}\left(L_1^{*} + L_2^{*}\right)\right] \tag{114b}$$

$$K_{13} = -\left[\left(\frac{A_{12}}{R} + \frac{c_4 L_2^{*}}{R}\right)\left(\frac{L}{m\pi}\right)^2 + B_{11} + \left(B_{12} + 2B_{66} - \frac{c_2}{R}D_{66} + 3B_{11}\tau^2 - 6B_{16}\tau + \frac{c_2}{R}D_{16}\tau\right)\left(\frac{nL}{m\pi R}\right)^2\right] \tag{114c}$$

$$K_{22} = \left(A_{66} + \frac{3c_2}{R} B_{66} + \frac{9c_2}{4R^2} D_{66} - \frac{c_1}{4}\left(L_1^* + L_2^* \right) \right) \left[1 + \left(\frac{nL}{m\pi R} \right)^2 \tau^2 \right] +$$
$$\left(A_{22} + \frac{2c_2}{R} B_{22} + \frac{c_2}{R^2} D_{22} \right) \left(\frac{nL}{m\pi R} \right)^2 - \left(c_2 - c_4 \right) \frac{L_2^*}{R^2} \left(\frac{L}{m\pi} \right)^2 - \left(2A_{26} + \frac{5c_2}{R} B_{26} + \frac{3c_2}{R^2} D_{26} \right) \left(\frac{nL}{m\pi R} \right)^2 \tau \tag{114d}$$

$$K_{23} = \left(\frac{nL}{m\pi R} \right) \left\{ \frac{1}{R} \left(A_{22} + \frac{c_2}{R} B_{22} - \left[A_{26} + \frac{3c_2}{2R} B_{26} \right] \tau - c_2 L_3^* \tau + \left(c_4 - c_2 \right) L_2^* \right) \left(\frac{L}{m\pi} \right)^2 + \right.$$
$$\left(B_{12} + 2B_{66} + \frac{c_2}{R} \left[D_{12} + 3D_{66} \right] \right) \left(1 + \left(\frac{nL}{m\pi R} \right)^2 \tau^2 \right) + \tag{114e}$$
$$\left. + \left(B_{22} + \frac{c_2}{R} D_{22} - 3 \left[B_{26} + \frac{7c_2}{6R} D_{26} \right] \tau \right) \left(\frac{nL}{m\pi R} \right)^2 - \left(B_{16} + \frac{3c_2}{2R} D_{16} \right) \left(3 + \left(\frac{nL}{m\pi R} \right)^2 \tau^2 \right) \tau \right\}$$

$$K_{33} = \frac{A_{22} + c_4 L_2^*}{R^2} \left(\frac{L}{m\pi} \right)^4 + \frac{2}{R} \left(\frac{L}{m\pi} \right)^2 \left[B_{12} + \left(B_{22} + B_{12}\tau^2 - 2B_{26}\tau \right) \left(\frac{nL}{m\pi R} \right)^2 \right] - \left(\frac{L}{m\pi} \right)^2 L_1^* +$$
$$D_{11} \left(1 + 6 \left(\frac{nL}{m\pi R} \right)^2 \tau^2 + \left(\frac{nL}{m\pi R} \right)^4 \tau^4 \right) + 2 \left(D_{12} + 2D_{66} \right) \left(\frac{nL}{m\pi R} \right)^2 \left(1 + \left(\frac{nL}{m\pi R} \right)^2 \tau^2 \right) + D_{22} \left(\frac{nL}{m\pi R} \right)^4 \tag{114f}$$
$$- 4D_{16} \left(\frac{nL}{m\pi R} \right)^2 \left(3 + \left(\frac{nL}{m\pi R} \right)^2 \tau^2 \right) \tau - 4D_{26} \left(\frac{nL}{m\pi R} \right)^4 \tau - \left(L_1^* \tau^2 + L_2^* + 2L_3^* \tau \right) \left(\frac{L}{m\pi} \right)^2 \left(\frac{nL}{m\pi R} \right)^2$$

and

$$G_{11} = \frac{c_1}{4} \left(L_1 + L_2 \right) \left(\frac{nL}{m\pi R} \right)^2 \tag{115a}$$

$$G_{12} = \frac{c_1}{4} \left(L_1 + L_2 \right) \left(\frac{nL}{m\pi R} \right) \tag{115b}$$

$$G_{13} = \frac{c_4 L_2}{R} \left(\frac{L}{m\pi} \right)^2 \tag{115c}$$

$$G_{22} = \left(c_2 - c_4 \right) \frac{L_2}{R^2} \left(\frac{L}{m\pi} \right)^2 + \frac{c_1}{4} \left(L_1 + L_2 \right) \left(1 + \left(\frac{nL}{m\pi R} \right)^2 \tau^2 \right) \tag{115d}$$

$$G_{23} = \left[\frac{c_2}{R} \left(L_2 + L_3 \tau \right) - \frac{c_4 L_2}{R} \right] \left(\frac{L}{m\pi} \right)^2 \left(\frac{nL}{m\pi R} \right) \tag{115e}$$

$$G_{33} = \left(\frac{L}{m\pi}\right)^2 \left[L_1 + \left(L_1 \tau^2 + L_2 + 2L_3 \tau \right) \left(\frac{nL}{m\pi R} \right)^2 - \frac{c_4 L_2}{R^2} \left(\frac{L}{m\pi} \right)^2 \right] \tag{115f}$$

Nontrivial solutions to equation (113) is also given by (82) through (84). The critical value of the loading parameter, $\tilde{p}_{cr}$, is the smallest positive value that satisfies equation (113) for values of $m \in \{1, 2, 3, ...\}$, $n \in \{0, 1, 2, , ...\}$, and real numbers τ. The corresponding values of the wave numbers, m and n, are denoted by m_{cr} and n_{cr}, respectively. The corresponding value of the skewedness parameter is denoted by τ_{cr}.

Upon obtaining the critical value of the loading parameter, $\tilde{p}_{cr}$, the skewedness parameter, τ_{cr}, and the corresponding wave numbers, m_{cr} and n_{cr}, the buckling mode (eigenvector) is obtained by substituting these values into equations (114) and (115). The resulting expressions are then substituted into equations (113), which becomes

$$\begin{bmatrix} K_{11}^{cr} & K_{12}^{cr} & K_{13}^{cr} \\ K_{12}^{cr} & K_{22}^{cr} & K_{23}^{cr} \\ K_{13}^{cr} & K_{23}^{cr} & K_{33}^{cr} \end{bmatrix} \begin{Bmatrix} \bar{u} \\ \bar{v} \\ \frac{m\pi}{L}\bar{w} \end{Bmatrix} = \tilde{p}_{cr} \begin{bmatrix} G_{11}^{cr} & G_{12}^{cr} & G_{13}^{cr} \\ G_{12}^{cr} & G_{22}^{cr} & G_{23}^{cr} \\ G_{13}^{cr} & G_{23}^{cr} & G_{33}^{cr} \end{bmatrix} \begin{Bmatrix} \bar{u} \\ \bar{v} \\ \frac{m\pi}{L}\bar{w} \end{Bmatrix} \tag{116}$$

where the superscript "cr" indicates that the coefficients given by equations (114) and (115) have been evaluated for $m = m_{cr}$, $n = n_{cr}$, and $\tau = \tau_{cr}$. Only two of the three equations given by matrix equation (116) are independent. Using the first and third equations to find $\bar{u}$ and $\bar{v}$ in terms of $\bar{w}$ yields

$$\bar{u} = \frac{m_{cr}\pi}{L} \frac{\left(K_{12}^{cr} - \tilde{p}_{cr}G_{12}^{cr}\right)\left(K_{33}^{cr} - \tilde{p}_{cr}G_{33}^{cr}\right) - K_{13}^{cr}\left(K_{23}^{cr} - \tilde{p}_{cr}G_{23}^{cr}\right)}{\left(K_{11}^{cr} - \tilde{p}_{cr}G_{11}^{cr}\right)\left(K_{23}^{cr} - \tilde{p}_{cr}G_{23}^{cr}\right) - K_{13}^{cr}\left(K_{12}^{cr} - \tilde{p}_{cr}G_{12}^{cr}\right)} \bar{w} \tag{117a}$$

$$\bar{v} = -\frac{m_{cr}\pi}{L} \frac{\left(K_{11}^{cr} - \tilde{p}_{cr}G_{11}^{cr}\right)\left(K_{33}^{cr} - \tilde{p}_{cr}G_{33}^{cr}\right) - \left(K_{13}^{cr}\right)^2}{\left(K_{11}^{cr} - \tilde{p}_{cr}G_{11}^{cr}\right)\left(K_{23}^{cr} - \tilde{p}_{cr}G_{23}^{cr}\right) - K_{13}^{cr}\left(K_{12}^{cr} - \tilde{p}_{cr}G_{12}^{cr}\right)} \bar{w} \tag{117b}$$

Substituting these two expressions into equations (108) give the buckling mode in terms of the unknown amplitude, $\bar{w}$; i. e.,

$$\overset{(1)}{u}_x = \frac{m_{cr}\pi}{L} \frac{\left(K_{12}^{cr} - \tilde{p}_{cr}G_{12}^{cr}\right)\left(K_{33}^{cr} - \tilde{p}_{cr}G_{33}^{cr}\right) - K_{13}^{cr}\left(K_{23}^{cr} - \tilde{p}_{cr}G_{23}^{cr}\right)}{\left(K_{11}^{cr} - \tilde{p}_{cr}G_{11}^{cr}\right)\left(K_{23}^{cr} - \tilde{p}_{cr}G_{23}^{cr}\right) - K_{13}^{cr}\left(K_{12}^{cr} - \tilde{p}_{cr}G_{12}^{cr}\right)} \bar{w} \cos\left(\frac{m_{cr}\pi x}{L}\right) \cos\left(\frac{n_{cr}}{R}\left(y - \tau_{cr}x\right)\right) \tag{118a}$$

$$\overset{(1)}{u}_y = -\frac{m_{cr}\pi}{L}\frac{\left(K_{11}^{cr}-\tilde{p}_{cr}G_{11}^{cr}\right)\left(K_{33}^{cr}-\tilde{p}_{cr}G_{33}^{cr}\right)-\left(K_{13}^{cr}\right)^2}{\left(K_{11}^{cr}-\tilde{p}_{cr}G_{11}^{cr}\right)\left(K_{23}^{cr}-\tilde{p}_{cr}G_{23}^{cr}\right)-K_{13}^{cr}\left(K_{12}^{cr}-\tilde{p}_{cr}G_{12}^{cr}\right)}\bar{w}\sin\left(\frac{m_{cr}\pi x}{L}\right)\sin\left(\frac{n_{cr}}{R}\left(y-\tau_{cr}x\right)\right) \quad (118b)$$

$$\overset{(1)}{w} = \bar{w}\,\sin\left(\frac{m_{cr}\pi x}{L}\right)\cos\left(\frac{n_{cr}}{R}\left(y-\tau_{cr}x\right)\right) \quad (118c)$$

For axisymmetric buckling modes, given by $n_{cr} = 0$, equation (108b) indicates that $\overset{(1)}{u}_y = 0$. In addition; $K_{12}^{cr} = 0$, $K_{23}^{cr} = 0$, $G_{11}^{cr} = 0$, $G_{12}^{cr} = 0$, and $G_{23}^{cr} = 0$. Thus, equation (116) reduces to

$$\begin{bmatrix} K_{11}^{cr} & K_{13}^{cr} \\ K_{13}^{cr} & K_{33}^{cr} \end{bmatrix}\begin{Bmatrix} \bar{u} \\ \frac{m_{cr}\pi}{L}\bar{w} \end{Bmatrix} = \tilde{p}_{cr}\begin{bmatrix} G_{11}^{cr} & G_{13}^{cr} \\ G_{13}^{cr} & G_{33}^{cr} \end{bmatrix}\begin{Bmatrix} \bar{u} \\ \frac{m_{cr}\pi}{L}\bar{w} \end{Bmatrix} \quad (119)$$

Only one of these two equations are independent. Using the first equation to find $\bar{u}$ in terms of $\bar{w}$ yields

$$\bar{u} = -\frac{m_{cr}\pi}{L}\,\frac{K_{13}^{cr}-\tilde{p}_{cr}G_{13}^{cr}}{K_{11}^{cr}}\,\bar{w} \quad (120)$$

Substituting this expression into equation (108a) gives

$$\overset{(1)}{u}_x = -\frac{m_{cr}\pi}{L}\,\frac{K_{13}^{cr}-\tilde{p}_{cr}G_{13}^{cr}}{K_{11}^{cr}}\,\bar{w}\cos\left(\frac{m_{cr}\pi x}{L}\right)\cos\left(\frac{n_{cr}}{R}\left(y-\tau_{cr}x\right)\right) \quad (121)$$

The Cartesian coordinates of the deformed (buckling mode) shell, (x*, y*, z*), are given by equations (94) and (95).

Results and Comparisons

Comparisons with results published in the technical literature and corresponding results obtained from the classical and Rayleigh-Ritz solutions of the present study are presented subsequently, in numerous tables, for complete circular cylinders with the classical simply supported boundary conditions applied at each end. The approximate Rayleigh-Ritz solution is used when shell-wall anisotropy or torsion loads are present in a given case. Only uniform loads are considered that include axial compression, external pressure, hydrostatic pressure, and torsion. The hydrostatic pressure load corresponds to the uniform external pressure plus the induced axial compression associated with caps on the cylinders ends ($L_1 = 0.5$ and $L_2 = 1$). In the following discussion, the applied pressure q_{ext} is denoted by p, for convenience.

For each set of tabular results obtained in the present study, buckling modes are also reported. Specifically, for results obtained from the classical solution presented herein, the buckling mode is given in the form (m, n), where m is the number of axial half waves and n is the number of full circumferential waves (see figure 4). For results obtained from the approximate Rayleigh-Ritz solution presented herein, the buckling mode is given in the form (m, n, τ), where τ is the parameter that quantifies how much a buckle pattern is skewed.

First, results and comparisons are presented for unstiffened, monocoque isotropic cylinders. Then similar comparisons are presented for cylinders stiffened by uniform arrays of rings, stringers, or rings and stringers. For each of these stiffened shells, homogenized constitutive equations are used in the analyses and a large range of stiffener properties are examined. Next, results are presented for unstiffened cylinders made of laminated-composite materials. Results for several wall constructions are presented that include the full extent of possible anisotropies. For each case, results obtained in the present study by using Donnell's equations, Sanders' equations, and Sanders' equations with the nonlinear rotations about the surface normal-vector field neglected are generally presented. In describing results for this latter set of equations, the phrase, "nonlinear rotations about the normal are neglected," is used for convenience herein. For cylinders subjected to pressure loads, results are generally presented with and without "live" pressure.

Unstiffened Isotropic Cylinders

Axial compression loads. Comparisons for unstiffened isotropic cylinders subjected to uniform axial compression are shown in Tables 1-5. The results in Table 1 show the predicted values of $\frac{\sigma_x^{cr}}{E}\left(1-\nu^2\right)$ obtained by Dym[29] and obtained in the present study as a function of $\frac{L}{mR}$ and the circumferential wave number n, where m is the number of axial half waves forming the buckling mode and L is the cylinder length. In addition, the results were calculated for the Poisson's ratio $\nu = 0.30$, a radius R = 4 in. and a thickness h defined by R/h = 91.287. The results of reference 29 include values of $\frac{\sigma_x^{cr}}{E}\left(1-\nu^2\right)$ obtained by using Flugge's equations[18], the Koiter-Budiansky equations,[22, 24] and Donnell's equations[17] for values of n = 1, 2, 3, and 4; where the largest differences between the results of the three sets of equations are most likely to occur. Moreover, the results are independent of the modulus of elasticity, E.

The results in Table 1 indicate that the values of $\frac{\sigma_x^{cr}}{E}\left(1-\nu^2\right)$ predicted by Dym and the present study by using Donnell's equations are nearly identical. Similarly, the results predicted herein by using Sanders' equations are, for the most part, within 1% of the corresponding results given by Dym that are based on Flugge's equations and the Koiter-Budiansky equations. In contrast, differences of between 11% and 15% are noted for cases with n = 1 and $\frac{L}{mR} = 10$, which correspond to column-like buckling modes. The most notable difference, 42%, is found for the cases with n = 4 and $\frac{L}{mR} = 90$. All other differences are between 1% and 6%. For the most part, these results indicate that Sanders' equations, Flugge's equations and the Koiter-Budiansky equations yield solutions with practically the same level of fidelity.

Comparisons of the values predicted herein for the critical value of the applied stress resultant with those predicted by Sheinman and Simitses[30] and by Simitses et. al.,[31] obtained by using Donnell's equations, are shown in Table 2. These results are for cylinders with a radius R = 4 in., a modulus $E = 10.5 \times 10^6$ psi, and Poisson's ratio $\nu = 0.3$. Moreover, results are given for selected values of the cylinder length-to-radius ratio given by $1 \le L/R \le 10$ and selected values of the radius-to-thickness ratio given by $80 \le R/h \le 1000$. The two sets of results presented in this table, that are based on Donnell's equations, exhibit differences less than 0.2%. In addition, the results obtained in the present study indicate that the differences in the corresponding predictions obtained by using Donnell's equations and Sanders' equations range from about 1% to 20%, with the largest differences being exhibit by the long cylinders. Similarly, the results indicate differences in the corresponding predictions obtained by using Donnell's equations and Sanders' equations, with nonlinear rotations about the normal neglected, range from about 0.5% to 11%.

Comparisons of the values predicted herein for the nondimensional buckling load $\sqrt{3\left(1-\nu^2\right)}\,\frac{N_x^{cr}R}{Eh^2}$ with those predicted by Zou and Foster[32] and by Xiang et. al.,[33] obtained by using Flügge's equations and Timoshenko's equations,[34] are shown in Table 3. This particular nondimensional buckling load is obtained by dividing the critical value of the applied axial stress resultant by the corresponding value obtained by appyling Donnell's equations to an infinitely long cylinder (for example, see equation (42b) of reference 35). Moreover, the results in this table are for cylinders with a thickness $h = 0.1$ inch, a modulus $E = 10.5 \times 10^6$ psi, and Poisson's ratio $\nu = 0.3$.

The results in Table 3 indicate that the nondimensional buckling loads predicted herein by using Donnell's equations are practically identical to the value for the corresponding infinitely long cylinder given by $\frac{6\,Eh^2}{10\,R}$. In addition, the results indicate that the nondimensional buckling loads predicted herein by using Sanders' equations are within 1% of the correspondinge results presented in references 32 and 33 and obtained by using either Flügge's equations or Timoshenko's equations. The results also show that neglecting the nonlinear rotations about the normal yields predictions that are as much as 7% higher than the corresponding result obtained by using Sanders' equations.

Predicted values of the nondimensional buckling load $\frac{N_x^{cr}L^2}{\pi^2 D}$ obtained in the present study and obtained by Yamaki and Kodama[36] are presented in Table 4 for selected values of Batdorf's parameter,[37] $Z = \frac{L^2}{Rh}\sqrt{1-\nu^2}$, in the range of $0 \le Z \le 1000$. A pictorial representation of the Z parameter, taken from reference 36, is shown in figure 7 for a value of $Z \approx 150$. The results in this table indicate nearly identical predictions for the two sets of results based on Donnell's equations. Moreover, the results based on Sanders' equation, with and without nonlinear rotations about the normal neglected, differ from the corresponding results obtained by using Donnell's equations by at most 1.1%.

Comparisons of the values predicted herein for the nondimensional buckling load $\sqrt{3\left(1-\nu^2\right)}\,\frac{N_x^{cr}R}{Eh^2}$ with those predicted by Yamaki and Kodama,[38] obtained by using Flügge's equations, are shown in Table 5. Specifically, results are given for cylinders with a Poisson's ratio $\nu = 0.30$, R/h = 100, and $0.15 \le L/R \le 100$. These results show differences of less than 1% between the predictions obtained by Yamaki and Kodama using Flügge's equations and the predictions obtained herein with Sanders' equations. The results also show that Donnell's equations and Sanders' equations with nonlinear rotations about the normal neglected predict buckling resistances that are greater than those predicted by Flügge's and Sanders' equations. Moreover, Donnell's equations predict the greatest buckling resistance over the entire range of L/R examined.

The differences in the buckling resistance predictions obtained in the present study by using Donnell's equations, Sanders' equations, and Sanders' equations with nonlinear rotations about the normal neglected are illustrated in figures 8-20 for cylinders with selected radius-to-thickness ratios in the range $50 \le R/h \le 1000$, with a Poisson's ratio $\nu = 0.30$, and with $E = 10.0 \times 10^6$ psi. Specifically, results are presented in figures 8-10 for cylinders with R/h = 50. In figures 8 and 9, the buckling resistance is measured by the nondimensional buckling coefficient $\frac{N_x^{cr}Rh}{\pi^2 D}$ for values of $0.2 \le L/R \le 50$ and $0.2 \le L/R \le 8$, respectively, where $D = \frac{Eh^3}{12\left(1-\nu^2\right)}$ is the principal shell bending stiffness. The mostly horizontal red line in figures 8 and 9 corresponds to results obtained by using Donnell's equations. The horizontal part corresponds to the widely used formula for the critical stress of an infinitely long cylinder given by

$$\sigma^*{}_x^{cr} = \frac{1}{\sqrt{3\left(1-\nu^2\right)}}\,\frac{Eh}{R} \tag{122}$$

The corresponding buckling coefficient is given by $\frac{N_x^{cr}Rh}{\pi^2 D} = \frac{4}{\pi^2}\sqrt{3\left(1-\nu^2\right)}$, which for $\nu = 0.30$ gives $\frac{N_x^{cr}Rh}{\pi^2 D} = 0.67$. The black and the blue festoon curves in each figure corresponds to results obtained by using Sanders' equations and Sanders' equations with nonlinear rotations about the normal neglected, respectively. The rightmost branch of these two festoon curves shown in figure 8 correspond to a column-like shell-buckling mode given by the wave numbers m = n = 1, and the graph coordinates for the first column-like shell-buckling mode are (25.5, 0.41). The gray curve in figure 8 corresponds to buckling coefficients obtained by using the Euler column-buckling formula

$$\sigma_{Euler}^{cr} = \frac{\pi^2 E R^2}{2L^2} \tag{123}$$

for a simply supported thin-walled tubular beam with length L, cross-sectional radius R, and thickness h that is deformed into a single half wave along its length. The results in figure 10 indicate the percent difference in the buckling loads with respect to the results obtained by using

Sanders' equations. For example, points of the red curve are obtained by computing the absolute value of the difference between buckling loads obtained by using Donnell's and Sanders' equations and then dividing the result by the corresponding buckling load obtained from Sanders' equations. The blue curve is obtained in a similar manner with the results obtained by using Donnell's equations replaced with the results obtained by using Sanders' equations with nonlinear rotations about the normal neglected.

Results similar to those presented in figures 8-10 are presented in figures 11-13 for cylinders with R/h = 100, in figures 14-16 for those with R/h = 500, and in figures 17-19 for those with R/h = 1000. In figure 11 (R/h = 100), the first column-like shell-buckling mode predicted by Sanders' equations is given by the graph coordinates (36.3, 0.41). In figures 14 (R/h = 500) and 17 (R/h = 1000), the first column-like shell-buckling modes are given by the graph coordinates (81.5, 0.41) and (115.3, 0.41), respectively, and are not shown.

The buckling-coefficient plots in figures 8-18 show significant differences in the buckling resistance predictions obtained from the three set of equations, with the black curves (Sanders' equations) generally exhibiting the lowest corresponding values of buckling resistance. Moreover, the differences are generally more pronounced as the cylinder length increases. The results obtained by using Sanders'equations predict a transition to a column buckling mode at significantly smaller values of L/R than the corresponding results obtained by using Sanders equations with nonlinear rotations about the normal neglected. The results obtained by using Donnell's equations predict no transition at all. The curves giving the percent differences in the buckling loads shown in figures 10, 13, 16, and 19 exhibit pronounced variations with the cylinder aspect ratio that results from the festoon curves predicted by the three sets of buckling equations being out of phase. The commonality of the curves shown in these four figures is illustrated in figure 20. This commonality was found by normalizing the cylinder aspect ratio shown as the abscissa in figures 10, 13, 16, and 19 by the corresponding value at which the first column-like shell-buckling mode occurs, L_{Euler}/R, that is predicted by Sanders' equations. As seen in figure 20, this normalization effectively eliminates the dependence of the curves on R/h for all practical purposes. The general trend is a significant increase in the bucking-load differences as the cylinder length approaches approximately 45% of the corresponding length at which a column-like cylinder buckling mode occurs. However, smaller differences occur due to the pronounced variations in the curves with L/L_{Euler}.

A concise representation of the buckling behavior predicted by Sanders' equations is shown in figure 21 that is made possible by the nature of the results predicted by Donnell's equations shown by the buckling-coefficient plots in figures 8-18. In particular, the curves based on Donnell's equations attenuate rapidly to a horizontal straight line as the cylinder aspect ratio becomes larger than approximately 0.6 for R/h = 50, and this attenuation becomes more pronounced as R/h increases. This property was found by Mikulas et. al.[39] to provide a concise representation of the buckling results by defining the ordinate as the buckling stress predicted by Sanders' equations, σ_x^{cr}, divided by the attenuated buckling stress predicted by Donnell's equations, σ^{*cr}_x, given by equation (122). In addition, the abscissa is defined by $\sqrt{\frac{\sigma^{*cr}_x}{\sigma^{cr}_{Euler}}}$, where the stress in the denomenator is the Euler-buckling stress given by equation (123). The more

explicit form of the abscissa is given by

$$\sqrt{\frac{\sigma^{*\,cr}_{x}}{\sigma^{cr}_{Euler}}} = \sqrt{\frac{2}{\pi^2\sqrt{3\left(1-\nu^2\right)}}\frac{h}{R}}\,\frac{L}{R} \tag{124}$$

With this representation, the black festoon curves shown in figures 8-18 become the red curves shown in figure 21. The solid blue curve shown in figure 21 corresponds to column buckling predicted by Euler's buckling equation, and it nearly overlaps the red curve. The slight differences in the red and blue curves appear as a result of the additional cross-section flexibility inherent to shell theory. Based on results obtained by using Sanders' equations, the cylinders buckle into the column-like mode (m = n = 1) at the approximate graph coordinates (1.27, 0.61). Using these coordinates with equations (122) and (123) yields the corresponding formula $\sigma^{cr}_{Euler} = 0.37\,\frac{Eh}{R}$ for the corresponding critical stress and $\frac{L_{Euler}}{R} = 3.63\sqrt{\frac{R}{h}}$ for the corresponding cylinder length, L_{Euler}. The values of the ordinate, 0.61, also corresponds to the value $\frac{N^{cr}_{x}Rh}{\pi^2 D} = 0.41$.

The four red curves shown in figure 21 effectively represent a single "master" curve to within the accuracy of the material properties used to calculate the results. Four additional sets of curves were obtained for values of $\nu = 0.20$, $\nu = 0.40$, $E = 5.0 \times 10^6$ psi, and $E = 30.0 \times 10^6$ psi. These additional curves were practically identical to the corresponding curves appearing in figure 21. Values of the buckling stress ratio for these curves are presented in Table 6. To demonstrate the utilility of figure 21, the abscissa $\sqrt{\frac{\sigma^{*\,cr}_{x}}{\sigma^{cr}_{Euler}}}$ is given in figures 22 and 23 as a function of R/h and for selected values of L/R. Overall, the results in figure 21 also indicate that differences as large as 20% may occur for values of the abscissa given by $0.22 < \sqrt{\frac{\sigma^{*\,cr}_{x}}{\sigma^{cr}_{Euler}}} < 0.36$. The largest differences are approximately 40% for values of the abscissa greater than 0.5.

Uniform external pressure loads. Results for unstiffened isotropic cylinders subjected to uniform external pressure are given in Tables 7-17. In these tables, Poisson's ratio $\nu = 0.30$ unless specified otherwise. First, predicted values of the nondimensional buckling pressure $\frac{p^{cr}RL^2}{\pi^2 D}$ obtained in the present study and obtained by Yamaki[40] are presented in Table 7 for selected values of Batdorf's Z parameter[37] in the range of $0 \le Z \le 100,000$. The results in this table that correspond to the present study were obtained by using the thickness $h = 0.1$ in. and $R/h = 1000$. In addition, the results obtained by using Sanders' equations, with and without nonlinear rotations about the normal, include the effect of a live pressure load.

The results in Table 7 indicate the buckling pressures obtained by Yamaki, that are based on Donnell's equations, differ by less than 0.5% from the corresponding results obtained in the present study, with a few exceptions. For Z = 3000 and 10000, the corresponding results differ by about 1% and 1.5%, respectively. For Z = 15000 and 30000, the corresponding results differ by

about 0.7% and 2.9%, respectively. Likewise, for Z = 50000 and 70000, the corresponding results differ by about 1.3% and 1.6%, respectively. For Z = 100000, the corresponding results differ by about 0.8%. The results also indicate that the buckling pressures predicted by Sanders' equations, with and without rotations about the normal neglected, differ very little from the corresponding results obtained by using Donnell's equations. The lowest predictions of the buckling resistance are obtained by using Sanders' equations with nonlinear rotations about the normal included.

Comparisons of the buckling pressures predicted in the present study with those predicted by Vodenitcharova and Ansourian,[41] obtained by using Flügge's equations, and by Showkati and Ansourian,[42] obtained by using a finite element method, are shown in Table 8. Results are given in this table for $0.5 \le L/R \le 5$ and $300 \le R/h \le 3000$, and were obtained by using the thickness h = 0.01 m, the modulus E = 200 GPa, the Poisson's ratio $\nu = 0.30$. In addition, the results obtained by using Donnell's equations and finite element analyses correspond to a dead pressure load. The results obtained by using Flügge's and Sanders' equations correspond to a live pressure load.

The results in Table 8 indicate the buckling pressures obtained by Vodenitcharova and Ansourian, that are based on Flügge's equations, differ by less than 0.1% from the corresponding results obtained in the present study with Sanders'equations, and predict the same number of circumferential waves in the buckling mode. Similarly, the buckling pressures obtained by Showkati and Ansourian from finite element analyses differ by less than 0.1% from the corresponding results obtained in the present study with Sanders'equations for all cases with L/R = 1 and 2, with one exception. That is, for L/R = 1 and R/h = 300, the difference is about 1.4%. For L/R = 0.5 and 5, the differences decrease from about 4.8% to 1% as R/h increases from 300 to 3000. For L/R = 3, the differences decrease from about 2% to 0.8% as R/h increases from 300 to 3000. In addition, the finite element analyses predict, for the most part, the same number of circumferential waves in the buckling mode as Sanders'equations.

The results in Table 8 also show that the results obtained in the present study by using Donnell's equations and by using Sanders' equations, neglecting nonlinear rotations about the normal, differ from the corresponding results obtained by using Sanders' equations by less than 1% with only a few exceptions. For L/R = 3 and R/h = 300, the difference is 1.4%. For L/R = 5, the differences are about 1.8%, 1.7%, and 1.1% for R/h = 300, 500, and 100, respectively. For nearly all the results obtained in the present study, the same buckling mode is predicted by the three different analyses for each case.

Predicted values of the nondimensional buckling pressure $\frac{p^{cr}R^3}{D}$ obtained in the present study and obtained by Wang and Billington,[43] by using Flügge's and Timoshenko's equations, are shown in Tables 9-14 for $1 \le L/R \le 250$. In particular, results are given in Tables 9-11 for a Poisson's ratio $\nu = 0.30$ and for R/h = 10, 100, and 1000, respectively. Results are given in Tables 12-14 for a Poisson's ratio $\nu = 0$ and for R/h = 10, 100, and 1000, respectively. In all these tables, the results obtained by using Donnell's equations correspond to a dead pressure load. The results obtained by using Flügge's, Timoshenko's, and Sanders' equations correspond to a live pressure load.

The results in Tables 9-14 indicate that the results obtained by Wang and Billington, by using

Flugge's equations, are within approximately 1% of the corresponding results obtained in the present study, by using Sanders' equations, with one curious exception. This exception appears in Table 14 for L/R = 9 and corresponds to about a 9% difference. In most of the cases, however the agreement is less than a fraction of 1%. The results in Tables 9-14 also indicate that the results obtained by Wang and Billington by using Timoshenko's equations are within approximately 3.5% of the corresponding results obtained in the present study by using Sanders' equations, with two exceptions. These exceptions are given in Tables 11 and 14 for L/R = 50 and 9, respectively, and correspond to differences of about 5% and 9%, respectively.

Further examination of Tables 9-14 also indicates that the results obtained by using Sanders' equations neglecting nonlinear rotations about the normal differ from the corresponding results obtained by using Sanders' equations by less than 3%, with many of the cases showing significantly better agreement. In contrast, the tables generally show larger differences between the results obained by using Sanders' equations and the corresponding results obtained by using Donnell's equations. In particular, the differences tend to increase as L/R increases, with a maximum difference of about 34%.

Predicted values of the nondimensional buckling pressure $\frac{p^{cr}R}{Eh} \times 10^6$ obtained in the present study and obtained by Brush and Almroth[17] using Flügge's equations are shown in Table 15 for selected values of $\pi/16 \le L/R \le 32\pi$ and for R/h = 100, 400, and 1000. Corresponding results obtained by Brush and Almroth are also given that are based on a set of nonshallow shell equations that neglect the effects of linear and nonlinear rotations about the normal. All results in this table are for a live pressure load except those obtained by using Donnell's equations. The results show agreement to within 0.2% for the predictions obtained from Flügge's equations and both forms of Sanders' equations. The nonshallow shell results of Brush and Almroth agree to with 1.5% of the corresponding results obtained by using Sanders' equations for $L/R \ge \pi/4$. For the remaining values of L/R in the table, the agreement is to within 3% except for the very-short-shell case with $L/R = \pi/16$ and R/h = 100, which exhibits a difference of 48%. In contrast, the results obtained by using Donnell's equations agree with the corresponding results from Sanders' equations to within approximately 1% for $L/R \le \pi/2$ and to within 5% for $L/R = 2\pi$. For $L/R > 2\pi$, differences as large as 63% are noted.

Nondimensional buckling pressures $\frac{p^{cr}R}{Eh} \times 10^6$ obtained in the present study and obtained by Simitses and Aswani[44] by using the Budiansky-Koiter equations[22, 24] and by using Donnell's equations are shown in Table 16 for selected values of $\pi/3 \le L/R \le 100\pi$ and for R/h = 35, 200, and 1000. All results in this table are for a live pressure load except those obtained by using Donnell's equations. The results show agreement to within 1% for the predictions obtained from the Budiansky-Koiter equations and both forms of Sanders' equations used in the present study. Similarly, the corresponding results based on Donnell's equations from reference 43 and the present study are within approximately 1%. Moreover, the results indicate that significant differences occur if Donnell's equations are used instead of Sanders' equations for most of the shells with $L/R \ge 9\pi$. The largest difference is about 34%.

Values of the nondimensional buckling pressures $\frac{p^{cr}R^2\sqrt{3\left(1-\nu^2\right)}}{Eh^2}$ obtained in the present study and obtained by Soong,[45] by using Sanders' equations and Donnell's equations, are shown in Table 17 for selected values of $0.5 \le L/R \le 40$ and for R/h = 100, 300, 500, 700, 1100, 1500, and 1900. Results obtained in the present study by using Sanders' equations are given in this table for live and dead pressure loads. All results in the table based on Donnell's equations are for dead pressures loads. It is noteworthy to point out that Soong uses a variant of Sanders' equations that have geometric stiffnesses that are different from those used in the present study. This variant of Sanders' equations was derived previously by Hoff & Soong.[46]

The results shown in Table 17 indicate that buckling pressures obtained in the present study by using Sanders' equations with live pressure are to a large extent identical to the corresponding results obtained by Soong. For the few results that differ, the difference is less than 1%. Similarly, the buckling pressures obtained in the present study by using Donnells' equations with dead pressure are almost identical to the corresponding results obtained by Soong, and the few differences are less than 0.1%. The results in Table 17 also show that significant differences between predictions based on live and dead pressure loads arise as the shells become longer and thicker. The maximum difference for this case is about 33%.

The differences in the buckling resistance predictions obtained in the present study by using Donnell's and Sanders' equations with dead pressure and Sanders' equations with live pressure are illustrated in figures 24-27 for cylinders with radius-to-thickness ratio R/h = 50, 100, 500, and 1000, respectively, and with a Poisson's ratio $\nu = 0.30$. In these figures, the buckling resistance is measured by the nondimensional buckling pressure $\frac{p^{cr}R^3}{D}$ for values of $0.2 \le L/R \le 50$. The black festoon curves in each figure correspond to results obtained by using Sanders equations with live pressure and approaches a value of three as L/R approaches 50, with the faster convergence being exhibited by the cylinder with R/h = 50. The blue and red festoon curves in each figure correspond to results obtained by using Sanders equations with dead pressure and Donnell's equationswith dead pressure, respectively. These two curves approach a value of four as L/R approaches 50.

The results in figures 24-27 exhibit significant differences in the buckling resistance predictions obtained from the three set of equations, with the black curves generally exhibiting the lowest values of buckling resistance. The highest values of buckling resistance are obtained by using Sanders' equation with dead pressure. In addition, the results obtained by using Donnell's equations predicted, for many cases, nearly the same level of buckling resistance as the corresponding results obtained by using Sanders' equation with dead pressure. More specifically, the percent difference in the buckling pressures with respect to the results obtained by using Sanders' equations with live pressure are shown in figures 28-31 for R/h = 50, 100, 500, and 1000, respectively. In particular, points of the red curves are obtained by computing the absolute value of the difference between buckling pressures obtained by using Donnell's equations with dead pressure and then dividing the result by the corresponding buckling load obtained from Sanders' equations with live pressure. The blue curve is obtained in a similar manner with the results obtained by using Donnell's equations replaced with the results obtained by using Sanders' equations with dead pressure.

The results in figures 28-31 show some significant differences in the buckling resistance predictions obtained from the three set of equations. The smaller differences occur for the shorter cylinders and the differences become less pronounced as R/h increases. The commonality of the curves shown in these four figures is illustrated in figure 32. This commonality was found by normalizing the cylinder length-to-radius ratio, shown as the abscissa in figures 28-31, by the corresponding value at which the first mode occurs with $m = 1$ and $n = 2$, denoted by $L_{(1,2)}/R$, that is predicted by Sanders' equations with live pressure. As seen in figure 32, this normalization effectively eliminates the dependence of the curves on R/h for all practical purposes. Moreover, Sanders' equations with dead pressure exhibit larger differences than the corresponding cases obtained by using Donnell's equations with dead pressure. For shorter cylinders with $L/L_{(1,2)} \le 4$, the differences are less than 8%. In contrast, differences in excess of 20% occur for the cylinders with $L/L_{(1,2)} > 1.6$.

A concise representation of the buckling behavior predicted by using Donnell's equations with dead pressure and Sanders'equations with live pressure is presented in figure 33. The corresponding results in figures 24-27 are shown in figure 33 by also using an affine mapping of the abscissa and ordinate. In particular, the ordinate is defined as the buckling-pressure ratio $\frac{p_{\infty}^{cr}}{p^{cr}}$, where

$$p_{\infty}^{cr} = \frac{1}{4\left(1-\nu^2\right)} \frac{Eh^3}{R^3} \tag{124}$$

is the buckling pressure obtained by applying Sanders' equations with live pressure to an infinitely long cylinder. In particular, equation (124) is obtained by from the condition that $\frac{p^{cr}R^3}{D} \to 3$ as $\frac{L}{R} \to \infty$. The abscissa is defined by $\frac{L}{R}\sqrt{\frac{h}{R}}$. With this representation, the black curves shown in figures 24-27 become the black, nearly identical, curves shown in figure 33. Similarly, the red curves shown in figures 24-27 become the red, nearly identical, curves shown in figure 33.

The nearly identical group of black curves and group of red curves shown in figure 33 each represent a single "master" curve to within the accuracy of the material properties used to calculate the results. Overall, these results indicate that differences as large as 33.3% may occur for values of the abscissa greater than 2. Similar curves were obtained for values of $\nu = 0.10$, 0.20, and 0.40 and for values of $E = 5.0 \times 10^6$ psi, 30.0×10^6 psi, and 40.0×10^6 psi. These additional curves were practically identical to the corresponding curves appearing in figure 33.

Uniform hydrostatic pressure loads. Results for unstiffened isotropic cylinders subjected to uniform hydrostatic pressure are shown in Tables 18-21. In these tables, Poisson's ratio ν = 0.30 unless specified otherwise. First, predicted values of the nondimensional buckling pressure $\frac{p^{cr}RL^2}{\pi^2 D}$ obtained in the present study and obtained by Yamaki,[40] by using Donnell's equations, are

presented in Table 18 for selected values of Batdorf's parameter,[36] $Z = \frac{L^2}{Rh}\sqrt{1-\nu^2}$, in the range of $0 \le Z \le 100000$ (see figure 7). The results obtained in the present study were computed for a thickness h = 0.1 in. and a radius-to-thickness ratio R/h = 1000. In addition, the results obtained from Donnell's equations are for a dead pressure loading, whereas the results based on Sanders' equations are for live pressure loads. The results in this table indicate nearly identical predictions for the two sets of results based on Donnell's equations, with most differences being less than 0.5%, and the largest being about 1.6%. Moreover, the results based on Sanders' equations, with and without nonlinear rotations about the normal neglected, differ from the corresponding results obtained by using Donnell's equations by about 2.4%.

Values of the nondimensional buckling pressure $\frac{p^{cr}R}{Eh} \times 10^3$ obtained in the present study and obtained by Fan et. al.,[47] using Flügge's and Donnell's equations; by Sobel,[48] using Donnell's equations; and by Ashour and Sobel,[49] using Sanders' equations, are presented in Table 19 for R/h = 100 and selected values of $0.5 \le L/R \le 10$. The results obtained from Donnell's equations are for a dead pressure loading, whereas the results based on Sanders' and Flügge's equations are for live pressure loads. Analysis of the results in this table reveals that buckling pressures predicted by Flügge's equations are within 0.1% of the corresponding results obtained in the present study by using Sanders' equations with live pressure. Similarly, all results in the table that are based on Donnell's equations are within 0.1% of the corresponding results obtained in the present study by using Donnells' equations. The table also shows that using a dead pressure load instead of a live pressure load yields differences between 6% and 12% in the results based on Sanders' equations for shells with $L/R \ge 4$. In addition, neglecting the nonlinear rotations about the normal in Sanders equations with live pressure is seen to have a very small effect. Comparing the corresponding results obtained in the present study by using Sanders' equations with live pressure and Donnell's equations with dead pressure indicates differences less than 5% for L/R < 9. For L/R = 9 and 10, the differences are approximately 7% and 9%, respectively.

Values of the nondimensional buckling pressures $\frac{p^{cr}R^2\sqrt{3\left(1-\nu^2\right)}}{Eh^2}$ obtained in the present study and obtained by Soong[45] by using Sanders' equations and Donnell's equations are shown in Table 20 for selected values of $0.5 \le L/R \le 40$ and for R/h = 100, 300, 500, 700, 1100, 1500, and 1900. Results obtained in the present study by using Sanders' equations are given in this table for live and dead pressure loads. All results in the table based on Donnell's equations are for dead pressures loads. The results presented in this table indicate that buckling pressures obtained in the present study by using Sanders' equations with live pressure are to a large extent identical to the corresponding results obtained by Soong. For the few results that differ, the difference is less than 0.3%. Similarly, the buckling pressures obtained in the present study by using Donnells' equations with dead pressure are identical to the corresponding results obtained by Soong. The results in Table 20 also show that significant differences between predictions based on live and dead pressure loads arise as the shells become longer and thicker. The maximum difference for this case is about 33%.

Predicted values of the nondimensional buckling pressure $\frac{p^{cr}R^3}{D}$ obtained in the present study and obtained by Singer et al.,[50, 51] using Donnell's equations, are shown in Table 21 for selected values of $0.4 \le L/R \le 10$ and for 19 values of R/h between, and including, 50 and 2000. Results obtained in the present study by using Sanders' equations are given in this table for live pressure loads and the results based on Donnell's equations are for dead pressures loads. The results presented in this table indicate that buckling pressures obtained in the present study by using Donnell's equations are almost identical to the corresponding results obtained by Singer et al., with the largest difference being about 0.04%. The results in Table 21 also show that differences in the corresponding results obtained in the present study by using Sanders' equations with and without nonlinear rotations about the normal are less than 0.1%. Likewise, the differences in the corresponding results obtained in the present study by using Sanders' equations and Donnell's equations are for the most part less than 1%, with a maximum difference of approximately 1.8%.

The differences in the buckling resistance predictions obtained in the present study by using Donnell's and Sanders' equations with dead pressure and Sanders' equations with live pressure are illustrated in figures 34-37 for cylinders with R/h = 50, 100, 500, and 1000, respectively, and with a Poisson's ratio $\nu = 0.30$. In these figures, the buckling resistance is also measured by the nondimensional buckling pressure $\frac{p^{cr}R^3}{D}$ for values of $0.2 \le L/R \le 50$. The black festoon curves in each figure correspond to results obtained by using Sanders' equations with live pressure and approaches a value of three as L/R increases without bound, with the faster convergence being exhibited by the cylinder with R/h = 50. The blue festoon curves in each figure correspond to results obtained by using Sanders' equations with dead pressure and approach a value of four as L/R increases without bound. The red festoon curve in each figure corresponds to results obtained by using Donnell's equations with dead pressure.

The results in figures 34-37 show significant differences in the buckling resistance predictions obtained from the three set of equations, with the black curves generally exhibiting the lowest values of buckling resistance, particularly for $L/R < 30$. The highest values of buckling resistance are generally obtained by using Sanders' equation with dead pressure. A direct quantitative depiction of the differences between buckling predictions obtained by using the three different sets of equations is presented in figures 38-41. More specifically, the percent difference in the buckling pressures with respect to the results obtained by using Sanders' equations with live pressure are shown in figures 38-41 for R/h = 50, 100, 500, and 1000, respectively. Points of the red curves are obtained by computing the absolute value of the difference between buckling pressures obtained by using Donnell's equations with dead pressure and then dividing the result by the corresponding buckling load obtained from Sanders' equations with live pressure. The blue curve is obtained in a similar manner with the results obtained by using Donnell's equations replaced with the results obtained by using Sanders' equations with dead pressure.

The results in figures 38-41 show some significant differences in the buckling resistance predictions obtained from the three set of equations. The smaller differences occur for the shorter cylinders and the differences become less pronounced as R/h increases, in a manner similar to that

seen for the cylinders subjected to external pressure. The commonality of the curves shown in figures 38-41 is illustrated in figure 42. This commonality was also found by normalizing the cylinder aspect ratio shown as the abscissa in figures 34-37 by the corresponding value at which the first mode occurs with $m = 1$ and $n = 2$, denoted by $L_{(1,2)}/R$, that is predicted by Sanders' equations with live pressure. As seen in figure 42, this normalization also effectively eliminates the dependence of the curves on R/h for all practical purposes. Moreover, Sanders' equations with dead pressure exhibit larger differences than the corresponding cases obtained by using Donnell's equations with dead pressure, for the most part. For shorter cylinders with $L/L_{(1,2)} \leq 4$, the differences are less than 8%. In contrast, differences in excess of 20% occur for the cylinders with $L/L_{(1,2)} > 1.6$.

A concise representation of the buckling behavior predicted by using Donnell's equations with dead hydrostatic pressure and Sanders'equations with live hydrostatic pressure is presented in figure 43. The corresponding results in figures 34-37 are shown in figure 43 by also using the same abscissa and ordinate that appears in figure 33 for cylinders subjected to external pressure. With this representation, the black and red curves shown in figures 34-37 become the nearly identical black and the nearly identical red curves, respectively, shown in figure 43.

Like for the case of external pressure, the nearly identical group of black curves and group of red curves shown in figure 43 each represent a single "master" curve to within the accuracy of the material properties used to calculate the results. Altogether, these results indicate that extremely large differences in the buckling resistance predicted by the two sets of equations occur for values of the abscissa greater than about 1.5. Similar curves were obtained for values of $\nu = 0.10$, 0.20, and 0.40 and for values of $E = 5.0 \times 10^6$ psi, 30.0×10^6 psi, and 40.0×10^6 psi. These additional curves were also practically identical to the corresponding curves appearing in figure 43.

Axial compression and fixed internal pressure loads. No relevant tabular data for this case were found in the present study. However, in a study presented by Hutchinson,[52] based on Donnell's equations, the formula

$$\frac{\sigma_x^{cr}}{\sigma^*{}_x^{cr}} = 1 + \frac{1}{2}\,\bar{q} \tag{125a}$$

where $\sigma^*{}_x^{cr}$ is given by equation (122) and

$$\bar{q} = \frac{q_{int}}{E}\sqrt{3\left(1-\nu^2\right)}\left(\frac{R}{h}\right)^2 \tag{125b}$$

is given that is in complete agreement with the corresponding results of the present study. This formula is obtained by noting that the stress at buckling, σ_x^{cr}, is the buckling stress of the corresponding unpressurized cylinder plus the axial tension stress caused by the internal pressure, $\frac{q_{int}R}{2}$. In addition, when the internal pressure vanishes, the buckling predictions obtained in the present study correspond to compression-loaded cylinders, which have been shown herein to be, for the most part, in excellent agreement with corresponding published results.

The differences in the buckling resistance predictions obtained in the present study by using Donnell's and Sanders' equations with dead internal pressure and Sanders' equations with live internal pressure are illustrated in figures 44-47 for cylinders with radius-to-thickness ratio R/h = 50, 100, 500, and 1000, respectively, and with a Poisson's ratio $\nu = 0.30$. In these figures, the buckling resistance is measured by the nondimensional buckling coefficient $\frac{N_x^{cr} Rh}{\pi^2 D}$ for values of $0.2 \le L/R \le 50$. Several curves are presented in each figure for values of the nondimensional internal pressure in the range $0 \le \bar{q} \le 1$. The solid black curves in each figure correspond to results obtained by using Sanders equations with live internal pressure, with the lowest festoon curve corresponding to results for unpressurized cylinders $(\bar{q} = 0)$. In figures 44 and 45, a portion of the solid black curve obtained by using Sanders' equations is shown that corresponds to column-like buckling modes with one half wave along the cylinder length. In addition, a solid gray curve is shown in these two figures that corresponds to results obtained from the Euler column-buckling equation for a thin-walled tube. The red curves in each figure corresponds to results obtained by using Donnell's equations with dead pressure.

The results in figures 44-47 show that as the internal pressure increases, the curves based on Sanders' equations generally transition from festoon curves to a horizontal straight line, and the buckling resistance increases. For the thicker cylinders with R/h = 50 and 100, the black curves transition to a monotonically decreasing parabola-like curve associated with column buckling as the values of L/R increase. In all cases, the results based on Donnell's equations are horizontal straight (red) lines.

Careful analysis of the curves shown in figures 44-47 reveals that as the internal pressure increases, the differences between the corresponding results obtained by using Sanders' and Donnell's equations disappear. Moreover, this trend is accelerated as R/h increases. The results also show substantial differences in the buckling resistance predictions obtained from the two sets of equations for the thicker shells with R/h = 50 and 100. For the thinner shells, figures 27 and 28 show no differences in the buckling predictions for the pressurized cylinders obtained from the two sets of equations.

A set of "master" curves the for internal-pressure-loaded cylinders, corresponding to the results in figures 44-47, is presented in figure 48. These curves were obtained by noting that the ordinate and abscissa should be similar to those shown in figure 21 for unpressurized cylinders $(\bar{q} = 0)$. After a number of attempts, the curves in figures 44-47 were found to come into near coalescence by first expressing the buckling stress obtained from Euler's buckling formula for a simply supported column deformed into a single half wave as

$$\sigma_{Euler}^{cr} = \frac{\pi^2 E R^2}{2L^2} - \frac{q_{int}}{2}\left(\frac{R}{h}\right) \tag{126}$$

where the second term is the axial prestress caused by the enclosed internal pressure. Then, like before, the ordinate is defined as the buckling stress ratio $\frac{\sigma_x^{cr}}{\sigma^*{}_x^{cr}}$, where

$$\sigma^{*\,cr}_{x} = \frac{1}{\sqrt{3\left(1-\nu^2\right)}}\,\frac{Eh}{R}\left(1+\frac{\bar{q}}{2}\right) \tag{127}$$

is the buckling stress obtained by applying Donnell's equations to an infinitely long, pressurized cylinder, given by equations (125). The abscissa is also defined by $\sqrt{\frac{\sigma^{*\,cr}_{x}}{\sigma^{cr}_{Euler}}}$, as before, but uses equations (126) and (127). After algebraic simplification, it is found that

$$\sqrt{\frac{\sigma^{*\,cr}_{x}}{\sigma^{cr}_{Euler}}} = \frac{L}{R}\sqrt{\frac{h}{R}\,\frac{\left(2+\bar{q}\right)}{\pi^2\sqrt{3\left(1-\nu^2\right)}-\left(\frac{L}{R}\right)^2\left(\frac{h}{R}\right)\bar{q}}} \tag{128}$$

By using this representation, it was found that the solid black curves shown in figures 44-47 become the red, nearly identical, curves shown in figure 48 when $\left(\frac{R}{h}\right)\bar{q}$ is used as the nondimensional internal-pressure parameter. Similar curves were obtained for values of $\nu = 0.10$, 0.20, and 0.40 and for values of $E = 5.0 \times 10^6$ psi, 30.0×10^6 psi, and 40.0×10^6 psi. These additional curves were practically identical to the corresponding curves appearing in figure 48. Altogether, the results in figure 48 give a very complete, compact representation of a very broad range of problem variables.

Torsion loads. Results for unstiffened isotropic cylinders with Poisson's ratio $\nu = 0.30$ and subjected to uniform torsional shear at the cylinder ends are shown in Tables 22-23. Specifically, predicted values of the shear-buckling coefficient $\frac{N^{cr}_{xy}L^2}{\pi^2 D}$ obtained in the present study and obtained by Batdorf, et.al.,[53] Yamaki,[54] and Yamaki and Kodama[55] using Donnell's equations are presented in Table 23 for selected values of Batdorf's Z parameter,[37] $Z = \frac{L^2}{Rh}\sqrt{1-\nu^2}$, in the range of $0 \le Z \le 100000$ (see figure 7). The results obtained in the present study in Table 22 were computed for a thickness $h = 0.1$ inch and $R/h = 100$. Predicted values of the shear-buckling coefficient $\frac{N^{cr}_{xy}R^2}{D}$ obtained in the present study and obtained by Baruch, et.al.,[56, 57] using Donnell's equations are presented in Table 23 for selected values of $0.35 \le L/R \le 3$ and $100 \le R/h \le 2000$. For both tables, the results of the present study are based on the approximate three-parameter, approximate Rayleigh-Ritz solution given by equations (108), that include the number of axial half waves m, the number of full circumferential waves n, and the skewedness parameter τ as the unknowns.

The results presented in Tables 22 and 23 indicate that the approximate three-parameter Rayleigh-Ritz solution presented herein is, for the most part, inadequate for predicting shear buckling loads of isotropic cylindrical shells. However, for values of $Z < 40$, the differences predicted by the analysis of the present study and those of references 52-56 are between 6% to 10%. In addition, the approximate three-term Rayleigh-Ritz solution presented herein gives the same result obtained by Timoshenko and Gere[34] (see p. 382-383) for an infinitely long plate ($Z = 0$).

Uniform hydrostatic pressure and torsion loads. Predicted values of the nondimensional buckling pressure, $\frac{p^{cr}R}{Eh} \times 10^3$, obtained in the present study and obtained by Fan, et al.[58] by using Donnell's and Flügge's equations are presented in Table 24 for R/h = 100 and selected values of $0.5 \le L/R \le 10$. The results based on Donnell's equations are for dead hydrostatic pressure and the results based on Flügge's and Sanders' equations are for live hydrostatic pressure. In addition, the results of the present study are based on the approximate three-parameter Rayleigh-Ritz solution given by equations (108). The results obtained by Fan, et al. are based on an exact solution of the differential equations governing the behavior.

The results in Table 24 indicate that the differences between the buckling pressures obtained herein, by using Sanders' equations, and obtained by Fan, et al., by using Flügge's equations, are less that 4.5%, and the differences decrease to about 1.2% as L/R increases to a value of 10. Likewise, the buckling pressures obtained herein and by Fan, et al. by using Donnell's equations are less that 4.4%, and the differences decrease to about 1.6% as L/R increases to a value of 10. The results of the present study shown in Table 24 also indicate that neglecting nonlinear rotations about the normal in Sanders' equations produces differences in the buckling loads of less than 1%. In contrast, the differences between the results obtained by using Sanders' equations and Donnell's equations in the present study range from less than 1% at L/R = 0.5 to less than about 5% at L/R = 6.0. For L/R = 10.0, the difference is about 8.6%. The corresponding differences between the results of Fan, et al. obtained by using Flügge's and Donnell's equations are nearly identical to those obtained in the present study. Altogether, the results of Tables 22-24 indicate that the approximate three-parameter Rayleigh-Ritz solution presented herein may be much more applicable to isotropic cylinders subjected to combined hydrostatic pressure and torsion than to cylinders subjected to pure torsion loads.

Stiffened Isotropic Cylinders

Axial compression loads. Comparisons for stiffened isotropic cylinders subjected to uniform axial compression are presented in Tables 25-54. In particular, the results in Tables 25 and 26 show the predicted values of the nondimensional buckling load $\frac{N_x^{cr}}{E\bar{h}}$ obtained by Block, Card, and Mikulas[59] and obtained in the present study for ring-and-stringer-stiffened cylinders and stringer-stiffened cylinders, respectively, with a cylinder radius R = 200.0 inches, wall thickness is h = 0.10 inch, a Young's modulus $E = 10 \times 10^6$ psi and a Poisson's ratio $\nu = 0.32$. More specifically, results are presented for cylinders with 503 stringers, which corresponds to a stringer spacing $d_s = 2.50$ inches. The results in Table 25 are for cylinders with length L = 200.0 in. and with internal rings and external stringers, internal rings and internal stringers, and external rings and external stringers. The results in Table 25 are presented for selected values of the ring spacing d_r divided by the cylinder radius. The results in Table 26 are for cylinders with either internal or external stringers and are given for selected values of the length-to-radius ratio $0.15 \le L/R \le 0.50$. The corresponding eccentricities of the rings and stringers are denoted by the values of e_r and e_s, respectively, presented in the tables. The rings have an I-shaped cross-section (figure 49a) with an area $A_r = 0.78$ in^2, a centroidal moment of inertia $I_r = 1.9786$ in^4, and a torsion constant $J_r =$

0.0026 in^4. The stringers have a Z-shaped cross-section (figure 49b) with an area $A_s = 0.36$ in^2, a centroidal moment of inertia $I_s = 0.2112$ in^4, and a torsion constant $J_s = 0.0012$ in^4. In the definition of the nondimensional buckling load appearing in these tables, N_x^{cr} is the value of the applied axial stress resultant at buckling and $\bar{h} = \frac{A_s}{d_s} + h$ is an equivalent cylinder wall thickness with a value of 0.24 inch.

The results presented in Table 25 for the ring-and-stringer-stiffened cylinders indicate that the nondimensional buckling loads obtained in the present study and by Block, Card, and Mikulas by using Donnell's equations are identical with three exceptions. Differences of approximately 0.02%, 0.03% and 3.4% are exhibited by the results for the cylinders with external rings and external stringers for $d_r/R = 0.05$, 0.10, and 0.25, respectively. The results obtained in the present study by using Sanders' equations indicate that neglecting the nonlinear rotations about the normal produces differences that are at most 0.6%. In addition, differences in predictions based on Sanders' and Donnell's equations are for the most part less than 1%. Differences of about 1.5% are noted for the cylinders with internal rings and internal stringers for $d_r/R = 0.20$ and 0.25.

The results presented in Table 26 for the stringer-stiffened cylinders indicate that the nondimensional buckling loads obtained in the present study and in reference 59 using Donnell's equations are also identical for the most part and that the differences that exist are less than 0.2%. The results in Table 26 obtained in the present study by using Sanders' equations indicate that neglecting the nonlinear rotations about the normal produces differences that are at most 0.5%. Similarly, differences in the predictions based on Sanders' and Donnell's equations are also at most 0.5%.

Results are presented in Table 27 that show the predicted values of the nondimensional buckling load $\frac{N_x^{cr}}{A_{11}}$ obtained by Block, Card, and Mikulas[59] and obtained in the present study for ring-stiffened cylinders with a circumferentially corrugated cylinder wall, as shown in figure 49c. An example of a similar corrugated cylinder is shown in figure 50. These corrugated cylinders have a cylinder radius R = 200.0 inches, a length L = 200.0 inches, a Young's modulus $E = 10 \times 10^6$ psi and a Poisson's ratio $\nu = 0.32$. The rings have the cross-sectional dimensions shown in figure 49a and the ring eccentricity is given by

$$e_r = \pm \frac{1}{2}\left(w_c \sin\alpha + h_c + D_r\right) \tag{129}$$

where the plus and minus signs in front of the parenthesis correspond to external and internal rings, respectively. The results in Table 27 are presented for selected values of the ratio of the ring spacing to the cylinder radius, d_r/R. The nonzero equivalent-plate stiffnesses used in the calculations are given by

$$A_{11} = \frac{2Eh_c}{1 + \cos\alpha} \tag{130a}$$

$$A_{22} = \frac{EA_r}{d_r} \tag{130b}$$

$$A_{66} = \frac{Eh_c}{4(1+\nu)}(1+\cos\alpha) \tag{130c}$$

$$B_{22} = A_{22}e_r \tag{130d}$$

$$D_{11} = \frac{w_c^2}{6} A_{11} \sin^2\alpha \tag{130e}$$

$$D_{22} = \frac{E}{d_r}\left(I_r + A_r e_r^2\right) \tag{130f}$$

$$D_{66} = \frac{EJ_r}{8(1+\nu)d_r} \tag{130g}$$

The rings have an I-shaped cross-section with an area $A_r = 0.78$ in^2, a centroidal moment of inertia $I_r = 1.9786$ in^4, and a torsion constant $J_r = 0.0026$ in^4. The ring eccentricity was found to be given by $e_r = \pm 3.812$ in.

The results in Table 27 indicate exact agreement between the nondimensional buckling loads predicted in the presented study and in reference 59 otained by applying Donnell's equations to the corrugated cylinders with external rings. Moreover, because the buckling mode is axisymmetric, the results based on Donnell's and Sanders' equations are identical. For the cylinders with internal rings, the results indicate differences between the nondimensional buckling loads obtained herein and in reference 59 that are approximately 0.4%. Differences between the results obtained herein by using Donnell's and Sanders' equations are at most 0.3%.

Results are presented in Table 28 that show the predicted values of the buckling load N_x^{cr} obtained by Hedgepeth and Hall,[60] by Singer, et al.,[61] and obtained in the present study for the cylinders with 60, either internal or external, stringers with a rectangular cross-section that were originally studied by Card and Jones.[62, 63] The cylinder, in a buckled form, and the stringer details are shown in figure 51. The results obtained in reference 60 are based on a variant of Sanders' equations in which certain nonlinear terms in the equilibrium equations are neglected. The results obtained in reference 61 are based on Donnell's equations and include results that show the effects of neglecting the torsional stiffness of the stringers ($J_s = 0$). The cylinders have a radius $R = 9.55$ in., lengths $L = 38.00$ and 23.75 in., a Young's modulus $E = 10.5 \times 10^6$ psi and a Poisson's ratio $\nu = 0.32$. Each stringer has width of $w_s = 0.097$ in. and a depth $D_s = 0.33 - h$ in., where h is the cylinder wall thickness given in the table. Moreover, the external and internal stringer have eccentricities $e_s = 0.165$ in. and $e_s = -0.165$ in., respectively, with respect to the midsurface of the cylinder, and the stringer spacing is given by $d_s = 1.0$ in. In the present study, the torsion constant used for each stringer is given by

$$J_s = \frac{1}{3} w_s^3 D_s \tag{131}$$

Results for the same cylinder obtained in the present study and by Card and Jones[63] are presented in Table 29. These results are based on the more exact expression for the torsion constant given by the theory of elasticity; that is,

$$J_s = w_s^3 D_s \left[\frac{1}{3} - \frac{64}{\pi^5} \frac{w_s}{D_s} \operatorname{Tanh}\left(\frac{\pi D_s}{2 w_s} \right) \right] \tag{132}$$

The results presented in Table 28 indicate that the buckling loads obtained in the present study and in reference 61 by using Donnell's equations differ by about 2%. In addition, the results presented in reference 61, obtained by using Donnell's equations, show that neglecting the torsional stiffness of the stringers yields buckling resistance predictions that are between 12% and 15% lower for the cylinders with external stringers and between 18% and 20% lower for the cylinders with internal stringers. Corresponding results obtained in the present study predict nearly the same reductions in buckling resistance associated with neglecting the torsional stiffness of the stringers and a similar trend is indicated in reference 63. The results in Table 28 obtained in the present study by using Sanders' equations and obtained by Hedgepeth and Hall by using a variant of Sanders' equations show differences of about 0.5% and 2.3% for the cylinders with external stringers and lengths equal to 38 in. and 23.57 in., respectively. Moreover, differences of about 4.9% and 1.4% are exhibited by the cylinders with internal stringers and lengths equal to 38 in. and 23.57 in., respectively. The results in Table 28 obtained in the present study by using Sanders' equations indicate that neglecting the nonlinear rotations about the normal produces differences between approximately 2-4%. Similarly, differences in the predictions based on Sanders' and Donnell's equations are between 3% and 8%.

The results in Table 29, for the more accurate representation of the torsional stiffness of the stringers, show differences of less than 0.2% in the corresponding buckling loads obtained by Card and Jones and in the present study by using Donnell's equations. The results in this table, obtained in the present study by using Sanders' equations, indicate that neglecting the nonlinear rotations about the normal also produces differences between approximately 2-4%. Similarly, differences in the predictions based on Sanders' and Donnell's equations are between 3% and 8%.

Results are presented in Tables 30 and 31 that show the predicted values of the buckling load N_x^{cr} obtained by Hedgepeth and Hall,[60] by Card and Jones,[63] and obtained in the present study for the cylinders with 60, either internal or external, Z-shaped stringers that were originally studied by Peterson and Dow[64] and by Card.[62] The cylinder is shown in a buckled form in figure 52. The results obtained in reference 60 are also based on a variant of Sanders' equations in which certain nonlinear terms in the equilibrium equations are neglected. The results obtained in reference 63 are based on Donnell's equations. Results obtained in the present study include results that show the effects of neglecting the torsional stiffness of the stringers ($J_s = 0$). Each cylinder has a stringer spacing is given by $d_s = 1.24$ in., a Young's modulus $E = 10.5 \times 10^6$ psi and a Poisson's ratio $\nu = 0.32$. The results in Table 30 are based on a cylinder radius $R = 15.80$ in. and a length $L = 59.0$

in., and several cylinder-wall thicknesses h that are presented in the table. This radius was initially reported by Card[62] and is slightly different from the radius R = 15.92 in. used in Table 31 and reported later by Card and Jones.[63] Each stringer has a depth $D_s = 0.54$ in., a wall thickness $h_s = 0.040$ in., and flange thicknesses $w_{f1} = 0.375$ in. and $w_{f2} = 0.22$ in., as shown in the figure 52. The stringer eccentricities are given by the values of e_s indicated in the tables. In the present study, the stringer area was calculated by using

$$A_s = \left(w_{f1} + w_{f2} + D_s - 2h_s\right)h_s \tag{133a}$$

and the stringer eccentricity shown in figure 33 was obtained by using

$$e_s = \pm\left[\frac{w_{f1}\left(h + h_s\right) + w_{f2}\left(2D_s + h - h_s\right) + \left(D_s - 2h_s\right)\left(D_s + h\right)}{w_{f1} + w_{f2} + D_s - 2h_s}\right] \tag{133b}$$

where the plus and minus signs in front of the bracket correspond to external and internal stringers, respectively. Similarly, the centroidal moment of inertia was calculated by using

$$\begin{aligned} I_s^c = {} & \frac{h_s^3}{12}\left(w_{f1} + w_{f2}\right) + \frac{h_s}{12}\left(D_s - 2h_s\right)^3 + w_{f1}h_s\left[e_s - \frac{1}{2}\left(h + h_s\right)\right]^2 \\ & + w_{f2}h_s\left[D_s - e_s + \frac{1}{2}\left(h - h_s\right)\right]^2 + h_s\left(D_s - 2h_s\right)\left[\frac{1}{2}\left(h + D_s\right) - e_s\right]^2 \end{aligned} \tag{133c}$$

and the torsion constant used for each stringer is given by

$$J_s = \frac{h_s^3}{3}\left(w_{f1} + w_{f2} + D_s - 2h_s\right) \tag{133d}$$

The results in Table 30 that were obtained in the present study by using Sanders' equations and obtained by Hedgepeth and Hall by using variant of Sanders' equations show a difference in predicted buckling loads of approximately 0.3% and 4% for the cylinders with internal and external Z-shaped stringers, respectively. The results of the present study obtained by using Sanders' equations indicate that neglecting the nonlinear rotations about the normal yields differences in the buckling loads of about 3%. Corresponding differences in results obtained from Sanders' and Donnell's equations are predicted to be approximately 5-6%.

The results in Table 31 show differences between 0.7% and 4.4% in the buckling loads obtained in the present study and in reference 63 that are based on Donnell's equations. Moreover, reductions in the buckling loads of about 0.8-2.2% are predicted by the results of the present study when the torsional stiffness of the stringers is neglected. A corresponding 1% difference is noted in reference 63. The results of the present study that were obtained by using Sanders' equations indicate that neglecting the nonlinear rotations about the normal yields differences in the buckling loads that are between approximately 0.7% and 2.1%. Similarly, the differences between corresponding buckling loads obtained by using Sanders' and Donnell's equations range from 1.1% to 6.2%.

Results are presented in Tables 32-49 that show the predicted values of the buckling coefficient $\frac{2N_x^{cr} R^2}{D}$ obtained by Singer, Baruch, and Harari[61, 65] and obtained in the present study for generic stringer-stiffened isotropic cylinders, for a broad range of cylinder geometries. In particular, results are given for length-to-radius ratios $0.25 \le L/R \le 20$ and for radius-to-thickness ratios $50 \le R/h \le 50000$. The generic stringer properties are given by $\frac{A_s}{d_s h} = 0.5$, $\frac{I_s^c}{d_s h^3} = 5,$ and $J_s = 0$, where A_s is the cross-sectional area, d_s is the stringer spacing, I_s^c is the centroidal moment of inertia, and J_s is the torsion constant. The results in Table 32 are for cylinders with stringers that are centrally located such that the centroid of the stiffener coincides with the middle surface of the cylinder. For this case, the nondimensional stiffener eccentricity is given by $e_s/h = 0$. The results in Table 33 are for cylinders with external and internal stringers, respectively, with $e_s/h =$ +2 and -2, respectively. Likewise, the results in Tables 34 and 35 are for cylinders with $e_s/h =$ +5 and -5, and the results in Table 36 are for cylinders with $e_s/h = +10$ and -10. In the buckling coefficient appearing in the tables, $D = \frac{Eh^3}{12\left(1-\nu^2\right)}$ is the principal bending stiffness of the cylinder wall, E is Young's modulus, and ν is Poisson's ratio. A value of $\nu = 0.3$ was used to generate the results shown in the tables.

The results in Table 32, for the cylinders with centrally located stringers, show differences less than approximately 0.01% in the buckling loads obtained in the present study and in reference 65 by using Donnell's equations. The results of the present study obtained by using Sanders' equations indicate that neglecting the nonlinear rotations about the normal yields differences in the buckling loads that are between approximately 0.4% and 1.5%. Similarly, the differences between corresponding buckling loads obtained by using Sanders' and Donnell's equations range from 0.7% to 2.8%.

The results in Table 33, for the cylinders with external stringers ($e_s/h = + 2$), show differences less than approximately 0.01% in the buckling loads obtained in the present study and in reference 65 by using Donnell's equations. The results of the present study obtained by using Sanders' equations indicate that neglecting the nonlinear rotations about the normal yields small differences in the buckling loads that are between approximately 0.4% and 1.5%. Similarly, the results also show that the differences between corresponding buckling loads obtained by using Sanders' and Donnell's equations range from 0.8% to about 3%.

The results in Table 33, for the cylinders with internal stringers ($e_s/h = - 2$), show differences less than approximately 0.05% in the buckling loads obtained in the present study and in reference 65 by using Donnell's equations. Moreover, the differences in buckling coefficients that result from neglecting nonlinear rotations about the normal in Sanders' equations range between about 0.5% and 2.5%, and the differences between the results obtained by using Sanders' and Donnell's equations range from 1% to about 3.5%.

The results in Table 34, for the cylinders with external stringers ($e_s/h = + 5$), show differences

less than approximately 0.11% in the buckling loads obtained in the present study and in reference 65 by using Donnell's equations. For many of the cases, the results obtained herein and in reference 65 are identical. The results of the present study obtained by using Sanders' equations indicate that neglecting the nonlinear rotations about the normal yields differences in the buckling loads that are between approximately 0% and 11%. More specifically, for the relatively short, thick cylinder with L/R = 0.25 and R/h = 50, the difference is about 6%. In contrast, the cylinders with $0.35 \le L/R \le 1$ and $50 \le R/h \le 50000$, exhibit differences in buckling loads less than 1%. Similarly, the cylinders with L/R = 1.5 and 2, and with $50 \le R/h \le 2000$ exhibit differences between 0.6 and 2%. The longer cylinders considered, with $4 \le L/R \le 20$ and $50 \le R/h \le 2000$, exhibit differences between 1.5% and 11%.

The results in Table 34 also show that the differences between corresponding buckling loads obtained by using Sanders' and Donnell's equations range from 0% to about 23%. In particular, the relatively short, thick cylinder with L/R = 0.25 and R/h = 50, exhibits a difference of about 6%. The cylinders with $0.35 \le L/R \le 1$ and $50 \le R/h \le 50000$, exhibit differences in buckling loads less than 1.1%. Similarly, the cylinders with L/R = 1.5 and 2, and with $50 \le R/h \le 2000$ exhibit differences between 1.3 and 4%. The longer cylinders with $4 \le L/R \le 20$ and $50 \le R/h \le 2000$, exhibit differences between 2.7% and 23%.

The results in Table 35, for the cylinders with internal stringers ($e_s/h = -5$), show differences less than approximately 0.6% in the buckling loads obtained in the present study and in reference 65 by using Donnell's equations. Like for the cylinders with external stringers, many of the results obtained herein and in reference 65 are identical. The results of the present study obtained by using Sanders' equations indicate that neglecting the nonlinear rotations about the normal yields differences in the buckling loads that are between approximately 0.02% and 15% for the very broad range of cylinder geometries considered. For the relatively short, thick cylinders with L/R = 0.25 and 0.35, and with R/h = 50, the differences are about 15% and 7%, respectively. In contrast, the cylinders with $0.5 \le L/R \le 1$ and $50 \le R/h \le 50000$, exhibit differences in buckling loads that range from 0.2% to 5%. Similarly, the cylinders with L/R = 1.5 and 2, and with $50 \le R/h \le 2000$ exhibit differences between about 0.3 and 5%. The longer cylinders considered, with $4 \le L/R \le 20$ and $50 \le R/h \le 2000$, exhibit differences between 0.3% and 10%.

The results in Table 35 also show that the differences between corresponding buckling loads obtained by using Sanders' and Donnell's equations range from 0.03% to about 20%. For the relatively short, thick cylinders with L/R = 0.25 and 0.35, and with R/h = 50, differences of about 15% and 8% are predicted, respectively. The cylinders with $0.5 \le L/R \le 1$ and $50 \le R/h \le 50000$, exhibit differences in buckling loads between about 0.3% and 5%, with the thicker cylinders exhibiting the larger differences. Similarly, the cylinders with L/R = 1.5 and 2, and with $50 \le R/h \le 2000$ exhibit differences between 0.7 and 7%, with the thicker cylinders also exhibiting the larger differences. The longer cylinders with $4 \le L/R \le 20$ and $50 \le R/h \le 2000$, exhibit differences between 0.7% and 20%.

The results in Table 36, for the cylinders with external stringers ($e_s/h = +10$), show differences less than approximately 0.04% in the buckling loads obtained in the present study and in reference 65 by using Donnell's equations. The results of the present study obtained by using Sanders' equations indicate that neglecting the nonlinear rotations about the normal yields

differences in the buckling loads that are less than approximately 3%. Moreover, for the cylinders with L/R = 0.5 and 1, the differences are less than about 0.5%. The results in Table 36 also show that the differences between corresponding buckling loads obtained by using Sanders' and Donnell's equations range from 0.03% to about 6%, with differences less than 0.7% for the cylinders with L/R = 0.5 and 1.

The results in Table 36, for the cylinders with internal stringers ($e_s/h = -10$), also show very small differences, less than approximately 0.03%, in the buckling loads obtained in the present study and in reference 65 by using Donnell's equations. In addition, the results obtained herein predict differences between 0.7% and 9% if the nonlinear rotations about the normal are neglected. Similarly, using Donnell's equations instead of Sanders equations produces buckling-coefficient differences between 0.8% and 10%.

Results for cases similar to those presented in Tables 34 ($e_s/h = +5$) and 35 ($e_s/h = -5$) for cylinders with $\frac{A_s}{d_s h} = 0.5$, $\frac{I_s^c}{d_s h^3} = 5$, and $J_s = 0$ are presented in Table 37 for stringer-stiffened cylinders with a much higher centroidal moment of inertia for the stringers, given by $\frac{I_s^c}{d_s h^3} = 15$. Similar results are presented in Table 38 for cylinders with $\frac{A_s}{d_s h} = 1.5$, $\frac{I_s^c}{d_s h^3} = 5$, and $J_s = 0$. In these two tables, values of the buckling coefficient $\frac{2N_x^{cr} R^2}{D}$ are presented for cylinder geometries that include $0.5 \le L/R \le 3$ and $50 \le R/h \le 1000$. The results in Tables 37 and 38, for both the cylinders with the stiffer external stringers ($e_s/h = +5$) and for the cylinders with the stiffer internal stringers ($e_s/h = -5$), show differences much less than approximately 1% in the buckling loads obtained in the present study and in reference 65 by using Donnell's equations. In addition, the results obtained herein predict differences less than 3.5% and mostly less than 5% if nonlinear rotations about the normal are neglected in the analysis of the cylinders with external and internal stiffeners, respectively. The largest difference is less than 8% when nonlinear rotations about the normal are neglected in the analysis of the cylinders with internal stiffeners. Similarly, using Donnell's equations instead of Sanders equations produces buckling-coefficient differences that are mostly less than 5%, with a maximum difference of approximately 10%.

Results are presented in Table 39 for short shells with $L/R = 1$, $250 \le R/h \le 1000$, $\frac{A_s}{d_s h} = 1.5$, $\frac{I_s^c}{d_s h^3} = 5$, $J_s = 0$, and with relatively high degrees of stiffener eccentricity given by $e_s/h = \pm 7$ and ± 10. Likewise, results are presented in Table 40 for short shells with $L/R = 2$, $R/h = 500$ and 1000, $\frac{I_s^c}{d_s h^3} = 5$, $J_s = 0$, $e_s/h = \pm 10$, and with $\frac{A_s}{d_s h} = 1.5$, 3, and 5. The results in these two tables show differences less than 0.1% in the buckling loads obtained in the present study and in reference 61 by using Donnell's equations, with one minor exception that exhibits a 4.1% difference and two major exceptions that exhibit very large differences. Specifically, the results

presented in reference 61 for $\frac{A_s}{d_s h} = 0.5$ and $e_s/h = \pm 10$ are significantly different from the corresponding results obtained in the present study for R/h = 500. However, the corresponding results obtained in the present study for R/h = 1000 are less than 0.05% different from the results of reference 61. This nearly identical agreement suggests the presence of a typographical error in reference 61. The results obtained herein that are given in Tables 39 and 40 also predict differences less than 2.5% when the nonlinear rotations about the normal are neglected in the use of Sanders' equations. Similarly, using Donnell's equations instead of Sanders equations produces buckling-coefficient differences that are less than 3.2%.

Results are presented in Table 41 for shells with L/R = 0.5 and R/h = 100, L/R = 2 and R/h = 500, and L/R = 4 and R/h = 2000. For each case, the stringer eccentricity varies according to $-10 \le e_s/h \le 10$ and the stringer properties are fixed at $\frac{A_s}{d_s h} = 1.5$, $\frac{I_s^c}{d_s h^3} = 5$, and $J_s = 0$. These results show differences less than 0.02% in the buckling loads obtained in the present study and in reference 65 by using Donnell's equations. The results obtained herein that are given in Table 41 predict differences less than 5%, and mostly less than 2%, when the nonlinear rotations about the normal are neglected in the use of Sanders' equations. Similarly, using Donnell's equations instead of Sanders' equations produces buckling-coefficient differences that are less than 5.1%.

Results are presented in Tables 42 and 43 for shells with L/R = 0.5 and R/h = 100, L/R = 2 and R/h = 500, and L/R = 4 and R/h = 2000, and with the stringer eccentricities $e_s/h = 5$ and -5, respectively. For each case, the stringer properties are fixed at $\frac{I_s^c}{d_s h^3} = 5$ and $J_s = 0$, and the stringer area varies according to $0.1 \le \frac{A_s}{d_s h} \le 1.5$. Similar results are presented in Tables 44 and 45 in which the stringer properties are fixed at $\frac{A_s}{d_s h} = 0.5$ and $J_s = 0$, and the stringer moment of inertia varies according to $1 \le \frac{I_s^c}{d_s h^3} \le 20$. These results show differences less than 0.05%, and for the most part much smaller, in the buckling loads obtained in the present study and in reference 65 by using Donnell's equations. The results obtained herein that are given in Tables 42-45 predict differences less than 2.3% when the nonlinear rotations about the normal are neglected in the use of Sanders' equations. Similarly, using Donnell's equations instead of Sanders' equations produces buckling-coefficient differences that are less than 4.4%.

Results are presented in Tables 46 and 47 for shells with the stringer eccentricities $e_s/h = 5$ and -5, respectively. These results include combinations of L/R = 0.5, 1, and 4 and R/h = 50, 250, 2000, and 5000. For each case, the stringer properties are fixed at $\frac{A_s}{d_s h} = 0.5$ and $\frac{I_s^c}{d_s h^3} = 5$, and results are given for selected value of the stringer torsional-stiffness parameter $\frac{G_s J_s}{d_s D} = 0$, 5, 10, 20, and 40. These results also show differences less than 0.05%, and for the most part much smaller, in the buckling loads obtained in the present study and in reference 66 by using Donnell's

equations. The results obtained herein that are given in Tables 46 and 47 predict differences less than 5% when the nonlinear rotations about the normal are neglected in the use of Sanders' equations. Similarly, using Donnell's equations instead of Sanders' equations produces buckling-coefficient differences that are less than 10.2%.

Results for shells with the stringer eccentricities $e_s/h = 5$ and -5 are also presented in Tables 48 and 49, respectively, for values of Poisson's ratio $\nu = 0$, 0.3, and 0.5. These results include selected combinations of $L/R = 0.35$, 0.5, and 1 and $R/h = 50$, 250, 500, 2000, and 5000. For each case, the stringer properties are fixed at $\frac{A_s}{d_s h} = 0.5$, $\frac{I_s^c}{d_s h^3} = 5$, and $J_s = 0$. These results also show differences less than 0.03%, and for the most part much smaller, in the buckling loads obtained in the present study and in reference 65 by using Donnell's equations with one exception. The results in Table 49 for $L/R = 1$, $R/h = 2000$, and $\nu = 0$ differ by about 5%. The results obtained herein that are given in Table 48 predict differences less than 2% for the cylinders with external stringers when the nonlinear rotations about the normal are neglected in the use of Sanders' equations. In contrast, the results in Table 49 show differences up to 10% for the cylinders with internal stringers when the nonlinear rotations about the normal are neglected. Similarly, using Donnell's equations instead of Sanders' equations produces buckling-coefficient differences that are less than 2% for the cylinders with external stringers and up to 10% for the cylinders with internal stringers.

Tables 50 and 51 show the geometric parameters and predicted buckling loads, respectively, obtained by Singer, Arbocz, and Babcock[66] and obtained in the present study for ring-stiffened and stringer-stiffened isotropic cylinders. The cylinders identified with the letter "A" are made of aluminum with a Young's modulus $E = 10 \times 10^6$ psi and a Poisson's ratio $\nu = 0.3$. The cylinders identified with the letters "B" are made of brass with a Young's modulus $E = 15.3 \times 10^6$ psi and a Poisson's ratio $\nu = 0.3$. The results include cylinders with length-to-radius ratios $1.28 \le L/R \le 1.88$ and radius-to-thickness ratios $377 \le R/h \le 517$. The generic stringer properties given by $\frac{A_s}{d_s h}$ and $\frac{I_s^c}{d_s h^3}$, and the corresponding ring properties $\frac{A_r}{d_r h}$ and $\frac{I_r^c}{d_r h^3}$, are also given in Table 50 along with their corresponding eccentricities e_s and e_r normalized by the cylinder wall thickness, h. All of the cylinders have external stiffeners. In the stiffener parameters, A_s is the stringer cross-sectional area, d_s is the stringer spacing, I_s^c is the stringer centroidal moment of inertia. Likewise, A_r is the ring cross-sectional area, d_r is the ring spacing, I_r^c is the ring centroidal moment of inertia. For all the results in Table 51, the torsional stiffnesses of the rings and stringers have been neglected.

The results in Table 51 show differences less than 4%, and for the most part much smaller, in the buckling loads obtained in the present study and in reference 66 by using Donnell's equations. In addition, the results predict differences less than 1.2% when the nonlinear rotations about the normal are neglected in the use of Sanders' equations. Moreover, using Donnell's equations instead of Sanders' equations produces buckling-load differences that are less than 2.5%. In many cases, no differences are exhibited by the three sets of results. This attribute is due

to the fact that the three sets of equations used to calculate the buckling loads are identical for shells that buckle into axisymmetric modes (n = 0).

Results are presented in Tables 52-54 that show the predicted values of the buckling coefficient $\frac{2N_x^{cr}R^2}{D}$ obtained by Singer, Baruch, and Harari[61, 65] and obtained in the present study for relatively short, generic ring-stiffened isotropic cylinders with L/R = 0.5, a Young's modulus $E = 10 \times 10^6$ psi, and a Poisson's ratio $\nu = 0.3$. In Table 52, results are given for R/h = 250, $\frac{A_r}{d_r h} = 0.5$, $J_s = 0$, $\frac{I_r^c}{d_r h^3} = 2$ and 40, and $e_r/h = \pm 1$. These results show that the buckling loads obtained in the present study and in references 61 and 65 by using Donnell's equations are indentical. Moreover, corresponding results were obtained in the present study by using Sanders' equations with and without nonlinear rotations about the normal that differ by at most 0.03% from those shown in Table 52. In Table 53, results are given for R/h = 250, $\frac{A_r}{d_r h} = 0.5$, $J_s = 0$, $e_r/h = 0$, and $2 \le \frac{I_r^c}{d_r h^3} \le 200$. This table also shows complete agreement between the results of references 61 and 65 and the present study, which are based on Donnell's equations, and these results also differ by less than 0.03% from the corresponding results obtained by using Sanders' equations with and without nonlinear rotations about the normal. In Table 54, results are given for $\frac{A_r}{d_r h} = 0.5$, $\frac{I_r^c}{d_r h^3} = 5$, $J_s = 0$, $e_r/h = \pm 5$, and $50 \le R/h \le 2000$. This table also shows differences between the results of references 61 and 65 and the present study, which are based on Donnell's equations, that are at most 3% for R/h = 50 and $e_r/h = +5$ and less than 1% otherwise. These results obtained in the present study by using Donnell's equations also differ by less than 1% from the corresponding results obtained by using Sanders' equations with and without nonlinear rotations about the normal.

The differences in the buckling resistance predictions obtained in the present study by using Donnell's equations, Sanders' equations, and Sanders' equations with nonlinear rotations about the normal neglected are illustrated in figures 53-94 for stringer-stiffened and for ring-stiffened cylinders with radius-to-thickness ratios R/h =50 and 500, with Poisson's ratio $\nu = 0.30$, and with Young's modulus $E = 10.0 \times 10^6$ psi. The buckling resistance is measured by the nondimensional coefficient $\frac{N_x^{cr}Rh}{\pi^2 D}$ for values of $0.2 \le L/R \le 50$, where $D = \frac{Eh^3}{12(1-\nu^2)}$ is the principal shell-wall bending stiffness. Parameters that are used to represent the results in these figures are obtained by expressing equations (65) as

$$\begin{bmatrix} A_{11} & A_{12} & A_{16} \\ A_{12} & A_{22} & A_{26} \\ A_{16} & A_{26} & A_{66} \end{bmatrix} = A \begin{bmatrix} 1 + \frac{E_s A_s}{d_s A} & \nu & 0 \\ \nu & 1 + \frac{E_r A_r}{d_r A} & 0 \\ 0 & 0 & \frac{1-\nu}{2} \end{bmatrix} \qquad (134a)$$

$$\begin{bmatrix} B_{11} & B_{12} & B_{16} \\ B_{12} & B_{22} & B_{26} \\ B_{16} & B_{26} & B_{66} \end{bmatrix} = Ah \begin{bmatrix} \frac{E_s A_s}{d_s A}\frac{e_s}{h} & 0 & 0 \\ 0 & \frac{E_r A_r}{d_r A}\frac{e_r}{h} & 0 \\ 0 & 0 & 0 \end{bmatrix} \tag{134b}$$

$$\begin{bmatrix} D_{11} & D_{12} & D_{16} \\ D_{12} & D_{22} & D_{26} \\ D_{16} & D_{26} & D_{66} \end{bmatrix} = \tag{134c}$$

$$D \begin{bmatrix} 1 + \frac{E_s I_s^c}{d_s D} + \frac{12 E_s A_s}{d_s A}\left(\frac{e_s}{h}\right)^2 & \nu & 0 \\ \nu & 1 + \frac{E_r I_r^c}{d_r D} + \frac{12 E_r A_r}{d_r A}\left(\frac{e_r}{h}\right)^2 & 0 \\ 0 & 0 & \frac{(1-\nu)}{2}\left[1 + \frac{G_s J_s}{2d_s(1-\nu)D} + \frac{G_r J_r}{2d_r(1-\nu)D}\right] \end{bmatrix}$$

where $A = \frac{Eh}{1-\nu^2}$ is the principal membrane stiffness of the shell wall. Thus, $\frac{E_s A_s}{d_s A}$ and $\frac{E_r A_r}{d_r A}$ are the ratios of the smeared-stringer and smeared-ring membrane stiffnesses to the principal membrane stiffness of the shell wall, respectively. Likewise, $\frac{E_s I_s^c}{d_s D}$ and $\frac{E_r I_r^c}{d_r D}$ are the ratios of the smeared-stringer and smeared-ring bending stiffnesses to the principal bending stiffness of the shell wall, respectively. Moreover, $\frac{G_s J_s}{2d_s(1-\nu)D}$ and $\frac{G_r J_r}{2d_r(1-\nu)D}$ are the ratios of the smeared-stringer and smeared-ring twisting stiffnesses to the twisting stiffness of the shell wall, respectively. The parameters $\frac{e_s}{h}$ and $\frac{e_r}{h}$ are the normalized stringer and ring eccentricities, respectively.

The red curves in figures 53-94 corresponds to results obtained by using Donnell's equations. The black and the blue curves corresponds to results obtained by using Sanders' equations and Sanders' equations with nonlinear rotations about the normal neglected, respectively. These results correspond to a wide range of stringer configurations, as indicated in each figure. As a frame of reference, the baseline case is taken as $\frac{E_s A_s}{d_s A} = 1$, $\frac{E_s I_s^c}{d_s D} = 1$, $\frac{G_s J_s}{2d_s(1-\nu)D} = 0$, and $\frac{e_s}{h} = 0$ for stringer-stiffened cylinders. Similarly, the baseline case is taken as $\frac{E_r A_r}{d_r A} = 1$, $\frac{E_r I_r^c}{d_r D} = 1$, $\frac{G_r J_r}{2d_r(1-\nu)D} = 0$, and $\frac{e_r}{h} = 0$ for ring-stiffened cylinders. The right-most branch of the black and the blue festoon curves shown in figures 53, 55, 57, 59, 61, 63, 65, 67, and 69 correspond to a column-like shell-buckling mode given by the wave numbers m = n = 1, and the graph coordinates for the first column-like shell-buckling mode are indicated in the figures. The corresponding gray curve that appears in these figures corresponds to buckling coefficients

obtained by using the Euler column-buckling formula

$$N^{cr}_{x,\,Euler} = \frac{\pi \tilde{E} I}{2RL^2} \tag{135}$$

for a simply supported thin-walled tubular beam with length L, cross-sectional radius R, and thickness h that is deformed into a single half wave along its length. In this expression, $N^{cr}_{x,\,Euler}$ is the Euler buckling load divided by $2\pi R$ and $\tilde{E}I$ is the column bending stiffness. More specifically, for the ring-stiffened cylinders considered herein, the contribution of the rings to the column bending stiffness is neglected and the column bending stiffness is approximated by $E\pi R^3 h$. In contrast, for the stringer-stiffened cylinders, $\tilde{E}I$ is taken as the column bending stiffness of the composite cross-section formed by the cylinder wall and a finite number of uniformly distributed stringer cross-sections given by $\frac{2\pi R}{d_s}$. Noting that the column bending stiffness $\tilde{E}I$ is the same about either of the two cross-section axes that pass through the geometric center, it follows that

$$\tilde{E}I = \frac{1}{2}\int\int_A E(r,\theta)\, r^2 dA \tag{136}$$

where A denotes the cross-sectional area, (r, θ) are corresponding polar coordinates, and $E(r, \theta)$ signifies the fact that the cylinder wall and the stringers may, in general, have different values for Young's modulus. Next, equation (136) is partitioned into

$$\tilde{E}I = \frac{E}{2}\int\int_{A_{cyl}} r^2 dA + \frac{N_s E_s}{2}\int\int_{A_s} r^2 dA \tag{137}$$

where A_{cyl} is the cross-sectional area of the cylinder wall and $N_s = \frac{2\pi R}{d_s}$ is the number of stringer cross-sections. The coordinate transformation $r = R + \zeta$ is applied to the first integral, with $-\frac{h}{2} \le \zeta \le \frac{h}{2}$ and $dA = (R + \zeta)d\zeta\, d\theta$, and the parallel-axis theorem is applied to the second integral to get

$$\tilde{E}I = \pi R^3 hE\left(1 + \frac{h^2}{4R^2}\right) + \frac{N_s E_s}{2}\left[A_s\left(R + e_s\right)^2 + P_s^c\right] \tag{138}$$

where P_s^c is the centroidal polar moment of inertia of the stringers. Equation (138) is approximated herein by presuming that $\frac{h^2}{4R^2} << 1$ and $P_s^c << A_s\left(R + e_s\right)^2$, which yields

$$\tilde{EI} = \pi R^3 hE\left[1 + \frac{E_s A_s}{E d_s h}\left(1 + \frac{e_s}{R}\right)^2\right] \tag{139}$$

Now, substituting equation (139) into equation (135) gives

$$\frac{N_{x,\,Euler}^{cr} Rh}{\pi^2 D} = \frac{6R^3}{L^2 h}\left[1 - \nu^2 + \frac{E_s A_s}{A d_s}\left(1 + \frac{e_s}{R}\right)^2\right] \tag{140}$$

for the stringer-stiffened cylinders. For the ring-stiffened cylinders,

$$\frac{N_{x,\,Euler}^{cr} Rh}{\pi^2 D} = \frac{6R^3}{L^2 h}\left(1 - \nu^2\right) \tag{141}$$

Several plots that indicate the percent difference in the buckling loads with respect to the results obtained by using Sanders' equations are included in figures 53-81. Points of the red curves appearing in these plots are obtained by computing the absolute value of the difference between buckling loads obtained by using Donnell's and Sanders' equations and then dividing the result by the corresponding buckling load obtained from Sanders' equations. The blue curve is obtained in a similar manner with the results obtained by using Donnell's equations replaced with the results obtained by using Sanders' equations with nonlinear rotations about the normal neglected.

The results in figures 53-72, for the stringer-stiffened cylinders with R/h = 50, show significant differences in the buckling resistance predictions obtained from the three set of equations, with the black curves (Sanders' equations) generally exhibiting the lowest corresponding values of buckling resistance. Additionally, the differences are generally more pronounced as the cylinder length increases. Like for the unstiffened-cylinder results presented herein, the results obtained by using Sanders' equations predict a transition to a column buckling mode at significantly smaller values of L/R than the corresponding results obtained by using Sanders' equations with nonlinear rotations about the normal neglected. The results obtained by using Donnell's equations predict no transition at all. In addition, the Euler column-buckling modes predicted by equation (140) are in close agreement with the corresponding results predicted by Sanders' equations. Moreover, the buckling loads predicted by equation (140) are slightly greater than the corresponding buckling loads predicted by Sanders' equations. This difference is attributed to the cross-section flexibility inherent to shell theory.

For the baseline stringer-configuration given by $\frac{E_sA_s}{d_sA} = 1$, $\frac{E_sI_s^c}{d_sD} = 1$, $\frac{G_sJ_s}{2d_s(1-\nu)D} = 0$, and $\frac{e_s}{h} =$ 0 and shown in figures 53 and 54, the differences between the corresponding results predicted by Donnell's and Sanders' equations, and between the two sets of Sanders' equations, are less than 4% for L/R < 9. As L/R increase beyond ten, the differences increase to values greater than 20%, except for the aspect ratios of approximately $18 \le L/R \le 22$. The largest differences occur for approximately L/R > 31, where Donnell's equations and Sanders' equations with nonlinear rotations about the normal neglected fail to predict a column-like buckling mode.

Relative to the baseline stringer-configuration, the results in figures 53-70, and other results obtained in the present study that are not presented herein, exhibit the following trends. First, increasing the smeared extentional stiffness of the stringers, relative to that of the skin, by increasing $\frac{E_sA_s}{d_sA}$ from the baseline value of one reduces substantially the differences between the corresponding results predicted by Donnell's and Sanders' equations, and by both set of Sanders' equations, for all values of L/R in which Sanders' equations do not yield a column-like buckling mode (figures 55-58). In particular, for $\frac{E_sA_s}{d_sA} = 2$, the differences do not exceed 12% and for the most part do not exceed 3%. As the value of this extentional-stiffness parameter is increased to four, the differences do not exceed approximately 2%. Next, increasing the smeared bending stiffness of the stringers (figures 59 and 60), relative to that of the skin, by increasing $\frac{E_sI_s^c}{d_sD}$ from the baseline value of one to a value of ten increases substantially the differences between the corresponding results predicted by Donnell's and Sanders' equations for all values of $0.4 \le L/R \le 50$. A similar trend is noted for the differences between the corresponding results obtained by using the two sets of Sanders' equations, especially for $L/R \le 10$.

Increasing the smeared torsional stiffness of the stringers (figures 61-64), relative to that of the skin, by increasing $\frac{G_sJ_s}{2d_s(1-\nu)D}$ from the baseline value of zero generally increases the differences between the corresponding results predicted by Donnell's and Sanders' equations for L/R > 10. In contrast, increasing this parameter generally reduces the differences between the corresponding results predicted by the two sets of Sanders' equations. For both cases, the differences exceed 20%. For the shorter cylnders with L/R < 10, increasing $\frac{G_sJ_s}{2d_s(1-\nu)D}$ from zero to one, generally increases the differences between the corresponding results predicted by Donnell's and Sanders' equations and by the two sets of Sanders' equations. However, increasing $\frac{G_sJ_s}{2d_s(1-\nu)D}$ to a value of ten significantly reduces the differences between the corresponding results predicted by all three sets of equations. For L/R < 4, the differences are less than 5%.

The results in figures 65-72 indicate that increasing the outward stringer eccentricity from the baseline value of zero up to a value of ten, signficantly increases the differences in the corresponding results predicted by Donnell's and Sanders' equations and by the two sets of Sanders' equations. In addition, Donnell's equations tend to produce much bigger differences

than Sanders' equations with nonlinear rotations about the normal neglected. Furthermore, for $\frac{e_s}{h} = 10$, very large differences are predicted for the extremely short cylinders. The results in figures 65-72 also indicate that increasing the inward stringer eccentricity from the baseline value of zero to a value of $\frac{e_s}{h} = -10$ has a somewhat different effect. In particular, changing $\frac{e_s}{h}$ from 0 to -1 increases the differences predicted by Donnell's and Sanders' equations, and by the two sets of Sanders' equations, from a maximum of about 4% to about 8% for L/R < 10. In contrast, the two sets of differences are reduced substantially in the range of L/R > 10. Increasing the inward eccentricity to $\frac{e_s}{h} = -10$ has a much different effect; that is, the two sets of differences increase greatly as the full range of L/R considered. Additionally, very large differences are predicted for the extremely short cylinders.

The results in figures 73-81, for the shells with R/h = 500, show much smaller differences in the buckling resistance predictions, over a larger range of L/R, obtained from the three set of equations, for the most part, than the corresponding shells with R/h = 50 and do not exhibit column-like buckling modes. For example, the baseline stringer-configuration shown in figure 73 exhibits negligible differences for values of L/R ≤ 30. For values of L/R >30, the differences increase substantially, reaching maximums of about 32% and 25% for the differences obtained by using Donnell's and Sanders' equations and by using the two sets of Sanders' equations, respectively. Likewise, for $\frac{E_sA_s}{d_sA} = 2$, the differences shown in figure 74 do not exceed 1% for L/R ≤ 40 and never exceed 10%. For $\frac{E_sI_s^c}{d_sD} = 10$, the differences shown in figure 75 do not exceed 2% for L/R ≤ 8. Moreover, for 8 < L/R < 28, the largest differences between the corresponding results predicted by Donnell's and Sanders' equations, and by the two sets of Sanders' equations, are approximately 18% and 12%, respectively. Furthermore, for L/R ≥ 28, the largest differences between the corresponding results predicted by Donnell's and Sanders' equations, and by the two sets of Sanders' equations, are approximately 56% and 25%, respectively.

For the cylinders with R/h = 500 and $\frac{G_sJ_s}{2d_s(1-\nu)D} = 1$, the differences between the corresponding results predicted by both sets of equations, shown in figure 76, are less than 4% for L/R ≤ 14. In the range 14 < L/R ≤ 29, difference as large as 14% are seen. Beyond L/R = 29, the differences between the corresponding results predicted by Donnell's and Sanders' equations, and by the two sets of Sanders' equations, exhibit a maximum of about 50% and 25%, respectively. In a manner similar to that seen for the cylinders with R/h = 50, the results in figure 77 show that increasing $\frac{G_sJ_s}{2d_s(1-\nu)D}$ to a value of ten increases the differences between the corresponding results predicted by all three sets of equations in the range of L/R > 7. Comparing the results in figures 68 and 78 for cylinders with $\frac{e_s}{h} = 1$ indicates that increasing R/h from 50 to 500 significantly reduces the differences between the corresponding results predicted by both sets of equations. Differences less than 10% are noted for L/R < 8. Similarly, the results in figures 69 and

80 for cylinders with $\frac{e_s}{h} = 10$ show a similar trend. The results for cylinders with $\frac{e_s}{h} = -1$ and -10, shown in figures 67 and 71 for R/h =50 and in 79 and 81 for R/h = 500, indicate a very pronounced reduction in the differences associated with increasing R/h. Differences less than 1% and less than about 6% are noted in the range of L/R < 32 for the cylinders with R/h = 500 and with $\frac{e_s}{h} =$ -1 and -10, respectively.

The results in figures 82-90, for the ring-stiffened cylinders with R/h = 50, also show significant differences in the buckling resistance predictions obtained from the three set of equations, with the black curves (Sanders' equations) generally exhibiting the lowest corresponding values of buckling resistance. Like for the stringer-stiffened cylinders, the differences are generally more pronounced as the cylinder length increases and the results obtained by using Sanders' equations predict a transition to a column buckling mode at significantly smaller values of L/R than the corresponding results obtained by using Sanders' equations with the nonlinear rotations about the normal neglected. Moreover, the results obtained by using Donnell's equations also predict no transition at all. The Euler column-buckling modes predicted by equation (141) for the ring-stiffened cylinders are also in close agreement with the corresponding results predicted by Sanders' equations. In contrast to the results for the stringer-stiffened cylinders, the buckling loads predicted by equation (141) for ring-stiffened cylinders are slightly less, for the most part, than the corresponding buckling loads predicted by Sanders' equations. This difference is attributed to the neglect of contributions made by the rings to the stiffness associated with column bending.

For the baseline ring-configuration given by $\frac{E_r A_r}{d_r A} = 1$, $\frac{E_r I_r^c}{d_r D} = 1$, $\frac{G_r J_r}{2d_r(1-\nu)D} = 0$, and $\frac{e_r}{h} = 0$ and shown in figure 82, the differences between the corresponding results predicted by Donnell's and Sanders' equations, and between the two sets of Sanders' equations, are less than 4% for L/R < 6. As L/R increases beyond six, the differences increase to values greater than 20%, except for the length-to-radius ratios of approximately $12 \le L/R \le 16$. The largest differences occur for approximately L/R > 23, where Donnell's equations and Sanders' equations with the nonlinear rotations about the normal neglected fail to predict a column-like buckling mode.

Relative to the baseline stringer-configuration, the results in figures 83-90, and other results obtained in the present study that are not presented herein, exhibit the following trends. First, increasing the smeared extentional stiffness of the rings, relative to that of the skin, by increasing $\frac{E_r A_r}{d_r A}$ from the baseline value of one to a value of four has a relatively small effect on the differences between the corresponding results predicted by Donnell's and Sanders' equations, and by both set of Sanders' equations. In particular, for $\frac{E_r A_r}{d_r A} = 4$, the differences are almost the same as that for the baseline case. Next, increasing the smeared bending stiffness of the rings (figure 84), relative to that of the skin, by increasing $\frac{E_r I_r^c}{d_r D}$ from the baseline value of one to a value of ten eliminates the differences between the corresponding results predicted by Donnell's and Sanders' equations for all values of L/R < 17.5, which corresponds to shell buckling modes. A similar

trend is noted for the corresponding results obtained by using the two sets of Sanders' equations for approximately $L/R < 26$.

Increasing the smeared torsional stiffness of the rings (figures 85 and 86), relative to that of the skin, by increasing $\frac{G_r J_r}{2d_r(1-\nu)D}$ from the baseline value of zero generally increases the differences between the corresponding results predicted by both sets of equations for approximately $L/R > 6$, with differences exceeding 20%. For the shorter cylnders with $L/R < 6$, increasing $\frac{G_r J_r}{2d_r(1-\nu)D}$ from zero to one, generally increases the differences between the corresponding results predicted by Donnell's and Sanders' equations and by the two sets of Sanders' equations. However, increasing $\frac{G_r J_r}{2d_r(1-\nu)D}$ to a value of ten significantly reduces the differences between the corresponding results predicted by all three sets of equations. For approximately $L/R < 5$, the differences are less than 5%. The results in figures 87-90 indicate that increasing the magnitude of the ring eccentricity, outward or inward, from the baseline value of zero up to a value of ten, eliminates the differences in the corresponding results predicted by Donnell's and Sanders' equations and by the two sets of Sanders' equations that correspond to cylinder buckling modes. For the column-like buckling modes, large differences are present for both cases.

Results for ring-stiffened shells with $R/h = 500$ were obtained in the present study for $0.2 \le L/R \le 50$ and for the same values of the nondimensional parameters used in figures 82-90. For each case, no column-like buckling modes were predicted and the buckling resistance predictions obtained from the three set of equations exhibit much smaller differences over a larger range of L/R, for the most part, than the corresponding cylinders with $R/h = 50$. For example, results for the baseline ring-configuration shown in figure 91 exhibit no appreciable differences for values of approximately $L/R \le 22$. For values of $L/R > 22$, the differences in the results obtained by using Donnell's and Sanders' equations and by using the two sets of Sanders' equations increase substantially, reaching magnitudes in excess of 20% at approximately $L/R = 25$. The results in figure 92 for $\frac{E_r A_r}{d_r A} = 2$ exhibit practically the same trend. For $\frac{E_r I_r^c}{d_r D} = 10$, the results obtained in the present study by using the three sets of equations show no appreciable differences with $\frac{N_x^{cr} R h}{\pi^2 D} = 0.90$ over the full range of L/R except for approximately $L/R < 0.5$.

For the ring-stiffened cylinders with $R/h = 500$ and $\frac{G_r J_r}{2d_r(1-\nu)D} = 1$, the differences between the corresponding results predicted by both sets of equations, shown in figure 93, are less than about 3% for $L/R \le 10$. In the range $10 < L/R \le 22$, difference less than about 13% are seen. Beyond $L/R = 22$, the differences between the corresponding results predicted by Donnell's and Sanders' equations, and by the two sets of Sanders' equations, exhibit a maximum of about 50% and 25%, respectively. Comparing the results in figures 93 and 94 shows that increasing $\frac{G_s J_s}{2d_s(1-\nu)D}$ to a value of ten increases the differences between the corresponding results predicted

by all three sets of equations, particularly in the range of L/R > 20. For the cylinders with eccentric rings, no appreciable difference were found for $\frac{e_s}{h}$ = -1, -10, and 10. For $\frac{e_s}{h}$ = 1, no differences were also found for approximately L/R ≤ 20 and all other differences are less than 5%. Moreover, the response curves are for the most part constant valued with $\frac{N_x^{cr}Rh}{\pi^2 D}$ = 0.69, 0.97, 0.67, and 0.97 for $\frac{e_s}{h}$ = -1, 1, -10, and 10, respectively.

Uniform external pressure loads. Results for ring-stiffened isotropic cylinders subjected to uniform external pressure are presented in Tables 55 and 56 for selected values of the radius-to-thickness ratios 50 ≤ R/h ≤ 2000 and the length-to-radius ratio 0.5 ≤ L/R ≤ 2. Specifically, the predicted values of the nondimensional buckling pressure $\frac{p^{cr}R^3}{D}$ obtained by Singer, Baruch, and Harari[50, 51] and obtained in the present study are shown for cylinders with the generic ring properties are given by $\frac{A_r}{d_r h} = 0.5$, $\frac{I_r^c}{d_r h^3} = 5$, and $J_r = 0$, where A_r is the cross-sectional area, d_r is the ring spacing, I_r^c is the centroidal moment of inertia, and J_r is the torsion constant. Moreover, results are given for cylinders with either external or internal rings having the eccentricites $e_r/h = +0.5$ and -0.5, respectively. The results in Table 55 are for very short cylinders with L/R = 0.5 and a Poisson's ratio $\nu = 0.3$. In contrast, the results in Table 56 are for cylinders with L/R =1 and 2, and for values of Poisson's ratio $\nu = 0$, 0.3, and 0.5. In the nondimensional buckling pressure appearing in the tables, $D = \frac{Eh^3}{12\left(1-\nu^2\right)}$ is the principal bending stiffness of the cylinder wall, E is Young's modulus, and ν is Poisson's ratio. In addition, the results based on Donnell's equations correspond to dead pressure loads, whereas those based on Sanders' equations are for live pressure loads.

The results in Tables 55 and 56 show differences less than 0.1% in the nondimensional buckling pressures obtained in the present study and in references 50 and 51 by using Donnell's equations. Additionally, the results of the present study obtained by using Sanders' equations indicate that neglecting the nonlinear rotations about the normal yields differences in the buckling loads that are less than approximately 5%. Similarly, the differences between corresponding buckling loads obtained by using Sanders' and Donnell's equations are less than approximately 6%.

The differences in the buckling resistance predictions obtained in the present study by using Donnell's equations (red curves), Sanders equations with dead pressure (blue curves), and Sanders equations with live pressure (black curves) are illustrated in figures 95-109 for stringer-stiffened and for ring-stiffened cylinders with radius-to-thickness ratios R/h =50 and 500, with Poisson's ratio $\nu = 0.30$, and with Young's modulus $E = 10.0 \times 10^6$ psi. The buckling resistance is measured by the nondimensional pressure $\frac{p^{cr}R^3}{D}$ for values of 0.2 ≤ L/R ≤ 50. In calculating these results, the circumferential wave numbers n = 0 and n = 1 were not used. These two wave

numbers correspond to axisymmetric deformation modes and column-buckling modes that are inconsistent with the presence of only uniform external pressure loads.

For the baseline stringer-configuration given by $\frac{E_sA_s}{d_sA} = 1$, $\frac{E_sI_s^c}{d_sD} = 1$, $\frac{G_sJ_s}{2d_s(1-\nu)D} = 0$, and $\frac{e_s}{h} = 0$ and shown in figure 95 for the cylinders with R/h = 50, the differences between the corresponding results predicted by Donnell's and Sanders' equations with live pressure, and between the two sets of Sanders' equations, are less than about 6% for $L/R \le 5$. For $5 < L/R < 12$, differences are large as 12% are found. As L/R increase beyond 12, the curves obtained by using Donnell's equations and by using Sanders' equations with dead pressure asymptotically approach the value $\frac{p^{cr}R^3}{D} = 4$, which is the asymptotic value of the corresponding unstiffened cylinder. In contrast, the curve obtained by using Sanders' equations with live pressure asymptotically approaches the value $\frac{p^{cr}R^3}{D} = 3$, which is also the asymptotic value of the corresponding unstiffened cylinder. These asymptotic results correspond to a maximum difference of 33% and to the $m = 1$ and $n = 2$ flattened-cylinder buckling mode illustrated in figure 95. It is noteworthy that overall, Donnell's equations tend to predict buckling pressures that are closer to the corresponding results predicted by Sanders' equations with live pressure.

Results were also obtained in the present study for stringer-stiffened cylinders with R/h = 50 and with the baseline configuration modified as follows. First, curves similar to those shown in figure 95 were obtained in which the value $\frac{E_sA_s}{d_sA} = 2$ was used with the baseline set of parameters. Then, seven similar sets of curves were obtained by modifying the baseline set of parameters such that $\frac{E_sI_s^c}{d_sD} = 10$, $\frac{G_sJ_s}{2d_s(1-\nu)D} = 1$ and 10, and $\frac{e_s}{h}$ = -1, 1, -10, and 10. For all sets of curve obtained, the plots were very similar to those shown in figure 95, including the asymptotic behavior of the curves for large values of L/R. Thus, it appears that the stringer configuration has a relatively small effect on the buckling pressure, likely due to the pressure load producing only circumferential compression prior to buckling. As a result of this similarity, the differences between the corresponding results predicted by Donnell's and Sanders' equations with live pressure, and between the two sets of Sanders' equations for the eight additional sets of curves not shown herein are similar to those exhibited by the curves shown in figure 95.

Results for the baseline stringer-configuration given by $\frac{E_sA_s}{d_sA} = 1$, $\frac{E_sI_s^c}{d_sD} = 1$, $\frac{G_sJ_s}{2d_s(1-\nu)D} = 0$, and $\frac{e_s}{h} = 0$ are shown in figure 96 for stringer-stiffened cylinders with R/h = 500. For these cylinders, the differences between the corresponding results predicted by Donnell's and Sanders' equations with live pressure, and between the two sets of Sanders' equations, are less than about 5% for approximately $L/R \le 10$. For approximately $10 < L/R \le 18$, the differences are less than 8%, and for $18 < L/R \le 38$, the differences are less than 12%. In the range $L/R > 38$, differences are large as 33% are found.

Results were also obtained in the present study for stringer-stiffened cylinders with R/h =500 and with the baseline configuration modified in the same way as described for the cylinders with R/h = 50. Specifically, curves similar to those shown in figure 96 were obtained in which the value $\frac{E_s A_s}{d_s A} = 2$ was used with the rest of the baseline parameters fixed. Additionally, seven similar sets of curves were obtained by modifying the baseline set of parameters such that $\frac{E_s I_s^c}{d_s D} = 10$, $\frac{G_s J_s}{2d_s(1-\nu)D} = 1$ and 10, and $\frac{e_s}{h}$ = -1, 1, -10, and 10. For all sets of curve obtained, the plots were very similar to those shown in figure 96. As a result of this similarity, the differences between the corresponding results predicted by Donnell's and Sanders' equations with live pressure, and between the two sets of Sanders' equations for the eight additional sets of curves not shown herein are similar to those exhibited by the curves shown in figure 96.

Results for cylinders with R/h = 50 and with the baseline ring-configuration given by $\frac{E_r A_r}{d_r A} = 1$, $\frac{E_r I_r^e}{d_r D} = 1$, $\frac{G_r J_r}{2d_r(1-\nu)D} = 0$, and $\frac{e_r}{h} = 0$ are shown in figure 97. The differences between the corresponding results predicted by Donnell's and Sanders' equations, and between the two sets of Sanders' equations, are less than 6% for L/R < 3. For $3 \le L/R < 8$, differences are large as 12% are found. As L/R increase beyond 8, the curves obtained by using Donnell's equations and by using Sanders' equations with dead pressure asymptotically approach the value $\frac{p^{cr} R^3}{D} = 8$. In contrast, the curve obtained by using Sanders' equations with live pressure asymptotically approaches the value $\frac{p^{cr} R^3}{D} = 6$. These asymptotic results also correspond to a maximum difference of 33% and to the $m = 1$ and $n = 2$ flattened-cylinder buckling mode illustrated in figure 97. Like for the stringer-stiffened cylinders, Donnell's equations tend to predict buckling pressures for the ring-stiffened cylinders that are closer to the corresponding results predicted by Sanders' equations with live pressure.

Results similar to those shown in figure 97 were obtained for cylinders with R/h = 50 and with the baseline ring-configuration modified such that $\frac{E_r A_r}{d_r A} = 2$. Likewise, results were also obtained for cylinders with R/h = 50 and with the baseline ring-configuration modified such that $\frac{G_r J_r}{2d_r(1-\nu)D} = 1$. Both sets of results exhibit practically the same buckling predictions, relative differences, and asymptotic responses as the baseline case shown in figure 97. Results for R/h = 50 and the baseline ring-configuration modified such that $\frac{G_r J_r}{2d_r(1-\nu)D} = 10$ are shown in figure 98. These results vary slightly from the corresponding baseline results and exhibit nearly the same relatives differences and asymptotic responses.

In contrast, results are presented in figure 99, for cylinders with R/h = 50 and with the

baseline ring-configuration modified such that $\frac{E_r I_r^c}{d_r D} = 10$, that show large increases in the predicted buckling pressures, compared to the corresponding baseline results. For this ring configuration, differences between the corresponding results predicted by Donnell's and Sanders' equations, and between the two sets of Sanders' equations, are less than 6% for $L/R < 2$. For $2 \leq L/R < 6$, differences are large as 12% are found. As L/R increases beyond 6, the curves obtained by using Donnell's equations and by using Sanders' equations with dead pressure asymptotically approach the value $\frac{p^{cr}R^3}{D} = 44$, whereas, the curve obtained by using Sanders' equations with live pressure asymptotically approaches the value $\frac{p^{cr}R^3}{D} = 33$. Results similar to those shown in figure 99 were obtained for cylinders with R/h = 50 and with the baseline ring-configuration modified such that $e_r/h = 1$ and - 1, and are shown in figures 100 and 101, respectively. These results for eccentric rings vary in magnitude somewhat from the corresponding results in figure 99 but exhibit nearly the same relatives differences. For the cylinders with $e_r/h = 1$, the curves obtained by using Donnell's equations and by using Sanders' equations with dead pressure asymptotically approach the value $\frac{p^{cr}R^3}{D} = 30$, whereas, the curve obtained by using Sanders' equations with live pressure asymptotically approaches the value $\frac{p^{cr}R^3}{D} = 22$. Moreover, at $L/R \leq 50$, the $m = 1$ and $n = 2$ flattened-cylinder buckling mode is absent from the responses. For the cylinders with $e_r/h = - 1$, the curves obtained by using Donnell's equations and by using Sanders' equations with dead pressure asymptotically approach the value $\frac{p^{cr}R^3}{D} = 32$, whereas, the curve obtained by using Sanders' equations with live pressure asymptotically approaches the value $\frac{p^{cr}R^3}{D} = 24$. For this ring configuration, the $m = 1$ and $n = 2$ flattened-cylinder buckling modes occur for approximately $L/R \geq 7$.

Results are presented in figure 102 for cylinders with R/h = 50 and with the baseline ring-configuration modified such that $e_r/h = 10$. The results show massive increases in the predicted buckling pressures with ring eccentricity, compared to the corresponding baseline results. For this ring configuration, the differences between the corresponding results predicted by Donnell's and Sanders' equations are as much as about 30% for $L/R < 2$. As L/R increase beyond 2, the differences increase to about 60%. The differences between the corresponding results predicted by the two sets of Sanders' equations are as much as about 19% for $L/R < 2$, and as L/R increase beyond 2, the differences increase to about 50%. In addition, the curves obtained by using Donnell's equations, by using Sanders' equations with dead pressure, and by using Sanders' equations with live pressure asymptotically approach the values $\frac{p^{cr}R^3}{D} = 2295$, 2132, and 1426, respectively.

Results are presented in figure 103 for cylinders with R/h = 50 and with the baseline ring-

configuration modified such that $e_r/h = -10$. These results also show massive increases in the predicted buckling pressures with ring eccentricity, compared to the corresponding baseline results. The differences between the corresponding results predicted by Donnell's and Sanders' equations, and between the two sets of Sanders' equations, are for the most part less than 10% for $2 \le L/R \le 50$. However, for $L/R < 2$, differences are large as about 14% are found. As L/R approaches 50, the curves obtained by using Donnell's equations and by using Sanders' equations with dead pressure asymptotically approach the value $\frac{p^{cr}R^3}{D} = 2408$. The curve obtained by using Sanders' equations with live pressure asymptotically approaches the value $\frac{p^{cr}R^3}{D} = 2202$. These asymptotic results also correspond to the $m = 1$ and $n = 2$ flattened-cylinder buckling mode.

Results for cylinders with $R/h = 500$ and with the baseline ring-configuration given by $\frac{E_rA_r}{d_rA} = 1$, $\frac{E_rI_r^c}{d_rD} = 1$, $\frac{G_rJ_r}{2d_r(1-\nu)D} = 0$, and $\frac{e_r}{h} = 0$ are shown in figure 104. The differences between the corresponding results predicted by Donnell's and Sanders' equations, and between the two sets of Sanders' equations, are less than about 6% for $L/R \le 12$. For $12 < L/R \le 26$, the differences are less than approximately 12%. As L/R increases beyond 26, differences are large as about 33% are found. Additionally, the results shown in figure 104 correspond to the $m = 1$ and $n = 2$ flattened-cylinder buckling mode for values of approximately $30 < L/R \le 50$. Additional calculations were made for $L/R \ge 500$ that revealed the curves obtained by using Donnell's equations and by using Sanders' equations with dead pressure asymptotically approach the value $\frac{p^{cr}R^3}{D} = 8$. Similarly, the curve obtained by using Sanders' equations with live pressure asymptotically approaches the value $\frac{p^{cr}R^3}{D} = 6$.

Results similar to those shown in figure 104 were obtained for cylinders with $R/h = 500$ and with the baseline ring-configuration modified such that $\frac{E_rA_r}{d_rA} = 2$. Likewise, results were also obtained for cylinders with $R/h = 500$ and with the baseline ring-configuration modified such that $\frac{G_rJ_r}{2d_r(1-\nu)D} = 1$ and 10. All three sets of results exhibit practically the same buckling predictions, relative differences, and asymptotic responses as the baseline case shown in figure 104. In contrast, results are presented in figure 105, for cylinders with $R/h = 500$ and with the baseline ring-configuration modified such that $\frac{E_rI_r^c}{d_rD} = 10$ that exhibit a different trend. That is, these results exhibit greater predicted buckling pressures, compared to the corresponding baseline results of figure 104. For this ring configuration, differences between the corresponding results predicted by Donnell's and Sanders' equations, and between the two sets of Sanders' equations, are less than approximately 7% for $L/R \le 8$. For $8 < L/R < 18$, differences are large as 14% are found. As L/R increase beyond 18, the curves obtained by using Donnell's equations and by using Sanders' equations with dead pressure asymptotically approach the value $\frac{p^{cr}R^3}{D} = 44$, whereas, the

curve obtained by using Sanders' equations with live pressure asymptotically approaches the value $\frac{p^{cr}R^3}{D} = 33$.

Results similar to those shown in figure 105 were obtained for cylinders with $R/h = 500$ and with the baseline ring-configuration modified such that $e_r/h = 1$ and -1 and are shown in figures 106 and 107, respectively. These results for cylinders with eccentric rings vary in magnitude somewhat from the corresponding results in figure 105 but exhibit nearly the same relatives differences. For the cylinders with $e_r/h = 1$, the curves obtained by using Donnell's equations and by using Sanders' equations with dead pressure asymptotically approach the value $\frac{p^{cr}R^3}{D} = 30.9$, whereas, the curve obtained by using Sanders' equations with live pressure asymptotically approaches the value $\frac{p^{cr}R^3}{D} = 23.1$. These asymptotic values do not correspond to the $m = 1$ and $n = 2$ flattened-cylinder buckling mode for very large values of L/R. For the cylinders with $e_r/h = -1$, the curves obtained by using Donnell's equations and by using Sanders' equations with dead pressure asymptotically approach the value $\frac{p^{cr}R^3}{D} = 32$, whereas, the curve obtained by using Sanders' equations with live pressure asymptotically approaches the value $\frac{p^{cr}R^3}{D} = 24$. For this case, the asymptotic values do correspond to the $m = 1$ and $n = 2$ flattened-cylinder buckling mode.

Results are presented in figure 108 for cylinders with $R/h = 500$ and with the baseline ring-configuration modified such that $e_r/h = 10$. The results show massive increases in the predicted buckling pressures with ring eccentricity, compared to the corresponding baseline results shown in figure 104. For this ring configuration, the differences between the corresponding results predicted by Donnell's and Sanders' equations are as much as about 10% for approximately $L/R < 4$. As L/R increase beyond 4, the differences increase to about 35%. The differences between the corresponding results predicted by the two sets of Sanders' equations are as much as about 13% for $L/R < 4$, and as L/R increase beyond 4, the differences increase to about 34%. In addition, the curves obtained by using Donnell's equations, by using Sanders' equations with dead pressure, and by using Sanders' equations with live pressure asymptotically approach the values $\frac{p^{cr}R^3}{D} = 2295$, 2285, and 1691, respectively. These asymptotic values do not correspond to the $m = 1$ and $n = 2$ flattened-cylinder buckling mode.

Results are presented in figure 109 for cylinders with $R/h = 500$ and with the baseline ring-configuration modified such that $e_r/h = -10$. These results also show massive increases in the predicted buckling pressures with ring eccentricity, compared to the corresponding baseline results. The differences between the corresponding results predicted by Donnell's and Sanders' equations, and between the two sets of Sanders' equations, are for the most part less than 10% for $0.2 \le L/R \le 6$. However, for $L/R > 6$, differences are large as about 30% are found. As L/R approaches 50, the curves obtained by using Donnell's equations and by using Sanders' equations

with dead pressure asymptotically approach the value $\frac{p^{cr}R^3}{D} = 2408$. The curve obtained by using Sanders' equations with live pressure asymptotically approaches the value $\frac{p^{cr}R^3}{D} = 1842$. These asymptotic results correspond to the $m = 1$ and $n = 2$ flattened-cylinder buckling mode.

The results in figures 95 and 96, and other results obtained in the present study, indicate that the stringer properties have no effect on the asymptotic response of the cylinders loaded by uniform external pressure. In contrast, the results in figures 97-109, and other results obtained in the present study, show that the ring properties have a significant effect. Moreover, the results indicate that the asymptotic results correspond to the $m = 1$ and $n = 2$ flattened-cylinder buckling mode in almost all cases. The exceptions are for cylinders with external eccentric rings (see figures 100, 102, 106, and 108). A closed-form expression for the asymptotic response of extremely long cylinders that buckle into the $m = 1$ and $n = 2$ flattening modes, based on Sanders' equations with live pressure, was obtained in the present study as follows. First, the cylinder length L is expressed as $L = R/å$, such that $å \rightarrow 0$ as $L/R \rightarrow \infty$. Next, $L = R/å$ is substituted into equations (83) to eliminate L from equation (82). Equation (82) is then multiplied through by the largest power of $å$ appearing in any of its denominators. Then, the limit of equation (82) is found as $å \rightarrow 0$ and the resulting equation is solved for the loading parameter. This process yields

$$\frac{p_{\infty}^{cr} R^3}{\sqrt{D_{11}D_{22}}} = 3 \sqrt{\frac{D_{22}}{D_{11}}} \left(\frac{1 - \frac{B_{22}^2}{A_{22}D_{22}}}{1 + \frac{2B_{22}}{A_{22}R} + \frac{D_{22}}{A_{22}R^2}} \right) \tag{142}$$

where the stiffness terms are given by equations (134). For a monocoque isotropic cylinder, this equation reduces to

$$\frac{p_{\infty}^{cr} R^3}{D} = 3\left(1 + \frac{h^2}{12R^2} \right)^{-1} \tag{143}$$

For Donnell's equations, and for Sanders' equations with dead pressure, this process yields

$$\frac{p_{\infty}^{cr} R^3}{\sqrt{D_{11}D_{22}}} = 4 \sqrt{\frac{D_{22}}{D_{11}}} \left(1 - \frac{B_{22}^2}{A_{22}D_{22}} \right) \tag{144}$$

Equations (142) and (144) yield results that are in exact agreement with the corresponding asymptotic results presented herein except for the cylinders with eccentric external rings. For these exceptions, differences are expected since they did not buckle into the $m = 1$ and $n = 2$ flattened-cylinder mode. With one exception, the differences in the corresponding asymptotic results obtained by using Donnell's equations, Sanders' equations with dead pressure, Sanders' equations with live pressure, and equations (142) and (144) are less than approximately 5%. A difference of 13% was found between the result predicted by Sanders' equations with dead

pressure and equation (144) for the cylinder with $R/h = 50$ and $e_r/h = 10$.

Uniform hydrostatic pressure loads. Results for ring-stiffened isotropic cylinders subjected to uniform hydrostatic pressure are presented in Tables 57 and 58 for selected values of the radius-to-thickness ratios $50 \le R/h \le 2000$ and the length-to-radius ratio $0.4 \le L/R \le 10$. Specifically, the predicted values of the nondimensional buckling pressure $\frac{p^{cr}R^3}{D}$ obtained by Singer, Baruch, and Harari[50, 51] and obtained in the present study are shown for cylinders with the generic ring properties are given by $\frac{A_r}{d_r h} = 0.5$, $\frac{I_r^c}{d_r h^3} = 5,$ and $J_r = 0$, where A_r is the cross-sectional area, d_r is the ring spacing, I_r^c is the centroidal moment of inertia, and J_r is the torsion constant. Moreover, the results in Table 57 and 58 are for cylinders with $e_r/h = +0.5$ (outward) and -0.5 (inward), respectively. In addition, the results based on Donnell's equations correspond to dead pressure loads, whereas those based on Sanders' equations are for live pressure loads. The results in these tables show differences less than 0.1% in the nondimensional buckling pressures obtained in the present study and in references 50 and 51 by using Donnell's equations, and in many cases are in complete agreement. Additionally, the results of the present study obtained by using Sanders' equations indicate that neglecting the nonlinear rotations about the normal yields differences in the buckling loads that are less than approximately 2%. Similarly, the differences between corresponding buckling loads obtained by using Sanders' and Donnell's equations are less than approximately 6%, and in many cases are less than 2%.

Results are presented in Table 59 that show the predicted values of the nondimensional buckling pressure $\frac{p^{cr}R^3}{D}$ obtained by Singer, Baruch, and Harari[50, 51] and obtained in the present study for generic stringer-stiffened isotropic cylinders, for a moderate range of cylinder geometries. In particular, results are given for length-to-radius ratios $0.5 \le L/R \le 3$ and for radius-to-thickness ratios in the range $50 \le R/h \le 2000$. The generic stringer properties are given by $\frac{A_s}{d_s h} = 0.5$, $\frac{I_s^c}{d_s h^3} = 5,$ and $J_s = 0$, where A_s is the cross-sectional area, d_s is the stringer spacing, I_s^c is the centroidal moment of inertia, and J_s is the torsion constant. Additionally, results are given for cylinders with either external or internal stringers having the eccentricities $e_s/h = +5$ and -5, respectively. Moreover, the results based on Donnell's equations correspond to dead pressure loads and those based on Sanders' equations are for live pressure loads. The results in this table also show differences less than 0.1% in the nondimensional buckling pressures obtained in the present study and in references 50 and 51 by using Donnell's equations. Additionally, the results of the present study obtained by using Sanders' equations indicate that neglecting the nonlinear rotations about the normal yields differences in the buckling loads that are less than approximately 2%. Similarly, the differences between corresponding buckling loads obtained by using Sanders' and Donnell's equations are less than approximately 1%.

The effects of variations in the ring section properties on the nondimensional buckling

pressure $\frac{p^{cr}R^3}{D}$ obtained by Singer, Baruch, and Harari[51] and obtained in the present study for generic ring-stiffened isotropic cylinders with $L/R = 0.5$ and $100 \le R/h \le 2000$ are presented in Tables 60 and 61 for eccentricities $e_r/h = +5$ and -5, respectively. The ranges of the ring section properties are given by $0.05 \le \frac{A_r}{d_r h} \le 0.8$ and $0.5 \le \frac{I_r^c}{d_r h^3} \le 8$. In addition, the results based on Donnell's equations correspond to dead pressure loads, whereas those based on Sanders' equations are for live pressure loads. The results in these tables show differences less than 0.1% in the nondimensional buckling pressures obtained in the present study and in reference 51 by using Donnell's equations, and in many cases are in complete agreement. Additionally, the results of the present study obtained by using Sanders' equations indicate that neglecting the nonlinear rotations about the normal yields differences in the buckling loads that are less than 1%. Likewise, the differences between corresponding buckling loads obtained by using Sanders' and Donnell's equations are less than 1%.

Results for the same section-property variations, radius-to-thickness ratios, and ring eccentricities used to generate Tables 60 and 61 are presented in Tables 62 and 63 for ring-stiffened isotropic cylinders with $L/R = 1$. Additionally, similar results are presented in Table 64 for ring-stiffened isotropic cylinders with $L/R = 2$ and $R/h = 1000$. For each table, the results based on Sanders' equations are for live pressure loads. The results in these three tables show identical predictions of the nondimensional buckling pressures obtained in the present study and in reference 51 by using Donnell's equations in almost every case. One notable exception appears in the last row Table 62, which corresponds to a 9% difference.Additionally, the results of the present study obtained by using Sanders' equations indicate that neglecting the nonlinear rotations about the normal yields differences in the buckling loads that are less than 3%, and in most cases less than 1%. Likewise, the differences between corresponding buckling loads obtained by using Sanders' and Donnell's equations are less than 5%, and in most cases less than 1%.

The effects of variations in the ring eccentricity on the nondimensional buckling pressure $\frac{p^{cr}R^3}{D}$ obtained by Singer, Baruch, and Harari[51] and obtained in the present study for generic ring-stiffened isotropic cylinders with $L/R = 0.5$ and with $R/h = 100$ and 1500 are presented in Table 65. Moreover, results are presented for selected values of the ring eccentricity given by $-8 \le e_r/h \le 8$. The ring section properties are given by $\frac{A_r}{d_r h} = 0.5$, $\frac{I_r^c}{d_r h^3} = 5$, and $J_r = 0$. In addition, the results based on Donnell's equations correspond to dead pressure loads, whereas those based on Sanders' equations are for live pressure loads. The results in this table show differences less than 0.1% in the nondimensional buckling pressures obtained in the present study and in reference 51 by using Donnell's equations, and in many cases are in complete agreement. In addition, the results of the present study obtained by using Sanders' equations indicate that neglecting the nonlinear rotations about the normal yields differences in the buckling loads that are less than 1%. Likewise, the differences between corresponding buckling loads obtained by using Sanders' and Donnell's equations are less than 1%.

Results similar to those given in Table 65 are presented in Table 66 for $L/R = 1$ and $50 \le R/h \le 2000$, and in Table 67 for $L/R = 2$ and $R/h = 1000$. The results in these tables show no differences in the nondimensional buckling pressures obtained in the present study and in reference 51 by using Donnell's equations, except for two cases which exhibit differences less than 0.1%. In addition, the results of the present study obtained by using Sanders' equations indicate that neglecting the nonlinear rotations about the normal yields differences in the buckling loads that are less than 1%, and in many cases much smaller. Likewise, the differences between corresponding buckling loads obtained by using Sanders' and Donnell's equations are less than 2%, and in many cases much smaller.

The combined effects of variations in the ring eccentricity and ring section properties on the nondimensional buckling pressure $\frac{p^{cr}R^3}{D}$ obtained by Singer, Baruch, and Harari[51] and obtained in the present study for generic ring-stiffened isotropic cylinders with $L/R = 1$ and for $R/h = 700$, 800, and 900 are presented in Table 68. The ranges of the stiffener section properties are given by $0.1 \le \frac{A_r}{d_r h} \le 0.8$ and $1 \le \frac{I_r^c}{d_r h^3} \le 8.$ Moreover, $J_r = 0$ and the ring eccentricity given by $-8 \le e_r/h \le 8$. In addition, the results based on Donnell's equations correspond to dead pressure loads, whereas those based on Sanders' equations are for live pressure loads. The results in this table also show differences less than 0.1% in the nondimensional buckling pressures obtained in the present study and in reference 51 by using Donnell's equations, and in many cases are in complete agreement. In addition, the results of the present study obtained by using Sanders' equations indicate that neglecting the nonlinear rotations about the normal yields differences in the buckling loads that are less than 1%. Likewise, the differences between corresponding buckling loads obtained by using Sanders' and Donnell's equations are less than 1%.

The effects of length-to-radius ratio L/R, for the range $0.5 \le L/R \le 3$, on the nondimensional buckling pressure $\frac{p^{cr}R^3}{D}$ obtained by Singer, Baruch, and Harari[51] and obtained in the present study for generic ring-stiffened isotropic cylinders are presented in Tables 69-71 for selected values of $500 \le R/h \le 200$. The results in Table 69 and 71 are for $\frac{A_r}{d_r h} = 0.5$, $\frac{I_r^c}{d_r h^3} = 5$, and for $e_r/h = \pm 8$ and ± 1, respectively. The results in Table 70 are for $\frac{A_r}{d_r h} = 0.8$, $\frac{I_r^c}{d_r h^3} = 8$, and $e_r/h = \pm 5$. For all three tables, the results are based on $J_r = 0$. For both tables, the results based on Donnell's equations correspond to dead pressure loads and those based on Sanders' equations are for live pressure loads.

The results in Tables 69-71 also show differences less than 0.1% in the nondimensional buckling pressures obtained in the present study and in reference 51 by using Donnell's equations, and in many cases are in complete agreement. In addition, the results of the present study obtained by using Sanders' equations indicate that neglecting the nonlinear rotations about the normal yields differences in the buckling loads that are less than approximately 1%. The differences between corresponding buckling loads obtained by using Sanders' and Donnell's equations are

less than 5%, and in many cases less than 1%.

Results are presented in Tables 72 and 73 that show the predicted values of the nondimensional buckling pressure $\frac{p^{cr}R^3}{D}$ obtained by Baruch and Singer[67] and obtained in the present study for isotropic cylinders stiffened by either stringers, rings, or rings and stringers. These results correspond to some very specific cylinder configurations. In particular, the results in Table 72 correspond to the wall thickness h = 0.1 in., R/h = 9.78761, L/R = 4.5391, and the stiffener spacings $d_s/R = d_r/R = 0.3360$. Moreover, one set of results appears in Table 72 for the stiffener properties $\frac{A_s}{d_s h} = \frac{A_r}{d_r h} = 0.1471$ and $\frac{12\, I_s^c}{d_s h^3} = \frac{12\, I_r^c}{d_r h^3} = 0.7819$, and stiffener eccentricites equal to ± 1.653. A second set appears for stringer-stiffened cylinders $\frac{A_s}{d_s h} = 0.2948$, $\frac{12\, I_s^c}{d_s h^3} = 6.330$, and $e_s/h = \pm 2.817$. The results in Table 73 correspond to the wall thickness h = 0.1 in., R/h = 9.79912, L/R = 4.5384, and the stiffener spacings $d_s/R = d_r/R = 0.3350$. The stiffener properties are given by $\frac{A_s}{d_s h} = \frac{A_r}{d_r h} = 0.2948$ and $\frac{12\, I_s^c}{d_s h^3} = \frac{12\, I_r^c}{d_r h^3} = 6.330$, and the stiffener eccentricites are equal to ± 2.817. For both tables, the results based on Donnell's equations correspond to dead pressure loads and those based on Sanders' equations are for live pressure loads.

The results in Tables 72 and 73 show differences less than approximately 0.5% in the nondimensional buckling pressures obtained in the present study and in reference 67 by using Donnell's equations. In addition, the results of the present study obtained by using Sanders' equations indicate that neglecting the nonlinear rotations about the normal yields differences in the buckling loads that are less than approximately 1%. The differences between corresponding buckling loads obtained by using Sanders' and Donnell's equations are between 2% and 5% for the cylinders properties in Table 72, and between approximately 3% and 13% for the cylinders properties in Table 73.

Results are presented in Table 74 that show the predicted buckling pressure obtained by McElman, Mikulas, and Stein[68] and obtained in the present study for isotropic cylinders stiffened by either stringers, rings, or rings and stringers. These results correspond to cylinder configurations with blade stiffeners. The cylinders have a wall thickness h = 0.028 in., a midsurface radius R = 9.55 in., and lengths L = 12, 24, 36, and 48 in. The length of 48 in. as reported as 60 in. in reference 69 and appears to be a mistake. The ring and stringer blades, have a thickness of 0.096 in., a height of 0.302 in., and are spaced 1.0 in. apart, on center. Moreover, the stiffeners are attached to either the inside or the outside of the cylinder, which corresponds to an eccentricity magnitude of 0.165 in. The torsional stiffness used in the calculations is given by one-third of the blade thickness cubed times the blade height. Additionally, the results based on Donnell's equations correspond to dead pressure loads and those based on Sanders' equations are for live pressure loads.

The results in Table 74 show differences less than approximately 6%, and less than 1% in most cases, in the nondimensional buckling pressures obtained in the present study and in

reference 68, by using Donnell's equations, with two curious exceptions. Specifically, for the two cylinders with $L = 12$ in. and no stringers, the differences are approximately 33% and 53%. In addition, the results of the present study obtained by using Sanders' equations indicate that neglecting the nonlinear rotations about the normal yields differences in the buckling loads that are less than approximately 2%. The differences between corresponding buckling loads obtained by using Sanders' and Donnell's equations increase with the cylinder length and are as large as approximately 14% for the cylinders with $L = 48$ in.

Results are presented in Table 75 that show the predicted values of the nondimensional buckling pressure $\frac{p^{cr}R}{Eh}\left(1-\nu^2\right)$ obtained by Tian et.al.[69] and obtained in the present study for isotropic cylinders stiffened by either internal or external blade-shaped rings. For these cylinders, $E = 10.0 \times 10^6$ psi, $\nu = 0.30$, and $R/h = 100$. The ring properties are given by $\frac{A_r}{d_r h} = 0.16384$, $\frac{I_r^c}{d_r h^3} = 1.01152$, and $J_r = 0$. The ring spacing is given by $d_r/R = 0.3$ and satisfies the relation $(N + 1)d_r/R = L/R$, where N is the number of rings. The ring eccentricities are given by $e_r/h = \pm 6.2633$.

The results in Table 75 show differences less than approximately 7% in the nondimensional buckling pressures obtained in the present study by using Sanders' equations with live pressure and in reference 69 by using a variant of Sanders' equations. In addition, the results of the present study obtained by using Sanders' equations with live pressure indicate that neglecting the nonlinear rotations about the normal yields differences in the buckling loads that are less than approximately 3%. The differences between corresponding buckling loads obtained by using Sanders' with live pressure and Donnell's equations with dead pressure are between approximately 3% and 34%.

The differences in the buckling resistance predictions obtained in the present study by using Donnell's equations (red curves), Sanders equations with dead pressure (blue curves), and Sanders equations with live pressure (black curves) are illustrated in figures 110-115 for stringer-stiffened and for ring-stiffened cylinders with radius-to-thickness ratios $R/h = 50$ and 500, with Poisson's ratio $\nu = 0.30$, and with Young's modulus $E = 10.0 \times 10^6$ psi. The buckling resistance is measured by the nondimensional pressure $\frac{p^{cr}R^3}{D}$ for values of $0.2 \le L/R \le 50$. In calculating these results, the circumferential wave numbers $n = 0$ and $n = 1$ were used due to the presence of axial compression. For the baseline stringer-configuration given by $\frac{E_s A_s}{d_s A} = 1$, $\frac{E_s I_s^c}{d_s D} = 1$, $\frac{G_s J_s}{2d_s(1-\nu)D} = 0$, and $\frac{e_s}{h} = 0$ and shown in figure 110 for the cylinders with $R/h = 50$, the blue and black response curves are practically identical to the corresponding curves shown in figure 95 for the corresponding cylinders subjected to uniform external pressure. Moreover, the red curves shown in figures 95 and 110 are practically identical for values of approximately $L/R < 36.5$. For larger values of L/R, the red curve obtained by using Donnell's equations deviates from the asymptotic response to a column-buckling mode ($m = n = 1$). It was also found that eliminating

the circumferential wave numbers $n = 0$ and $n = 1$ in the calculations based on Donnell's equations produced a red curve that is practically identical to the corresponding curve shown in figure 95 for uniform external pressure loads. By substituting $N^{cr}_{x,\,Euler} = \frac{p^{cr}R}{2}$ into equation (140), it is found that the column-like buckling modes are given by

$$\frac{p^{cr}R^3}{D} = \frac{12\pi^2R^4}{L^2h^2}\left[1 - \nu^2 + \frac{E_sA_s}{Ad_s}\left(1 + \frac{e_s}{R}\right)^2\right] \tag{145}$$

Results obtained by using this equation indicate that the branch of the red curve ($L/R \geq 36.5$) given by $m = n = 1$ does not correspond to the actual column-like buckling mode. Moreover, the results obtained by using Sander's equations indicate that the $m = n = 1$ solutions are erroneous.

Like for the cylinders loaded by external pressure, the differences between the corresponding results predicted by Donnell's and Sanders' equations with live hydrostatic pressure, and between the two sets of Sanders' equations, are also less than about 6% for $L/R \leq 5$. For $5 < L/R < 12$, differences are large as 12% are found. As L/R increase beyond 12, the curves obtained by using Sanders' equations with dead pressure asymptotically approach the value $\frac{p^{cr}R^3}{D} = 4$, which is the asymptotic value of the corresponding unstiffened cylinder. Additionally, the curve obtained by using Sanders' equations with live pressure asymptotically approaches the value $\frac{p^{cr}R^3}{D} = 3$, which is also the asymptotic value of the corresponding unstiffened cylinder. These asymptotic results correspond to a maximum difference of 33% and to the $m = 1$ and $n = 2$ flattened-cylinder buckling mode illustrated in figure 95.

Results were also obtained in the present study for stringer-stiffened cylinders with R/h =50 and with the various modified baseline configurations considered for the cylinders loaded by uniform external pressure. Specifically, eight additional sets of curves were obtained by modifying the baseline set of parameters such that $\frac{E_sA_s}{d_sA} = 2$, $\frac{E_sI^c_s}{d_sD} = 10$, $\frac{G_sJ_s}{2d_s(1-\nu)D} = 1$ and 10, and $\frac{e_s}{h}$ = -1, 1, -10, and 10. For each set of curves obtained by using Sanders' equations (blue and black curves), the plots were practically identical to the corresponding plots for the cylinders loaded by uniform external pressure, including the asymptotic behavior of the curves for large values of L/R. The corresponding red curves were also practically identical for the values of L/R with $m \neq n \neq 1$, like that shown in figure 110 for values of approximately $L/R < 37$. Thus, it appears that the stringer configuration also has a relatively small effect on the hydrostatic buckling pressure of the relatively long cylinders.

Results for the baseline stringer-configuration and the eight modifications were also obtained for stringer-stiffened cylinders with R/h = 500. For every stringer configuration, the response curves are practically identical to the response curves obtained for the corresponding cylinders loaded by uniform external pressure.

Results for cylinders with R/h = 50 and with the baseline ring-configuration given by $\frac{E_r A_r}{d_r A} = 1$, $\frac{E_r I_r^c}{d_r D} = 1$, $\frac{G_r J_r}{2d_r(1-\nu)D} = 0$, and $\frac{e_r}{h} = 0$ are shown in figure 111. The blue and black response curves are practically identical to the corresponding curves shown in figure 97 for the corresponding cylinders subjected to uniform external pressure. Moreover, the red curves shown in figures 97 and 111 are practically identical for values of approximately L/R < 25.8. For larger values of L/R, the red curve obtained by using Donnell's equations deviates from the asymptotic response to a column-buckling mode (m = n = 1). It was also found that eliminating the circumferential wave numbers n = 0 and n = 1 in the calculations based on Donnell's equations produced a red curve that is practically identical to the corresponding curve shown in figure 97 for uniform external pressure loads. By substituting $N^{cr}_{x,\,Euler} = \frac{p^{cr}R}{2}$ into equation (141), it is found that the column-like buckling modes are given by

$$\frac{p^{cr}R^3}{D} = \frac{12\pi^2 R^4}{L^2 h^2}\left(1-\nu^2\right) \tag{146}$$

Results obtained by using this equation indicate that the branch of the red curve (L/R ≥ 25.8) given by m = n = 1 does not correspond to a column-like buckling mode. Moreover, the results obtained by using Sander's equations indicate that the m = n = 1 solutions are erroneous.

Results similar to those shown in figure111 were obtained for cylinders with R/h = 50 and with the baseline ring-configuration modified such that $\frac{E_r A_r}{d_r A} = 2$. Likewise, results were also obtained for cylinders with R/h = 50 and with the baseline ring-configuration modified such that $\frac{E_r I_r^c}{d_r D} = 10$, $\frac{G_r J_r}{2d_r(1-\nu)D} = 1$, $\frac{G_r J_r}{2d_r(1-\nu)D} = 10$, $e_r/h = 1$, and $e_r/h = -1$. For each of these six cases, curves that are practically identical to to corresponding curves for external-pressure-loaded cylinders were obtained for the results based on Sanders' equations. Moreover, practically identical curves were obtained for the results based on Donnell's equations when the m = n = 1 solutions are omitted.

In contrast to the previous ring configurations, results are presented in figures 112 and 113 for cylinders with R/h = 50 and with the baseline ring-configuration modified such that e_r/h = 10 and - 10, respectively. The curves shown in these two figures, for cylinders with significant ring eccentricity, are substantially different from the corresponding curves obtained herein for the external-pressure-loaded cylinders. The differences between the corresponding results predicted by Donnell's and Sanders' equations, and between the two sets of Sanders' equations, shown in figure 112 are practically negligible for values of approximately L/R < 8 and L/R < 10, respectively. However, as L/R increases beyond these values, differences between the corresponding results predicted by Donnell's and Sanders' equations, and between the two sets of Sanders' equations, as large as about 40% and 90%, respectively, are found. The differences

between the corresponding results predicted by Donnell's and Sanders' equations, and between the two sets of Sanders' equations, shown in figure 113 are also practically negligible for values of approximately $L/R < 22$ and $L/R < 12$, respectively. For $L/R \geq 22$, the differences between the corresponding results predicted by Donnell's and Sanders' equations do not exceed approximately 5%. However, the differences in the results obtained from the two sets of Sanders' equations increase monotonically for $L/R \geq 12$, with a difference of approximately 95% for $L/R = 50$.

Results for cylinders with $R/h = 500$ and with the baseline ring-configuration given by $\frac{E_r A_r}{d_r A} = 1$, $\frac{E_r I_r^c}{d_r D} = 1$, $\frac{G_r J_r}{2d_r(1-\nu)D} = 0$, and $\frac{e_r}{h} = 0$ were also obtained in the present study. In addition, results were obtained for cylinders with $R/h = 500$ and with the baseline ring-configuration modified such that $\frac{E_r A_r}{d_r A} = 2$, $\frac{E_r I_r^c}{d_r D} = 10$, $\frac{G_r J_r}{2d_r(1-\nu)D} = 1$, $\frac{G_r J_r}{2d_r(1-\nu)D} = 10$, $e_r/h = 1$, and $e_r/h = -1$. For each of these seven cases, curves that are practically identical to to corresponding curves for external-pressure-loaded cylinders were obtained for the results based on Sanders' equations and for those based on Donnell's equations. Results are presented in figures 114 and 115 for cylinders with $R/h = 500$ and with the baseline ring-configuration modified such that $e_r/h = 10$ and -10, respectively. The results shown in figure 114 are practically identical to those shown in figure 108 for the corresponding cylinders loaded by uniform external pressure, for values of approximately $L/R > 2.4$. For values of $L/R \leq 2$, the differences in the results obtained from all three sets of equations were found to be negligible. Likewise, the results shown in figure 115 are practically identical to those shown in figure 109 for the corresponding cylinders loaded by uniform external pressure, for values of approximately $L/R > 5$. Moreover, the differences in the results obtained from all three sets of equations were found to be negligible for values of approximately $L/R > 5.2$.

Axial compression and pressure loads. Results are presented in Table 76 that show the predicted values of the critical loading parameter obtained by Schmit et.al.[70] and obtained in the present study for isotropic cylinders stiffened by internal blade-shaped rings and stringers. The cylinders have $E = 10.0 \times 10^6$ psi, $\nu = 0.333$, $R = 60$ in., and $L = 165.0$ in. Results for two cylinder configurations are given and the wall thicknesses and stiffener properties are given in Table 77. The torsion constant for the rings and stringers are given in terms of the stiffener properties by

$$J_r = J_s = \left(0.316 - 0.285\, e^{-0.49\frac{h_1}{t_1}}\right) t_1^3 h_1 \qquad (147)$$

The values of the critical loading parameter are given for selected values of uniform axial compression combined with either uniform internal or external pressure. Values are also given for pure axial compression. The results were computed by using a variant of Flügge's equations that are based on the work of Hedgepeth and Hall.[60]

The results in Table 76 show differences less than 1% in the critical loading parameter obtained in the present study by using Sanders' equations with live pressure and in reference 70 by using a variant of Flügge' equations. In addition, the results of the present study obtained by using Sanders' equations with live pressure indicate that neglecting the nonlinear rotations about

the normal yields differences in the critical loading parameters that are also less than 1%. The differences between the corresponding critical loading parameters obtained by using Sanders' equations with live pressure and Donnell's equations with dead pressure are also less than approximately 1%.

Torsion loads. Results obtained by Baruch et al[56, 57] and obtained in the present study for cylinders subjected to uniform torsional shear loads and stiffened by ring, by stringers, or by rings and stringers are presented in Tables 78-86. For each case, the approximate Rayleigh-Ritz solution presented herein was used to compute the results of the present study. In particular, the predicted values of the nondimensional buckling load $\frac{N_{xy}^{cr} R^2}{D}$ are presented in Table 78-81 for selected values of the radius-to-thickness ratios $100 \le R/h \le 2000$ and the length-to-radius ratio $0.35 \le L/R \le 3$. These results correspond to ring-stiffened cylinders with the generic ring properties given by $\frac{A_r}{d_r h} = 0.5$, $\frac{I_r^c}{d_r h^3} = 2,$ and $J_r = 0$. Moreover, the results in Table 78 are for cylinders with $e_r/h = +1$ (outward) and - 1 (inward), respectively. Similar results are given in Table 79 for cylinders with $e_r/h = \pm 5$. The results in Tables 80 and 81 correspond to the generic ring properties given by $\frac{A_r}{d_r h} = 0.5$, $\frac{I_r^c}{d_r h^3} = 5,$ and $J_r = 0$ and for the eccentricities $e_r/h = \pm 1$ and ± 5, respectively.

Results showing the effects of variations in the ring eccentricity are presented in Table 82 for cylinders with $L/R = 1$ and 3, and with $R/h = 1000$. These results also correspond to the generic ring properties given by $\frac{A_r}{d_r h} = 0.5$, $\frac{I_r^c}{d_r h^3} = 5,$ and $J_r = 0$. Similar results showing the effects of variations in $\frac{A_r}{d_r h}$ and $\frac{I_r^c}{d_r h^3}$ are presented in Tables 83 and 84, respectively, for $e_r/h = \pm 5$.

Predicted values of the nondimensional buckling load $\frac{N_{xy}^{cr} R^2}{D}$ are presented for stringer stiffened cylinders in Table 85 for values of the radius-to-thickness ratios $R/h = 100$ and 1000 and for the length-to-radius ratio $0.5 \le L/R \le 3$. These results correspond to the generic stringer properties given by $\frac{A_s}{d_s h} = 0.5$, $\frac{I_s^c}{d_s h^3} = 5,$ and $J_s = 0$. Additionally, the results in Table 85 are for cylinders with $e_r/h = \pm 5$. Similar results are given in Table 86 for cylinders stiffened by rings and stringers for combinations of with $e_r/h = \pm 5$ and with $e_s/h = \pm 5$. The results in this Table correspond to the generic stiffener properties given by $\frac{A_s}{d_s h} = \frac{A_r}{d_r h} = 0.5$ $\frac{I_s^c}{d_s h^3} = \frac{I_r^c}{d_r h^3} = 5,$ and $J_s = J_r = 0$.

The results in Tables 78-86 indicate that the approximate Rayleigh-Ritz solution presented

herein is, for the most part, inadequate for predicting the shear-buckling loads of the cylinders considered. Differences significantly greater than 10% are found for many cylinder configurations and are indicated in the tables by the yellow highlighting.

Unstiffened Orthotropic and Laminated-Composite Cylinders

Results are presented subsequently that include results for laminated-composite cylinders. For these cylinders, the plies are presumed to have the same thickness unless noted otherwise. Moreover, the first ply in the stacking sequence is designated as the innermost ply, and ply orientation angles are measured with respect to the cylinders generators.

Axial compression loads. Comparisons for unstiffened orthotropic and laminated-composite cylinders subjected to uniform axial compression are shown in Tables 87-117. For homogeneous orthotropic cylinders and cross-ply laminated-composite cylinders, the results of the present study were obtained by using the classical solution described herein. For cylinders with angle plies, anisotropies associated with the A_{16}, A_{26}, B_{16}, B_{26}, D_{16}, and D_{26} constitutive terms appearing in equation (11) are generally present. These anisotropies are typically associated with skewed buckle patterns and, as a result, the classical solution is invalid. In the present study, the effects of these anisotropies are approximated by using the three-parameter Rayleigh-Ritz solution presented herein that utilizes the displacement functions defined by equations (108). It is important to note that when the skewedness parameter τ is set equal to zero, the Rayleigh-Ritz solution produce results that are identical to the classical solution. It is also important to note that when unbalanced angle plies are present, the A_{16} and A_{26} constitutive terms are generally nonzero and enforcement of zero-valued circumferential displacement boundary conditions produces a nonzero shearing stress resultant in the prebuckling state.

The results in Table 87 show the predicted values of the nondimensional buckling load $\frac{N_x^{cr}}{E_y h}\frac{R_2}{R_1}\left(\frac{R_2}{R_1}-1\right)^{-1}$ for specially orthotropic cylinders obtained by Kardomateas[71] and obtained in the present study as a function of the ratio of the outer radius to the inner radius, R_2/R_1. For these cylinders, the length is given by $L/R_2 = 5$ and the radius-to-thickness ratio R/h is given by

$$\frac{R}{h} = \frac{\frac{R_2}{R_1}+1}{2\left(\frac{R_2}{R_1}-1\right)} \tag{148}$$

In this table, results are given for $R_2/R_1 = 1.01$, 1.02, 104, and 1.05. The corresponding values of R/h are given by 100.5, 50.5, 25.5, and 20.5. In addition, the results were calculated for a homogeneous orthotropic material with the principal material properties $E_1 = 15$ GPa, $E_2 = 57$ Gpa, $G_{12} = 5.7$ GPa, and $\nu_{21} = 0.277$. The results of reference 71 that are presented in Table 87 include nondimensional buckling loads obtained by using the nonshallow shell equations given by Brush and Almroth[17] (see pp.157-159), that neglect linear and nonlinear rotations about the

normal, and by using Timoshenko's equations.[34]

The results in Table 87 indicate that the nondimensional buckling loads obtained by Kardomateas, by using Timoshenko's equations, and obtained in the present study, by using Sanders' equations, differ by less than 3.5%. Additionally, the nondimensional buckling loads obtained by Kardomateas, by using the nonshallow shell equations given in reference 17, and obtained in the present study, by using Sanders' equations with the nonlinear rotations about the normal neglected, differ by less than 2.5% for the two thinner cylinders and by about 18% for the two thicker cylinders.Moreover, the nondimensional buckling loads obtained by Kardomateas, by using the nonshallow shell equations given in reference 17, and obtained in the present study, by using Donnell's equations are nearly identical. The results obtained in the present study also indicate differences in the corresponding predictions obtained by using Donnell's equations and Sanders' equations that range from about 1% to 18%, with the largest differences being exhibited by the thicker cylinders. This same trend is exhibited by the two sets of results given by Kardomateas. Similarly, the results indicate differences in the corresponding predictions obtained by using Donnell's equations and Sanders' equations, neglecting nonlinear rotations about the normal, that range from about 0.3% to 14%, with the largest differences being exhibited by the thicker cylinders.

Comparisons of the values predicted herein for the nondimensional buckling load $\frac{N_x^{cr} L^2}{\pi^2 D_{11}}$ with those predicted by Jones and Morgan[72] and by Soldatos and Tzivanidis,[73] obtained by using Donnell's equations, are shown in Table 88 for cylinders with $(90/0)_m$ antisymmetric cross-ply laminated-composite walls. These results are for cylinders with a radius R = 10 in., a wall thickness h = 0.10 in., and for values of the stacking sequence index m = 1, 2, 3, and ∞. The first ply in the stacking sequence is the innermost ply and its major principal axis is 90 degrees from the cylinder axis. The lamina material properties are $E_1 = 30 \times 10^6$ psi, $E_2 = 0.75 \times 10^6$ psi, $G_{12} = 0.375 \times 10^6$ psi, and $\nu_{12} = 0.25$. The results presented in this table are for values of the cylinder length L = 1.00, 3.16, 10.00, and 31.63 in. Only results for the cylinders with L = 1.00 in. are given by Soldatos and Tzivanidis.

The results in Table 88 show that the differences between the predicted buckling loads obtained by Jones and Morgan, Soldatos and Tzivanidis, and the present study of less than 1% for the cylinders with L = 1.00 in. For the longer shells, substantially larger differences are seen that range from approximately 4% to 8%. From a private communication, it was found that Weaver[74] obtained results based on Donnell's equations for all cases shown in Table 88 that are practically identical to those obtained in the present study. The results obtained in the present study also indicate that neglecting nonlinear rotations about the normal in Sanders' equations yields differences less than 1%. Similarly, the differences between corresponding results obtained by using Sanders' equations and Donnell's equations are at most approximately 2%.

Values of the predicted nondimensional buckling load $\frac{N_x^{cr} L^2}{E_2 h^3}$ obtained by Soldatos and Tzivanidis,[73] by using Donnell's equations, and obtained in the present study are given in Table

89 for cylinders with $(0/90/0_m)$ unsymmetric cross-ply laminated-composite walls. These results are also for cylinders with a length $L = 1.0$ in., a radius $R = 10$ in., a wall thickness $h = 0.10$ in., and for values of the stacking sequence index $m = 1, 2, 4, 8, 18$, and 48. The major principal axis of the first ply is aligned with the cylinder axis, and the lamina material properties are the same as those used to generate Table 88. Inspection of Table 89 reveals that the results obtained by Soldatos and Tzivanidis are almost completely identical to the results obtained in the present study. The results in Table 89 also show neglecting nonlinear rotations about the normal in Sanders' equations produces negligible differences. Additionally, the differences between the corresponding results obtained by using Donnell's equations and Sanders'equations are less than 0.2%.

Results similar to those given in Table 89 are presented in Table 90 for cylinders with $(0_m / 90/0)$ unsymmetric cross-ply laminated-composite walls and for cylinders with all 0-degree plies. These results are also for cylinders with a length $L = 34.64$ in., a radius $R = 10$ in., a wall thickness $h = 0.12$ in., and for values of the stacking sequence index $m = 1, 8, 18$, and 48. Moreover, the lamina material properties are identical to those used in generating Table 89. Results obtained by Jones and Morgan[72] and by Shen,[75] obtained by using Donnell's equations, differ from the corresponding results obtained in the present study by 0.6%, at most, and are identical in several cases. The results in Table 90 also show neglecting nonlinear rotations about the normal in Sanders' equations produces differences less than 1%, and the differences between the corresponding results obtained by using Donnell's equations and Sanders'equations are less than 2.4%.

Additional results for cross-ply laminated-composite cylinders with the lamina material properties $E_1 = 30 \times 10^6$ psi, $E_2 = 0.75 \times 10^6$ psi, $G_{12} = 0.375 \times 10^6$ psi, and $\nu_{12} = 0.25$ are presented in Tables 91-93. In Tables 91 and 92, the nondimensional buckling load is given by $\frac{N_x^{cr} L^2}{E_2 h^3}$ and in Table 93 by $\frac{N_x^{cr} L^2}{A_{22} h^2}$, where A_{22} is the circumferential extensional stiffness. The results in Table 91 are for cylinders with $L/R = 1$ and $R/h = 10$, and the results in Table 92 are for cylinders with $L/R = 2$ and $R/h = 40$. The results in Table 93 are for selected values of $0.5 \le L \le 10$ and $1 \le R \le 10$ that correspond to two groups of results; that is, one with $L/R = 1/2$ and the other with $L/R = 1$. For all three tables, a wall thickness $h = 0.10$ in. was used to compute the results.

The results in Table 91 obtained by Khdeir et al.[76] using Donnell's equations differ from the corresponding results obtained in the present study by approximately 3% to 8%. In contrast, the results in Table 92 obtained by Nosier and Reddy[77] using Donnell's equations are identical to the corresponding results obtained in the present study. Likewise, the results in Table 93 obtained by Iu and Chia[78] using Donnell's equations are identical to the corresponding results obtained in the present study, with two exceptions. Specifically, for the cylinders with $L = R = 10.0$ in. and with $L = R = 5$ in. the differences with the corresponding results obtained in the present study are approximately 33% and 16%, respectively. From a private communication, it was found that Weaver[74] obtained results based on Donnell's equations for these two cases that are within approximately 0.2% of the corresponding results obtained in the present study.

The results in Table 91 also indicate that neglecting nonlinear rotations about the normal in Sanders' equations produces differences between approximately 2% to 6%, and the differences between the corresponding results obtained by using Donnell's equations and Sanders'equations range from approximately 4% to 17%. In contrast, the results in Table 92 indicate that neglecting nonlinear rotations about the normal in Sanders' equations produces differences of approximately 1%, and the differences between the corresponding results obtained by using Donnell's equations and Sanders'equations range from approximately 3% to 4%. The results in Table 93 indicate that neglecting nonlinear rotations about the normal in Sanders' equations produces differences less than 2%, and mostly less than 1%. The differences between the corresponding results obtained by using Donnell's equations and Sanders'equations range from approximately 1% to 6%.

Values of the applied stress resultant at buckling, N_x^{cr}, obtained by Han and Simitses,[79] by using Donnell's equations, and obtained in the present study are given in Table 94 for unidirectional laminated-composite cylinders with either all 0-degree or all 90-degree plies. These results are also for cylinders with a radius R equal to either 4.0 in. or 7.5 in., a wall thickness h = 0.0212 in., and L/R = 1, 2, 5, and 10. The lamina material properties are $E_1 = 30 \times 10^6$ psi, $E_2 = 2.7 \times 10^6$ psi, $G_{12} = 0.65 \times 10^6$ psi, and $\nu_{12} = 0.21$. This table shows that the results obtained by Han and Simitses differ from the corresponding results obtained in the present study by less than 0.6%. The results in Table 94 also show neglecting nonlinear rotations about the normal in Sanders' equations produces negligible differences. Additionally, the differences between the corresponding results obtained by using Donnell's equations and Sanders'equations are less than 0.8%.

Results are presented in Table 95 that show the predicted buckling load obtained by Geier et al.,[80] Meyer-Piening et al.,[81] Geier and Singh,[82] and obtained in the present study for selected laminated-composite cylinders. These results are also for cylinders with a length L = 510 mm, a radius R = 250 mm, and a wall thickness h = 1.25 mm. The lamina material properties are E_1 = 123,550 MPa, E_2 = 8,708 MPa, G_{12} = 5,695 MPa, and $\nu_{12} = 0.32$. The results given in the table that were obtained by Geier et al. and Meyer-Piening et al. are based on Donnell's equations and neglect the A_{16}, A_{26}, B_{16}, B_{26}, D_{16}, and D_{26} anisotropic stiffnesses. In addition, results obtained by Meyer-Piening et al. that are based on Sanders' kinematic equations and that include the B_{16}, B_{26}, D_{16}, and D_{26} anisotropic stiffnesses are presented in the table, along with results obtained from a refined theory used by Geier and Singh that uses equations similar to those of Flügge,[18] but includes transverse-shearing deformations.

The results in Table 95 exhibit differences less than 1% between the buckling loads obtained in references 81 and 82, that are based on Donnell's equations, with the corresponding results obtained in the present study. Similarly, the results from references 82 and 83 exhibit differences less than 2% and 1%, respectively, from the corresponding results obtained in the present study that are based on Sanders' equations. The results in Table 95 also show that neglecting nonlinear rotations about the normal in Sanders' equations produces differences less than 3%. Additionally, the differences between the corresponding results obtained by using Donnell's equations and Sanders'equations are less than approximately 5%.

Predictions of the applied stress resultant at buckling, N_x^{cr}, obtained by Khot and Venkayya,[83] by using Donnell's equations, and obtained in the present study are given in Tables 96 and 97 for (0/-θ/+θ) and (90/-θ/+θ) three-ply laminated-composite cylinders. These results are for cylinders with a radius $R = 6.0$ in., a wall thickness $h = 0.036$ in., and a length $L = 12.5$ in. Moreover, the results in Table 96 are for glass-epoxy cylinders with the lamina material properties $E_1 = 7.5 \times 10^6$ psi, $E_2 = 3.5 \times 10^6$ psi, $G_{12} = 1.25 \times 10^6$ psi, and $\nu_{12} = 0.25$. The results in Table 97 are for boron-epoxy cylinders with the lamina material properties $E_1 = 40 \times 10^6$ psi, $E_2 = 4.5 \times 10^6$ psi, $G_{12} = 1.5 \times 10^6$ psi, and $\nu_{12} = 0.25$. Futhermore, the results obtained by Khot and Venkayya are based on an approximate analysis that uses the buckle pattern given by equation (108c) with a stress-function formulation that ignores some of the simply supported boundary conditions addressed in the present study. The approximate solutions used in the present study and in reference 83 use the skewedness parameter τ in equations (108) to account for cylinder wall anisotropies.

The results that are based on Donnell's equations in Table 96, obtained by Khot and Venkayya, for the glass-epoxy cylinders exhibit differences less than 2% from the corresponding results obtained in the present study. The results in Table 96 also show neglecting nonlinear rotations about the normal in Sanders' equations produces differences less than approximately 1%. In addition, the differences between the corresponding results obtained by using Donnell's equations and Sanders'equations are less than approximately 2%. However, the results in Table 97, obtained by Khot and Venkayya for the boron-epoxy cylinders, exhibit differences as large as 13% from the corresponding results obtained in the present study. The results in Table 97 also show neglecting nonlinear rotations about the normal in Sanders' equations produces differences less than approximately 1%, and the differences between the corresponding results obtained by using Donnell's equations and Sanders'equations are less than approximately 1%.

Results for the same three-ply glass-epoxy cylinders investigated by Khot and Venkayya, and shown in Table 96, were also obtained by Arbocz[84] using an approximate analytical formulation that is similar to that used by Khot and Venkayya. The results for the (0/-θ/+θ) and (90/-θ/+θ) cylinders were found to be within approximately 5% and 3%, respectively, of the corresponding results obtained in the present study. Results for the boron-epoxy cylinders presented in Table 97 were also obtained by Arbocz.[84] In particular, the results for the (0/-θ/+θ) and (90/-θ/+θ) cylinders were found to be within approximately 19% and 16%, respectively, of the corresponding results obtained in the present study. Arbocz[85] also obtained results for an eight-ply $(\pm 45/0/90)_s$ laminated-composite cylinder, using same approximate analysis based on Donnell's equations, that are presented in Table 98 along with corresponding results obtained in the present study. This cylinder has a radius $R = 8.0$ in., a wall thickness $h = 0.04$ in., and a length $L = 14.0$ in. The lamina material properties used to obtain these results are $E_1 = 18.5111 \times 10^6$ psi, $E_2 = 1.64 \times 10^6$ psi, $G_{12} = 0.8706 \times 10^6$ psi, and $\nu_{12} = 0.300235$. The results in Table 98 show a difference less than 0.3% between the buckling load obtained by Arbocz and the correspond results obtained herein that is based on Donnell's equations. The results in Table 98 also show that neglecting nonlinear rotations about the normal in Sanders' equations produces differences less than approximately 2%, and the differences between the corresponding results obtained by using Donnell's equations and Sanders'equations are less than approximately 4%.

Results are presented in Table 99 that show the predicted buckling stress (kgf/mm^2) obtained by Uemura and Kasuya[86] and obtained in the present study for selected cross-ply and angle-ply laminated-composite cylinders with a wall thickness $h = 1$ mm, a radius $R = 100$ mm, and a length $L = 600$ mm. The lamina properties used to obtain these results are $E_1 = 13,940$ kgf/mm^2, $E_2 = 833$ kgf/mm^2, $G_{12} = 484$ kgf/mm^2, $\nu_{12} = 0.316$, and the ply thickness = 0.125 mm. For the cross-ply cylinders, Uemura and Kasuya obtained results by substituting displacement functions equivalent to equations (77) into the Donnell-type differential equations governing buckling. For the angle-ply cylinders, Uemura and Kasuya obtained results by using the Rayleigh-Ritz method. For both solution methods, anisotropies associated with the B_{16}, B_{26}, D_{16}, and D_{26} constitutive terms are unaccounted for in the analyses. In contrast, the results shown in this table for the present study that were obtained by using the approximate Rayleigh-Ritz solution, which includes these anisotropies. For comparison purposes, results are also shown in this table for the present study that correspond to the classical solution ($\tau = 0$), which neglects these anisotropies, and are shown in red.

The results in Table 99 show differences less than 6% between the buckling load obtained by Uemura and Kasuya and the correspond results obtained herein that are based on Donnell's equations and neglect the anisotropies associated with the B_{16}, B_{26}, D_{16}, and D_{26} constitutive terms. Results obtained herein for the $(+20_4/-20_4)$, $(+45_4/-45_4)$, and $(+70_4/-70_4)$ cylinders by using the approximate Rayleigh-Ritz solution predict reductions in the buckling stress equal to approximately 33%, 33%, and 15%, respectively. The results in Table 99 also show that neglecting nonlinear rotations about the normal in Sanders' equations can produces differences in the corresponding results as large as approximately 21%. Likewise, the differences between the corresponding results obtained by using Donnell's equations and Sanders'equations are as large as approximately 32%.

Results obtained by Uemura and Kasuya[86] for cylinders with $h = 0.5$ mm, $R = 100$ mm, and $L = 300$ mm, that are similar to those in Table 99, are presented in Table 100. The results in Table 100 show no differences between the buckling load obtained by Uemura and Kasuya and the correspond results obtained herein that are based on Donnell's equations that neglect the anisotropies associated with the B_{16}, B_{26}, D_{16}, and D_{26} constitutive terms, except for one case. A difference of approximately 5% is found for the $(\pm 70)_2$ cylinder. Results obtained herein for the $(+20_2/-20_2)$, $(+45_2/-45_2)$, and $(\pm 70)_2$ cylinders by using the approximate Rayleigh-Ritz solution based on Donnell's equations predict reductions in the buckling stress equal to approximately 42%, 20%, and 7%, respectively. The results in Table 100 also show that neglecting nonlinear rotations about the normal in Sanders' equations produces differences between the corresponding results that are less than approximately 6%. However, the differences between the corresponding results obtained by using Donnell's equations and Sanders'equations are as large as approximately 15% for the $(\pm 70)_2$ cylinders.

Predicted buckling loads (kN/m) obtained by Sun[87] and herein are presented in Table 101 for selected laminated-composite cylinders made entirely from the three different material types indicated in the table. These cylinders have a wall thickness $h = 0.5$ mm, a radius $R = 82.5$ mm, and a length $L = 143.6$ mm. For these cylinders, Sun obtained results by substituting displacement

functions identical to equations (77) into the Donnell-type differential equations governing buckling, which effectively neglects the effects of anisotropies associated with the B_{16}, B_{26}, D_{16}, and D_{26} constitutive terms in the analysis. Like in the previous two tables, the results shown in Table 101 for the present study were obtained by using the approximate Rayleigh-Ritz solution, which includes these anisotropies. Additional results are also shown in this table, in red, for the present study that correspond to the classical solution ($\tau = 0$), which neglects these anisotropies.

The results in Table 101 show differences less than 2% between the buckling load obtained by Sun and the corresponding results obtained herein that are based on Donnell's equations and that neglect the anisotropies associated with the B_{16}, B_{26}, D_{16}, and D_{26} constitutive terms. Results obtained herein by using the approximate Rayleigh-Ritz solution, including the anisotropies, predict reductions in the buckling stress less than about 3%. The results in Table 101 also show that neglecting nonlinear rotations about the normal in Sanders' equations produces differences in the corresponding results that are less than approximately 3%. The differences between the corresponding results obtained by using Donnell's equations and Sanders'equations are less than approximately 4%.

Results obtained by Sun[87] for selected laminated-composite cylinders with $h = 0.5$ mm and $R = 82.5$ mm, and for several lengths, that are similar to those in Table 101, are presented in Table 102. The results in this table show differences less than 1% between the buckling loads obtained by Sun and the correspond results obtained herein that are based on Donnell's equations and that neglect the anisotropies associated with the B_{16}, B_{26}, D_{16}, and D_{26} constitutive terms. Results obtained herein by using the approximate Rayleigh-Ritz solution, including the anisotropies, predict reductions in the buckling stress less than about 1%. The results in Table 102 also show that neglecting nonlinear rotations about the normal in Sanders' equations produces differences in the results less than approximately 5%. The differences between the corresponding results obtained by using Donnell's equations and Sanders'equations are less than approximately 8%, and in several cases less than 5%.

Additional results obtained by Sun[87] for $(0_2/\pm 60_2)_m$ laminated-composite cylinders made of the type 2 material are presented in Table 103 for values of $m = 10$, 20, 40, 80, and 160. For these cylinders, $h = 0.5$ mm, $R = 82.5$ mm, and $L = 143.6$ mm. The results in this table show no differences between the buckling load obtained by Sun and the corresponding results obtained herein that are based on Donnell's equations. Moreover, results obtained herein by using the approximate Rayleigh-Ritz solution, including the anisotropies, predict no reductions in the buckling loads. The results in Table 103 also show that neglecting nonlinear rotations about the normal in Sanders' equations produces differences in the corresponding that are results less than approximately 3%. The differences between the corresponding results obtained by using Donnell's equations and Sanders'equations are less than approximately 4%.

Buckling loads obtained by Smerdov[88] and in the present study, normalized by $N^* = 104.7$ kN/m, are presented in Tables 104-107 for a variety of selected laminated-composite cylinders with the lamina material properties $E_1 = 146$ GPa, $E_2 = 10.8$ GPa, $G_{12} = 5.78$ GPa, and $\nu_{12} = 0.29$. These cylinders also have a wall thickness $h = 0.5$ mm, a radius $R = 82.5$ mm, and a length $L = 143.6$ mm. Like Sun, Smerdov's results were obtained by substituting displacement functions

identical to equations (77) into the Donnell-type differential equations governing buckling. Thus, Smerdov's analysis also neglects the effects of the anisotropies associated with the B_{16}, B_{26}, D_{16}, and D_{26} constitutive terms. Once again, the results shown in Tables 104-107 for the present study were obtained by using the approximate Rayleigh-Ritz solution, which includes these anisotropies. Additional results are also shown in this table, in red, for the present study that correspond to the classical solution ($\tau = 0$), which neglects these anisotropies.

The results in Tables 104-107 show no differences between the buckling load obtained by Smerdov and the corresponding results obtained herein that are based on Donnell's equations and neglect the anisotropies associated with the B_{16}, B_{26}, D_{16}, and D_{26} constitutive terms. The results in these tables also show a relatively small effect of neglecting nonlinear rotations about the normal in Sanders' equations. The differences between the corresponding results obtained by using Donnell's equations and Sanders'equations are less than approximately 9%, 6%, 6%, and 4% in Tables 104-107, respectively. However, the results obtained herein by using the approximate Rayleigh-Ritz solution with Sanders' equations, including the anisotropies, predict substantial reductions in the buckling loads for several laminates. Specifically, the $(\pm 71/0_2)$, $(\pm 19.5/90_2)$, and $(90_2/\pm 50.5)$ laminates in Table 104 are predicted to have buckling-load reductions due to anisotropy equal to 37%, 22%, and 21%, respectively. Likewise, the $(90_2/0_2/\pm 49)$ laminate in Table 105 and the $(90_2/\pm 31/\pm 31/90_2)$ and $(90_2/\pm 32.5/0_2/90_2)$ laminates in Table 106 are predicted to have buckling-load reductions equal to approximately 11%, 14%, and 11%, respectively.

Additional results obtained by Smerdov[88] and herein that are similar to the results in Tables 104-107 are presented in Tables 108-113 for a variety of laminated-composite cylinders with thinness ratios ranging from $50 \le R/h \le 1000$. These cylinders are also made of laminae with the material properties $E_1 = 146$ GPa, $E_2 = 10.8$ GPa, $G_{12} = 5.78$ GPa, and $\nu_{12} = 0.29$. However, the results correspond to cylinders with a radius R = 1000 mm and lengths given by L/R = 1 and 3. The normalization term N* is defined as N_x^{cr} for the corresponding $[0_2/(\pm 60)_2]_{160}$ laminated cylinder and the value for each cylinder is listed in the tables. Like for Smerdov's results presented in Tables 104-107, the results in Tables 108-113 were obtained by substituting displacement functions identical to equations (77) into the Donnell-type differential equations governing buckling, and inherently neglect the effects ofthe anisotropies associated with the B_{16}, B_{26}, D_{16}, and D_{26} constitutive terms.

The results in Tables 108-113 show, for the most part, no differences between the buckling loads obtained by Smerdov and the corresponding results obtained herein that are based on Donnell's equations and that neglect the anisotropies associated with the B_{16}, B_{26}, D_{16}, and D_{26} constitutive terms. The few contrary cases exhibited differences less than approximately 1.5%. The results in these tables also show a relatively small effect of neglecting nonlinear rotations about the normal in Sanders' equations. For most cases, the differences are less than 3%, and the largest difference is approximately 7%. The differences between the corresponding results obtained herein by using Donnell's equations and Sanders'equations are less than approximately 5%, 9%, 5%, 16%, 3%, and 9% in Tables 108-113, respectively. The results obtained herein by using the approximate Rayleigh-Ritz solution with Sanders' equations, including the anisotropies, predict reductions in the buckling loads that are less than 2%.

Normalized buckling loads obtained by Smerdov[88] and herein are presented in Tables 114-116 for a variety of laminated-composite cylinders with lamina moduli ratios ranging from $2 \le E_1/E_2 \le 10{,}000$. The corresponding lamina material properties are given by $E_1 = 146$ GPa, $E_2/G_{12} = 2$, and $\nu_{12} = 0.29$. In addition, the results correspond to cylinders with a radius $R = 1000$ mm, a thinness ration $R/h = 150$, and a length given by $L/R = 1$. The normalization term N* is also defined for these cylinders as N_x^{cr} for the corresponding $[0_2/(\pm 60)_2]_{160}$ laminated cylinder and the value for each cylinder is listed in the tables. Furthermore, Smernov's results in Tables 114-116 were obtained from the Donnell-type classical solution that inherently neglects the effects ofthe anisotropies associated with the B_{16}, B_{26}, D_{16}, and D_{26} constitutive terms. Again, the results shown in Tables 114-116 for the present study were obtained by using the approximate Rayleigh-Ritz solution, which includes these anisotropies. Additional results are also shown in this table, in red, for the present study that correspond to the classical solution ($\tau = 0$), which neglects these anisotropies.

The results in Tables 114-116 also show, for the most part, no differences between the buckling load obtained by Smerdov and the corresponding results obtained herein that are based on Donnell's equations and neglect the anisotropies associated with the B_{16}, B_{26}, D_{16}, and D_{26} constitutive terms. The few contrary cases exhibited differences less than approximately 1%, with one curious exception. Smerdov's result in the second row of Table 114 is listed as 0.91 and the corresponding result obtained in the present study is 0.71; a difference of approximately 28%. Based on the excellent agreement for all the other cases, it is likely that Smedov's result is a typographical error. The results in these tables also show an unimportant effect of neglecting nonlinear rotations about the normal in Sanders' equations. Similarly, the differences between the corresponding results obtained herein by using Donnell's equations and Sanders' equations are less than approximately 4%. The results obtained herein by using the approximate Rayleigh-Ritz solution with Sanders' equations, including the anisotropies, predict reductions in the buckling loads that are less than 2% in almost all cases. However, the results given for $E_1/E_2 = 100$ and 10,000 in Table 114 exhibit buckling load reductions of approximately 133% and 254%, respectively.

Buckling loads obtained by Wong and Weaver[89] and herein are presented in Table 117 for selected laminated-composite cylinders with the lamina material properties $E_1 = 161$ GPa, $E_2 = 11.5$ GPa, $G_{12} = 7.169$ GPa, and $\nu_{12} = 0.349$. These cylinders have a wall thickness $h = 0.125$ mm, a radius $R = 80$ mm, and a length $L = 150$ mm. The results given by Wong and Weaver were obtained by using a radial displacement function equivalent to equation (108c) with $m = 1$, and a corresponding stress function with the Donnell-type equilibrium and compatibility differential equations governing buckling. This solution is approximate in that it does not satisfy the simply supported boundary conditions considered herein. More accurate results obtained from finite element analyses conducted by Wong and Weaver are also given in Table 117.

The results in Table 117 indicates differences between the buckling load obtained by Wong and Weaver and the corresponding results obtained herein that are based on Donnell's equations that are less than approximately 5%, and in several cases less than 2%. The results in this table also show a negligible effect of neglecting nonlinear rotations about the normal in Sanders'

equations. Similarly, the differences between the corresponding results obtained herein by using Donnell's equations and Sanders' equations are less than approximately 1%. It is noteworty that the differences between the finite element results and the corresponding results obtained in the present study are, for the most part, less than approximately 5%. The exception is exhibited by the results for the $(90/-45_2/0)_S$ cylinder which is approximately 11%.

Differences in the buckling resistance predictions obtained in the present study by using Donnell's equations, Sanders equations, and Sanders equations with nonlinear rotations about the normal neglected are illustrated in figures 116-121 for $[(\pm 30)_6]_s$, $[(\pm 45)_6]_s$, and $[(\pm 60)_6]_s$ laminated-composite cylinders with radius-to-thickness ratios R/h =50 and 500. The lamina material properties used to obtain these results are $E_1 = 30 \times 10^6$ psi, $E_2 = 0.75 \times 10^6$ psi, $G_{12} = 0.375 \times 10^6$ psi, and $\nu_{12} = 0.25$. The buckling resistance is measured by the nondimensional coefficient $\frac{N_x^{cr} Rh}{\pi^2 \sqrt{D_{11} D_{22}}}$ for values of $0.2 \le L/R \le 50$, where D_{11} and D_{22} are the principal shell-wall bending stiffnesses appearing in equations (12c). For each laminate considered, it is presumed that the anisotropy associated with the D_{16} and D_{26} constitutive terms is negligible.

The red curves in figures 116-121 corresponds to results obtained by using Donnell's equations. The black and the blue curves corresponds to results obtained by using Sanders' equations and Sanders' equations with nonlinear rotations about the normal neglected, respectively. The rightmost branch of the black and the blue festoon curves shown in figures 116-118 and the black curve shown in figure 121 correspond to a column-like shell-buckling mode given by the wave numbers m = n = 1, and the graph coordinates for the first column-like shell-buckling mode are indicated in the figures. The corresponding gray curve that appears in these figures corresponds to buckling coefficients obtained by using the Euler column buckling formula given by equation (135) for a simply supported thin-walled tubular beam with length L, cross-sectional radius R, and thickness h that is deformed into a single half wave along its length. As stated previously herein, $N_{x,\,Euler}^{cr}$ is the Euler buckling load divided by $2\pi R$ and $\tilde{E}I$ is the column-bending stiffness. For the laminated-composite cylinders, the column-bending stiffness is approximated by $E_x \pi R^3 h$, where E_x is the effective axial stiffness of the shell given by

$$E_x = \frac{A_{11} A_{22} - A_{12}^2}{A_{22}\, h} \tag{149}$$

Using these results with equation (135) gives

$$\frac{N_{x,\,Euler}^{cr} Rh}{\pi^2 \sqrt{D_{11} D_{22}}} = \frac{R^3 h \left(A_{11} A_{22} - A_{12}^2 \right)}{2L^2 A_{22} \sqrt{D_{11} D_{22}}} \tag{150}$$

The results in figures 116-121, for the cylinders with R/h = 50 and 500, show significant differences in the buckling resistance predictions are obtained from the three set of equations, with

the black curves (Sanders' equations) generally exhibiting the lowest corresponding values of buckling resistance. In contrast, for the relatively short cylinders with R/h = 50, no differences are found for the $[(\pm 30)_6]_s$, $[(\pm 45)_6]_s$, and $[(\pm 60)_6]_s$ cylinders with approximately $L/R \leq 9$, $L/R \leq 5$, and $L/R \leq 3.6$, respectively. Likewise, for the relatively short cylinders with R/h = 500, no differences are also found for the $[(\pm 30)_6]_s$, $[(\pm 45)_6]_s$, and $[(\pm 60)_6]_s$ cylinders with approximately $L/R \leq 8.2$, $L/R \leq 4.5$, and $L/R \leq 3$, respectively. As the cylinder length increases, differences in excess of 20% are generally found, with some exceptions that are associated with the festoon nature of the blue and black curves. Like for monocoque and stiffened isotropic cylinders examined herein, the results obtained by using Sanders' equations predict a transition to a column buckling mode at significantly smaller values of L/R than the corresponding results obtained by using Sanders' equations with nonlinear rotations about the normal neglected. The results obtained by using Donnell's equations predict no transition at all. In addition, the Euler column-buckling modes predicted by equation (150) are in close agreement with the corresponding results predicted by Sanders' equations.

Uniform external pressure loads. Comparisons of the values predicted herein for the nondimensional buckling pressure $\frac{p^{cr}RL^2}{\pi^2 D_{11}}$ with those predicted by Jones and Morgan,[72] by using Donnell's equations, are shown in Table 118 for cylinders with $(90/0)_m$ cross-ply laminated-composite walls. These results are for cylinders with a radius R = 10 in., a wall thickness h = 0.10 in., and for values of the stacking sequence index m = 1, 2, and ∞. The first ply in the stacking sequence is the innermost ply and its major principal axis is 90 degrees from the cylinder axis. The lamina material properties are $E_1 = 30 \times 10^6$ psi, $E_2 = 0.75 \times 10^6$ psi, $G_{12} = 0.375 \times 10^6$ psi, and $\nu_{12} = 0.25$. The results presented in this table are for values of the cylinder length L = 1.00, 3.16, 10.00, and 31.63 in. Results obtained in the present study are also shown in this table that are based on Sanders' equations with live pressure, Sanders' equations with dead pressure, and Sanders' equations with dead pressure and nonlinear rotations about the normal neglected.

The results in Table 118 show that the differences between the predicted buckling pressures obtained by Jones and Morgan and the present study, based on Donnell's equations, are less than 2% for the cylinders with L = 1.00 in. For the longer shells, substantially larger differences are seen that range from approximately 3% to 6%. The results obtained in the present study also indicate that neglecting the effects of live pressure in Sanders' equations yields differences less than 3%, except for the cylinders with L = 31.63 in. which exhibit differences of about 4%-7%. Moreover, the same range of differences is obtained when both live pressure and nonlinear rotations about the normal are neglected in Sanders' equations. Surprisingly, the differences between the corresponding results obtained by using Sanders' equations with live pressure and Donnell's equations with dead pressure are at most approximately 2%.

Values of the nondimensional buckling pressure $\frac{p^{cr}RL^2}{E_2 h^3}$ obtained by Jones and Morgan,[72] Shen,[75] and obtained in the present study are presented in Table 119 for selected unsymmetric cross-ply cylinders with a radius R = 10 in., a wall thickness h = 0.10 in., and a length L = 34.64 in. The lamina material properties are also $E_1 = 30 \times 10^6$ psi, $E_2 = 0.75 \times 10^6$ psi, $G_{12} = 0.375 \times$

10^6 psi, and $\nu_{12} = 0.25$. These results are based on Donnell's equations with dead pressure. Additional results obtained in the present study are presented in Table 119 that are based on Sanders' equations with live pressure, Sanders' equations with dead pressure, and Sanders' equations with dead pressure and nonlinear rotations about the normal neglected.

The results in Table 119 show no differences between the predicted buckling pressures obtained by Jones and Morgan and the present study that are based on Donnell's equations. Moreover, differences between the predicted buckling pressures obtained by Shen and in the present study are less than approximately 3%. The results obtained in the present study also indicate that neglecting the effects of live pressure in Sanders' equations yields differences less than about 4%. Similar differences are obtained when both live pressure and nonlinear rotations about the normal are neglected in Sanders' equations. Once again, the differences between the corresponding results obtained by using Sanders' equations with live pressure and Donnell's equations with dead pressure are at most approximately 2%.

Predicted values of $p_{cr}R$ obtained by Sun[87] and herein are presented in Table 120 for selected laminated-composite cylinders made entirely from the three different material types indicated in the table. These cylinders have a wall thickness $h = 0.5$ mm, a radius $R = 82.5$ mm, and lengths $L = 45.4$, 143.6, and 321.1 mm. For these cylinders, Sun obtained results by substituting displacement functions identical to equations (77) into the Donnell-type differential equations governing buckling, which effectively neglects the effects of anisotropies associated with the B_{16}, B_{26}, D_{16}, and D_{26} constitutive terms in the analysis. Once again, the results shown in Table 120 for the present study were obtained by using the approximate Rayleigh-Ritz solution, which includes these anisotropies. Additional results are also shown in this table, in red, for the present study that correspond to the classical solution ($\tau = 0$), which neglects these anisotropies.

The results in this Table 120 show differences less than 0.3% between the buckling pressures obtained by Sun and the correspond results obtained herein that are based on Donnell's equations and neglect the anisotropies associated with the B_{16}, B_{26}, D_{16}, and D_{26} constitutive terms. Corresponding results obtained herein by using the approximate Rayleigh-Ritz solution, including the anisotropies, predict reductions in the buckling pressures less than about 1% and in many cases no reduction at all. Additional results obtained in the present study are given in Table 120 that are based on Sanders' equations with live pressure and Sanders' equations with live pressure and nonlinear rotations about the normal neglected. These results show that neglecting nonlinear rotations about the normal in Sanders' equations, with live pressure, produces differences in the results that are less than 1% for all cases. The differences between the corresponding results obtained by using Donnell's equations and Sanders'equations with live pressure are less than approximately 3% for all cases. Corresponding results obtained herein by using the approximate Rayleigh-Ritz solution, including the anisotropies, predict reductions in the corresponding buckling pressures less than about 1% and in many cases no reduction at all.

Values of the buckling pressures obtained by Simitses and Anastasiadis[90] and obtained in the present study are given in Tables 121-124 for selected infinitely long laminated-composite cylinders with a radius $R = 19.05$ cm. In particular, results are presented in Tables 121 and 122 for symmetric cross-ply cylinders with radius-to-thickness ratios $R/h = 15$ and 10, respectively.

Similarly, results are presented in Tables 123 and 124 for symmetric angle-ply cylinders with radius-to-thickness ratios $R/h = 15$ and 10, respectively. The lamina material properties (boron-epoxy) are $E_1 = 206.844 \times 10^9$ Pa, $E_2 = 18.6159 \times 10^9$ Pa, $G_{12} = 4.48162 \times 10^9$ Pa, and $\nu_{12} = 0.21$. The results obtained by Simitses and Anastasiadis are based on Sanders' equations with dead pressure and nonlinear rotations about the normal neglected. Additional results obtained in the present study are given in Tables 121-124 that are based on Donnell's equations with dead pressure, Sanders' equations with live pressure, Sanders' equations with dead pressure, and Sanders' equations with dead pressure and nonlinear rotations about the normal neglected. For each case obtained in the present study, a value of $L/R = 100$ was used in the calculations.

The results in Tables 121-124 indicate differences between the corresponding results obtained by Simitses and Anastasiadis and in the present study, that are based on Sanders' equations with dead pressure and nonlinear rotations about the normal neglected, are less than 2% and, for the most part, less than a fraction of 1%. In addition, the results obtained in the present study indicate negligible differences between the corresponding results obtained by using Donnell's equations with dead pressure, Sanders' equations with dead pressure, and Sanders' equations with dead pressure and nonlinear rotations about the normal neglected for every case. Moreover, the results indicate differences of approximately 33% between the results based on these three sets of equations and the corresponding results based on Sanders' equations with live pressure. The results presented in Tables 123 and 124, for the angle-ply cylinders, that were obtained herein by using the approximate Rayleigh-Ritz solution with the D_{16} and D_{26} anisotropies included, indicate reductions in the buckling pressures that are at most approximately 4%. For most cases, these differences are less than 1%. Additional results are also shown in this table, in red, for the present study that correspond to the classical solution ($\tau = 0$), which neglects these anisotropies.

Normalized buckling pressures obtained by Smerdov[91] and in the present study are shown in Tables 125-130 for a variety of selected laminated-composite cylinders with the lamina material properties $E_1 = 146$ GPa, $E_2 = 10.8$ GPa, $G_{12} = 5.78$ GPa, and $\nu_{12} = 0.29$. These cylinders have a wall thickness $h = 0.5$ mm and a radius $R = 82.5$ mm. Moreover, the results in Tables 125-130 are for length-to-radius ratios $L/R = 0.5$, 1, 1.74, 3, 5, and 10, respectively. Smerdov's results were obtained by substituting displacement functions identical to equations (77) into a variational statement that is based on Flügge's cylinder-buckling kinematics and that include the effects of live pressure.[28] As a result, Smerdov's analysis neglects the effects of the anisotropies associated with the B_{16}, B_{26}, D_{16}, and D_{26} constitutive terms. The results shown in Tables 125-130 for the present study were obtained by using the approximate Rayleigh-Ritz solution, which includes these anisotropies. Additional results are also shown in this table, in red, for the present study that correspond to the classical solution ($\tau = 0$), which neglects these anisotropies.

The results in Tables 125-130 indicate differences between the corresponding results obtained by Smerdov, using Flügge-type equations with live pressure, and in the present study, by using Sanders' equations with live pressure, are less than 1.5% and, for the most part, are nonexistent. In addition, the results obtained in the present study for the cylinders with $L/R = 0.5$ and 1 (Tables 125 and 126) indicate differences between the corresponding results obtained by using Donnell's equations with dead pressure and Sanders' equations with live pressure that are

less than 2%, for all table entries, and in many cases substantially smaller. Similar differences are found for these short cylinders between Sanders' equations without live pressure and with nonlinear rotations about the normal neglected and Sanders' equations with live pressure, and between Sanders' equations with and without live pressure. For the cylinders with L/R = 1.74 and 3 (Tables 127 and 128), the maximum difference obtained between Sanders' equations with live pressure and either of Donnell's equations with dead pressure, Sanders' equations without live pressure and with nonlinear rotations about the normal neglected, and Sanders' equations without live pressure increases to about 5% for all table entries. For the cylinders with L/R = 5 and 10 (Tables 129 and 130), the maximum difference increases to approximately 7% and 13%, respectively.

Most of laminate constructions shown in Tables 125-130 are unbalanced (nonzero A_{16} and A_{26} constitutive terms) and, as a result, experience a uniform torsional displacement under the application of uniform external pressure. Thus, strict adherence to the boundary conditions considered herein, for the prebuckling and buckling states implies that shearing stresses are induced into these cylinders by restraining the circumferential displacements at the ends. In addition, no restraint of axial displacement is present for these boundary conditions. For the simplified membrane prebuckling stress state considered herein, the induced uniform shearing stress resultant is found by first setting the shearing strain and axial stress resultant equal to zero, neglecting the B-matrix terms associated with the presence of a uniform radial displacement field, and setting the thermal terms equal to zero in equation (21a). The resulting equations are then solved and equations (28) are used to get the loading parameter associated with the induced shearing stresses

$$L_3 = \frac{A_{12}A_{16} - A_{11}A_{26}}{A_{11}A_{22} - A_{12}^2} L_2 \tag{151}$$

The values of L_3 obtained from this equation are shown in Tables 125-130 along with the results that were obtained by using the approximate Rayleigh-Ritz solution with the anisotropies included. For the cylinders with L/R = 0.5 and 1 (Tables 125 and 126) the approximate analysis predicts reductions in the buckling pressures due to wall anisotropies that are as large as approximately 9% and 22%, respectively. These reductions in the buckling pressures are based on comparing Smerdov's results and the corresponding results based on Sanders' equations with live pressure. Similarly, for the cylinders with L/R = 1.74 and 3 (Tables 127 and 128), the reductions in the buckling pressures due to wall anisotropies are as large as approximately 62% and 5%, respectively. For the cylinders with L/R = 5 and 10 (Tables 129 and 130), the predicted reductions are approximately 36% and 16%, respectively.

The differences in the buckling resistance predictions obtained in the present study by using Donnell's equations (red curves), Sanders equations with dead pressure (blue curves), and Sanders equations with live pressure (black curves) are illustrated in figures 122-127 for $[(\pm 30)_6]_s$, $[(\pm 45)_6]_s$, and $[(\pm 60)_6]_s$ laminated-composite cylinders with radius-to-thickness ratios R/h =50 and 500. The lamina material properties used to obtain these results are $E_1 = 30 \times 10^6$ psi, $E_2 =$

0.75×10^6 psi, $G_{12} = 0.375 \times 10^6$ psi, and $\nu_{12} = 0.25$. The buckling resistance is measured by the nondimensional coefficient $\frac{p^{cr}R^3}{\sqrt{D_{11}D_{22}}}$ for values of $0.2 \le L/R \le 50$, where D_{11} and D_{22} are the principal shell-wall bending stiffnesses appearing in equations (12c). For each laminate considered, it is presumed that the anisotropy associated with the D_{16} and D_{26} constitutive terms is negligible. In calculating results for cylinders subjected to uniform external pressure, the circumferential wave numbers $n = 0$ and $n = 1$ are typically not used because these two wave numbers correspond to axisymmetric deformation modes and column-buckling modes that are inconsistent with the uniform external pressure loading. However, the two wave numbers were included in the calculation of the subsequent results to facilitate the presentation of results for cylinders subjected to hydrostatic pressure.

For the $[(\pm 30)_6]_s$ cylinders with $R/h = 50$, shown in figure 122, the differences between the corresponding results predicted by Donnell's and Sanders' equations with live pressure, and between the two sets of Sanders' equations, are less than about 7% for $L/R \le 5$. For $5 < L/R < 12$, differences are large as approximately14% are found. As L/R increase beyond 12, the differences are generally much larger. It is important to note that the rightmost branch of the red festoon curve corresponds to $m = n = 1$. Upon eliminating these solutions, the red curve becomes coincident with the blue curve. Thus, for values of $L/R > 30$, the curves obtained by using Donnell's equations and by using Sanders' equations with dead pressure asymptotically approach the approximate value $\frac{p^{cr}R^3}{\sqrt{D_{11}D_{22}}} = 1.6$. In contrast, the curve obtained by using Sanders' equations with live pressure asymptotically approaches the approximate value $\frac{p^{cr}R^3}{\sqrt{D_{11}D_{22}}} = 1.2$. These asymptotic results correspond to a maximum difference of approximately 33% and to the $m = 1$ and $n = 2$ flattened-cylinder buckling mode.

Results similar to those in figure 122 are presented in figures 123 and 124 for the $[(\pm 45)_6]_s$, and $[(\pm 60)_6]_s$ cylinders with $R/h = 50$, respectively. The rightmost branch of the red festoon curves in these two figures also corresponds to $m = n = 1$, and upon eliminating these solutions, each red curves becomes coincident with the corresponding blue curve. For the $[(\pm 45)_6]_s$ cylinders (figure 123), the differences between the corresponding results predicted by Donnell's and Sanders' equations with live pressure, and between the two sets of Sanders' equations, are less than about 6% for $L/R \le 2$. For $2 < L/R < 7$, differences become as large as approximately12%, and as L/R increases beyond 7, the differences increase substantially. For values of $L/R > 20$, the curves obtained by using Donnell's equations and by using Sanders' equations with dead pressure asymptotically approach the approximate value $\frac{p^{cr}R^3}{\sqrt{D_{11}D_{22}}} = 4$. In contrast, the curve obtained by using Sanders' equations with live pressure asymptotically approaches the approximate value $\frac{p^{cr}R^3}{\sqrt{D_{11}D_{22}}} = 3$. These asymptotic results correspond to a maximum difference of approximately 33% and to the $m = 1$ and $n = 2$ flattened-cylinder

buckling mode.

For the $[(\pm 60)_6]_s$ cylinders shown in figure 124, the differences between the corresponding results predicted by Donnell's and Sanders' equations with live pressure, and between the two sets of Sanders' equations, are also less than about 6% for $L/R \le 2$. For $2 < L/R < 5$, differences become as large as approximately12%, and as L/R increases beyond 5, the differences increase substantially. For values of $L/R > 14$, the curves obtained by using Donnell's equations and by using Sanders' equations with dead pressure asymptotically approach the approximate value $\frac{p^{cr}R^3}{\sqrt{D_{11}D_{22}}} = 10.2$. In contrast, the curve obtained by using Sanders' equations with live pressure asymptotically approaches the approximate value $\frac{p^{cr}R^3}{\sqrt{D_{11}D_{22}}} = 7.7$. These asymptotic results also correspond to a maximum difference of approximately 33% and to the $m = 1$ and $n = 2$ flattened-cylinder buckling mode.

Results for the $[(\pm 30)_6]_s$ cylinders with $R/h = 500$, shown in figure 125, indicate that the differences between the corresponding results predicted by Donnell's and Sanders' equations with live pressure, and between the two sets of Sanders' equations, are less than about 7% for $L/R \le 18$. For approximately $18 < L/R < 39$, differences are large as approximately12% are found. For $39 \le L/R \le 50$, the differences between the corresponding results predicted by Donnell's and Sanders' equations with live pressure are at most 10%, whereas the differences between the corresponding results predicted by the two sets of Sanders' equations increase to approximately 34%. However, results for the $[(\pm 45)_6]_s$ cylinders with $R/h = 500$, shown in figure 126, indicate that the differences between the corresponding results predicted by Donnell's and Sanders' equations with live pressure are less than about 7% for $L/R \le 12$. The differences predicted between the two sets of Sanders' equations, are less than about 7% for approximately $L/R < 10$. In the range $10 \le L/R < 21$, differences between cooresponding results obtained from the two sets of Sanders' equations are large as approximately12% are found. The differences in the corresponding results obtained from Donnell's and Sanders' equations with live pressure are mostly less than 10%. For $21 \le L/R \le 50$, the differences between the corresponding results predicted by the two sets of Sanders' equations are, for the most part, approximately 33%. The differences between the corresponding results predicted by Donnell's and Sanders' equations with live pressure in this range increase from less than 1% to 30% as L/R increases.

Results for the $[(\pm 60)_6]_s$ cylinders with $R/h = 500$, shown in figure 127, indicate that the differences between the corresponding results predicted by Donnell's and Sanders' equations with live pressure, and between the two sets of Sanders' equations, are less than about 6% for $L/R \le 7$. For approximately $7 < L/R < 15$, differences are large as approximately12% are found. For $15 \le L/R \le 50$, the differences between the corresponding results predicted by the two sets of Sanders' equations are, for the most part, also approximately 33%. The differences between the corresponding results predicted by Donnell's and Sanders' equations with live pressure in this range also increase from less than 1% to 30% as L/R increases. It is important to note that the rightmost branch of the red festoon curve shown in figure 127 also corresponds to $m = n = 1$.

Uniform hydrostatic pressure loads. Values of the hydrostatic buckling pressures obtained by Perry and Miller[92] and obtained in the present study are presented in Tables 131-133 for selected symmetric and unsymmetric cross-ply cylinders with a wall thickness $h = 0.12$ in. The lamina material properties are $E_1 = 19 \times 10^6$ psi, $E_2 = 1.5 \times 10^6$ psi, $G_{12} = 1.0 \times 10^6$ psi, and $\nu_{12} = 0.28$. Moreover, the results in Tables 131 and 132 are for cylinders with $L/R = 6.050$ and $R/h = 25$. The results in Tables 133 are for cylinders with $L/R = 6.555$ and $R/h = 38$. The results obtained by Perry and Miller that are presented in these tables are based on Donnell's equations with dead pressure. Additional results obtained by Perry and Miller that are presented Table 133 were obtained from finite element analyses with dead pressure loads. Perry and Miller indicate in reference 93 that the finite element analyses were not completely converged and errors in the range of 3%-5% were expected. Values of the D_{22} constitutive term were also given by Perry and Miller that were matched exactly in the present study. Additional results obtained in the present study are also presented in Tables 131-133 that are based on Sanders' equations with live pressure, Sanders' equations with live pressure and nonlinear rotations about the normal are neglected, and Donnell's equations with dead pressure.

The results in Table 131 show differences between the predicted buckling pressures obtained by Perry and Miller and the corresponding results obtained in the present study that range from 2%-5%. In contrast, the results in Tables 132 and 133 show differences that range from approximately 1%-14% and 2%-10%, respectively. The finite element results obtained by Perry and Miller and the results obtained in the present study by using Sanders' equations with live pressure and nonlinear rotations about the normal neglected show differences that range from approximately 2%-10%. The results obtained in the present study and shown in Tables 131-133 also indicate that neglecting the effects of live pressure in Sanders' equations yields differences as large as about 3%, 0.5%, and 26%, respectively. Similarly, the differences between the corresponding results obtained by using Sanders' equations with live pressure and Donnell's equations with dead pressure are at most approximately 10%, 5%, and 15%, respectively, in these three tables.

Results obtained by Perry and Miller[92] and obtained in the present study are given in Table 134 for $[90_6/\pm\theta/0_4]_S$ laminated-composite cylinders made of the same lamina material as the cylinders in Tables 131-133 and with a wall thickness $h = 0.12$ in. The results in Table 134 are also for cylinders with $L/R = 6.050$ and $R/h = 25$, and correspond to values of $\theta = 0$, 15, 30, 45, 60, 75, and 90 degrees. One set of the results obtained by Perry and Miller is based on Donnell's equations with dead pressure and the other set was obtained from finite element analyses with dead pressure loads. Additional results obtained in the present study are also presented in Tables 134 that are based on Sanders' equations with live pressure, Sanders' equations with dead pressure, and Donnell's equations with dead pressure.

The results in Table 134 show differences between the predicted buckling pressures obtained by Perry and Miller and the corresponding results obtained in the present study, based on Donnell's equations with dead pressure, that range from approximately 2%-3%. However, the results in Table 134 also show differences between the predicted buckling pressures obtained by Perry and Miller, from finite element analyses, and the corresponding results obtained in the present study, based on Sanders' equations with dead pressure, that range from approximately

0.6%-8%. Since the $[90_6/\pm\theta/0_4]_S$ cylinder possess some anisotropies, results were obtained in the present study by using the approximate Rayleigh-Ritz analysis based on Sanders' equations with dead pressure. The results of these analyses are identical to the corresponding results shown in Table 134. The results obtained in the present study and shown in Table 134 also indicate that neglecting the effects of live pressure in Sanders' equations yields differences of about 27%. In contrast, the differences between the corresponding results obtained by using Sanders' equations with live pressure and Donnell's equations with dead pressure are less than 5%.

Normalized buckling pressures obtained by Smerdov[91] and in the present study are shown in Tables 135-140 for a variety of selected laminated-composite cylinders with the lamina material properties $E_1 = 146$ GPa, $E_2 = 10.8$ GPa, $G_{12} = 5.78$ GPa, and $\nu_{12} = 0.29$. These cylinders have a wall thickness $h = 0.5$ mm and a radius $R = 82.5$ mm. In particular, the results in Tables 135-140 are for length-to-radius ratios $L/R = 0.5$, 1, 1.74, 3, 5, and 10, respectively. Smerdov's results were obtained by substituting displacement functions identical to equations (77) into a variational statement that is based on Flügge's cylinder-buckling kinematics[28] and that includes the effects of live pressure, but neglects the effects of the anisotropies associated with the B_{16}, B_{26}, D_{16}, and D_{26} constitutive terms. The results shown in Tables 135-140 for the present study were obtained by using the approximate Rayleigh-Ritz solution, which includes these anisotropies. Additional results are also shown in this table, in red, for the present study that correspond to the classical solution ($\tau = 0$), which neglects these anisotropies.

The results in Tables 135-140 indicate differences between the corresponding results obtained by Smerdov, using Flügge-type equations with live pressure, and in the present study, by using Sanders' equations with live pressure, are less than 1.5% and, to a large extent, are nonexistent. In addition, the results obtained in the present study for the cylinders with $L/R = 0.5$ and 1 (Tables 135 and 136) indicate differences between the corresponding results obtained by using Donnell's equations with dead pressure and Sanders' equations with live pressure that are less than 1%, for all table entries, and in many cases smaller. Similar differences are found for these short cylinders between Sanders' equations without dead pressure and with nonlinear rotations about the normal neglected and Sanders' equations with live pressure, and between Sanders' equations with and without live pressure. For the cylinders with $L/R = 1.74$ and 3 (Tables 137 and 138), the maximum difference obtained between Sanders' equations with live pressure and either of Donnell's equations with dead pressure, Sanders' equations without dead pressure and with nonlinear rotations about the normal neglected, and Sanders' equations without live pressure is about 5% for all table entries. For the cylinders with $L/R = 5$ and 10 (Tables 139 and 140), the maximum differences are approximately 7% and 13%, respectively.

Most of laminate constructions shown in Tables 135-140 are unbalanced (nonzero A_{16} and A_{26} constitutive terms) and, as a result, experience a uniform torsional displacement under the application of uniform hydrostatic pressure. Thus, strict adherence to the boundary conditions considered herein, for the prebuckling and buckling states, implies that shearing stresses are induced into these cylinders by restraining the circumferential displacement at the ends. For the simplified membrane prebuckling stress state considered herein, the induced uniform shearing stress resultant is found by first setting the shearing strain equal to zero, neglecting the B-matrix terms associated with the presence of a uniform radial displacement field, and setting the thermal terms equal to zero in equation (21a). The resulting equations are then solved and equations (28)

are used to get the loading parameter associated with the induced shearing stresses

$$L_3 = \frac{(A_{12}A_{26} - A_{22}A_{16})L_1 + (A_{12}A_{16} - A_{11}A_{26})L_2}{A_{11}A_{22} - A_{12}^2} \tag{152}$$

The values of L_3 obtained from this equation are shown in Tables 135-140 along with the results that were obtained in the present study by using the approximate Rayleigh-Ritz solution with the anisotropies included. For the cylinders with L/R = 0.5 and 1 (Tables 135 and 136) the approximate analysis predicts reductions in the buckling pressures due to wall anisotropies that are as large as approximately 7% and 32%, respectively. These reductions in the buckling pressures are based on comparing Smerdov's results and the corresponding results based on Sanders' equations with live pressure. Similarly, for the cylinders with L/R = 1.74 and 3 (Tables 137 and 138), the reductions in the buckling pressures due to wall anisotropies that are as large as approximately 76% and 48%, respectively. For the cylinders with L/R = 5 and 10 (Tables 139 and 140), the predicted reductions are as large as approximately 41% and 18%, respectively.

Buckling pressures obtained by Fan et al.[93] and in the present study are given in Table 141 for a laminated composite cylinder with a radius R = 250.625 mm, a wall thickness h = 1.25 mm, and a length L = 530 mm. In addition to uniform hydrostatic pressure, results are also given for combined hydrostatic pressure and torsion defined by $L_1 = 0.5$, $L_2 = 1$, and $L_3 = 1$. The cylinder-wall laminate construction is defined by the stiffnesses indicated in the table.

The results in Table 141 indicate differences between the corresponding results obtained by Fan et al., using Flügge-type equations with live pressure, and obtained in the present study, by using Sanders' equations with live pressure, are less than approximately 1%. In addition, differences between the corresponding results obtained in the present study by using Donnell's equations with dead pressure and Sanders' equations with live pressure that are less than about 1%. Moreover, the results show that neglecting the nonlinear rotations about the normal in Sanders' equations with live pressure has negligible effects.

Differences in the buckling resistance predictions were obtained in the present study by using Donnell's equations, Sanders equations with dead pressure, and Sanders equations with live pressure for the hydrostatic-pressure loads. In particular, results were obtained for the $[(\pm 30)_6]_s$, $[(\pm 45)_6]_s$, and $[(\pm 60)_6]_s$ laminated-composite cylinders with radius-to-thickness ratios R/h =50 and 500 that have been described previously herein. In calculating results for this loading condition, the circumferential wave numbers n = 0 and n = 1 were included because of the presence of axial compression. The results obtained for these cylinders are identical to the results presented in figures 122-127, including the rightmost branch of the red festoon curves in these figures that correspond to the column-buckling mode given by m = n = 1.

Concluding Remarks

A detailed, complete exposition of the nonlinear and linear-bifurcation buckling equations for elastic, geometrically perfect, right-circular cylindrical shells subjected to combined loads has been presented. The loads include compression, shear, and "live" external and hydrostatic pressure in which the pressure remains normal to the shell surface during deformation. Moreover, the loads are partitioned into one group that produces a stable prebuckling stress state prior to the application of a second group that leads to buckling. The analysis includes elastic constitutive equations that are applicable to stiffened or unstiffened cylinders made from isotropic or laminated-composite materials. Complete sets of equations have been presented for the nonlinear boundary-value problem of shell buckling and the corresponding prebuckling and linear-bifurcation buckling problems. In addition, a variational statement for linear-bifurcation buckling has been presented that includes live pressure loads. These sets of equations are based on Sanders' nonlinear equations for the practical case of shell deformations with "small" strains and "moderately small" rotations, and negligible transverse shearing deformations. In addition, these sets of equations contain Donnell's quasi-shallow shell equations as a special case.

In addition to a general Rayleigh-Ritz formulation for linear-bifurcation buckling, a detailed three-parameter approximate Rayleigh-Ritz solution and a classical solution to the corresponding boundary-eigenvalue-problem have been presented for the case of simply supported edges, in which the circumferential and radial displacements are constrained. Extensive comparisons of results obtained from these solutions with published results spanning nearly fifty years have also been presented. These comparisons are for a wide variety of cylinder constructions that include isotropic cylinders with, and without, a regular array of rings and stringers, and unstiffened cylinders made of laminated-composite materials. Moreover, results for numerous laminated-composite cylinders have been presented that include a wide variety of shell-wall orthotropies and anisotropies. For almost all of the results that have been presented, the comparisons show that the approximate Rayleigh-Ritz and classical solutions generally predict the buckling behavior accurately. In some cases, such as cylinders subjected to torsion, the comparisons indicate that the three-parameter approximate Rayleigh-Ritz solution is inadequate. Numerous comparisons have also been presented that clearly show the descepancies between the results obtained by using Donnell's equations and variants of Sanders' equations, as a function of cylinder geometry, stiffnener properties, and material composition. For some cases, nondimensional parameters have been identified and "master" curves have been presented that faciliate concise representation of a very broad range of results. Overall, the detail and completeness of the presentation and results should make confident-use of the equations accessable to design engineers with a less specialized background, and provide a "stand-alone" reference document. Moreover, the comprehensive set of comparisons with previously published results should add confidence to their usage.

References

1. Nemeth, M. P. and Starnes, J. H., Jr.: The NASA Monographs on Shell Stability Design Recommendations - A Review and Suggested Improvements. NASA TP-1998-206290, January 1998.

2. Hilburger, M. W., Britt, V. O., and Nemeth, M. P.: Buckling Behavior of Compression-Loaded Quasi-isotropic Curved Panels with a Circular Cutout. *International Journal of Solids and Structures*, Vol. 38, No. 9, 2001, pp. 1495-1522.

3. Hilburger, M. W., Nemeth, M. P., and Starnes, J. H., Jr.: Nonlinear and Buckling Behavior of Curved Panels Subjected to Combined Loads. Presented at the AIAA/ASME/ASCE/AHS/ASC 42nd Structures, Structural Dynamics, and Materials Conference, Seattle, WA, AIAA Paper No. 2001-1398, April 16-19, 2001.

4. Hilburger, M. W.; Nemeth, M. P.; Riddick, J. C.; and Thornburg, R. P.: Compression-Loaded Composite Panels With Elastic Edge Restraints and Initial Prestress. NASA/TP-2005-213906, August 2005.

5. Nemeth, M. P., Britt, V. O., Collins, T. J., and Starnes, J. H., Jr.: Nonlinear Analysis of the Space Shuttle Super-Lightweight External Fuel Tank. NASA TP 3616, December, 1996.

6. Nemeth, M. P., Britt, V. O., Young, R. D., Collins, T. J., and Starnes, J. H., Jr.: Nonlinear Behavior of Space Shuttle Superlightweight Liquid-Oxygen Tank Under Prelaunch Loads. *Journal of Spacecraft and Rockets*, Vol. 36, No.6, November-December, 1999, pp. 788-803.

7. Nemeth, M. P., Young, R. D., Collins, T. J., and Starnes, J. H., Jr.: Nonlinear Behavior of Space Shuttle Superlightweight Liquid-Oxygen Tank Under End-of-Flight Loads. *Journal of Spacecraft and Rockets*, Vol. 36, No.6, November-December, 1999, pp. 828-835.

8. Young, R. D., Nemeth, M. P., Collins, T. J., and Starnes, J. H., Jr.: Nonlinear Behavior of Space Shuttle Superlightweight Liquid-Oxygen Tank Under Booster Ascent Loads. *Journal of Spacecraft and Rockets*, Vol. 36, No.6, November-December, 1999, pp. 820-827.

9. Nemeth, M. P., Young, R. D., Collins, T. J., and Starnes, J. H., Jr.: Effects of Welding-Induced Imperfections on Behavior of Space Shuttle Superlightweight Liquid-Oxygen Tank. *Journal of Spacecraft and Rockets*, Vol. 36, No.6, November-December, 1999, pp. 812-819.

10. Nemeth, M. P., Young, R. D., Collins, T. J., and Starnes, J. H., Jr.: Effects of Initial Geometric Imperfections on the Nonlinear Response of the Space Shuttle Superlightweight Liquid-Oxygen Tank. *International Journal of Non-Linear Mechanics*, Vol. 37, No.4-5, June, 2002, pp. 723-744.

11. Starnes, J. H., Jr. ; Hilburger, M. W.; and Nemeth, M. P.: The Effects of Initial Imperfections on the Buckling of Composite Shells. *Composite Structures: Theory and Practice*, ASTM STP 1383, 2000, pp. 529-550.

12. Hilburger, M. W. and Starnes, J. H., Jr.: Effects of Imperfections on the Buckling Response of Compression-Loaded Composite Shells. *International Journal of Non-Linear Mechanics*, Vol. 37, No.4-5, June, 2002, pp. 623-643.

13. Hilburger, M. W. and Starnes, J. H., Jr.: Effects of Imperfections on the Buckling Response of Composite Shells. *Thin-Walled Structures*, vol. 42, 2004, pp. 369-397.

14. Hilburger, M. W. and Starnes, J. H., Jr.: Parametric Study on the Response of Compression-Loaded Composite Shells with Geometric and Material Imperfections. NASA/TM-2004-212676, September, 2004.

15. Hilburger, M. W. and Starnes, J. H., Jr.: Buckling and Failure of Compression-Loaded Composite Cylindrical Shells with Geometric and Material Imperfections. NASA/TM-2004-212677, September, 2004.

16. Hilburger, M. W.; Nemeth, M. P.; and Starnes, J. H., Jr.: Shell Buckling Design Criteria Based on Manufacturing Imperfection Signatures. *AIAA Journal*, vol. 44, no. 3, pp. 654-663, 2006.

17. Brush, D. O.; and Almroth, B.: *Buckling of Bars, Plates, and Shells*. McGraw-Hill, 1975.

18. Flügge, W.: *Stresses in Shells*. Second ed., Springer-Verlag, 1973.

19. Sanders, J. L.; Jr.: Nonlinear Theories for Thin Shells. *Quarterly of Applied Mathematics*, vol. 21, no. 1, 1963, pp. 21-36.

20. Sanders, J. L.; Jr.: An Improved First-Approximation Theory for Thin Shells. NASA TR R-24, February, 1959.

21. Kraus, H.: *Thin Elastic Shells*. John Wiley & Sons, Inc., 1967.

22. Budiansky, B.: Notes on Nonlinear Shell Theory. *Journal of Applied Mechanics*, vol. 35, no. 2, 1968, pp. 393-401.

23. Cohen, G. A.: Conservativeness of a Normal Pressure Field Acting on a Shell. *AIAA Journal*, vol. 4, no. 10, 1966, p. 1886.

24. Koiter, W. T.: General Equations of Elastic Stability for Thin Shells. D. Muster, ed., Proceedings- Symposium on the Theory of Shells, Lloyd Hamilton Donnell 70th Anniversary Volume, University of Houston, Houston, 1967, pp. 187-227.

25. Sheinman, I. and Tene, Y.: Potential Energy of a Normal Pressure Field Acting on an Arbitrary Shell. *AIAA Journal*, vol. 11, no. 8, 1973, p. 1216.

26. Cohen, G. A. : Computer Analysis of Asymmetric Buckling of Ring-Stiffened Orthotropic Shells of Revolution. *AIAA Journal*, vol. 6, no. 1, 1968, pp. 141-149.

27. Jones, R. M.: *Mechanics of Composite Materials*. Second ed., Taylor & Francis, 1999.

28. Nemeth, M. P.: A Treatise on Equivalent-Plate Stiffnesses for Stiffened Laminated-Composite Plates and Plate-Like Lattices. NASA/TP-2011-216882, January, 2011.

29. Dym, C. L.: On the Buckling of Cylinders in Axial Compression. *Journal of Applied Mechanics*, June, 1973, pp. 565-568.

30. Sheinman, I. and Simitses, G. J.: Buckling and Postbuckling of Imperfect Cylindrical Shells Under Axial Compression. *Computers and Structures*, vol. 17, no. 2, 1983, pp. 277-285.

31. Simitses, G. J.; Shaw, D,; and Sheinman, I.: Stability of Cylindrical Shells by Various Nonlinear Shell Theories. *Z. Angew. Math. u. Mech.*, vol. 65, no. 3, 1985, pp. 159-166.

32. Zou, R. D. and Foster, C. G.: Simple Solution for Buckling of Orthotropic Circular Cylindrical Shells. *Thin-Walled Structures*, vol. 22, 1995, pp. 143-158.

33. Xiang, Y.; Wang, C. M.; Lim, C. W.; and Kitipornchai, S.: Buckling of Intermediate Ring Supported Cylindrical Shells Under Axial Compression. *Thin-Walled Structures*, vol. 43, 2005, pp. 427-443.

34. Timoshenko, S. P. and Gere, J. M.: *Theory of Elastic Stability*. Second ed., McGraw-Hill, 1961.

35. Nemeth, M. P. and Mikulas, M. M., Jr.: Simple Formulas and Results for Buckling-Resistance and Stiffness Design of Compression-Loaded Laminated-Composite Cylinders. NASA/TP-2009-215778, August, 2009.

36. Yamaki, N. and Kodama, S.: Buckling of Circular Cylindrical Shells Under Compression-Report 1. Reports of the Institute of High Speed Mechanics, vol. 23, no. 229, 1971.

37. Batdorf, S. B.: A Simplified Method of Elastic-Stability Analysis for Thin Cylindrical Shells. NACA TR-874, March, 1947.

38. Yamaki, N. and Kodama, S.: Buckling of Circular Cylindrical Shells Under Compression-Report 2. Reports of the Institute of High Speed Mechanics, vol. 24, no. 239, 1971.

39. Mikulas, M. M., Jr.; Nemeth, M. P.; Oremont, L.; and Jegley, D. C.: Effect of Boundary Conditions on the Axial Compression Buckling of Homogeneous Orthotropic Composite Cylinders in the Long Column Range. Presented at the AIAA/ASME/ASCE/AHS/ASC 52nd Structures, Structural Dynamics, and Materials Conference, Denver, CO, AIAA Paper No. 2011-2126, April 4-7, 2011.

40. Yamaki, N.: Buckling of Circular Cylindrical Shells Under External Pressure. Reports of the Institute of High Speed Mechanics, vol. 20, no. 196, 1968-1969.

41. Vodenitcharova, T. and Ansourian, P.: Buckling of Circular Cylindrical Shells Subject to Uniform Lateral Pressure. *Engineering Structures*, vol. 18, no. 8, 1996, pp. 604-614.

42. Showkati, H. and Ansourian, P.: Influence of Primary Boundary Conditions on the Buckling of Shallow Cylindrical Shells. *Journal of Constructional Steel Research*, vol. 36, no. 1, 1996, pp. 53-75.

43. Wang, Y. and Billington, D. P.: Buckling of Cylindrical Shells by Wind Pressure. *Journal of the Engineering Mechanics Division*, ASCE, vol. 100, no, EM5, 1974, pp. 1005-1023.

44. Simitses, G. J. and Aswani, M.: Buckling of Thin Cylinders Under Uniform Lateral Loading. *Journal of Applied Mechanics*, vol. 41, no. 3, 1974, pp. 827-829.

45. Soong, T.-C.: Buckling of Cylindrical Shell Under Pressure by Using Sanders' Theory. *AIAA Journal*, vol. 5, no. 5, 1967, pp. 1049-1052.

46. Hoff, N. J. and Soong, T.-C.: Buckling of Circular Cylindrical Shells in Axial Compression. *International Journal of Mechanical Sciences*, vol. 7, 1965, pp. 489-520.

47. Fan, S. R.; Geier, B.; Rohwer, K.; and Liu, D. C.: Stability of Layered Anisotropic Cylindrical Shells under Combined Loading. *Zeitschrift fur Flugwissenschaften und Weltraumforschung*, vol. 7, no. 5, 1983, pp. 293-301.

48. Sobel, L. H.: Effects of Boundary Conditions on the Stability of Cylinders Subject to Lateral and Axial Pressures. *AIAA Journal*, vol. 2, no. 8, 1964, pp. 1437-1440.

49. Ashour, H. A. and Sobel, L. H.: Buckling of Prismatic Structures Under Biaxial Loading. *Computers & Structures*, vol. 12, 1980, pp. 749-758.

50. Singer, J.; Baruch, M.; and Harari, O.: Inversion of the Eccentricity Effect in Stiffened Cylindrical Shells Buckling Under External Pressure. *Journal of Mechanical Engineering Science*, vol. 8, no. 4, 1966, pp. 363-373.

51. Singer, J.; Baruch, M.; and Harari, O.: Further Remarks on the Effect of Eccentricity of Stiffeners on the General Instability of Stiffenerd Cylindrical Shells. TAE Report 42 (revised), Technion Research and Development Foundation, 1965.

52. Hutchinson, J.: Axial Buckling of Pressurized Imperfect Cylindrical Shells. *AIAA Journal,* vol. 3, no. 8, 1965, pp. 1461-1466.

53. Batdorf, S. B.; Stein, M.; and Schildcrout, M.: Critical Stress of Thin-Walled Cylinders in Torsion. NACA TN 1344, June 1947.

54. Yamaki, N.: *Elastic Stability of Circular Cylindrical Shells*. North-Holland, 1984.

55. Yamaki, N. and Kodama, S.: Buckling of Cylindrical Shells Under Torsion. Report 2, Reports of the Institute of High Speed Mechanics, vol. 18, 1966-1967.

56. Baruch, M.; Singer, J.; and Weller, T.: Effect of Eccentricity of Stiffeners on the General Instability of Cylindrical Shells Under Torsion. *Israel Journal of Technology*, vol. 4, no. 1, 1966, pp. 144-154.

57. Baruch, M.; Singer, J.; and Weller, T.: Effect of Eccentricity of Stiffeners on the General Instability of Stiffened Cylindrical Shells Under Torsion. TAE Report 43, Technion Research and Development Foundation, 1965.

58. Fan, S. R.; Geier, B.; Rohwer, K.; and Liu, D. C.: Stability of Layered Anisotropic Cylindrical Shells under Combined Loading. *Zeitschrift fur Flugwissenschaften und Weltraumforschung*, vol. 7, no. 5, 1983, pp. 293-301.

59. Block, D. L.; Card, M. F.; and Mikulas, M. M., Jr.: Buckling of Eccentrically Stiffened Orthotropic Cylinders. NASA TN D-2960, August, 1965.

60. Hedgepeth, J. M. and Hall, D. B.: Stability of Stiffened Cylinders. *AIAA Journal,* vol. 3, no. 12, 1965, pp. 2275-2286.

61. Singer, J.;Baruch, M.; and Harari, O.: On the Stability of Eccentrically Stiffened Cylindrical Shells Under Axial Compression. *International Journal of Solids and Structures,* vol. 3, 1967, pp. 445-470.

62. Card, M. F.: Preliminary Results of Compression Tests on Cylinders with Eccentric Longitudinal Stiffeners. NASA TM X-1004, September, 1964.

63. Card, M. F. and Jones, R. M.: Experimental and Theoretical Results for Buckling of Eccentrically Stiffened Cylinders. NASA TN D-3639, October, 1966.

64. Peterson, J. P. and Dow, M. B.: Compression Tests on Circular Cylinders Stiffened Longitudinally by Closely Spaced Z-Section Stringers. NASA MEMO 2-12-59L, 1959.

65. Singer, J.; Baruch, M.; and Harari, O.: On the Stability of Eccentrically Stiffened Cylindrical Shells Under Axial Compression. TAE Report 44, Technion Research and Development Foundation, 1965

66. Singer, J.; Arbocz, J.; and Babcock, C. D.: Buckling of Imperfect Stiffened Cylindrical Shells Under Axial Compression. *AIAA Journal*, vol. 9, no. 1, 1971, pp. 68-75.

67. Baruch, M. and Singer, J.: Effect of Eccentricity of Stiffeners on the General Instability of Stiffened Cylindrical Shells under Hydrostatic Pressure. *Journal of Mechanical Engineering Science*, vol. 5, no. 1, 1963, pp. 23-27.

68. McElman, J. A.; Mikulas, M. M., Jr.; and Stein, M.: Static and Dynamic Effects of Eccentric Stiffening of Plates and Cylindrical Shells. *AIAA Journal*, vol. 4, no. 5, 1966, pp. 887-894.

69. Tian, J.; Wang, C. M.; and Swaddiwudhipong, S.: Elastic Buckling Analysis of Ring-Stiffened Cylindrical Shells Under General Pressure Loading via the Ritz Method. *Thin-Walled Structures*, vol. 35, 1999, pp. 1-24.

70. Schmit, L. A., Jr.; Morrow, W. M., II; Kicher, T. P.: A Structural Synthesis Capability for Integrally Stiffened Cylindrical Shells. AIAA/ASME 9th Structures, Structural Dynamics, and Materials Conference, Palm Springs, CA, April 1-3, 1968, AIAA Paper No. 68-327.

71. Kardomateas, G. A.: Bifurcation of Equilibrium in Thick Orthotropic Cylindrical Shells Under Axial Compression. *Journal of Applied Mechanics*, vol. 62, 1995, pp. 43-52.

72. Jones, R. M. and Morgan, H. S.: Buckling and Vibration of Cross-Ply Laminated Circular Cylindrical Shells. *AIAA Journal*, vol. 13, no. 5, 1975, pp. 664-671.

73. Soldatos, K. P. and Tzivanidis, G. J.: Buckling and Vibration of Cross-Ply Laminated Non-Circular Cylindrical Shells. *Journal of Sound and Vibration*, vol. 82, no. 3, 1982, pp. 425-434.

74. Weaver, P. M.: Private communication. University of Bristol, United Kingdom, 2011.

75. Shen, Hui-Shen: Postbuckling Analysis of Stiffened Laminated Cylindrical Shells Under Combined External Liquid Pressure and Axial Compression. *Engineering Structures*, vol. 20, no. 8, 1998, pp. 738-751.

76. Khdeir, A. A.; Reddy, J. N.; and Frederick, D.: A Study of Bending, Vibration and Buckling of Cross-Ply Circular Cylindrical Shells with Various Shell Theories. *International Journal of Engineering Science*, vol. 27, no. 11, 1989, pp. 1337-1351.

77. Nosier, A. and Reddy, J. N.: Vibration and Stability Analyses of Cross-Ply Laminated Circular Cylindrical Shells. *Journal of Sound and Vibration*, vol. 157, no. 1, 1992, pp. 139-159.

78. Iu, V. P. and Chia, C. Y.: Effect of Transverse Shear on Nonlinear Vibration and Postbuckling of Anti-Symmetric Cross-Ply Imperfect Cylindrical Shells. *International Journal of Mechanical Sciences*, vol. 30, no. 10, 1988, pp. 705-718.

79. Han, B. and Simitses, G. J.: Analysis of Anisotropic Laminated Cylindrical Shells Subjected to Destabilizing Loads, Part II: Numerical Results. *Composite Structures*, vol. 19, 1991, pp. 183-205.

80. Geier, B.; Meyer-Piening, H.-R.; and Zimmermann, R.: On the Influence of Laminate Stacking on Buckling of Composite Cylindrical Shells Subjected to Axial Compression. *Composite Structures*, vol. 55, 2002, pp. 467-474.

81. Meyer-Piening, H.-R.; Farshad, M.; Geier, B.; and Zimmermann, R.: Buckling Loads of CFRP Composite Cylinders under Combined Axial and Torsion Loading - Experiments and Computations. *Composite Structures*, vol. 53, 2001, pp. 427-435.

82. Geier, B. and Singh, G.: Some Simple Solutions for Buckling Loads of Thin and Moderately Thick Cylindrical Shells and Panels Made of Laminated Composite Material. *Aerospace Science and Technology*, vol. 1, 1997, pp. 47-63.

83. Khot, N. S. and Venkayya, V. B.: Effect of Fiber Orientation on Initial Postbuckling Behavior and Imperfection Sensitivity of Composite Cylindrical Shells. AFFDL-TR-70-125, Wright-Patterson Air Force Base, Ohio, 1970.

84. Arbocz, J.: The Effect of Initial Imperfections on Shell Stability - A Review. Delft University of Technology Report LR-618, The Netherlands, 1991.

85. Arbocz, J.: On a High-Fidelity Hierarchial Approach to Buckling Load Calculations. European Conference on Spacecraft Structures, Materials & Mechanical Testing 2005, Noordwijk, The Netherlands, May 10-12, 2005 (ESA SP-581, August 2005).

86. Uemura, M. and Kasuya, H.: Coupling Effect on Axial Compressive Buckling of Laminated Composite Cylindrical Shells. *Progress in Science and Engineering of Composites*, T. Hayashi, K. Kawata, and S. Umekawa, eds., Japan Society for Composite Materials, 1982, pp. 583-590.

87. Sun, G.: A Practical Approach to Optimal Design of Laminated Cylindrical Shells for Buckling. *Composites Science and Technology*, vol. 36, 1989, pp. 243-253.

88. Smerdov, A. A.: A Computational Study in Optimum Formulations of Optimization Problems on Laminated Cylindrical Shells for Buckling, I. Shells Under Axial Compression. *Composites Science and Technology*, vol. 60, 2000, pp. 2057-2066.

89. Wong, K. F. W. and Weaver, P. M.: Approximate Solution for the Compression Buckling of Fully Anisotropic Cylindrical Shells. *AIAA Journal*, vol. 43, no. 12, 2005, pp. 2639-2645.

90. Simitses, G. J. and Anastasiadis, J. S.: Shear Deformable Theories for Cylindrical Laminates-Equilibrium and Buckling with Applications. *AIAA Journal*, vol. 30, no. 3, 1992, pp. 826-834.

91. Smerdov, A. A.: A Computational Study in Optimum Formulations of Optimization Problems on Laminated Cylindrical Shells for Buckling, II. Shells Under External Pressure. *Composites Science and Technology*, vol. 60, 2000, pp. 2067-2076.

92. Perry, T. and Miller, Z.: A Study of Jones' Equation for Buckling of Laminated Composite Cylinders Under External Hydrostatic Pressure. *Journal of Ship Research*, vol. 37, no. 3, 1993, pp. 239-252.

93. Fan, S. R.; Geier, B.; Rohwer, K.; and Liu, D. C.: Stability of Layered Anisotropic Cylindrical Shells under Combined Loading. *Zeitschrift fur Flugwissenschaften und Weltraumforschung*, vol. 7, no. 5, 1983, pp. 293-301.

Table 1. Nondimensional buckling stress, $\frac{\sigma_x^{cr}}{E}\left(1-\nu^2\right)$, for isotropic cylinders with simply supported edges and subjected to axial compression ($\nu = 0.30$, R = 4.0 in., R/h = 91.287)

Wave number, n	$\frac{L}{mR}$	Ref. 29			Present study	
		Flügge	Koiter-Budiansky	Donnell	Donnell	Sanders
1	0.01	0.98698	0.98692	0.98697	0.98699	0.98698
	0.10	0.01080	0.01081	0.10810	0.10810	0.01081
	1.00	0.07549	0.07244	0.07614	0.07614	0.07546
	10.00	0.04609	0.03539	0.07452	0.07453	0.04016
	90.00	0.00055	0.00055	0.00933	0.00933	0.00055
2	0.01	0.98704	0.98698	0.98705	0.98705	0.98704
	0.10	0.01086	0.01086	0.01086	0.01086	0.01086
	1.00	0.04591	0.04324	0.04688	0.04688	0.04588
	10.00	0.00510	0.00501	0.00705	0.00705	0.00509
	90.00	0.05919	0.05917	0.13146	0.13146	0.05867
3	0.01	0.98714	0.98708	0.98715	0.98715	0.98714
	0.10	0.01095	0.01095	0.01096	0.01096	0.01096
	1.00	0.02492	0.02373	0.02558	0.02559	0.02491
	10.00	0.00696	0.00693	0.00947	0.00947	0.00695
	90.00	0.47289	0.47284	0.66496	0.66496	0.45138
4	0.01	0.98728	0.98722	0.98729	0.98729	0.98728
	0.10	0.01108	0.01108	0.01108	0.01109	0.01108
	1.00	0.01372	0.01327	0.01410	0.01410	0.01371
	10.00	0.02207	0.02204	0.02660	0.02661	0.02204
	90.00	1.7382	1.7382	2.1013	2.1013	1.2268

Table 2. Buckling load N_x^{cr} (lb/in.), for isotropic† cylinders with simply supported edges, and subjected to axial compression (R = 4 in.)

L/R	R/h	Refs. 30 and 31	Present study		
		Donnell	Donnell	Sanders*	Sanders
1	1000	25.45	25.42 (16,19)[a]	25.28 (1,13)	25.15 (1,13)
	500	101.81	101.68 (10,17)	100.94 (1,11)	100.23 (1,11)
	250	407.23	406.72 (9,4)	401.86 (1,9)	397.95 (1,9)
	80	3977.0	3971.8 (5,3)	3930.4 (2,8)	3906.8 (2,8)
2	188.7	714.94	713.89 (14,8)	695.83 (1,6)	679.27 (1,6)
5	250	407.23	406.71 (28,14)	394.08 (1,4)	371.91 (1,4)
	188.7	714.94	713.88 (38,5)	669.52 (1,4)	631.84 (1,4)
10	250	407.23	406.72 (35,14)	363.44 (1,3)	327.76 (1,3)
	188.7	714.94	713.88 (21,11)	644.75 (1,3)	581.43 (1,3)

[a] Numbers in parentheses, (m,n), indicate the number of axial half-waves and circumferential waves, respectively.
* Nonlinear rotations about the normal are neglected.

† $E = 10.5 \times 10^6$ psi, $\nu = 0.30$

Table 3. Nondimensional buckling load $\sqrt{3(1-\nu^2)}\,\frac{N_x^{cr}R}{Eh^2}$ for isotropic† cylinders with simply supported edges and subjected to axial compression (h = 0.1 in.)

R/h	L/R	Refs. 32 and 33		Present study		
		Flügge	Timoshenko	Donnell	Sanders*	Sanders
100	1	0.960713 (7)	0.962416 (7)[a]	1.00150 (3,9)[b]	0.981971 (1,7)	0.968204 (1,7)
	5	0.901542 (3)	0.904858 (3)	1.00003 (16,9)	0.981971 (5,7)	0.91319 (1,3)
	10	0.883810 (4)	0.886141 (4)	1.00008 (15,8)	0.942039 (3,4)	0.891808 (3,4)
500	1	0.984007 (11)	0.984486 (11)	1.00004 (13,0)	0.992698 (1,11)	0.985727 (1,11)
	5	0.923693 (5)	0.924240 (5)	1.00007 (1,5)	0.961337 (1,5)	0.925434 (1,5)
	10	0.923693 (5)	0.924240 (5)	1.00001 (15,13)	0.961337 (2,5)	0.925434 (2,5)

[a] Number in parentheses, (n) indicate the number of circumferential waves, n
[b] Numbers in parentheses, (m,n), indicate the number of axial half-waves and circumferential waves, respectively.
* Nonlinear rotations about the normal are neglected.

† $E = 10.5 \times 10^6$ psi, $\nu = 0.30$.

Table 4. Nondimensional buckling load $\frac{N_x^{cr} L^2}{\pi^2 D}$ for isotropic cylinders with simply supported edges and subjected to uniform axial compression ($\nu = 0.30$)

Batdorf-Z parameter†	Ref. 35	Present study		
	Donnell	Donnell	Sanders*	Sanders
0	1.0000	1.0000 (1,0)[a]	1.0000 (1,0)	1.0000 (1,0)
0.5	1.0308	1.0308 (1,0)	1.0308 (1,0)	1.0308 (1,0)
1	1.1232	1.1232 (1,0)	1.1232 (1,0)	1.1232 (1,0)
2	1.4928	1.4928 (1,0)	1.4928 (1,0)	1.4928 (1,0)
5	3.5099	3.5101 (1,25)	3.5092 (1,25)	3.5088 (1,25)
10	7.0197	7.0213 (1,29)	7.0174 (1,29)	7.0155 (1,29)
20	14.039	14.040 (2,25)	14.028 (1,28)	14.021 (1,28)
50	35.099	35.099 (4,12)	35.083 (2,29)	35.072 (2,29)
70	49.138	49.139 (3,28)	49.058 (1,23)	48.999 (1,23)
100	70.197	70.198 (4,27)	70.140 (2,27)	70.098 (2,27)
150	105.30	105.30 (7,11)	105.09 (1,20)	104.90 (1,20)
200	140.39	140.40 (8,12)	140.32 (1,19)	140.02 (1,19)
250	175.49	175.49 (7,25)	175.16 (1,18)	174.73 (1,18)
300	210.59	210.59 (10,9)	209.90 (1,17)	209.31 (1,17)
350	245.69	245.69 (11,5)	245.27 (2,22)	244.93 (2,22)
400	280.79	280.79 (3,25)	279.72 (1,16)	278.80 (1,16)
450	315.89	315.89 (11,19)	315.23 (2,21)	314.72 (2,21)
500	350.99	350.99 (13,8)	349.89 (1,15)	348.57 (1,15)
600	421.18	421.19 (14,11)	420.37 (2,20)	419.58 (2,20)
700	491.38	491.39 (15,12)	488.99 (1,14)	486.81 (1,14)
800	561.58	561.58 (16,12)	560.53 (3,22)	558.96 (1,14)
900	631.78	631.78 (4,24)	629.92 (1,13)	626.63 (1,13)
1000	701.97	701.97 (14,25)	697.95 (1,13)	694.27 (1,13)

[a] Numbers in parentheses, (m,n), indicate the number of axial half-waves and circumferential waves, respectively.

* Nonlinear rotations about the normal are neglected.

† $Z = \frac{L^2}{Rh}\sqrt{1-\nu^2}$ and $D = \frac{Eh^3}{12(1-\nu^2)}$

Table 5. Nondimensional buckling load $\sqrt{3(1-\nu^2)}\,\frac{N_x^{cr}R}{Eh^2}$ for isotropic cylinders with simply supported edges and subjected to uniform axial compression ($\nu = 0.30$, $R/h = 100$)

	Ref. 38	Present study		
L/R	Flügge	Donnell	Sanders*	Sanders
0.150	1.0395 (1,0)[a]	1.0404 (1,0)	1.0404 (1,0)	1.0404 (1,0)
0.160	1.0110 (1,0)	1.0119 (1,0)	1.0119 (1,0)	1.0119 (1,0)
0.165	1.0034 (1,0)	1.0043 (1,0)	1.0043 (1,0)	1.0043 (1,0)
0.168	1.0007 (1,0)	1.0016 (1,0)	1.0016 (1,0)	1.0016 (1,0)
0.169	0.9998 (1,1)	1.0010 (1,0)	1.0010 (1,0)	1.0010 (1,0)
0.170	0.9992 (1,1)	1.0005 (1,0)	1.0005 (1,0)	1.0005 (1,0)
0.171	0.9991 (1,1)	1.0002 (1,0)	1.0002 (1,0)	1.0002 (1,0)
0.173	0.9992 (1,1)	1.0000 (1,1)	1.0000 (1,1)	1.0000 (1,1)
0.174	0.9990 (1,2)	1.0000 (1,1)	0.9999 (1,2)	0.9999 (1,2)
0.175	0.9990 (1,2)	1.0000 (1,2)	0.9999 (1,2)	0.9999 (1,2)
0.176	0.9990 (1,2)	1.0001 (1,2)	0.9999 (1,3)	0.9998 (1,3)
0.177	0.9989 (1,3)	1.0000 (1,3)	0.9998 (1,3)	0.9997 (1,3)
0.178	0.9988 (1,3)	1.0000 (1,3)	0.9997 (1,3)	0.9997 (1,3)
0.179	0.9989 (1,3)	1.0001 (1,3)	0.9998 (1,3)	0.9997 (1,3)
0.180	0.9988 (1,4)	1.0002 (1,4)	0.9998 (1,4)	0.9996 (1,4)
0.182	0.9985 (1,4)	1.0000 (1,4)	0.9995 (1,4)	0.9994 (1,4)
0.184	0.9987 (1,4)	1.0002 (1,4)	0.9997 (1,4)	0.9995 (1,4)
0.186	0.9984 (1,5)	1.0002 (1,5)	0.9995 (1,5)	0.9992 (1,5)
0.188	0.9981 (1,5)	1.0000 (1,5)	0.9992 (1,5)	0.9990 (1,5)
0.190	0.9983 (1,5)	1.0001 (1,5)	0.9993 (1,5)	0.9990 (1,5)
0.192	0.9986 (1,6)	1.0005 (1,5)	0.9997 (1,5)	0.9994 (1,6)
0.196	0.9978 (1,6)	1.0001 (1,6)	0.9989 (1,6)	0.9985 (1,6)
0.200	0.9979 (1,6)	1.0002 (1,6)	0.9990 (1,6)	0.9985 (1,6)
0.205	0.9978 (1,7)	1.0007 (1,7)	0.9990 (1,7)	0.9984 (1,7)
0.210	0.9970 (1,7)	1.0000 (1,7)	0.9983 (1,7)	0.9976 (1,7)
0.215	0.9972 (1,7)	1.0003 (1,7)	0.9985 (1,7)	0.9977 (1,7)
0.22	0.9981 (1,7)	1.0014 (1,7)	0.9995 (1,7)	0.9987 (1,7)
0.23	0.9961 (1,8)	1.0002 (1,8)	0.9976 (1,8)	0.9966 (1,8)

[a] Numbers in parentheses, (m,n), indicate the number of axial half-waves and circumferential waves, respectively.
* Nonlinear rotations about the normal are neglected.

Table 5. Continued

L/R	Ref. 38	Present study		
	Flügge	Donnell	Sanders*	Sanders
0.24	0.9959 (1,8)[a]	1.0002 (1,8)	0.9975 (1,8)	0.9963 (1,8)
0.25	0.9970 (1,8)	1.0017 (1,8)	0.9987 (1,8)	0.9974 (1,8)
0.26	0.9965 (1,9)	1.0022 (1,9)	0.9983 (1,9)	0.9968 (1,9)
0.30	0.9929 (1,9)	1.0000 (1,9)	0.9952 (1,9)	0.9930 (1,9)
0.34	0.9915 (1,9)	1.0002 (1,9)	0.9944 (1,9)	0.9915 (1,9)
0.40	0.9888 (1,9)	1.0000 (1,9)	0.9926 (1,9)	0.9887 (1,9)
0.44	0.9877 (1,9)	1.0006 (1,9)	0.9921 (1,9)	0.9874 (1,9)
0.50	0.9903 (1,9)	1.0017 (2,8)	0.9955 (1,9)	0.9899 (1,9)
0.54	0.9961 (1,8)	1.0002 (3,4)	0.9970 (2,9)	0.9952 (2,9)
0.60	0.9848 (1,8)	1.0000 (2,9)	0.9920 (1,8)	0.9844 (1,8)
0.65	0.9796 (1,8)	1.0001 (1,8)	0.9874 (1,8)	0.9792 (1,8)
0.70	0.9794 (1,8)	1.0000 (4,2)	0.9878 (1,8)	0.9789 (1,8)
0.72	0.9808 (1,8)	1.0002 (2,9)	0.9895 (1,8)	0.9803 (1,8)
0.76	0.9865 (1,8)	1.0001 (2,9)	0.9932 (2,9)	0.9860 (1,8)
0.80	0.9888 (2,9)	1.0000 (2,9)	0.9926 (2,9)	0.9887 (2,9)
0.82	0.9884 (2,9)	1.0000 (2,9)	0.9924 (2,9)	0.9882 (2,9)
0.85	0.9825 (1,7)	1.0000 (4,7)	0.9921 (2,9)	0.9820 (1,7)
0.90	0.9736 (1,7)	1.0000 (3,9)	0.9858 (1,7)	0.9730 (1,7)
0.95	0.9690 (1,7)	1.0000 (1,7)	0.9817 (1,7)	0.9684 (1,7)
1.00	0.9689 (1,7)	1.0002 (3,9)	0.9820 (1,7)	0.9682 (1,7)
1.04	0.9718 (1,7)	1.0000 (6,1)	0.9853 (1,7)	0.9712 (1,7)
1.10	0.9813 (1,7)	1.0001 (6,4)	0.9937 (3,9)	0.9806 (1,7)
1.15	0.9890 (2,8)	1.0001 (3,9)	0.9931 (3,9)	0.9886 (2,8)
1.18	0.9864 (2,8)	1.0000 (6,6)	0.9928 (3,9)	0.9860 (2,8)
1.20	0.9827 (1,6)	1.0000 (3,9)	0.9920 (2,8)	0.9820 (1,6)
1.30	0.9606 (1,6)	1.0001 (2,8)	0.9812 (1,6)	0.9613 (1,6)
1.40	0.9538 (1,6)	1.0000 (8,2)	0.9735 (1,6)	0.9530 (1,6)
1.45	0.9539 (1,6)	1.0000 (8,4)	0.9740 (1,6)	0.9531 (1,6)
1.50	0.9567 (1,6)	1.0000 (5,9)	0.9771 (1,6)	0.9559 (1,6)

[a] Numbers in parentheses, (m,n), indicate the number of axial half-waves and circumferential waves, respectively.
* Nonlinear rotations about the normal are neglected.

Table 5. Continued

L/R	Ref. 38	Present study		
	Flügge	Donnell	Sanders*	Sanders
1.60	0.9699 (1,6)[a]	1.0000 (9,3)	0.9912 (1,6)	0.9691 (1,6)
1.70	0.9825 (2,7)	1.0000 (9,5)	0.9921 (4,9)	0.9820 (2,7)
1.75	0.9776 (2,7)	1.0000 (10,2)	0.9895 (2,7)	0.9769 (2,7)
1.8	0.9708 (1,5)	1.0000 (6,9)	0.9858 (2,7)	0.9700 (1,5)
2.0	0.9372 (1,5)	1.0000 (5,9)	0.9676 (1,5)	0.9364 (1,5)
2.1	0.9308 (1,5)	1.0000 (12,2)	0.9614 (1,5)	0.9299 (1,5)
2.2	0.9304 (1,5)	1.0000 (7,9)	0.9615 (1,5)	0.9295 (1,5)
2.4	0.9457 (1,5)	1.0000 (6,9)	0.9780 (1,5)	0.9448 (1,5)
2.6	0.9612 (2,6)	1.0000 (15,1)	0.9812 (2,6)	0.9613 (2,6)
2.7	0.9564 (2,6)	1.0000 (9,9)	0.9759 (2,6)	0.9557 (2,6)
2.8	0.9538 (2,6)	1.0000 (16,2)	0.9735 (2,6)	0.9530 (2,6)
3.0	0.9250 (1,4)	1.0000 (10,9)	0.9749 (1,4)	0.9241 (1,4)
3.2	0.9018 (1,4)	1.0000 (18,3)	0.9509 (1,4)	0.9007 (1,4)
3.4	0.8902 (1,4)	1.0000 (18,5)	0.9395 (1,4)	0.8892 (1,4)
3.7	0.8919 (1,4)	1.0000 (12,9)	0.9422 (1,4)	0.8910 (1,4)
4.0	0.9126 (1,4)	1.0000 (10,9)	0.9647 (1,4)	0.9117 (1,4)
4.2	0.9308 (2,5)	1.0000 (24,2)	0.9614 (2,5)	0.9299 (2,5)
4.4	0.9304 (2,5)	1.0000 (11,9)	0.9615 (2,5)	0.9295 (2,5)
4.7	0.9399 (2,5)	1.0000 (20,8)	0.9720 (2,5)	0.9391 (2,5)
5.0	0.9142 (1,3)	1.0000 (29,0)	0.9820 (5,7)	0.9132 (1,3)
5.6	0.8425 (1,3)	1.0000 (32,2)	0.9292 (1,3)	0.8416 (1,3)
6.0	0.8172 (1,3)	1.0000 (15,9)	0.9020 (1,3)	0.8163 (1,3)
6.5	0.8049 (1,3)	1.0000 (33,6)	0.8892 (1,3)	0.8041 (1,3)
7.0	0.8104 (1,3)	1.0000 (40,2)	0.8958 (1,3)	0.8094 (1,3)
8.0	0.8620 (1,3)	1.0000 (45,3)	0.9538 (1,3)	0.8610 (1,3)
9.0	0.9250 (3,4)	1.0000 (52,0)	0.9636 (4,5)	0.9241 (3,4)
9.5	0.9045 (3,4)	1.0000 (45,7)	0.9540 (3,4)	0.9037 (3,4)
10	0.8934 (3,4)	1.0000 (33,9)	0.9420 (3,4)	0.8918 (3,4)

[a] Numbers in parentheses, (m,n), indicate the number of axial half-waves and circumferential waves, respectively.
* Nonlinear rotations about the normal are neglected.

Table 5. Concluded

L/R	Ref. 38	Present study		
	Flügge	Donnell	Sanders*	Sanders
12	0.7172 (1,2)[a]	1.0000 (30,9)	0.8898 (1,2)	0.7162 (1,2)
14	0.6313 (1,2)	1.0000 (35,9)	0.7845 (1,2)	0.6304 (1,2)
16	0.6034 (1,2)	1.0000 (40,9)	0.7507 (1,2)	0.6025 (1,2)
18	0.6134 (1,2)	1.0000 (45,9)	0.7638 (1,2)	0.6125 (1,2)
20	0.6505 (1,2)	1.0000 (50,9)	0.8105 (1,2)	0.6496 (1,2)
22	0.7008 (1,2)	1.0000 (55,9)	0.8831 (1,2)	0.7075 (1,2)
24	0.7172 (2,2)	1.0000 (60,9)	0.8898 (2,2)	0.7162 (2,2)
28	0.6313 (2,2)	1.0001 (20,6)	0.7845 (2,2)	0.6304 (2,2)
30	0.6116 (2,2)	1.0002 (31,7)	0.7606 (2,2)	0.6108 (2,2)
32	0.6034 (2,2)	1.0000 (23,6)	0.7507 (2,2)	0.6025 (2,2)
35	0.6084 (2,2)	1.0000 (37,7)	0.7570 (2,2)	0.6072 (2,2)
40	0.5065 (1,1)	1.0000 (19,5)	0.8100 (3,2)	0.5060 (1,1)
60	0.2258 (1,1)	1.0002 (29,5)	0.4505 (1,1)	0.2258 (1,1)
80	0.1272 (1,1)	1.0000 (13,3)	0.2540 (1,1)	0.1272 (1,1)
100	0.08145 (1,1)	1.0003 (16,3)	0.16275 (1,1)	0.08144 (1,1)

[a] Numbers in parentheses, (m,n), indicate the number of axial half-waves and circumferential waves, respectively.
* Nonlinear rotations about the normal are neglected.

Table 6. Buckling stress ratio $\frac{\sigma_x^{cr}}{\sigma^*_x{}^{cr}}$ for isotropic cylinders with simply supported edges, and subjected to axial compression ($\nu = 0.30$)

$\sqrt{\frac{\sigma^*_x{}^{cr}}{\sigma^{cr}_{Euler}}}$	Radius-to-Thickness Ratio, R/h			
	50	100	500	1000
0.01	1.10	0.99	0.99	0.99
0.02	0.99	0.99	0.99	0.98
0.03	0.98	0.98	0.97	0.97
0.04	0.96	0.99	0.96	0.96
0.05	0.99	0.95	0.96	0.97
0.06	0.95	0.98	0.96	0.96
0.07	0.94	0.94	0.96	0.96
0.08	0.96	0.93	0.92	0.92
0.09	0.97	0.96	0.95	0.94
0.10	0.92	0.95	0.96	0.97
0.11	0.90	0.91	0.92	0.93
0.12	0.89	0.89	0.89	0.89
0.13	0.91	0.89	0.88	0.88
0.14	0.93	0.91	0.90	0.90
0.15	0.95	0.93	0.93	0.92
0.16	0.95	0.93	0.92	0.92
0.17	0.91	0.94	0.93	0.93
0.18	0.87	0.89	0.91	0.92
0.19	0.85	0.86	0.87	0.87
0.20	0.83	0.83	0.84	0.84
0.21	0.81	0.82	0.82	0.82
0.22	0.81	0.81	0.81	0.81
0.23	0.81	0.80	0.80	0.80
0.24	0.81	0.81	0.80	0.80
0.25	0.82	0.81	0.81	0.81
0.26	0.84	0.83	0.82	0.82
0.27	0.85	0.84	0.83	0.83
0.28	0.87	0.86	0.85	0.85
0.29	0.90	0.88	0.87	0.87
0.30	0.92	0.91	0.90	0.90
0.31	0.91	0.93	0.93	0.92
0.32	0.90	0.92	0.92	0.92
0.33	0.90	0.91	0.92	0.92
0.34	0.89	0.90	0.91	0.91
0.35	0.88	0.89	0.90	0.90
0.36	0.85	0.87	0.88	0.89
0.37	0.82	0.83	0.85	0.85
0.38	0.79	0.81	0.82	0.82
0.39	0.77	0.78	0.79	0.79
0.40	0.75	0.76	0.77	0.77
0.41	0.73	0.74	0.74	0.75
0.42	0.71	0.72	0.72	0.72
0.43	0.69	0.70	0.71	0.71
0.44	0.68	0.68	0.69	0.69
0.45	0.67	0.67	0.67	0.68
0.46	0.65	0.66	0.66	0.66
0.47	0.65	0.65	0.65	0.65
0.48	0.64	0.64	0.64	0.64
0.49	0.63	0.63	0.63	0.63
0.50	0.62	0.62	0.62	0.62

Table 6. Continued

$\sqrt{\frac{\sigma^{*cr}_x}{\sigma^{cr}_{Euler}}}$	Radius-to-Thickness Ratio, R/h			
	50	100	500	1000
0.51	0.62	0.62	0.62	0.62
0.52	0.61	0.61	0.61	0.61
0.53	0.61	0.61	0.61	0.61
0.54	0.61	0.61	0.61	0.61
0.55	0.61	0.60	0.60	0.6
0.56	0.60	0.60	0.60	0.6
0.57	0.60	0.60	0.60	0.6
0.58	0.60	0.60	0.60	0.6
0.59	0.61	0.60	0.60	0.6
0.60	0.61	0.60	0.60	0.6
0.61	0.61	0.61	0.60	0.6
0.62	0.61	0.61	0.61	0.61
0.63	0.62	0.61	0.61	0.61
0.64	0.62	0.62	0.61	0.61
0.65	0.62	0.62	0.62	0.62
0.66	0.63	0.63	0.62	0.62
0.67	0.63	0.63	0.63	0.63
0.68	0.64	0.64	0.63	0.63
0.69	0.65	0.64	0.64	0.64
0.70	0.65	0.65	0.65	0.65
0.71	0.66	0.66	0.65	0.65
0.72	0.67	0.66	0.66	0.66
0.73	0.68	0.67	0.67	0.67
0.74	0.68	0.68	0.68	0.68
0.75	0.69	0.69	0.68	0.68
0.76	0.70	0.70	0.69	0.69
0.77	0.71	0.71	0.70	0.7
0.78	0.72	0.72	0.71	0.71
0.79	0.73	0.73	0.72	0.72
0.80	0.74	0.74	0.73	0.73
0.81	0.74	0.75	0.74	0.74
0.82	0.73	0.74	0.74	0.75
0.83	0.72	0.73	0.73	0.73
0.84	0.71	0.72	0.72	0.72
0.85	0.70	0.71	0.71	0.72
0.86	0.69	0.70	0.71	0.71
0.87	0.69	0.69	0.70	0.7
0.88	0.68	0.68	0.69	0.69
0.89	0.67	0.68	0.68	0.68
0.90	0.67	0.67	0.67	0.68
0.91	0.66	0.66	0.67	0.67
0.92	0.65	0.66	0.66	0.66
0.93	0.65	0.65	0.66	0.66
0.94	0.65	0.65	0.65	0.65
0.95	0.64	0.64	0.65	0.65
0.96	0.64	0.64	0.64	0.64
0.97	0.63	0.63	0.64	0.64
0.98	0.63	0.63	0.63	0.63
0.99	0.63	0.63	0.63	0.63
1.00	0.62	0.62	0.62	0.62

Table 6. Concluded

$\sqrt{\frac{\sigma^{*cr}_x}{\sigma^{cr}_{Euler}}}$	Radius-to-Thickness Ratio, R/h			
	50	100	500	1000
1.01	0.62	0.62	0.62	0.62
1.02	0.62	0.62	0.62	0.62
1.03	0.62	0.62	0.62	0.62
1.04	0.61	0.61	0.61	0.61
1.05	0.61	0.61	0.61	0.61
1.06	0.61	0.61	0.61	0.61
1.07	0.61	0.61	0.61	0.61
1.08	0.61	0.61	0.61	0.61
1.09	0.61	0.60	0.60	0.60
1.10	0.61	0.60	0.60	0.60
1.11	0.60	0.60	0.60	0.60
1.12	0.60	0.60	0.60	0.60
1.13	0.60	0.60	0.60	0.60
1.14	0.60	0.60	0.60	0.60
1.15	0.60	0.60	0.60	0.60
1.16	0.60	0.60	0.60	0.60
1.17	0.60	0.60	0.60	0.60
1.18	0.61	0.60	0.60	0.60
1.19	0.61	0.60	0.60	0.60
1.20	0.61	0.60	0.60	0.60
1.21	0.61	0.61	0.60	0.60
1.22	0.61	0.61	0.60	0.60
1.23	0.61	0.61	0.61	0.61
1.24	0.61	0.61	0.61	0.61
1.25	0.61	0.61	0.61	0.61
1.26	0.62	0.61	0.61	0.61
1.27	0.61	0.61	0.61	0.61
1.28	0.60	0.61	0.61	0.61
1.29	0.59	0.60	0.60	0.60
1.30	0.58	0.59	0.59	0.59
1.31	0.57	0.58	0.58	0.58
1.32	0.56	0.57	0.57	0.57
1.33	0.56	0.56	0.56	0.56
1.34	0.55	0.55	0.56	0.56
1.35	0.54	0.54	0.55	0.55
1.36	0.53	0.54	0.54	0.54
1.37	0.52	0.53	0.53	0.53
1.38	0.52	0.52	0.52	0.52
1.39	0.51	0.51	0.52	0.52
1.40	0.50	0.51	0.51	0.51

Table 7. Nondimensional buckling pressure $\frac{p^{cr}RL^2}{\pi^2 D}$ for isotropic cylinders with simply supported edges and subjected to uniform external pressure ($\nu = 0.30$)

Batdorf-Z parameter†	Ref. 40	Present study		
	Donnell	Donnell	Sanders* Live pressure	Sanders Live pressure
0	4.0000	4.0000 (1,970)[a]	4.0000 (1,970)	4.0000 (1,970)
1	4.0299	4.0300 (1,98)	4.0301 (1,98)	4.0300 (1,98)
1.5	4.0650	4.0651 (1,82)	4.0653 (1,82)	4.0651 (1,82)
2	4.1106	4.1107 (1,72)	4.1109 (1,72)	4.1107 (1,72)
3	4.2240	4.2242 (1,62)	4.2245 (1,62)	4.2242 (1,62)
4	4.3549	4.3549 (1,56)	4.3552 (1,56)	4.3549 (1,56)
5	4.4935	4.4938 (1,52)	4.4942 (1,52)	4.4938 (1,52)
7	4.7753	4.7755 (1,48)	4.7758 (1,48)	4.7753 (1,48)
10	5.1836	5.1840 (1,44)	5.1841 (1,44)	5.1836 (1,44)
15	5.8045	5.8047 (1,40)	5.8046 (1,40)	5.8039 (1,40)
20	6.3594	6.3614 (1,37)	6.3612 (1,37)	6.3603 (1,37)
30	7.3266	7.3272 (1,34)	7.3264 (1,34)	7.3253 (1,34)
40	8.1629	8.1630 (1,32)	8.1615 (1,32)	8.1603 (1,32)
50	8.9093	8.9178 (1,30)	8.9161 (1,30)	8.9138 (1,30)
70	10.218	10.221 (1,28)	10.218 (1,28)	10.216 (1,28)
100	11.883	11.884 (1,26)	11.878 (1,26)	11.876 (1,26)
150	14.190	14.202 (1,24)	14.193 (1,24)	14.190 (1,24)
200	16.142	16.145 (1,22)	16.133 (1,22)	16.130 (1,22)
300	19.426	19.428 (1,20)	19.410 (1,20)	19.406 (1,20)
400	22.199	22.217 (1,19)	22.191 (1,19)	22.186 (1,19)
500	24.645	24.664 (1,18)	24.631 (1,18)	24.626 (1,18)
700	28.894	28.988 (1,16)	28.949 (1,16)	28.943 (1,16)
1000	34.254	34.255 (1,15)	34.190 (1,15)	34.183 (1,15)

[a] Numbers in parentheses, (m,n), indicate the number of axial half-waves and circumferential waves, respectively.
* Nonlinear rotations about the normal are neglected.

† $Z = \frac{L^2}{Rh}\sqrt{1-\nu^2}$ and $D = \frac{Eh^3}{12(1-\nu^2)}$

Table 7. Concluded

Batdorf-Z parameter†	Ref. 40	Present study		
	Donnell	Donnell	Sanders* Live pressure	Sanders Live pressure
1500	41.634	41.806 (1,14)[a]	41.693 (1,14)	41.686 (1,14)
2000	47.858	48.009 (1,13)	47.860 (1,13)	47.852 (1,13)
3000	58.301	58.899 (1,12)	58.661 (1,12)	58.652 (1,12)
4000	67.106	67.387 (1,11)	67.084 (1,11)	67.073 (1,11)
5000	74.864	74.935 (1,10)	74.612 (1,10)	74.598 (1,10)
7000	88.329	88.981 (1,9)	88.584 (1,9)	88.565 (1,9)
10 000	105.31	106.95 (1,9)	106.13 (1,9)	106.11 (1,9)
15 000	128.67	129.62 (1,8)	128.44 (1,8)	128.42 (1,8)
20 000	148.36	148.97 (1,7)	147.75 (1,7)	147.72 (1,7)
30 000	181.40	186.90 (1,7)	184.32 (1,7)	184.30 (1,7)
40 000	209.26	209.33 (1,6)	206.66 (1,6)	206.62 (1,6)
50 000	233.80	236.80 (1,6)	232.75 (1,6)	232.72 (1,6)
70 000	276.39	280.88 (1,5)	277.36 (1,5)	277.30 (1,5)
100 000	330.09	332.84 (1,5)	324.97 (1,5)	324.92 (1,5)

[a] Numbers in parentheses, (m,n), indicate the number of axial half-waves and circumferential waves, respectively.

* Nonlinear rotations about the normal are neglected.

† $Z = \frac{L^2}{Rh}\sqrt{1-\nu^2}$ and $D = \frac{Eh^3}{12(1-\nu^2)}$

Table 8. Buckling pressure ($\times 10^{-4}$ MPa) for isotropic cylinders with simply supported edges and subjected to external pressure (E = 200 GPa, $\nu = 0.30$, h = 0.01 m)

L/R	R/h	Ref. 41	Ref. 42	Present study		
		Flügge Live pressure	FEM[¢]	Donnell	Sanders* Live pressure	Sanders Live pressure
0.5	300	2766.2 (15)[a]	2632.0 (15)	2769.0 (1,15)[b]	2766.7 (1,5)	2765.1 (1,15)
	500	---	716.2 (17)	743.10 (1,18)	742.56 (1,18)	742.03 (1,18)
	1000	---	123.6 (21)	126.49 (1,21)	126.40 (1,21)	126.37 (1,21)
	1500	---	44.4 (23)	45.213 (1,24)	45.178 (1,24)	45.173 (1,24)
	2000	---	21.48 (25)	21.821 (1,25)	21.809 (1,25)	21.806 (1,25)
	3000	7.816 (28)	7.74 (28)	7.822 (1,28)	7.818 (1,28)	7.817 (1,28)
1	300	1269.6 (11)	1251.0 (11)	1273.5 (1,11)	1269.9 (1,11)	1269.1 (1,11)
	500	348.43 (13)	346.1 (13)	349.45 (1,13)	348.48 (1,13)	348.35 (1,13)
	1000	60.488 (15)	60.16 (15)	60.600 (1,5)	60.494 (1,15)	60.481 (1,15)
	1500	21.767 (17)	21.72 (17)	21.804 (1,17)	21.768 (1,17)	21.766 (1,17)
	2000	10.559 (18)	10.54 (18)	10.574 (1,18)	10.560 (1,18)	10.559 (1,18)
	3000	3.810 (20)	3.809 (20)	3.815 (1,20)	3.811 (1,20)	3.811 (1,20)
2	300	607.33 (8)	612.0 (8)	611.80 (1,8)	607.50 (1,8)	607.12 (1,8)
	500	---	169.4 (9)	169.18 (1,9)	168.29 (1,9)	168.22 (1,9)
	1000	---	29.74 (11)	29.675 (1,11)	29.550 (1,11)	29.545 (1,11)
	1500	---	10.74 (12)	10.712 (1,12)	10.677 (1,12)	10.676 (1,12)
	2000	---	5.221 (13)	5.208 (1,13)	5.193 (1,13)	5.192 (1,13)
	3000	1.884 (14)	1.895 (14)	1.889 (1,14)	1.885 (1,14)	1.885 (1,14)
3	300	407.17 (7)	414.7 (7)	412.62 (1,7)	407.27 (1,7)	407.07 (1,7)
	500	---	115.2 (8)	114.16 (1,7)	113.55 (1,7)	113.50 (1,7)
	1000	---	19.75 (9)	19.645 (1,9)	19.519 (1,9)	19.515 (1,9)
	1500	---	7.149 (10)	7.115 (1,10)	7.077 (1,10)	7.076 (1,10)
	2000	---	3.500 (11)	3.487 (1,11)	3.470 (1,11)	3.470 (1,11)
	3000	1.251 (12)	1.261 (12)	1.256 (1,12)	1.251 (1,12)	1.251 (1,12)
5	300	235.34 (5)	244.8 (5)	239.43 (1,5)	235.42 (1,5)	235.27 (1,5)
	500	---	67.8 (6)	66.984 (1,6)	65.902 (1,6)	65.881 (1,6)
	1000	---	11.85 (7)	11.727 (1,7)	11.599 (1,7)	11.597 (1,7)
	1500	---	4.327 (8)	4.299 (1,8)	4.257 (1,8)	4.257 (1,8)
	2000	---	2.092 (8)	2.071 (1,8)	2.057 (1,8)	2.057 (1,8)
	3000	0.744 (9)	0.754 (9)	0.748 (1,9)	0.744 (1,9)	0.744 (1,9)

[a] Number in parentheses, (n) indicate the number of circumferential waves, n
[b] Numbers in parentheses, (m,n), indicate the number of axial half-waves and circumferential waves, respectively.
* Nonlinear rotations about the normal are neglected.
[¢] Results obtained by using a finite element method.

Table 9. Nondimensional buckling pressure $\frac{p^{cr}R^3}{D}$ for isotropic cylinders with R/h = 10, simply supported edges, and subjected to external pressure ($\nu = 0.30$)

L/R	Ref. 43		Present study		
	Flügge Live pressure	Timoshenko Live pressure	Sanders Live pressure	Sanders* Live pressure	Donnell
1	51.46 (1,5)	51.46 (1,5)	51.37 (1,5)	51.82 (1,5)	51.76 (1,4)
2	20.10 (1,3)	20.03 (1,3)	20.04 (1,3)	20.48 (1,3)	20.23 (1,3)
3	11.94 (1,3)	12.00 (1,3)	11.89 (1,3)	12.03 (1,3)	12.76 (1,3)
4	9.82 (1,3)	9.87 (1,3)	9.79 (1,3)	9.86 (1,3)	10.20 (1,2)
5	6.83 (1,2)	6.89 (1,2)	6.79 (1,2)	6.98 (1,2)	7.03 (1,2)
6	5.08 (1,2)	5.15 (1,2)	5.04 (1,2)	5.15 (1,2)	5.69 (1,2)
7	4.25 (1,2)	4.30 (1,2)	4.22 (1,2)	4.29 (1,2)	5.04 (1,2)
8	3.81 (1,2)	3.85 (1,2)	3.79 (1,2)	3.83 (1,2)	4.69 (1,2)
9	3.56 (1,2)	3.59 (1,2)	3.54 (1,2)	3.57 (1,2)	4.49 (1,2)
10	3.40 (1,2)	3.43 (1,2)	3.39 (1,2)	3.42 (1,2)	4.36 (1,2)
50	3.01 (1,2)	3.01 (1,2)	3.00 (1,2)	3.01 (1,2)	4.01 (1,2)
100	3.00 (1,2)	3.00 (1,2)	3.00 (1,2)	3.00 (1,2)	4.00 (1,2)
150	3.00 (1,2)	3.00 (1,2)	3.00 (1,2)	3.00 (1,2)	4.00 (1,2)
200	3.00 (1,2)	3.00 (1,2)	3.00 (1,2)	3.00 (1,2)	4.00 (1,2)
250	3.00 (1,2)	3.00 (1,2)	3.00 (1,2)	3.00 (1,2)	4.00 (1,2)

[b] Numbers in parentheses, (m,n), indicate the number of axial half-waves and circumferential waves, respectively.
* Nonlinear rotations about the normal are neglected.

[‡] Results calculated for live pressure load.

Table 10. Nondimensional buckling pressure $\frac{p^{cr}R^3}{D}$ for isotropic cylinders with R/h = 100, simply supported edges, and subjected to external pressure ($\nu = 0.30$)

L/R	Ref. 43		Present study		
	Flügge Live pressure	Timoshenko Live pressure	Sanders Live pressure	Sanders* Live pressure	Donnell
1	115.24 (1,8)[b]	115.73 (1,8)	115.19 (1,8)	115.41 (1,8)	115.72 (1,8)
2	52.95 (1,6)	53.57 (1,6)	52.91 (1,6)	53.00 (1,6)	53.58 (1,6)
3	34.28 (1,5)	34.79 (1,5)	34.25 (1,5)	34.31 (1,5)	34.95 (1,5)
4	26.30 (1,4)	26.97 (1,4)	26.28 (1,4)	26.34 (1,4)	26.66 (1,4)
5	20.02 (1,4)	20.35 (1,4)	20.01 (1,4)	20.04 (1,4)	20.76 (1,4)
6	17.62 (1,4)	17.79 (1,4)	17.61 (1,4)	17.62 (1,4)	18.49 (1,4)
7	14.96 (1,3)	15.47 (1,3)	14.94 (1,3)	14.99 (1,3)	15.22 (1,3)
8	12.19 (1,3)	12.51 (1,3)	12.18 (1,3)	12.20 (1,3)	12.75 (1,3)
9	10.68 (1,3)	10.89 (1,3)	10.67 (1,3)	10.69 (1,3)	11.41 (1,3)
10	9.80 (1,3)	9.95 (1,3)	9.80 (1,3)	9.81 (1,3)	10.63 (1,3)
50	3.04 (1,2)	3.04 (1,2)	3.04 (1,2)	3.04 (1,2)	4.03 (1,2)
100	3.00 (1,2)	3.00 (1,2)	3.00 (1,2)	3.00 (1,2)	4.00 (1,2)
150	3.00 (1,2)	3.00 (1,2)	3.00 (1,2)	3.00 (1,2)	4.00 (1,2)
200	3.00 (1,2)	3.00 (1,2)	3.00 (1,2)	3.00 (1,2)	4.00 (1,2)
250	3.00 (1,2)	3.00 (1,2)	3.00 (1,2)	3.00 (1,2)	4.00 (1,2)

[b] Numbers in parentheses, (m,n), indicate the number of axial half-waves and circumferential waves, respectively.
* Nonlinear rotations about the normal are neglected.

Table 11. Nondimensional buckling pressure $\frac{p_{cr}R^3}{D}$ for isotropic cylinders with R/h = 1000, simply supported edges, and subjected to external pressure ($\nu = 0.30$)

L/R	Ref. 43		Present study		
	Flügge Live pressure	Timoshenko Live pressure	Sanders Live pressure	Sanders* Live pressure	Donnell
1	330.25 (1,15)[b]	335.77 (1,15)	330.23 (1,15)	330.29 (1,15)	330.87 (1,15)
2	161.33 (1,11)	164.28 (1,11)	161.31 (1,11)	161.34 (1,11)	162.03 (1,11)
3	106.56 (1,9)	108.68 (1,9)	106.55 (1,9)	106.57 (1,9)	107.26 (1,9)
4	80.03 (1,8)	81.46 (1,8)	80.03 (1,8)	80.04 (1,8)	80.79 (1,8)
5	63.32 (1,7)	64.66 (1,7)	63.32 (1,7)	63.33 (1,7)	64.03 (1,7)
6	53.37 (1,6)	55.01 (1,6)	53.37 (1,6)	53.38 (1,6)	53.88 (1,6)
7	45.06 (1,6)	45.97 (1,6)	45.06 (1,6)	45.07 (1,6)	45.79 (1,6)
8	40.98 (1,6)	41.52 (1,6)	40.98 (1,6)	40.99 (1,6)	41.73 (1,5)
9	34.95 (1,5)	35.96 (1,5)	34.95 (1,5)	34.95 (1,5)	35.52 (1,5)
10	31.23 (1,5)	31.90 (1,5)	31.23 (1,5)	31.24 (1,5)	31.95 (1,5)
50	6.54 (1,2)	6.89 (1,2)	6.55 (1,2)	6.55 (1,2)	6.66 (1,2)
100	3.22 (1,2)	3.24 (1,2)	3.22 (1,2)	3.22 (1,2)	4.17 (1,2)
150	3.04 (1,2)	3.05 (1,2)	3.04 (1,2)	3.04 (1,2)	4.03 (1,2)
200	3.01 (1,2)	3.01 (1,2)	3.01 (1,2)	3.01 (1,2)	4.01 (1,2)
250	3.00 (1,2)	3.00 (1,2)	3.01 (1,2)	3.01 (1,2)	4.00 (1,2)

[b] Numbers in parentheses, (m,n), indicate the number of axial half-waves and circumferential waves, respectively.
* Nonlinear rotations about the normal are neglected.

Table 12. Nondimensional buckling pressure $\frac{p^{cr}R^3}{D}$ for isotropic cylinders with R/h = 10, simply supported edges, and subjected to external pressure ($\nu = 0$)

L/R	Ref. 43		Present study		
	Flügge Live pressure	Timoshenko Live pressure	Sanders Live pressure	Sanders* Live pressure	Donnell
1	51.72 (1,5)[b]	52.16 (1,5)	51.84 (1,5)	52.29 (1,5)	52.48 (1,5)
2	20.64 (1,3)	20.99 (1,3)	20.75 (1,3)	21.21 (1,3)	20.78 (1,3)
3	12.04 (1,3)	12.14 (1,3)	12.06 (1,3)	12.21 (1,3)	12.90 (1,3)
4	9.84 (1,3)	9.90 (1,3)	9.84 (1,3)	9.92 (1,3)	10.68 (1,2)
5	7.08 (1,2)	7.11 (1,2)	7.10 (1,2)	7.30 (1,2)	7.25 (1,2)
6	5.19 (1,2)	5.23 (1,2)	5.20 (1,2)	5.31 (1,2)	5.80 (1,2)
7	4.30 (1,2)	4.34 (1,2)	4.31 (1,2)	4.37 (1,2)	5.10 (1,2)
8	3.84 (1,2)	3.87 (1,2)	3.84 (1,2)	3.89 (1,2)	4.73 (1,2)
9	3.57 (1,2)	3.60 (1,2)	3.57 (1,2)	3.61 (1,2)	4.51 (1,2)
10	3.41 (1,2)	3.43 (1,2)	3.41 (1,2)	3.44 (1,2)	4.37 (1,2)
50	3.01 (1,2)	3.01 (1,2)	3.00 (1,2)	3.01 (1,2)	4.01 (1,2)
100	3.00 (1,2)	3.00 (1,2)	3.00 (1,2)	3.00 (1,2)	4.00 (1,2)
150	3.00 (1,2)	3.00 (1,2)	3.00 (1,2)	3.00 (1,2)	4.00 (1,2)
200	3.00 (1,2)	3.00 (1,2)	3.00 (1,2)	3.00 (1,2)	4.00 (1,2)
250	3.00 (1,2)	3.00 (1,2)	3.00 (1,2)	3.00 (1,2)	4.00 (1,2)

[b] Numbers in parentheses, (m,n), indicate the number of axial half-waves and circumferential waves, respectively.
* Nonlinear rotations about the normal are neglected.

Table 13. Nondimensional buckling pressure $\frac{p_{cr}R^3}{D}$ for isotropic cylinders with R/h = 100, simply supported edges, and subjected to external pressure ($\nu = 0$)

L/R	Ref. 43		Present study		
	Flügge Live pressure	Timoshenko Live pressure	Sanders Live pressure	Sanders* Live pressure	Donnell
1	118.24 (1,8)[b]	118.86 (1,9)	118.28 (1,8)	118.50 (1,8)	118.73 (1,8)
2	54.18 (1,6)	54.27 (1,6)	54.19 (1,6)	54.28 (1,6)	54.82 (1,6)
3	35.05 (1,5)	35.09 (1,5)	35.05 (1,5)	35.11 (1,5)	35.72 (1,5)
4	27.27 (1,4)	27.30 (1,4)	27.28 (1,4)	27.34 (1,4)	27.59 (1,4)
5	20.42 (1,4)	20.44 (1,4)	20.42 (1,4)	20.46 (1,4)	21.15 (1,4)
6	17.81 (1,4)	17.82 (1,4)	17.81 (1,4)	17.83 (1,4)	18.68 (1,4)
7	15.59 (1,3)	15.60 (1,3)	15.59 (1,3)	15.64 (1,3)	15.80 (1,3)
8	12.56 (1,3)	12.57 (1,3)	12.56 (1,3)	12.59 (1,3)	13.09 (1,3)
9	10.91 (1,3)	10.92 (1,3)	10.91 (1,3)	10.93 (1,3)	11.62 (1,3)
10	9.96 (1,3)	9.96 (1,3)	9.95 (1,3)	9.97 (1,3)	10.77 (1,3)
50	3.05 (1,2)	3.05 (1,2)	3.05 (1,2)	3.05 (1,2)	4.04 (1,2)
100	3.00 (1,2)	3.00 (1,2)	3.00 (1,2)	3.00 (1,2)	4.00 (1,2)
150	3.00 (1,2)	3.00 (1,2)	3.00 (1,2)	3.00 (1,2)	4.00 (1,2)
200	3.00 (1,2)	3.00 (1,2)	3.00 (1,2)	3.00 (1,2)	4.00 (1,2)
250	3.00 (1,2)	3.00 (1,2)	3.00 (1,2)	3.00 (1,2)	4.00 (1,2)

[b] Numbers in parentheses, (m,n), indicate the number of axial half-waves and circumferential waves, respectively.
* Nonlinear rotations about the normal are neglected.

Table 14. Nondimensional buckling pressure $\frac{p_{cr}R^3}{D}$ for isotropic cylinders with R/h = 1000, simply supported edges, and subjected to external pressure ($\nu = 0$)

L/R	Ref. 43		Present study		
	Flügge Live pressure	Timoshenko Live pressure	Sanders Live pressure	Sanders* Live pressure	Donnell
1	338.74 (1,15)[b]	338.93 (1,15)	338.75 (1,15)	338.81 (1,15)	339.35 (1,15)
2	164.90 (1,11)	164.93 (1,11)	164.91 (1,11)	164.94 (1,11)	165.59 (1,11)
3	108.96 (1,9)	108.98 (1,9)	108.96 (1,9)	108.98 (1,9)	109.64 (1,9)
4	81.59 (1,8)	81.60 (1,8)	81.59 (1,8)	81.60 (1,8)	82.33 (1,8)
5	64.76 (1,7)	64.76 (1,7)	64.76 (1,7)	64.77 (1,7)	65.44 (1,7)
6	55.13 (1,6)	55.14 (1,6)	55.13 (1,6)	55.14 (1,6)	55.59 (1,6)
7	46.01 (1,6)	46.02 (1,6)	46.01 (1,6)	46.02 (1,6)	46.72 (1,6)
8	41.54 (1,6)	41.55 (1,6)	41.54 (1,6)	41.55 (1,6)	42.37 (1,6)
9	39.14 (1,6)	39.15 (1,6)	36.00 (1,5)	36.01 (1,5)	36.54 (1,5)
10	31.93 (1,5)	31.93 (1,5)	31.93 (1,5)	31.93 (1,5)	32.62 (1,5)
50	6.90 (1,2)	6.90 (1,2)	6.90 (1,2)	6.90 (1,2)	6.92 (1,2)
100	3.25 (1,2)	3.25 (1,2)	3.25 (1,2)	3.25 (1,2)	4.18 (1,2)
150	3.05 (1,2)	3.05 (1,2)	3.05 (1,2)	3.05 (1,2)	4.04 (1,2)
200	3.02 (1,2)	3.02 (1,2)	3.02 (1,2)	3.02 (1,2)	4.01 (1,2)
250	3.01 (1,2)	3.01 (1,2)	3.01 (1,2)	3.01 (1,2)	4.00 (1,2)

[b] Numbers in parentheses, (m,n), indicate the number of axial half-waves and circumferential waves, respectively.
* Nonlinear rotations about the normal are neglected.

Table 15. Buckling pressure $\frac{p^{cr}R}{Eh} \times 10^{6}$ for isotropic cylinders with simply supported edges, and subjected to uniform external pressure ($\nu = 0.30$)

L/R	R/h	Ref. 17, p.165		Present study		
		Flügge Live pressure	Brush and Almroth^ Live pressure	Sanders Live pressure	Sanders* Live pressure	Donnell
32π	1000	0.2947 (2)[a]	0.2947 (2)	0.2948 (1,2)[b]	0.2948 (1,2)	0.3814 (1,2)
	400	1.738 (2)	1.738 (2)	1.738 (1,2)	1.738 (1,2)	1.525(1,1)
	100	27.51 (2)	27.51 (2)	27.51 (1,2)	27.51 (1,2)	10.13 (1,1)
8π	1000	1.111 (3)	1.111 (3)	1.111 (1,3)	1.111 (1,3)	1.161 (1,3)
	400	4.972 (3)	4.971 (3)	4.971 (1,3)	4.972 (1,3)	5.503 (1,3)
	100	32.80 (2)	32.79 (2)	32.78 (1,2)	32.82 (1,2)	40.70 (1,2)
2π	1000	4.610 (6)	4.609 (6)	4.610 (1,6)	4.611 (1,6)	4.664 (1,6)
	400	18.11 (5)	18.10 (5)	18.10 (1,5)	18.11 (1,5)	18.52 (1,5)
	100	157.7 (4)	157.7 (4)	157.6 (1,4)	157.8 (1,4)	165.9 (1,4)
π/2	1000	18.95(12)	18.94(12)	18.94 (1,12)	18.95 (1,12)	19.00 (1,12)
	400	76.27 (10)	76.24 (10)	76.26 (1,10)	76.29 (1,10)	76.70 (1,10)
	100	634.5 (7)	632.8 (7)	634.1 (1,7)	635.1 (1,7)	641.2 (1,7)
π/4	1000	38.94 (17)	38.91 (17)	38.94 (1,17)	38.94 (1,17)	39.00 (1,17)
	400	159.9 (14)	159.5 (13)	159.8 (1,13)	159.9 (1,14)	160.2 (1,13)
	100	1395.0 (9)	1374.0 (9)	1394.7 (1,9)	1397.2 (1,9)	1399.6 (1,9)
π/8	1000	82.42 (24)	82.05 (24)	82.41 (1,24)	82.43 (1,24)	82.48 (1,24)
	400	348.8 (19)	343.6 (19)	348.8 (1,19)	348.9 (1,19)	349.2 (1,19)
	100	3383.0 (13)	3299.0 (13)	3382.9 (1,13)	3387.0 (1,13)	3388.2 (1,13)
π/16	1000	185.3 (33)	180.9 (33)	185.3 (1,33)	185.4 (1,33)	185.4 (1,33)
	400	845.6 (25)	824.5 (25)	845.6 (1,25)	845.9 (1,25)	845.9 (1,25)
	100	10110.0 (18)	14960.0 (18)	10109.9 (1,18)	10117.9 (1,18)	10109.3 (1,18)

[a] Number in parentheses, (n) indicate the number of circumferential waves, n
[b] Numbers in parentheses, (m,n), indicate the number of axial half-waves and circumferential waves, respectively.
* Nonlinear rotations about the normal are neglected.
^ All rotations about the normal are neglected.

Table 16. Buckling pressure $\frac{p^{cr}R}{Eh} \times 10^{6}$ for isotropic cylinders with simply supported edges, and subjected to uniform external pressure ($\nu = 0.30$)

R/h	L/R	Ref. 44		Present study		
		Budiansky-Koiter[20,22] Live pressure	Donnell	Sanders Live pressure	Sanders* Live pressure	Donnell
35	π/3	70.5175 (1,6)[b]	70.9200 (1,6)	70.5714 (1,6)	70.9020 (1,6)	71.1133 (1,6)
	π	20.0807 (1,4)	20.9160 (1,4)	20.1123 (1,4)	20.1875 (1,4)	20.9554 (1,4)
	3π	6.44560 (1,2)	6.63478 (1,2)	6.48657 (1,2)	6.54450 (1,2)	6.66815 (1,2)
	9π	3.06322 (1,2)	4.04066 (1,2)	3.06374 (1,2)	3.06688 (1,2)	4.05639 (1,2)
	15π	3.01306 (1,2)	4.01094 (1,2)	3.01308 (1,2)	3.01419 (1,2)	4.01301 (1,2)
	100π	3.00000 (1,2)	4.00000 (1,2)	2.99997 (1,2)	3.00000 (1,2)	4.00020 (1,2)
200	π/3	147.483 (1,10)	148.198 (1,10)	147.855 (1,10)	147.968 (1,10)	148.589 (1,10)
	π	46.0042 (1,6)	46.7699 (1,6)	46.1230 (1,6)	46.1609 (1,6)	46.8907 (1,6)
	3π	16.2343 (1,3)	16.3429 (1,3)	16.3439 (1,3)	16.3689 (1,3)	16.4415 (1,3)
	9π	4.38325 (1,2)	5.04407 (1,2)	4.40153 (1,2)	4.40606 (1,2)	5.05858 (1,2)
	15π	3.18545 (1,2)	4.14115 (1,2)	3.18719 (1,2)	3.18838 (1,2)	4.14341 (1,2)
	100π	3.00000 (1,2)	4.00000 (1,2)	3.00025 (1,2)	3.00028 (1,2)	4.00027 (1,2)
1000	π/3	313.523 (1,15)	314.207 (1,15)	314.448 (1,15)	314.506 (1,15)	315.155 (1,15)
	π	102.096 (1,9)	102.789 (1,9)	102.303 (1,9)	102.320 (1,9)	103.062 (1,9)
	3π	33.0159 (1,5)	33.6668 (1,5)	33.1282 (1,5)	33.1344 (1,5)	33.7747 (1,5)
	9π	10.5828 (1,3)	11.2230 (1,3)	10.5852 (1,3)	10.5870 (1,3)	11.3016 (1,3)
	15π	7.40602 (1,2)	7.29077 (1,2)	7.49330 (1,2)	7.49607 (1,2)	7.37179 (1,2)
	100π	3.00000 (1,2)	4.00000 (1,2)	3.00245 (1,2)	3.00247 (1,2)	4.00191 (1,2)

[b] Numbers in parentheses, (m,n), indicate the number of axial half-waves and circumferential waves, respectively.
* Nonlinear rotations about the normal are neglected.

Table 17. Nondimensional buckling pressure $\frac{p^{cr}R^2\sqrt{3(1-\nu^2)}}{Eh^2}$ for isotropic cylinders with simply supported edges and subjected to uniform external pressure ($\nu = 0.30$)

R/h	L/R	Ref. 45		Present study		
		Sanders Live pressure	Donnell	Sanders	Sanders Live pressure	Donnell
100	0.5	0.4035 (11)[a]	0.4047 (11)	0.4062 (11)	0.4040 (1,11)[b]	0.4047 (1,11)
	1	0.1741 (8)	0.1751 (8)	0.1765 (1,8)	0.1743 (1,8)	0.1751 (1,8)
	2	0.0799 (6)	0.0811(6)	0.0821 (1,6)	0.0801 (1,6)	0.0811 (1,6)
	4	0.0397 (4)	0.0403 (4)	0.0423 (1,4)	0.0398 (1,4)	0.0403 (1,4)
	10	0.0148 (3)	0.0161 (3)	0.0166 (1,3)	0.0148 (1,3)	0.0161 (1,3)
	20	0.00667 (2)	0.00768 (2)	0.00887 (1,2)	0.00668 (1,2)	0.00768 (1,2)
	40	0.00468 (2)	0.00617 (2)	0.00624 (1,2)	0.00469 (1,2)	0.00617 (1,2)
300	0.5	0.2055 (15)	0.2058 (15)	0.2063 (1,15)	0.2056 (1,15)	0.2059 (1,15)
	1	0.0943 (11)	0.0947 (11)	0.0951 (1,11)	0.0944 (1,11)	0.0947 (1,11)
	2	0.0451 (8)	0.0455 (8)	0.0458 (1,8)	0.0451 (1,8)	0.0455 (1,8)
	4	0.0223(6)	0.0227 (6)	0.0229 (1,6)	0.0223 (1,6)	0.0227 (1,6)
	10	0.00890 (4)	0.00933 (4)	0.00949 (1,4)	0.00890 (1,4)	0.00933 (1,4)
	20	0.00452 (3)	0.00498 (3)	0.00508 (1,3)	0.00452 (1,3)	0.00498 (1,3)
	40	0.00191 (2)	0.00232 (2)	0.00254 (1,2)	0.00191 (1,2)	0.00232 (1,2)
500	0.5	0.1532 (18)	0.1535 (18)	0.1537 (1,18)	0.1533 (1,18)	0.1535 (1,18)
	1	0.0719 (13)	0.0722 (13)	0.0723 (1,13)	0.0719 (1,13)	0.0722 (1,13)
	2	0.0347 (9)	0.0349 (9)	0.0352 (1,9)	0.0347 (1,9)	0.0349 (1,9)
	4	0.0176 (7)	0.0178 (6)	0.0179 (1,7)	0.0176 (1,7)	0.0178 (1,6)
	10	0.00667 (4)	0.00684 (4)	0.00711 (1,4)	0.00667 (1,4)	0.00684 (1,4)
	20	0.00321 (3)	0.00342 (3)	0.00361 (1,3)	0.00321 (1,3)	0.00342 (1,3)
	40	0.00156 (2)	0.00170 (2)	0.00208 (1,2)	0.00156 (1,2)	0.00170 (1,2)
700	0.5	0.1270 (19)	0.1271 (19)	0.1273 (1,19)	0.1270 (1,19)	0.1272 (1,19)
	1	0.0601 (14)	0.0603 (14)	0.0604 (1,14)	0.0601 (1,14)	0.0603 (1,14)
	2	0.0292 (10)	0.0294 (10)	0.0295 (1,10)	0.0292 (1,10)	0.0294 (1,10)
	4	0.0144 (7)	0.0145 (7)	0.0147 (1,7)	0.0144 (1,7)	0.0145 (1,7)
	10	0.00597 (5)	0.00616 (5)	0.00622 (1,5)	0.00597 (1,5)	0.00616 (1,5)
	20	0.00282 (3)	0.00292 (3)	0.00317 (1,3)	0.00282 (1,3)	0.00292 (1,3)
	40	0.00156 (2)	0.00155 (2)	0.00202 (1,3)	0.00157 (1,2)	0.00155 (1,2)

[a] Numbers in parentheses, (n), indicate the number of circumferential waves.
[b] Numbers in parentheses, (m,n), indicate the number of axial half-waves and circumferential waves, respectively.

Table 17. Concluded

R/h	L/R	Ref. 45		Present study		
		Sanders Live pressure	Donnell	Sanders	Sanders Live pressure	Donnell
1100	0.5	0.0991 (22)[a]	0.0992 (22)	0.0993 (1,22)[b]	0.0991 (1,22)	0.0992 (1,22)
	1	0.0477 (16)	0.0478 (16)	0.0478 (1,16)	0.0477 (1,16)	0.0478 (1,16)
	2	0.0232 (11)	0.0233 (11)	0.0234 (1,11)	0.0232 (1,11)	0.0233 (1,11)
	4	0.0115 (8)	0.0116 (8)	0.0116 (1,8)	0.0115 (1,8)	0.0116 (1,8)
	10	0.00450 (5)	0.00459 (5)	0.00469 (1,5)	0.00450 (1,5)	0.00459 (1,5)
	20	0.00236 (4)	0.00248 (4)	0.00251 (1,4)	0.00236 (1,4)	0.00248 (1,4)
	40	0.00121 (3)	0.00133 (3)	0.00136 (1,3)	0.00121 (1,3)	0.00133 (1,3)
1500	0.5	0.0840 (24)	0.0840 (24)	0.0841 (1,24)	0.0840 (1,24)	0.0840 (1,24)
	1	0.0405 (17)	0.0405 (17)	0.0406 (1,17)	0.0405 (1,17)	0.0405 (1,17)
	2	0.0198 (12)	0.0199 (12)	0.0200 (1,12)	0.0198 (1,12)	0.0199 (1,12)
	4	0.0099 (9)	0.0100 (9)	0.0101 (1,9)	0.0100 (1,9)	0.0100 (1,9)
	10	0.00404 (5)	0.00407 (5)	0.00420 (1,6)	0.00404 (1,5)	0.00407 (1,5)
	20	0.00191 (4)	0.00199 (4)	0.00204 (1,4)	0.00191 (1,4)	0.00199 (1,4)
	40	0.00095 (3)	0.00104 (3)	0.00107 (1,3)	0.00095 (1,3)	0.00104 (1,3)
1900	0.5	0.0739 (25)	0.0740 (25)	0.0740 (1,25)	0.0739 (1,25)	0.0740 (1,25)
	1	0.0358 (18)	0.0359 (18)	0.0359 (1,18)	0.0358 (1,18)	0.0359 (1,18)
	2	0.0176 (13)	0.0177 (13)	0.0177 (1,13)	0.0176 (1,13)	0.0177 (1,13)
	4	0.00871 (9)	0.00876 (9)	0.00882 (1,9)	0.00871 (1,9)	0.00876 (1,9)
	10	0.00347 (6)	0.00353 (6)	0.00357 (1,6)	0.00347 (1,6)	0.00353 (1,6)
	20	0.00169 (4)	0.00174 (4)	0.00181 (1,4)	0.00169 (1,4)	0.00174 (1,4)
	40	0.000820 (3)	0.000881 (3)	0.000925 (1,3)	0.000822 (1,3)	0.000881 (1,3)

[a] Numbers in parentheses, (n), indicate the number of circumferential waves.
[b] Numbers in parentheses, (m,n), indicate the number of axial half-waves and circumferential waves, respectively.

Table 18. Nondimensional buckling pressure $\frac{p^{cr}RL^2}{\pi^2 D}$ for isotropic cylinders with simply supported edges and subjected to uniform hydrostatic pressure ($\nu = 0.30$)

Batdorf-Z parameter†	Ref. 47	Present study		
	Donnell	Donnell	Sanders* Live pressure	Sanders Live pressure
0	2.0000	2.0000 (1,0)[a]	2.0000 (1,0)	2.0000 (1,0)
1	2.1774	2.1775 (1,40)	2.1776 (1,40)	2.1775 (1,40)
1.5	2.3173	2.3174 (1,43)	2.3175 (1,43)	2.3174 (1,43)
2	2.4571	2.4571 (1,44)	2.4573 (1,44)	2.4571 (1,44)
3	2.7204	2.7204 (1,44)	2.7206 (1,44)	2.7203 (1,44)
4	2.9601	2.9603 (1,44)	2.9604 (1,44)	2.9600 (1,44)
5	3.1797	3.1797 (1,43)	3.1798 (1,43)	3.1794 (1,43)
7	3.5727	3.5732 (1,42)	3.5732 (1,42)	3.5727 (1,42)
10	4.0815	4.0817 (1,40)	4.0816 (1,40)	4.0809 (1,40)
15	4.7947	4.7960 (1,37)	4.7957 (1,37)	4.7948 (1,37)
20	5.4028	5.4053 (1,36)	5.4046 (1,36)	5.4035 (1,36)
30	6.4307	6.4307 (1,33)	6.4294 (1,33)	6.4281 (1,33)
40	7.3016	7.3022 (1,31)	7.3004 (1,31)	7.2988 (1,31)
50	8.0710	8.0733 (1,30)	8.0706 (1,30)	8.0689 (1,30)
70	9.4092	9.4137 (1,28)	9.4097 (1,28)	9.4076 (1,28)
100	11.100	11.110 (1,26)	11.104 (1,26)	11.100 (1,26)
150	13.429	13.449 (1,23)	13.441 (1,23)	13.436 (1,23)
200	15.395	15.396 (1,22)	15.383 (1,22)	15.379 (1,22)
300	18.694	18.695 (1,20)	18.675 (1,20)	18.670 (1,20)
400	21.477	21.516 (1,19)	21.488 (1,19)	21.482 (1,19)
500	23.929	23.968 (1,18)	23.933 (1,18)	23.926 (1,18)
700	28.185	28.246 (1,16)	28.205 (1,16)	28.196 (1,16)
1000	33.553	33.553 (1,15)	33.486 (1,15)	33.477 (1,15)

[a] Numbers in parentheses, (m,n), indicate the number of axial half-waves and circumferential waves, respectively.

* Nonlinear rotations about the normal are neglected.

† $Z = \frac{L^2}{Rh}\sqrt{1-\nu^2}$ and $D = \frac{Eh^3}{12(1-\nu^2)}$

Table 18. Concluded

Batdorf-Z parameter†	Ref. 47	Present study		
	Donnell	Donnell	Sanders* Live pressure	Sanders Live pressure
1500	40.939	41.147 (1,14)	41.033 (1,14)	41.023 (1,14)
2000	47.167	47.349 (1,13)	47.199 (1,13)	47.187 (1,13)
3000	57.614	58.206 (1,11)	58.024 (1,12)	58.011 (1,11)
4000	66.422	66.740 (1,11)	66.432 (1,11)	66.416 (1,11)
5000	74.182	74.236 (1,10)	73.909 (1,10)	73.888 (1,10)
7000	87.650	88.248 (1,9)	87.845 (1,9)	87.818 (1,9)
10 000	104.63	106.33 (1,9)	105.51 (1,9)	105.48 (1,9)
15 000	127.99	128.98 (1,9)	127.80 (1,8)	127.77 (1,8)
20 000	147.69	148.25 (1,7)	147.03 (1,7)	146.99 (1,7)
30 000	180.73	186.30 (1,7)	183.72 (1,7)	183.68 (1,7)
40 000	208.59	208.65 (1,6)	205.97 (1,6)	205.91 (1,6)
50 000	233.13	236.19 (1,6)	232.13 (1,6)	232.08 (1,6)
70 000	275.72	280.12 (1,5)	276.58 (1,5)	276.49 (1,5)
100 000	329.42	332.22 (1,5)	324.33 (1,5)	324.25 (1,5)

[a] Numbers in parentheses, (m,n), indicate the number of axial half-waves and circumferential waves, respectively.

* Nonlinear rotations about the normal are neglected.

† $Z = \frac{L^2}{Rh}\sqrt{1-\nu^2}$ and $D = \frac{Eh^3}{12(1-\nu^2)}$

Table 19. Nondimensional buckling pressure $\frac{p^{cr}R}{Eh} \times 10^3$ for isotropic cylinders with R/h = 100, simply supported edges, and subjected to uniform hydrostatic pressure ($\nu = 0.30$)

L/R	Ref. 48		Ref. 49	Ref. 50	Present study		
	Flugge Live pressure	Donnell	Donnell	Sanders	Sanders Live pressure	Sanders* Live pressure	Donnell
0.5	2.096 (11)[a]	2.106 (11)	2.106 (11)		2.098 (1,11)[b]	2.102 (1,11)	2.106 (1,11)
0.6			1.715 (10)		1.708 (1,10)	1.711 (1,10)	1.715 (1,10)
0.75			1.344 (9)		1.337 (1,9)	1.341 (1,9)	1.344 (1,9)
1.0	0.9776 (8)	0.9838 (8)	0.9838 (8)	0.9890	0.9773 (1,8)	0.9773 (1,8)	0.9839 (1,8)
1.5			0.6417 (7)		0.6343 (1,7)	0.6357 (1,7)	0.6417 (1,7)
2.0	0.4679 (6)	0.4744 (6)	0.4744 (6)	0.4790	0.4676 (1,6)	0.4688 (1,6)	0.4744 (1,6)
3.0	0.3066 (5)	0.3132 (5)	0.3132 (5)		0.3064 (1,5)	0.3072 (1,5)	0.3132 (1,5)
4.0			0.2395 (4)	0.2502	0.2355 (1,4)	0.2364 (1,4)	0.2396 (1,4)
5.0			0.1878 (4)	0.1920	0.1807 (1,4)	0.1811 (1,4)	0.1878 (1,4)
6.0	0.1598 (4)	0.1679 (4)	0.1679 (4)	0.1690	0.1597 (1,4)	0.1599 (1,4)	0.1679 (1,4)
7.0			0.1378 (3)		0.1350 (1,3)	0.1355 (1,3)	0.1378 (1,3)
8.0			0.1158 (3)	0.1236	0.1104 (1,3)	0.1107 (1,3)	0.1158 (1,3)
9.0			0.1038 (3)		0.09693 (1,3)	0.09717 (1,3)	0.1038 (1,3)
10.0	0.08916 (3)	0.09678 (3)	0.09678 (3)	0.0999	0.08912 (1,3)	0.08930 (1,3)	0.09677 (1,3)

[a] Number in parentheses, (n), indicates the number of circumferential waves.
[a] Numbers in parentheses, (m,n), indicate the number of axial half-waves and circumferential waves, respectively.
* Nonlinear rotations about the normal are neglected.

Table 20. Nondimensional buckling pressure $\frac{p_{cr}R^2\sqrt{3(1-\nu^2)}}{Eh^2}$ for isotropic cylinders with simply supported edges, and subjected to uniform hydrostatic pressure ($\nu = 0.30$)

R/h	L/R	Ref. 45		Present study		
		Sanders Live pressure	Donnell	Sanders	Sanders Live pressure	Donnell
100	0.5	0.3465 (11)[a]	0.3479 (11)	0.3483 (1,11)[b]	0.3466 (1,11)	0.3479 (1,11)
	1	0.1614 (8)	0.1626 (8)	0.1634 (1,8)	0.1615 (1,8)	0.1626 (1,8)
	2	0.0772 (6)	0.0784 (6)	0.0792 (1,6)	0.0773 (1,6)	0.0784 (1,6)
	4	0.0389 (4)	0.0396 (4)	0.0413 (1,4)	0.0389(1,4)	0.0396 (1,4)
	10	0.0147 (3)	0.0160 (3)	0.0165 (1,3)	0.0147 (1,3)	0.0160 (1,3)
	20	0.00664 (2)	0.00766 (2)	0.00881 (1,2)	0.00664 (1,2)	0.00766 (1,2)
	40	0.00468 (2)	0.00616 (2)	0.00623 (1,2)	0.00468 (1,2)	0.00616 (1,2)
300	0.5	0.1889 (15)	0.1893 (15)	0.1895 (1,15)	0.1889 (1,15)	0.1893 (1,15)
	1	0.0906 (11)	0.0910 (11)	0.0913 (1,11)	0.0906 (1,11)	0.0910 (1,11)
	2	0.0443 (8)	0.0446 (8)	0.0449 (1,8)	0.0443 (1,8)	0.0446 (1,8)
	4	0.0221 (6)	0.0225 (6)	0.0227 (1,6)	0.0221(1,6)	0.0225 (1,6)
	10	0.00887 (4)	0.00931 (4)	0.00946 (1,4)	0.00887 (1,4)	0.00931 (1,4)
	20	0.00451 (3)	0.00497 (3)	0.00507 (1,3)	0.00451 (1,3)	0.00497 (1,3)
	40	0.00191 (2)	0.00232 (2)	0.00254 (1,2)	0.00191 (1,2)	0.00232 (1,2)
500	0.5	0.1442 (17)	0.1444 (17)	0.1446 (1,17)	0.1442 (1,17)	0.1444 (1,17)
	1	0.0699 (13)	0.0701 (13)	0.0703 (1,13)	0.0699 (1,13)	0.0701 (1,13)
	2	0.0342 (1,9)	0.0344 (1,9)	0.0346 (1,9)	0.0342 (1,9)	0.0344 (1,9)
	4	0.0174 (7)	0.0176 (6)	0.0178 (1,7)	0.0174 (1,7)	0.0176 (1,6)
	10	0.00664 (4)	0.00682 (4)	0.00708 (1,4)	0.00664 (1,4)	0.00682 (1,4)
	20	0.00320 (3)	0.00342 (3)	0.00360 (1,3)	0.00320 (1,3)	0.00342 (1,3)
	40	0.00156 (2)	0.00170 (2)	0.00208 (1,2)	0.00156 (1,2)	0.00170 (1,2)
700	0.5	0.1204 (19)	0.1206 (19)	0.1207 (1,19)	0.1204 (1,19)	0.1206 (1,19)
	1	0.0587 (14)	0.0588 (14)	0.0589 (1,14)	0.0587 (1,14)	0.0588 (1,14)
	2	0.0289 (10)	0.0290 (10)	0.0292 (1,10)	0.0289 (1,10)	0.0290 (1,10)
	4	0.0143 (7)	0.0144 (7)	0.0146 (1,7)	0.0143 (1,7)	0.0144 (1,7)
	10	0.00596 (5)	0.00615 (5)	0.00621 (1,5)	0.00596 (1,5)	0.00615 (1,5)
	20	0.00282 (3)	0.00291 (3)	0.00317 (1,3)	0.00282 (1,3)	0.00291 (1,3)
	40	0.00156 (2)	0.00155 (2)	0.00202 (1,3)	0.00156 (1,2)	0.00155 (1,2)

[a] Numbers in parentheses, (n), indicate the number of circumferential waves.
[b] Numbers in parentheses, (m,n), indicate the number of axial half-waves and circumferential waves, respectively.

Table 20. Concluded

R/h	L/R	Ref. 45		Present study		
		Sanders Live pressure	Donnell	Sanders	Sanders Live pressure	Donnell
1100	0.5	0.0952 (22)[a]	0.0953 (22)	0.0954 (1,22)[b]	0.0952 (1,22)	0.0953 (1,22)
	1	0.0468 (16)	0.0469 (16)	0.0469 (1,16)	0.0468 (1,16)	0.0469 (1,16)
	2	0.0230 (11)	0.0231 (11)	0.0232 (1,11)	0.0230 (1,11)	0.0231 (1,11)
	4	0.0114 (8)	0.0115 (8)	0.0116 (1,8)	0.0114 (1,8)	0.0115 (1,8)
	10	0.00449 (5)	0.00458 (5)	0.00468 (1,5)	0.00449 (1,5)	0.00458 (1,5)
	20	0.00236 (4)	0.00248 (4)	0.00251 (1,4)	0.00236 (1,4)	0.00248 (1,4)
	40	0.00121 (3)	0.00133 (3)	0.00136 (1,3)	0.00121 (1,3)	0.00133 (1,3)
1500	0.5	0.0811 (23)	0.0812 (23)	0.0812 (1,23)	0.0811 (1,23)	0.0812 (1,23)
	1	0.0397 (17)	0.0398 (17)	0.0399 (1,17)	0.0398 (1,17)	0.0398 (1,17)
	2	0.0197 (12)	0.0197 (12)	0.0198 (1,12)	0.0197 (1,12)	0.0197 (1,12)
	4	0.00992 (9)	0.0100 (9)	0.0100 (1,9)	0.00992 (1,9)	0.0100 (1,9)
	10	0.00403 (5)	0.00407 (5)	0.00419 (1,6)	0.00403 (1,5)	0.00407 (1,5)
	20	0.00191 (4)	0.00198 (4)	0.00203(1,4)	0.00191 (1,4)	0.00198 (1,4)
	40	0.00095 (3)	0.00104 (3)	0.00107 (1,3)	0.00095 (1,3)	0.00104 (1,3)
1900	0.5	0.0717 (25)	0.0717 (25)	0.0718 (1,25)	0.0717 (1,25)	0.0717 (1,25)
	1	0.0353 (18)	0.0353 (18)	0.0354 (1,18)	0.0353 (1,18)	0.0353 (1,18)
	2	0.0175 (13)	0.0176 (13)	0.0176 (1,13)	0.0175 (1,13)	0.0176 (1,13)
	4	0.00868 (9)	0.00873 (9)	0.00878 (1,9)	0.00868 (1,9)	0.00873 (1,9)
	10	0.00347 (6)	0.00353 (6)	0.00357 (1,6)	0.00347 (1,6)	0.00353 (1,6)
	20	0.00169 (4)	0.00174 (4)	0.00181 (1,4)	0.00169 (1,4)	0.00174 (1,4)
	40	0.000820 (3)	0.000881 (3)	0.000924 (1,3)	0.000822 (1,3)	0.000881 (1,3)

[a] Numbers in parentheses, (n), indicate the number of circumferential waves.
[b] Numbers in parentheses, (m,n), indicate the number of axial half-waves and circumferential waves, respectively.

Table 21. Nondimensional buckling pressure $\frac{p^{cr}R^3}{D}$ for isotropic cylinders with simply supported edges and subjected to uniform hydrostatic pressure ($\nu = 0.30$)

R/h	L/R	Ref. 51 and 52 Donnell	Present Study		
			Donnell	Sanders* Live pressure	Sanders Live pressure
50	0.5	173.2	173.2 (1,9)[b]	172.9 (1,9)	172.3 (1,9)
	1	78.48	78.48 (1,7)	77.90 (1,7)	77.59 (1,7)
	1.5	51.14	51.14 (1,6)	50.44 (1,6)	50.24 (1,6)
75	0.65	150.7	150.7 (1,9)	150.3 (1,9)	149.9 (1,9)
	0.8	120.3	120.3 (1,8)	120.0 (1,8)	119.6 (1,8)
100	0.5	229.9	229.9 (1,11)	229.6 (1,11)	229.1 (1,11)
	1	107.4	107.4 (1,8)	107.0 (1,8)	106.7 (1,8)
	1.5	70.07	70.07 (1,7)	69.42 (1,7)	69.27 (1,7)
	2	51.81	51.81 (1,6)	51.19 (1,6)	51.07 (1,6)
150	0.8	164.4	164.4 (1,10)	163.9 (1,10)	163.7 (1,10)
200	1	148.6	148.6 (1,10)	148.0 (1,10)	147.8 (1,10)
250	0.5	345.9	345.9 (1,14)	345.5 (1,14)	345.2 (1,14)
	1	166.8	166.8 (1,11)	166.1 (1,11)	166.0 (1,11)
	1.5	109.3	109.3 (1,9)	108.6 (1,9)	108.5 (1,9)
	2	82.14	82.14 (1,8)	81.39 (1,8)	81.32 (1,8)
	3	53.97	53.97 (1,6)	53.46 (1,6)	53.39 (1,6)
300	1	180.4	180.4 (1,11)	179.8 (1,11)	179.7 (1,11)
400	1	207.2	207.2 (1,12)	206.6 (1,12)	206.5 (1,12)
475	0.65	352.7	352.7 (1,15)	352.2 (1,15)	352.0 (1,15)
500	0.5	477.2	477.2 (1,17)	476.7 (1,17)	476.5 (1,17)
	1	231.7	231.7 (1,13)	231.0 (1,13)	230.9 (1,13)
	1.5	153.8	153.8 (1,10)	153.3 (1,10)	153.2 (1,10)
	2	113.7	113.7 (1,9)	113.1 (1,9)	113.0 (1,9)
	3	77.05	77.05 (1,7)	76.62 (1,7)	76.57 (1,7)
550	0.8	305.7	305.7 (1,14)	305.2 (1,14)	305.0 (1,14)
600	1	252.8	252.8 (1,13)	252.2 (1,13)	252.1 (1,13)
700	1	272.2	272.1 (1,14)	271.5 (1,14)	271.4 (1,14)

[b] Numbers in parentheses, (m,n), indicate the number of axial half-waves and circumferential waves, respectively.
* Nonlinear rotations about the normal are neglected.

Table 21. Concluded

R/h	L/R	Ref. 51 and 52 Donnell	Present Study		
			Donnell	Sanders* Live pressure	Sanders Live pressure
750	0.6	476.4	476.4 (1,18)[b]	475.8 (1,18)	475.6 (1,18)
	0.7	406.7	406.7 (1,17)	406.1 (1,17)	405.9 (1,17)
	0.8	354.5	354.5 (1,16)	353.9 (1,16)	353.7 (1,16)
	0.9	313.6	313.6 (1,15)	312.9 (1,15)	312.8 (1,15)
	1	281.2	281.2 (1,14)	280.6 (1,14)	280.5 (1,14)
800	1	290.9	290.9 (1,14)	290.3 (1,14)	290.2 (1,14)
900	1	307.7	307.8 (1,15)	307.2 (1,15)	307.1 (1,15)
1000	0.5	661.1	661.1 (1,21)	660.5 (1,21)	660.3 (1,21)
	0.6	547.8	547.8 (1,19)	547.3 (1,19)	547.1 (1,19)
	0.7	466.5	466.5 (1,18)	465.9 (1,18)	465.7 (1,18)
	0.8	406.8	406.8 (1,17)	406.1 (1,17)	406.0 (1,17)
	0.9	360.4	360.4 (1,16)	359.8 (1,16)	359.7 (1,16)
	1	323.8	323.8 (1,15)	323.2 (1,15)	323.1 (1,15)
	1.5	215.9	215.9 (1,12)	215.4 (1,12)	215.3 (1,12)
	2	160.4	160.4 (1,11)	159.7 (1,11)	159.7 (1,11)
	3	106.5	106.5 (1,9)	105.8 (1,9)	105.8 (1,9)
1500	0.5	804.9	804.9 (1,23)	804.3 (1,23)	804.2 (1,23)
2000	0.4	1163	1163 (1,28)	1162 (1,82)	1162 (1,28)
	0.5	924.0	924.0 (1,25)	923.4 (1,25)	923.2 (1,25)
	0.6	765.9	765.9 (1,23)	765.3 (1,23)	765.2 (1,23)
	0.7	655.5	655.5 (1,22)	654.9 (1,22)	654.8 (1,22)
	0.9	506.2	506.2 (1,19)	505.6 (1,19)	505.5 (1,19)
	1	454.9	454.9 (1,18)	454.3 (1,18)	454.2 (1,18)
	1.5	301.9	301.9 (1,15)	301.2 (1,15)	301.2 (1,15)
	2	225.8	225.8 (1,13)	225.2 (1,13)	225.1 (1,13)
	2.5	181.9	181.9 (1,12)	181.1 (1,12)	181.1 (1,12)
	3	151.6	151.6 (1,11)	150.9 (1,11)	150.9 (1,11)
	4	112.6	112.6 (1,9)	112.0 (1,9)	112.0 (1,9)
	6	76.80	76.80 (1,8)	76.00 (1,8)	75.99 (1,8)
	10	45.21	45.21 (1,6)	44.47 (1,6)	44.46 (1,6)

[b] Numbers in parentheses, (m,n), indicate the number of axial half-waves and circumferential waves, respectively.
* Nonlinear rotations about the normal are neglected.

Table 22. Nondimensional buckling coefficients $\frac{N_{xy}^{cr} L^2}{\pi^2 D}$ for isotropic cylinders with R/h = 100, simply supported edges, and subjected to unform torsion ($\nu = 0.30$)

Batdorf-Z parameter	Ref. 54	Refs. 55 (p. 51) and 56	Present study			Percent difference
	Donnell	Donnell	Donnell	Sanders*	Sanders	
0	5.34	5.34	5.66 (1,inf, .71)[a,#]			6.0
1	5.41	5.34	5.72 (1,26,.70)	5.72 (1,26,.70)	5.72 (1,26,.70)	5.7
1.5	---	5.45	5.78 (1,21,.71)			6.1
2	---	5.53	5.87 (1,19,.70)			6.1
3	---	5.73	6.09 (1,17,.68)			6.3
4	---	5.96	6.34 (1,15,.69)			6.4
5	6.22	---	6.62 (1,14,.69)	6.63 (1,14,.69)	6.63 (1,14,.69)	6.4
7	---	6.72	7.21 (1,13,.67)			7.3
10	7.55	7.52	8.09 (1,13,.63)	8.10 (1,13,.63)	8.10 (1,13,.63)	7.2
15	---	8.84	9.57 (1,12,.61)			8.3
20	---	10.13	11.04 (1,12,.58)	11.05 (1,12,.58)	11.05 (1,12,.58)	9.0
30	12.69	---	13.83 (1,11,.55)			9.0
40	---	14.96	16.61 (1,11,.52)			11.0
50	---	17.22	19.30 (1,10,.49)			12.1
100	27.86	27.51	32.23 (1,10,.44)			17.2
200	---	45.27	56.61 (1,9,.37)	56.59 (1,9,.37)	56.59 (1,9,.37)	25.0
300	61.47	---	80.25 (1,8,.31)			30.6
500	---	89.27	126.97 (1,8,.30)	126.90 (1,8,0.29)	126.90 (1,8,0.29)	42.2
1,000	153.0	150.2	240.5 (1,7,.23)			57.2
2,000	---	253.0	464.36 (1,6,.17)	464.18 (1,6,.17)	464.18 (1,6,.17)	83.5
5,000	---	504.5	1129 (1,5,.12)	1129 (1,5,.12)	1129 (1,5,.12)	123.8
10,000	851.9	849.9	2228 (1,5,0.12)			161.5
100,000	4800	---	21,922 (1,4,.08)	22,057 (1,5,.12)	22,057 (1,5,.12)	359.5

[a] Numbers in parentheses, (m,n,τ), indicate the number of axial half-waves, the number of circumferential waves, and the values of the skewedness parameter, respectively

* Nonlinear rotations about the normal are neglected

[#] same as Timoshenko and Gere[34]

Table 23. Nondimensional buckling coefficients $\frac{N_{xy}^{cr} R^2}{D}$ for isotropic cylinders with simply supported edges and subjected to unform torsion ($\nu = 0.30$)

L/R	R/h	Refs. 57 and 58	Present study			Percent difference
		Donnell	Sanders	Sanders*	Donnell	
0.35	100	642.7 (12)[a]	694.2 (1,12,.64)[b]	694.2 (1,12,.64)	693.3 (1,12,.64)	7.9
0.4	100	551.8 (12)	595.4 (1,12,.61)	595.4 (1,12,.61)	594.9 (1,12,.61)	7.8
0.5	100	438.7 (11)	479.6 (1,11,.57)	479.6 (1,11,.57)	479.1 (1,11,.57)	9.2
	250	764.9 (15)	859.7 (1,16,.48)	859.7 (1,16,.48)	859.6 (1,16,.48)	12.4
	500	1234 (20)	1456 (1,21,.41)	1456 (1,21,.41)	1456 (1,21,.41)	18.0
	1000	2041 (25)	2593 (1,27,.34)	2593 (1,27,.34)	2593 (1,27,.34)	27.0
	2000	3418 (31)	4790 (1,34,.28)	4790 (1,34,.28)	4790 (1,34,.28)	40.1
1.0	100	263.5 (9)	306.2 (1,10,.44)	306.2 (1,10,.44)	306.4 (1,10,.44)	16.3
	250	511.7 (13)	649.0 (1,13,.32)	649.0 (1,13,.32)	649.0 (1,13,.32)	26.8
	500	854.7 (16)	1198 (1,17,.27)	1198 (1,17,.27)	1198 (1,17,.28)	40.2
	1000	1437 (19)	2270 (1,22,.23)	2270 (1,22,.23)	2270 (1,22,.23)	60.0
	2000	2419 (24)	4380 (1,28,.19)	4380 (1,28,.19)	4380 (1,28,.19)	81.1
1.5	100	209.9 (8)	263.9 (1,9,.37)	263.9 (1,9,.37)	264.1 (1,9,.37)	25.8
	250	414.7 (11)	592.3 (1,12,.27)	592.3 (1,12,.27)	592.4 (1,12,.27)	42.9
	500	698.7 (13)	1127 (1,15,.21)	1127 (1,15,.21)	1127 (1,15,.22)	61.3
	1000	1176 (16)	2179 (1,19,.17)	2179 (1,19,.17)	2178 (1,19,.17)	85.2
	2000	1979 (20)	4264 (1,24,.14)	4264 (1,24,.14)	4264 (1,24,.14)	115.5
2.0	100	181.6 (7)	244.8 (1,8,.30)	244.8 (1,8,.30)	244.9 (1,8,.30)	34.9
	250	359.7 (10)	567.4 (1,11,.23)	567.4 (1,11,.23)	567.5 (1,11,.23)	57.8
	500	604.9 (12)	1095 (1,14,.19)	1095 (1,14,.19)	1095 (1,14,.19)	81.0
	1000	1020 (14)	2139 (1,17,.14)	2139 (1,17,.14)	2139 (1,17,.14)	109.7
	2000	1717 (17)	4213 (1,22,.12)	4213 (1,22,.12)	4213 (1,22,.12)	145.4
3.0	100	148.1 (6)	228.4 (1,7,.23)	228.4 (1,7,.23)	228.6 (1,7,.23)	54.4
	250	293.9 (8)	545.4 (1,10,.19)	545.6 (1,10,.19)	545.6 (1,10,.19)	85.6
	500	494.8 (10)	1066 (1,12,.14)	1066 (1,12,.14)	1066 (1,12,.14)	115.4
	1000	833.3 (12)	2102 (1,15,.11)	2102 (1,15,.11)	2102 (1,15,.11)	152.3
	2000	1404 (14)	4166 (1,19,.09)	4166 (1,19,.09)	4166 (1,19,.09	196.7

[a] Numbers in parentheses indicate the number of circumferential waves, n
[b] Numbers in parentheses, (m,n,τ), indicate the number of axial half-waves, the number of circumferential waves, and the values of the skewedness parameter, respectively
* Nonlinear rotations about the normal are neglected.

Table 24. Nondimensional buckling pressure $\frac{p^{cr}R}{Eh} \times 10^3$ for isotropic cylinders with R/h = 100, simply supported edges, and subjected to uniform hydrostatic pressure and torsion ($\nu = 0.30$)

L/R	Ref. 59		Present study		
	Flügge	Donnell	Sanders	Sanders*	Donnell
0.5	1.666 (11)[a]	1.672 (11)	1.730 (1,11,.24)[b]	1.745 (1,11,.24)	1.747 (1,11,.24)
1.0	0.8557 (8)	0.8597 (8)	0.8939 (1,8,.10)	0.8959 (1,8,.10)	0.8984 (1,8,.10)
2.0	0.4390 (6)	0.4442 (6)	0.4531 (1,6,0.03)	0.4541 (1,6,.03)	0.4591 (1,6,.04)
3.0	0.2944 (5)	0.3001 (5)	0.3018 (1,5,.02)	0.3025 (1,5,.02)	0.3081 (1,5,.02)
6.0	0.1553 (4)	0.1627 (4)	0.1592 (1,4,.01)	0.1595 (1,4,.01)	0.1671 (1,4,.01)
10.0	0.08798 (3)	0.09524 (3)	0.08909 (1,3,.00)	0.08928 (1,3,.00)	0.09678 (1,3,.00)

[a] Numbers in parentheses indicate the number of circumferential waves, n
[b] Numbers in parentheses, (m,n,τ), indicate the number of axial half-waves, the number of circumferential waves, and the values of the skewedness parameter, respectively
* Nonlinear rotations about the normal are neglected.

Table 25. Nondimensional buckling loads $\frac{N_x^{cr}}{E\bar{h}}$ for isotropic† cylinders with simply supported edges, subjected to axial compression, and stiffened by rings and stringers#

Ring spacing, d_r/R	Ref. 60 Donnell	Present study		
		Donnell	Sanders*	Sanders
Internal rings with eccentricity e_r = - 2.05 in. and external stringers with eccentricity e_s = 1.05 in.				
0.05	0.004111 (3,7)[a]	0.004112 (3,7)	0.004099 (3,7)	0.004096 (3,7)
0.10	0.003836 (3,7)	0.003837 (3,7)	0.003830 (3,7)	0.003827 (3,7)
0.20	0.003629 (3,8)	0.003629 (3,8)	0.003623 (3,8)	0.003621 (3,8)
0.25	0.003574 (3,8)	0.003574 (3,8)	0.003569 (3,8)	0.003567 (3,8)
Internal rings with eccentricity e_r = - 2.05 in. and internal stringers with eccentricity e_s = -1.05 in.				
0.05	0.003764 (3,7)	0.003764 (3,7)	0.003741 (3,7)	0.003728 (3,7)
0.10	0.003430 (3,7)	0.003430 (3,7)	0.003415 (3,8)	0.003404 (3,8)
0.20	0.002988 (2,7)	0.002988 (2,7)	0.002960 (2,8)	0.002945 (2,8)
0.25	0.002779 (2,8)	0.002779 (2,8)	0.002753 (2,8)	0.002738 (2,8)
External rings with eccentricity e_r = 2.05 in. and external stringers with eccentricity e_s = 1.05 in.				
0.05	0.005970 (3,6)	0.005970 (4,5)	0.005953 (4,5)	0.005946 (4,5)
0.10	0.005121 (3,6)	0.005121 (4,5)	0.005114 (4,5)	0.005111 (4,5)
0.20	0.004467 (3,7)	0.004467 (3,7)	0.004453 (3,7)	0.004447 (3,7)
0.25	0.004137 (3,8)	0.004283 (3,8)	0.004269 (3,8)	0.004264 (3,8)

[a] Numbers in parentheses, (m,n), indicate the number of axial half-waves and circumferential waves, respectively.
* Nonlinear rotations about the normal are neglected.

† $E = 10 \times 10^6$ psi, $\nu = 0.32$, R = 200.0 in., L = 200.0 in., h = 0.10 in.

Stringer properties: spacing d_s = 2.50 in. , area A_s = 0.36 in^2, I_s = 0.2112 in^4, J_s = 0.0012 in^4

Ring properties: A_r = 0.78 in^2, I_r = 1.9786 in^4, J_r = 0.0026 in^4, $\bar{h} = \frac{A_s}{d_s} + h = 0.24$ in.

Table 26. Nondimensional buckling loads $\frac{N_x^{cr}}{E\bar{h}}$ for stringer-stiffened[#] isotropic[†] cylinders with simply supported edges and subjected to axial compression

Length-to-radius ratio, L/R	Ref. 60 Donnell	Present study		
		Donnell	Sanders*	Sanders
External stringers with eccentricity e_s = 1.05 in.				
0.15	0.007043 (1,0)[a]	0.007043 (1,0)	0.007043 (1,0)	0.007043 (1,0)
0.20	0.004739 (1,8)	0.004739 (1,8)	0.004739 (1,8)	0.004739 (1,8)
0.25	0.003614 (1,18)	0.003614 (1,18)	0.003614 (1,18)	0.003614 (1,18)
0.30	0.002814 (1,25)	0.002814 (1,25)	0.002813 (1,25)	0.002813 (1,25)
0.35	0.002243 (1,27)	0.002243 (1,27)	0.002243 (1,27)	0.002243 (1,27)
0.40	0.001843 (1,27)	0.001842 (1,27)	0.001842 (1,27)	0.001842 (1,27)
0.45	0.001554 (1,26)	0.001554 (1,26)	0.001554 (1,26)	0.001553 (1,26)
0.50	0.001340 (1,25)	0.001340 (1,25)	0.001339 (1,25)	0.001339 (1,25)
Internal stringers with eccentricity e_s = - 1.05 in.				
0.15	0.006747 (1,21)	0.006747 (1,21)	0.006747 (1,21)	0.006717 (1,21)
0.20	0.003804 (1,20)	0.003804 (1,20)	0.003804 (1,20)	0.003789 (1,20)
0.25	0.002443 (1,19)	0.002443 (1,19)	0.002443 (1,19)	0.002434 (1,19)
0.30	0.001706 (1,18)	0.001706 (1,18)	0.001706 (1,18)	0.001700 (1,18)
0.35	0.001262 (1,18)	0.001262 (1,18)	0.001261 (1,18)	0.001257 (1,18)
0.40	0.000975 (1,18)	0.000975 (1,18)	0.000975 (1,18)	0.000972 (1,18)
0.45	0.000780 (1,18)	0.000780 (1,18)	0.000780 (1,18)	0.000778 (1,18)
0.50	0.000641 (1,17)	0.000642 (1,17)	0.000641 (1,17)	0.000639 (1,17)

[a] Numbers in parentheses, (m,n), indicate the number of axial half-waves and circumferential waves, respectively.
* Nonlinear rotations about the normal are neglected.

[†] $E = 10 \times 10^6$ psi, $\nu = 0.32$, R = 200.0 in., h = 0.10 in.

[#] Stringer properties: spacing d_s = 2.50 in. , area A_s = 0.36 in^2, I_s = 0.2112 in^4, J_s = 0.0012 in^4, $\bar{h} = \frac{A_s}{d_s} + h = 0.24$ in.

Table 27. Nondimensional buckling loads $\frac{N_x^{cr}}{A_{11}}$ for isotropic[†] cylinders with simply supported edges, subjected to axial compression, with a corrugated shell wall, and stiffened by rings[#]

Ring spacing, d_r/R	Ref. 60 Donnell	Present study		
		Donnell	Sanders*	Sanders
External rings with eccentricity e_r = 3.812 in.				
0.20	0.004289 (2,0)[a]	0.004289 (2,0)	0.004289 (2,0)	0.004289 (2,0)
0.25	0.003826 (2,0)	0.003826 (2,0)	0.003826 (2,0)	0.003826 (2,0)
0.50	0.002900 (2,0)	0.002900 (2,0)	0.002900 (2,0)	0.002900 (2,0)
Internal rings with eccentricity e_r = -3.812 in.				
0.20	0.001491 (1,6)	0.001496 (1,6)	0.001493 (1,6)	0.001492 (1,6)
0.25	0.001324 (1,6)	0.001329 (1,6)	0.001327 (1,6)	0.001327 (1,6)
0.50	0.000967 (1,6)	0.000971 (1,6)	0.000971 (1,6)	0.000971 (1,6)

[a] Numbers in parentheses, (m,n), indicate the number of axial half-waves and circumferential waves, respectively.
* Nonlinear rotations about the normal are neglected.

[†] $E = 10 \times 10^6$ psi, $\nu = 0.32$, R = 200.0 in., L = 200.0 in., h = 0.10 in.

[#] Ring properties: $A_r = 0.78$ in^2, $I_r = 1.9786$ in^4, $J_r = 0.0026$ in^4

Table 28. Buckling load N_x^{cr} (lbs/in.) for isotropic† cylinders with simply supported edges, subjected to axial compression, and stiffened by internal or external blade stringers (figure 51)

Length, in.	Cylinder wall thickness, h, in.	Ref. 61 Sanders**	Ref. 62 Donnell $J_s = 0$	Ref. 62 Donnell	Present study			
					Donnell $J_s = 0$	Donnell	Sanders*	Sanders
External stringers with eccentricity $e_s = 0.165$ in.								
38.00	0.0283	1115 (6)[a]	1043 (6)	1193 (6)	1029 (1,6)[b]	1173 (1,6)	1137 (1,6)	1109 (1,6)
23.75	0.0275	1354 (7)	1183 (7)	1389 (7)	1171 (1,7)	1368 (1,7)	1346 (1,7)	1324 (1,7)
Internal stringers with eccentricity $e_s = -0.165$ in.								
38.00	0.0277	689 (5)	587 (7)	719 (5)	580 (2,7)	707 (1,5)	681 (1,5)	657 (1,5)
23.75	0.0280	725 (6)	611 (7)	765 (6)	602 (1,7)	752 (1,6)	733 (1,6)	715 (1,6)

[a] Numbers in parentheses indicate the number of circumferential waves, n
[b] Numbers in parentheses, (m,n), indicate the number of axial half-waves and circumferential waves, respectively.
* Nonlinear rotations about the normal are neglected.
† $E = 10.5 \times 10^6$ psi, $\nu = 0.32$, R = 9.55 in., stringer spacing $d_s = 1.0$ in.
** Selected terms are neglected in Sanders' nonlinear equilibrium equations.

Table 29. Buckling load N_x^{cr} (lbs/in.) for isotropic† cylinders with simply supported edges, subjected to axial compression, and stiffened by internal or external blade stringers (figure 51)

Length, in.	Cylinder wall thickness, h, in.	Ref. 64 Donnell	Present study		
			Donnell	Sanders*	Sanders
External stringers with eccentricity $e_s = 0.165$ in.					
38.00	0.0283	1145	1144 (1,6)[b]	1110 (1,6)	1083 (1,6)
23.75	0.0275	1326	1328 (1,7)	1308 (1,7)	1287 (1,7)
Internal stringers with eccentricity $e_s = -0.165$ in.					
38.00	0.0277	687	687(1,5)	662 (1,5)	639 (1,5)
23.75	0.0280	722	723 (1,6)	705 (1,6)	688 (1,6)

[b] Numbers in parentheses, (m,n), indicate the number of axial half-waves and circumferential waves, respectively.
* Nonlinear rotations about the normal are neglected.
† $E = 10.5 \times 10^6$ psi, $\nu = 0.32$, R = 9.55 in., stringer spacing $d_s = 1.0$ in.
** Selected terms are neglected in Sanders' nonlinear equilibrium equations.

Table 30. Buckling load N_x^{cr} (lbs/in.) for isotropic† cylinders with simply supported edges, subjected to axial compression, and stiffened by internal or external Z-shaped stringers (figure 32)

Thickness, in.	Stringer eccentricity, e_s, in.	Ref. 61 Sanders**	Present study		
			Donnell	Sanders*	Sanders
0.0410	0.2538	1125 (6)[a]	1231 (1,6)[b]	1203 (1,6)	1173 (1,6)
0.0401	-0.2533	735 (6)	779 (1,6)	753 (1,6)	733 (1,6)

[a] Numbers in parentheses indicate the number of circumferential waves, n
[b] Numbers in parentheses, (m,n), indicate the number of axial half-waves and circumferential waves, respectively.
* Nonlinear rotations about the normal are neglected.
† $E = 10.5 \times 10^6$ psi, $\nu = 0.32$, R = 15.80 in., L = 59.0 in., stringer spacing d_s = 1.24 in.
** Selected terms are neglected in Sanders' nonlinear equilibrium equations.

Table 31. Buckling load N_x^{cr} (lbs/in.) for isotropic† cylinders with simply supported edges, subjected to axial compression, and stiffened by internal or external Z-shaped stringers (figure 32)

Length, in.	Thickness, h, in.	Stringer eccentricity, e_s, in.	Ref. 64 Donnell	Present study			
				Donnell $J_s = 0$	Donnell	Sanders $J_s = 0$	Sanders
59.00	0.0410	0.2538	1193	1213 (1,6)[b]	1223 (1,6)	1157 (1,6)	1166 (1,6)
59.00	0.0401	-0.2533	766	759 (1,6)	769 (1,6)	715 (1,6)	724 (1,6)
41.83	0.0391	0.2528	1283	1310 (1,7)	1324 (1,7)	1271 (1,7)	1284 (1,7)
41.83	0.0401	-0.2533	773	766 (1,7)	779 (1,7)	734 (1,7)	747 (1,7)
29.68	0.0392	0.2529	1574	1606 (1,9)	1629 (1,9)	1577 (1,9)	1599 (1,9)
29.68	0.0403	-0.2534	838	832 (1,8)	851 (1,8)	809 (1,8)	826 (1,8)
20.77	0.0395	0.2530	2068	2133 (1,10)	2162 (1,10)	2111 (1,10)	2138 (1,10)
20.77	0.0401	-0.2533	1027	1035 (1,9)	1058 (1,9)	1016 (1,9)	1038 (1,9)

[b] Numbers in parentheses, (m,n), indicate the number of axial half-waves and circumferential waves, respectively.
† $E = 10.5 \times 10^6$ psi, $\nu = 0.32$, R = 15.92 in., stringer spacing d_s = 1.24 in.

Table 32. Nondimensional buckling coefficient $\frac{2N_x^{cr} R^2}{D}$ for isotropic cylinders with simply supported edges, central stringers,[#] and subjected to axial compression ($\nu = 0.3$)

L/R	R/h	Central stringers, $e_s/h = 0$			
		Ref. 66 Donnell	Present Study		
			Donnell	Sanders*	Sanders
0.5	50	4991 (1,6)[b]	4991 (1,6)	4984 (1,6)	4956 (1,6)
	100	5714 (1,9)	5714 (1,9)	5701 (1,9)	5674 (1,9)
1	50	1814 (1,6)	1814 (1,6)	1794 (1,6)	1768 (1,6)
	100	2561 (1,7)	2561 (1,7)	2535 (1,7)	2505 (1,7)
	250	4914 (1,9)	4914 (1,9)	4875 (1,9)	4833 (1,9)
	500	8865 (1,11)	8865 (1,11)	8810 (1,11)	8753 (1,11)
	1000	16860 (1,14)	16861 (1,14)	16774 (1,14)	16701 (1,14)
2	500	8219 (1,8)	8219 (1,8)	8108 (1,8)	7997 (1,8)
	2000	32410 (1,12)	32411 (1,12)	32170 (1,12)	31960 (1,12)
4	2000	32410 (2,12)	32411 (2,12)	32170 (2,12)	31827 (1,8)

[b] Numbers in parentheses, (m,n), indicate the number of axial half-waves and circumferential waves, respectively
* Nonlinear rotations about the normal are neglected.

[#] $\frac{A_s}{d_s h} = 0.5$, $\frac{I_s^c}{d_s h^3} = 5$, and $J_s = 0$

Table 33. Nondimensional buckling coefficient $\frac{2N_x^{cr}R^2}{D}$ for isotropic stringer-stiffened[#] cylinders with simply supported edges, and subjected to axial compression ($\nu = 0.3$)

		Ref. 66 Donnell	Present Study		
			Donnell	Sanders*	Sanders
L/R	R/h	External stringers, $e_s/h = +2$			
1	50	2434 (1,6)[b]	2434 (1,6)	2415 (1,6)	2394 (1,6)
	100	3402 (1,7)	3402 (1,7)	3377 (1,7)	3345 (1,7)
	250	6196 (1,9)	6196 (1,9)	6154 (1,10)	6108 (1,9)
	500	10620 (1,11)	10619 (1,11)	10560 (1,12)	10498 (1,11)
	1000	19120 (1,14)	19119 (1,14)	19032 (1,14)	18952 (1,14)
2	1000	17340 (1,10)	17342 (1,10)	17173 (1,10)	17016 (1,10)
3	1000	16900 (1,8)	16898 (1,8)	16658 (1,8)	16416 (1,8)
		Internal stringers, $e_s/h = -2$			
1	50	1866 (1,5)	1867 (1,5)	1850 (1,5)	1804 (1,5)
	100	2443 (1,7)	2443 (1,7)	2416 (1,7)	2380 (1,7)
	250	4395 (1,9)	4395 (1,9)	4355 (1,9)	4314 (1,9)
	500	7901 (1,11)	7901 (1,11)	7845 (1,11)	7792 (1,11)
	1000	15320 (1,13)	15324 (1,13)	15248 (1,13)	15171 (1,13)
2	1000	15320 (2,13)	15324 (2,13)	15196 (1,10)	15056 (1,10)
3	1000	15190 (2,11)	15186 (2,11)	15068 (2,11)	14956 (2,11)

[b] Numbers in parentheses, (m,n), indicate the number of axial half-waves and circumferential waves, respectively
* Nonlinear rotations about the normal are neglected.

[#] $\frac{A_s}{d_s h} = 0.5$, $\frac{I_s^c}{d_s h^3} = 5$, and $J_s = 0$

Table 34. Nondimensional buckling coefficient $\frac{2N_x^{cr} R^2}{D}$ for isotropic cylinders with simply supported edges, external stringers,[#] and subjected to axial compression ($\nu = 0.3$)

L/R	R/h	External stringers, $e_s/h = +5$			
		Ref. 66 Donnell	Present Study		
			Donnell	Sanders*	Sanders
0.25	50	46360 (1,3)[b]	46362 (1,3)	46364 (1,3)	43638 (1,8)
0.35	50	23650 (1,0)	23649 (1,0)	23649 (1,0)	23582 (1,3)
0.5	50	12110 (1,0)	12097 (1,0)	12097 (1,0)	12097 (1,0)
	100	14830 (1,5)	14833 (1,5)	14831 (1,5)	14829 (1,5)
	250	20050 (1,12)	20050 (1,12)	20032 (1,12)	20010 (1,12)
	500	26440 (1,16)	26435 (1,16)	26405 (1,16)	26365 (1,16)
	1000	37640 (1,19)	37640 (1,19)	37597 (1,19)	37538 (1,19)
	2000	58020 (1,24)	58019 (1,24)	57953 (1,24)	57881 (1,24)
1	50	4659 (1,5)	4659 (1,5)	4646 (1,5)	4629 (1,5)
	100	6016 (1,7)	6016 (1,7)	5992 (1,7)	5955 (1,7)
	250	9411 (1,10)	9411 (1,10)	9365 (1,10)	9310 (1,10)
	500	14500 (1,12)	14505 (1,12)	14440 (1,12)	14368 (1,12)
	1000	24030 (1,14)	24031 (1,14)	23945 (1,14)	23847 (1,14)
	2000	42280 (1,17)	42284 (1,17)	42160 (1,17)	42033 (1,17)
	5000	94870 (1,21)	94866 (1,21)	94680 (1,21)	94483 (1,21)
	50000	847600 (1,38)	847582 (1,38)	846989 (1,38)	846408 (1,38)
1.5	50	2805 (1,5)	2805 (1,5)	2778 (1,5)	2738 (1,5)
	100	3961 (1,6)	3961 (1,6)	3922 (1,6)	3864 (1,6)
	250	6985 (1,8)	6985 (1,8)	6920 (1,8)	6842 (1,8)
2	100	3193 (1,6)	3193 (1,6)	3129 (1,6)	3069 (1,6)
	250	6008 (1,7)	6008 (1,7)	5922 (1,7)	5826 (1,7)
	500	10700 (1,8)	10704 (1,8)	10594 (1,8)	10454 (1,8)
	2000	36590 (1,12)	36592 (1,12)	36352 (1,12)	36116 (1,12)

[b] Numbers in parentheses, (m,n), indicate the number of axial half-waves and circumferential waves, respectively
* Nonlinear rotations about the normal are neglected.

[#] $\frac{A_s}{d_s h} = 0.5$, $\frac{I_s^c}{d_s h^3} = 5$, and $J_s = 0$

Table 34. Concluded

L/R	R/h	External stringers, $e_s/h = +5$			
		Ref. 66 Donnell	Present Study		
			Donnell	Sanders*	Sanders
4	50	1326 (1,3)[b]	1326 (1,3)	1265 (1,3)	1166 (1,3)
	100	2191 (1,4)	2191 (1,4)	2083 (1,4)	1977 (1,4)
	250	4843 (1,5)	4843 (1,5)	4677 (1,5)	4512 (1,5)
	500	9148 (1,6)	9148 (1,6)	8910 (1,6)	8683 (1,6)
	1000	17610 (1,7)	17609 (1,7)	17286 (1,7)	16955 (1,7)
	2000	34930 (1,8)	34929 (1,8)	34509 (1,8)	33995 (1,8)
6	250	4550 (1,4)	4550 (1,4)	4316 (1,4)	4077 (1,4)
	1000	17270 (1,6)	17272 (1,6)	16746 (1,6)	16305 (1,6)
10	500	8713 (1,4)	8713 (1,4)	8077 (1,4)	7611 (1,4)
20	500	8713 (2,4)	8713 (2,4)	7846 (1,3)	7068 (1,3)

[b] Numbers in parentheses, (m,n), indicate the number of axial half-waves and circumferential waves, respectively
* Nonlinear rotations about the normal are neglected.

$\frac{A_s}{d_s h} = 0.5,\ \frac{I_s^c}{d_s h^3} = 5,$ and $J_s = 0$

Table 35. Nondimensional buckling coefficient $\frac{2N_x^{cr} R^2}{D}$ for isotropic cylinders with simply supported edges, internal stringers,[#] and subjected to axial compression ($\nu = 0.3$)

L/R	R/h	Internal stringers, $e_s/h = -5$			
		Ref. 66 Donnell	Present Study		
			Donnell	Sanders*	Sanders
0.25	50	46640 (1,8)[b]	46643 (1,8)	46624 (1,8)	40688 (1,10)
0.35	50	23890 (1,7)	23886 (1,7)	23870 (1,7)	22216 (1,7)
0.5	50	11800 (1,6)	11800 (1,6)	11786 (1,6)	11210 (1,6)
	100	12050 (1,8)	12054 (1,8)	12038 (1,8)	11791 (1,8)
	250	12980 (1,11)	12984 (1,11)	12964 (1,11)	12858 (1,11)
	500	15030 (1,14)	15033 (1,14)	15006 (1,14)	14937 (1,14)
	1000	20000 (1,17)	19996 (1,17)	19959 (1,17)	19900 (1,17)
	2000	31590 (1,21)	31589 (1,21)	31537 (1,21)	31475 (1,21)
1	50	3156 (1,5)	3156 (1,5)	3139 (1,5)	3013 (1,5)
	100	3551 (1,6)	3551 (1,6)	3529 (1,6)	3446 (1,6)
	250	5045 (1,9)	5045 (1,9)	5005 (1,9)	4950 (1,9)
	500	7933 (1,11)	7933 (1,11)	7877 (1,11)	7819 (1,11)
	1000	14300 (1,13)	14302 (1,13)	14226 (1,13)	14152 (1,13)
	2000	28080 (1,16)	28080 (1,16)	27968 (1,16)	27869 (1,16)
	5000	70650 (2,28)	70647 (2,28)	70560 (2,28)	70474 (2,28)
	50000	701900 (5,80)	701987 (5,80)	701875 (5,80)	701769 (5,80)
1.5	50	1648 (1,4)	1648 (1,4)	1627 (1,4)	1547 (1,4)
	100	2160 (1,6)	2160 (1,6)	2120 (1,6)	2067 (1,6)
	250	3908 (1,7)	3908 (1,7)	3857 (1,7)	3790 (1,7)
2	100	1673 (1,5)	1673 (1,5)	1625 (1,5)	1570 (1,5)
	250	3693 (1,7)	3693 (1,7)	3607 (1,7)	3541 (1,7)
	500	7020 (1,8)	7020 (1,8)	6909 (1,8)	6812 (1,8)
	2000	28080 (2,16)	28080 (2,16)	27968 (2,16)	27869 (2,16)

[b] Numbers in parentheses, (m,n), indicate the number of axial half-waves and circumferential waves, respectively
* Nonlinear rotations about the normal are neglected.

[#] $\frac{A_s}{d_s h} = 0.5$, $\frac{I_s^c}{d_s h^3} = 5$, and $J_s = 0$

Table 35. Concluded

L/R	R/h	Internal stringers, $e_s/h = -5$			
		Ref. 66 Donnell	Present Study		
			Donnell	Sanders*	Sanders
4	50	731.7 (1,3)[b]	731.7 (1,3)	669.5 (1,3)	609.5 (1,3)
	100	1454 (1,4)	1454 (1,4)	1346 (1,4)	1272 (1,4)
	250	3608 (1,5)	3608 (1,5)	3441 (1,5)	3316 (1,5)
	500	7020 (2,8)	7020 (2,8)	6909 (2,8)	6812 (2,8)
	1000	14200 (3,12)	14192 (3,12)	14081 (3,12)	13992 (3,12)
	2000	28080 (4,16)	28080 (4,16)	27968 (4,16)	27869 (4,16)
6	250	3670 (1,4)	3670 (1,4)	3436 (1,4)	3242 (1,4)
	1000	14050 (4,11)	14054 (4,11)	13936 (4,11)	13831 (4,11)
10	500	7020 (5,8)	7020 (5,8)	6909 (5,8)	6812 (5,8)
20	500	7020 (10,8)	7020 (10,8)	6909 (10,8)	6800 (1,3)

[b] Numbers in parentheses, (m,n), indicate the number of axial half-waves and circumferential waves, respectively
* Nonlinear rotations about the normal are neglected.

$\frac{A_s}{d_s h} = 0.5,\ \frac{I_s^c}{d_s h^3} = 5,$ and $J_s = 0$

Table 36. Nondimensional buckling coefficient $\frac{2N_x^{cr}R^2}{D}$ for isotropic stringer-stiffened[#] cylinders with simply supported edges and subjected to axial compression ($\nu = 0.3$)

		Ref. 66 Donnell	Present Study		
L/R	R/h		Donnell	Sanders*	Sanders
		External stringers, $e_s/h = +10$			
0.5	250	49160 (1,10)[b]	49160 (1,10)	49149 (1,10)	49145 (1,10)
	500	59540 (1,16)	59545 (1,16)	59516 (1,16)	59472 (1,16)
1	50	11420 (1,3)	11418 (1,3)	11414 (1,3)	11413 (1,3)
	100	13980 (1,7)	13984 (1,7)	13962 (1,7)	13930 (1,7)
	250	18640 (1,10)	18645 (1,10)	18599 (1,10)	18519 (1,10)
	500	24960 (1,12)	24962 (1,12)	24898 (1,12)	24790 (1,12)
	1000	36280 (1,14)	36283 (1,14)	36196 (1,15)	36058 (1,14)
2	100	5659 (1,6)	5659 (1,6)	5595 (1,6)	5504 (1,6)
	150	6886 (1,6)	6886 (1,6)	6822 (1,6)	6698 (1,6)
	1000	23800 (1,10)	23805 (1,10)	23636 (1,10)	23426 (1,10)
3	100	3824 (1,5)	3824 (1,5)	3727 (1,5)	3617 (1,5)
	150	4862 (1,5)	4862 (1,5)	4765 (1,5)	4618 (1,5)
	1000	20840 (1,8)	20841 (1,8)	20601 (1,8)	20305 (1,8)
		Internal stringers, $e_s/h = -10$			
0.5	250	33810 (1,9)	33812 (1,9)	33795 (1,9)	33266 (1,9)
	500	34870 (1,12)	34866 (1,12)	34844 (1,12)	34580 (1,12)
1	50	8413 (1,4)	8413 (1,4)	8398 (1,4)	7722 (1,4)
	100	8653 (1,5)	8653 (1,5)	8635 (1,5)	8292 (1,5)
	250	9479 (1,8)	9479 (1,8)	9446 (1,8)	9298 (1,8)
	500	11460 (1,10)	11461 (1,10)	11413 (1,10)	11306 (1,10)
	1000	16610 (1,12)	16611 (1,12)	16545 (1,12)	16440 (1,12)
2	100	2713 (1,5)	2713 (1,5)	2665 (1,5)	2562 (1,5)
	150	3139 (1,5)	3139 (1,5)	3091 (1,5)	2982 (1,5)
	1000	13710 (1,9)	13712 (1,9)	13573 (1,9)	13418 (1,9)
3	100	1711 (1,4)	1711 (1,4)	1647 (1,4)	1556 (1,4)
	150	2390 (1,5)	2390 (1,5)	2293 (1,5)	2208 (1,5)
	1000	13800 (1,8)	13796 (1,8)	13557 (1,8)	13356 (1,8)

[b] Numbers in parentheses, (m,n), indicate the number of axial half-waves and circumferential waves, respectively
* Nonlinear rotations about the normal are neglected.

[#] $\frac{A_s}{d_s h} = 0.5,\ \frac{I_s^c}{d_s h^3} = 5,\ \text{and}\ J_s = 0$

Table 37. Nondimensional buckling coefficient $\frac{2N_x^{cr} R^2}{D}$ for isotropic stringer-stiffened[#] cylinders with simply supported edges and subjected to axial compression ($\nu = 0.3$)

L/R	R/h	External stringers, $e_s/h = +5$			
		Ref. 66 Donnell	Present Study		
			Donnell	Sanders*	Sanders
0.5	250	28670 (1,12)	28672 (1,12)	28654 (1,12)	28623 (1,12)
	500	35060 (1,16)	35058 (1,16)	35027 (1,16)	34974 (1,16)
1	50	6814 (1,5)	6814 (1,5)	6802 (1,5)	6776 (1,5)
	100	8172 (1,7)	8172 (1,7)	8148 (1,7)	8097 (1,7)
	250	11570 (1,10)	11567 (1,10)	11520 (1,10)	11453 (1,10)
	500	16660 (1,12)	16660 (1,12)	16595 (1,12)	16513 (1,12)
	1000	26190 (1,14)	26187 (1,14)	26100 (1,14)	25993 (1,14)
2	100	3732 (1,6)	3732 (1,6)	3668 (1,6)	3598 (1,6)
	150	4661 (1,6)	4661 (1,6)	4597 (1,6)	4505 (1,6)
	1000	19910 (1,10)	19912 (1,10)	19743 (1,10)	19565 (1,10)
3	100	2798 (1,5)	2798 (1,5)	2702 (1,5)	2616 (1,5)
	150	3630 (1,5)	3630 (1,5)	3534 (1,5)	3419 (1,5)
	1000	18440 (1,8)	18440 (1,8)	18201 (1,8)	17937 (1,8)
L/R	R/h	Internal stringers, $e_s/h = -5$			
		Ref. 66 Donnell	Present Study		
			Donnell	Sanders*	Sanders
0.5	250	21610 (1,11)	21606 (1,11)	21586 (1,11)	21410 (1,11)
	500	23660 (1,14)	23655 (1,14)	23628 (1,14)	23519 (1,14)
1	50	5312 (1,5)	5312 (1,5)	5294 (1,5)	5077 (1,5)
	100	5706 (1,6)	5706 (1,6)	5684 (1,6)	5551 (1,6)
	250	7201 (1,9)	7201 (1,9)	7161 (1,9)	7082 (1,9)
	500	10090 (1,11)	10088 (1,11)	10032 (1,11)	9959 (1,11)
	1000	16460 (1,13)	16458 (1,13)	16382 (1,13)	16296 (1,13)
2	100	2211 (1,5)	2211 (1,5)	2164 (1,5)	2091 (1,5)
	150	2878 (1,6)	2878 (1,6)	2813 (1,6)	2744 (1,6)
	1000	14970 (1,10)	14970 (1,10)	14801 (1,10)	14663 (1,10)
3	100	1713 (1,4)	1713 (1,4)	1649 (1,4)	1564 (1,4)
	150	2395 (1,5)	2395 (1,5)	2298 (1,5)	2217 (1,5)
	1000	14920 (1,8)	14918 (1,8)	14678 (1,8)	14463 (1,8)

[b] Numbers in parentheses, (m,n), indicate the number of axial half-waves and circumferential waves, respectively
* Nonlinear rotations about the normal are neglected

[#] $\frac{A_s}{d_s h} = 0.5$, $\frac{I_s^c}{d_s h^3} = 15$, and $J_s = 0$

Table 38. Nondimensional buckling coefficient $\frac{2N_x^{cr} R^2}{D}$ for isotropic stringer-stiffened[#] cylinders with simply supported edges, and subjected to axial compression ($\nu = 0.3$)

L/R	R/h	External stringers, $e_s/h = +5$			
		Ref. 66 Donnell	Present Study		
			Donnell	Sanders*	Sanders
0.5	250	33470 (1,9)	33474 (1,9)	33466 (1,9)	33465 (1,9)
	500	47010 (1,15)	47013 (1,15)	46988 (1,15)	46970 (1,15)
1	50	7376 (1,3)	7376 (1,3)	7372 (1,3)	7372 (1,3)
	100	10580 (1,7)	10584 (1,7)	10563 (1,7)	10555 (1,7)
	250	16590 (1,10)	16586 (1,10)	16542 (1,10)	16493 (1,10)
	500	24690 (1,13)	24691 (1,13)	24617 (1,13)	24542 (1,13)
	1000	38880 (1,15)	38879 (1,15)	38781 (1,15)	38667 (1,15)
2	100	5387 (1,6)	5387 (1,6)	5324 (1,6)	5258 (1,6)
	150	6966 (1,7)	6966 (1,7)	6882 (1,7)	6803 (1,7)
	1000	28630 (1,11)	28630 (1,11)	28427 (1,11)	28228 (1,11)
3	100	4017 (1,5)	4017 (1,5)	3922 (1,5)	3821 (1,5)
	150	5526 (1,5)	5526 (1,5)	5430 (1,5)	5282 (1,5)
	1000	25800 (1,9)	25802 (1,9)	25501 (1,9)	25218 (1,9)
L/R	R/h	Internal stringers, $e_s/h = -5$			
		Ref. 66 Donnell	Present Study		
			Donnell	Sanders*	Sanders
0.5	250	18110 (1,9)	18113 (1,9)	18097 (1,9)	17845 (1,9)
	500	19350 (1,12)	19348 (1,12)	19326 (1,12)	19193 (1,12)
1	50	4492 (1,4)	4492 (1,4)	4477 (1,4)	4169 (1,4)
	100	4738 (1,6)	4738 (1,6)	4715 (1,6)	4564 (1,6)
	250	5716 (1,8)	5716 (1,8)	5683 (1,8)	5601 (1,8)
	500	8222 (1,10)	8222 (1,10)	8174 (1,10)	8103 (1,10)
	1000	14310 (1,13)	14308 (1,13)	14232 (1,13)	14158 (1,13)
2	100	1789 (1,5)	1789 (1,5)	1741 (1,5)	1678 (1,5)
	150	2421 (1,6)	2421 (1,6)	2356 (1,6)	2295 (1,6)
	1000	14310 (2,13)	14308 (2,13)	14232 (2,13)	14158 (2,13)
3	100	1476 (1,4)	1476 (1,4)	1412 (1,4)	1340 (1,4)
	150	2159 (1,5)	2159 (1,5)	2062 (1,5)	1990 (1,5)
	1000	14310 (3,13)	14308 (3,13)	14232 (3,13)	14158 (3,13)

[b] Numbers in parentheses, (m,n), indicate the number of axial half-waves and circumferential waves, respectively
* Nonlinear rotations about the normal are neglected.

[#] $\frac{A_s}{d_s h} = 1.5$, $\frac{I_s^c}{d_s h^3} = 5$, and $J_s = 0$

Table 39. Nondimensional buckling coefficient $\frac{2N_x^{cr} R^2}{D}$ for isotropic stringer-stiffened[#] cylinders with simply supported edges, and subjected to axial compression ($\nu = 0.3$, $L/R = 1$)

R/h	e_s/h	Ref. 62 Donnell	Present Study		
			Donnell	Sanders*	Sanders
250	7	23380 (10)[a]	24376 (1,10)[b]	24332 (1,10)	24285 (1,10)
	-7	8432 (7)	8432 (1,7)	8405 (1,7)	8243 (1,7)
	10	39700 (10)	39707 (1,10)	39664 (1,10)	39633 (1,10)
	–10	14780 (7)	14781 (1,7)	14752 (1,7)	14394 (1,7)
500	7	33900 (13)	33897 (1,13)	33823 (1,13)	33737 (1,13)
	-7	10150 (10)	10148 (1,10)	10100 (1,10)	10002 (1,10)
	10	51720(13)	51722 (1,13)	51649 (1,13)	51551 (1,13)
	–10	15730 (9)	15731 (1,9)	15691 (1,9)	15491 (1,9)
1000	7	50060 (15)	50062 (1,15)	49964 (1,15)	49829 (1,15)
	-7	15180 (13)	15176 (1,13)	15100 (1,13)	15016 (1,13)
	10	70690 (16)	70695 (1,16)	70585 (1,16)	70433 (1,16)
	–10	19240 (12)	19243 (1,12)	19177 (1,12)	19046 (1,12)

[a] Numbers in parentheses indicate the number of circumferential waves, n
[b] Numbers in parentheses, (m,n), indicate the number of axial half-waves and circumferential waves, respectively
* Nonlinear rotations about the normal are neglected.

[#] $\frac{A_s}{d_s h} = 1.5$, $\frac{I_s^c}{d_s h^3} = 5$, and $J_s = 0$

Table 40. Nondimensional buckling coefficient $\frac{2N_x^{cr} R^2}{D}$ for isotropic stringer-stiffened[#] cylinders with simply supported edges and subjected to axial compression ($\nu = 0.3$, $L/R = 2$)

$A_s/(d_s h)$	e_s/h	Ref. 62 Donnell	Present Study		
			Donnell	Sanders*	Sanders
1.5	10	25890 (9)[a]	25888 (1,9)[b]	25751 (1,9)	25529 (1,9)
	−10	7471 (8)	7471 (1,8)	7361 (1,8)	7250 (1,8)
3	10	39650 (10)	39654 (1,10)	39487 (1,10)	39269 (1,10)
	−10	7597 (7)	7597 (1,7)	7510 (1,7)	7370 (1,7)
5	10	81770 (12)	54735 (1,10)	54568 (1,10)	54356 (1,10)
	−10	13970 (10)	7636 (1,7)	7549 (1,7)	7407 (1,7)
5 (R/h=1000)	10	---	81773 (1,12)	81534 (1,12)	81202 (1,12)
	−10	---	13974 (1,10)	13805 (1,10)	13673 (1,10)

[a] Numbers in parentheses indicate the number of circumferential waves, n
[b] Numbers in parentheses, (m,n), indicate the number of axial half-waves and circumferential waves, respectively
* Nonlinear rotations about the normal are neglected.

[#] $\frac{I_s^c}{d_s h^3} = 5$, $J_s = 0$, and $\frac{R}{h} = 500$ unless noted otherwise

Table 41. Nondimensional buckling coefficient $\frac{2N_x^{cr} R^2}{D}$ for isotropic stringer-stiffened[#] cylinders with simply supported edges and subjected to axial compression ($\nu = 0.3$)

L/R	R/h	e_s/h	Ref. 66 Donnell	Present Study		
				Donnell	Sanders*	Sanders
0.5	100	0	5714 (9)[a]	5714 (1,9)[b]	5701 (1,9)	5674 (1,9)
		1	6344 (9)	6344 (1,9)	6332 (1,9)	6314 (1,9)
		–1	5729 (9)	5729 (1,9)	5715 (1,9)	5676(1,9)
		3	9477 (8)	9477 (1,8)	9469 (1,8)	9461 (1,8)
		–3	7641 (8)	7642 (1,8)	7628 (1,8)	7529 (1,8)
		7	21460 (0)	21459(1,0)	21459 (1,0)	21459 (1,0)
		–7	18810 (7)	18811 (1,7)	18797 (1,7)	18226 (1,7)
		10	35220 (0)	35219(1,0)	35219 (1,0)	35219 (1,0)
		-10	33400 (6)	33399 (1,6)	33386 (1,6)	31808 (1,6)
2	500	0	8219 (8)	8219 (1,8)	8108 (1,8)	7997 (1,8)
		1	8613 (8)	8613 (1,8)	8503 (1,8)	8387 (1,8)
		–1	7876 (8)	7876 (1,8)	7766 (1,8)	7659 (1,8)
		3	9556 (8)	9556 (1,8)	9445 (1,8)	9319 (1,8)
		–3	7345 (8)	7345 (1,8)	7235 (1,8)	7134 (1,8)
		10	14300 (9)	14300 (1,9)	14162 (1,9)	14014 (1,9)
		-10	7107 (8)	7108 (1,8)	6997 (1,8)	6895 (1,8)
4	2000	0	32410 (12)	32411 (2,12)	32170 (2,12)	31827 (1,8)
		1	33140 (12)	33141 (2,12)	32722 (1,8)	32234 (1,8)
		–1	31480 (14)	31479 (3,14)	31330 (3,14)	31184 (3,14)
		3	34010 (8)	34009 (1,8)	33589 (1,8)	33089 (1,8)
		–3	29350 (18)	29350 (5,18)	29259 (5,18)	29166 (4,16)
		7	35900 (8)	35902 (1,8)	35483 (1,8)	34955 (1,8)
		–7	27570 (14)	27566 (3,14)	27417 (3,14)	27287 (3,14)
		10	37460 (8)	37462 (1,8)	37042 (1,8)	36492 (1,8)
		-10	27190 (14)	27191 (3,14)	27042 (3,14)	26912 (3,14)

[a] Numbers in parentheses indicate the number of circumferential waves, n
[b] Numbers in parentheses, (m,n), indicate the number of axial half-waves and circumferential waves, respectively
* Nonlinear rotations about the normal are neglected.

[#] $\frac{A_s}{d_s h} = 0.5$, $\frac{I_s^c}{d_s h^3} = 5$, and $J_s = 0$

Table 42. Nondimensional buckling coefficient $\frac{2N_x^{cr} R^2}{D}$ for isotropic stringer-stiffened[#] cylinders with simply supported edges, and subjected to axial compression ($\nu = 0.3$)

L/R	R/h	$A_s/(d_s h)$	External stringers, $e_s/h = +5$			
			Ref. 66 Donnell	Present Study		
				Donnell	Sanders*	Sanders
0.5	100	0.1	8064 (9)[a]	8064 (1,9)[b]	8052 (1,9)	8027 (1,9)
		0.3	12020 (8)	12023 (1,8)	12015 (1,8)	12007 (1,8)
		0.5	14830 (5)	14833 (1,5)	14831 (1,5)	14829 (1,5)
		0.7	16530 (2)	16533 (1,2)	16533 (1,2)	16531 (1,2)
		1.0	18040 (0)	18038 (1,0)	18038 (1,0)	18038 (1,0)
		1.5	19750 (0)	19754 (1,0)	19754 (1,0)	19754 (1,0)
2	500	0.1	7689 (8)	7689 (1,8)	7579 (1,8)	7472 (1,8)
		0.3	9224 (8)	9224 (1,8)	9114 (1,8)	8990 (1,8)
		0.5	10700 (8)	10704 (1,8)	10594 (1,8)	10454 (1,8)
		1.0	13650 (9)	13652 (1,9)	13514 (1,9)	13378 (1,9)
		1.5	16260 (9)	16258 (1,9)	16121 (1,9)	15968 (1,9)
4	2000	0.1	28210 (8)	28211 (1,8)	27792 (1,8)	27373 (1,8)
		0.3	31590 (8)	31587 (1,8)	31167 (1,8)	30700 (1,8)
		0.5	34930 (8)	34929 (1,8)	34509 (1,8)	33995 (1,8)
		0.7	37720 (9)	37722 (1,9)	37192 (1,9)	36752 (1,9)
		1.0	41070 (9)	41071 (1,9)	40541 (1,9)	40065 (1,9)
		1.5	46570 (9)	46568 (1,9)	46038 (1,9)	45503 (1,9)

[a] Numbers in parentheses indicate the number of circumferential waves, n
[b] Numbers in parentheses, (m,n), indicate the number of axial half-waves and circumferential waves, respectively
* Nonlinear rotations about the normal are neglected.

[#] $\frac{I_s^c}{d_s h^3} = 5$ and $J_s = 0$

Table 43. Nondimensional buckling coefficient $\frac{2N_x^{cr} R^2}{D}$ for isotropic stringer-stiffened[#] cylinders with simply supported edges and subjected to axial compression ($\nu = 0.3$)

L/R	R/h	$A_s/(d_s h)$	Internal stringers, $e_s/h = -5$			
			Ref. 66 Donnell	Present Study		
				Donnell	Sanders*	Sanders
0.5	100	0.1	7293 (8)[a]	7293 (1,8)[b]	7279 (1,9)	7215 (1,8)
		0.3	9963 (8)	9963 (1,8)	9949 (1,8)	9801 (1,8)
		0.5	12050 (8)	12054 (1,8)	12038 (1,8)	11791 (1,8)
		0.7	13650 (7)	13649 (1,7)	13635 (1,7)	13282 (1,7)
		1.0	15490 (7)	15491 (1,7)	15477 (1,7)	14977 (1,7)
		1.5	17660 (6)	17655 (1,6)	17641 (1,7)	16926 (1,7)
2	500	0.1	6925 (8)	6925 (1,8)	6814 (1,8)	6717 (1,8)
		0.3	6973 (8)	6973 (1,8)	6863 (1,8)	6765 (1,8)
		0.5	7020 (8)	7020 (1,8)	6909 (1,8)	6812 (1,8)
		1.0	7130 (8)	7130 (1,8)	7019 (1,8)	6921 (1,8)
		1.5	7230 (8)	7230 (1,8)	7120 (1,8)	7022 (1,8)
4	2000	0.1	27390 (11)	27389 (2,11)	26970 (1,8)	26564 (1,8)
		0.3	27900 (16)	27893 (4,16)	27774 (3,14)	27642 (3,14)
		0.5	28080 (16)	28080 (4,16)	27968 (4,16)	27869 (4,16)
		0.7	28260 (16)	28260 (4,16)	28148 (4,16)	28049 (4,16)
		1.0	28410 (18)	28409 (5,18)	28317 (5,18)	28238 (5,18)
		1.5	28450 (18)	28447 (5,18)	28355 (5,18)	28277 (5,18)

[a] Numbers in parentheses indicate the number of circumferential waves, n
[b] Numbers in parentheses, (m,n), indicate the number of axial half-waves and circumferential waves, respectively
* Nonlinear rotations about the normal are neglected.

[#] $\frac{I_s^c}{d_s h^3} = 5$ and $J_s = 0$

Table 44. Nondimensional buckling coefficient $\frac{2N_x^{cr} R^2}{D}$ for isotropic stringer-stiffened[#] cylinders with simply supported edges and subjected to axial compression ($\nu = 0.3$)

L/R	R/h	$I_s/(d_s h^3)$	External stringers, $e_s/h = +5$			
			Ref. 66 Donnell	Present Study		
				Donnell	Sanders*	Sanders
0.5	100	1	11380 (5)[a]	11384 (1,5)[b]	11382 (1,5)	11381 (1,5)
		3	13110 (5)	13109 (1,5)	13106 (1,5)	13105 (1,5)
		10	19140 (5)	19144 (1,5)	19142 (1,5)	19139 (1,5)
		15	23460 (5)	23455 (1,5)	23453 (1,5)	23452 (1,5)
		20	27770 (5)	27766 (1,5)	27764 (1,5)	27763 (1,5)
2	500	1	10490 (8)	10489 (1,8)	10379 (1,8)	10241 (1,8)
		3	10600 (8)	10597 (1,8)	10486 (1,8)	10347 (1,8)
		10	10970 (8)	10974 (1,8)	10864 (1,8)	10720 (1,8)
		15	11240 (8)	11243 (1,8)	11133 (1,8)	10985 (1,8)
4	2000	1	34880 (8)	34875 (1,8)	34455 (1,8)	33942 (1,8)
		3	34900 (8)	34902 (1,8)	34482 (1,8)	33969 (1,8)
		10	35000 (8)	34996 (1,8)	34577 (1,8)	34062 (1,8)
		15	35060 (8)	35064 (1,8)	34644 (1,8)	34128 (1,8)
		20	35130 (8)	35131 (1,8)	34711 (1,8)	34194 (1,8)

[a] Numbers in parentheses indicate the number of circumferential waves, n
[b] Numbers in parentheses, (m,n), indicate the number of axial half-waves and circumferential waves, respectively
* Nonlinear rotations about the normal are neglected.

[#] $\frac{A_s}{d_s h} = 0.5$ and $J_s = 0$

Table 45. Nondimensional buckling coefficient $\frac{2N_x^{cr} R^2}{D}$ for isotropic stringer-stiffened[#] cylinders with simply supported edges and subjected to axial compression ($\nu = 0.3$)

L/R	R/h	$I_s/(d_s h^3)$	Internal stringers, $e_s/h = -5$			
			Ref. 66 Donnell	Present Study		
				Donnell	Sanders*	Sanders
0.5	100	1	8605 (8)[a]	8605 (1,8)[b]	8589 (1,8)	8415 (1,8)
		3	10330 (8)	10329 (1,8)	10314 (1,8)	10103 (1,8)
		10	16360 (8)	16365 (1,8)	16349 (1,8)	16010 (1,8)
		15	20680 (8)	20676 (1,8)	20660 (1,8)	20227 (1,8)
		20	24990 (8)	24987 (1,8)	24971 (1,8)	24443 (1,7)
2	500	1	6804 (8)	6804 (1,8)	6694 (1,8)	6599 (1,8)
		3	6912 (8)	6912 (1,8)	6802 (1,8)	6706 (1,8)
		10	7289 (8)	7289 (1,8)	7179 (1,8)	7078 (1,8)
		15	7559 (8)	7559 (1,8)	7448 (1,8)	7343 (1,8)
4	2000	1	26930 (19)	26928 (6,19)	26856 (6,19)	26790 (6,19)
		3	27650 (16)	27648 (4,16)	27537 (4,16)	27439 (4,16)
		10	29010 (14)	29008 (3,14)	28859 (3,14)	28723 (3,14)
		15	29610 (14)	29614 (3,14)	29466 (3,14)	29326 (3,14)
		20	30220 (14)	30220 (3,14)	30072 (3,14)	29917 (2,12)

[a] Number in parentheses indicate the number of circumferential waves, n
[b] Numbers in parentheses, (m,n), indicate the number of axial half-waves and circumferential waves, respectively
* Nonlinear rotations about the normal are neglected.

[#] $\frac{A_s}{d_s h} = 0.5$ and $J_s = 0$

Table 46. Nondimensional buckling coefficient $\frac{2N_x^{cr} R^2}{D}$ for isotropic stringer-stiffened[#] cylinders with simply supported edges and subjected to axial compression ($\nu = 0.3$)

L/R	R/h	Torsional stiffness, $G_sJ_s/(d_sD)$	External stringers, $e_s/h = +5$			
			Ref. 66 Donnell	Present Study		
				Donnell	Sanders*	Sanders
0.5	250	0	20050	20050 (1,12)[b]	20032 (1,12)	20010 (1,12)
		20	24370	24374 (1,9)	24316 (1,9)	24279 (1,9)
	2000	0	58020	58019(1,24)	57953 (1,24)	57881 (1,24)
		20	78270	78269 (1,22)	78140 (1,22)	78028 (1,22)
1	50	0	4659	4659 (1,5)	4646 (1,5)	4629 (1,5)
		20	5460	5460 (1,4)	5411 (1,4)	5383 (1,4)
	250	0	9411	9411 (1,10)	9365 (1,10)	9310 (1,10)
		20	12790	12787 (1,9)	12680 (1,9)	12593 (1,9)
	2000	0	42280	42284 (1,17)	42160 (1,17)	42033 (1,17)
		20	53060	53058 (1,16)	52870 (1,16)	52693 (1,16)
	5000	0	94870	94866 (1,21)	94680 (1,21)	94483 (1,21)
		20	112500	112506 (1,21)	112241 (1,21)	112008 (1,21)
4	250	0	4843	4843 (1,5)	4677 (1,5)	4512 (1,5)
		20	5843	5843 (1,5)	5600 (1,5)	5403 (1,5)

[b] Numbers in parentheses, (m,n), indicate the number of axial half-waves and circumferential waves, respectively
* Nonlinear rotations about the normal are neglected.

[#] $\frac{A_s}{d_s h} = 0.5$ and $\frac{I_s^c}{d_s h^3} = 5$

Table 47. Nondimensional buckling coefficient $\frac{2N_x^{cr}R^2}{D}$ for isotropic stringer-stiffened[#] cylinders with simply supported edges and subjected to axial compression ($\nu = 0.3$)

L/R	R/h	Torsional stiffness, $G_sJ_s/(d_sD)$	Internal stringers, $e_s/h = -5$			
			Ref. 66 Donnell	Present Study		
				Donnell	Sanders*	Sanders
0.5	250	0	12980	12984 (1,11)[b]	12964 (1,11)	12858 (1,11)
		5	14020	14025 (1,10)	13987 (1,10)	13865 (1,10)
		10	15020	15025 (1,10)	14968 (1,10)	14837 (1,10)
		20	16680	16683 (1,9)	16592 (1,9)	16437 (1,9)
		40	19500	19498 (1,8)	19342 (1,8)	19151 (1,8)
	2000	0	31590	31589 (1,21)	31537 (1,21)	31475 (1,21)
		5	36000	35999 (1,21)	35928 (1,21)	35857 (1,21)
		10	40330	40326 (1,20)	40239 (1,20)	40154 (1,20)
		20	48330	48326 (1,20)	48200 (1,20)	48099 (1,20)
		40	62980	62981 (1,19)	62783 (1,19)	62640 (1,19)
1	50	0	3156	3156 (1,5)	3139 (1,5)	3013 (1,5)
		5	3406	3406 (1,5)	3368 (1,5)	3232 (1,5)
		10	3611	3611 (1,4)	3561 (1,4)	3401 (1,4)
		20	3931	3931 (1,4)	3844 (1,4)	3670 (1,4)
		40	4571	4571 (1,4)	4410 (1,4)	4207 (1,4)
	250	0	5045	5045 (1,9)	5005 (1,9)	4950 (1,9)
		5	5744	5744 (1,8)	5692 (1,8)	5619 (1,8)
		10	6384	6384 (1,8)	6313 (1,8)	6232 (1,8)
		20	7664	7664 (1,8)	7554 (1,8)	7458 (1,8)
		40	9842	9842 (1,7)	9666 (1,7)	9521 (1,7)
	2000	0	28080	28080 (1,16)	27968 (1,16)	27869 (1,16)
		5	30640	30640 (1,16)	30509 (1,16)	30400 (1,16)
		10	33200	33200 (1,16)	33049 (1,16)	32931 (1,16)
		20	37840	37838 (1,15)	37662 (1,15)	37511 (1,15)
		40	46840	46838 (1,15)	46583 (1,15)	46398 (1,15)

[b] Numbers in parentheses, (m,n), indicate the number of axial half-waves and circumferential waves, respectively
* Nonlinear rotations about the normal are neglected.

[#] $\frac{A_s}{d_sh} = 0.5$ and $\frac{I_s^c}{d_sh^3} = 5$

Table 47. Concluded

L/R	R/h	Torsional stiffness, $G_sJ_s/(d_sD)$	Internal stringers, $e_s/h = -5$			
			Ref. 66 Donnell	Present Study		
				Donnell	Sanders*	Sanders
1	5000	0	70650	70647 (2,28)	70560 (2,28)	70474 (2,28)
		5	76060	76057 (1,20)	75867 (1,20)	75684 (1,20)
		10	80060	80057 (1,20)	79848 (1,20)	79654 (1,20)
		20	88060	88057 (1,20)	87808 (1,20)	87603 (1,20)
		40	103700	103705 (1,19)	103394 (1,19)	103129 (1,19)
4	250	0	3608	3608 (1,5)	3441 (1,5)	3316 (1,5)
		5	3858	3858 (1,5)	3672 (1,5)	3539 (1,5)
		10	4108	4108 (1,5)	3903 (1,5)	3761 (1,5)
		20	4608	4608 (1,5)	4364 (1,5)	4205 (1,5)
		40	5608	5608 (1,5)	5286 (1,5)	5094 (1,5)

[b] Numbers in parentheses, (m,n), indicate the number of axial half-waves and circumferential waves, respectively
* Nonlinear rotations about the normal are neglected.

$\frac{A_s}{d_s h} = 0.5$ and $\frac{I_s^c}{d_s h^3} = 5$

Table 48. Nondimensional buckling coefficient $\frac{2N_x^{cr} R^2}{D}$ for isotropic stringer-stiffened[#] cylinders with simply supported edges and subjected to axial compression

L/R	R/h	Poisson's ratio, ν	External stringers, $e_s/h = +5$			
			Ref. 66 Donnell	Present Study		
				Donnell	Sanders*	Sanders
0.35	50	0	26690	26688 (1,0)	26688 (1,0)	26687 (1,0)
		0.3	23650	23649 (1,0)	23649 (1,0)	23582 (1,3)
		0.5	19540	19536 (1,3)	19538 (1,3)	19174 (1,5)
0.5	50	0	14230	14232 (1,0)	14232 (1,0)	14232 (1,0)
		0.3	12130	12097 (1,0)	12097 (1,0)	12097 (1,0)
		0.5	9699	9699 (1,0)	9699 (1,0)	9699 (1,0)
	100	0	17480	17479 (1,7)	17473 (1,7)	17469 (1,7)
		0.3	14830	14833 (1,5)	14831 (1,5)	14829(1,5)
		0.5	11660	11664 (1,4)	11662 (1,4)	11661 (1,4)
1	50	0	5299	5299 (1,6)	5281 (1,6)	5256 (1,6)
		0.3	4659	4659 (1,5)	4646 (1,5)	4629 (1,5)
		0.5	3759	3759 (1,5)	3747 (1,5)	3736 (1,5)
	100	0	6737	6737 (1,8)	6706 (1,8)	6664 (1,8)
		0.3	6016	6016 (1,7)	5992 (1,7)	5955 (1,7)
		0.5	4967	4967 (1,7)	4943 (1,7)	4916 (1,7)
	250	0	10310	10311 (1,10)	10264 (1,10)	10200 (1,10)
		0.3	9411	9411 (1,10)	9365 (1,10)	9310 (1,10)
		0.5	8027	8027 (1,9)	7989 (1,9)	7937 (1,9)
	500	0	15690	15694 (1,12)	15628 (1,12)	15547 (1,12)
		0.3	14500	14505 (1,12)	14440 (1,12)	14368 (1,12)
		0.5	12600	12600 (1,11)	12544 (1,11)	12475 (1,11)
	2000	0	44990	44986 (1,17)	44862 (1,17)	44725 (1,17)
		0.3	42280	42284 (1,17)	42160 (1,17)	42033 (1,17)
		0.5	37610	37610 (1,16)	37499 (1,16)	37375 (1,16)
	5000	0	100600	100621 (1,21)	100434 (1,21)	100215 (1,21)
		0.3	94870	94866 (1,21)	94680 (1,21)	94482 (1,21)
		0.5	85210	85209 (1,21)	85023 (1,21)	84847 (1,21)

[b] Numbers in parentheses, (m,n), indicate the number of axial half-waves and circumferential waves, respectively
* Nonlinear rotations about the normal are neglected.

[#] $\frac{A_s}{d_s h} = 0.5$, $\frac{I_s^c}{d_s h^3} = 5$, and $J_s = 0$

Table 49. Nondimensional buckling coefficient $\frac{2N_x^{cr} R^2}{D}$ for isotropic stringer-stiffened[#] cylinders with simply supported edges, and subjected to axial compression

L/R	R/h	Poisson's ratio, ν	Internal stringers, $e_s/h = -5$			
			Ref. 66 Donnell	Present Study		
				Donnell	Sanders*	Sanders
0.35	50	0	26070	26071 (1,5)[b]	26063 (1,5)	25016 (1,6)
		0.3	23890	23886 (1,7)	23870 (1,7)	22216 (1,7)
		0.5	19860	19862 (1,7)	19842 (1,8)	18038 (1,8)
0.5	50	0	12860	12860 (1,5)	12851 (1,5)	12417 (1,5)
		0.3	11800	11800 (1,6)	11786 (1,6)	11210 (1,6)
		0.5	9830	9830 (1,6)	9815 (1,6)	9240 (1,6)
	100	0	13070	13075 (1,7)	13063 (1,7)	12841 (1,7)
		0.3	12050	12054 (1,8)	12038 (1,8)	11791 (1,8)
		0.5	10070	10066 (1,8)	10050 (1,8)	9816 (1,8)
1	50	0	3421	3421 (1,5)	3404 (1,5)	3284 (1,5)
		0.3	3156	3156 (1,5)	3139 (1,5)	3013 (1,5)
		0.5	2660	2660 (1,5)	2642 (1,5)	2527 (1,5)
	100	0	3811	3811 (1,6)	3790(1,6)	3707 (1,6)
		0.3	3551	3551 (1,6)	3529 (1,6)	3446 (1,6)
		0.5	3027	3027 (1,6)	3005 (1,6)	2931 (1,6)
	250	0	5348	5348 (1,9)	5308 (1,9)	5251 (1,9)
		0.3	5045	5045 (1,9)	5005 (1,9)	4950 (1,9)
		0.5	4425	4425 (1,8)	4392 (1,8)	4335 (1,8)
	500	0	8350	8350 (1,11)	8294 (1,11)	8234 (1,11)
		0.3	7933	7933 (1,11)	7877 (1,11)	7819 (1,11)
		0.5	7103	7103 (1,10)	7055 (1,10)	6995 (1,10)
	2000	0	28140	29488 (1,16)	29376 (1,16)	29271 (1,16)
		0.3	28080	28080 (1,16)	27968 (1,16)	27869 (1,16)
		0.5	25640	25638 (1,16)	25527 (1,16)	25436 (1,16)
	5000	0	74300	74298 (2,28)	74211 (2,28)	74121 (2,28)
		0.3	70650	70647 (2,28)	70560 (2,28)	70474 (2,28)
		0.5	63890	63887 (2,27)	63806 (2,27)	63722 (2,27)

[b] Numbers in parentheses, (m,n), indicate the number of axial half-waves and circumferential waves, respectively
* Nonlinear rotations about the normal are neglected.

[#] $\frac{A_s}{d_s h} = 0.5$, $\frac{I_s^e}{d_s h^3} = 5$, and $J_s = 0$

Table 50. Geometric properties of aluminum and brass stiffened cylinders given in reference 67

Ring-Stiffened Shells							
Shell	$h \times 10^3$, in.	R/h	L/R	d_r, in.	$\frac{A_r}{d_r h}$	e_r/h	$\frac{I_r^c}{d_r h^3}$
AR-1	9.29	431	1.31	0.250	0.205	1.13	0.0288
AR-2	9.50	421	1.31	0.250	0.198	1.11	0.0262
AR-3	10.05	398	1.31	0.250	0.305	1.55	0.1287
AR-4	10.43	384	1.31	0.250	0.293	1.52	0.1189
AR-5	8.38	477	1.31	0.250	0.315	1.54	0.1266
AR-6	8.46	473	1.31	0.250	0.307	1.51	0.1160
AR-7	8.26	484	1.44	0.320	0.248	1.43	0.0738
AR-9	8.32	481	1.88	0.250	0.678	2.88	1.6326
AR-10	8.80	455	1.38	0.250	0.630	2.78	1.3711
AR-11	8.13	492	1.35	0.200	0.777	2.63	1.5527
AR-12	10.43	384	1.40	0.180	0.575	2.28	0.7978
BR-1	10.55	379	1.31	0.250	0.193	1.04	0.0199
BR-4	10.61	377	1.28	0.300	0.156	1.09	0.0208
Stringer-Stiffened Shells							
Shell	$h \times 10^3$, in.	R/h	L/R	d_s, in.	$A_s/(d_s h)$	e_s/h	$I_s/(d_s h^3)$
AS-2	7.74	517	1.38	0.316	0.506	1.72	0.2466
AS-3	11.05	362	1.38	0.316	0.330	1.29	0.0679
AS-4	10.21	392	1.38	0.316	0.235	1.07	0.0248

Table 51. Buckling load N_x^{cr} (lb.in) for aluminum and brass stiffened cylinders with simply supported edges and subjected to axial compression

Shell	Ref. 67 Donnell	Present Study		
		Donnell	Sanders*	Sanders
AR-1	143.2	143.5 (16,0)[b]	143.5 (16,0)	143.5 (16,0)
AR-2	149.7	149.6 (16,0)	149.6 (16,0)	149.6 (16,0)
AR-3	174.6	174.6 (16,0)	174.6 (16,0)	174.6 (16,0)
AR-4	187.2	187.0 (16,0)	187.0 (16,0)	187.0 (16,0)
AR-5	122.1	122.0 (18,0)	122.0 (18,0)	122.0 (18,0)
AR-6	123.9	123.9 (18,0)	123.9 (18,0)	123.9 (18,0)
AR-7	115.4	115.5 (19,0)	115.5 (19,0)	115.5 (19,0)
AR-9	136.0	135.6 (27,0)	135.6 (27,0)	135.6 (27,0)
AR-10	149.8	149.5 (19,0)	149.5 (19,0)	149.5 (19,0)
AR-11	133.3	133.3 (20,0)	133.3 (20,0)	133.3 (20,0)
AR-12	206.7	206.4 (18,0)	206.4 (18,0)	206.4 (18,0)
AS-2	123.8	121.8 (1,10)	120.7 (1,10)	119.7 (1,10)
AS-3	219.8	224.7 (1,9)	222.0 (1,9)	219.7 (1,9)
AS-4	173.5	180.2 (1,9)	178.1 (1,9)	176.2 (1,9)
BR-1	281.7	282.0 (15,0)	282.0 (15,0)	282.0 (15,0)
BR-4	280.3	280.2 (15,0)	280.2 (15,0)	280.2 (15,0)

[b] Numbers in parentheses, (m,n), indicate the number of axial half-waves and circumferential waves, respectively

Table 52. Nondimensional buckling coefficient $\frac{2N_x^{cr} R^2}{D}$ for isotropic ring-stiffened[#] cylinders with simply supported edges, and subjected to axial compression ($\nu = 0.3$, L/R = 0.5, R/h = 250).

$I_r/(d_r h^3)$	External rings, $e_r/h = +1$		Internal rings, $e_r/h = -1$	
	Refs. 62 and 66 Donnell	Present Study Donnell	Refs. 62 and 66 Donnell	Present Study Donnell
2	4048 (5,0)[b]	4048 (5,0)	3854 (5,7)	3854 (5,7)
40	4048 (5,0)	4048 (5,0)	4030 (5,2)	4030 (5,2)

[b] Numbers in parentheses, (m,n), indicate the number of axial half-waves and circumferential waves, respectively
* Nonlinear rotations about the normal are neglected. $A_r/(d_r h) = 0.5$

[#] $\frac{A_r}{d_r h} = 0.5$ and $J_s = 0$

Table 53. Nondimensional buckling coefficient $\frac{2N_x^{cr} R^2}{D}$ for isotropic ring-stiffened[#] cylinders with simply supported edges, and subjected to axial compression ($\nu = 0.3$, L/R = 0.5, R/h = 250)

$I_r/(d_r h^3)$	Refs. 62 and 66 Donnell	Present Study Donnell
2	4016 (5,5)[b]	4016 (5,5)
5	4033 (5,3)	4033 (5,3)
20	4044 (5,2)	4044 (5,2)
40	4046 (5,1)	4046 (5,1)
200	4048 (5,0)	4048 (5,0)

[b] Numbers in parentheses, (m,n), indicate the number of axial half-waves and circumferential waves, respectively
* Nonlinear rotations about the normal are neglected.

[#] $\frac{A_r}{d_r h} = 0.5$, $e_r/h = 0$, and $J_s = 0$

Table 54. Nondimensional buckling coefficient $\frac{2N_x^{cr} R^2}{D}$ for isotropic ring-stiffened[#] cylinders with simply supported edges, and subjected to axial compression ($\nu = 0.3$, $L/R = 0.5$).

R/h	External rings, $e_r/h = +5$		Internal rings, $e_r/h = -5$	
	Refs. 62 and 66 Donnell	Present Study Donnell	Refs. 62 and 66 Donnell	Present Study Donnell
50	809.4 (2,0)[b]	834.5 (2,0)	714.8 (2,3)	718.4 (2,3)
100	1619 (3,0)	1633 (3,0)	1420 (3,4)	1421 (3,4)
250	4048 (5,0)	4048 (5,0)	3578 (5,6)	3578 (5,6)
500	8094 (6,0)	8103 (7,0)	7063 (6,8)	7063 (6,8)
1000	16190 (9,0)	16194 (10,0)	14050 (9,11)	14049 (9,11)
2000	32380 (13,0)	32411 (14,0)	28080 (13,16)	28083 (13,16)

[b] Numbers in parentheses, (m,n), indicate the number of axial half-waves and circumferential waves, respectively

[#] $\frac{A_r}{d_r h} = 0.5$, $\frac{I_r^e}{d_r h^3} = 5$, and $J_s = 0$

Table 55. Nondimensional buckling pressure $\frac{p_{cr}R^3}{D}$ for isotropic ring-stiffened[#] cylinders with L/R = 0.5, simply supported edges, and subjected to uniform external pressure ($\nu = 0.3$ and $e_r/h = \pm 5$)

R/h	External rings, $e_r/h = +5$			
	Ref. 52 Donnell	Present Study		
		Donnell	Sanders* Live pressure	Sanders Live pressure
50	4664	4664 (1,4)[b]	4724 (1,4)	4480 (1,4)
100	6997	6997 (1,5)	7067 (1,5)	6865 (1,5)
250	11430	11429 (1,7)	11429 (1,7)	11300 (1,7)
500	16410	16406 (1,9)	16352 (1,9)	16267 (1,9)
1000	23470	23472 (1,11)	23402 (1,11)	23344 (1,11)
2000	33410	33413 (1,13)	33350 (1,13)	33307 (1,13)
R/h	Internal rings, $e_r/h = -5$			
	Ref. 52 Donnell	Present Study		
		Donnell	Sanders* Live pressure	Sanders Live pressure
50	2803	2803 (1,4)	2854 (1,4)	2847 (1,4)
100	4589	4589 (1,5)	4649 (1,5)	4635 (1,5)
250	9094	9094 (1,7)	9136 (1,7)	9118 (1,7)
500	14470	14472 (1,8)	14549 (1,8)	14517 (1,8)
1000	22830	22829 (1,10)	22879 (1,10)	22850 (1,10)
2000	34900	34898 (1,13)	34890 (1,13)	34869 (1,13)

[b] Numbers in parentheses, (m,n), indicate the number of axial half-waves and circumferential waves, respectively
* Nonlinear rotations about the normal are neglected.

[#] $\frac{A_r}{d_r h} = 0.5$, $\frac{I_r^c}{d_r h^3} = 5$, and $J_s = 0$

Table 56. Effect of Poisson's ratio on nondimensional buckling pressure $\frac{p_{cr}R^3}{D}$ for isotropic ring-stiffened[#] cylinders with simply supported edges and subjected to uniform external pressure ($e_r/h = \pm 5$)

R/h	L/R	Poisson's ratio, ν	External rings, $e_r/h = +5$			
			Refs. 51 and 52 Donnell	Present Study		
				Donnell	Sanders* Live pressure	Sanders Live pressure
50	1	0	3175	3175 (1,3)[b]	3150 (1,4)	3028 (1,4)
		0.3	2643	2643 (1,3)	2650 (1,4)	2532 (1,4)
		0.5	2071	2071 (1,3)	2102 (1,4)	1996 (1,3)
750	1	0	12720	12717 (1,7)	12676 (1,8)	12643 (1,7)
		0.3	10370	10370 (1,7)	10331 (1,7)	10292 (1,7))
		0.5	8036	8036 (1,7)	7997 (1,7)	7967 (1,7)
2000	2	0	10340	10335 (1,7)	10229 (1,7)	10218 (1,7)
		0.3	8517	8517 (1,7)	8416 (1,7)	8407 (1,7)
		0.5	6660	6660 (1,7)	6574 (1,7)	6567 (1,7)
R/h	L/R	Poisson's ratio, ν	Internal rings, $e_r/h = -5$			
			Refs. 51 and 52 Donnell	Present Study		
				Donnell	Sanders* Live pressure	Sanders Live pressure
50	1	0	1971	1971 (1,3)	2136 (1,3)	2096 (1,3)
		0.3	1883	1883 (1,3)	1969 (1,3)	1941 (1,3)
		0.5	1612	1612 (1,3)	1643 (1,3)	1624 (1,3)
750	1	0	11010	11014 (1,7)	11029 (1,7)	11003 (1,7)
		0.3	11120	11123 (1,7)	11127 (1,7)	11104 (1,7)
		0.5	9950	9950 (1,7)	9945 (1,7)	9925 (1,7)
2000	2	0	9967	9967 (1,7)	9884 (1,7)	9874 (1,7)
		0.3	10210	10208 (1,7)	10130 (1,7)	10121 (1,7)
		0.5	9283	9283 (1,7)	9215 (1,7)	9208 (1,7)

[b] Numbers in parentheses, (m,n), indicate the number of axial half-waves and circumferential waves, respectively
* Nonlinear rotations about the normal are neglected.

[#] $\frac{A_r}{d_r h} = 0.5$, $\frac{I_r^e}{d_r h^3} = 5$, and $J_s = 0$

Table 57. Nondimensional buckling pressure $\frac{p^{cr}R^3}{D}$ for isotropic ring-stiffened[#] cylinders with simply supported edges and subjected to uniform hydrostatic pressure ($\nu = 0.3$ and $e_r/h = +5$)

R/h	L/R	External rings, $e_r/h = +5$			
		Refs. 51 and 52 Donnell	Present Study		
			Donnell	Sanders* Live pressure	Sanders Live pressure
50	0.5	834.5 (2,0)[b]	834.5 (2,0)	838.4 (2,0)	838.4 (2,0)
	1	825.4 (5,0)	825.4 (5,0)	827.9 (5,0)	827.9 (5,0)
	1.5	810.9 (7.0)	810.9 (7,0)	813.7 (7,0)	813.7 (7,0)
75	0.65	1241 (4,0)	1241 (4,0)	1243 (4,0)	1243 (4,0)
	0.8	1240 (4,0)	1240 (4,0)	1244 (4,0)	1244 (4,0)
100	0.5	1633 (3,0)	1633 (3,0)	1636 (3,0)	1636 (3,0)
	1	1633 (6,0)	1633 (6,0)	1636 (6,0)	1636 (6,0)
	1.5	1624 (10,0)	1624 (10,0)	1627 (10,0)	1627 (10,0)
	2	1620 (13,0)	1620 (13,0)	1586 (1,3)	1526 (1,3)
150	0.8	2438 (6,0)	2438 (6,0)	2442 (6,0)	2441 (6,0)
250	0.5	4048 (5,0)	4048 (5,0)	4052 (5,0)	4052 (5,0)
	1	4048 (10,0)	4048 (10,0)	4052 (10,0)	4052 (10,0)
	1.5	3774 (1,4)	3774 (1,4)	3689 (1,5)	3650 (1,5)
	2	2757 (1,4)	2757 (1,4)	2669 (1,4)	2633 (1,4)
	3	1954 (1,3)	1954 (1,3)	1937 (1,3)	1899 (1,3)
475	0.65	7691 (9,0)	7691 (9,0)	7694 (9,0)	7694 (9,0)
500	0.5	8103 (7,0)	8103 (7,0)	8106 (7,0)	8106 (7,0)
	1	7680 (1,6)	7680 (1,6)	7639 (1,7)	7590 (1,6)
	1.5	5366 (1,5)	5366 (1,5)	5339 (1,5)	5292 (1,5)
	2	4083 (1,5)	4083 (1,5)	3974 (1,5)	3950 (1,5)
	3	2734 (1,4)	2734 (1,4)	2637 (1,4)	2619 (1,4)
550	0.8	8904 (12,0)	8904 (12,0)	8907 (12,0)	8907 (12,0)

[b] Numbers in parentheses, (m,n), indicate the number of axial half-waves and circumferential waves, respectively
* Nonlinear rotations about the normal are neglected.

[#] $\frac{A_r}{d_r h} = 0.5$, $\frac{I_r^c}{d_r h^3} = 5$, and $J_s = 0$

Table 57. Concluded

R/h	L/R	External rings, $e_r/h = +5$			
		Refs. 51 and 52 Donnell	Present Study		
			Donnell	Sanders* Live pressure	Sanders Live pressure
750	0.6	12190 (11,0)[b]	12190 (11,0)	12193 (11,0)	12193 (11,0)
	0.7	12150 (12,0)	12154 (12,0)	12158 (12,0)	12158 (12,0)
	0.8	11410 (1,8)	11415 (1,8)	11336 (1,8)	11284 (1,8)
	0.9	10490 (1,8)	10486 (1,8)	10382 (1,8)	10340 (1,8)
	1	9421 (1,7)	9421 (1,7)	9362 (1,7)	9314 (1,7)
1000	0.5	16190 (10,0)	16194 (10,0)	16197 (10,0)	16197 (10,0)
	0.6	16190 (12,0)	16194 (12,0)	16197 (12,0)	16197 (12,0)
	0.7	15100 (1,9)	15098 (1,9)	15032 (1,9)	14977 (1,9)
	0.8	13560 (1,9)	13559 (1,9)	13460 (1,9)	13418 (1,9)
	0.9	12110 (1,8)	12112 (1,8)	12047 (1,8)	12002 (1,8)
	1	11030 (1,8)	11029 (1,8)	10936 (1,8)	10901 (1,8)
	1.5	7814 (1,6)	7814 (1,6)	7720 (1,7)	7699 (1,7)
	2	5887 (1,6)	5887 (1,6)	5776 (1,6)	5760 (1,6)
	3	4029 (1,5)	4030 (1,5)	3914 (1,5)	3903 (1,5)
2000	0.4	32480 (11,0)	32484 (11,0)	32488 (11,0)	32488 (11,0)
	0.5	29920 (1,13)	29918 (1,13)	29836 (1,13)	29786 (1,13)
	0.6	25490 (1,12)	25487 (1,12)	25403 (1,12)	25360 (1,12)
	0.7	22170 (1,11)	22174 (1,11)	22099 (1,11)	22059 (1,11)
	1	16120 (1,9)	16125 (1,9)	16069 (1,9)	16037 (1,9)
	1.5	10930 (1,8)	10934 (1,8)	10834 (1,8)	10817 (1,8)
	2	8308 (1,7)	8308 (1,7)	8204 (1,7)	8192 (1,7)
	3	5777 (1,6)	5777 (1,6)	5659 (1,6)	5652 (1,6)
	4	4226 (1,5)	4226 (1,5)	4121 (1,5)	4114 (1,5)
	6	2806 (1,4)	2806 (1,4)	2711 (1,4)	2706 (1,4)
	10	1688 (1,3)	1688 (1,3)	1614 (1,3)	1611 (1,3)

[b] Numbers in parentheses, (m,n), indicate the number of axial half-waves and circumferential waves, respectively
* Nonlinear rotations about the normal are neglected.

$\frac{A_r}{d_r h} = 0.5$, $\frac{I_r^e}{d_r h^3} = 5$, and $J_s = 0$

Table 58. Nondimensional buckling pressure $\frac{p^{cr}R^3}{D}$ for isotropic ring-stiffened[#] cylinders with simply supported edges and subjected to uniform hydrostatic pressure ($\nu = 0.3$ and $e_r/h = -5$)

R/h	L/R	Internal rings, $e_r/h = -5$			
		Refs. 51 and 52 Donnell	Present Study		
			Donnell	Sanders* Live pressure	Sanders Live pressure
50	0.5	644.9 (2,3)[b]	644.9 (2,3)	646.9 (2,3)	646.3 (2,3)
	1	644.9 (4,3)	644.9 (4,3)	646.9 (4,3)	646.3 (4,3)
	1.5	644.9 (6,3)	644.9 (6,3)	646.9 (6,3)	646.3 (6,3)
75	0.65	979.1 (3,3)	979.1 (3,3)	983.4 (3,3)	982.7 (3,3)
	0.8	982.3 (4,3)	982.3 (4,3)	985.8 (4,3)	985.3 (4,3)
100	0.5	1303 (3,4)	1303 (3,4)	1306 (3,4)	1305 (3,4)
	1	1288 (5,4)	1288 (5,4)	1292 (5,4)	1291 (5,4)
	1.5	1280 (8,4)	1280 (8,4)	1283 (8,4)	1282 (8,4)
	2	1281 (11,4)	1281 (11,4)	1284 (11,4)	1283 (11,4)
150	0.8	1926 (5,5)	1926 (5,5)	1929 (5,5)	1928 (5,5)
250	0.5	3228 (4,6)	3228 (4,6)	3232 (4,6)	3231 (4,6)
	1	3224 (9,6)	3224 (9,6)	3227 (9,6)	3226 (9,6)
	1.5	3211 (13,6)	3211 (13,6)	3214 (13,6)	3214 (13,6)
	2	3044 (1,4)	3044 (1,4)	2998 (1,4)	2974 (1,4)
	3	2252 (1,3)	2252 (1,3)	2259 (1,3)	2227 (1,3)
475	0.65	6108 (8,9)	6108 (8,9)	6110 (8,9)	6110 (8,9)
500	0.5	6398 (6,9)	6398 (6,9)	6401 (6,9)	6400 (6,9)
	1	6398 (12,9)	6398 (12,9)	6401 (12,9)	6400 (12,9)
	1.5	5897 (1,5)	5897 (1,5)	5901 (1,5)	5867 (1,5)
	2	4660 (1,5)	4660 (1,5)	4590 (1,5)	4572 (1,5)
	3	3230 (1,4)	3230 (1,4)	3160 (1,4)	3144 (1,4)
550	0.8	7054 (10,9)	7054 (10,9)	7058 (10,9)	7057 (10,9)

[b] Numbers in parentheses, (m,n), indicate the number of axial half-waves and circumferential waves, respectively
* Nonlinear rotations about the normal are neglected.

[#] $\frac{A_r}{d_r h} = 0.5$, $\frac{I_r^c}{d_r h^3} = 5$, and $J_s = 0$

Table 58. Concluded

R/h	L/R	Internal rings, $e_r/h = -5$			
		Refs. 51 and 52 Donnell	Present Study		
			Donnell	Sanders* Live pressure	Sanders Live pressure
750	0.6	9603 (9,11)[b]	9603 (9,11)	9606 (9,11)	9605 (9,11)
	0.7	9607 (10,11)	9607 (10,11)	9610 (10,11)	9609 (10,11)
	0.8	9603 (12,11)	9603 (12,11)	9606 (12,11)	9605 (12,11)
	0.9	9600 (13,11)	9600 (13,11)	9603 (13,11)	9603 (13,11)
	1	9603 (15,11)	9603 (15,11)	9606 (15,11)	9605 (15,11)
1000	0.5	12860 (8,13)	12861 (8,13)	12864 (8,13)	12863 (8,13)
	0.6	12810 (10,13)	12809 (10,13)	12812 (10,13)	12811 (10,13)
	0.7	12810 (12,13)	12807 (12,13)	12809 (12,13)	12809 (12,13)
	0.8	12820 (14,13)	12823 (14,13)	12826 (14,13)	12825 (14,13)
	0.9	12810 (15,13)	12809 (15,13)	12812 (15,13)	12811 (15,13)
	1	12180 (1,8)	12176 (1,8)	12128 (1,8)	12106 (1,8)
	1.5	8956 (1,7)	8956 (1,7)	8879 (1,7)	8863 (1,7)
	2	6881 (1,6)	6881 (1,6)	6800 (1,6)	6786 (1,6)
	3	4779 (1,5)	4779 (1,5)	4685 (1,5)	4675 (1,5)
2000	0.4	25660 (10,18)	25655 (10,18)	25658 (10,18)	25658 (10,18)
	0.5	25590 (12,18)	25592 (12,18)	25595 (12,18)	25594 (12,18)
	0.6	25620 (14,18)	25618 (14,18)	25621 (14,18)	25620 (14,18)
	0.7	24380 (1,11)	24380 (1,11)	24346 (1,11)	24320 (1,11)
	1	18520 (1,9)	18512 (1,9)	18487 (1,9)	18461 (1,9)
	1.5	12920 (1,8)	12921 (1,8)	12849 (1,8)	12833 (1,8)
	2	9957 (1,7)	9957 (1,7)	9876 (1,7)	9863 (1,7)
	3	6912 (1,6)	6912 (1,6)	6810 (1,6)	6803 (1,6)
	4	5179 (1,5)	5179 (1,5)	5086 (1,5)	5079 (1,5)
	6	3500 (1,4)	3500 (1,4)	3413 (1,4)	3407 (1,4)
	10	2150 (1,3)	2150 (1,3)	2080 (1,3)	2076 (1,3)

[b] Numbers in parentheses, (m,n), indicate the number of axial half-waves and circumferential waves, respectively
* Nonlinear rotations about the normal are neglected.

$\frac{A_r}{d_r h} = 0.5$, $\frac{I_r^c}{d_r h^3} = 5$, and $J_r = 0$

Table 59. Nondimensional buckling pressure $\frac{p_{cr}R^3}{D}$ for isotropic stringer-stiffened[#] cylinders with simply supported edges and subjected to uniform hydrostatic pressure ($\nu = 0.3$ and $e_s/h = \pm 5$)

R/h	L/R	External stringers, $e_s/h = +5$			
		Refs. 51 and 52 Donnell	Present Study		
			Donnell	Sanders* Live pressure	Sanders Live pressure
50	0.5	1113	1113 (1,23)[b]	1112 (1,23)	1112 (1,23)
100	1	301.1	301.2 (1,12)	301.2 (1,12)	301.2 (1,12)
	1.5	147.8	147.8 (1,9)	147.6 (1,9)	147.5 (1,9)
	2	93.36	93.39 (1,7)	93.28 (1,7)	93.17 (1,7)
2000	3	176.2	176.2 (1,11)	175.6 (1,11)	175.6 (1,11)
R/h	L/R	Internal stringers, $e_s/h = -5$			
		Refs. 51 and 52 Donnell	Present Study		
			Donnell	Sanders* Live pressure	Sanders Live pressure
50	0.5	1086	1086 (1,22)	1087 (1,22)	1085 (1,22)
100	1	254.4	254.5 (1,10)	255.1 (1,11)	254.8 (1,10)
	1.5	111.2	111.2 (1,7)	111.5 (1,7)	111.3 (1,7)
	2	66.42	66.40 (1,6)	66.24 (1,6)	66.06 (1,6)
2000	3	158.9	158.9 (1,11)	158.2 (1,11)	158.2 (1,11)

[b] Numbers in parentheses, (m,n), indicate the number of axial half-waves and circumferential waves, respectively
* Nonlinear rotations about the normal are neglected.

[#] $\frac{A_s}{d_s h} = 0.5$, $\frac{I_s^e}{d_s h^3} = 5$, and $J_s = 0$

Table 60. Effect of section properties on nondimensional buckling pressure $\frac{p_{cr}R^3}{D}$ for isotropic ring-stiffened cylinders with L/R = 0.5, simply supported edges, and subjected to uniform hydrostatic pressure ($\nu = 0.3$ and $e_r/h = +5$)

R/h	$A_r/(d_r\, h)$	$I_r/(d_r\, h^3)$	External rings, $e_r/h = +5$			
			Ref. 52 Donnell	Present Study		
				Donnell	Sanders* Live pressure	Sanders Live pressure
100	0.1	1	1382 (3,2)[b]	1382 (3,2)	1385 (3,2)	1385 (3,2)
	0.3	3	1510 (3,0)	1510 (3,0)	1513 (3,0)	1513 (3,0)
	0.5	5	1633 (3,0)	1633 (3,0)	1636 (3,0)	1636 (3,0)
	0.8	8	1817 (3,0)	1817 (3,0)	1821 (3,0)	1821 (3,0)
1000	0.05	0.5	4903 (1,14)	4903 (1,14)	4895 (1,14)	4889 (1,14)
	0.1	1	7642 (1,13)	7624 (1,13)	7606 (1,13)	7595 (1,13)
	0.3	3	14950 (1,11)	14947 (1,11)	14908 (1,11)	14866 (1,11)
	0.5	5	16190 (10,0)	16194 (10,0)	16197 (10,0)	16197 (10,0)
	0.8	8	17780 (11,0)	17783 (11,0)	17786 (11,0)	17786 (11,0)
1500	0.05	0.5	6176 (1,16)	6176 (1,16)	6166 (1,16)	6161 (1,16)
	0.1	1	9640 (1,14)	9640 (1,14)	9627 (1,14)	9616 (1,14)
	0.5	5	24340 (12,0)	24336 (12,0)	24339 (12,0)	24339 (12,0)
	0.8	8	26600 (13,0)	26601 (13,0)	26604 (13,0)	26604 (13,0)
2000	0.1	1	11340 (1,16)	11340 (1,16)	11318 (1,16)	11310 (1,16)
	0.3	3	22390 (1,14)	22395 (1,14)	22337 (1,14)	22309 (1,14)
	0.5	5	29920 (1,13)	29918 (1,13)	29836 (1,13)	29786 (1,13)
	0.8	8	35470 (12,17)	35468 (15,0)	35471 (15,0)	35471 (15,0)

[b] Numbers in parentheses, (m,n), indicate the number of axial half-waves and circumferential waves, respectively
* Nonlinear rotations about the normal are neglected.

Table 61. Effect of section properties on nondimensional buckling pressure $\frac{p_{cr}R^3}{D}$ for isotropic ring-stiffened cylinders with L/R = 0.5, simply supported edges, and subjected to uniform hydrostatic pressure ($\nu = 0.3$ and $e_r/h = -5$)

R/h	$A_r/(d_r h)$	$I_r/(d_r h^3)$	Internal rings, $e_r/h = -5$			
			Ref. 52 Donnell	Present Study		
				Donnell	Sanders* Live pressure	Sanders Live pressure
100	0.1	1	1200 (2,5)[b]	1200 (2,5)	1205 (2,5)	1203 (2,5)
	0.3	3	1273 (3,4)	1273 (3,4)	1276 (3,4)	1276 (3,4)
	0.5	5	1303 (3,4)	1303 (3,4)	1306 (3,4)	1305 (3,4)
	0.8	8	1348 (3,4)	1348 (3,4)	1350 (3,4)	1350 (3,4)
1000	0.05	0.5	5033 (1,14)	5033 (1,14)	5027 (1,14)	5023 (1,14)
	0.1	1	7805 (1,13)	7805 (1,13)	7794 (1,13)	7787 (1,13)
	0.3	3	12420 (8,13)	12425 (8,13)	12429 (8,13)	12428 (8,13)
	0.5	5	12860 (8,13)	12861 (8,13)	12864 (8,13)	12863 (8,13)
	0.8	8	13340 (9,12)	13339 (9,12)	13342 (9,12)	13341 (9,12)
1500	0.05	0.5	6421 (1,16)	6421 (1,16)	6412 (1,16)	6409 (1,16)
	0.1	1	10010 (1,14)	10013 (1,14)	10005 (1,14)	9997 (1,14)
	0.5	5	19250 (10,16)	19248 (10,16)	19250 (10,16)	19250 (10,16)
	0.8	8	19990 (11,15)	19993 (11,15)	19996 (11,15)	19996 (11,15)
2000	0.1	1	11950 (1,15)	11953 (1,15)	11946 (1,15)	11938 (1,15)
	0.3	3	23490 (1,13)	23492 (1,13)	23485 (1,13)	23463 (1,13)
	0.5	5	25590 (12,18)	25592 (12,18)	25595 (12,18)	25594 (12,18)
	0.8	8	26650 (12,17)	26650 (12,17)	26653 (12,17)	26652 (12,17)

[b] Numbers in parentheses, (m,n), indicate the number of axial half-waves and circumferential waves, respectively
* Nonlinear rotations about the normal are neglected.

Table 62. Effect of section properties on nondimensional buckling pressure $\frac{p_{cr}R^3}{D}$ for isotropic ring-stiffened cylinders with L/R = 1, simply supported edges, and subjected to uniform hydrostatic pressure ($\nu = 0.3$ and $e_r/h = +5$)

R/h	$A_r/(d_r h)$	$I_r/(d_r h^3)$	External rings, $e_r/h = +5$			
			Ref. 52 Donnell	Present Study		
				Donnell	Sanders* Live pressure	Sanders Live pressure
50	0.1	1	689.0 (1,4)[b]	689.0 (1,4)	675.6 (1,4)	658.5 (1,4)
	0.5	5	825.4 (5,0)	825.4 (5,0)	827.9 (5,0)	827.9 (5,0)
	0.8	8	891.8 (5,0)	891.8 (5,0)	894.5 (5,0)	894.5 (5,0)
100	0.1	1	1095 (1,5)	1095 (1,5)	1080 (1,5)	1065 (1,5)
	0.5	5	1633 (6,0)	1633 (6,0)	1636 (6,0)	1636 (6,0)
	0.8	8	1780 (7,0)	1780 (7,0)	1783 (7,0)	1783 (7,0)
200	0.05	0.5	1101 (1,7)	1101 (1,7)	1089 (1,7)	1084 (1,7)
	0.1	1	1669 (1,6)	1669 (1,6)	1655 (1,6)	1642 (1,6)
	0.5	5	3238 (9,0)	3238 (9,0)	3241 (9,0)	3241 (9,0)
	0.8	8	3566 (9,0)	3566 (9,0)	3569 (9,0)	3569 (9,0)
300	0.05	0.5	1379 (1,7)	1379 (1,7)	1374 (1,7)	1369 (1,7)
	0.1	1	2131 (1,7)	2131 (1,7)	2110 (1,7)	2100 (1,7)
	0.5	5	4857 (11,0)	4857 (11,0)	4861 (11,0)	4861 (11,0)
	0.8	8	5332 (12,0)	5332 (12,0)	5335 (12,0)	5335 (12,0)
400	0.05	0.5	1597 (1,8)	1597 (1,8)	1588 (1,8)	1583 (1,8)
	0.1	1	2517 (1,7)	2517 (1,7)	2507 (1,7)	2496 (1,7)
	0.5	5	6478 (13,0)	6478 (13,0)	6482 (13,0)	6454 (1,6)
	0.8	8	7107 (13,0)	7107 (13,0)	7110 (13,0)	7110 (13,0)
500	0.1	1	2835 (1,8)	2835 (1,8)	2814 (1,8)	2806 (1,8)
	0.3	3	5599 (1,7)	5599 (1,7)	5542 (1,7)	5513 (1,7)
	0.5	5	7680 (1,6)	7680 (1,6)	7639 (1,7)	7590 (1,6)
	0.8	8	9654 (1,6)	8867 (15,0)	8870 (15,0)	8870 (15,0)

[b] Numbers in parentheses, (m,n), indicate the number of axial half-waves and circumferential waves, respectively.
* Nonlinear rotations about the normal are neglected.

Table 63. Effect of section properties on nondimensional buckling pressure $\frac{p^{cr}R^3}{D}$ for isotropic ring-stiffened cylinders with L/R = 1, simply supported edges, and subjected to external hydrostatic pressure ($\nu = 0.3$ and $e_r/h = -5$)

R/h	$A_r/(d_r\, h)$	$I_r/(d_r\, h^3)$	Internal rings, $e_r/h = -5$			
			Ref. 52 Donnell	Present Study		
				Donnell	Sanders* Live pressure	Sanders Live pressure
50	0.1	1	589.6 (3,4)[b]	589.6 (3,4)	591.9 (3,4)	590.4 (3,4)
	0.5	5	644.9 (4,3)	644.9 (4,3)	646.9 (4,3)	646.3 (4,3)
	0.8	8	675.1 (4,3)	675.1 (4,3)	676.5 (4,3)	675.9 (4,3)
100	0.1	1	1063 (1,5)	1063 (1,5)	1055 (1,5)	1047 (1,5)
	0.5	5	1288 (5,4)	1288 (5,4)	1292 (5,4)	1291 (5,4)
	0.8	8	1348 (6,4)	1348 (6,4)	1350 (6,4)	1350 (6,4)
200	0.05	0.5	1127 (1,7)	1127 (1,7)	1118 (1,7)	1114 (1,7)
	0.1	1	1685 (1,6)	1685 (1,6)	1676 (1,6)	1668 (1,6)
	0.5	5	2580 (8,6)	2580 (8,6)	2582 (8,6)	2581 (8,6)
	0.8	8	2691 (8,5)	2691 (8,5)	2695 (8,5)	2694 (8,5)
300	0.05	0.5	1418 (1,7)	1418 (1,7)	1416 (1,7)	1411 (1,7)
	0.1	1	2206 (1,7)	2206 (1,7)	2192 (1,7)	2185 (1,7)
	0.5	5	3844 (9,7)	3844 (9,7)	3847 (9,7)	3846 (9,7)
	0.8	8	4017 (10,7)	4017 (10,7)	4019 (10,7)	4019 (10,7)
400	0.05	0.5	1662 (1,8)	1662 (1,8)	1655 (1,8)	1651 (1,8)
	0.1	1	2617 (1,7)	2617 (1,7)	2612 (1,7)	2603 (1,7)
	0.5	5	5133 (11,8)	5123 (11,8)	5126 (11,8)	5125 (11,8)
	0.8	8	5331 (11,8)	5331 (11,8)	5333 (11,8)	5333 (11,8)
500	0.1	1	2991 (1,8)	2991 (1,8)	2976 (1,8)	2969 (1,8)
	0.3	3	5914 (1,7)	5914 (1,7)	5886 (1,7)	5869 (1,7)
	0.5	5	6398 (12,9)	6398 (12,9)	6401 (12,9)	6400 (12,9)
	0.8	8	6674 (12,9)	6674 (12,9)	6676 (12,9)	6675 (12,9)

[b] Numbers in parentheses, (m,n), indicate the number of axial half-waves and circumferential waves, respectively
* Nonlinear rotations about the normal are neglected.

Table 64. Effect of section properties on nondimensional buckling pressure $\frac{p_{cr}R^3}{D}$ for isotropic ring-stiffened cylinders with L/R = 2, simply supported edges, and subjected to uniform hydrostatic pressure ($\nu = 0.3$ and $e_r/h = \pm 5$)

R/h	$A_r/(d_r h)$	$I_r/(d_r h^3)$	External rings, $e_r/h = +5$			
			Ref. 52 Donnell	Present Study		
				Donnell	Sanders* Live pressure	Sanders Live pressure
1000	0.05	0.5	1380 (1,7)[b]	1380 (1,7)	1372 (1,7)	1370 (1,7)
	0.1	1	2158 (1,7)	2158 (1,7)	2134 (1,7)	2130 (1,7)
	0.3	3	4274 (1,6)	4275 (1,6)	4218 (1,6)	4205 (1,6)
	0.5	5	5887 (1,6)	5887 (1,6)	5776 (1,6)	5760 (1,6)
	0.8	8	7682 (1,5)	7682 (1,5)	7636 (1,5)	7594 (1,5)
R/h	$A_r/(d_r h)$	$I_r/(d_r h^3)$	Internal rings, $e_r/h = -5$			
			Ref. 52 Donnell	Present Study		
				Donnell	Sanders* Live pressure	Sanders Live pressure
1000	0.05	0.5	1496 (1,7)	1496 (1,7)	1489 (1,7)	1487 (1,7)
	0.1	1	2380 (1,7)	2380 (1,7)	2358 (1,7)	2355 (1,7)
	0.3	3	4959 (1,6)	4959 (1,6)	4915 (1,6)	4904 (1,6)
	0.5	5	6881 (1,6)	6881 (1,6)	6800 (1,6)	6786 (1,6)
	0.8	8	9227 (1,5)	9227 (1,5)	9168 (1,6)	9150 (1,6)

[b] Numbers in parentheses, (m,n), indicate the number of axial half-waves and circumferential waves, respectively
* Nonlinear rotations about the normal are neglected.

Table 65. Effect of ring eccentricity on nondimensional buckling pressure $\frac{p^{cr}R^3}{D}$ for isotropic ring-stiffened[#] cylinders with L/R = 0.5, simply supported edges, and subjected to uniform hydrostatic pressure ($\nu = 0.3$).

R/h	e_r/h	Ref. 52 Donnell	Present Study		
			Donnell	Sanders* Live pressure	Sanders Live pressure
100	0	1519 (3,4)[b]	1519 (3,4)	1521 (3,4)	1520 (3,4)
	1	1594 (3,3)	1594 (3,3)	1597 (3,3)	1596 (3,3)
	–1	1443 (3,5)	1443 (3,5)	1445 (3,5)	1444 (3,5)
	2	1632 (3,0)	1632 (3,1)	1635 (3,1)	1635 (3,1)
	–2	1384 (3,5)	1384 (3,5)	1386 (3,5)	1384 (3,5)
	5	1633 (3,0)	1633 (3,0)	1636 (3,0)	1636 (3,0)
	–5	1303 (3,4)	1303 (3,4)	1306 (3,4)	1305 (3,4)
	8	1633 (3,0)	1633 (3,0)	1636 (3,0)	1636 (3,0)
	-8	1305 (3,3)	1305 (3,3)	1309 (3,3)	1308 (3,3)
1500	0	13170 (1,13)	13165 (1,13)	13154 (1,13)	13138 (1,13)
	0.5	13250 (1,13)	13253 (1,13)	13240 (1,13)	13223 (1,13)
	–0.5	13350 (1,13)	13353 (1,13)	13342 (1,13)	13327 (1,13)
	1	13620 (1,13)	13617 (1,13)	13600 (1,13)	13582 (1,13)
	–1	13820 (1,13)	13816 (1,13)	13805 (1,13)	13790 (1,13)
	3	17830 (1,13)	17828 (1,13)	17779 (1,13)	17751 (1,13)
	–3	18340 (1,12)	18343 (1,12)	18342 (1,12)	18320 (1,12)
	5	24340 (12,0)	24336 (12,0)	24339 (12,0)	24339 (12,0)
	–5	19250 (10,16)	19248 (10,16)	19250 (10,16)	19250 (10,16)
	8	24340 (12,0)	24336 (12,0)	24339 (12,0)	24339 (12,0)
	-8	19140 (11,13)	19139 (11,13)	19142 (11,13)	19141 (11,13)

[b] Numbers in parentheses, (m,n), indicate the number of axial half-waves and circumferential waves, respectively
* Nonlinear rotations about the normal are neglected.

[#] $\frac{A_r}{d_r h} = 0.5$, $\frac{I_r^c}{d_r h^3} = 5$, and $J_r = 0$

Table 66. Effect of ring eccentricity on nondimensional buckling pressure $\frac{p^{cr}R^3}{D}$ for isotropic ring-stiffened[#] cylinders with L/R = 1, simply supported edges, and subjected to uniform hydrostatic pressure ($\nu = 0.3$).

R/h	e_r/h	Ref. 52 Donnell	Present Study		
			Donnell	Sanders* Live pressure	Sanders Live pressure
50	1	806.8 (4,2)[b]	806.8 (4,2)	809.7 (4,3)	807.7 (4,3)
	–1	716.0 (4,3)	716.0 (4,3)	718.9 (4,3)	717.6 (4,3)
	5	825.4 (5,0)	825.4 (5,0)	827.9 (5,0)	827.9 (5,0)
	–5	644.9 (4,3)	644.9 (4,3)	646.9 (4,3)	646.3 (4,3)
	8	825.4 (5,0)	825.4 (5,0)	827.9 (5,0)	827.9 (5,0)
	-8	654.3 (4,2)	654.3 (4,2)	658.4 (4,2)	658.0 (4,2)
100	1	1556 (1,4)	1556 (1,4)	1528 (1,5)	1508 (1,5)
	–1	1434 (5,5)	1434 (5,5)	1437 (5,5)	1434 (5,5)
	5	1633 (6,0)	1633 (6,0)	1636 (6,0)	1636 (6,0)
	–5	1288 (5,4)	1288 (5,4)	1292 (5,4)	1291 (5,4)
	8	1633 (6,0)	1633 (6,0)	1636 (6,0)	1636 (6,0)
	-8	1305 (6,3)	1305 (6,3)	1309 (6,3)	1308 (6,3)
600	0	4347 (1,8)	4347 (1,8)	4319 (1,8)	4308 (1,8)
	0.5	4367 (1,8)	4367 (1,8)	4337 (1,8)	4325 (1,8)
	–0.5	4436 (1,8)	4436 (1,8)	4409 (1,8)	4398 (1,8)
	1	4496 (1,8)	4496 (1,8)	4462 (1,8)	4449 (1,8)
	–1	4633 (1,8)	4633 (1,8)	4605 (1,8)	4595 (1,8)
	5	8335 (1,7)	8335 (1,7)	8242 (1,7)	8197 (1,7)
	–5	7681 (13,10)	7681 (13,10)	7684 (13,10)	7683 (13,10)
	6.5	9721 (16,0)	9721 (16,0)	9724 (16,0)	9724 (16,0)
	–6.5	7643 (13,9)	7643 (13,9)	7646 (13,9)	7646 (13,9)
	8	9721 (16,0)	9721 (16,0)	9724 (16,0)	9724 (16,0)
	-8	7658 (13,8)	7658 (13,8)	7662 (13,8)	7661 (13,8)
2000	8	26340 (1,9)	26339 (1,9)	26129 (1,9)	26071 (1,9)
	-8	25465 (24,15)	25465 (24,15)	25468 (24,15)	25468 (24,15)

[b] Numbers in parentheses, (m,n), indicate the number of axial half-waves and circumferential waves, respectively
* Nonlinear rotations about the normal are neglected.

[#] $\frac{A_r}{d_r h} = 0.5$, $\frac{I_r^c}{d_r h^3} = 5$, and $J_r = 0$

Table 67. Effect of ring eccentricity on nondimensional buckling pressure $\frac{p^{cr}R^3}{D}$ for isotropic ring-stiffened[#] cylinders with L/R = 2, simply supported edges, and subjected to uniform hydrostatic pressure ($\nu = 0.3$).

R/h	e_r/h	Ref. 52 Donnell	Present Study		
			Donnell	Sanders* Live pressure	Sanders Live pressure
1000	0	3166 (1,6)	3166 (1,6)	3131 (1,7)	3127 (1,7)
	0.5	3149 (1,6)	3149 (1,6)	3133 (1,7)	3127 (1,6)
	–0.5	3248 (1,6)	3248 (1,6)	3217 (1,7)	3212 (1,7)
	1	3195 (1,6)	3195 (1,6)	3178 (1,6)	3170 (1,6)
	–1	3394 (1,6)	3394 (1,6)	3379 (1,6)	3371 (1,6)
	3	4026 (1,6)	4026 (1,6)	3978 (1,6)	3967 (1,6)
	–3	4622 (1,6)	4622 (1,6)	4585 (1,6)	4575 (1,6)
	5	5887 (1,6)	5887 (1,6)	5776 (1,6)	5760 (1,6)
	–5	6881 (1,6)	6881 (1,6)	6800 (1,6)	6786 (1,6)
	6.5	7681 (1,5)	7681 (1,5)	7636 (1,5)	7594 (1,5)
	–6.5	9183 (1,5)	9183 (1,5)	9124 (1,6)	9106 (1,6)
	8	9416 (11,5)	9416 (1,5)	9288 (1,5)	9236 (1,5)
	-8	11269 (1,5)	11263 (1,5)	11198 (1,5)	11153 (1,5)

[b] Numbers in parentheses, (m,n), indicate the number of axial half-waves and circumferential waves, respectively
* Nonlinear rotations about the normal are neglected.

[#] $\frac{A_r}{d_r h} = 0.5$, $\frac{I_r^c}{d_r h^3} = 5$, and $J_r = 0$

Table 68. Effect of ring eccentricity and section properties on nondimensional buckling pressure $\frac{p^{cr}R^3}{D}$ for isotropic ring-stiffened# cylinders with L/R = 1, simply supported edges, and subjected to uniform hydrostatic pressure ($\nu = 0.3$)

R/h	e_r/h	$A_r/(d_r\, h)$	$I_r/(d_r\, h^3)$	Ref. 52 Donnell	Present Study		
					Donnell	Sanders* Live pressure	Sanders Live pressure
700	1	0.1	1	1641 (1,10)	1641 (1,10)	1634 (1,10)	1632 (1,10)
	3	0.3	3	4603 (1,8)	4603 (1,8)	4576 (1,8)	4562 (1,8)
	8	0.8	8	12420 (18,0)	12419 (18,0)	12423 (18,0)	12423 (18,0)
	–1	0.1	1	1685 (1,10)	1685 (1,10)	1679 (1,10)	1677 (1,10)
	–3	0.3	3	4935 (1,8)	4935 (1,8)	4919 (1,8)	4908 (1,8)
	–8	0.8	8	9109 (15,9)	9109 (15,9)	9111 (15,9)	9111 (15,9)
800	1	0.1	1	1765 (1,10)	1765 (1,10)	1759 (1,10)	1757 (1,10)
	3	0.3	3	5005 (1,8)	5005 (1,8)	4986 (1,8)	4971 (1,8)
	8	0.8	8	14190 (19,0)	14187 (19,0)	14191 (19,0)	14191 (19,0)
	–1	0.1	1	1815 (1,10)	1815 (1,10)	1809 (1,10)	1807 (1,10)
	–3	0.3	3	5385 (1,8)	5385 (1,8)	5375 (1,8)	5363 (1,8)
	–8	0.8	8	10420 (16,9)	10422 (16,9)	10425 (16,9)	10425 (16,9)
900	1	0.1	1	1896 (1,11)	1896 (1,11)	1888 (1,11)	1886 (1,11)
	3	0.3	3	5338 (1,9)	5338 (1,9)	5301 (1,9)	5290 (1,9)
	8	0.8	8	15960 (20,0)	15962 (20,0)	15965 (20,0)	15965 (20,0)
	–1	0.1	1	1949 (1,11)	1949 (1,11)	1941 (1,11)	1939 (1,11)
	–3	0.3	3	5783 (1,9)	5783 (1,9)	5757 (1,9)	5749 (1,9)
	–8	0.8	8	11700 (17,10)	11699 (17,10)	11701 (17,10)	11701 (17,10)

[b] Numbers in parentheses, (m,n), indicate the number of axial half-waves and circumferential waves, respectively
* Nonlinear rotations about the normal are neglected.

Table 69. Effect of length-to-radius ratio on nondimensional buckling pressure $\frac{p^{cr}R^3}{D}$ for isotropic ring-stiffened[#] cylinders with L/R = 1, simply supported edges, and subjected to uniform hydrostatic pressure ($\nu = 0.3$ and $e_r/h = \pm 8$)

R/h	L/R	External rings, $e_r/h = +8$			
		Ref. 52 Donnell	Present Study		
			Donnell	Sanders* Live pressure	Sanders Live pressure
500	1.5	8103 (21,0)[b]	8103 (21,0)	8106 (21,0)	8106 (21,0)
	1.6	8095 (23,0)	8095 (23,0)	7889 (1,5)	7817 (1,5)
	1.7	7810 (1,5)	7810 (1,5)	7581 (1,5)	7518 (1,5)
	1.8	7600 (1,5)	7599 (1,5)	7352 (1,5)	7296 (1,5)
	2.2	5961 (1,4)	5961 (1,4)	5835 (1,4)	5769 (1,4)
	2.4	5482 (1,4)	5482 (1,4)	5308 (1,4)	5255 (1,4)
1000	3	6487 (1,4)	6487 (1,4)	6401 (1,4)	6360 (1,4)

R/h	L/R	Internal rings, $e_r/h = -8$			
		Ref. 52 Donnell	Present Study		
			Donnell	Sanders* Live pressure	Sanders Live pressure
500	1.5	6388 (18,8)	6388 (18,8)	6390 (18,8)	6390 (18,8)
	1.6	6391 (20,8)	6391 (20,8)	6393 (20,8)	6393 (20,8)
	1.7	6387 (21,8)	6387 (21,8)	6389 (21,8)	6389 (21,8)
	1.8	6385 (22,8)	6385 (22,8)	6388 (22,8)	6387 (22,8)
	2.2	6385 (27,8)	6385 (27,8)	6388 (27,8)	6387 (27,8)
	2.4	6386 (29,8)	6386 (29,8)	6325 (1,4)	6283 (1,4)
1000	3	8076 (1,4)	8076 (1,4)	8034 (1,4)	7993 (1,4)

[b] Numbers in parentheses, (m,n), indicate the number of axial half-waves and circumferential waves, respectively
* Nonlinear rotations about the normal are neglected.

[#] $\frac{A_r}{d_r h} = 0.5$, $\frac{I_r^c}{d_r h^3} = 5$, and $J_r = 0$

Table 70. Effect of length-to-radius ratio on nondimensional buckling pressure $\frac{p^{cr}R^3}{D}$ for isotropic ring-stiffened[#] cylinders with L/R = 1, simply supported edges, and subjected to uniform hydrostatic pressure ($\nu = 0.3$ and $e_r/h = \pm 5$).

R/h	L/R	External rings, $e_r/h = +5$			
		Ref. 52 Donnell	Present Study		
			Donnell	Sanders* Live pressure	Sanders Live pressure
2000	0.6	32980 (1,11)[b]	32983 (1,11)	32893 (1,11)	32817 (1,11)
	0.7	28900 (1,11)	28897 (1,11)	28751 (1,11)	28696 (1,11)
	0.9	22980 (1,9)	22984 (1,9)	22906 (1,9)	22851 (1,9)
	2	10990 (1,6)	10991 (1,6)	10937 (1,6)	10907 (1,6)
R/h	L/R	Internal rings, $e_r/h = -5$			
		Ref. 52 Donnell	Present Study		
			Donnell	Sanders* Live pressure	Sanders Live pressure
2000	0.6	26640 (15,17)	26639 (15,17)	26642 (15,17)	26641 (15,17)
	0.7	26630 (17,17)	26634 (17,17)	26637 (17,17)	26636 (17,17)
	0.9	26080 (1,9)	26077 (1,9)	26053 (1,9)	26014 (1,9)
	2	13330 (1,7)	13334 (1,7)	13203 (1,7)	13188 (1,7)

[b] Numbers in parentheses, (m,n), indicate the number of axial half-waves and circumferential waves, respectively
* Nonlinear rotations about the normal are neglected.

[#] $\frac{A_r}{d_r h} = 0.8$, $\frac{I_r^c}{d_r h^3} = 8$, and $J_r = 0$

Table 71. Effect of length-to-radius ratio on nondimensional buckling pressure $\frac{p^{cr}R^3}{D}$ for isotropic ring-stiffened[#] cylinders with L/R = 1, simply supported edges, and subjected to uniform hydrostatic pressure ($\nu = 0.3$ and $e_r/h = \pm 1$).

R/h	L/R	External rings, $e_r/h = +1$			
		Ref. 52 Donnell	Present Study		
			Donnell	Sanders* Live pressure	Sanders Live pressure
500	0.5	6915 (1,10)[b]	6915 (1,10)	6890 (1,10)	6869 (1,10)
	0.6	---	6025 (1,9)	6006 (1,9)	5985 (1,9)
	0.7	5437 (1,8)	5437 (1,8)	5429 (1,8)	5407 (1,8)
2000	1	8697 (1,11)	8697 (1,11)	8660 (1,11)	8652 (1,11)
R/h	L/R	Internal rings, $e_r/h = -1$			
		Ref. 52 Donnell	Present Study		
			Donnell	Sanders* Live pressure	Sanders Live pressure
500	0.5	6742 (1,9)	6742 (1,9)	6746 (1,9)	6725 (1,9)
	0.6	5980 (1,9)	5980 (1,9)	5967 (1,9)	5951 (1,9)
	0.7	5420 (1,8)	5420 (1,8)	5417 (1,8)	5399 (1,8)
2000	1	9129 (1,11)	9129 (1,11)	9096 (1,11)	9089 (1,11)

[b] Numbers in parentheses, (m,n), indicate the number of axial half-waves and circumferential waves, respectively
* Nonlinear rotations about the normal are neglected.

[#] $\frac{A_r}{d_r h} = 0.5$, $\frac{I_r^c}{d_r h^3} = 5$, and $J_r = 0$

Table 72. Buckling pressure (psi) for isotropic[†] cylinders with simply supported edges, subjected to uniform hydrostatic pressure, and stiffened by rings and stringers

Stiffener properties[†]	Ring eccentricity, e_s/h	Stringer eccentricity, e_s/h	Ref. 68, Donnell	Present Study		
				Donnell	Sanders* Live pressure	Sanders Live pressure
$\frac{A_s}{d_s h} = 0.1471$	no rings	no stringers	102	101.8 (1,4)[b]	98.2 (1,4)	97.9 (1,4)
	1.653	no stringers	326	326.1 (1,3)	312.8 (1,3)	309.9 (1,3)
$\frac{A_r}{d_r h} = 0.1471$	-1.653	no stringers	370	369.8 (1,3)	358.7 (1,3)	355.7 (1,3)
	no rings	1.653	106	106.5 (1,4)	103.2 (1,4)	102.9 (1,4)
$\frac{12\, I_s^c}{d_s h^3} = 0.7819$	no rings	-1.653	103	103.0 (1,4)	99.4 (1,4)	99.1 (1,4)
	1.653	1.653	346	345.8 (1,3)	334.9 (1,3)	331.9 (1,3)
$\frac{12\, I_r^c}{d_r h^3} = 0.7819$	-1.653	-1.653	377	377.1 (1,3)	367.0 (1,3)	364.1 (1,3)
$J_s = 0$	1.653	-1.653	---	335.0 (1,3)	322.7 (1,3)	319.8 (1,3)
$J_r = 0$	-1.653	1.653	---	387.1 (1,3)	378.4 (1,3)	375.3 (1,3)
$\frac{A_s}{d_s h} = 0.2948$	no rings	2.817	115	115.0 (1,4)	112.3 (1,4)	112.0 (1,4)
$\frac{12\, I_s^c}{d_s h^3} = 6.330$	no rings	-2.817	103	103.1 (1,4)	99.5 (1,4)	99.3 (1,4)
$J_s = 0$						
$J_r = 0$						

[†] $E = 30 \times 10^6$ psi, $\nu = 0.30$, $h = 0.1$ in., $R/h = 9.78761$, $L/R = 4.5391$, and $d_s/R = d_r/R = 0.3360$

[b] Numbers in parentheses, (m,n), indicate the number of axial half-waves and circumferential waves, respectively

* Nonlinear rotations about the normal are neglected

Table 73. Buckling pressure (psi) for isotropic† cylinders with simply supported edges, subjected to uniform hydrostatic pressure, and stiffened by rings and stringers

Stiffener properties†	Ring eccentricity, e_s/h	Stringer eccentricity, e_s/h	Ref. 68, Donnell	Present Study		
				Donnell	Sanders* Live pressure	Sanders Live pressure
$\frac{A_s}{d_s h} = 0.2948$	no rings	no stringers	99	99.2 (1,4)[b]	95.7 (1,4)	95.4 (1,4)
	2.817	no stringers	1167	1167.4 (1,3)	1047.8 (1,3)	1037.1 (1,3)
$\frac{A_r}{d_r h} = 0.2948$	-2.817	no stringers	1299	1297.9 (1,3)	1206.3 (1,3)	1197.4 (1,3)
$\frac{12\, I_s^c}{d_s h^3} = 6.330$	no rings	2.817	112	112.2 (1,4)	109.6 (1,4)	109.3 (1,4)
	no rings	-2.817	101	100.5 (1,4)	97.1 (1,4)	96.8 (1,4)
$\frac{12\, I_r^c}{d_r h^3} = 6.330$	2.817	2.817	1221	1221.0 (1,3)	1107.1 (1,3)	1096.3 (1,3)
	-2.817	-2.817	1306	1305.6 (1,3)	1215.2 (1,3)	1206.5 (1,3)
$J_s = 0$						
$J_r = 0$	2.817	-2.817	---	1182.9 (1,3)	1064.5 (1,3)	1053.9 (1,3)
	-2.817	2.817	---	1335.5 (1,3)	1249.4 (1,3)	1240.6 (1,3)

† $E = 30 \times 10^6$ psi, $\nu = 0.30$, $h = 0.1$ in., $R/h = 9.79912$, $L/R = 4.5384$, and $d_s/R = d_r/R = 0.3350$

[b] Numbers in parentheses, (m,n), indicate the number of axial half-waves and circumferential waves, respectively

* Nonlinear rotations about the normal are neglected

Table 74. Buckling pressure (psi) for isotropic[†] cylinders with simply supported edges, subjected to hydrostatic pressure, and stiffened by internal or external blade[#] stiffeners

Length, in.	Ring eccentricity, e_s, in.	Stringer eccentricity, e_s, in.	Ref. 69 Donnell	Present Study		
				Donnell	Sanders* Live pressure	Sanders Live pressure
12.0	0.165	0.165	291	290 (1,5)[b]	286 (1,5)	284 (1,5)
	-0.165	0.165	251	250 (1,5)	250 (1,5)	249 (1,5)
	0.165	-0.165	221	220 (1,5)	214 (1,5)	211 (1,5)
	-0.165	-0.165	221	220 (1,5)	219 (1,5)	218 (1,5)
	0.165	no stringers	207	156 (16,0)	156 (16,0)	156 (16,0)
	-0.165	no stringers	215	141 (13,6)	141 (13,6)	141 (13,6)
	no rings	0.165	11.1	11.0 (1,14)	11.0 (1,14)	11.0 (1,14)
	no rings	-0.165	8.0	8.0 (1,10)	8.0 (1,10)	7.9 (1,10)
	no rings	no stringers	3.7	3.7 (1,10)	3.7 (1,10)	3.7 (1,10)
24.0	0.165	0.165	147	145 (1,4)	139 (1,4)	138 (1,4)
	-0.165	0.165	151	150 (1,4)	147 (1,4)	146 (1,4)
	0.165	-0.165	130	129 (1,4)	122 (1,4)	121 (1,4)
	-0.165	-0.165	141	140 (1,4)	136 (1,4)	136 (1,4)
	0.165	no stringers	121	120 (1,4)	113 (1,4)	112 (1,4)
	-0.165	no stringers	139	138 (1,4)	134 (1,4)	133 (1,4)
	no rings	0.165	3.7	3.6 (1,9)	3.6 (1,9)	3.6 (1,9)
	no rings	-0.165	2.7	2.6 (1,7)	2.6 (1,7)	2.6 (1,7)
	no rings	no stringers	1.9	1.8 (1,7)	1.8 (1,7)	1.8 (1,7)

[†] $E = 10.5 \times 10^6$ psi, $\nu = 0.30$, $h = 0.028$ in., $R/h = 95.5$, and $d_s = d_r = 1.0$ in.

[b] Numbers in parentheses, (m,n), indicate the number of axial half-waves and circumferential waves, respectively

* Nonlinear rotations about the normal are neglected

[#] Blade thickness = 0.096 in., blade height = 0.302 in.

Table 74. Concluded

Length, in.	Ring eccentricity, e_s, in.	Stringer eccentricity, e_s, in.	Ref. 69 Donnell	Present Study		
				Donnell	Sanders* Live pressure	Sanders Live pressure
36.0	0.165	0.165	96	96 (1,3)	93 (1,3)	92 (1,3)
	-0.165	0.165	104	104 (1,3)	102 (1,3)	101 (1,3)
	0.165	-0.165	86	86 (1,3)	81 (1,3)	80 (1,3)
	-0.165	-0.165	96	96 (1,3)	93 (1,3)	93 (1,3)
	0.165	no stringers	75	74 (1,3)	69 (1,3)	68 (1,3)
	-0.165	no stringers	90	90 (1,3)	87 (1,3)	86 (1,3)
	no rings	0.165	2.1	2.1 (1,7)	2.0 (1,7)	2.0 (1,7)
	no rings	-0.165	1.6	1.6 (1,6)	1.5 (1,6)	1.5 (1,6)
	no rings	no stringers	1.2	1.2 (1,6)	1.2 (1,6)	1.2 (1,6)
48.0	0.165	0.165	75	75 (1,3)	69 (1,3)	68 (1,3)
	-0.165	0.165	83	83 (1,3)	79 (1,3)	78 (1,3)
	0.165	-0.165	72	71 (1,3)	65 (1,3)	64 (1,3)
	-0.165	-0.165	81	80 (1,3)	75 (1,3)	75 (1,3)
	0.165	no stringers	67	67 (1,3)	60 (1,3)	59 (1,3)
	-0.165	no stringers	78	78 (1,3)	73 (1,3)	72 (1,3)
	no rings	0.165	1.4	1.4 (1,6)	1.4 (1,6)	1.4 (1,6)
	no rings	-0.165	1.2	1.2 (1,6)	1.1 (1,6)	1.1 (1,6)
	no rings	no stringers	0.9	0.9 (1,5)	0.9 (1,5)	0.9 (1,5)

† $E = 10.5 \times 10^6$ psi, $\nu = 0.30$, $h = 0.028$ in., $R/h = 95.5$, and $d_s = d_r = 1.0$ in.

[b] Numbers in parentheses, (m,n), indicate the number of axial half-waves and circumferential waves, respectively

* Nonlinear rotations about the normal are neglected

[#] Blade thickness = 0.096 in., blade height = 0.302 in.

Table 75. Buckling pressure $\frac{p^{cr}R}{Eh}\left(1-\nu^2\right) \times 10^4$ for isotropic† cylinders with simply supported edges, subjected to uniform hydrostatic pressure, and stiffened by external blade-shaped# rings

		External rings, e_r/h = + 6.2633			
L/R	Number of rings, N	Ref. 70 Sanders[c]	Present Study		
			Donnell	Sanders* Live pressure	Sanders Live pressure
3.0	9	51.7673(3)[a]	60.1467 (1,3)[b]	55.8764 (1,3)	54.7460 (1,3)
4.5	14	44.4317 (3)	45.6492 (1,2)	47.9593 (1,3)	47.4479 (1,3)
6.0	19	25.8902 (2)	30.4328 (1,2)	27.9813 (1,2)	27.1199 (1,2)
7.5	24	19.9256 (2)	26.1285 (1,2)	21.5441 (1,2)	21.0904 (1,2)
9.0	29	17.8466 (2)	24.7113 (1,2)	19.2910 (1,2)	18.9991 (1,2)
10.5	34	17.0418 (2)	24.2098 (1,2)	18.4030 (1,2)	18.1942 (1,2)
		Internal rings, e_r/h = - 6.2633			
L/R	Number of rings	Ref. 70 Sanders[c]	Present Study		
			Donnell	Sanders* Live pressure	Sanders Live pressure
3.0	9	65.0081 (3)	65.3831 (1,3)	62.4452 (1,3)	61.5725 (1,3)
4.5	14	54.2450 (2)	50.8856 (1,2)	53.2112 (1,3)	52.8178 (1,3)
6.0	19	33.2485 (2)	34.7730 (1,2)	32.9186 (1,2)	32.0360 (1,2)
7.5	24	26.2896 (2)	29.3944 (1,2)	25.4086 (1,2)	24.9420 (1,2)
9.0	29	23.4553 (2)	27.1795 (1,2)	22.3524 (1,2)	22.0576 (1,2)
10.5	34	22.1130 (2)	26.1162 (1,2)	20.8996 (1,2)	20.6930 (1,2)

[a] Number in parentheses indicate the number of circumferential waves, n
[b] Numbers in parentheses, (m,n), indicate the number of axial half-waves and circumferential waves, respectively
[c] The equations given in Ref. 70 appear to be a variant of Sanders' equations

* Nonlinear rotations about the normal are neglected

$\frac{A_r}{d_r h} = 0.16384$, $\frac{I_r^c}{d_r h^3} = 1.01152$, and $J_r = 0$

† $E = 30 \times 10^6$ psi, $\nu = 0.30$, R/h = 100, $(N+1)d_r/R = L/R$

Table 76. Critical loading parameter $\tilde{p}_{cr}$ for isotropic† cylinders with simply supported edges, subjected to uniform axial compression and pressure, and stiffened by internal blade-shaped rings and stringers

Cylinder configuration	Applied axial load, lbs/in.	Applied pressure, psi	Ref. 71 Flügge[a]	Present Study		
				Donnell	Sanders* Live pressure	Sanders Live pressure
1	700.0	0.	1.300 (15,9)[b]	1.307 (15,9)	1.304 (15,9)	1.303 (15,9)
	940.0	-2.0	1.003 (15,9)	1.008 (15,8)	1.006 (15,9)	1.005 (15,9)
	212.0	0.4	4.167 (14,9)	4.183 (15,9)	4.178 (15,9)	4.173 (14,9)
2	700.0	0.	1.255 (12,10)	1.266 (12,10)	1.263 (12,10)	1.261 (12,10)
	940.0	-2.0	1.001 (12,10)	1.012 (12,10)	1.008 (12,10)	1.006 (12,10)
	212.0	0.4	3.861 (1,5)	3.912 (11,10)	3.903 (11,10)	3.870 (1,5)

[a] Variant of Flugge's[28] equations based on the equations of Hedgepeth and Hall[60]

†$E = 10.0 \times 10^6$ psi, $\nu = 0.333$, R = 60.0 in., L = 165.0 in.

[b] Numbers in parentheses, (m,n), indicate the number of axial half-waves and circumferential waves, respectively

* Nonlinear rotations about the normal are neglected

Table 77. Cylinder wall and stiffener properties used in Table 76

Wall and stiffener properties, in.	Cylinder configuration	
	1	2
Wall thickness, h	0.0221	0.0229
Stringer thickness, t_l	0.0298	0.0513
Stringer height, h_l	0.347	0.351
Stringer spacing, d_s	0.849	0.986
Stringer eccentricity, e_s	- 0.1846	- 0.1870
Ring thickness, t_l	0.0092	0.0523
Ring height, h_l	1.93	0.906
Ring spacing, d_r	6.65	8.13
Ring eccentricity, e_r	- 0.9761	- 0.4645

Table 78. Nondimensional buckling coefficients $\frac{N_{xy}^{cr} R^2}{D}$ for isotropic ring-stiffened[#] cylinders with simply supported edges and subjected to uniform shear ($\nu = 0.30$)

L/R	R/h	External rings, $e_r/h = +1$			Internal rings, $e_r/h = -1$		
		Refs. 57 and 58 Donnell	Present Study Donnell	Percent differ-ence	Refs. 57 and 58 Donnell	Present Study Donnell	Percent differ-ence
0.4	100	1490(7)[a]	1652 (1,7,1.59)[b]	10.9	1226 (7)	1325 (1,7,1.52)	8.1
0.5	100	1336 (7)	1470 (1,7,1.56)	10.0	1093 (7)	1166 (1,7,1.53)	6.7
	250	2905 (10)	3185 (1,11,1.48)	9.6	2361 (10)	2494 (1,11,1.53)	5.6
	500	5475 (13)	6004 (1,15,1.42)	9.7	4519 (14)	4676 (1,15,1.52)	3.5
	1000	10320 (17)	11605 (1,20,1.29)	12.5	8810 (19)	9044 (1,20,1.47)	2.7
	2000	19140 (22)	22783 (1,28,1.23)	19.0	17590 (23)	17769 (1,29,1.48)	0.4
1.0	100	1114 (6)	1226 (1,7,1.46)	10.1	914.8 (6)	957.7 (1,7,1.53)	4.7
	250	2583 (9)	2901 (1,10,1.29)	12.3	2203 (10)	2261 (1,10,1.47)	2.6
	500	4786 (11)	5696 (1,14,1.23)	19.0	4412 (11)	4447 (1,14,1.45)	0.8
	1000	8695 (13)	11271 (1,19,1.09)	29.6	8441 (14)	8807 (1,20,1.45)	4.3
	2000	15500 (16)	22402 (1,26,.99)	44.5	15690 (17)	17542 (1,29,1.48)	11.8
1.5	100	1050 (6)	1171 (1,6,1.19)	11.5	896.1 (6)	918.1 (1,6,1.44)	2.5
	250	2370 (7)	2843 (1,10,1.24)	20.0	2188 (8)	2217 (1,10,1.46)	1.3
	500	4268 (9)	5631 (1,13,1.00)	31.9	4182 (10)	4402 (1,14,1.44)	5.3
	1000	7587 (11)	11192 (1,18,.93)	47.5	7738 (11)	8763 (1,20,1.45)	13.2
	2000	13310 (13)	22234 (1,18,.41)	67.0	13920 (14)	17499 (1,28,1.44)	25.7
2.0	100	982.7 (5)	1147 (1,6,1.13)	16.7	893.0 (5)	901.0 (1,6,1.41)	0.9
	250	2182 (7)	2822 (1,9,.95)	29.3	2110 (7)	2202 (1,10,1.45)	4.4
	500	3874 (8)	5600 (1,13,.99)	44.6	3931 (8)	4386 (1,14,1.44)	11.6
	1000	6817 (10)	11137 (1,13,.43)	63.4	7088 (10)	8747 (1,20,1.45)	23.4
	2000	11840 (12)	22027 (1,15,.24)	86.0	12550 (12)	17484 (1,28,1.44)	39.3
3.0	100	888.5 (4)	1129 (1,6,1.09)	26.7	864.0 (5)	888.6 (1,6,1.38)	2.8
	250	1914 (6)	2798 (1,9,.93)	46.2	1935 (6)	2191 (1,10,1.45)	13.2
	500	3337 (7)	5558 (1,9,.41)	66.6	3479 (7)	4375 (1,14,1.44)	25.8
	1000	5764 (8)	10993 (1,10,.25)	90.7	6133 (8)	8736 (1,20,1.45)	42.4
	2000	9941 (10)	21765 (1,12,.18)	118.9	10700 (10)	17472 (1,28,1.43)	63.3

[a] Numbers in parentheses indicate the number of circumferential waves, n
[b] (m,n, τ) indicate the number of axial half-waves, circumferential waves, and skewedness parameter, respectively
* Nonlinear rotations about the normal are neglected.

[#] $\frac{A_r}{d_r h} = 0.5$, $\frac{I_r^c}{d_r h^3} = 2$, and $J_r = 0$

Table 79. Nondimensional buckling coefficients $\frac{N_{xy}^{cr} R^2}{D}$ for isotropic ring-stiffened[#] cylinders with simply supported edges and subjected to uniform shear ($\nu = 0.30$)

L/R	R/h	External rings, $e_r/h = +5$			Internal rings, $e_r/h = -5$		
		Refs. 57 and 58 Donnell	Present Study Donnell	Percent difference	Refs. 57 and 58 Donnell	Present Study Donnell	Percent difference
0.35	100	3047 (5)[a]	3369 (1,5,2.87)[b]	10.6	1710 (5)	1855 (1,5,2.19)	8.5
0.4	100	2858 (5)	3149 (1,5,2.90)	10.2	1562 (5)	1687 (1,5,2.25)	8.0
0.5	100	2656 (5)	2893 (1,5,2.93)	8.9	1400 (5)	1492 (1,5,2.32)	6.6
	250	6233 (7)	6561 (1,8,2.93)	5.3	3100 (8)	3226 (1,8,2.41)	4.1
	500	12420 (10)	12621 (1,11,2.99)	1.6	5912 (11)	6088 (1,11,2.47)	3.0
	1000	24190 (13)	24715 (1,15,3.07)	2.2	11550 (15)	11837 (1,15,2.51)	2.5
	2000	45130 (17)	48948 (1,21,3.10)	8.5	23000 (21)	23323 (1,22,2.50)	1.4
1.0	100	2477 (5)	2552 (1,5,2.95)	3.0	1199 (5)	1237 (1,5,2.45)	3.2
	250	6058 (7)	6198 (1,7,3.26)	2.3	2921 (8)	2974 (1,8,2.47)	1.8
	500	11330 (8)	12261 (1,10,3.23)	8.2	5913 (10)	5831 (1,11,2.50)	-1.4
	1000	20510 (10)	24364 (1,15,3.07)	18.8	12460 (14)	11573 (1,15,2.52)	-7.1
	2000	36330 (13)	48595 (1,21,3.10)	33.8	30120 (18)	23066 (1,22,2.50)	-23.4
1.5	100	2451 (4)	2489 (1,5,2.96)	1.6	1163 (5)	1190 (1,5,2.47)	2.3
	250	5563 (6)	6130 (1,7,3.26)	10.2	2934 (7)	2927 (1,8,2.48)	-0.2
	500	10050 (7)	12194 (1,10,3.23)	21.3	6339 (10)	5783 (1,11,2.50)	-8.8
	1000	17780 (9)	24299 (1,15,3.07)	36.7	15760 (12)	11524 (1,15,2.53)	-26.9
	2000	31080 (11)	48530 (1,21,3.10)	56.1	32050 (12)	23018 (1,22,2.50)	-28.2
2.0	100	2317 (4)	2467 (1,5,2.96)	6.5	1150 (5)	1173 (1,5,2.48)	2.0
	250	5128 (5)	6106 (1,7,3.26)	19.1	3114 (7)	2911 (1,8,2.49)	-6.5
	500	9152 (6)	12170 (1,10,3.23)	33.0	7867 (8)	5766 (1,11,2.50)	-26.7
	1000	15910 (8)	24276 (1,15,3.07)	52.6	16180 (9)	11507 (1,15,2.53)	-28.9
	2000	27670 (10)	48465 (1,10,.24)	75.2	30220 (10)	23002 (1,22,2.50)	-23.9
3.0	100	2125 (3)	2451 (1,5,2.96)	15.3	1336 (4)	1162 (11,5,2.49)	-13.0
	250	4524 (4)	6090 (1,7,3.26)	34.6	3740 (6)	2899 (1,8,2.49)	-22.5
	500	7847 (5)	12153 (1,10,3.23)	54.9	8014 (6)	5755 (1,11,2.50)	-28.2
	1000	13530 (7)	24139 (1,7,.24)	78.4	14880 (7)	11495 (1,15,2.53)	-22.7
	2000	23090 (8)	47000 (1,8,.16)	103.6	26740 (8)	22990 (1,22,2.50)	-14.0

[a] Numbers in parentheses indicate the number of circumferential waves, n
[b] (m,n, τ) indicate the number of axial half-waves, circumferential waves, and skewedness parameter, respectively
* Nonlinear rotations about the normal are neglected

[#] $\frac{A_r}{d_r h} = 0.5$, $\frac{I_r^c}{d_r h^3} = 2$, and $J_r = 0$

Table 80. Nondimensional buckling coefficients $\frac{N_{xy}^{cr} R^2}{D}$ for isotropic ring-stiffened[#] cylinders with simply supported edges and subjected to uniform shear ($\nu = 0.30$)

L/R	R/h	External rings, $e_r/h = +1$			Internal rings, $e_r/h = -1$		
		Refs. 57 and 58 Donnell	Present Study Donnell	Percent difference	Refs. 57 and 58 Donnell	Present Study Donnell	Percent difference
0.4	100	1863 (6)[a]	2045 (1,6,2.06)[b]	9.8	1595 (6)	1729 (1,6,1.96)	8.4
0.5	100	1699 (6)	1843 (1,6,2.07)	8.5	1444 (6)	1543 (1,6,1.98)	6.9
	250	3835 (9)	4066 (1,9,2.09)	6.0	3217 (9)	3361 (1,9,2.03)	4.5
	500	7458 (12)	7761 (1,13,2.06)	4.1	6236 (12)	6386 (1,13,2.03)	2.4
	1000	15070 (17)	15141 (1,18,2.05)	0.5	12350 (17)	12425 (1,18,2.03)	0.6
	2000	28800 (20)	29915 (1,25,2.04)	3.9	25310 (23)	24520 (1,25,2.03)	-3.1
1.0	100	1522 (5)	1575 (1,6,2.05)	3.5	1268 (6)	1299 (1,6,2.02)	2.4
	250	3720 (8)	3785 (1,9,2.05)	1.7	3096 (9)	3106 (1,9,2.03)	0.3
	500	7199 (10)	7485 (1,13,2.03)	4.0	6357 (12)	6136 (1,13,2.03)	-3.5
	1000	13510 (12)	14858 (1,18,2.03)	10.0	12940 (13)	12171 (1,18,2.03)	-5.9
	2000	24670 (15)	29626 (1,25,2.03)	20.1	24450 (15)	24261 (1,25,2.03)	-0.8
1.5	100	1490 (5)	1526 (1,6,2.04)	2.4	1254 (6)	1254 (1,6,2.02)	0.0
	250	3571 (7)	3733 (1,9,2.04)	4.5	3256 (8)	3059 (1,9,2.03)	-6.1
	500	6674 (8)	7433 (1,13,2.03)	11.4	6430 (9)	6090 (1,13,2.03)	-5.3
	1000	12100 (10)	14806 (1,18,2.03)	22.4	12090 (10)	12124 (1,18,2.03)	0.3
	2000	21530 (12)	29573 (1,25,2.03)	37.4	21980 (12)	24212 (1,25,2.03)	10.2
2.0	100	1478 (5)	1508 (1,6,2.03)	2.0	1263 (5)	1238 (1,6,2.03)	-2.0
	250	3378 (6)	3715 (1,9,2.03)	10.0	3246 (6)	3043 (1,9,2.03)	-6.3
	500	6171 (7)	7415 (1,13,2.03)	20.2	6131 (8)	6074 (1,13,2.03)	-0.9
	1000	11010 (9)	14787 (1,18,2.03)	34.3	11180 (9)	12107 (1,18,2.03)	8.3
	2000	19370 (11)	29554 (1,25,2,03)	52.6	19990 (11)	24196 (1,25,2.03)	21.0
3.0	100	1368 (4)	1496 (1,6,2.03)	9.4	1301 (4)	1227 (1,6,2.03)	-5.7
	250	3025 (5)	3701 (1,9,2.03)	22.3	3022 (5)	3031 (1,9,2.03)	0.3
	500	5382 (6)	7403 (1,13,2.03)	37.6	5495 (6)	6063 (1,13,2.03)	10.3
	1000	9445 (7)	14774 (1,18,2.03)	56.4	9791 (7)	12095 (1,18,2.03)	23.5
	2000	16390 (9)	29541 (1,25,2.02)	80.2	17140 (9)	24,184 (1,25,2.03)	41.1

[a] Numbers in parentheses indicate the number of circumferential waves, n
[b] (m,n, τ) indicate the number of axial half-waves, circumferential waves, and skewedness parameter, respectively
* Nonlinear rotations about the normal are neglected

[#] $\frac{A_r}{d_r h} = 0.5$, $\frac{I_r^c}{d_r h^3} = 5$, and $J_r = 0$

Table 81. Nondimensional buckling coefficients $\frac{N_{xy}^{cr} R^2}{D}$ for isotropic ring-stiffened[#] cylinders with simply supported edges and subjected to uniform shear (ν = 0.30)

L/R	R/h	External rings, $e_r/h = +5$			Internal rings, $e_r/h = -5$		
		Refs. 57 and 58 Donnell	Present Study Donnell	Percent difference	Refs. 57 and 58 Donnell	Present Study Donnell	Percent difference
0.35	100	3196 (5)[a]	3509 (1,5,2.96)[b]	9.8	1887 (5)	2036 (1,5,2.34)	7.9
0.4	100	3010(5)	3288 (1,5,2.99)	9.2	1737 (5)	1863 (1,5,2.40)	7.3
0.5	100	2808 (5)	3030 (1,5,3.04)	7.9	1568 (5)	1663 (1,5,2.48)	6.1
	250	6522 (7)	6806 (1,7,3.34)	4.4	3441 (7)	3615 (1,7,2.69)	5.1
	500	12890 (10)	13123 (1,10,3.34)	1.8	6614 (10)	6830 (1,10,2.72)	3.3
	1000	26680 (13)	25759 (1,14,3.37)	-3.5	13010 (14)	13256 (1,15,2.68)	1.9
	2000	50670 (16)	51033 (1,20,3.35)	0.7	25880 (20)	26117 (1,21,2.70)	0.9
1.0	100	2613 (4)	2686 (1,4,3.66)	2.8	1361 (5)	1399 (1,5,2.62)	2.8
	250	6682 (7)	6440 (1,7,3.37)	-3.6	3245 (7)	3328 (1,7,2.75)	2.6
	500	12670 (8)	12758 (1,10,3.35)	0.7	6469 (10)	6545 (1,10,2.75)	1.2
	1000	23290 (10)	25392 (1,14,3.38)	9.0	14180 (14)	12983 (1,15,2.70)	-8.4
	2000	41890 (13)	50669 (1,20,3.35)	21.0	33200 (18)	25843 (1,21,2.71)	-22.2
1.5	100	2601 (4)	2613 (1,4,3.68)	0.5	1321 (5)	1350 (1,5,2.65)	2.2
	250	6286 (6)	6372 (1,7,3.38)	1.4	3264 (7)	3275 (1,7,2.76)	0.3
	500	11450 (7)	12691 (1,10,3.35)	10.8	7280 (10)	6493 (1,10,2.75)	-10.8
	1000	20540 (9)	25325 (1,14,3.38)	23.3	16280 (13)	12933 (1,15,2.70)	-20.6
	2000	36180 (11)	50602 (1,20,3.35)	39.9	36630 (12)	25792 (1,21,2.71)	-29.6
2.0	100	2605 (4)	2588 (1,4,3.68)	-0.7	1347 (5)	1333 (1,5,2.66)	-1.0
	250	5823 (5)	6348 (1,7,3.38)	9.0	3545 (7)	3256 (1,7,2.76)	-8.2
	500	10470 (6)	12667 (1,10,3.35)	21.0	9304 (8)	6474 (1,10,2.75)	-30.4
	1000	18510 (8)	25301 (1,14,3.38)	36.7	18370 (10)	12915 (1,15,2.70)	-29.7
	2000	32190 (9)	50578 (1,20,3.35)	57.1	34550 (10)	25774 (1,21,2.71)	-25.4
3.0	100	2390 (3)	2570 (1,4,3.69)	7.5	1423 (4)	1320 (1,5,2.66)	-7.2
	250	5166 (4)	6331 (1,7,3.38)	22.6	4098 (6)	3243 (1,7,2.77)	-20.9
	500	9051 (5)	12650 (1,10,3.35)	39.8	9158 (6)	6461 (1,10,2.76)	-29.4
	1000	15780 (6)	25284 (1,14,3.38)	60.2	17040 (7)	12903 (1,15,2.70)	-24.3
	2000	27130 (8)	50561 (1,20,3.35)	86.4	30610 (8)	25761 (1,21,2.71)	-15.8

[a] Numbers in parentheses indicate the number of circumferential waves, n
[b] (m,n, τ) indicate the number of axial half-waves, circumferential waves, and skewedness parameter, respectively
* Nonlinear rotations about the normal are neglected

[#] $\frac{A_r}{d_r h} = 0.5$, $\frac{I_r^c}{d_r h^3} = 5$, and $J_r = 0$

Table 82. Nondimensional buckling coefficients $\frac{N_{xy}^{cr} R^2}{D}$ for isotropic ring-stiffened[#] cylinders with simply supported edges and subjected to uniform shear (ν = 0.30, R/h = 1000)

L/R	e_r/h	External rings			Internal rings		
		Refs. 57 and 58 Donnell	Present Study Donnell	Percent differ-ence	Refs. 57 and 58 Donnell	Present Study Donnell	Percent differ-ence
1.0	1	13510 (12)[a]	14858 (1,18,2.03)[b]	10.0	12940 (13)	12171 (1,18,2.03)	-5.9
	3	17330 (11)	19914 (1,16,2.60)	14.9	13650 (14)	11998 (1,16,2.34)	-12.1
	5	23290 (10)	25392 (1,14,3.38)	9.0	14180 (14)	12983 (1,15,2.70)	-8.4
	8	34750 (9)	32731 (1,11,4.64)	-5.8	16820 (12)	15043 (1,13,3.25)	-10.6
3.0	1	9445 (7)	14774 (1,18,2.03)	56.4	9791 (7)	12095 (1,18,2.03)	23.5
	3	11730 (7)	19818 (1,16,2.59)	69.0	12650 (7)	11920 (1,16,2.34)	-5.8
	5	15780 (6)	25284 (1,14,3.38)	60.2	17040 (7)	12903 (1,15,2.70)	-24.3
	8	23630 (6)	32596 (1,11,4.65)	37.9	25050 (6)	14951 (1,13,3.26)	-40.3

[a] Numbers in parentheses indicate the number of circumferential waves, n
[b] (m,n, τ) indicate the number of axial half-waves, circumferential waves, and skewedness parameter, respectively
* Nonlinear rotations about the normal are neglected

[#] $\frac{A_r}{d_r h} = 0.5$, $\frac{I_r^c}{d_r h^3} = 5$, and $J_r = 0$

Table 83. Nondimensional buckling coefficients $\frac{N_{xy}^{cr} R^2}{D}$ for isotropic ring-stiffened[#] cylinders with simply supported edges and subjected to uniform shear (ν = 0.30, R/h = 1000)

L/R	$A_r/(d_r h)$	External rings, $e_r/h = +5$			Internal rings, $e_r/h = -5$		
		Refs. 57 and 58 Donnell	Present Study Donnell	Percent differ-ence	Refs. 57 and 58 Donnell	Present Study Donnell	Percent differ-ence
1.0	0.1	15890 (12)[a]	15220 (1,16,2.54)[b]	-4.2	13090 (15)	12287 (1,16,2.40)	-5.1
	0.5	23290 (10)	25392 (1,14,3.38)	9.0	14180 (14)	12983 (1,15,2.70)	-8.4
	1.0	28250 (10)	35287 (1,13,3.95)	24.9	14550 (13)	13236 (1,14,2.86)	-9.0
	1.5	31030 (9)	40978 (1,9,.50)	32.1	14750 (13)	13394 (1,14,2.92)	-9.2
3.0	0.1	11280 (7)	15136 (1,16,2.54)	34.2	11710 (7)	12209 (1,16,2.40)	4.3
	0.5	15780 (6)	25284 (1,14,3.38)	60.2	17040 (7)	12903 (1,15,2.70)	-24.3
	1.0	18360 (6)	31999 (1,6,.22)	74.3	20110 (7)	13151 (1,14,2.87)	-34.6
	1.5	19810 (6)	34747 (1,6,.23)	75.4	21740 (7)	13310 (1,14,2.93)	-38.8

[a] Number in parentheses indicate the number of circumferential waves, n
[b] (m,n, τ) indicate the number of axial half-waves, circumferential waves, and skewedness parameter, respectively
* Nonlinear rotations about the normal are neglected

[#] $\frac{I_r^c}{d_r h^3} = 5$ and $J_r = 0$

Table 84. Nondimensional buckling coefficients $\frac{N_{xy}^{cr} R^2}{D}$ for isotropic ring-stiffened[#] cylinders with simply supported edges and subjected to uniform shear ($\nu = 0.30$, $R/h = 1000$)

L/R	$I_r/(d_r h^3)$	External rings, $e_r/h = +5$			Internal rings, $e_r/h = -5$		
		Refs. 57 and 58 Donnell	Present Study Donnell	Percent difference	Refs. 57 and 58 Donnell	Present Study Donnell	Percent difference
1.0	1	19400 (11)[a]	23961 (1,15,3.02)[b]	23.5	11850 (15)	11073 (1,16,2.42)	-6.6
	2	20510 (10)	24364 (1,15,3.07)	18.8	12460 (14)	11573 (1,15,2.52)	-7.1
	3	21520 (10)	24752 (1,14,3.30)	15.0	13030 (14)	12054 (1,15,2.59)	-7.5
	5	23290 (10)	25392 (1,14,3.38)	9.0	14180 (14)	12983 (1,15,2.70)	-8.4
	8	26020 (10)	26311 (1,13,3.68)	1.1	15640 (13)	14156 (1,14,2.91)	-9.5
	10	27620 (10)	26809 (1,13,3.73)	-2.9	16560 (13)	14883 (1,14,2.99)	-10.1
3.0	1	12670 (7)	22979 (1,7,.22)	81.4	14090 (7)	11000 (1,16,2.42)	-21.9
	2	13530 (7)	24139 (1,7,.24)	78.4	14880 (7)	11495 (1,15,2.53)	-22.7
	3	14360 (7)	24644 (1,14,3.30)	71.6	15640 (7)	11975 (1,15,2.59)	-23.4
	5	15780 (6)	25284 (1,14,3.38)	60.2	17040 (7)	12903 (1,15,2.70)	-24.3
	8	17860 (6)	26197 (1,13,3.68)	46.7	19140 (7)	14069 (1,14,2.91)	-26.5
	10	19150 (6)	26694 (1,13,3.73)	39.5	20400 (6)	14794 (1,14,2.99)	-27.5

[a] Numbers in parentheses indicate the number of circumferential waves, n
[b] Numbers in parentheses, (m,n, τ), indicate the number of axial half-waves, circumferential waves, and skewedness parameter, respectively
* Nonlinear rotations about the normal are neglected

[#] $\frac{A_r}{d_r h} = 0.5$ and $J_r = 0$

Table 85. Nondimensional buckling coefficients $\frac{N_{xy}^{cr} R^2}{D}$ for isotropic stringer-stiffened[#] cylinders with simply supported edges and subjected to uniform shear ($\nu = 0.30$)

L/R	R/h	External stringers, $e_s/h = +5$			Internal stringers, $e_s/h = -5$		
		Refs. 57 and 58 Donnell	Present Study Donnell	Percent differ-ence	Refs. 57 and 58 Donnell	Present Study Donnell	Percent differ-ence
0.5	100	6556 (22)[a]	7360 (1,22,.16)[b]	12.3	6215 (20)	7035 (1,21,.16)	13.2
0.7	100	3102 (14)	3846 (1,16,.16)	24.0	3435 (16)	3528 (1,15,.15)	2.7
1.0	100	1782 (12)	1981 (1,12,.15)	11.2	1470 (10)	1687 (1,10,.15)	14.8
	1000	3255 (19)	3798 (1,20,.13)	16.7	2049 (17)	3001 (1,17,.12)	46.5
1.5	100	898.4 (9)	990.8 (1,9,.15)	10.3	650.3 (7)	770.3 (1,7,.15)	18.5
3.0	100	346.8 (6)	403.5 (1,6,.13)	16.3	222.8 (5)	316.7 (1,6,.13)	42.1
	1000	1204 (12)	2242 (1,14,.09)	86.2	872.8 (12)	2141 (1,13,.08)	145.3

[a] Numbers in parentheses indicate the number of circumferential waves, n

[b] Numbers in parentheses, (m,n, τ), indicate the number of axial half-waves, circumferential waves, and skewedness parameter, respectively

* Nonlinear rotations about the normal are neglected

[#] $\frac{A_s}{d_s h} = 0.5$, $\frac{I_s^c}{d_s h^3} = 5$, and $J_s = 0$

Table 86. Nondimensional buckling coefficients $\frac{N_{xy}^{cr} R^2}{D}$ for isotropic ring-and-stringer-stiffened[#] cylinders with simply supported edges and subjected to uniform shear ($\nu = 0.30$)

L/R	R/h	External stringers, $e_s/h = +5$ External rings, $e_r/h = +5$			Internal stringers, $e_s/h = -5$ Internal rings, $e_r/h = -5$		
		Refs. 57 and 58 Donnell	Present Study Donnell	Percent difference	Refs. 57 and 58 Donnell	Present Study Donnell	Percent difference
1.0	100	5980 (4)[a]	9266 (1,5,.60)[b]	54.9	8072 (4)	6489 (1,4,.56)	-19.6
	1000	23170 (9)	36731 (1,10,.49)	58.5	32060 (9)	26289 (1,10,.57)	-18.0
3.0	100	2352 (3)	3790 (1,3,.47)	61.1	3280 (3)	2675 (1,3,.55)	-18.4
	1000	17550 (7)	28299 (1,7,.27)	61.2	19230 (6)	22841 (1,9,.52)	18.8
		External stringers, $e_s/h = +5$ Internal rings, $e_r/h = -5$			Internal stringers, $e_s/h = -5$ External rings, $e_r/h = +5$		
1.0	100	6446(4)	7062 (1,4,.60)	9.6	6281 (4)	7143 (1,4,.54)	13.7
	1000	25180 (10)	28402 (1,10,.59)	12.8	26990 (10)	32262 (1,9,.42)	19.5
3.0	100	2578 (3)	2948 (1,3,.57)	14.4	2756 (3)	3262 (1,3,.45)	18.4
	1000	16940 (7)	23198 (1,9,.52)	36.9	19600 (7)	27430 (1,7,.27)	39.9

[a] Numbers in parentheses indicate the number of circumferential waves, n
[b] Numbers in parentheses, (m,n, τ), indicate the number of axial half-waves, circumferential waves, and skewedness parameter, respectively
* Nonlinear rotations about the normal are neglected.

[#] $\frac{A_s}{d_s h} = \frac{A_r}{d_r h} = 0.5$, $\frac{I_s^c}{d_s h^3} = \frac{I_r^c}{d_r h^3} = 5$, and $J_s = J_r = 0$

Table 87. Nondimensional buckling loads $\frac{N_x^{cr}}{E_y h} \frac{R_2}{R_1} \left(\frac{R_2}{R_1} - 1 \right)^{-1}$ for specially orthotropic[†] cylinders with simply supported edges and subjected to axial compression ($L/R_2 = 5$)

R_2 / R_1[a]	R/h	Ref. 73[c]	Ref. 72 Timoshenko	Present study		
				Donnell	Sanders*	Sanders
1.01	100.5	0.7971 (20,9)[b]	0.7895 (20,9)	0.8024 (20,9)	0.7970 (20,9)	0.7945 (20,9)
1.02	50.5	0.7957 (13,6)	0.7786 (13,6)	0.8063 (14,6)	0.7956 (13,6)	0.7897 (13,6)
1.04	25.5	0.8049 (8,4)	0.6811 (1,2)	0.8270 (9,4)	0.8044 (8,4)	0.7038 (1,2)
1.05	20.5	0.7904 (9,4)	0.6735 (1,2)	0.8168 (9,4)	0.7899 (9,4)	0.6949 (1,2)

[a] R_2 = outer radius, R_1 = inner radius
[b] Numbers in parentheses, (m,n), indicate the number of axial half-waves and circumferential waves, respectively
[c] Nonshallow shell equations given in reference 17 (pp. 157-159), which neglect rotations about the normal
* Nonlinear rotations about the normal are neglected

[†] $E_1 = 14$ GPa, $E_2 = 57$ Gpa, $G_{12} = 5.7$ GPa, and $\nu_{21} = 0.277$

Table 88. Nondimensional buckling loads $\frac{N_x^{cr} L^2}{\pi^2 D_{11}}$ for antisymmetric cross-ply cylinders[c] with simply supported edges and subjected to axial compression.

Length, in.	Lay up[†]	Ref. 74, Donnell	Ref. 73, Donnell	Present study		
				Donnell	Sanders*	Sanders
1.00	(90/0)	0.3605 (1,10)[b]	0.35636	.35775 (1,10)	.35770 (1,10)	.35761 (1,10)
	$(90/0)_2$	0.8745 (1,9)	0.87041	.87293 (1,9)	.87278 (1,9)	.87188 (1,9)
	$(90/0)_3$	0.9694 (1,9)		0.96829 (1,9)	0.96809 (1,9)	0.96685 (1,9)
	$(90/0)_\infty$	1.045 (1,9)	1.0408	1.0449 (1,9)	1.0446 (1,9)	1.0427 (1,9)
3.16	(90/0)		0.90101	.96149 (1,8)	.95858 (1,8)	.95689 (1,8)
	$(90/0)_2$		1.5857	1.6604 (1,7)	1.6527 (1,7)	1.6467 (1,7)
	$(90/0)_\infty$		1.7982	1.8747 (1,7)	1.8636 (1,7)	1.8549 (1,7)
10.00	(90/0)		8.7406	9.4671 (3,8)	9.4340 (3,8)	9.4171 (3,8)
	$(90/0)_2$		13.310	14.356 (2,6)	14.217 (2,6)	14.135 (2,6)
	$(90/0)_\infty$		14.567	15.614 (2,6)	15.421 (2,6)	15.316 (2,6)
31.63	(90/0)		86.153	92.683 (8,8)	92.191 (8,8)	92.017 (8,8)
	$(90/0)_2$		132.84	143.41 (6,6)	141.85 (6,6)	141.03 (6,6)
	$(90/0)_\infty$		145.37	155.92 (6,6)	153.78 (6,6)	152.73 (6,6)

[b] Numbers in parentheses, (m,n), indicate the number of axial half-waves and circumferential waves, respectively

[c] R = 10.0 in., h = 0.10 in

[†] $E_1 = 30 \times 10^6$ psi, $E_2 = 0.75 \times 10^6$ psi, $G_{12} = 0.375 \times 10^6$ psi, $\nu_{12} = 0.25$

* Nonlinear rotations about the normal are neglected

Table 89. Nondimensional buckling loads $\frac{N_x^{cr}L^2}{E_2h^3}$ for unsymmetric cross-ply cylinders[c] with simply supported edges and subjected to axial compression

Lay up[†]	Ref. 74, Donnell	Present study		
		Donnell	Sanders*	Sanders
(0/90/0)	32.359 (1,10)[b]	32.359 (1,10)	32.356 (1,10)	32.308 (1,10)
$(0/90/0_2)$	30.967 (1,10)	30.967 (1,10)	30.965 (1,10)	30.940 (1,10)
$(0/90/0_4)$	28.426 (1,10)	28.426 (1,10)	28.425 (1,10)	28.411 (1,9)
$(0/90/0_8)$	28.030 (1,8)	28.031 (1,8)	28.030 (1,8)	28.021 (1,8)
$(0/90/0_{18})$	29.557 (1,6)	29.557 (1,6)	29.557 (1,6)	29.552 (1,6)
$(0/90/0_{48})$	31.389 (1,1)	31.389 (1,0)	31.389 (1,0)	31.389 (1,0)

[b] Numbers in parentheses, (m,n), indicate the number of axial half-waves and circumferential waves, respectively

[c] R = 10.0 in., h = 0.10 in., and L = 1. in.

[†] $E_1 = 30 \times 10^6$ psi, $E_2 = 0.75 \times 10^6$ psi, $G_{12} = 0.375 \times 10^6$ psi, $\nu_{12} = 0.25$

* Nonlinear rotations about the normal are neglected

Table 90. Nondimensional buckling loads $\frac{N_x^{cr}L^2}{E_2h^3}$ for unsymmetric cross-ply cylinders[c] with simply supported edges and subjected to axial compression

Lay up[†]	Ref. 73, Donnell	Ref. 76, Donnell	Present study		
			Donnell	Sanders*	Sanders
(0)	1482.0	1481.75 (3,7)[b]	1482.0 (3,7)	1466.4 (3,7)	1458.8 (3,7)
(0/90/0)	1859.8	1853.96 (3,6)	1859.9 (3,6)	1833.0 (3,6)	1818.4 (3,6)
$(0_8/90/0)$	1987.2	1984.18 (4,7)	1987.2 (4,7)	1958.2 (4,7)	1943.6 (4,7)
$(0_{18}/90/0)$	2061.8	2050.42 (4,7)	2061.8 (4,7)	2031.3 (4,7)	2016.9 (4,7)
$(0_{48}/90/0)$	1957.4	1950.19 (4,7)	1957.4 (4,7)	1932.8 (4,7)	1917.5 (3,6)

[b] Numbers in parentheses, (m,n), indicate the number of axial half-waves and circumferential waves, respectively

[c] R = 10.0 in., h = 0.12 in., and L = 34.64 in.

[†] $E_1 = 30 \times 10^6$ psi, $E_2 = 0.75 \times 10^6$ psi, $G_{12} = 0.375 \times 10^6$ psi, $\nu_{12} = 0.25$

* Nonlinear rotations about the normal are neglected

Table 91. Nondimensional buckling loads $\frac{N_x^{cr} L^2}{E_2 h^3}$ for cross-ply cylinders with simply supported edges and subjected to axial compression (L/R = 1, R/ h = 10)

Lay up†	Ref. 77, Donnell	Present study		
		Donnell	Sanders*	Sanders
(0/90)	18.17	16.86 (1,3)[b]	15.17 (1,3)	14.38 (1,3)
(0/90/0)	41.86	40.57 (1,3)	39.96 (1,3)	38.91 (1,3)
$(0/90)_5$	33.95	31.66 (1,2)	30.15 (1,2)	28.39 (1,2)

[b] Numbers in parentheses, (m,n), indicate the number of axial half-waves and circumferential waves, respectively

† $E_1 = 30 \times 10^6$ psi, $E_2 = 0.75 \times 10^6$ psi, $G_{12} = 0.375 \times 10^6$ psi, $\nu_{12} = 0.25$

* Nonlinear rotations about the normal are neglected

Table 92. Nondimensional buckling loads $\frac{N_x^{cr} L^2}{E_2 h^3}$ for cross-ply cylinders with simply supported edges and subjected to axial compression (L/R = 2, R/ h = 40)

Lay up†	Ref. 78, Donnell	Present study		
		Donnell	Sanders*	Sanders
(0/90)	186.63 (6)	186.63 (4,6)	182.39 (4,6)	180.05 (4,6)
(0/90/0)	205.07 (6)	205.07 (2,6)	200.53 (2,6)	198.52 (2,6)

[b] Numbers in parentheses, (m,n), indicate the number of axial half-waves and circumferential waves, respectively

† $E_1 = 30 \times 10^6$ psi, $E_2 = 0.75 \times 10^6$ psi, $G_{12} = 0.375 \times 10^6$ psi, $\nu_{12} = 0.25$

* Nonlinear rotations about the normal are neglected

Table 93. Nondimensional buckling loads $\frac{N_x^{cr} L^2}{A_{22} h^2}$ for antisymmetric [90/0]† cross-ply cylinders with simply supported edges and subjected to axial compression

Length, in.	Radius, in.	Ref. 79, Donnell	Present study		
			Donnell	Sanders*	Sanders
5.0	10.0	1.964 (1,7)[b]	1.964 (1,7)	1.952 (1,7)	1.946 (1,7)
2.5	5.0	0.966 (1,6)	0.966 (1,6)	0.957 (1,6)	0.954 (1,6)
1.0	2.0	0.484 (1,4)	0.484 (1,4)	0.480 (1,4)	0.478 (1,4)
0.5	1.0	0.357 (1,3)	0.357 (1,3)	0.355 (1,3)	0.353 (1,3)
10.0	10.0	10.317 (3,6)	7.786 (3,8)	7.759 (3,8)	7.745 (3,8)
5.0	5.0	4.468 (2,5)	3.864 (2,6)	3.827 (2,6)	3.816 (2,6)
2.0	2.0	1.595 (1,3)	1.595 (1,3)	1.565 (1,3)	1.538 (1,3)
1.0	1.0	0.821 (1,3)	0.821 (1,3)	0.785 (1,3)	0.778 (1,3)

[b] Numbers in parentheses, (m,n), indicate the number of axial half-waves and circumferential waves, respectively

† $E_1 = 30 \times 10^6$ psi, $E_2 = 0.75 \times 10^6$ psi, $G_{12} = 0.375 \times 10^6$ psi, $\nu_{12} = 0.25$, and h = 0.10 in.

* Nonlinear rotations about the normal are neglected

Table 94. Buckling loads N_x^{cr} (lb/in) for unidirectional laminated cylinders with simply supported edges and subjected to axial compression.

Fiber angle, degrees†	Radius, R (in.)	L/R	Ref. 80, Donnell	Present study		
				Donnell	Sanders*	Sanders
0	4.0	2	231 (11)[a]	231.6 (4,11)[b]	230.6 (4,11)	230.1 (4,11)
0	4.0	5	229 (10)	229.8 (9,10)	228.7 (9,10)	228.2 (9,10)
0	4.0	10	229 (10)	229.7 (17,10)	228.6 (17,10)	228.0 (17,10)
90	4.0	1	229 (10)	229.8 (6,10)	228.7 (6,10)	228.2 (6,10)
90	4.0	2	229 (10)	229.8 (12,10)	228.7 (12,10)	228.2 (12,10)
0	7.5	2	123 (14)	122.3 (5,14)	122.0 (5,14)	121.9 (5,14)
0	7.5	5	123 (14)	122.3 (12,14)	122.0 (12,14)	121.8 (12,14)
90	7.5	1	122 (14)	122.3 (8,14)	122.0 (8,14)	121.8 (8,14)
90	7.5	2	123 (14)	122.3 (16,14)	122.0 (16,14)	121.8 (16,14)

[a] Number in parentheses, (n) indicate the number of circumferential waves, n

[b] Numbers in parentheses, (m,n), indicate the number of axial half-waves and circumferential waves, respectively

† $E_1 = 30 \times 10^6$ psi, $E_2 = 2.7 \times 10^6$ psi, $G_{12} = 0.65 \times 10^6$ psi, $\nu_{12} = 0.21$, and h = 0.0212 in.

* Nonlinear rotations about the normal are neglected

Table 95. Buckling loads (N/mm) for unsymmetrically laminated cylinders[#] with simply supported edges, and subjected to axial compression

Lay up[†]	Ref. 81, Donnell	Ref. 82, Donnell	Ref. 82, Sanders[@]	Ref. 83, Refined theory	Present study		
					Donnell	Sanders*	Sanders
$(0_2/\pm19/\pm37/\pm45/\pm51)$	114.5 (1,7)	114.6	108.2		114.8 (1,7)	112.3 (1,7)	110.15 (1,7)
$(\pm60/0_2/\pm68/\pm52/\pm37)$				174.6	183.8 (16,6)	180.0 (1,6)	175.7 (1,6)
$(\mp60/0_2/\mp68/\mp52/\mp37)$		184.0	173.2		183.8 (16,6)	180.0 (1,6)	175.7 (1,6)
$(\mp37/\mp52/\mp68/0_2/\mp60)$		143.9	139.4		143.7 (17,0)	143.7 (17,0)	141.5 (1,6)
$(\mp38/\mp68/90_2/\mp8/\mp53)$		163.6	153.4		163.3 (1,6)	159.1 (1,6)	155.2 (1,6)
$(\pm30/90_2/\pm22/\pm38/\pm53)$				174.6	183.8 (4,11)	180.0 (1,6)	175.6 (1,6)
$(\mp30/90_2/\mp22/\mp38/\mp53)$		184.0	174.4		183.8 (4,11)	180.0 (1,6)	175.6 (1,6)
$(\mp51/\mp45/\mp37/\mp19/0_2)$	62.54 (13,0)	62.39	62.39	62.52	62.72 (13,0)	62.72 (13,0)	62.72 (13,0)

[b] Numbers in parentheses, (m,n), indicate the number of axial half-waves and circumferential waves, respectively

[†] E_1 =123,550 MPa, E_2 = 8,708 MPa, G_{12} = 5,695 MPa, ν_{12} = 0.32

* Nonlinear rotations about the normal are neglected

[#] L = 510 mm, R = 250 mm, and h = 1.25 mm

[@] B_{16}, B_{26}, D_{16}, D_{26} included in the analysis; A_{16}, A_{26}, B_{16}, B_{26}, D_{16}, D_{26} neglected otherwise

Table 96 Buckling loads N_x^{cr} (lbs/in.) for (0/-θ/+θ) and (90/-θ/+θ) three-ply glass-epoxy cylinders[#] with simply supported edges and subjected to axial compression

(0/-θ/+θ)[†] cylinders				
Fiber angle, deg	Ref. 84, Donnell	Present study		
		Donnell	Sanders*	Sanders
0	492.52 (6,11,.000)[b]	491.60 (6,11,.000)	489.72 (6,11,.000)	488.70 (6,11,.000)
10	499.17 (6,11,-.085)	500.69 (6,11,-.008)	498.80 (6,11,-.008)	497.74 (6,11,-.008)
20	516.45 (7,12,-.006)	520.08 (7,12,.007)	518.31 (7,12,.006)	517.25 (6,12,.017)
30	534.73 (6,12,.083)	540.96 (6,12,.028)	538.55 (6,12,.027)	537.27 (6,12,.027)
40	542.00 (6,12,.122)	551.71 (6,12,.023)	549.03 (6,12,.022)	547.52 (6,12,.022)
50	536.68 (6,12,.091)	546.98 (6,12,-.002)	544.01 (6,12,-.003)	541.82 (5,11,-.021)
60	521.19 (7,12,.102)	528.83 (5,11,-.049)	525.28 (5,11,-.048)	523.02 (5,11,-.048)
70	502.47 (7,12,.048)	507.37 (7,12,-.031)	504.75 (7,12,-.031)	502.66 (5,11,-.062)
80	487.52 (6,11,-.001)	488.39 (6,11,-.033)	485.50 (6,11,-.033)	483.78 (6,11,-.033)
90	482.96 (6,11,.000)	480.82 (6,11,.000)	477.91 (6,11,.000)	472.22 (6,11,.000)
(90/-θ/+θ)[†] cylinders				
Fiber angle, deg	Ref. 84, Donnell	Present study		
		Donnell	Sanders*	Sanders
0	481.69 (8,11,.000)[b]	481.00 (8,11,.000)	479.80 (8,11,.000)	479.23 (8,11,.000)
10	485.96 (8,11,-.189)	485.34 (1,11,-1.212)	484.24 (1,11,-1.209)	483.77 (1,11,-1.208)
20	500.81 (8,11,-.314)	501.87 (1,11,-1.263)	500.73 (1,11,-1.261)	500.26 (1,11,-1.260)
30	522.24 (10,12,-.007)	525.35 (1,12,1.341)	524.72 (1,12,1.338)	524.44 (1,12,1.337)
40	536.89 (10,12,.161)	528.09(1,12,1.437)	527.52 (1,12,1.435)	527.26 (1,12,1.434)
50	535.69 (9,11,.470)	526.25 (1,12,1.504)	525.65 (1,12,1.502)	525.39 (1,12,1.501)
60	526.38 (9,11,.404)	522.16 (1,12,1.536)	521.47 (1,12,1.534)	521.17 (1,12,1.533)
70	511.98 (10,12,.164)	517.21 (1,12,1.529)	516.33 (1,12,1.526)	515.97 (1,12,1.525)
80	498.11 (9,11,.137)	500.43 (10,12,.003)	498.68 (10,12,.003)	497.87 (10,12,.003)
90	492.58 (9,11,.000)	491.63 (9,11,.000)	489.82 (9,11,.000)	488.83 (9,11,.000)

[b] Numbers in parentheses, (m,n, τ), indicate the number of axial half-waves, circumferential waves, and skewedness parameter, respectively

[†] $E_1 = 7.5 \times 10^6$ psi, $E_2 = 3.5 \times 10^6$ psi, $G_{12} = 1.25 \times 10^6$ psi, $\nu_{12} = 0.25$

* Nonlinear rotations about the normal are neglected

[#] L = 12.5 in., R = 6.0 in., and h = 0.036 in.

Table 97. Buckling loads N_x^{cr} (lbs/in.) for (0/-θ/+θ) and (90/-θ/+θ) three-ply boron-epoxy cylinders[#] with simply supported edges, and subjected to axial compression

(0/-θ/+θ)[†] cylinders				
Fiber angle, deg	Ref. 84, Donnell	Present study		
		Donnell	Sanders*	Sanders
0	834.31 (4,10,.000)[b]	830.00 (4,10,.000)	826.44 (4,10,.000)	824.44 (4,10,.000)
10	914.84 (4,11,-.132)	933.84 (4,11,-.045)	929.59 (4,11,-.045)	927.56 (4,11,-.045)
20	1113.9 (5,12,-.037)	1168.5 (1,11,-.708)	1164.9 (1,11,-.707)	1163.2 (1,11,-.706)
30	1277.4 (5,13,.159)	1417.3 (4,12,.015)	1409.6 (4,12,.013)	1404.8 (4,12,.013)
40	1307.6 (5,13,.100)	1472.6 (2,9,-.048)	1453.9 (2,9,-.047)	1439.6 (2,9,-.047)
50	1219.8 (6,13,.035)	1365.5 (3,10,-.105)	1349.6 (2,9,-.086)	1336.0 (2,9,-.085)
60	1081.4 (5,12,-.014)	1176.1 (4,11,-.232)	1166.6 (4,11,-.229)	1160.3 (4,11,-.227)
70	951.76 (6,12,-.216)	981.52 (4,11,-.380)	973.96 (4,11,-.375)	969.50 (4,11,-.374)
80	843.10 (7,11,-.118)	852.34 (7,11,-.198)	846.86 (7,11,-.196)	843.65 (7,11,-.196)
90	780.51 (8,11,.000)	774.15 (8,11,.000)	769.17 (8,11,.000)	766.49 (8,11,.000)
(90/-θ/+θ)[†] cylinders				
Fiber angle, deg	Ref. 84, Donnell	Present study		
		Donnell	Sanders*	Sanders
0	781.86 (7,11,.000)	776.07 (7,11,.000)	774.22 (7,11,.000)	773.46 (7,11,.000)
10	785.03 (6,10,-.465)	809.88 (1,10,-.919)	807.34 (1,10,-.917)	806.08 (1,10,-.917)
20	855.40 (7,11,-.552)	939.86 (5,11,-.799)	937.78 (5,11,-.799)	937.02 (5,11,-.799)
30	1001.8 (8,11,-.650)	1147.4 (1,15,1.058)	1146.8 (1,15,1.057)	1146.5 (1,15,1.056)
40	1216.6 (13,13,-.039)	1183.0 (1,15,1.250)	1182.5 (1,15,1.249)	1182.3 (1,15,1.249)
50	1302.8 (15,13,.199)	1187.3 (1,15,1.467)	1186.8 (1,15,1.466)	1186.5 (1,15,1.465)
60	1248.8 (14,13,.297)	1150.7 (1,14,1.737)	1150.1 (1,14,1.736)	1149.7 (1,14,1.735)
70	1096.7 (14,12,.180)	1078.4 (1,13,1.927)	1077.3 (1,13,1.924)	1076.7 (1,13,1.923)
80	920.42 (13,11,.059)	935.98 (12,11,-.057)	932.04 (12,11,-.058)	930.05 (12,11,-.058)
90	833.95 (11,10,.000)	829.98 (11,10,.000)	825.93 (11,10,.000)	823.80 (11,10,.000)

[b] Numbers in parentheses, (m,n, τ), indicate the number of axial half-waves, circumferential waves, and skewedness parameter, respectively

[†] $E_1 = 40 \times 10^6$ psi, $E_2 = 4.5 \times 10^6$ psi, $G_{12} = 1.5 \times 10^6$ psi, $\nu_{12} = 0.25$

* Nonlinear rotations about the normal are neglected

[#] L = 12.5 in., R = 6.0 in., and h = 0.036 in.

Table 98. Buckling loads N_x^{cr} (lbs/in.) for $(+45/-45/0/90)_s$[†] quasi-isotropic cylinders[#] with simply supported edges and subjected to axial compression

Ref. 86, Donnell	Present study		
	Donnell	Sanders*	Sanders
819.21 (1,7,.011)[b]	821.18 (1,7,.006)	802.81 (1,7,.006)	788.62 (1,7,.006)

[b] Numbers in parentheses, (m,n, τ), indicate the number of axial half-waves, circumferential waves, and skewedness parameter, respectively

[†] $E_1 = 18.5111 \times 10^6$ psi, $E_2 = 1.64 \times 10^6$ psi, $G_{12} = 0.8706 \times 10^6$ psi, $\nu_{12} = 0.300235$

* Nonlinear rotations about the normal are neglected

[#] L = 14.0 in., R = 8.0 in., and h = 0.04 in.

Table 99. Buckling stress σ_x^{cr} (kgf/mm^2) for laminated-composite[†] cylinders[#] with simply supported edges and subjected to axial compression

Laminate	Ref. 87, Donnell	Present study		
		Donnell	Sanders*	Sanders
$[(0/90)_2]_S$	16.0, n ≠ 0	15.43 (11,7,0)[b]	15.29 (11,7,0)	15.20 (11,7,0)
$0_4/90_4$	10.9, n ≠ 0	10.86 (17,9,0)	10.75 (17,9,0)	10.68 (17,9,0)
$(\pm 20)_4$	18.2, n = 0	18.20 (19,0,0)	18.02 (1,4,.00)	17.00 (1,4,.00)
$+20_4/-20_4$	18.2, n = 0	12.90 (10,8,.76)	12.84 (10,8,.76)	12.82 (10,8,.76)
	---	18.20 (19,0,0)	18.02 (1,4,0)	17.00 (1,4,0)
$(\pm 45)_4$	15.8, n = 0	15.76 (28,0,0)	15.69 (1,3,.00)	14.07 (1,3,.00)
$+45_4/-45_4$	15.8, n = 0	13.17 (1,3,.02)	11.78 (1,3,.02)	10.58 (1,3,.02)
	---	15.76 (28,0,0)	15.69 (1,3,.00)	14.07 (1,3,.00)
$(\pm 70)_4$	18.2, n = 0	18.99 (3,4,.02)	17.56 (2,3,.01)	14.61 (1,2,.00)
$+70_4/-70_4$	18.2, n = 0	14.11 (1,11,1.06)	13.78 (3,4,.08)	12.66 (1,3,.04)
		19.30 (3,4,0)	17.73 (2,3,0)	14.61 (1,2,0)
$[(\pm 70))_2]_S$	18.2, n = 0	19.30 (3,4,.00)	17.73 (2,3,.00)	14.61 (1,2,.00)

[b] Numbers in parentheses, (m,n, τ), indicate the number of axial half-waves, circumferential waves, and skewedness parameter, respectively

[†] $E_1 = 13,940$ kgf/mm^2, $E_2 = 833$ kgf/mm^2, $G_{12} = 484$ kgf/mm^2, $\nu_{12} = 0.316$, ply thickness = 0.125 mm

* Nonlinear rotations about the normal are neglected

[#] L = 600 mm, R = 100 mm, and h = 1 mm

Table 100. Buckling stress σ_x^{cr} (kgf/mm^2) for laminated-composite† cylinders with simply supported edges and subjected to axial compression

Laminate	Ref. 87, Donnell	Present study		
		Donnell	Sanders*	Sanders
$(+20_2/-20_2)$	9.11, n = 0	6.44 (7,11,.79)[b]	6.43 (7,11,.79)	6.43 (7,11,.79)
	---	9.11 (13,0,0)	9.11 (13,0,0)	9.11 (13,0,0)
$(\pm 45)_S$	7.88, n = 0	7.88 (20,0,0)	7.88 (20,0,0)	7.88 (20,0,0)
$(+45_2/-45_2)$	7.88, n = 0	7.10 (1,5,.03)	6.82 (1,5,.02)	6.55 (1,5,.02)
	---	7.88 (20,0,0)	7.88 (20,0,0)	7.88 (20,0,0)
$(\pm 70)_2$	9.10, n = 0	8.84 (1,4,.02)	8.22 (1,4,.02)	7.75 (1,4,.02)
	---	9.53 (1,4,0)	8.83 (1,4,0)	8.31 (1,4,0)

[b] Numbers in parentheses, (m,n, τ), indicate the number of axial half-waves, circumferential waves, and skewedness parameter, respectively

† E_1 = 13, 940 kgf/mm^2, E_2 = 833 kgf/mm^2, G_{12} = 484 kgf/mm^2, ν_{12} = 0.316, ply thickness = 0.125 mm

* Nonlinear rotations about the normal are neglected

$^{\#}$ L = 300 mm, R = 100 mm, and h = 0.5 mm

Table 101. Buckling load N_x^{cr} (kN/m) for laminated-composite cylinders with simply supported edges and subjected to axial compression

Material Type†	Laminate	Ref. 88, Donnell	Present study		
			Donnell	Sanders*	Sanders
1	$(\pm 33/90_2/0_2/\pm 52)$	---	132.8 (2,9,.03)[b]	130.5 (1,6,.01)	127.6 (1,6,.01)
		133.4 (1,6,0)	133.4 (2,9,0)	130.9 (1,6,0)	127.9 (1,6,0)
	$(\pm 59/0_2/90_2/\pm 30)$	---	126.2 (1,11,1.17)	125.8 (1,11,1.17)	125.6 (1,11,1.17)
		129.9 (13,4,0)	130.0 (11,8,0)	129.9 (10,9,0)	129.8 (10,9,0)
2	$(\pm 33/90_2/0_2/\pm 53)$	---	103.8 (3,10,.05)	101.8 (1,6,.01)	99.57(1,6,.01)
		104.1 (13,0,0)	103.9 (13,0,0)	102.0 (1,6,0)	99.78 (1,6,0)
	$(\pm 59/0_2/90_2/\pm 28)$	---	99.81 (1,11,1.23)	99.53 (1,11,1.22)	99.42 (1,11,1.22)
		101.7 (13,3,0)	101.7 (13,3,0)	101.7 (11,8,0)	101.6 (11,8,0)
3	$(\pm 30/\pm 78/\pm 3/\pm 55)$	---	58.42 (3,10,.02)	57.53 (1,6,.00)	56.23 (1,6,.00)
		58.54 (3,10,0)	58.48 (3,10,0)	57.53 (1,6,0)	56.23 (1,6,0)
	$(\pm 29/\pm 75/0_2/\pm 28)$	---	57.43 (2,9,.01)	56.73 (2,9,.01)	56.22 (1,7,.01)
		58.52 (3,10,0)	57.46 (2,9,0)	56.77 (2,9,0)	56.23 (1,9,0)

[b] Numbers in parentheses, (m,n, τ), indicate the number of axial half-waves, circumferential waves, and skewedness parameter, respectively

† Type 1: $E_1 = 207$ GPa, $E_2 = 5.17$ GPa, $G_{12} = 2.69$ GPa, $\nu_{12} = 0.25$
Type 2: $E_1 = 146$ GPa, $E_2 = 10.8$ GPa, $G_{12} = 5.78$ GPa, $\nu_{12} = 0.29$
Type 3: $E_1 = 51.5$ GPa, $E_2 = 24.0$ GPa, $G_{12} = 8.58$ GPa, $\nu_{12} = 0.25$

* Nonlinear rotations about the normal are neglected

L = 143.6 mm, R = 82.5 mm, and h = 0.5 mm

Table 102. Buckling load N_x^{cr} (kN/m) for laminated-composite cylinders[#] with simply supported edges and subjected to axial compression

Material Type[†]	Laminate and length, mm	Ref. 88, Donnell	Present study		
			Donnell	Sanders*	Sanders
1	(±33/±88/±19/±51)	---	134.2 (1,10,.04)[b]	133.09 (1,10,.04)	132.4 (1,10,.04)
	L = 45.4	134.6	134.7 (1,10,0)	133.6 (1,10,0)	132.8 (1,10,0)
	(±33/90$_2$/0$_2$/±52)	---	132.8 (2,9,.03)	130.5 (1,6,.01)	127.6 (1,6,.01)
	L = 143.6	133.4	133.4 (2,9,0)	130.9 (1,6,0)	127.9 (1,6,0)
	(±33/90$_2$/0$_2$/±61)	---	129.9 (2,6,.01)	126.2 (2,6,.01)	122.0 (1,4,.01)
	L = 321.1	130.4	130.5 (2,6,0)	126.8 (2,6,0)	122.1 (1,4,0)
2	(±32/±84/±15/±53)	---	103.6 (1,10,.05)	102.8 (1,10,.05)	102.2 (1,10,.05)
	L = 45.4	104.7	104.1 (1,10,0)	103.3 (1,10,0)	102.7 (1,10,0)
	(±33/±88/0$_2$/±53)	---	103.8 (3,10,.05)	101.7 (1,6,.01)	99.52 (1,6,.01)
	L = 143.6	104.1	104.2 (1,6,0)	102.0 (1,6,0)	99.78 (1,6,0)
	(±33/90$_2$/0$_2$/±63)	---	101.6 (2,6,.01)	98.74 (2,6,.01)	94.84 (1,4,.00)
	L = 321.1	102.0	102.0 (2,6,0)	99.10 (2,6,0)	94.84 (1,4,0)
3	(±33/±86/±19/±51)	---	58.49 (4,1,.08)	58.23 (1,10,.01)	57.90 (1,10,.01)
	L = 45.4	58.62	58.49 (4,9,0)	58.25 (1,10.0)	57.92 (1,10,0)
	(±33/±86/0$_2$/±59)	---	58.74 (3,10,.02)	57.47 (1,6,.00)	56.17 (1,6,.00)
	L = 143.6	58.57	58.79 (3,10,0)	57.47 (1,6,0)	56.17 (1,6,0)
	(±32/90$_2$/0$_2$/±68)	---	58.16 (2,6,.00)	56.50 (2,6,.00)	54.04 (1,4,.00)
	L = 321.1	58.14	58.16 (2,6,0)	56.50 (2,6,0)	54.04 (1,4,0)

[b] Numbers in parentheses, (m,n, τ), indicate the number of axial half-waves, circumferential waves, and skewedness parameter, respectively

[†] Type 1: E_1 = 207 GPa, E_2 = 5.17 GPa, G_{12} = 2.69 GPa, ν_{12} = 0.25
Type 2: E_1 = 146 GPa, E_2 = 10.8 GPa, G_{12} = 5.78 GPa, ν_{12} = 0.29
Type 3: E_1 = 51.5 GPa, E_2 = 24.0 GPa, G_{12} = 8.58 GPa, ν_{12} = 0.25

* Nonlinear rotations about the normal are neglected

[#] R = 82.5 mm, h = 0.5 mm

Table 103. Buckling load N_x^{cr} (kN/m) for $(0_2/\pm 60_2)_m$ laminated-composite[†] cylinders[#] with simply supported edges and subjected to axial compression

Stacking sequence index, m	Ref. 88, Donnell	Present study		
		Donnell	Sanders*	Sanders
10	---	102.4 (4,11,.01)[b]	101.6 (3,10,.01)	99.84 (1,6,.00)
	102.4	102.4 (4,11,0)	101.7 (4,11,0)	99.84 (1,6,0)
20	---	103.7 (4,11,.01)	102.8 (1,6,.00)	100.4 (1,6,.00)
	103.7	103.7 (4,11,0)	102.8 (1,6,0)	100.4 (1,6,0)
40	---	104.3 (4,11,.00)	103.0 (1,6,.00)	100.7 (1,6,.00)
	104.3	104.3 (4,11,0)	103.0 (1,6,0)	100.7 (1,6,0)
80	---	104.6 (3,10,.00)	103.2 (1,6,.00)	100.8 (1,6,.00)
	104.6	104.6 (3,10,0)	103.2 (1,6,0)	100.8 (1,6,0)
160	---	104.7 (3,10,.00)	103.2 (1,6,.00)	100.9 (1,6,.00)
	104.7	104.7 (3,10,0)	103.2 (1,6,0)	100.9 (1,6,0)

[b] Numbers in parentheses, (m,n, τ), indicate the number of axial half-waves, circumferential waves, and skewedness parameter, respectively

[†] Type 2: $E_1 = 146$ GPa, $E_2 = 10.8$ GPa, $G_{12} = 5.78$ GPa, $\nu_{12} = 0.29$

* Nonlinear rotations about the normal are neglected

[#] L = 143.6 mm, R = 82.5 mm, and h = 0.5 mm

Table 104. Buckling-load ratio $\frac{N_x^{cr}}{N^*}$ for laminated-composite cylinders[#] with simply supported edges and subjected to axial compression

Laminate[†]	Ref. 89, Donnell	Present study		
		Donnell	Sanders*	Sanders
$(0_2/\pm 39.5)$	---	0.58 (4,13,-.06)[b]	0.58 (4,13,-.06)	0.58 (4,13,-.06)
	0.59	0.59 (4,13,0)	0.58 (4,13,0)	0.58 (4,13,0)
(±30/±37)	---	0.64 (1,7,.02)	0.62 (1,7,.02)	0.61 (1,7,.02)
	0.65	0.65 (1,7,0)	0.64 (1,7,0)	0.62 (1,7,0)
(±45/±50.5)	---	0.55 (1,6,.02)	0.53 (1,6,.02)	0.52 (1,6,.02)
	0.59	0.59 (1,6,0)	0.56 (1,6,0)	0.55 (1,6,0)
(±60/±64.5)	---	0.55 (1,5,.03)	0.53 (1,5,.03)	0.51 (1,5,.03)
	0.58	0.58 (1,5,0)	0.56 (1,5,0)	0.53 (1,5,0)
$(90_2/\pm 50.5)$	---	0.48 (1,14,-1.49)	0.48 (1,14,-1.48)	0.48 (1,14,-1.48)
	0.58	0.58 (12,12,0)	0.58 (12,12,0)	0.58 (12,12,0)
$(\pm 71.5/0_2)$	---	0.46 (1,13,.63)	0.46 (1,13,.63)	0.46 (1,13,.63)
	0.63	0.63 (12,10,0)	0.63 (12,10,0)	0.63 (12,10,0)
(±21/±30)	---	0.69 (1,8,.02)	0.68 (1,8,.02)	0.67 (1,8,.01)
	0.70	0.70 (1,8,0)	0.69 (1,8,0)	0.68 (1,8,0)
(±13/±45)	---	0.65 (1,7,.02)	0.64 (1,7,.02)	0.63 (1,7,.02)
	0.67	0.67 (1,7,0)	0.66 (1,7,0)	0.64 (1,7,0)
(±77.5/±60)	---	0.62 (1,12,-2.34)	0.62 (1,12,-2.33)	0.62 (1,12,-2.33)
	0.68	0.68 (19,7,0)	0.68 (18,8,0)	0.68 (18,8,0)
$(\pm 19.5/90_2)$	---	0.50 (8,13,.66)	0.50 (8,13,.66)	0.50 (8,13,.66)
	0.63	0.63 (2,9,0)	0.62 (1,7,0)	0.61 (1,7,0)

[b] Numbers in parentheses, (m,n, τ), indicate the number of axial half-waves, circumferential waves, and skewedness parameter, respectively

[†] $E_1 = 146$ GPa, $E_2 = 10.8$ GPa, $G_{12} = 5.78$ GPa, $\nu_{12} = 0.29$

* Nonlinear rotations about the normal are neglected

[#] L = 143.6 mm, R = 82.5 mm, h = 0.5 mm, and N* = 104.7 kN/m

Table 105. Buckling-load ratio $\frac{N_x^{cr}}{N^*}$ for laminated-composite cylinders[#] with simply supported edges and subjected to axial compression

Laminate[†]	Ref. 89, Donnell	Present study		
		Donnell	Sanders*	Sanders
$(0_2/\pm47.5/0_2)$	---	0.55 (2,11,.06)[b]	0.55 (2,11,.06)	0.55 (2,11,.06)
	0.57	0.57 (2,11,0)	0.57 (2,11,0)	0.56 (2,11,0)
$(90_2/\pm43.5/90_2)$	---	0.50 (1,11,2.93)	0.50 (1,12,2.62)	0.50 (1,12,2.62)
	0.57	0.57 (18,11,0)	0.57 (18,11,0)	0.57 (18,11,0)
$(0_2/\pm32.5/90_2)$	---	0.54 (5,13,.10)	0.54 (5,13,.10)	0.53 (5,13,.10)
	0.55	0.55 (5,13,0)	0.54 (5,13,0)	0.54 (5,13,0)
$(90_2/\pm58/0_2)$	---	0.54 (11,13,.07)	0.54 (11,13,.07)	0.54 (11,13,.07)
	0.55	0.55 (11,13,0)	0.55 (11,13,0)	0.55 (11,13,0)
$(0_2/90_2/\pm40.5)$	---	0.52 (5,12,-.08)	0.52 (5,12,-.07)	0.52 (5,12,-.07)
	0.52	0.52 (4,11,0)	0.52 (4,11,0)	0.52 (4,11,0))
$(90_2/0_2/\pm49)$	---	0.47 (1,12,-1.35)	0.47 (1,12,-1.35)	0.47 (1,12,-1.35)
	0.52	0.52 (9,12,0)	0.52 (9,12,0)	0.52 (9,12,0)
$(\pm49.5/90_2/0_2)$	---	0.73 (1,7,.02)	0.71 (1,7,.02)	0.70 (1,7,.02)
	0.74	0.74 (14,0,0)	0.73 (1,7,0)	0.71 (1,7,0)
$(\pm30/0_2/90_2)$	---	0.74 (1,7,.01)	0.72 (1,7,.01)	0.71 (1,7,.01)
	0.74	0.74 (1,7,0)	0.72 (1,7,0)	0.71 (1,7,0)
$(\pm71/0_2/\pm71)$	---	0.63 (1,8,-3.71)	0.63 (1,8,-3.71)	0.63 (1,8,-3.71)
	0.64	0.64 (19,2,0)	0.64 (19,2,0)	0.64 (19,2,0)
$(\pm36.5/90_2/\pm36.5)$	---	0.76 (1,7,.01)	0.74 (1,7,.01)	0.73 (1,7,.01)
	0.77	0.77 (1,7,0)	0.75 (1,7,0)	0.73 (1,7,0)
$(0_2/\pm50/\pm38)$	---	0.67 (2,10,.04)	0.67 (2,10,.04)	0.66 (2,10,.04)
	0.68	0.68 (3,11,0)	0.68 (2,10,0)	0.67 (2,10,0)
$(90_2/\pm40/\pm52)$	---	0.67 (1,13,-1.61)	0.67 (1,13,-1.61)	0.67 (1,13,-1.61)
	0.68	0.68 (14,11,0)	0.68 (14,11,0)	0.68 (14,11,0)
$(\pm29/0_2/\pm49)$	---	0.78 (1,7,.02)	0.77 (1,7,.02)	0.75 (1,7,.02)
	0.79	0.79 (1,7,0)	0.77 (1,7,0)	0.76 (1,7,0)
$(\pm47/90_2/\pm29)$	---	0.81 (1,6,.01)	0.79 (1,6,.01)	0.77 (1,6,.01)
	0.81	0.81 (14,0,0)	0.79 (1,6,0)	0.77 (1,6,0)

[b] Numbers in parentheses, (m,n, τ), indicate the number of axial half-waves, circumferential waves, and skewedness parameter, respectively

[†] $E_1 = 146$ GPa, $E_2 = 10.8$ GPa, $G_{12} = 5.78$ GPa, $\nu_{12} = 0.29$ * Nonlinear rotations about the normal are neglected

[#] L = 143.6 mm, R = 82.5 mm, h = 0.5 mm, and N* = 104.7 kN/m

Table 106. Buckling-load ratio $\frac{N_x^{cr}}{N^*}$ for laminated-composite cylinders[#] with simply supported edges and subjected to axial compression

Laminate[†]	Ref. 89, Donnell	Present study		
		Donnell	Sanders*	Sanders
$0_2/90_2/\pm52/0_2$	---	0.54 (4,12,.02)[b]	0.54 (4,12,.02)	0.54 (4,12,.02)
	0.54	0.54 (4,12,0)	0.54 (4,12,0)	0.54 (4,12,0)
$0_2/\pm58.5/90_2/0_2$	---	0.62 (2,10,.06)	0.61 (2,10,.06)	0.61 (2,10,.06)
	0.63	0.63 (2,10,0)	0.62 (2,10,0)	0.62 (1,7,0)
$90_2/0_2/\pm37/90_2$	---	0.54 (11,12,.07)	0.54 (11,12,.07)	0.54 (11,12,.07)
	0.54	0.54 (11,12,0)	0.54 (11,12,0)	0.54 (11,12,0)
$90_2/\pm32.5/0_2/90_2$	---	0.56 (1,11,2.24)	0.56 (1,11,2.24)	0.56 (1,11,2.24)
	0.62	0.62 (15,9,0)	0.62 (14,10,0)	0.62 (14,10,0)
$0_2/\pm54/\pm54/0_2$	---	0.63 (1,8,.03)	0.62 (1,8,.03)	0.61 (1,8,.03)
	0.65	0.65 (2,10,0)	0.64 (1,8,0)	0.63 (1,8,0)
$90_2/\pm31/\pm31/90_2$	---	0.57 (1,10,2.77)	0.57 (1,11,2.45)	0.57 (1,11,2.45)
	0.65	0.65 (16,9,0)	0.65 (16,9,0)	0.65 (16,9,0)
$\pm67/0_4/\pm67$	---	0.71 (1,7,-3.47)	0.71 (1,7,-3.47)	0.71 (1,7,-3.47)
	0.72	0.72 (15,4,0)	0.72 (14,6,0)	0.72 (15,4,0)
$\pm29/90_4/\pm29$	---	0.77 (1,7,.01)	0.75 (1,7,.01)	0.73 (1,7,.01)
	0.77	0.77 (1,7,0)	0.75 (1,7,0)	0.73 (1,7,0)
$\pm48/0_2/90_2/\pm48$	---	0.90 (1,6,.01)	0.88 (1,6,.01)	0.86 (1,6,.01)
	0.91	0.91 (1,6,0)	0.89 (1,6,0)	0.86 (1,6,0)
$\pm36.5/90_2/0_2/\pm36.5$	---	0.91 (1,7,.01)	0.89 (1,7,.01)	0.88 (1,7,.01)
	0.91	0.91 (1,7,0)	0.89 (1,7,0)	0.88 (1,7,0)
$90_2/\pm42/90_2/0_2$	---	0.72 (1,12,1.11)	0.72 (1,12,1.11)	0.72 (1,12,1.11)
	0.76	0.76 (10,12,0)	0.76 (9,12,0)	0.76 (9,12,0)
$0_2/\pm47/\pm6/90_2$	---	0.75 (4,12,.09)	0.75 (4,12,.09)	0.74 (4,12,.09)
	0.76	0.76 (5,12,0)	0.76 (4,12,0)	0.75 (4,12,0)
$\pm59/0_2/90_2/\pm28$	---	0.95 (1,11,1.23)	0.95 (1,11,1.22)	0.95 (1,11,1.22)
	0.97	0.97 (13,3,0)	0.97 (11,8,0)	0.97 (11,8,0)
$\pm33/90_2/0_2/\pm52$	---	0.96 (1,9,2.04)	0.96 (1,9,2.04)	0.95 (1,6,.01)
	0.99	0.99 (13,0,0)	0.98 (1,6,0)	0.95 (1,6,0)

[b] Numbers in parentheses, (m,n, τ), indicate the number of axial half-waves, circumferential waves, and skewedness parameter, respectively

[†] $E_1 = 146$ GPa, $E_2 = 10.8$ GPa, $G_{12} = 5.78$ GPa, $\nu_{12} = 0.29$

* Nonlinear rotations about the normal are neglected

[#] L = 143.6 mm, R = 82.5 mm, h = 0.5 mm, and N* = 104.7 kN/m

Table 107. Buckling-load ratio $\frac{N_x^{cr}}{N^*}$ for laminated-composite cylinders with simply supported edges and subjected to axial compression

Laminate	Ref. 89, Donnell	Present study		
		Donnell	Sanders*	Sanders
$0_2/90_2/\pm43.5//\pm43.5/90_2/0_2$	---	0.75 (5,12,.03)[b]	0.75 (5,12,.03)	0.74 (4,11,.03)
	0.75	0.75 (5,12,0)	0.75 (5,12,0)	0.75 (4,11,0)
$90_2/0_2/\pm46.5//\pm46.5/0_2/90_2$	---	0.74 (1,12,1.47)	0.74 (1,12,1.47)	0.74 (1,12,1.47)
	0.75	0.75 (9,12,0)	0.75 (9,12,0)	0.75 (9,12,0)
$0_2/\pm56.5/90_4/\pm56.5/0_2$	---	0.70 (2,9,.03)	0.69 (2,9,.03)	0.68 (2,9,.03)
	0.70	0.70 (2,9,0)	0.69 (2,9,0)	0.69 (2,9,0)
$90_2/\pm35/0_4/\pm35/90_2$	---	0.67 (1,10,2.12)	0.67 (1,10,2.12)	0.67 (1,10,2.12)
	0.70	0.70 (12,10,0)	0.70 (12,10,0)	0.70 (12,10,0)
$0_2/90_2/\pm46.5/90_2/\pm46.5/0_2$	---	0.69 (4,11,.02)	0.68 (4,11,.02)	0.68 (4,11,.02)
	0.69	0.69 (4,11,0)	0.68 (4,11,0)	0.68 (4,11,0)
$0_2/90_2/\pm43.5/0_2/90_2/\pm43.5$	---	0.72 (5,11,.02)	0.71 (5,11,.02)	0.71 (5,11,.02)
	0.72	0.72 (5,11,0)	0.71 (5,11,0)	0.71 (5,11,0)
$\pm50.5/0_2/90_4/0_2/\pm50.5$	---	0.93 (3,10,.04)	0.92 (3,10,.04)	0.91 (1,6,.01)
	0.93	0.93 (3,10,0)	0.92 (3,10,0)	0.91 (1,6,0)
$\pm39/90_2/0_4/90_2/\pm39$	---	0.91 (1,9,2.00)	0.90 (1,9,2.00)	0.90 (1,9,1.99)
	0.92	0.92 (9,10,0)	0.92 (9,10,0)	0.92 (9,10,0)
$\pm46/0_2/90_2/0_2/90_2/\pm46$	---	0.94 (5,11,.06)	0.93 (5,11,.06)	0.92 (1,6,.01)
	0.94	0.94 (5,11,0)	0.94 (5,11,0)	0.92 (1,6,0)
$\pm43.5/90_2/0_2/90_2/0_2/\pm43.5$	---	0.92 (1,10,1.50)	0.92 (1,10,1.49)	0.92 (1,10,1.49)
	0.94	0.94 (9,10,0)	0.94 (7,11,0)	0.94 (7,11,0)
$\pm49/0_2/90_2/90_2/0_2/\pm55$	---	0.93 (4,10,.05)	0.92 (1,6,.01)	0.90 (1,6,.01)
	0.93	0.93 (4,10,0)	0.92 (1,6,0)	0.90 (1,6,0)
$\pm47/0_2/90_2/0_2/90_2/\pm39$	---	0.94 (5,11,.05)	0.93 (3,10,.04)	0.93 (1,6,.01)
	0.94	0.94 (5,11,0)	0.94 (3,10,0)	0.93 (1,6,0)
$\pm59/0_2/\pm26/\pm59/90_2/\pm26$	---	0.98 (3,10,.03)	0.96 (1,6,.01)	0.94 (1,6,.01)
	0.98	0.98 (1,6,0)	0.96 (1,6,0)	0.94 (1,6,0)
$\pm29/90_2/\pm64/\pm29/0_2/\pm64$	---	0.95 (1,10,1.74)	0.95 (1,11,1.49)	0.94 (1,11,1.49)
	0.98	0.98 (10,10,0)	0.98 (10,10,0)	0.98 (10,10,0)

[b] Numbers in parentheses, (m,n, τ), indicate the number of axial half-waves, circumferential waves, and skewedness parameter, respectively

† $E_1 = 146$ GPa, $E_2 = 10.8$ GPa, $G_{12} = 5.78$ GPa, $\nu_{12} = 0.29$

* Nonlinear rotations about the normal are neglected

L = 143.6 mm, R = 82.5 mm, h = 0.5 mm, and N* = 104.7 kN/m

Table 108. Buckling-load‡ ratio $\frac{N_x^{cr}}{N^*}$ for laminated-composite cylinders with simply supported edges and subjected to axial compression (L/R = 1)

R/h[#]	N*, N/m	Laminate[†]	Ref. 89, Donnell	Present study		
				Donnell	Sanders*	Sanders
50	13,842.3	±22/±40	---	0.84 (1,6,.05)[b]	0.82 (1,7,.05)	0.80 (1,6,.04)
			0.85	0.85 (3,0,0)	0.83 (1,6,0)	0.81 (1,6,0)
100	3,451.26	±23/±37	---	0.77 (1,8,.03)	0.76 (1,8,.03)	0.75 (1,8,.03)
			0.78	0.78 (1,8,0)	0.77 (1,8,0)	0.75 (1,8,0)
150	1,533.41	±22/±34	---	0.75 (1,9,.02)	0.74 (1,9,.02)	0.73 (1,9,.02)
			0.75	0.75 (1,9,0)	0.74 (1,9,0)	0.74 (1,9,0)
200	862.722	±22/±33	---	0.73 (1,10,.02)	0.72 (1,10,.02)	0.71 (1,10,.02)
			0.73	0.73 (1,10,0)	0.73 (1,10,0)	0.72 (1,10,0)
500	138.055	±19/±27	---	0.69 (1,14,.01)	0.69 (1,14,.01)	0.68 (1,14,.01)
			0.69	0.69 (1,14,0)	0.69 (1,14,0)	0.69 (1,14,0)
1000	34.5017	±13/±30	---	0.67 (1,16,.01)	0.67 (1,16,.01)	0.67 (1,16,.01)
			0.69	0.68 (1,16,0)	0.68 (1,16,0)	0.67 (1,16,0)

[b] Numbers in parentheses, (m,n, τ), indicate the number of axial half-waves, circumferential waves, and skewedness parameter, respectively

[†] E_1 = 146 GPa, E_2 = 10.8 GPa, G_{12} = 5.78 GPa, ν_{12} = 0.29

* Nonlinear rotations about the normal are neglected

[#] R = 1000.0 mm

Table 109. Buckling-load‡ ratio $\frac{N_x^{cr}}{N^*}$ for laminated-composite cylinders with simply supported edges and subjected to axial compression (L/R = 3)

R/h[#]	N*, N/m	Laminate[†]	Ref. 89, Donnell	Present study		
				Donnell	Sanders*	Sanders
50	13,842.3	±17/±27	---	0.68 (1,5,1.31)[b]	0.68 (1,5,1.30)	0.66 (1,4,.01)
			0.72	0.72 (7,0,0)	0.69 (1,4,0)	0.66 (1,4,0)
100	3,451.26	±16/±25	---	0.65 (1,8,1.04)	0.64 (1,8,1.04)	0.64 (1,8,1.04)
			0.69	0.69 (1,5,0)	0.67 (1,5,0)	0.65 (1,5,0)
150	1,533.41	±13/±35	---	0.67 (1,6,.01)	0.65 (1,6,.01)	0.63 (1,6,.01)
			0.68	0.68 (1,6,0)	0.66 (1,6,0)	0.64 (1,6,0)
200	862.722	±14/±31	---	0.68 (1,6,.01)	0.67 (1,6,.01)	0.65 (1,6,.01)
			0.69	0.69 (1,6,0)	0.67 (1,6,0)	0.65 (1,6,0)
500	138.055	±12/±33	---	0.67 (1,8,.01)	0.66 (1,8,.01)	0.65 (1,8,.01)
			0.68	0.68 (4,15,0)	0.67 (1,8,0)	0.66 (1,8,0)
1000	34.5017	±13/±30	---	0.67 (2,14,.01)	0.67 (2,14,.01)	0.67 (2,14,.01)
			0.68	0.68 (3,16,0)	0.67 (1,10,0)	0.67 (1,10,0)

[b] Numbers in parentheses, (m,n, τ), indicate the number of axial half-waves, circumferential waves, and skewedness parameter, respectively

[†] E_1 = 146 GPa, E_2 = 10.8 GPa, G_{12} = 5.78 GPa, ν_{12} = 0.29

* Nonlinear rotations about the normal are neglected

[#] R = 1000.0 mm

Table 110. Buckling-load[‡] ratio $\frac{N_x^{cr}}{N^*}$ for laminated-composite cylinders with simply supported edges and subjected to axial compression (L/R = 1)

R/h[#]	N*, N/m	Laminate[†]	Ref. 89, Donnell	Present study		
				Donnell	Sanders*	Sanders
50	13,842.3	$\pm 40/90_2/\pm 36$	---	0.97 (1,6,.03)[b]	0.94 (1,6,.03)	0.92 (1,6,.03)
			0.97	0.97 (1,6,0)	0.94 (1,6,0)	0.92 (1,6,0)
100	3,451.26	$\pm 42/90_2/\pm 27$	---	0.90 (1,7,.02)	0.89 (1,7,.02)	0.87 (1,7,.02)
			0.90	0.90 (1,7,0)	0.89 (1,7,0)	0.87 (1,7,0)
150	1,533.41	$\pm 45/90_2/\pm 34$	---	0.86 (1,8,.02)	0.85 (1,8,.02)	0.84 (1,8,.02)
			0.86	0.86 (1,8,0)	0.85 (1,8,0)	0.84 (1,8,0)
200	862.722	$\pm 45/90_2/\pm 35$	---	0.85 (1,9,.02)	0.83 (1,9,.02)	0.82 (1,9,.02)
			0.85	0.85 (1,9,0)	0.84 (1,9,0)	0.83 (1,9,0)
500	138.055	$\pm 49/90_2/\pm 37$	---	0.79 (1,11,.01)	0.78 (1,11,.01)	0.78 (1,11,.01)
			0.80	0.80 (1,11,0)	0.79 (1,11,0)	0.78 (1,11,0)
1000	34.5017	$\pm 50/90_2/\pm 34$	---	0.77 (1,13,.01)	0.76 (1,13,.01)	0.76 (1,13,.01)
			0.77	0.77 (20,0,0)	0.77 (1,13,0)	0.76 (1,13,0)

[b] Numbers in parentheses, (m,n, τ), indicate the number of axial half-waves, circumferential waves, and skewedness parameter, respectively

[†] $E_1 = 146$ GPa, $E_2 = 10.8$ GPa, $G_{12} = 5.78$ GPa, $\nu_{12} = 0.29$

* Nonlinear rotations about the normal are neglected

[#] R = 1000.0 mm

Table 111. Buckling-load[‡] ratio $\frac{N_x^{cr}}{N^*}$ for laminated-composite cylinders with simply supported edges and subjected to axial compression (L/R = 3)

R/h[#]	N*, N/m	Laminate[†]	Ref. 89, Donnell	Present study		
				Donnell	Sanders*	Sanders
50	13,842.3	$\pm 45/90_2/\pm 38$	---	0.86 (1,4,.02)[b]	0.78 (1,4,.02)	0.74 (1,4,.02)
			0.87	0.87 (1,4,0)	0.79 (1,4,0)	0.75 (1,4,0)
100	3,451.26	$\pm 46/90_2/\pm 25$	---	0.80 (1,5,.01)	0.76 (1,5,.01)	0.73 (1,5,.01)
			0.81	0.81 (1,4,0)	0.77 (1,5,0)	0.74 (1,4,0)
150	1,533.41	$\pm 49/90_2/\pm 40$	---	0.78 (1,5,.01)	0.74 (1,5,.01)	0.71 (1,5,.01)
			0.79	0.79 (1,5,0)	0.75 (1,5,0)	0.72 (1,5,0)
200	862.722	$\pm 51/90_2/\pm 35$	---	0.75 (1,5,.01)	0.72 (1,5,.01)	0.70 (1,5,.01)
			0.76	0.76 (1,5,0)	0.73 (1,5,0)	0.70 (1,5,0)
500	138.055	$\pm 50/90_2/\pm 31$	---	0.76 (1,7,.01)	0.74 (1,7,.01)	0.73 (1,6,.00)
			0.76	0.76 (1,6,0)	0.75 (1,6,0)	0.73 (1,6,0)
1000	34.5017	$\pm 51/90_2/\pm 34$	---	0.75 (1,8,.00)	0.74 (1,8,.00)	0.73 (1,8,.00)
			0.75	0.75 (1,8,0)	0.74 (1,8,0)	0.73 (1,8,0)

[b] Numbers in parentheses, (m,n, τ), indicate the number of axial half-waves, circumferential waves, and skewedness parameter, respectively

[†] $E_1 = 146$ GPa, $E_2 = 10.8$ GPa, $G_{12} = 5.78$ GPa, $\nu_{12} = 0.29$

* Nonlinear rotations about the normal are neglected

[#] R = 1000.0 mm

Table 112. Buckling-load[‡] ratio $\frac{N_x^{cr}}{N^*}$ for laminated-composite cylinders with simply supported edges and subjected to axial compression (L/R = 1)

R/h[#]	N*, N/m	Laminate[†]	Ref. 89, Donnell	Present study		
				Donnell	Sanders*	Sanders
50	13,842.3	±32/90$_2$/0$_2$/±53	---	0.99 (2,6,.17)[b]	0.97 (2,6,.17)	0.97 (1,6,.06)
			1.00	1.00 (2,6,0)	0.99 (1,6,0)	0.97 (1,6,0)
100	3,451.26	±33/90$_2$/0$_2$/±55	---	0.99 (1,7,.03)	0.97 (1,7,.03)	0.96 (1,7,.03)
			0.99	0.99 (1,7,0)	0.97 (1,7,0)	0.96 (1,7,0)
150	1,533.41	±33/90$_2$/0$_2$/±58	---	0.97 (1,8,2.37)	0.97 (1,8,2.37)	0.96 (1,8,.02)
			0.99	0.99 (1,8,0)	0.98 (1,8,0)	0.96 (1,8,0)
200	862.722	±33/90$_2$/0$_2$/±54	---	0.97 (1,10,2.03)	0.97 (1,10,2.03)	0.97 (1,10,2.02)
			0.99	1.00 (8,4,0)	0.98 (1,9,0)	0.97 (1,9,0)
500	138.055	±33/90$_2$/0$_2$/±62	---	0.94 (1,14,2.63)	0.94 (1,14,2.63)	0.94 (1,14,2.63)
			0.98	0.98 (1,11,0)	0.97 (1,11,0)	0.96 (1,11,0)
1000	34.5017	±32/90$_2$/0$_2$/±56	---	0.95 (1,23,1.97)	0.95 (1,23,1.97)	0.95 (1,23,1.96)
			0.97	0.98 (1,13,0)	0.97 (1,13,0)	0.96 (1,13,0)

[b] Numbers in parentheses, (m,n, τ), indicate the number of axial half-waves, circumferential waves, and skewedness parameter, respectively

[†] $E_1 = 146$ GPa, $E_2 = 10.8$ GPa, $G_{12} = 5.78$ GPa, $\nu_{12} = 0.29$

* Nonlinear rotations about the normal are neglected

[#] R = 1000.0 mm

Table 113. Buckling-load[‡] ratio $\frac{N_x^{cr}}{N^*}$ for laminated-composite cylinders with simply supported edges and subjected to axial compression (L/R = 3)

R/h[#]	N*, N/m	Laminate[†]	Ref. 89, Donnell	Present study		
				Donnell	Sanders*	Sanders
50	13,842.3	±33/90$_2$/0$_2$/±53	---	0.96 (1,5,2.03)[b]	0.95 (2,5,.03)	0.90 (1,4,.01)
			0.99	0.99 (2,5,0)	0.95 (2,5,0)	0.91(1,4,0)
100	3,451.26	±33/90$_2$/0$_2$/±58	---	0.94 (1,7,2.17)	0.94 (1,7,2.16)	0.91 (1,4,.01)
			0.99	0.99 (18,0,0)	0.96 (2,6,0)	0.91 (1,4,0)
150	1,533.41	±32/90$_2$/0$_2$/±62	---	0.93 (1,8,2.44)	0.93 (1,8,2.44)	0.91 (1,5,.01)
			0.99	0.99 (5,9,0)	0.95 (1,5,0)	0.91 (1,5,0)
200	862.722	±33/90$_2$/0$_2$/±55	---	0.95 (1,10,2.08)	0.95 (1,5,.01)	0.91 (1,5,.01)
			0.98	0.98 (2,7,0)	0.95 (1,5,0)	0.91 (1,5,0)
500	138.055	±31/90$_2$/0$_2$/±61	---	0.93 (1,16,2.07)	0.93 (1,16,2.07)	0.93 (1,16,2.07)
			0.97	0.97 (2,9,0)	0.96 (2,9,0)	0.95 (2,9,0)
1000	34.5017	±33/90$_2$/0$_2$/±58	---	0.94 (1,21,2.36)	0.94 (1,21,2.36)	0.94 (1,8,.00)
			0.98	0.97 (1,8,0)	0.95 (1,8,0)	0.94 (1,8,0)

[b] Numbers in parentheses, (m,n, τ), indicate the number of axial half-waves, circumferential waves, and skewedness parameter, respectively

[†] $E_1 = 146$ GPa, $E_2 = 10.8$ GPa, $G_{12} = 5.78$ GPa, $\nu_{12} = 0.29$

* Nonlinear rotations about the normal are neglected

[#] R = 1000.0 mm

Table 114. Buckling-load‡ ratio $\frac{N_x^{cr}}{N^*}$ for laminated-composite cylinders# with simply supported edges and subjected to axial compression (L/R = 1, R/h = 150)

E_1/E_2	N*, N/m	Laminate†	Ref. 89, Donnell	Present study		
				Donnell	Sanders*	Sanders
2	2723.48	±26/±34	---	0.98 (1,8,.01)[b]	0.97 (1,8,.01)	0.96 (1,8,.01)
			0.98	0.98 (1,8,0)	0.97 (1,8,0)	0.96 (1,8,0)
5	1876.75	±42/±38	---	0.71 (6,0,0)	0.71 (6,0,0)	0.71 (6,0,0)
			0.91	0.71 (6,0,0)	0.71 (6,0,0)	0.71 (6,0,0)
10	1598.78	±22/±34	---	0.79 (1,9,.02)	0.78 (1,9,.02)	0.77 (1,9,.02)
			0.79	0.80 (5,0,0)	0.79 (1,9,0)	0.78 (1,9,0)
15	1506.46	±21/±33	---	0.73 (1,9,.02)	0.72 (1,9,.02)	0.71 (1,9,.02)
			0.73	0.73 (1,9,0)	0.73 (1,9,0)	0.72 (1,9,0)
20	1460.34	±22/±34	---	0.68 (1,9,.02)	0.67 (1,9,.02)	0.67 (1,9,.02)
			0.69	0.69 (1,9,0)	0.68 (1,9,0)	0.67 (1,9,0)
50	1377.39	±23/±33	---	0.53 (1,10,.02)	0.52 (1,10,.02)	0.51 (1,10,.02)
			0.54	0.54 (1,10,0)	0.53 (1,10,0)	0.52 (1,10,0)
100	1349.76	$\pm 18/90_2$	---	0.21 (5,12,1.09)	0.21 (5,12,1.09)	0.21 (5,12,1.09)
			0.50	0.50 (1,9,0)	0.49 (1,9,0)	0.49 (1,9,0)
10,000	1322.40	$\pm 18/90_2$	---	0.13 (6,12,1.31)	0.13 (6,12,1.31)	0.13 (6,12,1.31)
			0.47	0.47 (1,9,0)	0.46 (1,9,0)	0.46 (1,9,0)

[b] Numbers in parentheses, (m,n, τ), indicate the number of axial half-waves, circumferential waves, and skewedness parameter, respectively

† $E_1 = 146$ GPa, $E_2/G_{12} = 2$, $\nu_{12} = 0.29$

* Nonlinear rotations about the normal are neglected

R = 1000.0 mm

Table 115. Buckling-load[‡] ratio $\frac{N_x^{cr}}{N^*}$ for laminated-composite cylinders[#] with simply supported edges and subjected to axial compression (L/R = 1, R/h = 150)

E_1/E_2	N*, N/m	Laminate[†]	Ref. 89, Donnell	Present study		
				Donnell	Sanders*	Sanders
2	2723.48	±61/90$_2$/±41	---	0.99 (1,8,.01)[b]	0.98 (1,8,.01)	0.96 (1,8,.01)
			0.99	0.99 (2,10,0)	0.98 (1,8,0)	0.97 (1,8,0)
5	1876.75	±49/90$_2$/±41	---	0.92 (1,8,.02)	0.90 (1,8,.02)	0.89 (1,8,.02)
			0.92	0.92 (1,8,0)	0.90 (1,8,0)	0.89 (1,8,0)
10	1598.78	±46/90$_2$/±36	---	0.87 (1,8,.02)	0.86 (1,8,.02)	0.85 (1,8,.02)
			0.88	0.88 (8,0,0)	0.86 (1,8,0)	0.85 (1,8,0)
15	1506.46	±44/90$_2$/±31	---	0.85 (1,8,.02)	0.84 (1,8,.02)	0.83 (1,8,.02)
			0.86	0.86 (1,8,0)	0.85 (1,8,0)	0.83 (1,8,0)
20	1460.34	±44/90$_2$/±33	---	0.84 (1,8,.02)	0.83 (1,8,.02)	0.82 (1,8,.02)
			0.85	0.85 (1,8,0)	0.83 (1,8,0)	0.82 (1,8,0)
50	1377.39	±43/90$_2$/±31	---	0.83 (1,8,.02)	0.81 (1,8,.02)	0.80 (1,8,.02)
			0.83	0.83 (1,8,0)	0.82 (1,8,0)	0.81 (1,8,0)
100	1349.76	±42/90$_2$/±27	---	0.82 (1,8,.02)	0.81 (1,8,.02)	0.80 (1,8,.02)
			0.82	0.82 (1,8,0)	0.81 (1,8,0)	0.80 (1,8,0)
10,000	1322.40	±42/90$_2$/±27	---	0.81 (1,9,.03)	0.80 (1,9,.02)	0.79 (1,9,.02)
			0.81	0.82 (1,8,0)	0.81 (1,8,0)	0.80 (1,8,0)

[b] Numbers in parentheses, (m,n, τ), indicate the number of axial half-waves, circumferential waves, and skewedness parameter, respectively

[†] E_1 = 146 GPa, E_2/G_{12} = 2, ν_{12} = 0.29

* Nonlinear rotations about the normal are neglected

[#] R = 1000.0 mm

Table 116. Buckling-load[‡] ratio $\frac{N_x^{cr}}{N^*}$ for laminated-composite cylinders[#] with simply supported edges and subjected to axial compression (L/R = 1, R/h = 150)

E_1/E_2	N*, N/m	Laminate[†]	Ref. 89, Donnell	Present study		
				Donnell	Sanders*	Sanders
2	2723.48	±33/90$_2$/0$_2$/±56	---	1.00 (1,8,.01)[b]	0.98 (1,8,.01)	0.97 (1,8,.01)
			1.00	1.00 (1,8,0)	0.98 (1,8,0)	0.97 (1,8,0)
5	1876.75	±33/90$_2$/0$_2$/±57	---	0.99 (1,8,.02)	0.98 (1,8,.02)	0.97 (1,8,.01)
			0.99	1.00 (1,8,0)	0.98 (1,8,0)	0.97(1,8,0)
10	1598.78	±33/90$_2$/0$_2$/±58	---	0.98 (1,8,2.37)	0.97 (1,8,.02)	0.96 (1,8,.02)
			0.99	0.99 (1,8,0)	0.98 (1,8,0)	0.97 (1,8,0)
15	1506.46	±33/90$_2$/0$_2$/±58	---	0.97 (1,8,2.37)	0.96 (1,8,2.37)	0.96 (1,8,.03)
			0.99	0.99 (1,8,0)	0.97 (1,8,0)	0.96 (1,8,0)
20	1460.34	±33/90$_2$/0$_2$/±58	---	0.96 (1,8,2.37)	0.96 (1,8,2.37)	0.96 (1,8,2.36)
			0.99	0.99 (1,8,0)	0.97 (1,8,0)	0.96 (1,8,0)
50	1377.39	±33/90$_2$/0$_2$/±58	---	0.95 (1,8,2.37)	0.95 (1,8,2.36)	0.95 (1,8,2.36)
			0.99	0.99 (1,8,0)	0.97 (1,8,0)	0.96 (1,8,0)
100	1349.76	±33/90$_2$/0$_2$/±58	---	0.94 (1,8,2.37)	0.94 (1,8,2.36)	0.94 (1,8,2.36)
			0.99	0.99 (1,8,0)	0.97 (1,8,0)	0.96 (1,8,0)
10,000	1322.40	±33/90$_2$/0$_2$/±58	---	0.94 (1,8,2.37)	0.94 (1,8,2.36)	0.94 (1,8,2.36)
			0.98	0.99 (1,8,0)	0.97 (1,8,0)	0.96 (1,8,0)

[b] Numbers in parentheses, (m,n, τ), indicate the number of axial half-waves, circumferential waves, and skewedness parameter, respectively

[†] E_1 = 146 GPa, E_2/G_{12} = 2, ν_{12} = 0.29

* Nonlinear rotations about the normal are neglected

[#] R = 1000.0 mm

Table 117. Buckling load (kN) for laminated-composite cylinders[#] with simply supported edges and subjected to axial compression

Stacking sequence[†]	Ref. 90 Donnell	Ref. 90 Finite element	Present study		
			Donnell	Sanders*	Sanders
$(90/-45/0/45)_S$	158	156.317	160.5 (1,8,-2.02)[b]	160.2 (1,8,-2.02)	160.1 (1,8,-2.02)
$(90/-45/0/45)_A$	172	169.239	179.2 (1,7,-2.18)	178.5 (1,7,-2.17)	178.3 (1,7,-2.17)
$(90/-45_2/0)_S$	138	130.388	144.9 (1,6,-3.67)	144.9 (1,6,-3.67)	144.9 (1,6,-3.67)
$(90_3/0)_T$	28.7	28.729	28.68 (9,11,0)	28.61 (9,11,0)	28.59 (9,11,0)
$(90/-45/45_2/0/-45_2/45)_T$	158	156.049	158.1 (10,0,0)	158.1 (10,0,0)	158.1 (10,0,0)
$(90/-45/0/\pm45/90/45/0)_T$	196	194.374	201.9 (1,8,-1.24)	201.1 (1,8,-1.23)	200.7 (1,8,-1.23)
$(90/-45/0/45/90/0/-45/45)_T$	190	186.415	193.1 (1,8,-1.36)	192.1 (1,8,-1.35)	191.7 (1,8,-1.35)
$(90/-45/0/\pm45/0/-45/90)_T$	170	175.600	175.5 (1,8,-2.24)	175.4 (1,8,-2.23)	175.4 (1,8,-2.23)
$(90/-45/0/45/0_2/90/-45)_T$	154	160.071	156.5 (1,9,-1.67)	156.3 (1,9,-1.67)	156.2 (1,9,-1.66)

[b] Numbers in parentheses, (m,n, τ), indicate the number of axial half-waves, circumferential waves, and skewedness parameter, respectively

[†] $E_1 = 161$ GPa, $E_2 = 11.5$ GPa, $G_{12} = 7.169$ GPa, $\nu_{12} = 0.349$

* Nonlinear rotations about the normal are neglected

[#] L = 150 mm, R = 80 mm, and h = 0.125 mm

Table 118. Nondimensional buckling pressures $\frac{p^{cr}RL^2}{\pi^2 D_{11}}$ for antisymmetric cross-ply cylinders[#] with simply supported edges and subjected to external pressure

Length, in.	Lay up[†]	Ref. 73, Donnell	Present study			
			Donnell	Sanders*	Sanders	Sanders, live pressure
1.00	(90/0)	0.73758	0.75092 (1,32)[b]	0.75003 (1,32)	0.74731 (1,32)	0.74671 (1,31)
	$(90/0)_2$	1.7685	1.7819 (1,31)	1.7816 (1,31)	1.7808 (1,31)	1.7790 (1,31)
	$(90/0)_\infty$	2.1121	2.1255 (1,31)	2.1277 (1,31)	2.1271 (1,31)	2.1251 (1,31)
3.16	(90/0)	0.89741	0.92873 (1,12)	0.93268 (1,12)	0.93256 (1,12)	0.92794 (1,12)
	$(90/0)_2$	1.9656	2.0029 (1,11)	2.0160 (1,11)	2.0142 (1,11)	1.9998 (1,11)
	$(90/0)_\infty$	2.3164	2.3531 (1,11)	2.3702 (1,11)	2.3661 (1,11)	2.3482 (1,11)
10.00	(90/0)	2.6910	2.8614 (1,7)	2.8886 (1,8)	2.8874 (1,8)	2.8558 (1,8)
	$(90/0)_2$	5.1606	5.4406 (1,6)	5.5494 (1,7)	5.5437 (1,7)	5.4261 (1,6)
	$(90/0)_\infty$	5.8367	6.1029 (1,6)	6.2393 (1,6)	6.2248 (1,6)	6.0619 (1,6)
31.63	(90/0)	10.788	11.257 (1,5)	11.509 (1,5)	11.502 (1,5)	11.106 (1,5)
	$(90/0)_2$	20.930	21.875 (1,4)	23.014 (1,4)	22.975 (1,4)	21.642 (1,4)
	$(90/0)_\infty$	23.750	24.580 (1,4)	25.718 (1,4)	25.672 (1,4)	24.129 (1,4)

[b] Numbers in parentheses, (m,n), indicate the number of axial half-waves and circumferential waves, respectively

[†] $E_1 = 30 \times 10^6$ psi, $E_2 = 0.75 \times 10^6$ psi, $G_{12} = 0.375 \times 10^6$ psi, $\nu_{12} = 0.25$

* Nonlinear rotations about the normal are neglected

[#] R = 10.0 in. and h = 0.10 in.

Table 119. Nondimensional buckling pressures $\frac{p^{cr}RL^2}{E_2h^3}$ for unsymmetric cross-ply cylinders[#] with simply supported edges and subjected to external pressure

Lay up[†]	Ref. 73, Donnell	Ref. 76, Donnell	Present study			
			Donnell	Sanders*	Sanders	Sanders, live pressure
(0)	55.90	55.81 (1,6)[b]	55.90 (1,6)	56.95 (1,6)	56.93 (1,6)	55.39 (1,6)
(0/90/0)	99.39	99.32 (1,5)	99.39 (1,5)	102.51 (1,5)	102.44 (1,5)	98.44 (1,5)
$(0_8/90/0)$	100.98	97.57 (1,5)	100.98 (1,6)	102.17 (1,6)	102.13 (1,6)	98.70 (1,6)
$(0_{18}/90/0)$	108.00	105.30 (1,5)	108.00 (1,5)	111.22 (1,6)	111.18 (1,6)	106.77 (1,5)
$(0_{48}/90/0)$	99.72	96.61 (1,5)	99.72 (1,6)	100.92 (1,6)	100.89 (1,6)	97.67 (1,6)

[b] Numbers in parentheses, (m,n), indicate the number of axial half-waves and circumferential waves, respectively

[†] $E_1 = 30 \times 10^6$ psi, $E_2 = 0.75 \times 10^6$ psi, $G_{12} = 0.375 \times 10^6$ psi, $\nu_{12} = 0.25$

* Nonlinear rotations about the normal are neglected

[#] L = 34.64 in., R = 10.0 in. and h = 0.12 in.

Table 120. Buckling load $p^{cr}R$ (kN/m) for laminated-composite cylinders[#] with simply supported edges and subjected to external pressure

Material Type[†]	Laminate and length, mm	Ref. 88, Donnell	Present study		
			Donnell	Sanders*, live pressure	Sanders, live pressure
1	$\pm 72/\pm 37/0_2/90_2$	---	48.23 (1,11,.05)[b]	48.21 (1,11,.05)	48.13 (1,11,.05)
	L = 45.4	48.58	48.60 (1,11,0)	48.58 (1,11,0)	48.40 (1,11,0)
	$90_2/\pm 26/\pm 19/\pm 83$	---	16.33 (1,6,.00)	16.19 (1,7,.01)	16.17 (1,7,.01)
	L = 143.6	16.32	16.33 (1,6,0)	16.20 (1,7,0)	16.18 (1,7,0)
	$90_2/\pm 7/\pm 27/\pm 82$	---	7.972 (1,5,.01)	7.752 (1,5,.01)	7.745 (1,5,.01)
	L = 321.1	7.977	7.977 (1,5,0)	7.756 (1,5,0)	7.749 (1,5,0)
2	$\pm 72/\pm 37/0_2/90_2$	---	36.39 (1,11,.04)	36.38 (1,11,.04)	36.32 (1,11,.04)
	L = 45.4	36.62	36.60 (1,11,0)	36.59 (1,11,0)	36.53 (1,11,0)
	$90_2/\pm 13/\pm 27/90_2$	---	12.13 (1,7,.00)	11.99 (1,7,.00)	11.98 (1,7,.00)
	L = 143.6	12.13	12.13 (1,7,0)	11.99 (1,7,0)	11.98 (1,7,0)
	$90_2/0_2/\pm 28/90_2$	---	5.851 (1,5,.00)	5.692 (1,5,.00)	5.687 (1,5,.00)
	L = 321.1	5.851	5.851 (1,5,0)	5.692 (1,5,0)	5.687 (1,5,0)
3	$\pm 86/\pm 47/0_2/90_2$	---	17.42 (1,12,.01)	17.39 (1,12,.01)	17.37 (1,12,.01)
	L = 45.4	17.41	17.42 (1,12,0)	17.40 (1,12,0)	17.38 (1,12,0)
	$90_2/0_2/0_2/90_2$	---	5.293 (1,7,.00)	5.252 (1,7,.00)	5.247 (1,7,.00)
	L = 143.6	5.292	5.293 (1,7,0)	5.252 (1,7,0)	5.247 (1,7,0)
	$90_2/0_2/0_2/90_2$	---	2.406 (1,5,.00)	2.352 (1,5,.00)	2.350 (1,5,.00)
	L = 321.1	2.401	2.406 (1,5,0)	2.352 (1,5,0)	2.350 (1,5,0)
	$90_2/90_2/0_2/90_2$	---	2.406 (1,5,.00)	2.348 (1,5,.00)	2.345 (1,5,.00)
	L = 321.1	2.401	2.406 (1,5,0)	2.348 (1,5,0)	2.345 (1,5,0)

[b] Numbers in parentheses, (m,n, τ), indicate the number of axial half-waves, circumferential waves, and skewedness parameter, respectively

[†] Type 1: $E_1 = 207$ GPa, $E_2 = 5.17$ GPa, $G_{12} = 2.69$ GPa, $\nu_{12} = 0.25$
Type 2: $E_1 = 146$ GPa, $E_2 = 10.8$ GPa, $G_{12} = 5.78$ GPa, $\nu_{12} = 0.29$
Type 3: $E_1 = 51.5$ GPa, $E_2 = 24.0$ GPa, $G_{12} = 8.58$ GPa, $\nu_{12} = 0.25$

* Nonlinear rotations about the normal are neglected

[#] R = 82.5 mm and h = 0.5 mm

Table 121. Critical external pressure (Pa x 10^{-6}) for infinitely long laminated-composite cylinders[#] with simply supported edges (L/R = 100, R/h =15)

Lay up[†]	Ref. 91, Sanders*	Present study			
		Donnell	Sanders*	Sanders	Sanders, live pressure
$(0_3)_S$	1847	1847 (1,2)[b]	1847 (1,2)	1847 (1,2)	1385 (1,2)
$(0_2/90)_S$	2537	2538 (1,2)	2538 (1,2)	2538 (1,2)	1904 (1,2)
$(0/90/0)_S$	6687	6686 (1,2)	6686 (1,2)	6685 (1,2)	5013 (1,2)
$(0/90_2)_S$	7377	7377 (1,2)	7377 (1,2)	7376 (1,2)	5532 (1,2)
$(90/0_2)_S$	14982	14981 (1,2)	14981 (1,2)	14980 (1,2)	11229 (1,2)
$(90/0/90)_S$	15671	15672 (1,2)	15672 (1,2)	15670 (2,2)	11750 (1,2)
$(90_2/0)_S$	19822	19820 (1,2)	19820 (1,2)	19816 (2,2)	14859 (1,2)
$(90_3)_S$	20512	20511 (1,2)	20511 (1,2)	20493 (5,2)	15379 (1,2)
$(0_2/90_2)_S$	4185	4180 (1,2)	4180 (1,2)	4179 (1,2)	3135 (1,2)
$(0/90/0/90)_S$	7680	7679 (1,2)	7679 (1,2)	7679 (1,2)	5759 (1,2)
$(0/90_2/0)_S$	9432	9429 (1,2)	9429 (1,2)	9428 (1,2)	7070 (1,2)
$(90/0_2/90)_S$	12934	12929 (1,2)	12929 (1,2)	12927 (1,2)	9693 (1,2)
$(90/0/90/0)_S$	14679	14679 (1,2)	14679 (1,2)	14677 (1,2)	11005 (1,2)
$(90_2/0_2)_S$	18181	18178 (1,2)	18178 (1,2)	18175 (2,2)	13627 (1,2)

[b] Numbers in parentheses, (m,n), indicate the number of axial half-waves and circumferential waves, respectively

[†] $E_1 = 206.844 \times 10^9$ Pa, $E_2 = 18.6159 \times 10^9$ Pa, $G_{12} = 4.48162 \times 10^9$ Pa, $\nu_{12} = 0.21$

* Nonlinear rotations about the normal are neglected

[#] R = 19.05 cm

Table 122. Critical external pressure (Pa x 10^{-6}) for infinitely long laminated-composite cylinders with simply supported edges (L/R = 100, R/h =10)

Lay up[†]	Ref. 91, Sanders*	Present study			
		Donnell	Sanders*	Sanders	Sanders, live pressure
$(0_3)_S$	6274	6232 (1,2)	6233 (1,2)	6232 (1,2)	4671 (1,2)
$(0_2/90)_S$	8618	8565 (1,2)	8566 (1,2)	8565 (1,2)	6423 (1,2)
$(0/90/0)_S$	22614	22564 (1,2)	22564 (1,2)	22562 (1,2)	16913 (1,2)
$(0/90_2)_S$	24959	24897 (1,2)	24897 (1,2)	24894 (1,2)	18666 (1,2)
$(90/0_2)_S$	50607	50561 (1,2)	50561 (1,2)	50551 (2,2)	37865 (1,2)
$(90/0/90)_S$	52952	52894 (1,2)	52894 (1,2)	52877 (3,2)	39637 (1,2)
$(90_2/0)_S$	66948	66892 (1,2)	66892 (1,2)	66859 (3,2)	50114 (1,2)
$(90_3)_S$	69223	69225 (1,2)	69225 (1,2)	69083 (7,2)	51878 (1,2)
$(0_2/90_2)_S$	14134	14106 (1,2)	14107 (1,2)	14105 (1,2)	10578 (1,2)
$(0/90/0/90)_S$	25924	25918 (1,2)	25918 (1,2)	25915 (1,2)	19429 (1,2)
$(0/90_2/0)_S$	31853	31823 (1,2)	31824 (1,2)	31820 (1,2)	23853 (1,2)
$(90/0_2/90)_S$	43644	43634 (1,2)	43635 (1,2)	43626 (2,2)	32697 (1,2)
$(90/0/90/0)_S$	49573	49540 (1,2)	49540 (1,2)	49529 (2,2)	37117 (1,2)
$(90_2/0_2)_S$	61363	61351 (1,2)	61351 (1,2)	61332 (3,2)	45954 (1,2)

[b] Numbers in parentheses, (m,n), indicate the number of axial half-waves and circumferential waves, respectively

[†] $E_1 = 206.844 \times 10^9$ Pa, $E_2 = 18.6159 \times 10^9$ Pa, $G_{12} = 4.48162 \times 10^9$ Pa, $\nu_{12} = 0.21$

* Nonlinear rotations about the normal are neglected

[#] R = 19.05 cm

Table 123. Critical external pressure (Pa x 10^{-6}) for infinitely long laminated-composite cylinders[#] with simply supported edges (L/R = 100, R/h =15)

Lay up[†]	Ref. 91, Sanders*	Present study			
		Donnell	Sanders*	Sanders	Sanders, live pressure
$(45_2/-45)_S$	6226	6149 (1,2,.01)[b]	6203 (1,2,.01)	6202 (1,2,.01)	4642 (1,2,.01)
		6234 (1,2,0)	6234 (1,2,0)	6234 (1,2,0)	4674 (1,2,0)
$(45/-45_2)_S$	6226	6234 (1,2,.00)	6234 (1,2,.00)	6234 (1,2,.00)	4674 (1,2,.00)
		6234 (1,2,0)	6234 (1,2,0)	6234 (1,2,0)	4674 (1,2,0)
$(-45/45/-45)_S$	6226	6232 (1,2,-.01)	6234 (1,2,.00)	6234 (1,2,.00)	4674 (1,2,.00)
		6234 (1,2,0)	6234 (1,2,0)	6234 (1,2,0)	4674 (1,2,0)
$(-45_2/45)_S$	6226	6149 (1,2,-.01)	6203 (1,2,-.01)	6202 (1,2,-.01)	4642 (1,2,-.01)
		6234 (1,2,0)	6234 (1,2,0)	6234 (1,2,0)	4674 (1,2,0)
$(-45_2/45_2)_S$	6226	6188 (1,2,-.01)	6234 (1,2,.00)	6234 (1,2,.00)	4674 (1,2,.00)
		6234 (1,2,0)	6234 (1,2,0)	6234 (1,2,0)	4674 (1,2,0)
$(45_2/-45_2)_S$	6226	6188 (1,2,.01)	6234 (1,2,.00)	6234 (1,2,.00)	4674 (1,2,.00)
		6234 (1,2,0)	6234 (1,2,0)	6234 (1,2,0)	4674 (1,2,0)
$(45/-45/45/-45)_S$	6226	6234 (1,2,.00)	6234 (1,2,.00)	6234 (1,2,.00)	4674 (1,2,.00)
		6234 (1,2,0)	6234 (1,2,0)	6234 (1,2,0)	4674 (1,2,0)
$(45/-45_2/45)_S$	6226	6234 (1,2,.00)	6234 (1,2,.00)	6234 (1,2,.00)	4674 (1,2,.00)
		6234 (1,2,0)	6234 (1,2,0)	6234 (1,2,0)	4674 (1,2,0)
$(30_2/-60)_S$	3144	3149 (1,2,.00)	3150 (1,2,.00)	3150 (1,2,.00)	2362 (1,2,.00)
		3149 (1,2,0)	3150 (1,2,0)	3150 (1,2,0)	2362 (1,2,0)
$(60_2/-30)_S$	11790	11518 (1,2,.02)	11620 (1,2,.01)	11619 (1,2,.01)	8673 (1,2,.02)
		11790 (1,2,0)	11791 (1,2,0)	11790 (1,2,0)	8839 (1,2,0)
$(30_2/-60_2)_S$	3964	3970 (1,2,0)	3971 (1,2,0)	3971 (1,2,0)	2978 (1,2,0)
		3970 (1,2,0)	3971 (1,2,0)	3971 (1,2,0)	2978 (1,2,0)
$(60_2/-30_2)_S$	10960	10802 (1,2,.02)	10851 (1,2,.01)	10850 (1,2,.01)	8118 (1,2,.01)
		10970 (1,2,0)	10970 (1,2,0)	10969 (1,2,0)	8223(1,2,0)

[b] Numbers in parentheses, (m,n, τ), indicate the number of axial half-waves, circumferential waves, and skewedness parameter, respectively

[†] $E_1 = 206.844 \times 10^9$ Pa, $E_2 = 18.6159 \times 10^9$ Pa, $G_{12} = 4.48162 \times 10^9$ Pa, $\nu_{12} = 0.21$

* Nonlinear rotations about the normal are neglected

[#] R = 19.05 cm

Table 124. Critical external pressure (Pa x 10^{-6}), for infinitely long laminated-composite cylinders[#] with simply supported edges (L/R = 100, R/h = 10)

Lay up[†]	Ref. 91, Sanders*	Present study			
		Donnell	Sanders*	Sanders	Sanders, live pressure
$(45_2/-45)_S$	21029	20427 (1,2,.02)[b]	20649 (1,2,.01)	20647 (1,2,.01)	15448 (1,2,.01)
		21038 (1,2,0)	21041 (1,2,0)	21039 (1,2,0)	15767 (1,2,0)
$(45/-45_2)_S$	21029	20918 (1,2,.01)	21000 (1,2,.01)	20997 (1,2,.01)	15763 (1,2,.01)
		21038 (1,2,0)	21041 (1,2,0)	21039 (1,2,0)	15767 (1,2,0)
$(-45/45/-45)_S$	21029	20873 (1,2,-.01)	20953 (1,2,-.01)	20950 (1,2,-.01)	15675 (1,2,-.01)
		21038 (1,2,0)	21041 (1,2,0)	21039 (1,2,0)	15767 (1,2,0)
$(-45_2/45)_S$	21029	20427 (1,2,-.02)	20649 (1,2,-.01)	20647 (1,2,-.01)	15448 (1,2,-.01)
		21038 (1,2,0)	21041 (1,2,0)	21039 (1,2,0)	15767 (1,2,0)
$(-45_2/45_2)_S$	21029	20682 (1,2,-.02)	20785 (1,2,-.01)	20783 (1,2,-.01)	15576 (1,2,-.01)
		21038 (1,2,0)	21041 (1,2,0)	21039 (1,2,0)	15767 (1,2,0)
$(45_2/-45_2)_S$	21029	20682 (1,2,.02)	20785 (1,2,.01)	20783 (1,2,.01)	15576 (1,2,.01)
		21038 (1,2,0)	21041 (1,2,0)	21039 (1,2,0)	15767 (1,2,0)
$(45/-45/45/-45)_S$	21029	20949 (1,2,.01)	21041 (1,2,.00)	21039 (1,2,.01)	15767 (1,2,.00)
		21038 (1,2,0)	21041 (1,2,0)	21039 (1,2,0)	15767 (1,2,0)
$(45/-45_2/45)_S$	21029	21038 (1,2,.01)	21041 (1,2,.00)	21039 (1,2,.00)	15767 (1,2,.00)
		21038 (1,2,0)	21041 (1,2,0)	21039 (1,2,0)	15767 (1,2,0)
$(30_2/-60)_S$	10617	10529 (1,2,.01)	10598 (1,2,.01)	10597 (1,2,.01)	7952 (1,2,.01)
		10629 (1,2,0)	10632 (1,2,0)	10630 (1,2,0)	7970 (1,2,0)
$(60_2/-30)_S$	39782	37856 (1,2,.05)	38457 (1,2,.03)	38448 (1,2,.03)	28591 (1,2,.03)
		39792 (1,2,0)	39795 (1,2,0)	39790 (1,2,0)	29814 (1,2,0)
$(30_2/-60_2)_S$	13444	13381 (1,2,.01)	13402 (1,2,.00)	13401 (1,2,.00)	10047 (1,2,.00)
		13400 (1,2,0)	13402 (1,2,0)	13401 (1,2,0)	10047 (1,2,0)
$(60_2/-30_2)_S$	37025	35809 (1,2,.03)	36183 (1,2,.02)	36177 (1,2,.02)	27003 (1,2,.02)
		37022 (1,2,0)	37024 (1,2,0)	37020 (1,2,0)	27734 (1,2,0)

[b] Numbers in parentheses, (m,n, τ), indicate the number of axial half-waves, circumferential waves, and skewedness parameter, respectively

[†] $E_1 = 206.844 \times 10^9$ Pa, $E_2 = 18.6159 \times 10^9$ Pa, $G_{12} = 4.48162 \times 10^9$ Pa, $\nu_{12} = 0.21$

* Nonlinear rotations about the normal are neglected

[#] R = 19.05 cm

Table 125. Buckling-pressure ratio $\frac{q_{ext}^{cr}}{q_{ext}^{*}}$ for laminated-composite cylinders[#] with simply supported edges and subjected to uniform external pressure (L/R = 0.5)

Laminate[†]	Ref. 92, Flügge live pressure	Present study				
		Induced shear, L_3[‡]	Donnell	Sanders*	Sanders	Sanders Live Pressure
68/54	---	-0.369312	0.88 (1,11,-.10)[b]	0.88 (1,11,-.11)	0.88 (1,11,-.11)	0.88 (1,11,-.11)
	0.90	0.	0.90 (1,12,0)	0.91 (1,12,0)	0.90 (1,12,0)	0.90 (1,12,0)
67.5/2.6/90	---	-0.144161	0.90 (1,12,.20)	0.91 (1,12,.20)	0.91 (1,12,.20)	0.90 (1,12,.20)
	0.98	0.	0.98 (1,11,0)	0.99 (1,12,0)	0.99 (1,12,0)	0.98 (1,11,0)
75/41.3/0/90	---	-0.162608	1.00 (1,12,.04)	1.01 (1,12,.04)	1.00 (1,12,.04)	1.00 (1,12,.04)
	1.00	0.	1.00 (1,12,0)	1.01 (1,12,0)	1.01 (1,12,0)	1.00 (1,12,0)

[b] Numbers in parentheses, (m,n, τ), indicate the number of axial half-waves, circumferential waves, and skewedness parameter, respectively

[†] $E_1 = 146$ GPa, $E_2 = 10.8$ GPa, $G_{12} = 5.78$ GPa, $\nu_{12} = 0.29$

* Nonlinear rotations about the normal are neglected

[#] R = 82.5 mm, h = 0.5 mm, and $q_{ext}^{*} = 488.4$ kPa

[‡] see equation (151)

Table 126. Buckling-pressure ratio $\frac{q_{ext}^{cr}}{q_{ext}^{*}}$ for laminated-composite cylinders[#] with simply supported edges and subjected to uniform external pressure (L/R = 1)

Laminate[†]	Ref. 92, Flügge live pressure	Present study				
		Induced shear, L_3[‡]	Donnell	Sanders*	Sanders	Sanders Live Pressure
77/52	---	-0.260874	0.69 (1,8,-.18)[b]	0.69 (1,8,-.18)	0.69 (1,8,-.18)	0.68 (1,8,-.18)
	0.83	0.	0.83 (1,8,0)	0.84 (1,8,0)	0.84 (1,8,0)	0.83 (1,8,0)
76.6/15.8/90	---	-0.090461	0.97 (1,8,-.01)	0.98 (1,8,-.01)	0.97 (1,8,-.01)	0.96 (1,8,-.01)
	0.96	0.	0.97 (1,8,0)	0.98 (1,8,0)	0.98 (1,8,0)	0.96 (1,8,0)
83.9/34.6/0/90	---	-0.085732	1.00 (1,8,-.04)	1.01 (1,8,-.04)	1.00 (1,8,-.04)	0.99 (1,8,-.04)
	1.00	0.	1.01 (1,8,0)	1.02 (1,9,0)	1.02 (1,9,0)	1.00 (1,8,0)

[b] Numbers in parentheses, (m,n, τ), indicate the number of axial half-waves, circumferential waves, and skewedness parameter, respectively

[†] $E_1 = 146$ GPa, $E_2 = 10.8$ GPa, $G_{12} = 5.78$ GPa, $\nu_{12} = 0.29$

* Nonlinear rotations about the normal are neglected

[#] R = 82.5 mm, h = 0.5 mm, and $q_{ext}^{*} = 245.2$ kPa

[‡] see equation (151)

Table 127. Buckling-pressure ratio $\frac{q_{ext}^{cr}}{q_{ext}^{*}}$ for laminated-composite cylinders[#] with simply supported edges and subjected to uniform external pressure (L/R = 1.74)

Laminate[†]	Ref. 92, Flügge live pressure	Present study				
		Induced shear, L_3[‡]	Donnell	Sanders*	Sanders	Sanders Live Pressure
0/90	---	0.				
	0.36	0.	0.36 (1,8,0)[b]	0.36 (1,8,0)	0.36 (1,8,0)	0.36 (1,8,0)
90/51.8	---	-0.103595	0.50 (1,6,-.13)	0.51 (1,6,-.13)	0.51 (1,6,-.13)	0.50 (1,6,-.13)
	0.81	0.	0.82 (1,6,0)	0.83 (1,7,0)	0.83 (1,7,0)	0.81 (1,6,0)
45/37.8	---	-0.372064	0.46 (1,7,-.03)	0.47 (1,7,-.04)	0.47 (1,7,-.04)	0.46 (1,7,-.03)
	0.48	0.	0.48 (1,7,0)	0.49 (1,8,0)	0.49 (1,8,0)	0.48 (1,7,0)
71.1/0	---	-0.276606	0.40 (1,8,.02)	0.41 (1,8,.02)	0.41 (1,8,.02)	0.40 (1,8,.02)
	0.40	0.	0.40 (1,8,0)	0.41 (1,8,0)	0.41 (1,8,0)	0.40 (1,8,0)
90_2	---	0.				
	0.72	0.	0.72 (1,5,0)	0.75 (1,5,0)	0.74 (1,5,0)	0.72 (1,5,0)
87.3/45	---	-0.103380	0.50 (1,6,-.13)	0.51 (1,6,-.13)	0.50 (1,6,-.13)	0.49 (1,6,-.13)
	0.75	0.	0.76 (1,7,0)	0.77 (1,7,0)	0.77 (1,7,0)	0.75 (1,7,0)
90/18/90	---	0.000911	0.88 (1,6,-.08)	0.90 (1,6,-.08)	0.89 (1,6,-.08)	0.87 (1,6,-.08)
	0.97	0.	0.97 (1,6,0)	0.99 (1,6,0)	0.99 (1,6,0)	0.97 (1,6,0)
90_2/60.3	---	-0.087745	0.59 (1,6,-.12)	0.60 (1,6,-.12)	0.60 (1,6,-.12)	0.58 (1,6,-.12)
	0.77	0.	0.78 (1,6,0)	0.79 (1,6,0)	0.78 (1,6,0)	0.77 (1,6,0)
90_3	---	0.				
	0.72	0.	0.72 (1,5,0)	0.75 (1,5,0)	0.74 (1,5,0)	0.72 (1,5,0)
78.3/90/78.3	---	-0.118371	0.73 (1,5,-.01)	0.75 (1,6,.01)	0.75 (1,6,.01)	0.72 (1,5,-.01)
	0.73	0.	0.73 (1,5,0)	0.75 (1,6,0)	0.75 (1,6,0)	0.72 (1,5,0)
76.2/0/76.2	---	-0.209942	0.97 (1,6,-.01)	0.99 (1,7,.01)	0.98 (1,7,.01)	0.97 (1,7,.01)
	0.97	0.	0.97 (1,6,0)	0.99 (1,7,0)	0.98 (1,7,0)	0.97 (1,6,0)
90/45/90	---	-0.042463	0.79 (1,6,-.05)	0.80 (1,6,-.05)	0.80 (1,6,-.05)	0.78 (1,6,-.05)
	0.84	0.	0.85 (1,6,0)	0.86 (1,6,0)	0.86 (1,6,0)	0.84 (1,6,0)

[b] Numbers in parentheses, (m,n, τ), indicate the number of axial half-waves, circumferential waves, and skewedness parameter, respectively

[†] E_1 = 146 GPa, E_2 = 10.8 GPa, G_{12} = 5.78 GPa, ν_{12} = 0.29

* Nonlinear rotations about the normal are neglected

[#] R = 82.5 mm, h = 0.5 mm, and q_{ext}^{*} = 146.2 kPa

[‡] see equation (151)

Table 127. Concluded

Laminate†	Ref. 92 Flügge live pressure	Present study				
		Induced shear, L_3‡	Donnell	Sanders*	Sanders	Sanders Live Pressure
90/18.9_2/90	---	-0.001421	0.86 (1,6,-.10)[b]	0.87 (1,6,-.10)	0.87 (1,6,-.10)	0.85 (1,6,-.10)
	0.99	0.	1.01 (1,7,0)	1.01 (1,7,0)	1.01 (1,7,0)	0.99 (1,7,0)
90/25.2/0/90	---	-0.017508	0.97 (1,6,-.06)	0.99 (1,7,-.04)	0.99 (1,7,-.04)	0.96 (1,6,-.06)
	0.99	0.	1.00 (1,7,0)	1.01 (1,7,0)	1.01 (1,7,0)	0.99 (1,7,0)
90/0/32.4/90	---	-0.036330	0.94 (1,6,-.07)	0.95 (1,6,-.07)	0.95 (1,6,-.07)	0.93 (1,6,-.07)
	0.99	0.	1.00 (1,7,0)	1.01 (1,7,0)	1.01 (1,7,0)	0.99 (1,7,0)
82.1/0_2/82.1	---	-0.115657	0.96 (1,6,.00)	0.97 (1,7,.01)	0.97 (1,7,.01)	0.96 (1,7,.01)
	0.96	0.	0.96 (1,6,0)	0.97 (1,7,0)	0.97 (1,7,0)	0.96 (1,6,0)
81/0/90/81	---	-0.090776	0.88 (1,6,.01)	0.89 (1,6,.01)	0.89 (1,6,.01)	0.87 (1,6,.01)
	0.87	0.	0.88 (1,6,0)	0.89 (1,6,0)	0.89 (1,6,0)	0.87 (1,6,0)
76.5/90/0/76.5	---	-0.133711	0.90 (1,6,-.01)	0.92 (1,6,-.01)	0.92 (1,6,-.01)	0.90 (1,6,-.01)
	0.90	0.	0.90 (1,6,0)	0.92 (1,6,0)	0.92 (1,6,0)	0.90 (1,6,0)

[b] Numbers in parentheses, (m,n, τ), indicate the number of axial half-waves, circumferential waves, and skewedness parameter, respectively

† E_1 = 146 GPa, E_2 = 10.8 GPa, G_{12} = 5.78 GPa, ν_{12} = 0.29

* Nonlinear rotations about the normal are neglected

R = 82.5 mm, h = 0.5 mm, and q_{ext}* = 146.2 kPa

‡ see equation (151)

Table 128. Buckling-pressure ratio $\frac{q_{ext}^{cr}}{q_{ext}^{*}}$ for laminated-composite cylinders[#] with simply supported edges and subjected to uniform external pressure (L/R = 3)

Laminate[†]	Ref. 92 , Flügge live pressure	Present study				
		Induced shear, L_3[‡]	Donnell	Sanders*	Sanders	Sanders Live Pressure
90/65	---	-0.142353	0.60 (1,5,-.09)[b]	0.61 (1,5,-.09)	0.61 (1,5,-.09)	0.59 (1,5,-.09)
	0.83	0.	0.84 (1,4,0)	0.86 (1,5,0)	0.86 (1,5,0)	0.83 (1,5,0)
90/12/90	---	0.001661	0.97 (1,5,-.04)	0.98 (1,5,-.04)	0.98 (1,5,-.04)	0.95 (1,5,-.04)
	0.99	0.	1.01 (1,5,0)	1.03 (1,5,0)	1.03 (1,5,0)	0.99 (1,5,0)
90/0/25.3/90	---	-0.017721	0.97 (1,5,-.04)	0.99 (1,5,-.04)	0.99 (1,5,-.04)	0.95 (1,5,-.04)
	1.00	0.	1.02 (1,5,0)	1.05 (1,5,0)	1.04 (1,5,0)	1.00 (1,5,0)

[b] Numbers in parentheses, (m,n, τ), indicate the number of axial half-waves, circumferential waves, and skewedness parameter, respectively

[†] $E_1 = 146$ GPa, $E_2 = 10.8$ GPa, $G_{12} = 5.78$ GPa, $\nu_{12} = 0.29$

* Nonlinear rotations about the normal are neglected

[#] R = 82.5 mm, h = 0.5 mm, and $q_{ext}^{*} = 84.51$ kPa

[‡] see equation (151)

Table 129. Buckling-pressure ratio $\frac{q_{ext}^{cr}}{q_{ext}^{*}}$ for laminated-composite cylinders[#] with simply supported edges and subjected to uniform external pressure (L/R = 5)

Laminate[†]	Ref. 92, Flügge live pressure	Present study				
		Induced shear, L_3[‡]	Donnell	Sanders*	Sanders	Sanders Live Pressure
90/68	---	-0.137763	0.64 (1,4,-.06)[b]	0.65 (1,4,-.05)	0.65 (1,4,-.05)	0.61 (1,4,-.05)
	0.83	0.	0.84 (1,3,0)	0.89 (1,4,0)	0.89 (1,4,0)	0.83 (1,4,0)
90/5/90	---	0.000967	1.02 (1,4,-.01)	1.05 (1,4,-.01)	1.05 (1,4,-.01)	0.98 (1,4,-.01)
	0.99	0.	1.03 (1,4,0)	1.06 (1,4,0)	1.06 (1,4,0)	0.99 (1,4,0)
90/0/20.2/90	---	-0.008699	0.99 (1,4,-.02)	1.02 (1,4,-.02)	1.02 (1,4,-.02)	0.96 (1,4,-.02)
	1.00	0.	1.03 (1,4,0)	1.07 (1,4,0)	1.07 (1,4,0)	1.00 (1,4,0)

[b] Numbers in parentheses, (m,n, τ), indicate the number of axial half-waves, circumferential waves, and skewedness parameter, respectively

[†] $E_1 = 146$ GPa, $E_2 = 10.8$ GPa, $G_{12} = 5.78$ GPa, $\nu_{12} = 0.29$

* Nonlinear rotations about the normal are neglected

[#] R = 82.5 mm, h = 0.5 mm, and $q_{ext}^{*} = 51.31$ kPa

[‡] see equation (151)

Table 130. Buckling-pressure ratio $\frac{q_{ext}^{cr}}{q_{ext}^{*}}$ for laminated-composite cylinders[#] with simply supported edges and subjected to uniform external pressure (L/R = 10)

Laminate[†]	Ref. 92, Flügge live pressure	Present study				
		Induced shear, L_3[‡]	Donnell	Sanders*	Sanders	Sanders Live Pressure
90/77	---	-0.096018	0.77 (1,2,-.01)[b]	0.85 (1,3,-.02)	0.85 (1,3,-.02)	0.75 (1,3,-.02)
	0.88	0.	0.84 (1,2,0)	0.98 (1,3,0)	0.98 (1,3,0)	0.87 (1,2,0)
90/0/90	---	0.				
	1.00	0.	1.08 (1,3,0)	1.12 (1,3,0)	1.12 (1,3,0)	1.00 (1,3,0)
90/0/13.1/90	---	-0.001822	1.04 (1,3,-.01)	1.09 (1,3,-.01)	1.09 (1,3,-.01)	0.97 (1,3,-.01)
	1.00	0.	1.06 (1,3,0)	1.12 (1,3,0)	1.12 (1,3,0)	0.99 (1,3,0)

[b] Numbers in parentheses, (m,n, τ), indicate the number of axial half-waves, circumferential waves, and skewedness parameter, respectively

[†] $E_1 = 146$ GPa, $E_2 = 10.8$ GPa, $G_{12} = 5.78$ GPa, $\nu_{12} = 0.29$

* Nonlinear rotations about the normal are neglected

[#] $R = 82.5$ mm, $h = 0.5$ mm, and $q_{ext}^{*} = 25.79$ kPa

[‡] see equation (151)

Table 131. Critical hydrostatic pressure p_{cr} (psi) for cross-ply laminated-composite cylinders[#] with simply supported edges

Laminate[†]	Ref. 93, Donnell	Present study		
		Donnell	Sanders* Live Pressure	Sanders Live Pressure
$(90_5/0)_T$	427.2	416.0 (1,2)[b]	418.7 (1,2)	408.4 (1,2)
$(90_3/0)_T$	407.6	399.5 (1,2)	426.8 (1,3)	418.4 (1,2)
$(90_2/0)_T$	394.0	376.5 (1,3)	346.7 (1,3)	345.3 (1,3)
$(90/0)_T$	276.4	265.0 (1,3)	248.7 (1,3)	247.8 (1,3)
$(90_5/0_2/90_5)_T$	568.9	550.1 (1,2)	512.2 (1,2)	499.2 (1,2)
$(90_3/0_2/90_3)_T$	600.0	581.6 (1,2)	556.3 (1,2)	543.1 (1,2)
$(90_2/0_2/90_2)_T$	622.4	604.7 (1,2)	591.2 (1,2)	577.9 (1,2)
$(90/0_2/90)_T$	639.5	623.6 (1,2)	633.8 (1,2)	620.9 (1,2)
$(90_3/0_6/90_3)_T$	644.4 (2)[a]	623.6 (1,2)	633.8 (1,2)	620.9 (1,2)
$(90_4/0_5/90_3)_T$	633.1 (2)	615.8 (1,2)	616.6 (1,2)	603.6 (1,2)
$(90_3/0_5/90_4)_T$	631.0 (2)	611.6 (1,2)	609.6 (1,2)	596.5 (1,2)
$(90_2/0_7/90_3)_T$	629.8 (2)	607.3 (1,2)	630.9 (1,2)	618.5 (1,2)
$(90_3/0_7/90_2)_T$	628.3 (2)	609.8 (1,2)	637.2 (1,2)	625.1 (1,2)
$(90_3/0_5/90/0/90_2)_T$	627.7 (2)	608.8 (1,2)	623.3 (1,2)	610.7 (1,2)
$(90_2/0/90/0_5/90_3)_T$	627.4 (2)	607.5 (1,2)	620.9 (1,2)	608.3 (1,2)
$(90_3/0/90/0_4/90_3)_T$	623.1 (2)	606.2 (1,2)	608.5 (1,2)	595.7 (1,2)
$(90_2/0_8/90_2)_T$	622.0 (2)	601.6 (1,2)	635.0 (1,3)	627.4 (1,2)
$(90_3/0_4/90/0/90_3)_T$	621.8 (2)	603.7 (1,2)	604.3 (1,2)	591.4 (1,2)

[a] Number in parentheses, (n), indicates the number of circumferential waves

[b] Numbers in parentheses, (m,n), indicate the number of axial half-waves and circumferential waves, respectively

[†] $E_1 = 19.0 \times 10^6$ psi, $E_2 = 1.5 \times 10^6$ psi, $G_{12} = 1.0 \times 10^6$ psi, $\nu_{12} = 0.28$

* Nonlinear rotations about the normal are neglected

[#] h = 0.12 in., L/R = 6.050, and R/h = 25

Table 132. Critical hydrostatic pressure p_{cr} (psi) for cross-ply laminated-composite cylinders[#] with simply supported edges

Laminate	Ref. 93 Donnell	Present study		
		Donnell	Sanders* Live Pressure	Sanders Live Pressure
$(0_2/90_2/0_8)_T$	138.4 (3)[a]	161.5 (1,3)[b]	156.1 (1,3)	155.6 (1,3)
$(0_4/90/0/90/0_5)_T$	137.5 (3)	135.5 (1,3)	131.6 (1,3)	131.1 (1,3)
$(0_4/90_3/0_5)_T$	137.3 (3)	133.6 (1,3)	129.4 (1,3)	128.9 (1,3)
$(0_2/90/0_9)_T$	136.3 (3)	160.4 (1,3)	155.4 (1,3)	154.9 (1,3)
$(0_7/90_2/0_3)_T$	130.1 (3)	140.8 (1,3)	135.2 (1,3)	134.6 (1,3)
$(0_8/90/0_3)_T$	129.4 (3)	143.2 (1,3)	138.1 (1,3)	137.6 (1,3)
$(0_3/90_2/0_7)_T$	123.5 (3)	141.8 (1,3)	137.9 (1,3)	137.4 (1,3)
$(0_3/90/0_8)_T$	120.1 (3)	143.0 (1,3)	139.4 (1,3)	138.9 (1,3)
$(0_6/90_2/0_4)_T$	118.5 (3)	129.4 (1,3)	125.5 (1,3)	125.0 (1,3)
$(0_4/90_2/0_6)_T$	115.3 (3)	129.9 (1,3)	126.8 (1,3)	126.3 (1,3)

[a] Number in parentheses, (n), indicates the number of circumferential waves

[b] Numbers in parentheses, (m,n), indicate the number of axial half-waves and circumferential waves, respectively

† $E_1 = 19.0 \times 10^6$ psi, $E_2 = 1.5 \times 10^6$ psi, $G_{12} = 1.0 \times 10^6$ psi, $\nu_{12} = 0.28$

* Nonlinear rotations about the normal are neglected

[#] h = 0.12 in., L/R = 6.050, and R/h = 25

Table 133. Critical hydrostatic pressure p_{cr} (psi) for cross-ply[†] composite cylinders[#] with simply supported edges

Laminate[†]	Ref. 93 Finite Elements	Ref. 93 Donnell	Present study		
			Donnell	Sanders	Sanders Live Pressure
$(90_{12})_T$	167.20	141.6	143.7 (1,2)[b]	157.7 (1,2)	124.8 (1,2)
$(90_{10}/0_2)_T$	160.22	150.1	151.2 (1,2)	171.3 (1,3)	154.1 (1,3)
$(90_9/0_3)_T$	133.82	135.0	137.6 (1,3)	139.5 (1,3)	125.6 (1,3)
$(90_8/0_4)_T$	113.50	110.6	112.6 (1,3)	115.3 (1,3)	104.0 (1,3)
$(90_6/0_6)_T$	89.22	81.22	82.48 (1,3)	86.31 (1,3)	78.09 (1,3)
$(90_4/0_8)_T$	82.00	71.76	72.77 (1,3)	77.33 (1,3)	70.14 (1,3)
$(90_3/0_9)_T$	82.44	71.73	72.71 (1,3)	77.55 (1,3)	70.38 (1,3)
$(90_2/0_{10})_T$	83.50	72.47	73.44 (1,3)	78.54 (1,3)	71.25 (1,3)
$(0_{12})_T$	45.61	42.54	43.23 (1,4)	43.87 (1,4)	41.21 (1,4)
$(0_2/90_{10})_T$	154.6	139.9	141.0 (1,2)	167.2 (1,3)	146.2 (1,2)
$(0_3/90_9)_T$	127.45	130.6	133.1 (1,3)	134.3 (1,3)	119.6 (1,3)
$(0_4/90_8)_T$	107.23	105.7	107.6 (1,3)	109.4 (1,3)	97.28 (1,3)
$(0_6/90_6)_T$	84.67	76.27	77.50 (1,3)	80.62 (1,3)	71.42 (1,3)
$(0_8/90_4)_T$	80.33	68.03	68.99 (1,3)	73.28 (1,3)	64.73 (1,3)
$(0_9/90_3)_T$	82.32	68.97	69.90 (1,3)	74.73 (1,3)	65.96 (1,3)
$(0_{10}/90_2)_T$	84.80	70.84	71.76 (1,3)	77.12 (1,3)	68.06 (1,3)

[b] Numbers in parentheses, (m,n), indicate the number of axial half-waves and circumferential waves, respectively

[†] $E_1 = 19.0 \times 10^6$ psi, $E_2 = 1.5 \times 10^6$ psi, $G_{12} = 1.0 \times 10^6$ psi, $\nu_{12} = 0.28$

[#] h = 0.12 in., L/R = 6.555, and R/h = 38

Table 134 Critical hydrostatic pressure p_{cr} (psi) for $[90_6/\pm\theta/0_4]_S$ laminated-composite[†] cylinders[#] with simply supported edges

Fiber angle, θ, deg	Ref. 93, Finite Elements	Ref. 93, Donnell	Present study		
			Donnell	Sanders	Sanders Live Pressure
90	739.6	622.4	604.7 (1,2)[b]	733.1 (1,2)	577.9 (1,2)
75	776.9	630.2	612.8 (1,2)	748.5 (1,2)[@]	590.8 (1,2)
60	835.7	642.2	625.8 (1,2)	775.4 (1,2)[@]	612.9 (1,2)
45	821.3	653.0	637.3 (1,2)	801.4 (1,2)[@]	633.5 (1,2)
30	810.7	659.4	644.1 (1,2)	818.8 (1,2)[@]	646.3 (1,2)
15	802.7	650.5	634.9 (1,2)	807.7 (1,2)[@]	635.7 (1,2)
0	775.0	639.5	623.6 (1,2)	790.4 (1,2)	620.9 (1,2)

[b] Numbers in parentheses, (m,n), indicate the number of axial half-waves and circumferential waves, respectively

[†] $E_1 = 19.0 \times 10^6$ psi, $E_2 = 1.5 \times 10^6$ psi, $G_{12} = 1.0 \times 10^6$ psi, $\nu_{12} = 0.28$

[#] h = 0.12 in., L/R = 6.050, and R/h = 25

[@] same result obtained using the approximate Rayleigh-Ritz solution including anisotropies

Table 135. Buckling-pressure ratio $\frac{q_{ext}^{cr}}{q_{ext}^{*}}$ for laminated-composite cylinders with simply supported edges and subjected to uniform hydrostatic pressure (L/R = 0.5)

Laminate	Ref. 92 , Flügge live pressure	Present study				
		Induced shear, L_3‡	Donnell	Sanders*	Sanders	Sanders Live Pressure
66/51	---	-0.533536	0.84 (1,10,-.25)	0.84 (1,10,-.25)	0.84 (1,10,-.25)	0.84 (1,10,-.25)
	0.90	0.	0.90 (1,11,0)	0.90 (1,11,0)	0.90 (1,11,0)	0.90 (1,11,0)
64.3/5.1/72.7	---	-0.351578	0.97 (1,12,.05)	0.98 (1,12,.05)	0.97 (1,12,.05)	0.97 (1,12,.05)
	0.98	0.	0.98 (1,11,0)	0.98 (1,12,0)	0.98 (1,11,0)	0.97 (1,11,0)
73.3/39.7/0/90	---	-0.241021	1.00 (1,12,.03)	1.01 (1,12,.03)	1.00 (1,12,.03)	1.00 (1,12,.03)
	1.00	0.	1.00 (1,11,0)	1.01 (1,12,0)	1.01 (1,12,0)	1.00 (1,11,0)

[b] Numbers in parentheses, (m,n, τ), indicate the number of axial half-waves, circumferential waves, and skewedness parameter, respectively

† $E_1 = 146$ GPa, $E_2 = 10.8$ GPa, $G_{12} = 5.78$ GPa, $\nu_{12} = 0.29$

* Nonlinear rotations about the normal are neglected

R = 82.5 mm, h = 0.5 mm, and $q_{ext}^{*} = 429.1$ kPa

‡ see equation (152)

Table 136. Buckling-pressure ratio $\frac{q_{ext}^{cr}}{q_{ext}^{*}}$ for laminated-composite cylinders with simply supported edges and subjected to uniform hydrostatic pressure (L/R = 1)

Laminate	Ref. 92, Flügge live pressure	Present study				
		Induced shear, L_3‡	Donnell	Sanders*	Sanders	Sanders Live Pressure
77/50	---	-0.455216	0.62 (1,8,-.23)	0.62 (1,8,-.23)	0.62 (1,8,-.23)	0.62 (1,8,-.22)
	0.83	0.	0.83 (1,8,0)	0.83 (1,8,0)	0.83 (1,8,0)	0.82 (1,8,0)
76.6/15.8/90	---	-0.197815	0.96 (1,8,-.03)	0.97 (1,8,-.03)	0.96 (1,8,-.03)	0.95 (1,8,-.03)
	0.96	0.	0.96 (1,8,0)	0.97 (1,8,0)	0.97 (1,8,0)	0.96 (1,8,0)
81.4/33.7/0/90	---	-0.179704	0.99 (1,8,-.04)	1.00 (1,8,-.04)	1.00 (1,8,-.04)	0.98 (1,8,-.04)
	1.00	0.	1.00 (1,8,0)	1.01 (1,8,0)	1.01 (1,8,0)	1.00 (1,8,0)

[b] Numbers in parentheses, (m,n, τ), indicate the number of axial half-waves, circumferential waves, and skewedness parameter, respectively

† $E_1 = 146$ GPa, $E_2 = 10.8$ GPa, $G_{12} = 5.78$ GPa, $\nu_{12} = 0.29$

* Nonlinear rotations about the normal are neglected

R = 82.5 mm, h = 0.5 mm, and $q_{ext}^{*} = 228.9$ kPa

‡ see equation (152)

Table 137. Buckling-pressure ratio $\frac{q_{ext}^{cr}}{q_{ext}^{*}}$ for laminated-composite cylinders[#] with simply supported edges and subjected to uniform hydrostatic pressure (L/R = 1.74)

Laminate[†]	Ref. 92, Flügge live pressure	Present study				
		Induced shear, L_3[‡]	Donnell	Sanders*	Sanders	Sanders Live Pressure
0/90	---	0.				
	0.36	0.	0.37 (1,8,0)[b]	0.37 (1,8,0)	0.37 (1,8,0)	0.36 (1,8,0)
90/50.7	---	-0.356041	0.46 (1,6,-.14)	0.47 (1,6,-.14)	0.47 (1,6,-.14)	0.46 (1,6,-.14)
	0.81	0.	0.81 (1,6,0)	0.82 (1,7,0)	0.82 (1,7,0)	0.81 (1,6,0)
45/37.2	---	-0.587877	0.46 (1,7,-.04)	0.46 (1,7,-.04)	0.46 (1,7,-.04)	0.45 (1,7,-.04)
	0.48	0.	0.49 (1,7,0)	0.49 (1,8,0)	0.49 (1,8,0)	0.48 (1,7,0)
71.1/0	---	-0.277316	0.41 (1,8,.02)	0.41 (1,8,.02)	0.41 (1,8,.02)	0.41 (1,8,.02)
	0.41	0.	0.41 (1,8,0)	0.41 (1,8,0)	0.41 (1,8,0)	0.41 (1,8,0)
90_2	---	0.				
	0.70	0.	0.71 (1,5,0)	0.72 (1,5,0)	0.72 (1,5,0)	0.70 (1,5,0)
87.3/45	---	-0.365204	0.46 (1,6,-.14)	0.47 (1,6,-.14)	0.47 (1,6,-.14)	0.46 (1,6,-.14)
	0.76	0.	0.77 (1,7,0)	0.77 (1,7,0)	0.77 (1,7,0)	0.76 (1,7,0)
90/18/90	---	-0.121069	0.86 (1,6,-.09)	0.87 (1,6,-.09)	0.87 (1,6,-.09)	0.85 (1,6,-.09)
	0.96	0.	0.97 (1,6,0)	0.98 (1,6,0)	0.98 (1,6,0)	0.96 (1,6,0)
90_2/60.3	---	-0.233385	0.57 (1,6,-.13)	0.57 (1,6,-.13)	0.57 (1,6,-.13)	0.56 (1,6,-.13)
	0.76	0.	0.77 (1,6,0)	0.78 (1,6,0)	0.78 (1,6,0)	0.76 (1,6,0)
90_3	---	0.				
	0.70	0.	0.71 (1,5,0)	0.72 (1,5,0)	0.72 (1,5,0)	0.70 (1,5,0)
78.3/90/78.3	---	-0.137759	0.71 (1,5,-.01)	0.73 (1,5,-.01)	0.72 (1,5,-.01)	0.70 (1,5,-.01)
	0.71	0.	0.71 (1,5,0)	0.73 (1,5,0)	0.72 (1,5,0)	0.70 (1,5,0)
74.8/0/74.8	---	-0.232609	0.97 (1,6,-.01)	0.98 (1,7,.01)	0.98 (1,7,.01)	0.96 (1,6,-.01)
	0.96	0.	0.97 (1,6,0)	0.98 (1,7,0)	0.98 (1,7,0)	0.96 (1,6,0)
90/45/90	---	-0.277721	0.77 (1,6,-.06)	0.77 (1,6,-.06)	0.77 (1,6,-.06)	0.75 (1,6,-.06)
	0.84	0.	0.85 (1,6,0)	0.86 (1,6,0)	0.85 (1,6,0)	0.83 (1,6,0)

[b] Numbers in parentheses, (m,n, τ), indicate the number of axial half-waves, circumferential waves, and skewedness parameter, respectively

[†] E_1 = 146 GPa, E_2 = 10.8 GPa, G_{12} = 5.78 GPa, ν_{12} = 0.29

* Nonlinear rotations about the normal are neglected

[#] R = 82.5 mm, h = 0.5 mm, and q_{ext}^{*} = 140.6 kPa

[‡] see equation (152)

Table 137. Concluded

Laminate†	Ref. 92, Flügge live pressure	Present study				
		Induced shear, L_3‡	Donnell	Sanders*	Sanders	Sanders Live Pressure
$90/18.9_2/90$	---	-0.139724	0.82 (1,6,-.11)[b]	0.84 (1,6,-.11)	0.83 (1,6,-.11)	0.81 (1,6,-.11)
	1.00	0.	1.01 (1,7,0)	1.02 (1,7,0)	1.02 (1,7,0)	1.00 (1,7,0)
90/25.2/0/90	---	-0.093677	0.95 (1,6,-.06)	0.97 (1,6,-.06)	0.97 (1,6,-.06)	0.95 (1,6,-.06)
	1.00	0.	1.01 (1,7,0)	1.02 (1,7,0)	1.01 (1,7,0)	1.00 (1,7,0)
90/0/32.4/90	---	-0.119703	0.92 (1,6,-.08)	0.93 (1,6,-.08)	0.93 (1,6,-.08)	0.91 (1,6,-.08)
	1.00	0.	1.01 (1,6,0)	1.02 (1,7,0)	1.02 (1,7,0)	1.00 (1,7,0)
$80.5/0_2/80.5$	---	-0.138623	0.96 (1,6,.00)	0.97 (1,7,.01)	0.97 (1,7,.01)	0.96 (1,7,.01)
	0.96	0.	0.96 (1,6,0)	0.98 (1,7,0)	0.97 (1,7,0)	0.96 (1,6,0)
81/0/90/81	---	-0.092047	0.87 (1,6,.02)	0.88 (1,6,.01)	0.88 (1,6,.01)	0.86 (1,6,.01)
	0.87	0.	0.87 (1,6,0)	0.89 (1,6,0)	0.88 (1,6,0)	0.86 (1,6,0)
76.5/90/0/76.5	---	-0.137759	0.90 (1,6,-.01)	0.91 (1,6,-.01)	0.91 (1,6,-.01)	0.89 (1,6,-.01)
	0.89	0.	0.90 (1,6,0)	0.91 (1,6,0)	0.91 (1,6,0)	0.89 (1,6,0)

[b] Numbers in parentheses, (m,n, τ), indicate the number of axial half-waves, circumferential waves, and skewedness parameter, respectively

† $E_1 = 146$ GPa, $E_2 = 10.8$ GPa, $G_{12} = 5.78$ GPa, $\nu_{12} = 0.29$

* Nonlinear rotations about the normal are neglected

$R = 82.5$ mm, $h = 0.5$ mm, and $q_{ext}^* = 140.6$ kPa

‡ see equation (152)

Table 138. Buckling-pressure ratio $\frac{q_{ext}^{cr}}{q_{ext}^{*}}$ for laminated-composite cylinders[#] with simply supported edges and subjected to uniform hydrostatic pressure (L/R = 3)

Laminate[†]	Ref. 92, Flügge live pressure	Present study				
		Induced shear, L_3[‡]	Donnell	Sanders*	Sanders	Sanders Live Pressure
90/64	---	-0.276649	0.58 (1,5,-.09)	0.58 (1,5,-.09)	0.58 (1,5,-.09)	0.56 (1,5,-.09)
	0.83	0.	0.84 (1,4,0)	0.86 (1,5,0)	0.86 (1,5,0)	0.83 (1,5,0)
90/12/90	---	-0.080207	0.96 (1,5,-.04)	0.98 (1,5,-.04)	0.97 (1,5,-.04)	0.94 (1,5,-.04)
	0.99	0.	1.01 (1,5,0)	1.03 (1,5,0)	1.02 (1,5,0)	0.99 (1,5,0)
90/0/25.3/90	---	-0.094055	0.96 (1,5,-.04)	0.98 (1,5,-.04)	0.98 (1,5,-.04)	0.94 (1,5,-.04)
	1.00	0.	1.02 (1,5,0)	1.04 (1,5,0)	1.04 (1,5,0)	1.00 (1,5,0)

[b] Numbers in parentheses, (m,n, τ), indicate the number of axial half-waves, circumferential waves, and skewedness parameter, respectively

[†] $E_1 = 146$ GPa, $E_2 = 10.8$ GPa, $G_{12} = 5.78$ GPa, $\nu_{12} = 0.29$

* Nonlinear rotations about the normal are neglected

[#] $R = 82.5$ mm, $h = 0.5$ mm, and $q_{ext}^{*} = 82.61$ kPa

[‡] see equation (152)

Table 139. Buckling-pressure ratio $\frac{q_{ext}^{cr}}{q_{ext}^{*}}$ for laminated-composite cylinders[#] with simply supported edges and subjected to uniform hydrostatic pressure (L/R = 5)

Laminate[†]	Ref. 92, Flügge live pressure	Present study				
		Induced shear, L_3[‡]	Donnell	Sanders*	Sanders	Sanders Live Pressure
90/67	---	-0.240788	0.62 (1,4,-.06)	0.63 (1,4,-.05)	0.63 (1,4,-.05)	0.59 (1,4,-.05)
	0.83	0.	0.84 (1,3,0)	0.88 (1,4,0)	0.88 (1,4,0)	0.83 (1,4,0)
90/4.9/90	---	-0.032581	1.02 (1,4,-.01)	1.05 (1,4,-.01)	1.04 (1,4,-.01)	0.98 (1,4,-.01)
	0.99	0.	1.03 (1,4,0)	1.06 (1,4,0)	1.05 (1,4,0)	0.99 (1,4,0)
90/0/20.2/90	---	-0.074562	0.99 (1,4,-.02)	1.02 (1,4,-.02)	1.02 (1,4,-.02)	0.96 (1,4,-.02)
	1.00	0.	1.03 (1,4,0)	1.07 (1,4,0)	1.07 (1,4,0)	1.00 (1,4,0)

[b] Numbers in parentheses, (m,n, τ), indicate the number of axial half-waves, circumferential waves, and skewedness parameter, respectively

[†] $E_1 = 146$ GPa, $E_2 = 10.8$ GPa, $G_{12} = 5.78$ GPa, $\nu_{12} = 0.29$

* Nonlinear rotations about the normal are neglected

[#] $R = 82.5$ mm, $h = 0.5$ mm, and $q_{ext}^{*} = 50.65$ kPa

[‡] see equation (152)

Table 140. Buckling-pressure ratio $\frac{q_{ext}^{cr}}{q_{ext}^{*}}$ for laminated-composite cylinders[#] with simply supported edges and subjected to uniform hydrostatic pressure (L/R = 10)

Laminate[†]	Ref. 92, Flügge live pressure	Present study				
		Induced shear, L_3[‡]	Donnell	Sanders*	Sanders	Sanders Live Pressure
90/76	---	-0.130924	0.76 (1,2,-.01)	0.83 (1,3,-.02)	0.83 (1,3,-.02)	0.74 (1,3,-.02)
	0.87	0.	0.84 (1,2,0)	0.98 (1,3,0)	0.98 (1,3,0)	0.87 (1,2,0)
90/0/90	---	0.				
	1.00	0.	1.08 (1,3,0)	1.12 (1,3,0)	1.12 (1,3,0)	1.00 (1,3,0)
90/0/13.1/90	---	-0.047625	1.04 (1,3,-.01)	1.09 (1,3,-.01)	1.09 (1,3,-.01)	0.97 (1,3,-.01)
	1.00	0.	1.06 (1,3,0)	1.12 (1,3,0)	1.11 (1,3,0)	0.99 (1,3,0)

[b] Numbers in parentheses, (m,n, τ), indicate the number of axial half-waves, circumferential waves, and skewedness parameter, respectively

[†] $E_1 = 146$ GPa, $E_2 = 10.8$ GPa, $G_{12} = 5.78$ GPa, $\nu_{12} = 0.29$

* Nonlinear rotations about the normal are neglected

[#] $R = 82.5$ mm, $h = 0.5$ mm, and $q_{ext}^{*} = 25.63$ kPa

[‡] see equation (152)

Table 141. Buckling pressure (N/mm^2) for a laminated-composite cylinders with simply supported edges and subjected to hydrostatic compression or to hydrostatic pressure and torsion

Loading	Ref. 94	Present study		
	Flügge Live Pressure	Sanders Live Pressure	Sanders* Live Pressure	Donnell
Hydrostatic pressure $L_1 = 0.5$, $L_2 = 1$	0.03766 (7)[a]	0.03722 (1,7,0)[b]	0.03727 (1,7,0)	0.03766 (1,7,0)
Hydrostatic pressure and torsion $L_1 = 0.5$, $L_2 = 1$, $L_3 = 1$	0.03613 (7)	0.03657 (1,7,.02)	0.03662 (1,7,.02)	0.03698 (1,7,.02)

[a] Number in parentheses, (n), indicates the number of circumferential waves

[b] Numbers in parentheses, (m,n, τ), indicate the number of axial half-waves, circumferential waves, and skewedness parameter, respectively

* Nonlinear rotations about the normal are neglected

[#] R = 250.625 mm, h = 1.25 mm, and L = 530 mm

[†] Laminate stiffnesses:

$A_{11} = 0.60278 \times 10^5$ N/mm
$A_{12} = 0.23801 \times 10^5$ N/mm
$A_{16} = 0.$ N/mm
$A_{22} = 0.65646 \times 10^5$ N/mm
$A_{26} = 0.$ N/mm
$A_{66} = 0.27417 \times 10^5$ N/mm

$B_{11} = 0.36680 \times 10^5$ N
$B_{12} = 0.16988 \times 10^5$ N
$B_{16} = 0.$ N
$B_{22} = 0.37798 \times 10^5$ N
$B_{26} = 0.$ N
$B_{66} = 0.19248 \times 10^5$ N

$D_{11} = 0.29772 \times 10^5$ N mm
$D_{12} = 0.15627 \times 10^5$ N mm
$D_{16} = 0.$ N mm
$D_{22} = 0.29353 \times 10^5$ N mm
$D_{26} = 0.$ N mm
$D_{66} = 0.17510 \times 10^5$ N mm

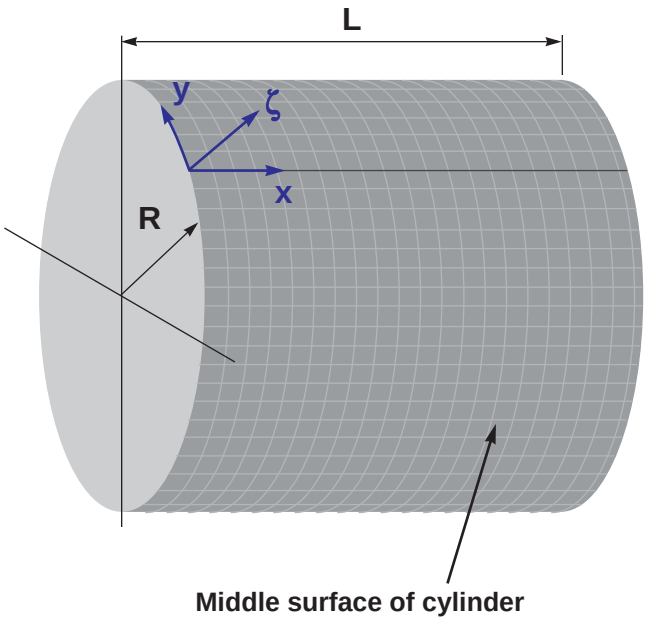

Figure 1. Geometry and coordinate system of a cylindrical shell.

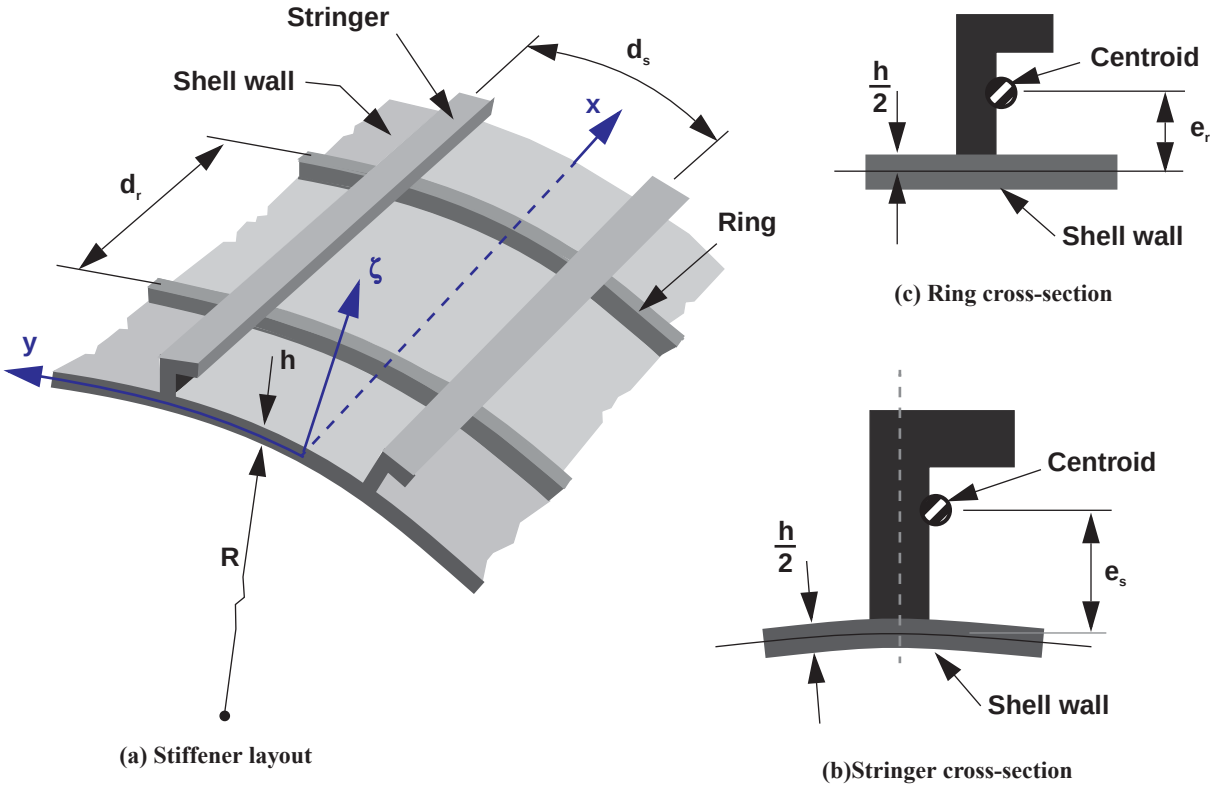

(a) Stiffener layout

(c) Ring cross-section

(b)Stringer cross-section

Figure 2. Stiffener details.

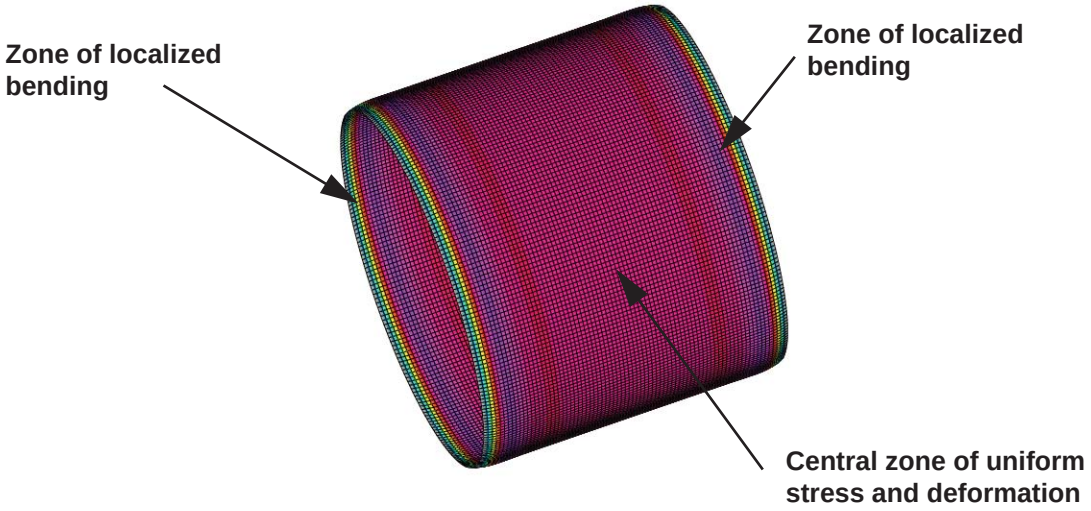

Figure 3. Circumfrential stress resultant distribution and localized-bending zones in a compression-loaded cylinder with ends restrained against radial displacement.

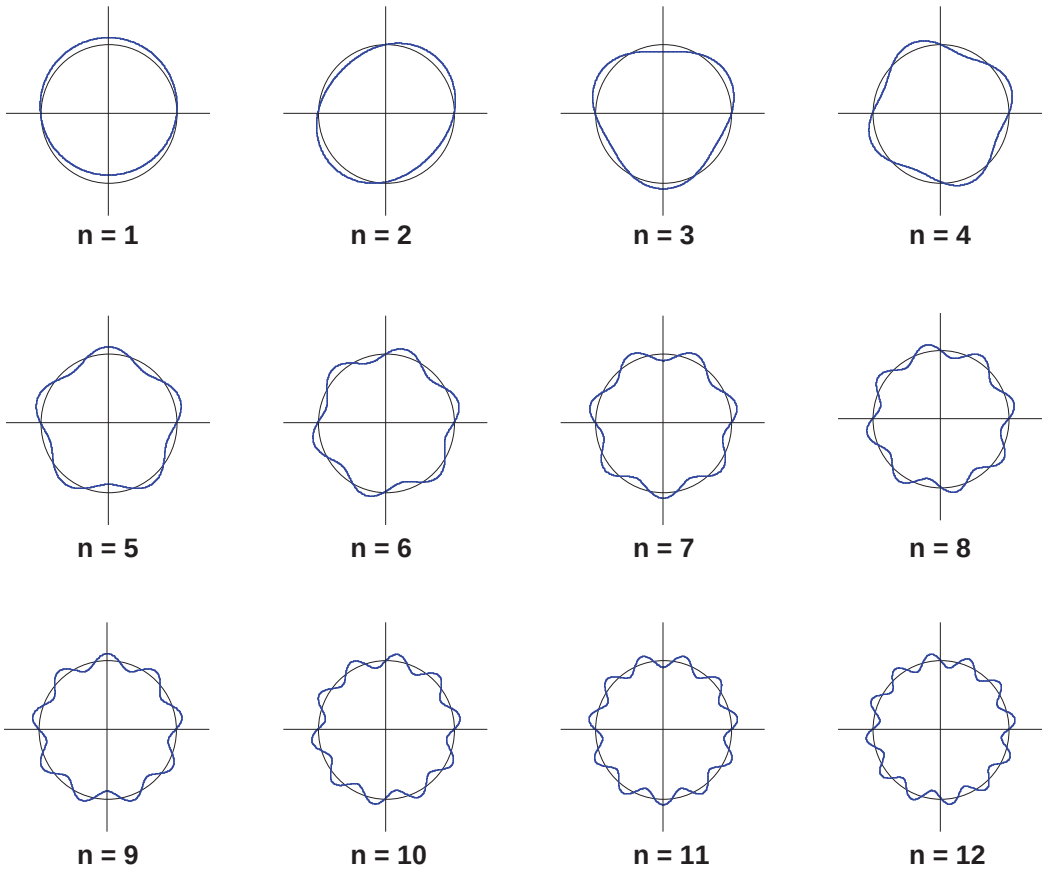

Figure 4. Circumferential waveforms used in equation (77c).

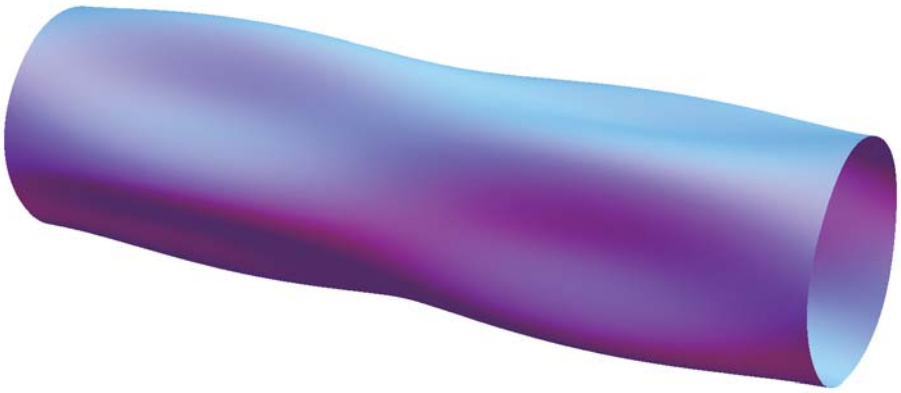

(a) Three-dimensional rendering of a buckling mode

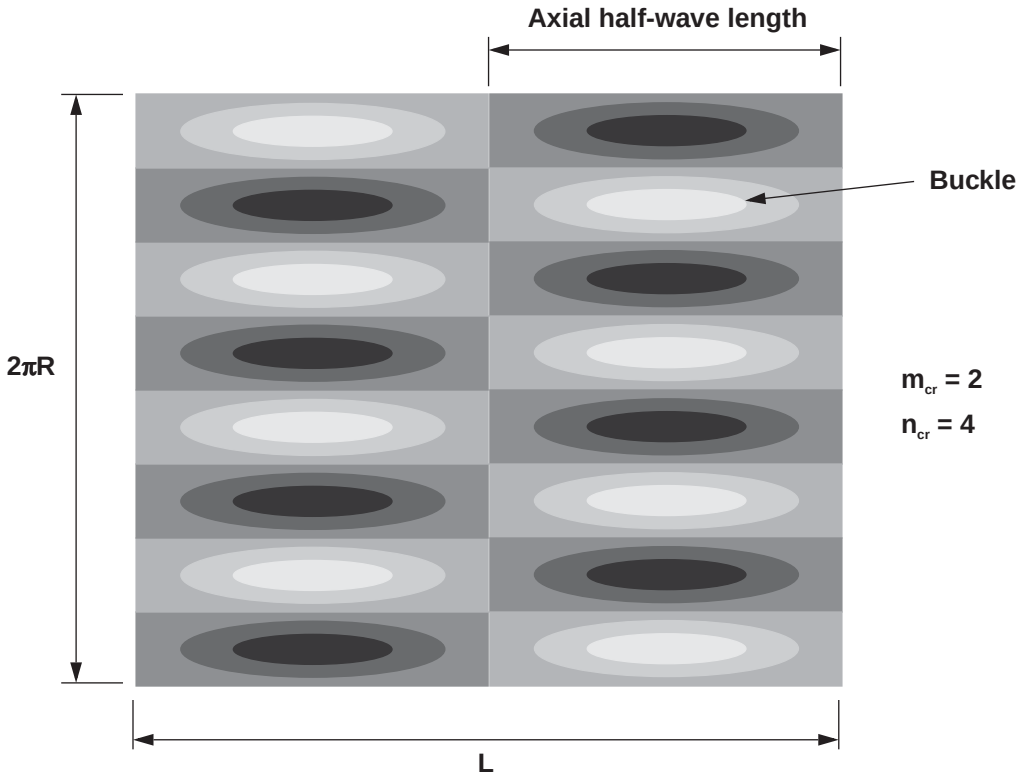

(b) Contour plot of the radial displacement

Figure 5. Typical buckle pattern of a compression-loaded cylinder.

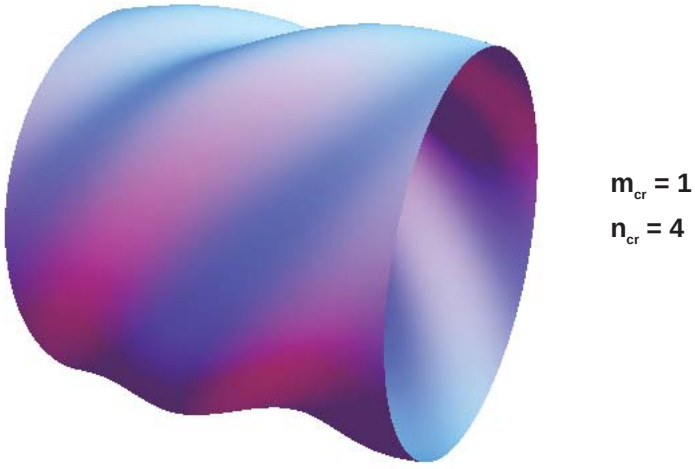

(a) Three-dimensional rendering of a skewed buckling mode

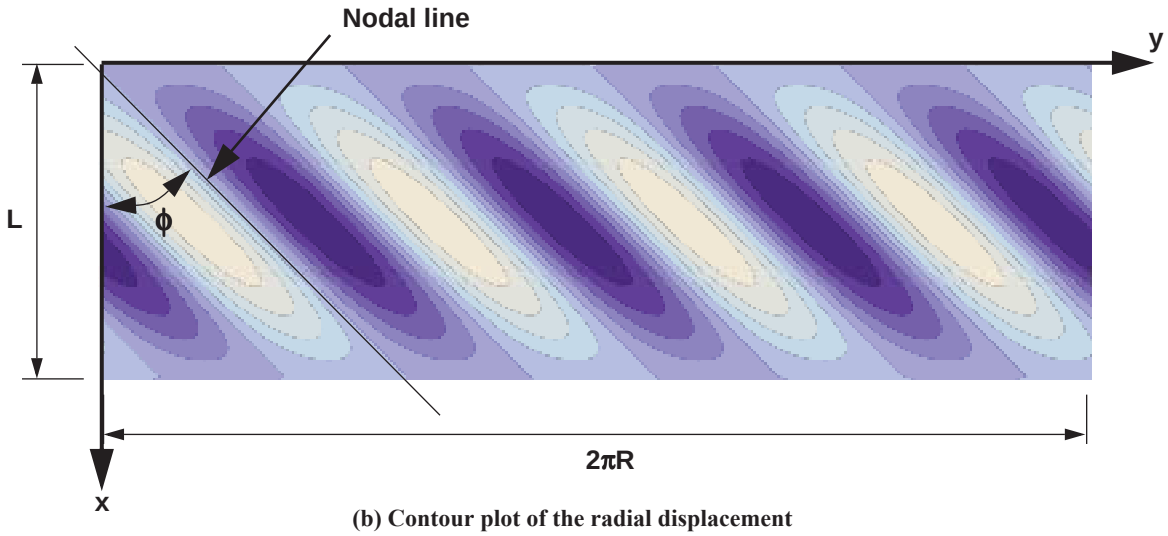

(b) Contour plot of the radial displacement

Figure 6. Typical skewed buckle pattern of a compression-loaded anisotropic cylinder or an orthotropic cylinder subjected to shear loads.

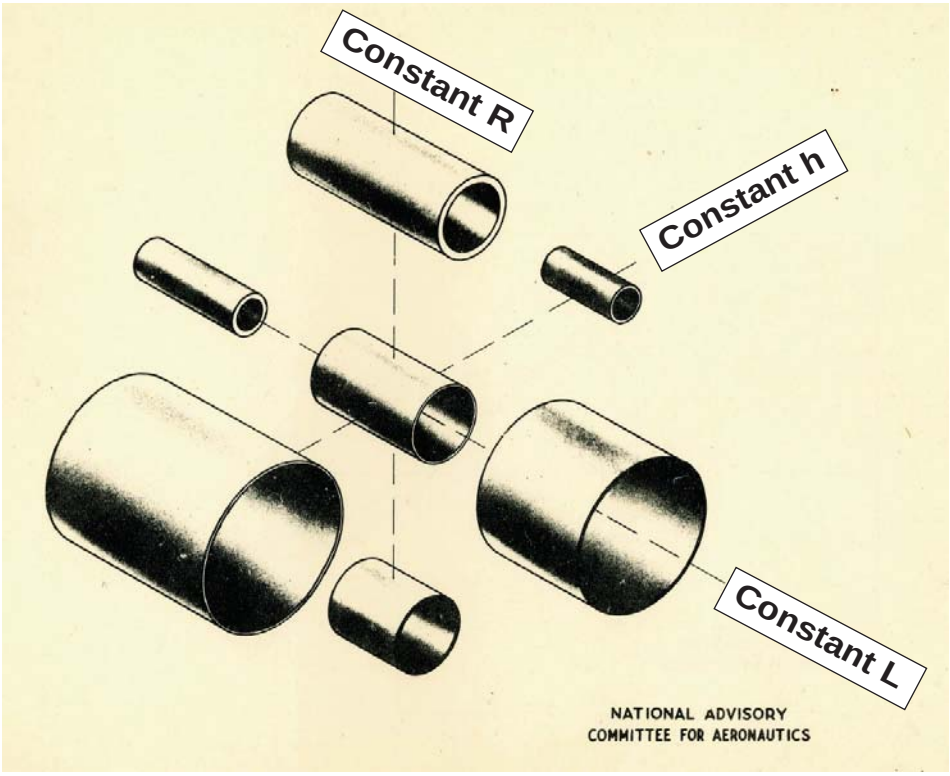

Figure 7. Representative cylinders corresponding to the same value of the Batdorf Z parameter (Z about 150).

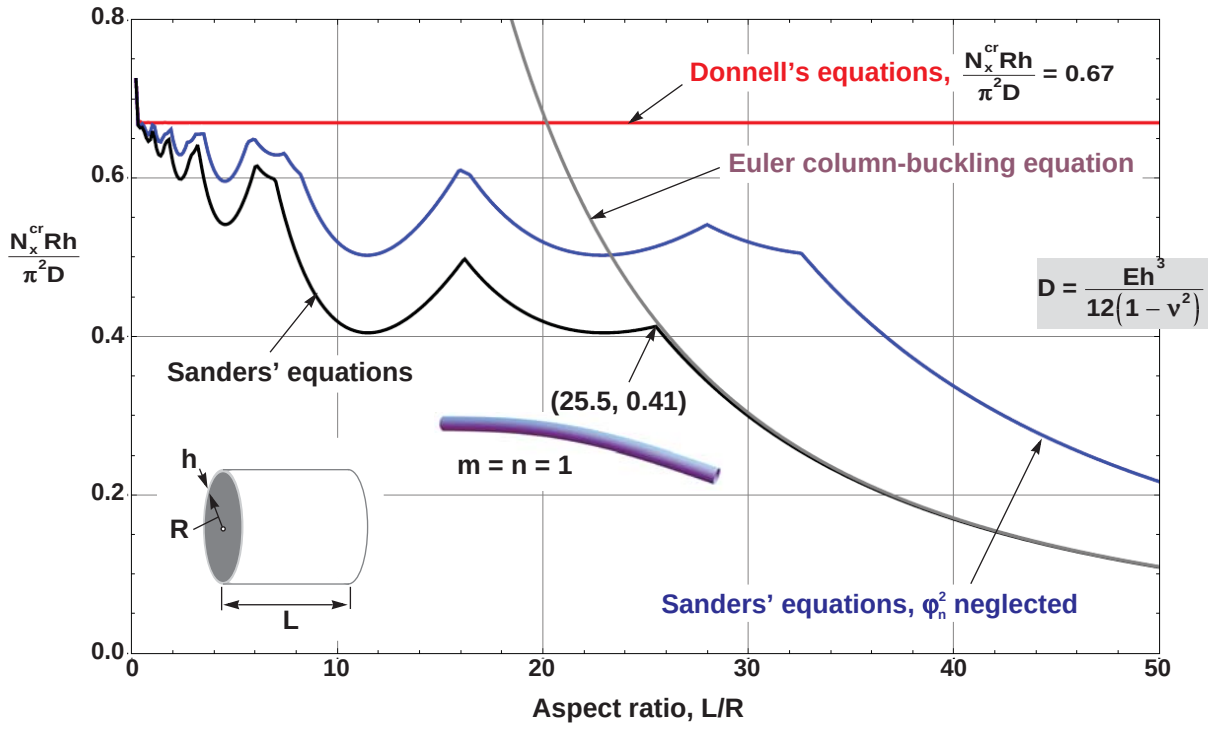

Figure 8. Nondimensional buckling loads for compression-loaded (N_x) isotropic cylinders with simply supported edges for R/h = 50 and L/R ≤ 50 (ν = 0.3).

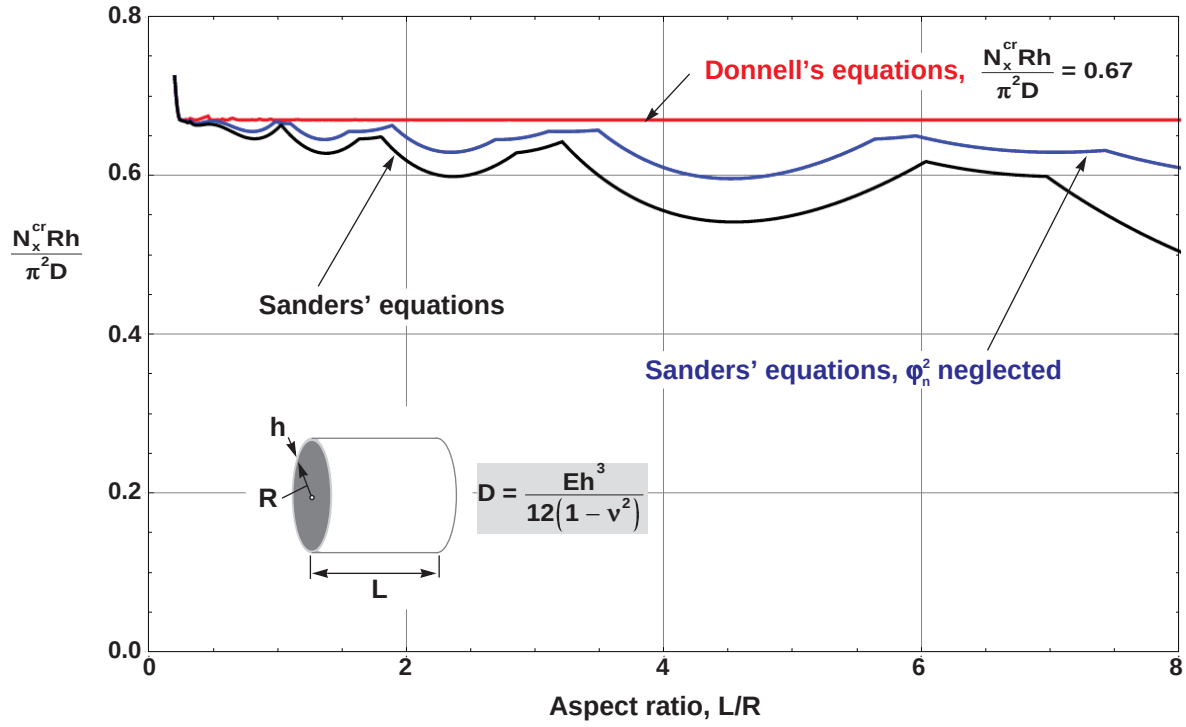

Figure 9. Nondimensional buckling loads for compression-loaded (N_x) isotropic cylinders with simply supported edges for R/h = 50 and L/R ≤ 8 (ν = 0.3).

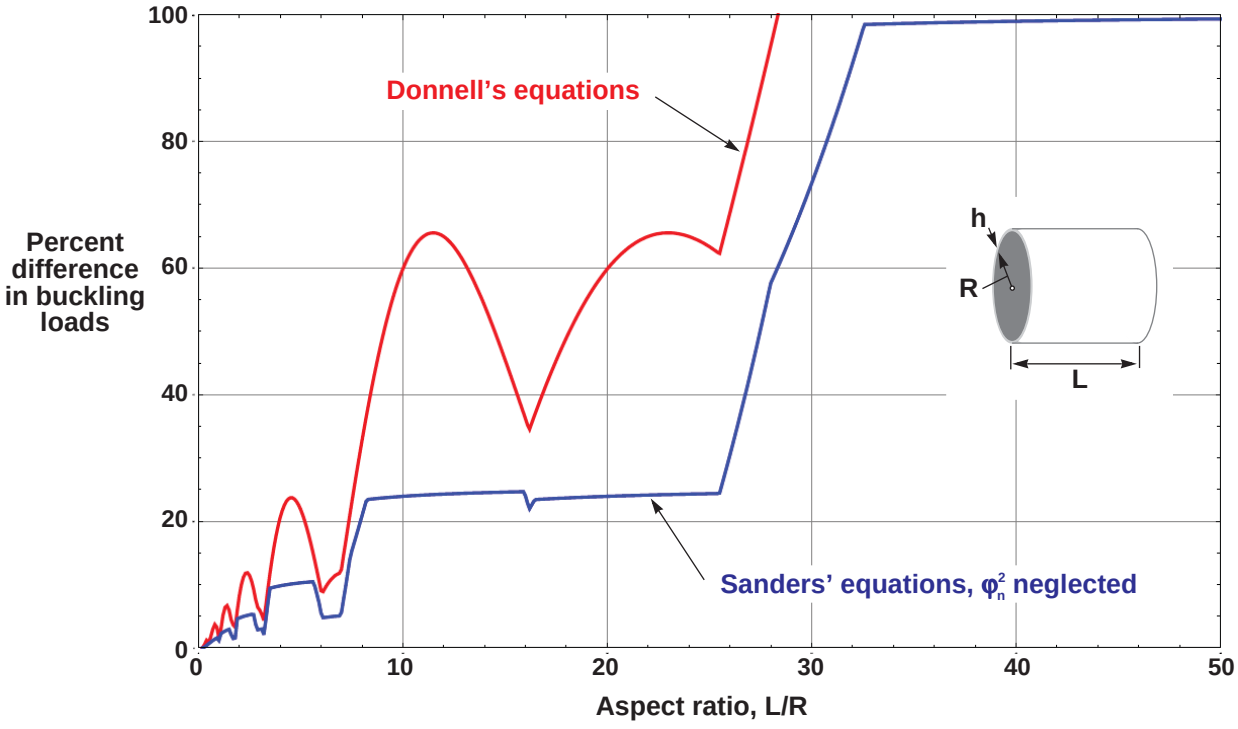

Figure 10. Difference in buckling loads, with respect to results based on Sanders' equations, for compression-loaded isotropic cylinders with simply supported edges for R/h = 50 and L/R ≤ 50 (ν = 0.3).

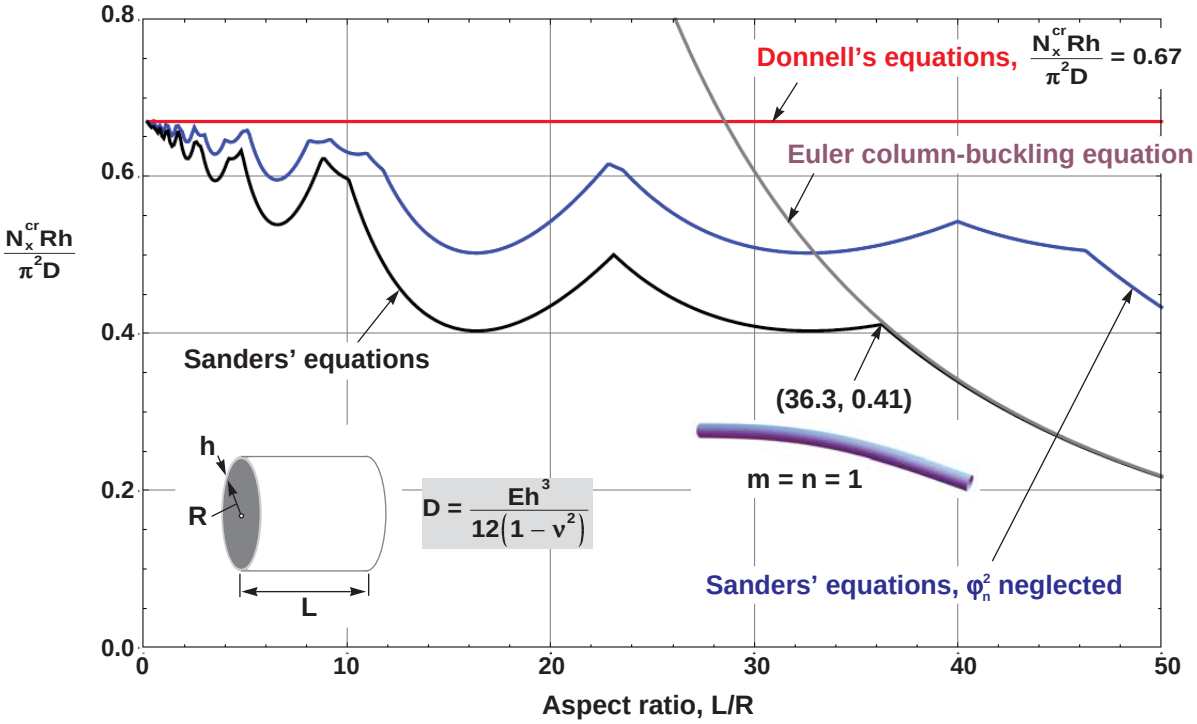

Figure 11. Nondimensional buckling loads for compression-loaded (N_x) isotropic cylinders with simply supported edges for R/h = 100 and L/R ≤ 50 (ν = 0.3).

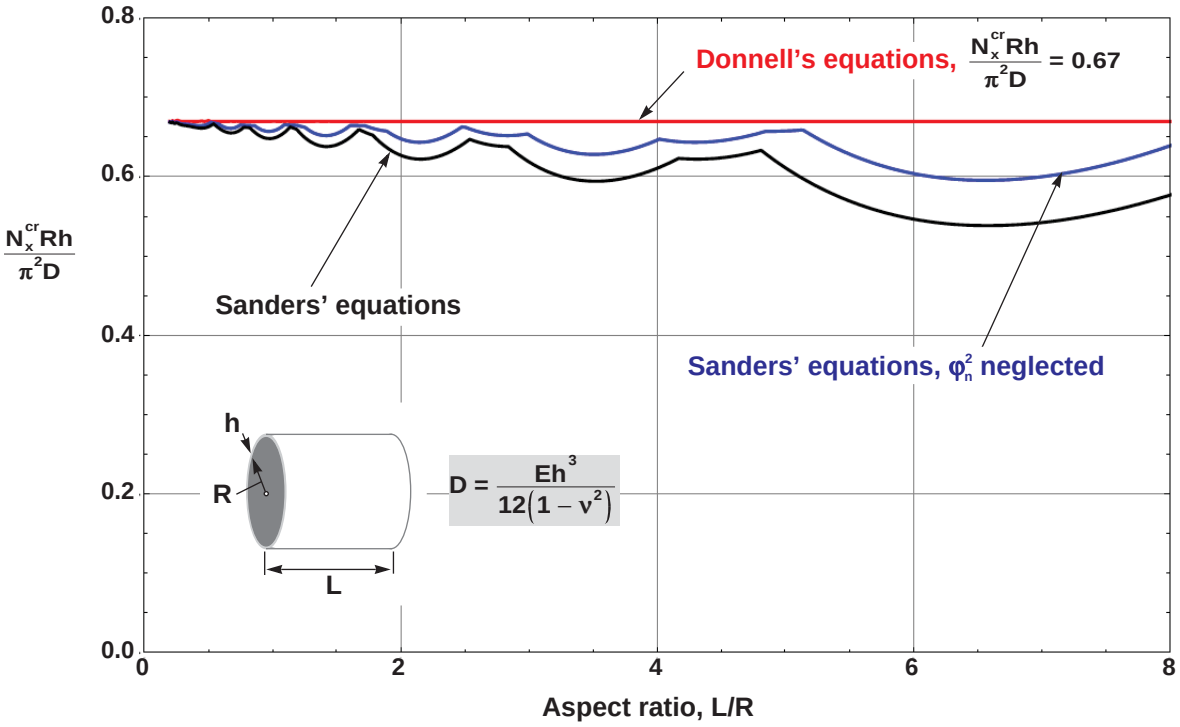

Figure 12. Nondimensional buckling loads for compression-loaded (N_x) isotropic cylinders with simply supported edges for R/h = 100 and L/R ≤ 8 (ν = 0.3).

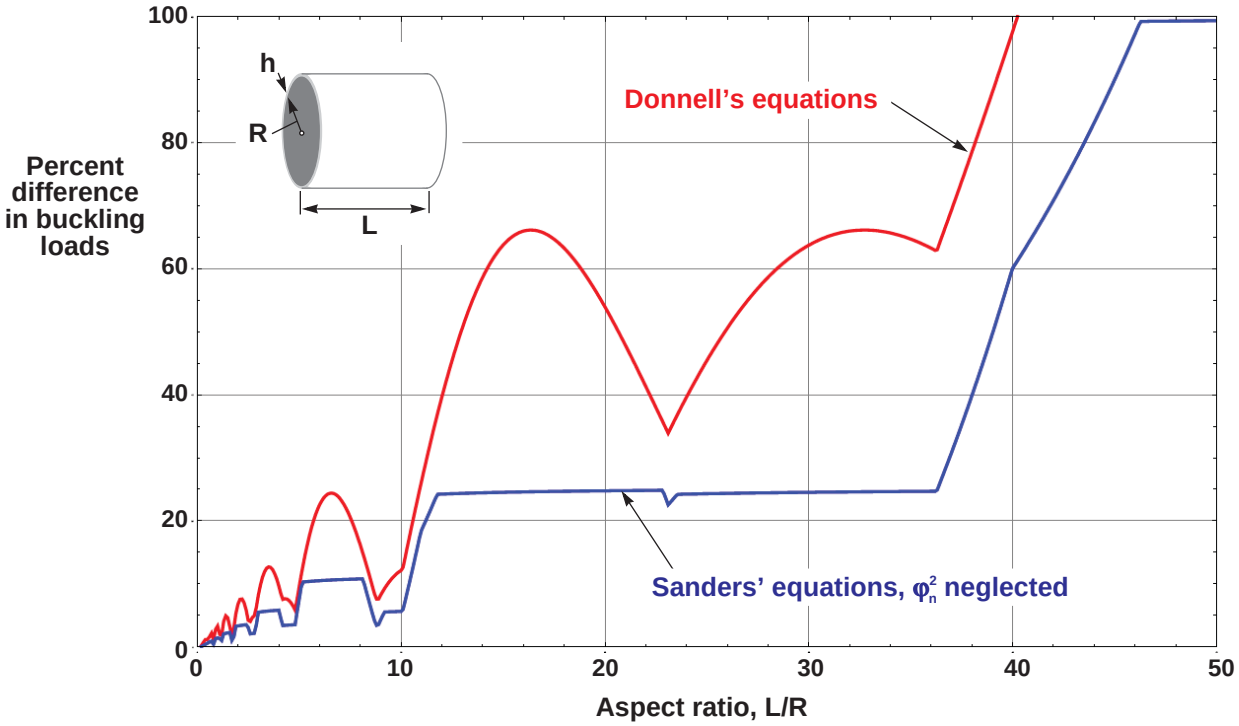

Figure 13. Difference in buckling loads, with respect to results based on Sanders' equations, for compression-loaded isotropic cylinders with simply supported edges for R/h = 100 and L/R ≤ 50 (ν = 0.3).

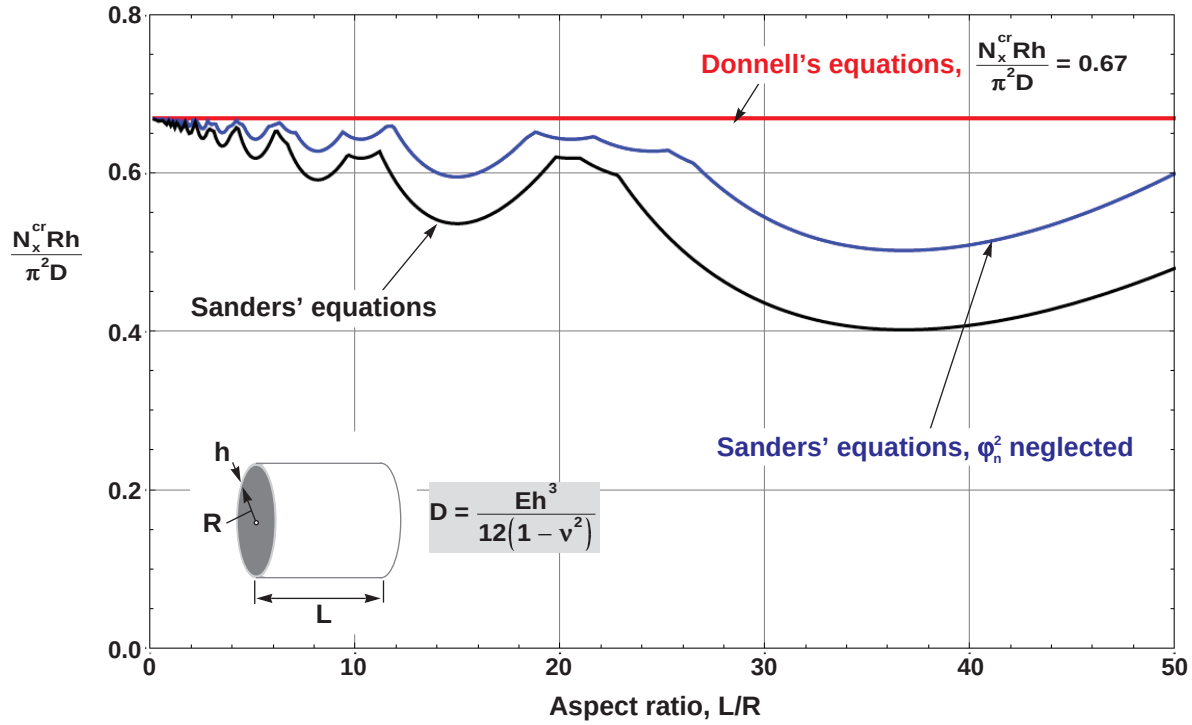

Figure 14. Nondimensional buckling loads for compression-loaded (N_x) isotropic cylinders with simply supported edges for R/h = 500 and L/R ≤ 50 (ν = 0.3).

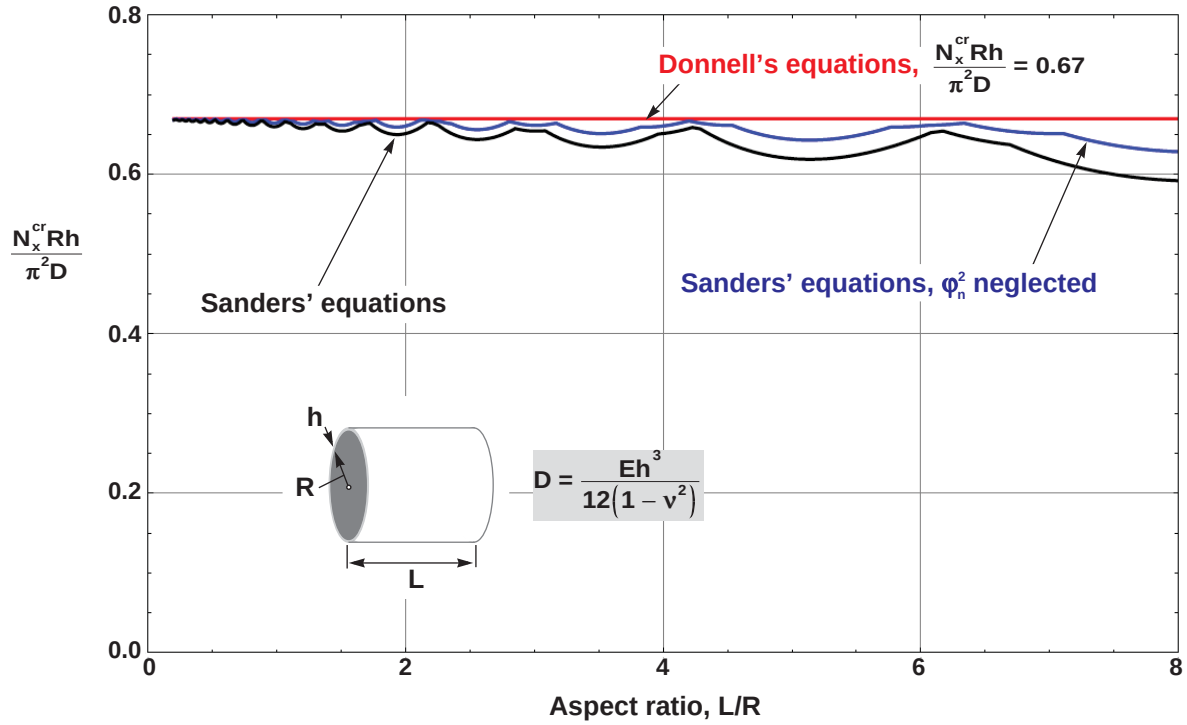

Figure 15. Nondimensional buckling loads for compression-loaded (N_x) isotropic cylinders with simply supported edges for R/h = 500 and L/R ≤ 8 (ν = 0.3).

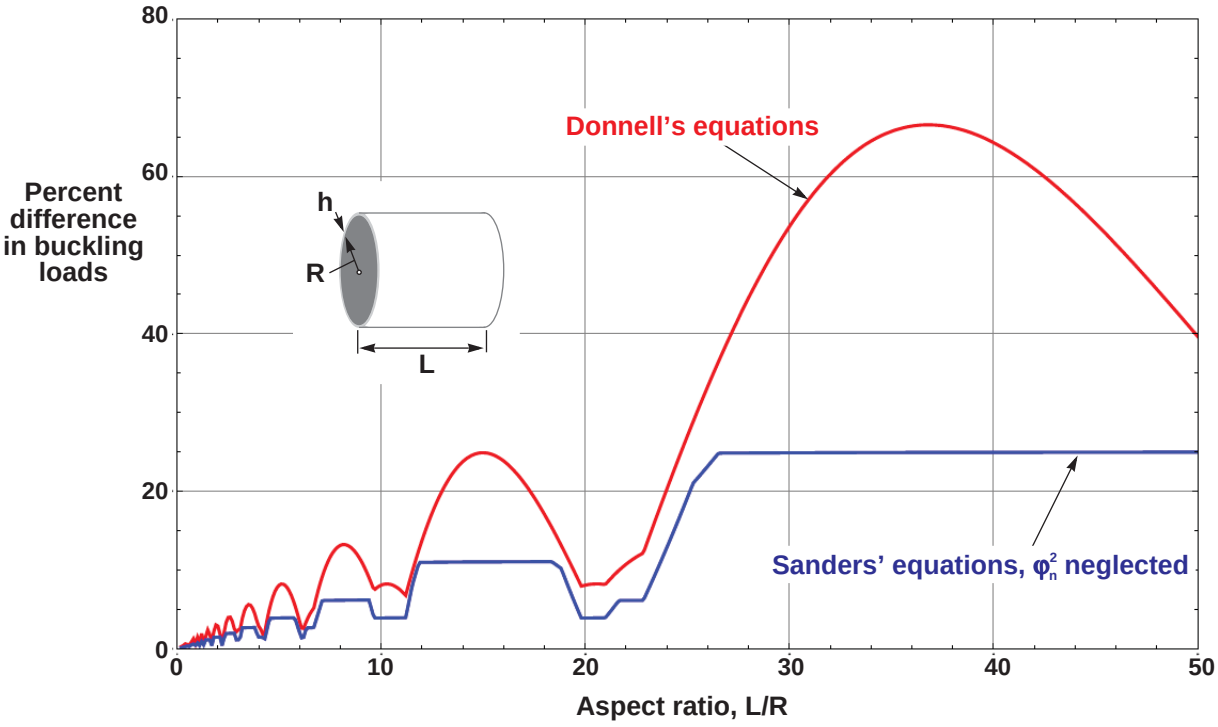

Figure 16. Difference in buckling loads, with respect to results based on Sanders' equations, for compression-loaded isotropic cylinders with simply supported edges for R/h = 500 and L/R ≤ 50 (ν = 0.3).

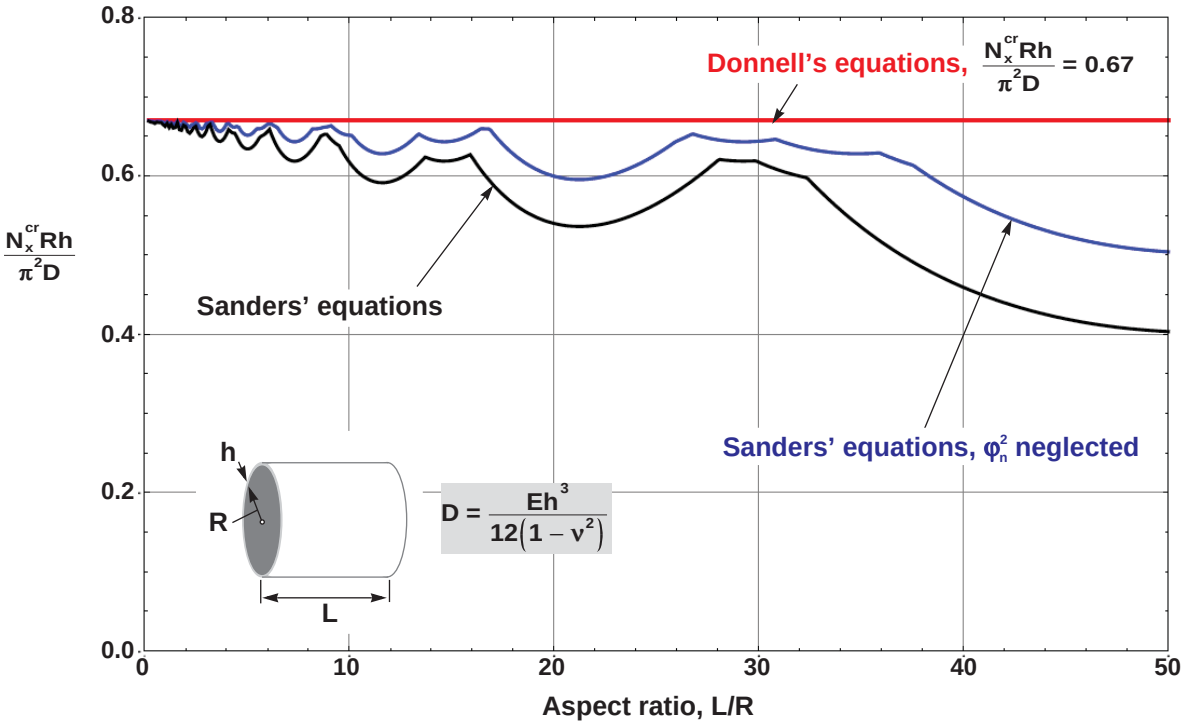

Figure 17. Nondimensional buckling loads for compression-loaded (N_x) isotropic cylinders with simply supported edges for R/h = 1000 and L/R ≤ 50 (ν = 0.3).

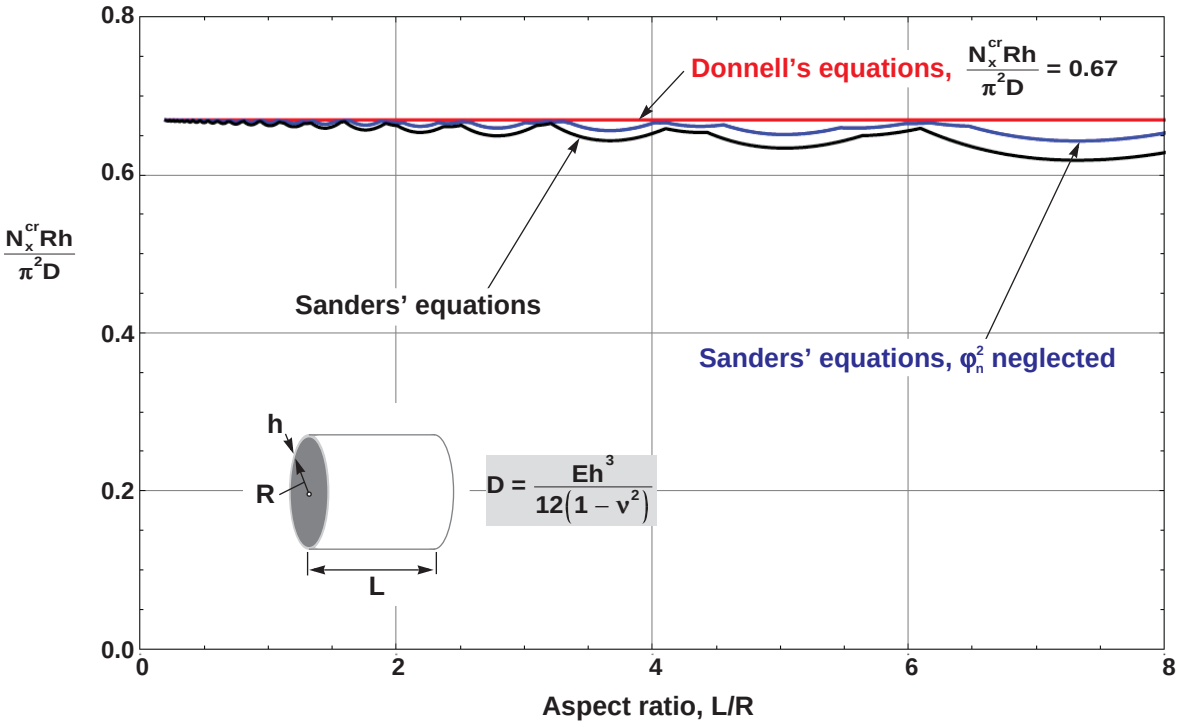

Figure 18. Nondimensional buckling loads for compression-loaded (N_x) isotropic cylinders with simply supported edges for R/h = 1000 and L/R ≤ 8 (ν = 0.3).

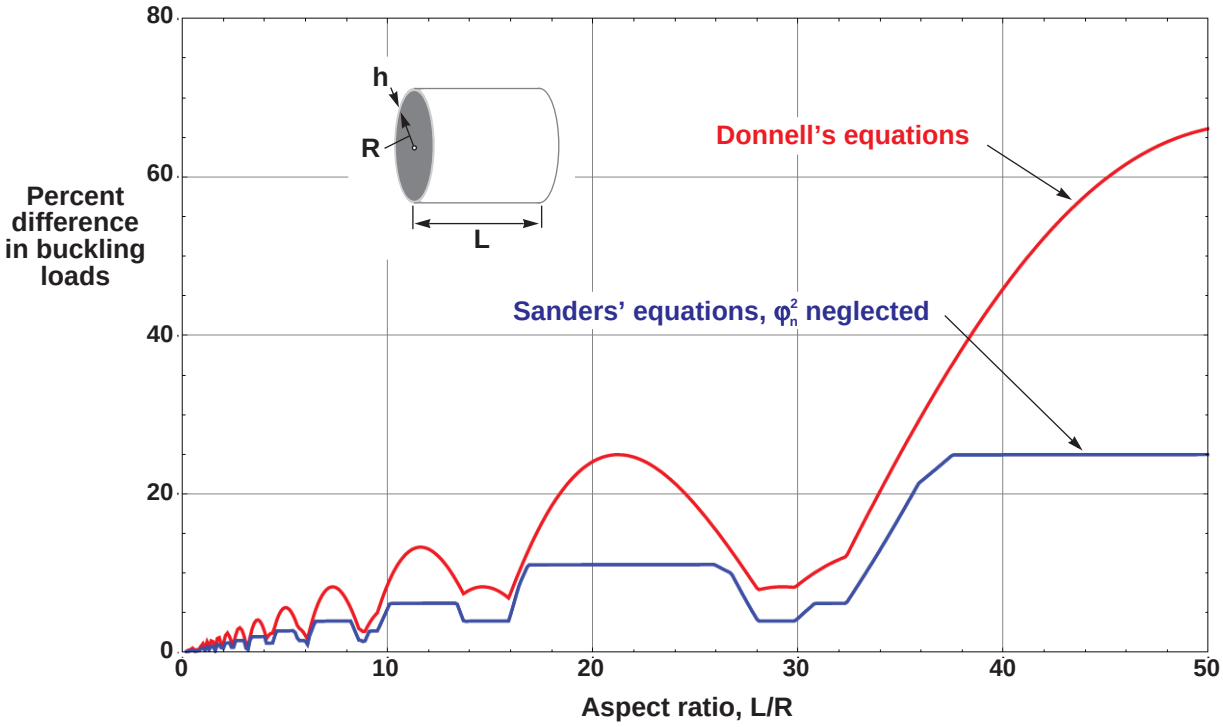

Figure 19. Difference in buckling loads, with respect to results based on Sanders' equations, for compression-loaded isotropic cylinders with simply supported edges for R/h = 1000 and L/R ≤ 50 (ν = 0.3).

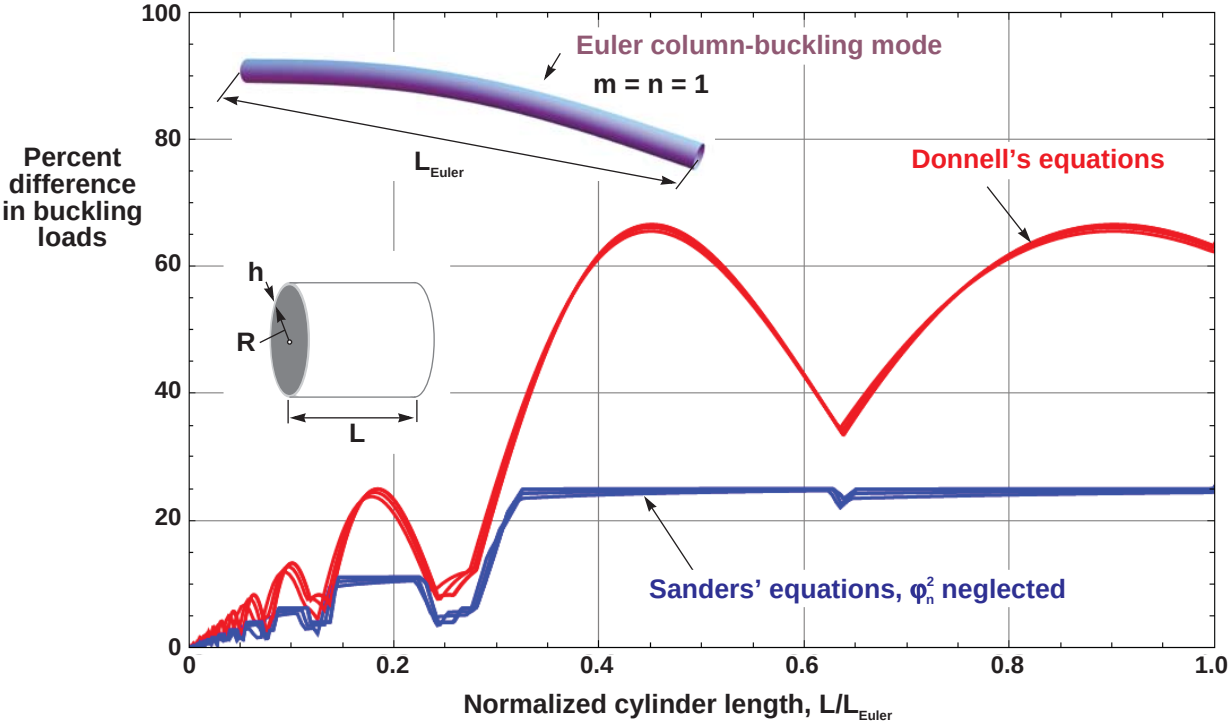

Figure 20. Difference in buckling loads, with respect to results based on Sanders' equations, for compression-loaded isotropic cylinders with simply supported edges for R/h = 50, 100, 500, and 1000 (ν = 0.3).

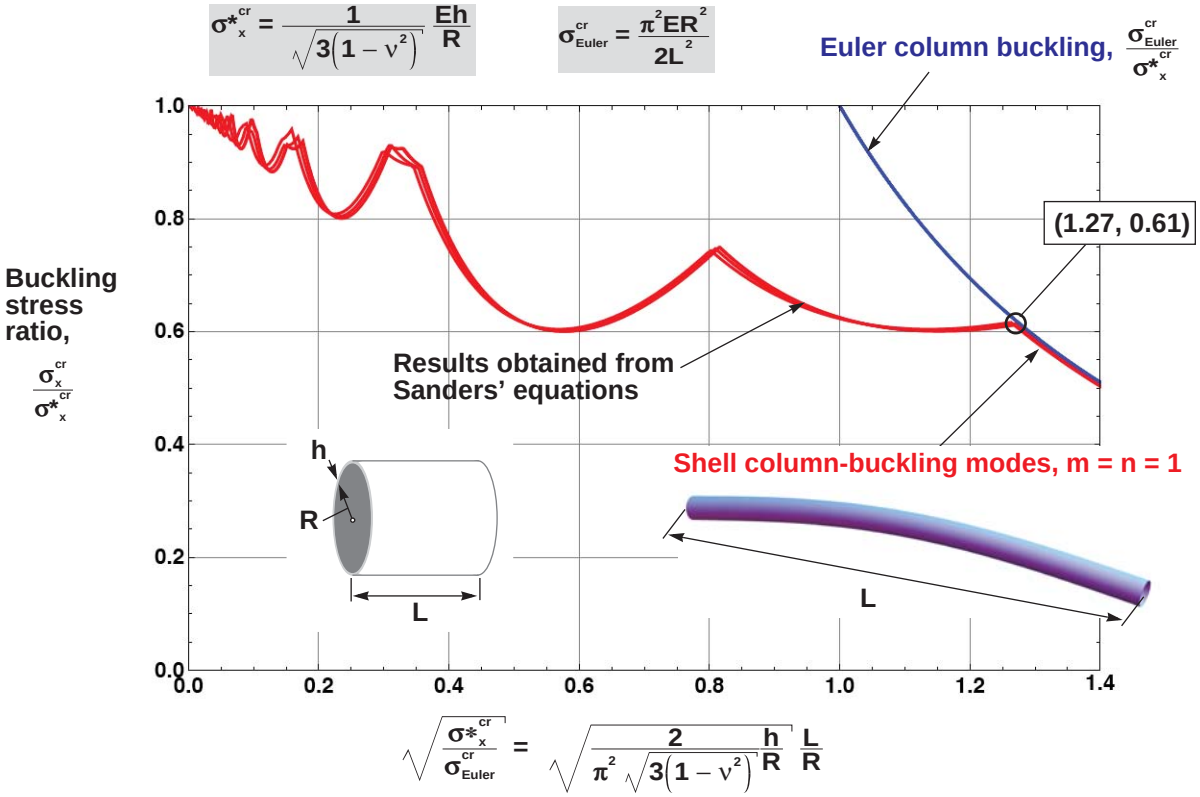

Figure 21. Nondimensional buckling stress ratios for compression-loaded isotropic cylinders with simply supported edges, for R/h = 50, 100, 500, and 1000 (ν = 0.3).

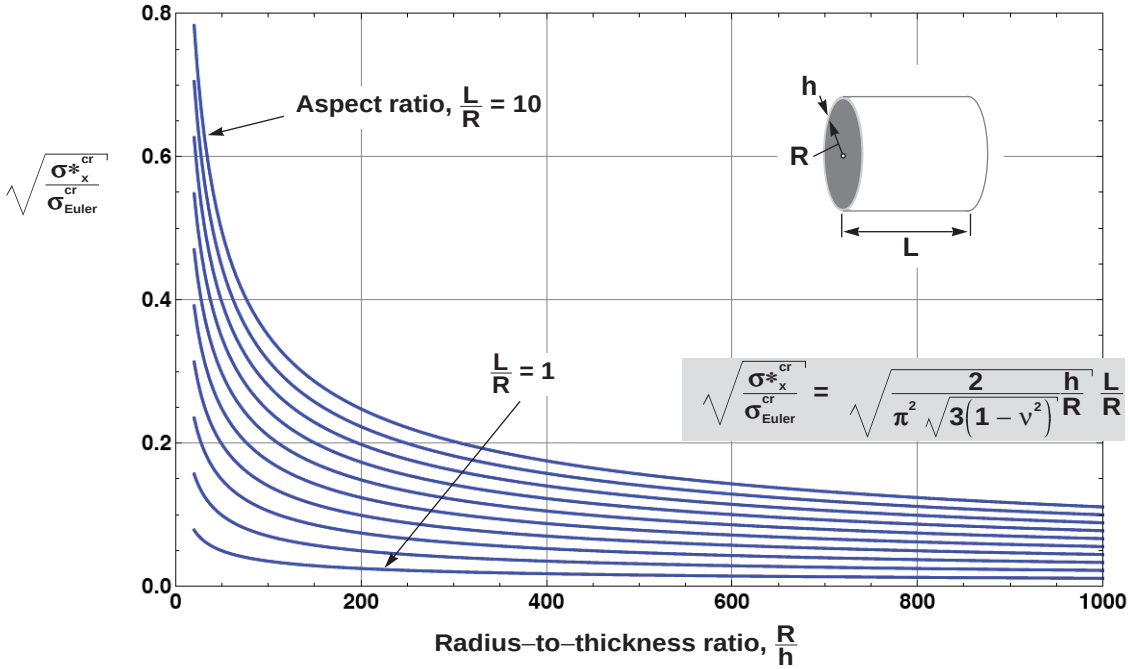

Figure 22. Values of the abscissa shown in figure 21 as a function of R/h and for select values of L/R (ν = 0.3).

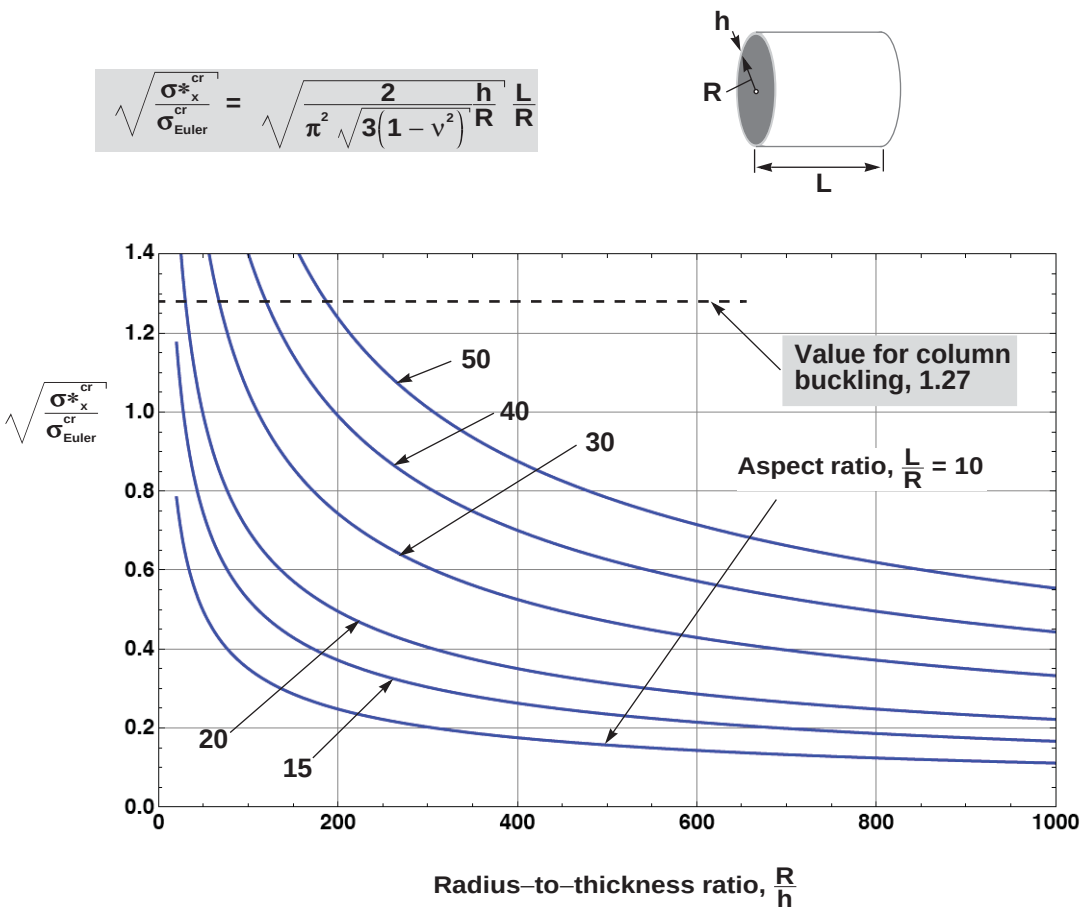

Figure 23. Values of the abscissa shown in figure 21 as a function of R/h and for select values of L/R (ν = 0.3).

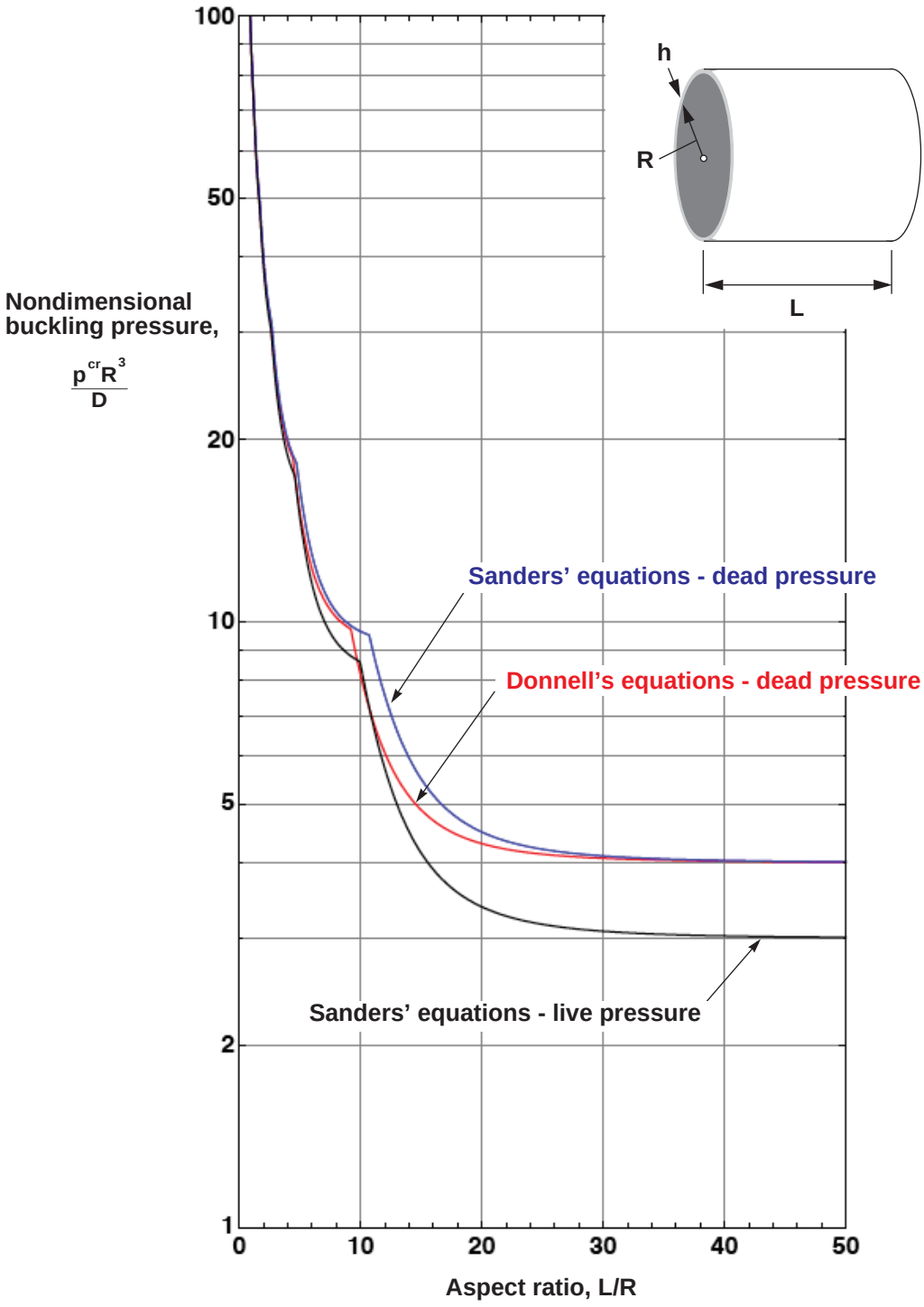

Figure 24. Nondimensional buckling loads for external-pressure-loaded isotropic cylinders with simply supported edges for R/h = 50 (ν = 0.3).

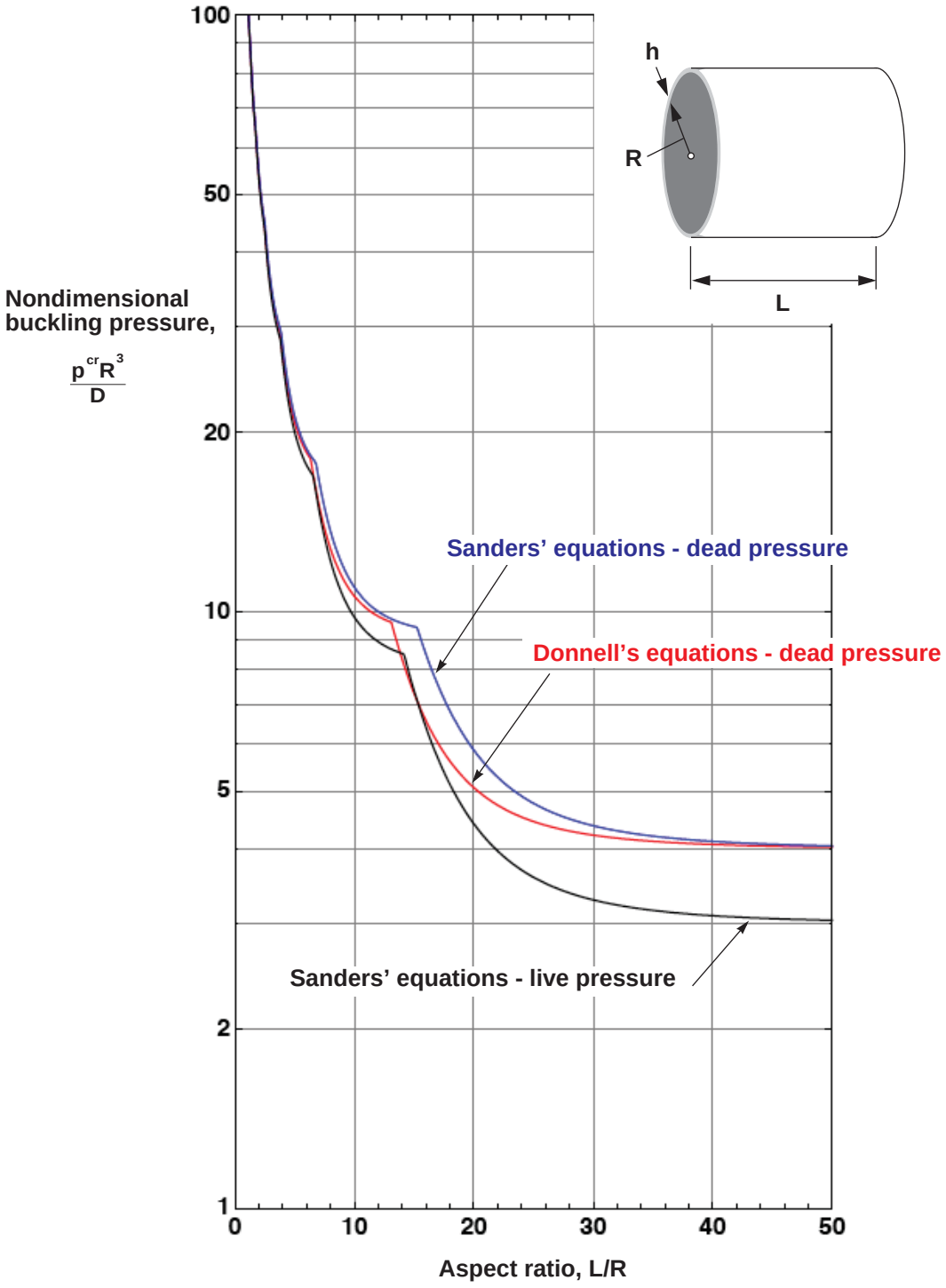

Figure 25. Nondimensional buckling loads for external-pressure-loaded isotropic cylinders with simply supported edges for R/h = 100 (ν = 0.3).

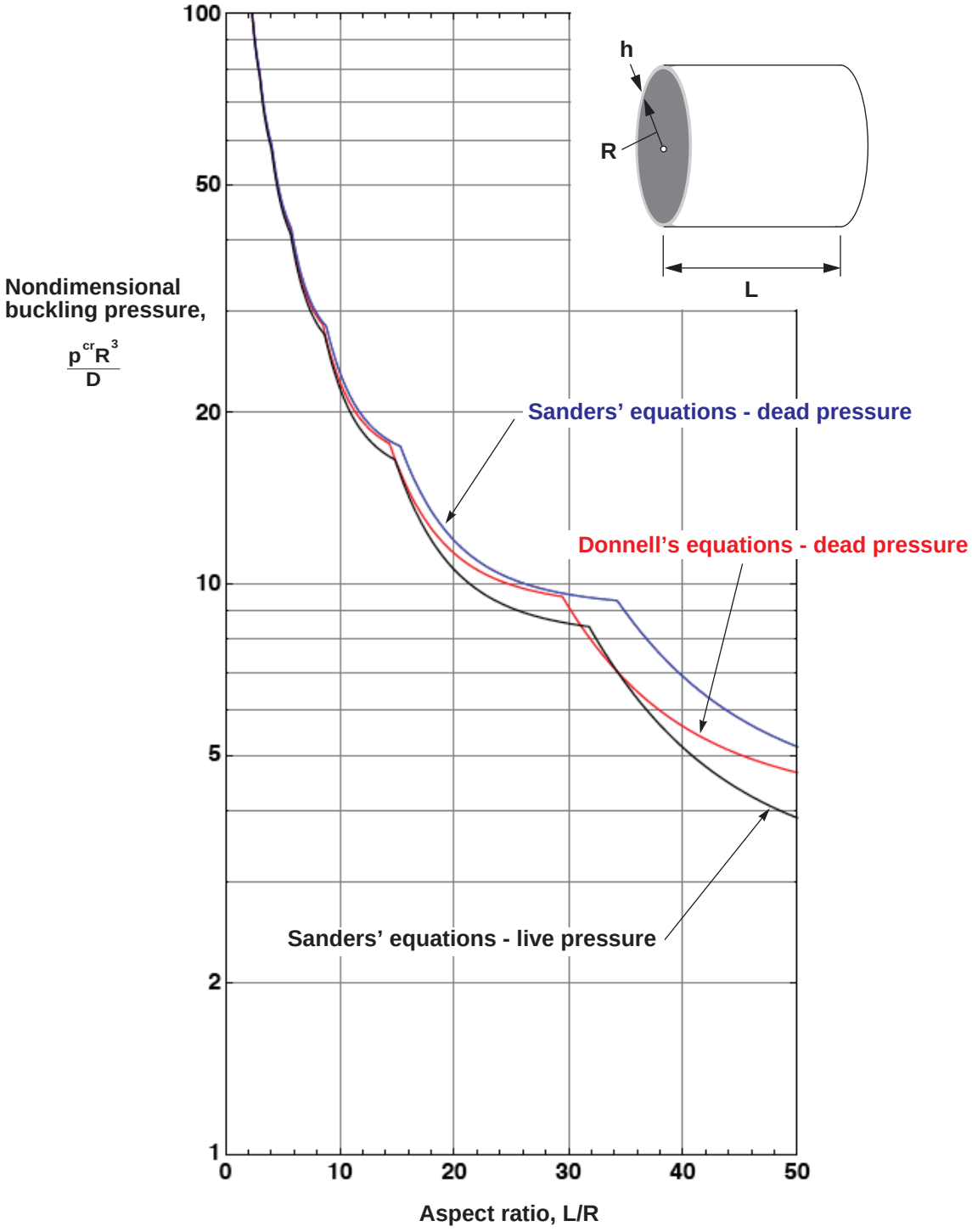

Figure 26. Nondimensional buckling loads for external-pressure-loaded isotropic cylinders with simply supported edges for R/h = 500 (ν = 0.3).

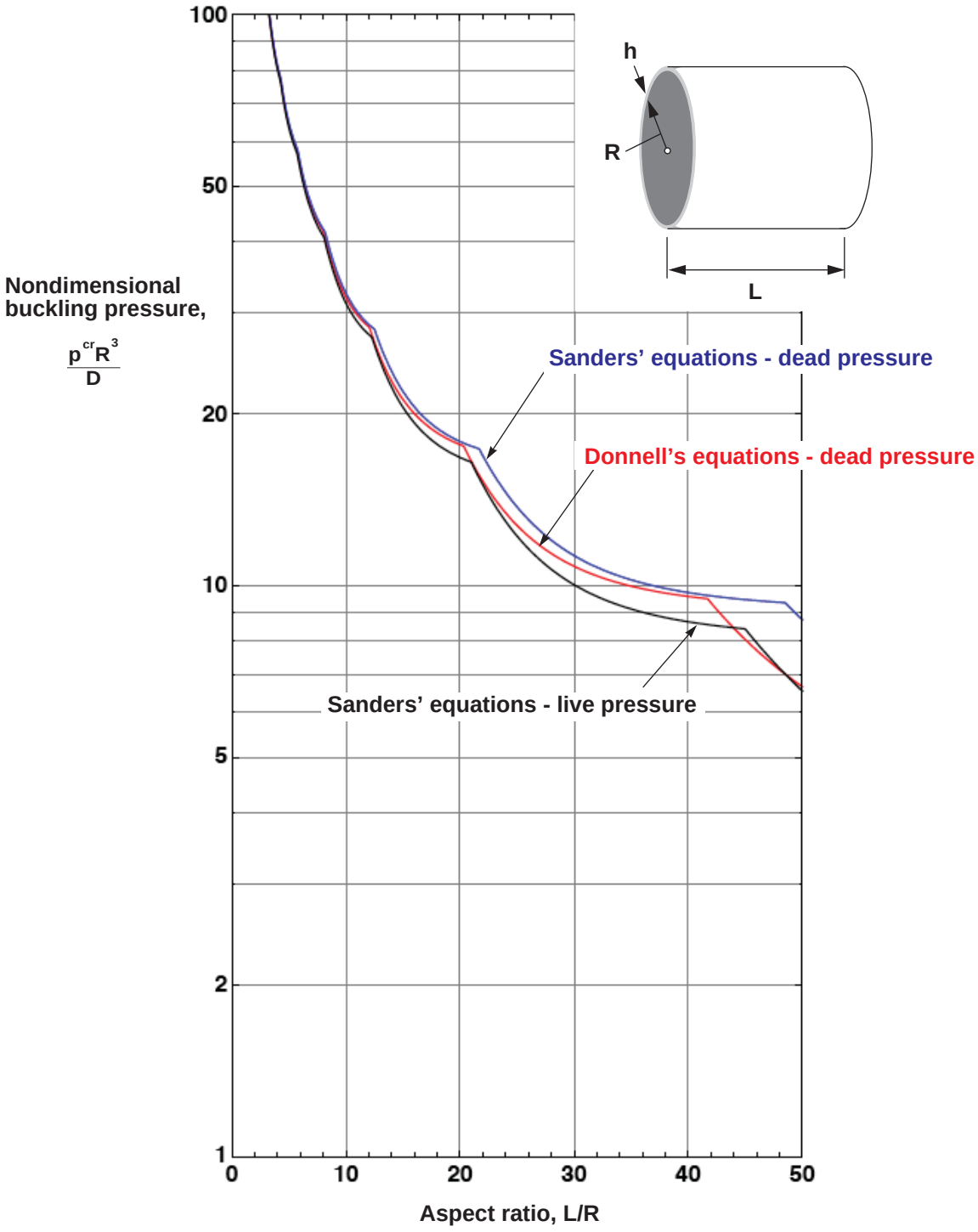

Figure 27. Nondimensional buckling loads for external-pressure-loaded isotropic cylinders with simply supported edges for R/h = 1000 (ν = 0.3).

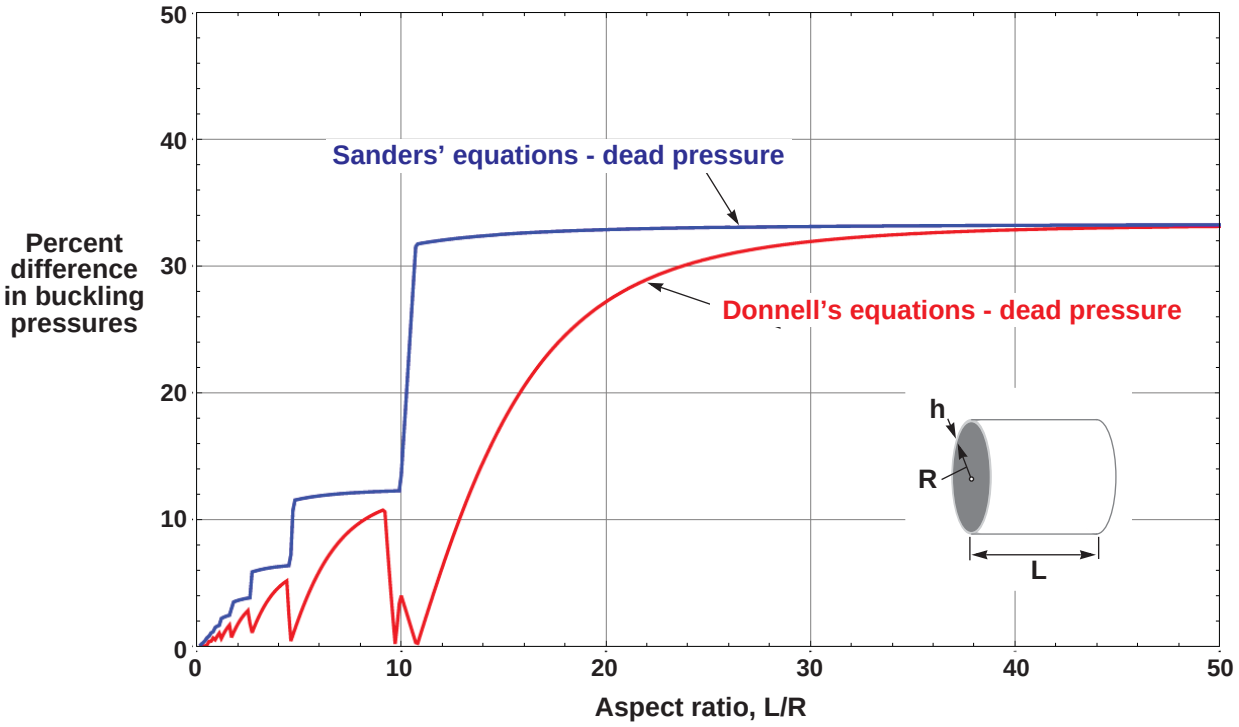

Figure 28. Differences in external buckling pressure, with respect to results based on Sanders' live-pressure equations, for isotropic cylinders with simply supported edges for R/h = 50 (ν = 0.3).

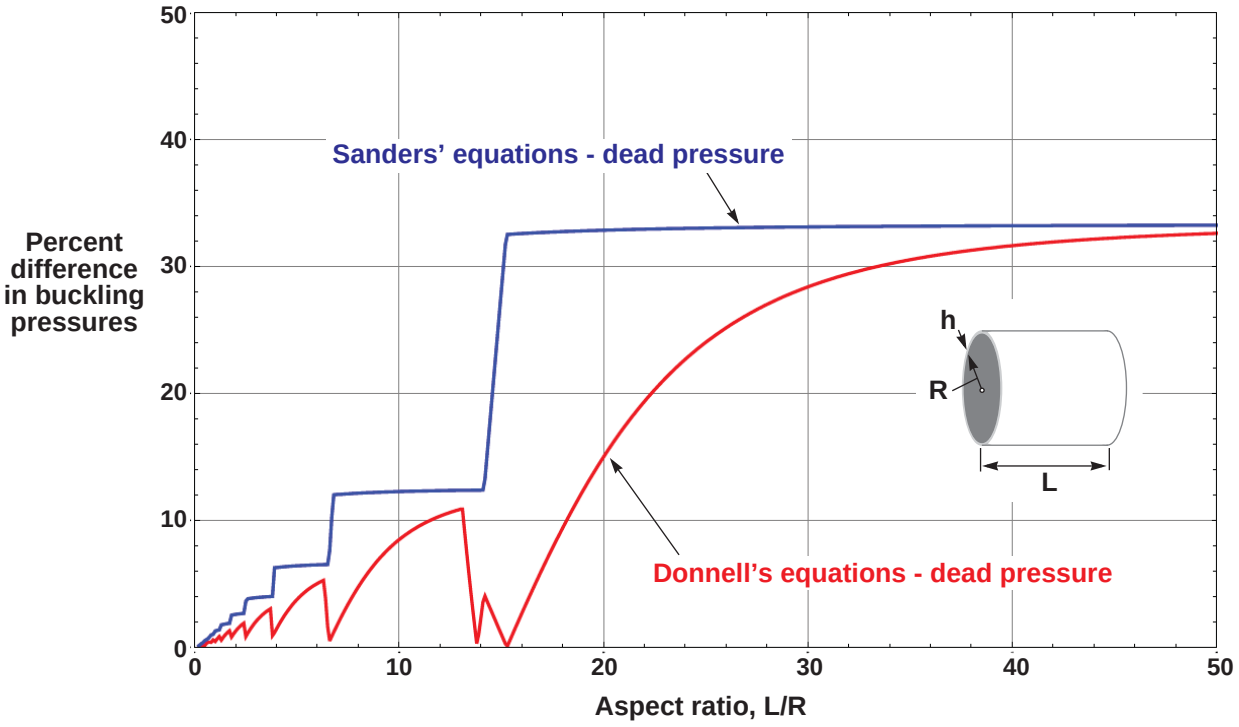

Figure 29. Differences in external buckling pressure, with respect to results based on Sanders' live-pressure equations, for isotropic cylinders with simply supported edges for R/h = 100 (ν = 0.3).

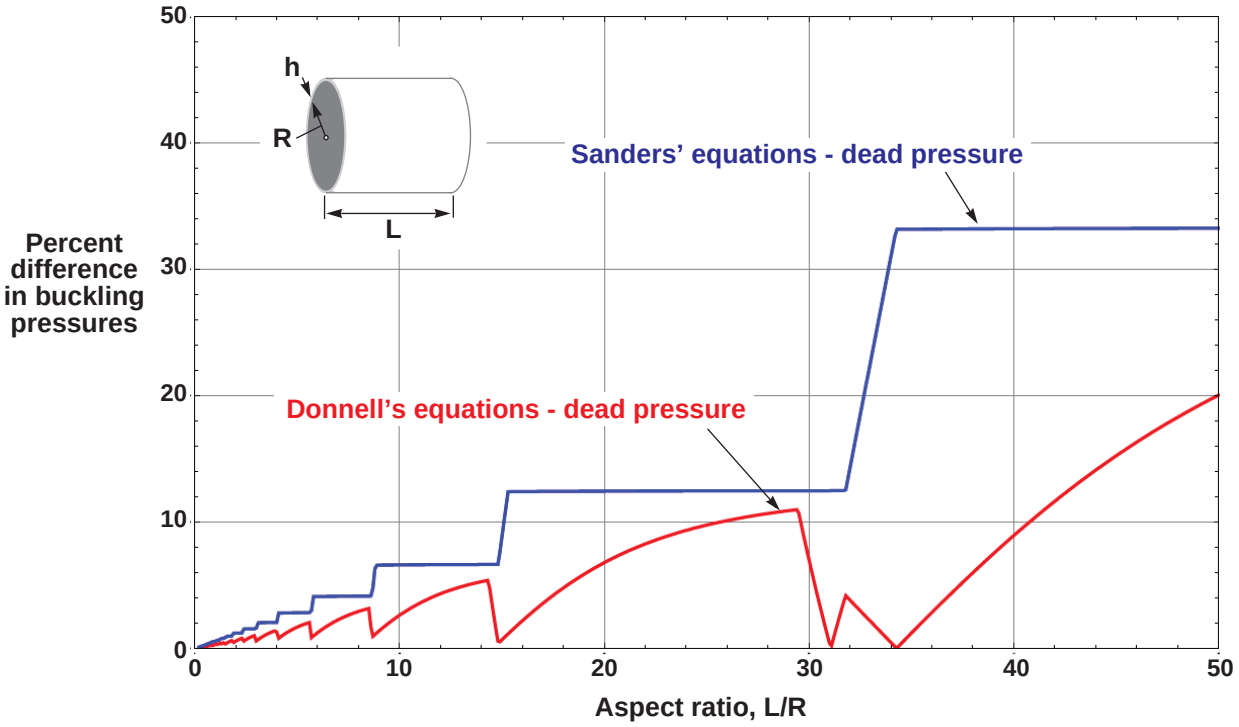

Figure 30. Differences in external buckling pressure, with respect to results based on Sanders' live-pressure equations, for isotropic cylinders with simply supported edges for R/h = 500 (ν = 0.3).

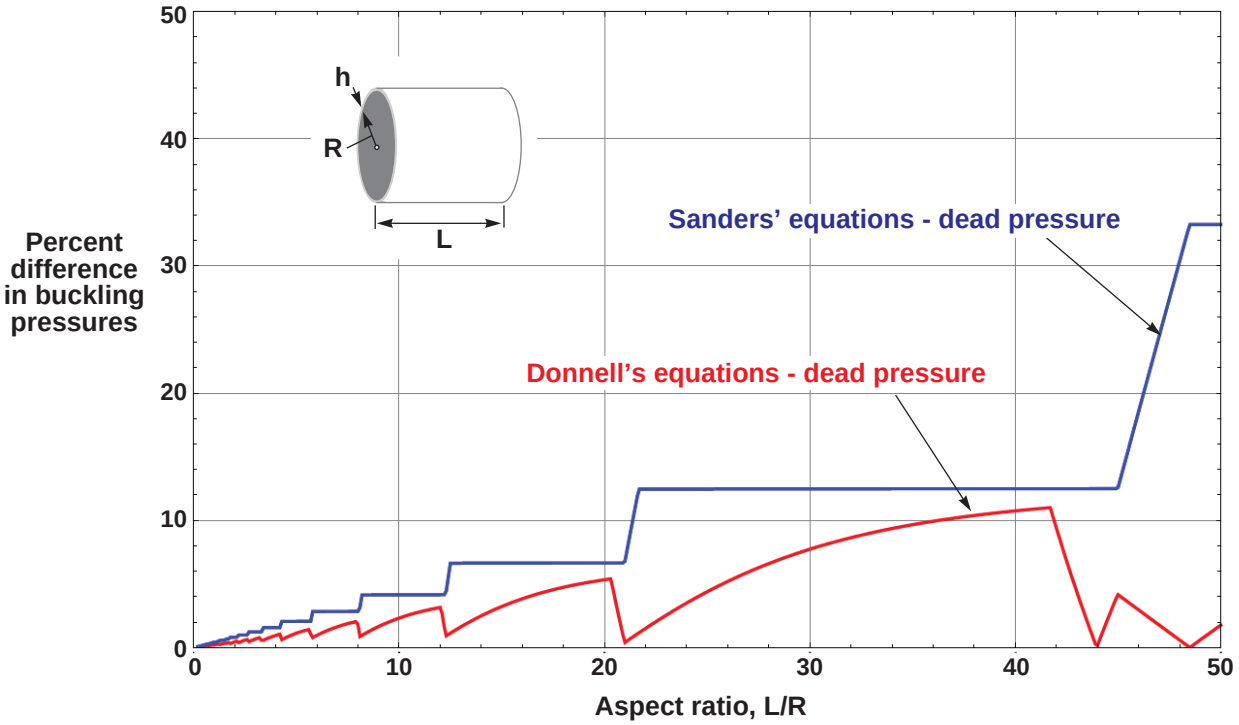

Figure 31. Differences in external buckling pressure, with respect to results based on Sanders' live-pressure equations, for isotropic cylinders with simply supported edges for R/h = 1000 (ν = 0.3).

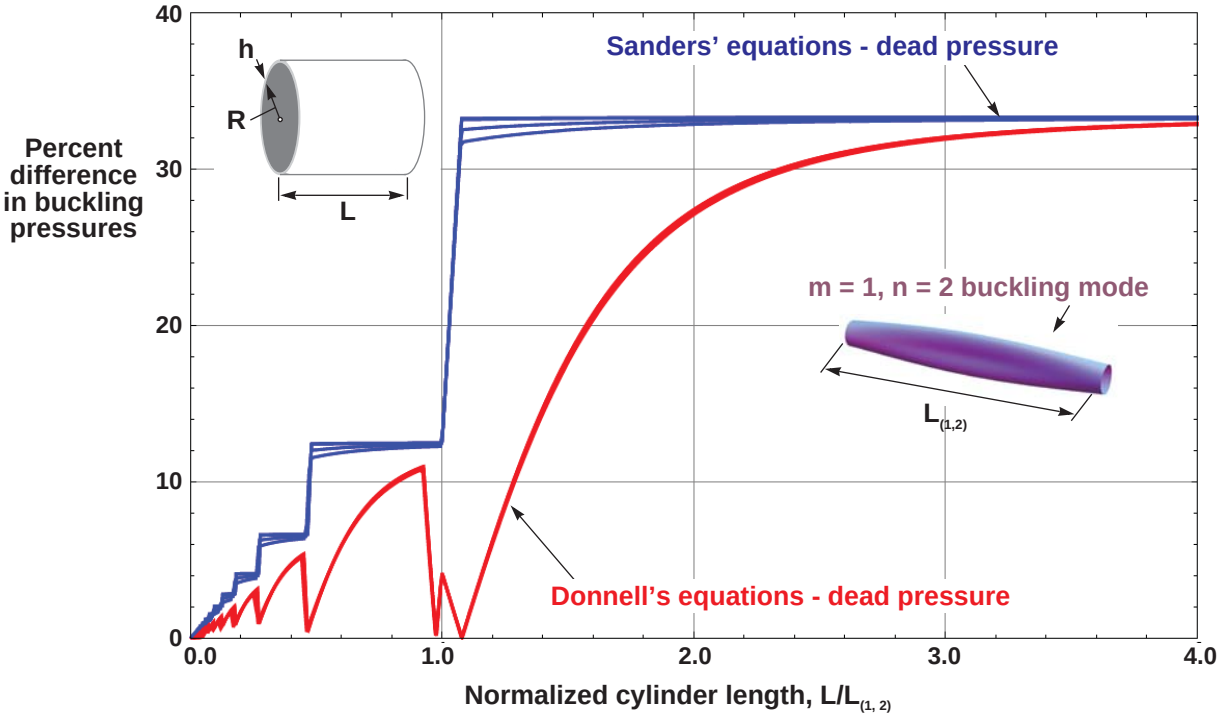

Figure 32. Difference in the external buckling pressures, with respect to results based on Sanders' live-pressure equations for isotropic cylinders with simply supported edges for R/h = 50, 100, 500, and 1000 (ν = 0.3).

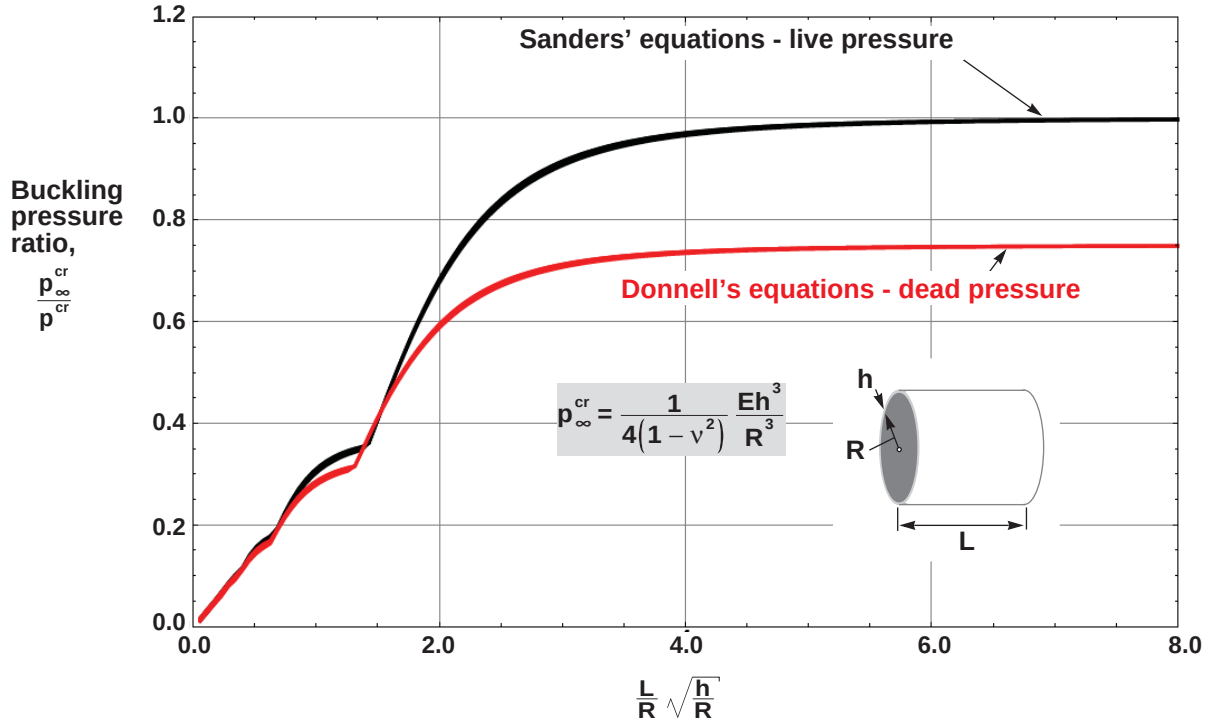

Figure 33. Nondimensional buckling pressure ratios for external-pressure-loaded isotropic cylinders with simply supported edges, for R/h = 50, 100, 500, and 1000 (ν = 0.3).

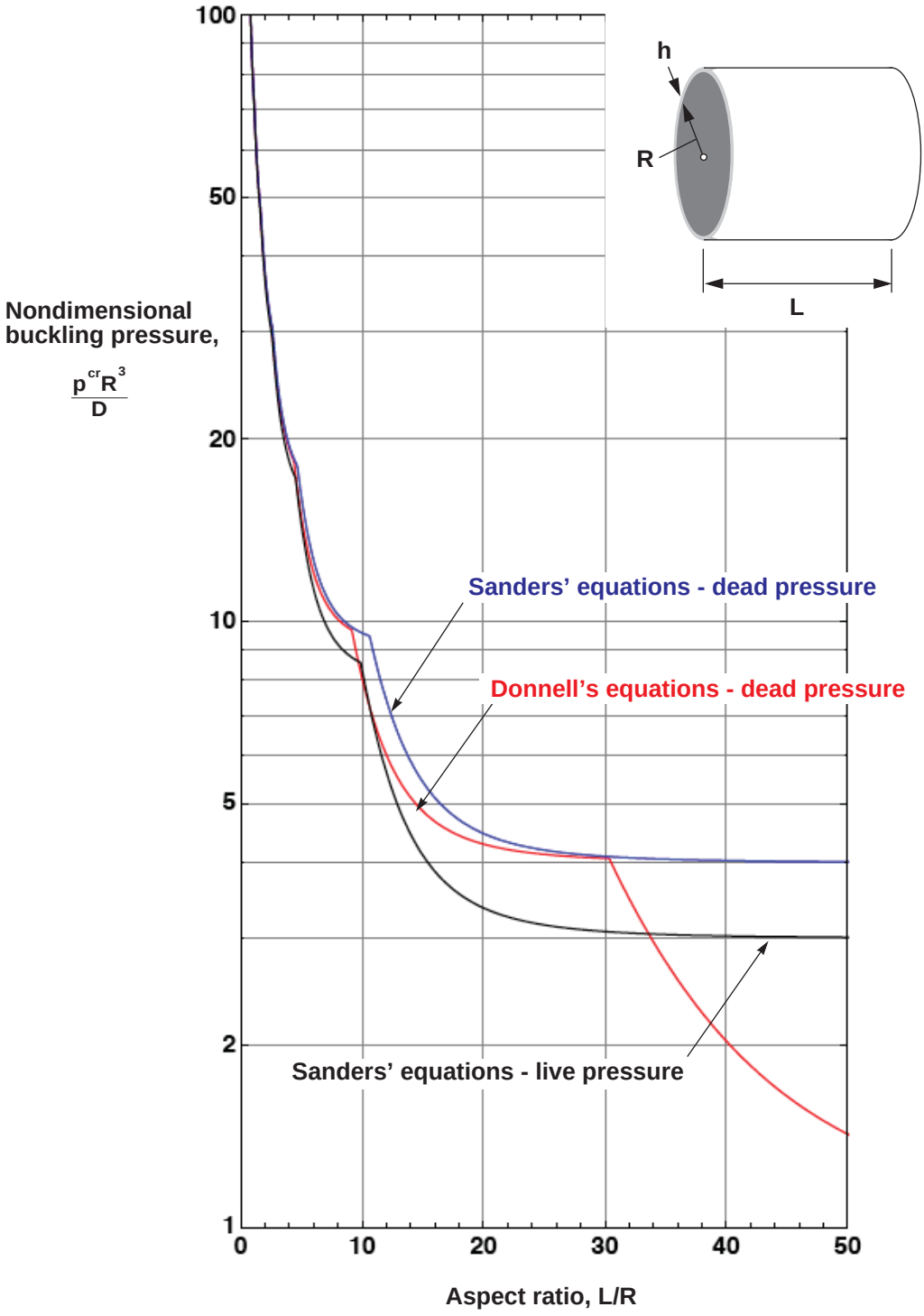

Figure 34. Nondimensional buckling loads for hydrostatic-pressure-loaded isotropic cylinders with simply supported edges for R/h = 50 (ν = 0.3).

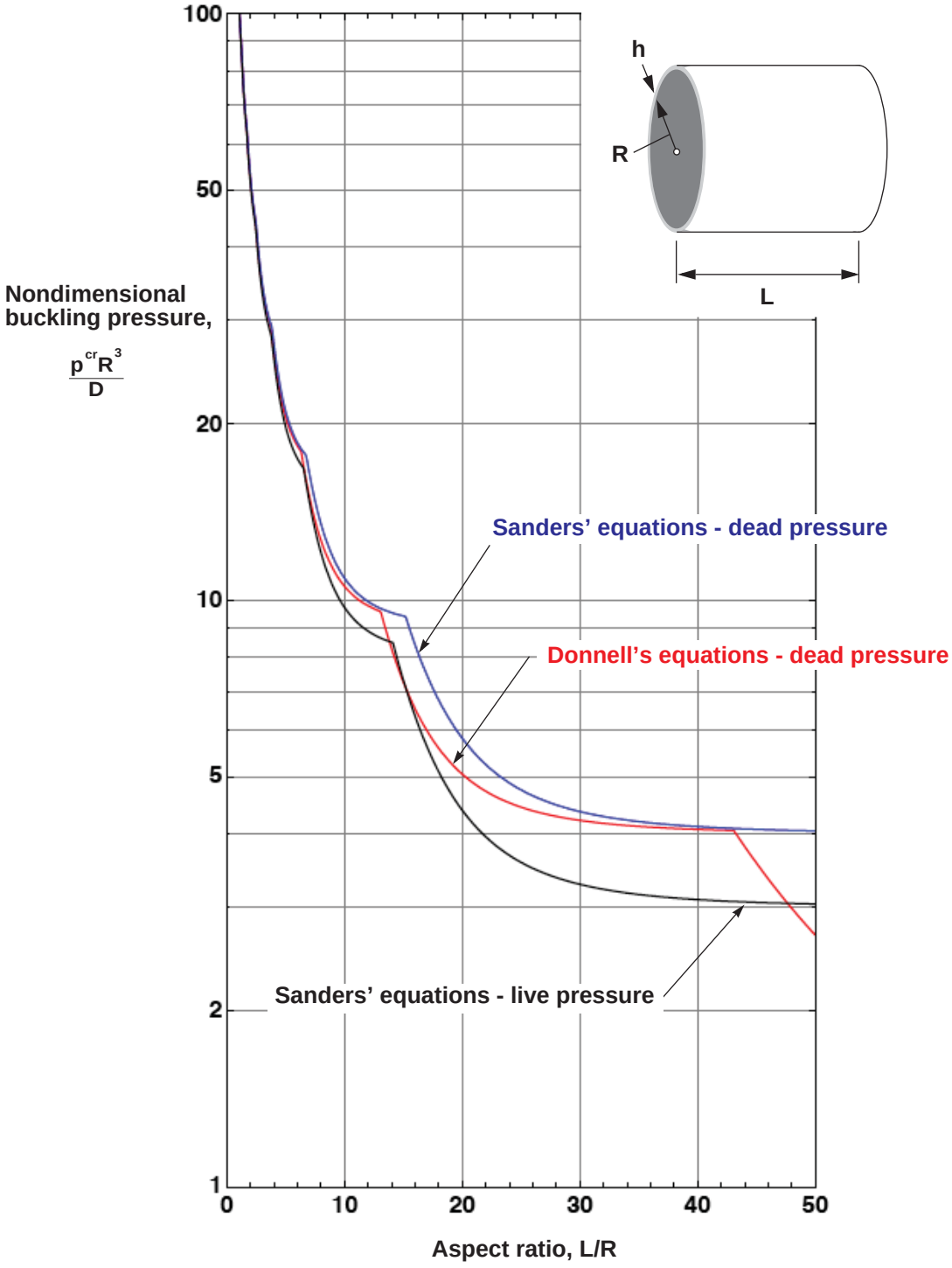

Figure 35. Nondimensional buckling loads for hydrostatic-pressure-loaded isotropic cylinders with simply supported edges for R/h = 100 (ν = 0.3).

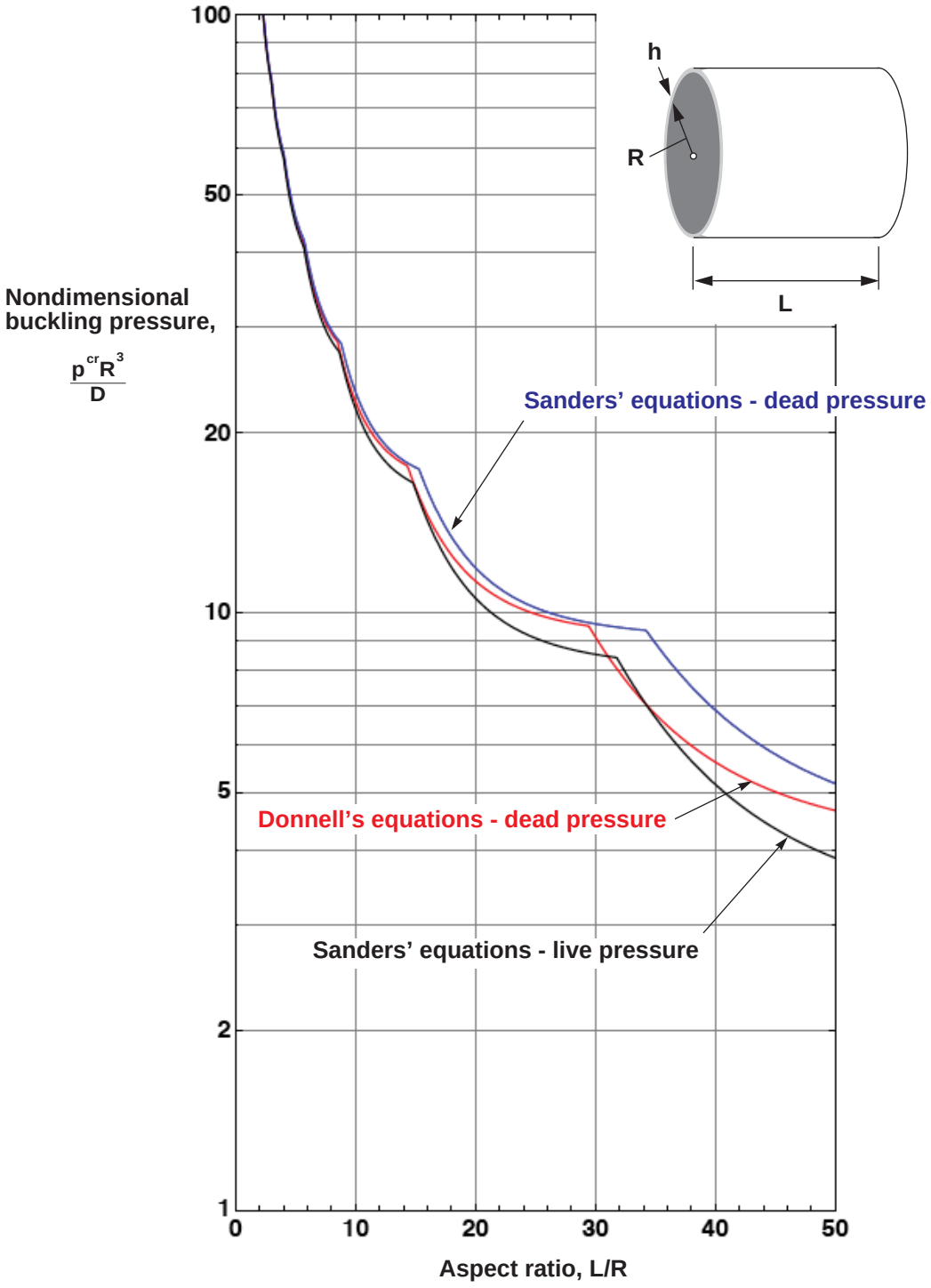

Figure 36. Nondimensional buckling loads for hydrostatic-pressure-loaded isotropic cylinders with simply supported edges for R/h = 500 (ν = 0.3).

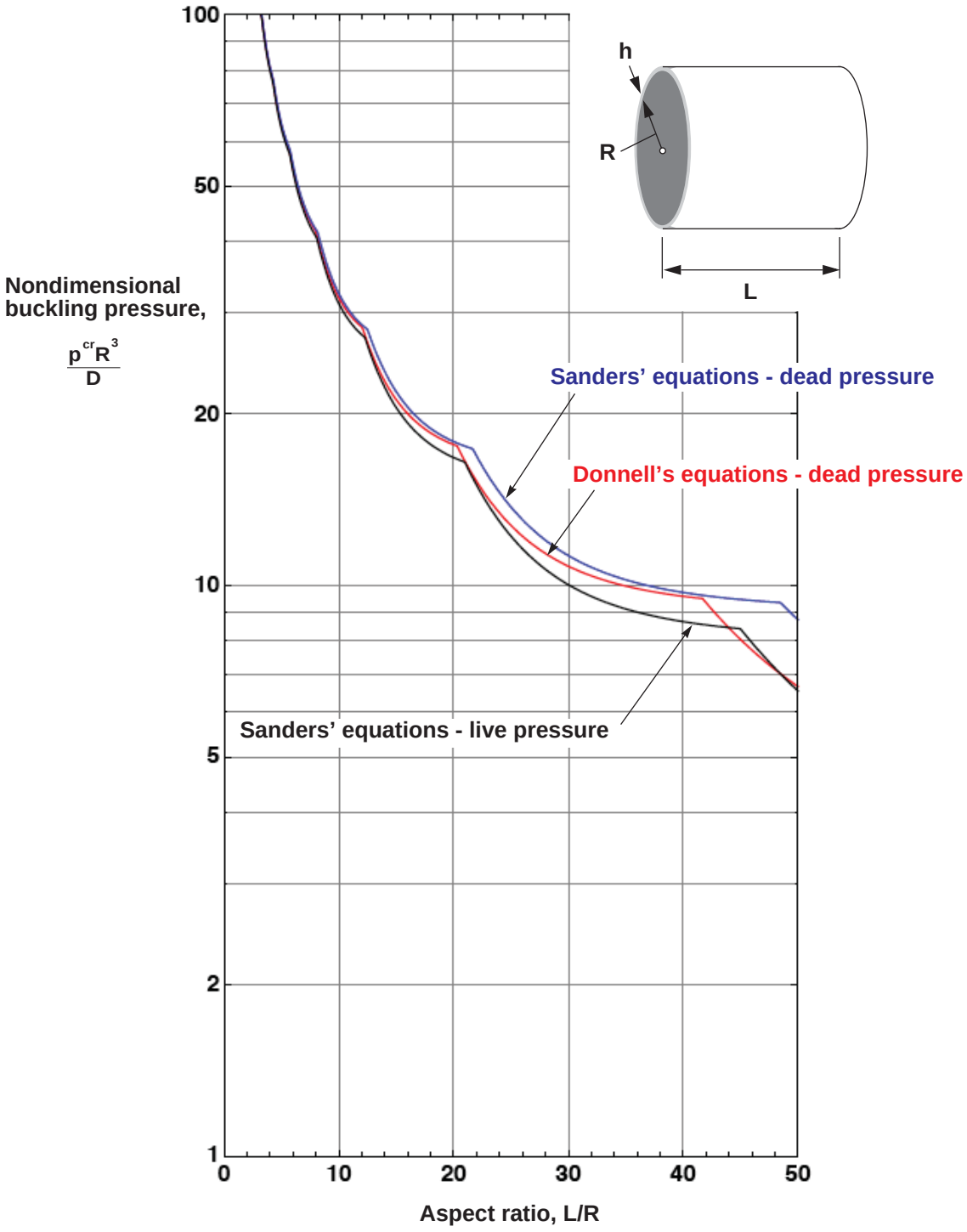

Figure 37. Nondimensional buckling loads for hydrostatic-pressure-loaded isotropic cylinders with simply supported edges for R/h = 1000 (ν = 0.3).

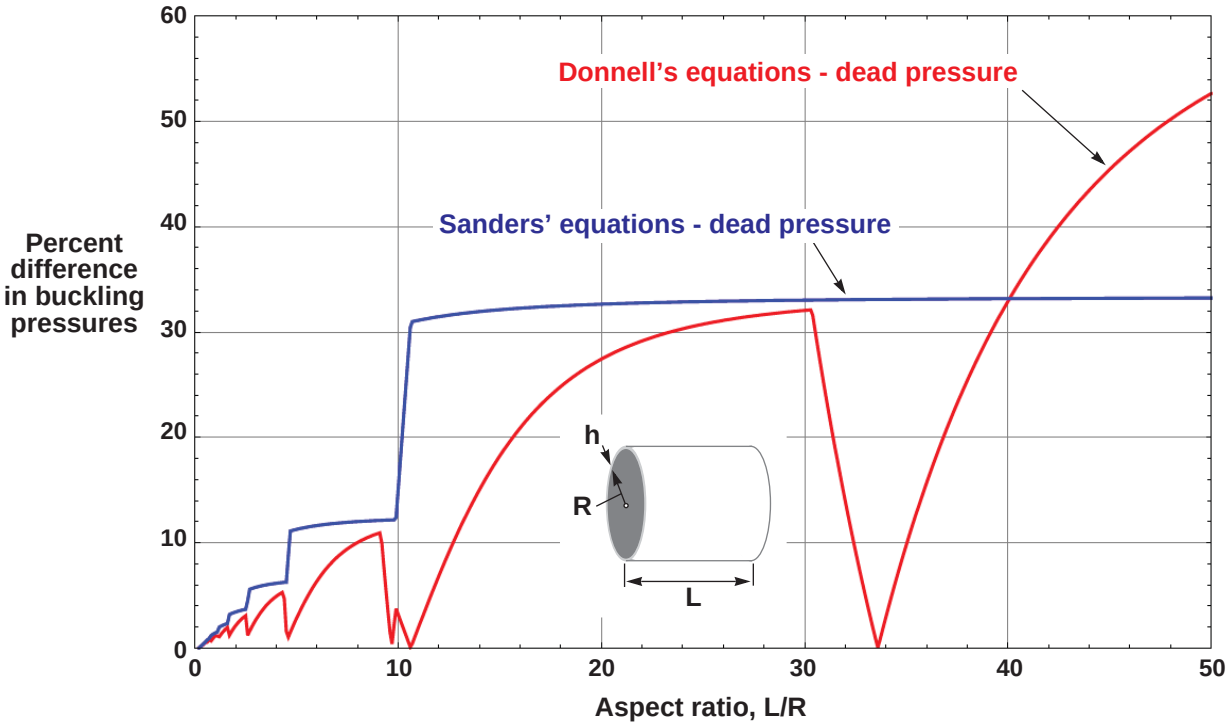

Figure 38. Differences in external hydrostatic buckling pressure, with respect to results based on Sanders' live-pressure equations, for isotropic cylinders with simply supported edges for R/h = 50 (ν = 0.3).

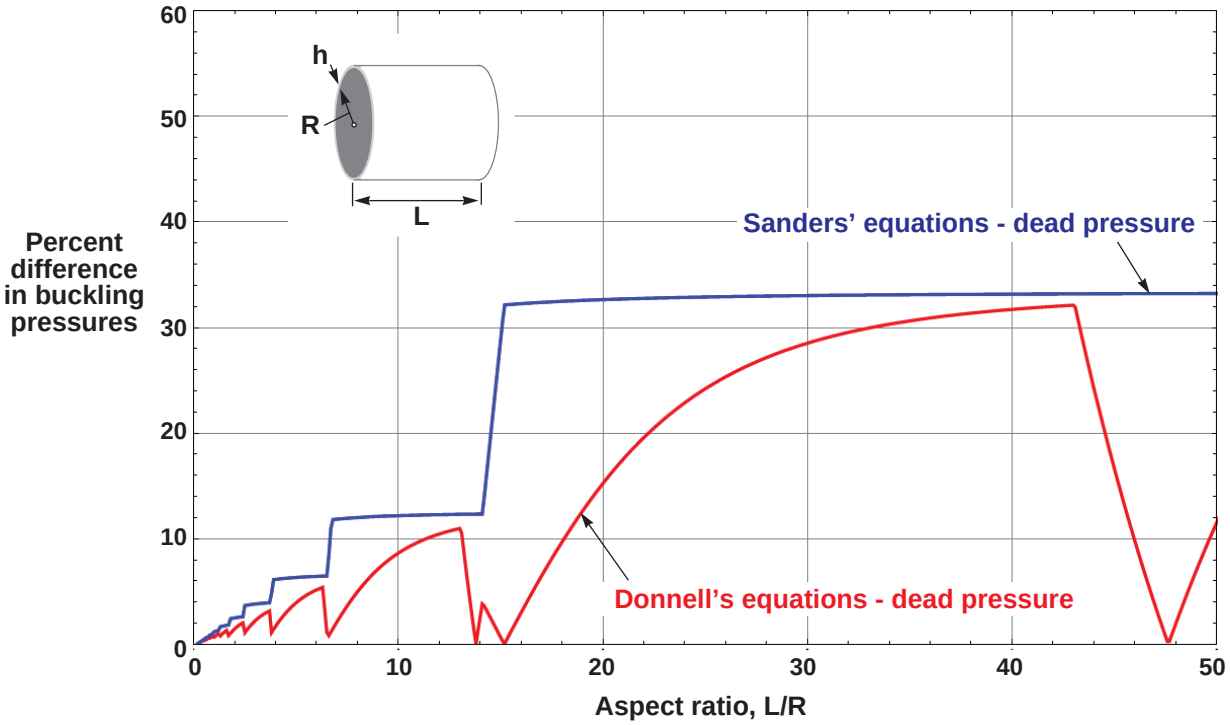

Figure 39. Differences in external hydrostatic buckling pressure, with respect to results based on Sanders' live-pressure equations, for isotropic cylinders with simply supported edges for R/h = 100 (ν = 0.3).

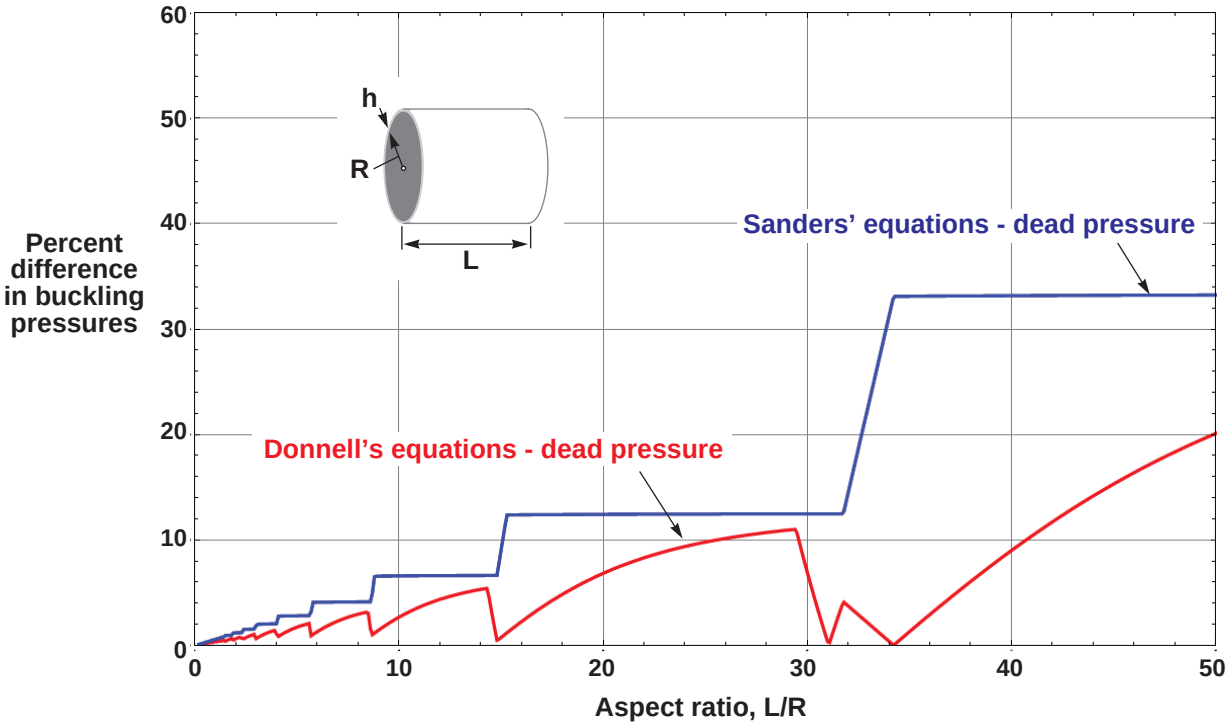

Figure 40. Differences in external hydrostatic buckling pressure, with respect to results based on Sanders' live-pressure equations, for isotropic cylinders with simply supported edges for R/h = 500 (ν = 0.3).

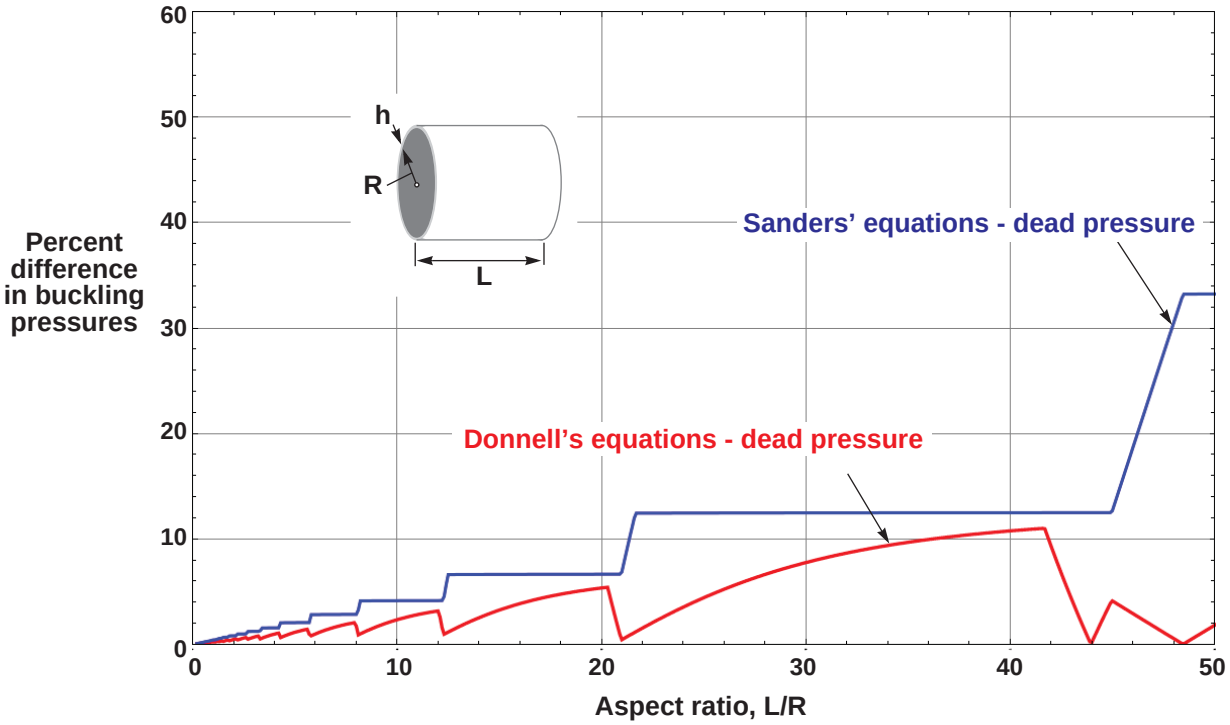

Figure 41. Differences in external hydrostatic buckling pressure, with respect to results based on Sanders' live-pressure equations, for isotropic cylinders with simply supported edges for R/h = 1000 (ν = 0.3).

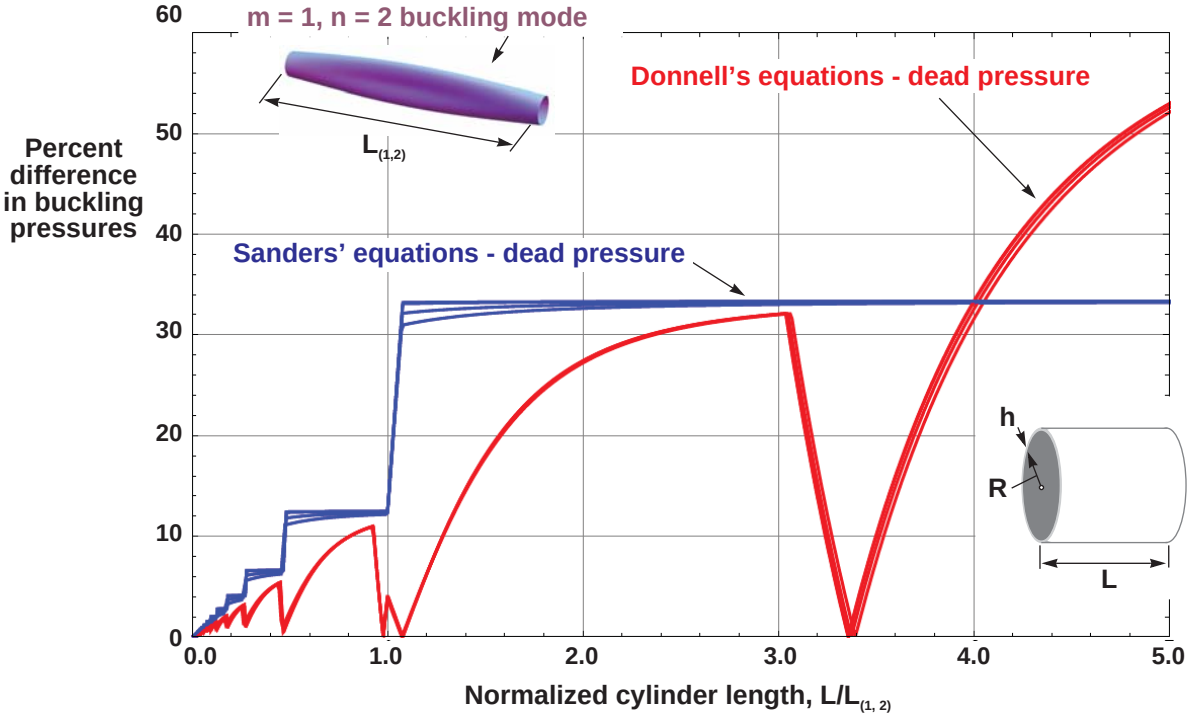

Figure 42. Difference in buckling loads, with respect to results based on Sanders' equations, for hydrostatic-pressure-loaded isotropic cylinders with simply supported edges for R/h = 50, 100, 500, and 1000 (ν = 0.3).

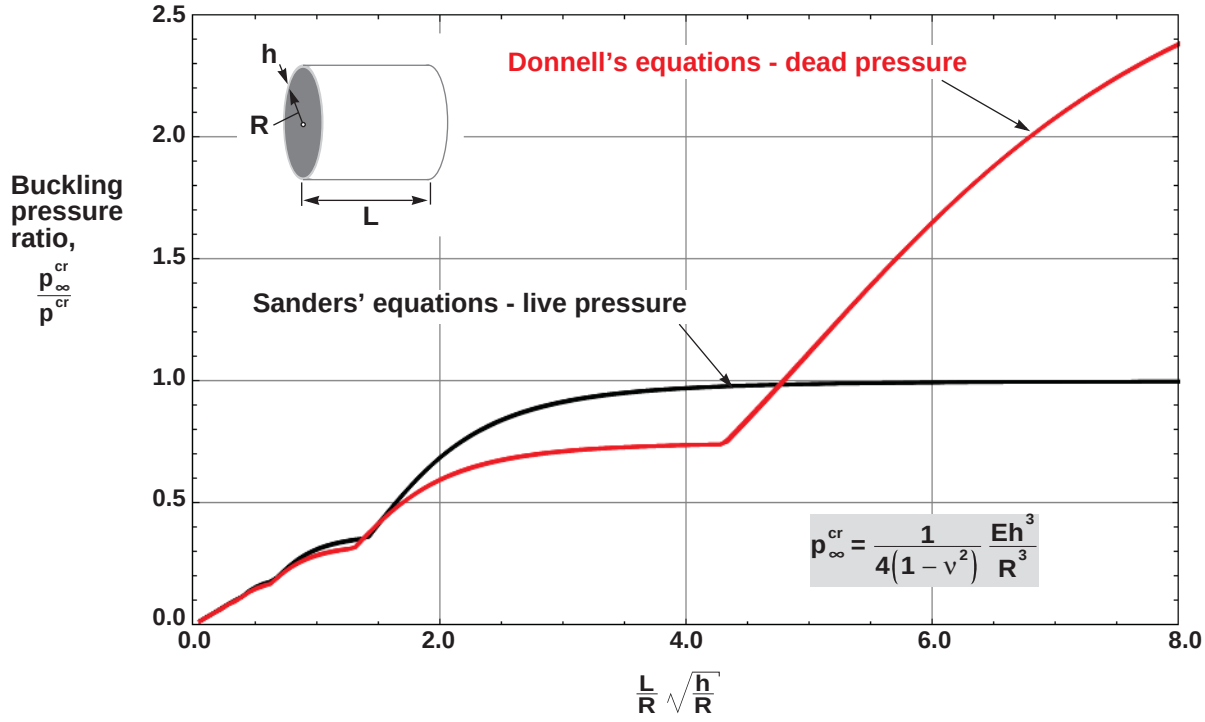

Figure 43. Nondimensional buckling pressure ratios for hydrostatic-pressure-loaded isotropic cylinders with simply supported edges, for R/h = 50, 100, 500, and 1000 (ν = 0.3).

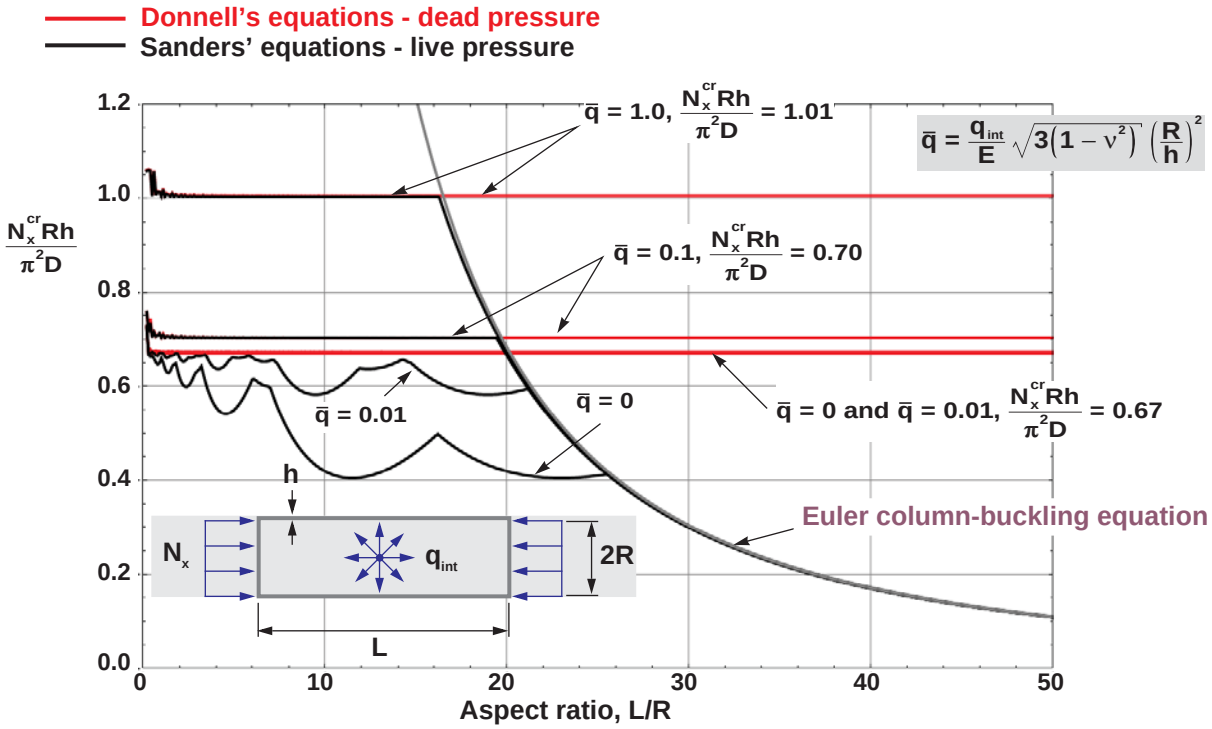

Figure 44. Nondimensional buckling loads for isotropic cylinders subected to axial compression and internal pressure and with simply supported edges for R/h = 50 (ν = 0.3).

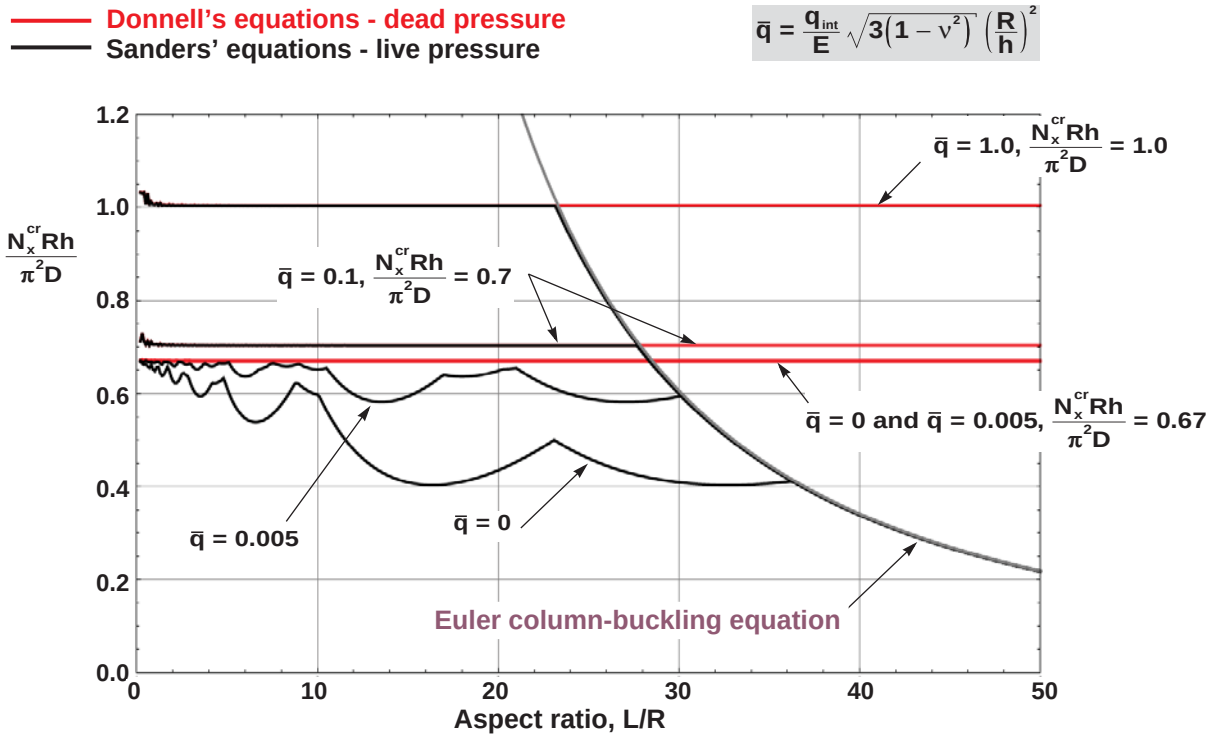

Figure 45. Nondimensional buckling loads for isotropic cylinders subected to axial compression and internal pressure and with simply supported edges for R/h = 100 (ν = 0.3).

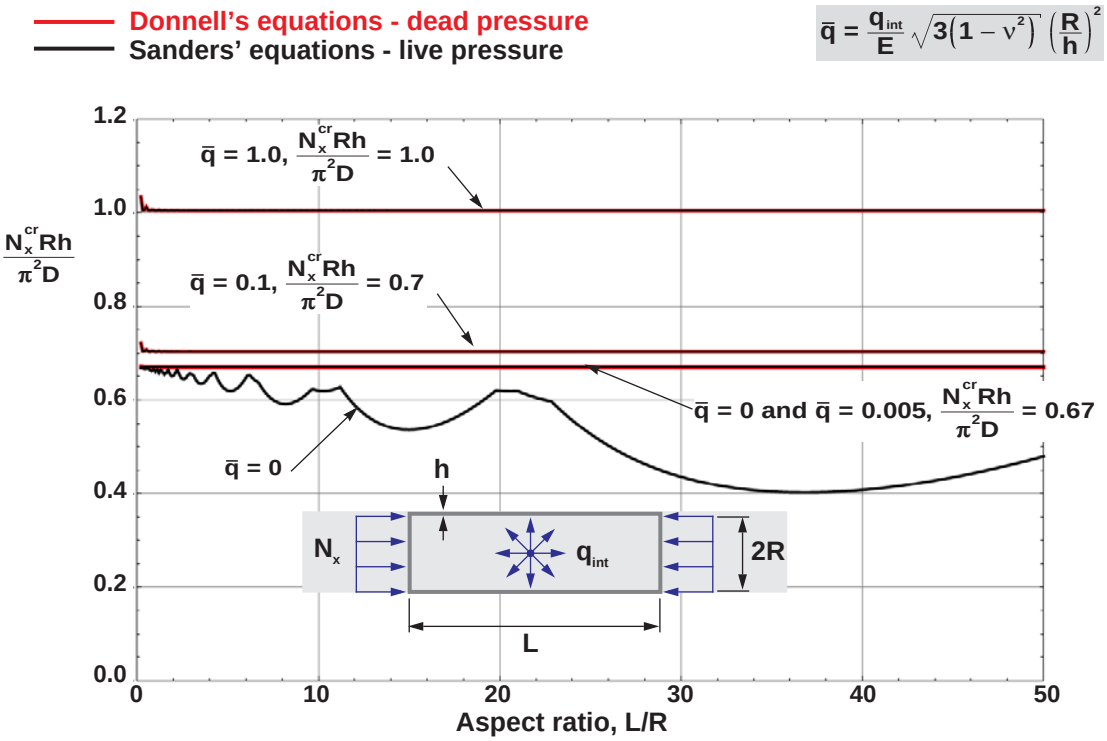

Figure 46. Nondimensional buckling loads for isotropic cylinders subected to axial compression and internal pressure and with simply supported edges for R/h = 500 (ν = 0.3).

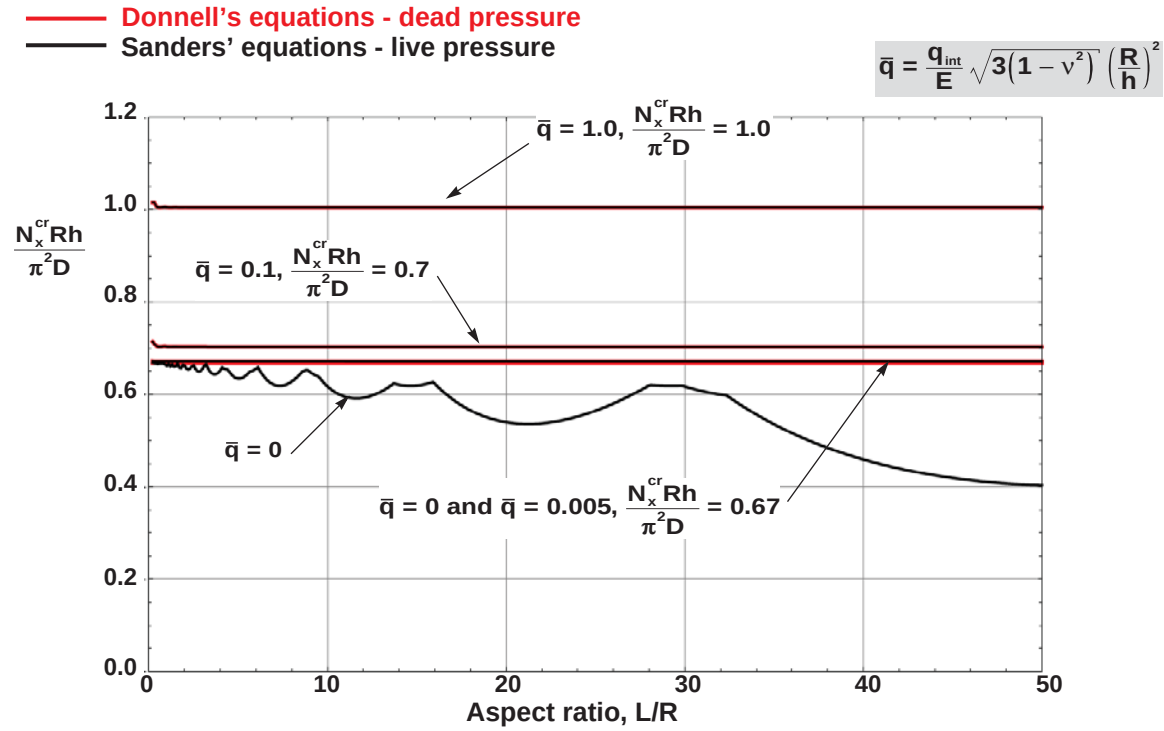

Figure 47. Nondimensional buckling loads for isotropic cylinders subected to axial compression and internal pressure and with simply supported edges for R/h =1000 (ν = 0.3).

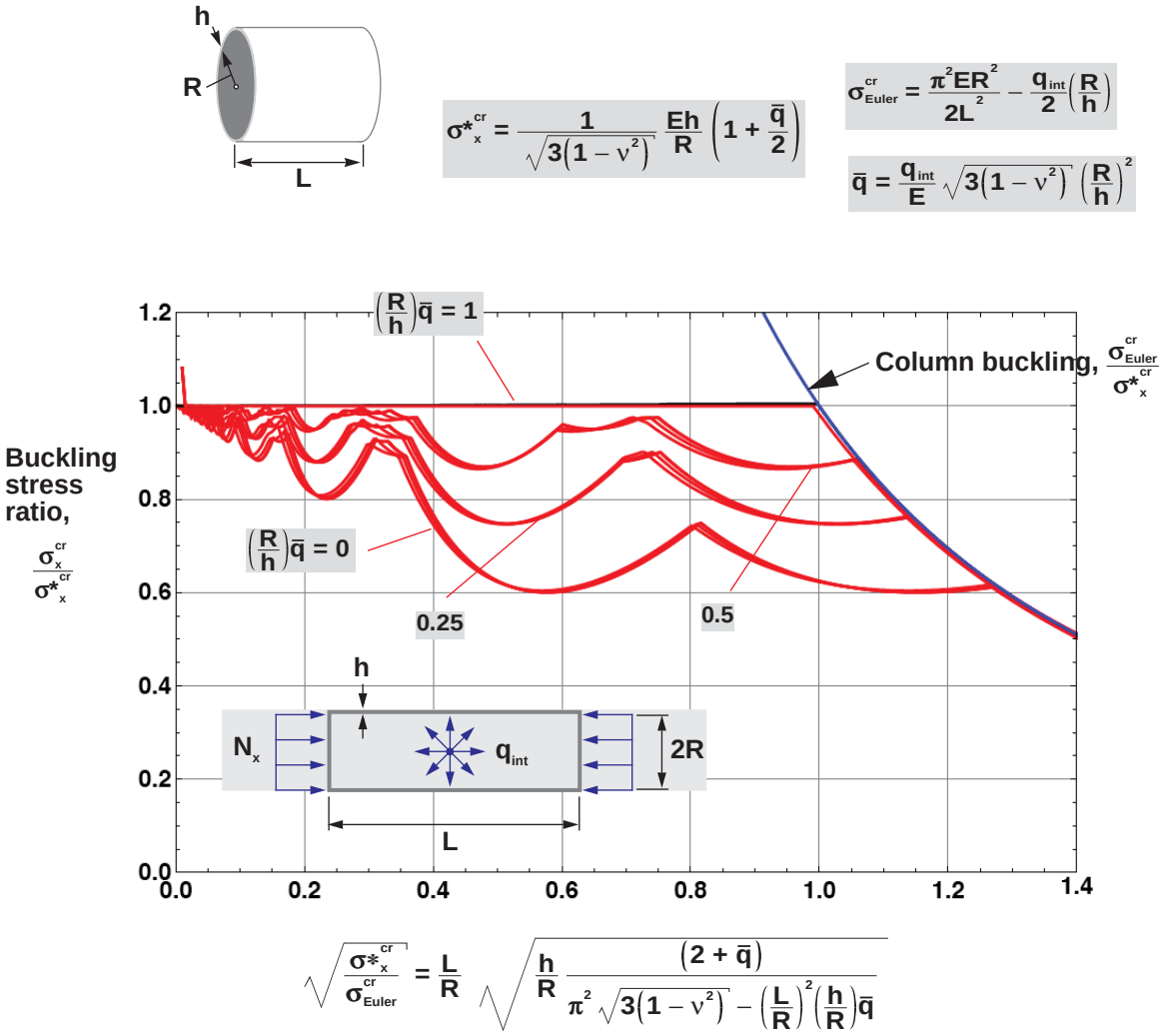

Figure 48. Nondimensional buckling stress ratios or isotropic cylinders subected to axial compression and internal pressure and with simply supported edges, for R/h = 50, 100, 500, and 1000 (ν = 0.3).

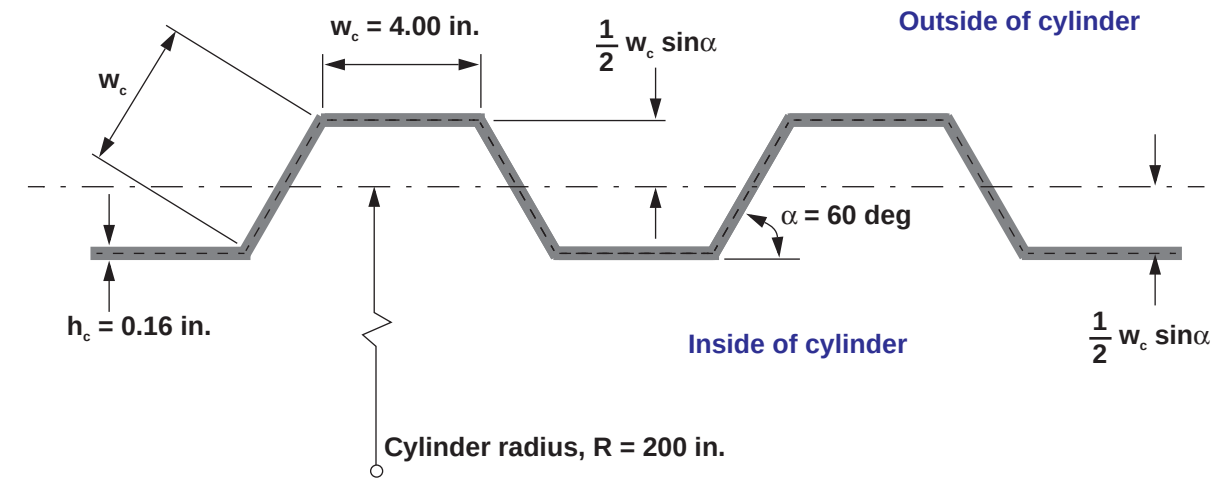

(c) Corrugated-wall cross-section

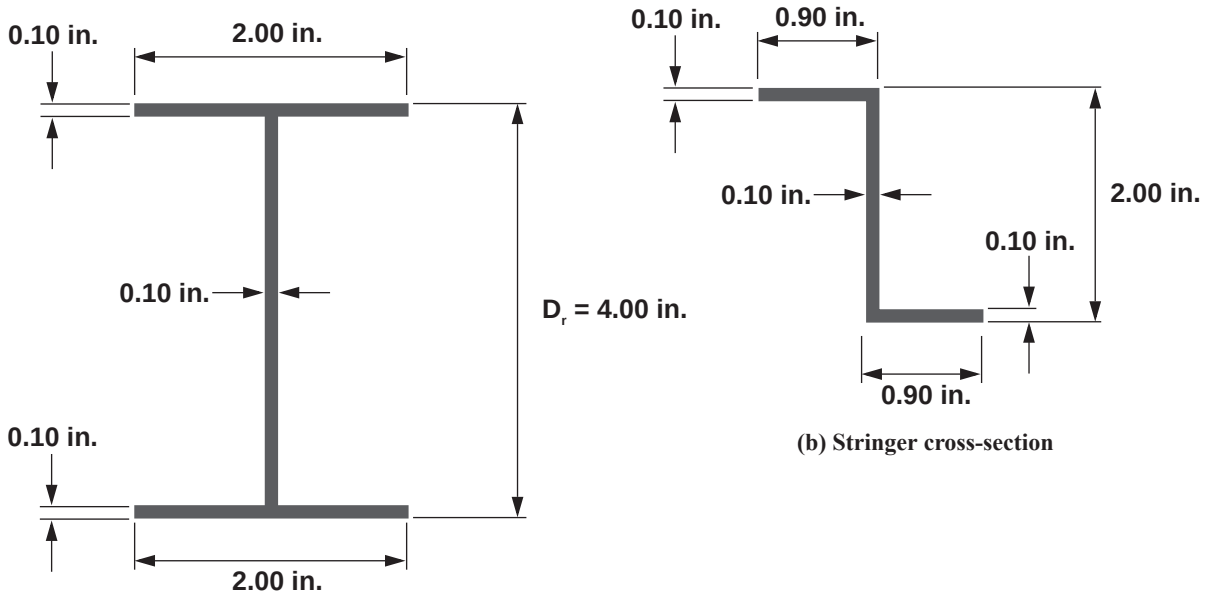

(a) Ring cross-section

(b) Stringer cross-section

Figure 49. Ring, stringer, and corrugated wall details for stiffened cylinders of reference 59.

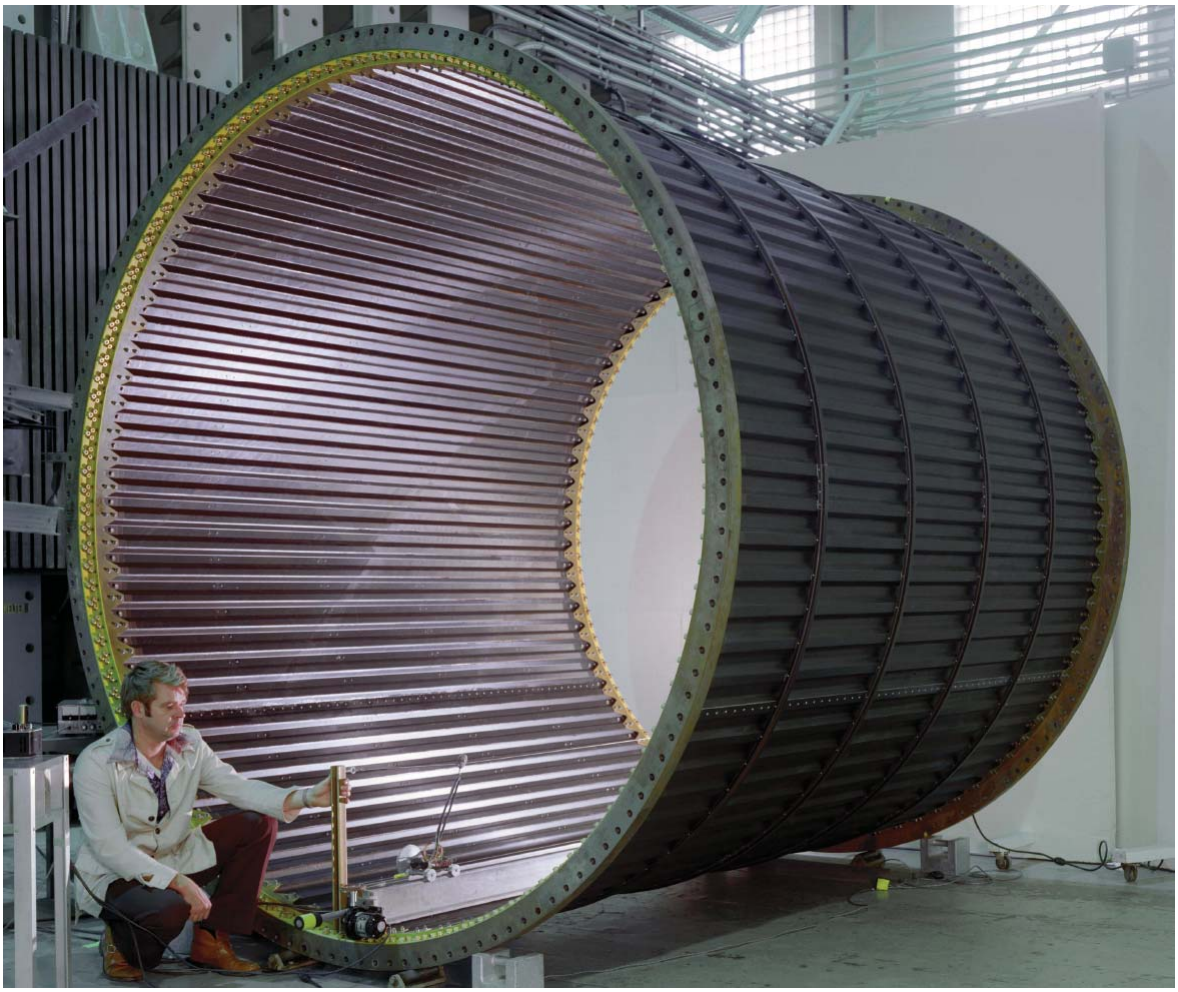

Figure 50. Corrugated cylinder with external rings (Dr. Randall C. Davis shown with the cylinder).

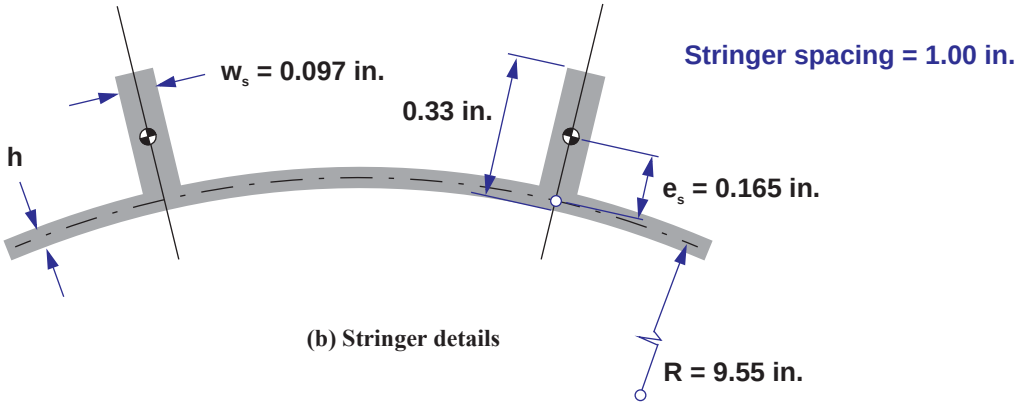

(b) Stringer details

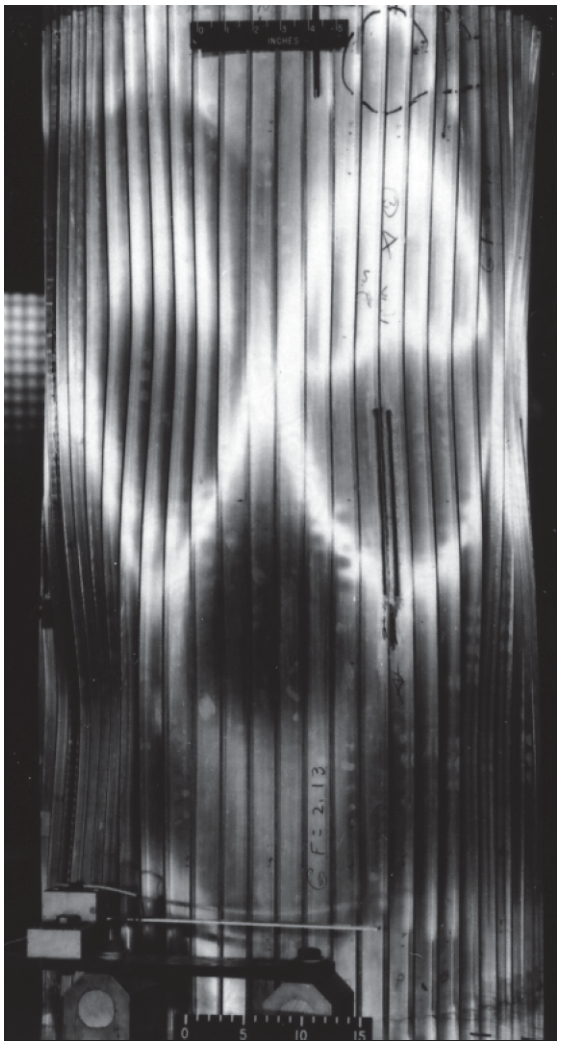

(a) Buckled cylinder

Figure 51. Buckled cylinder with rectangular external stringers and stringer details.

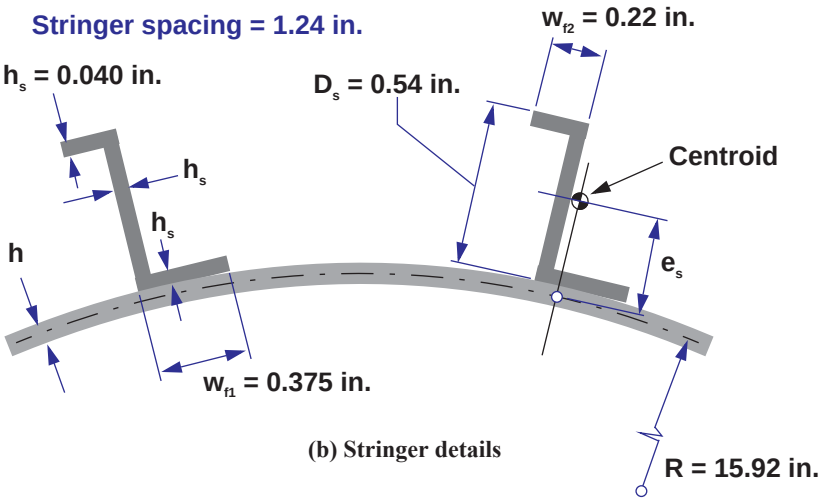

(b) Stringer details

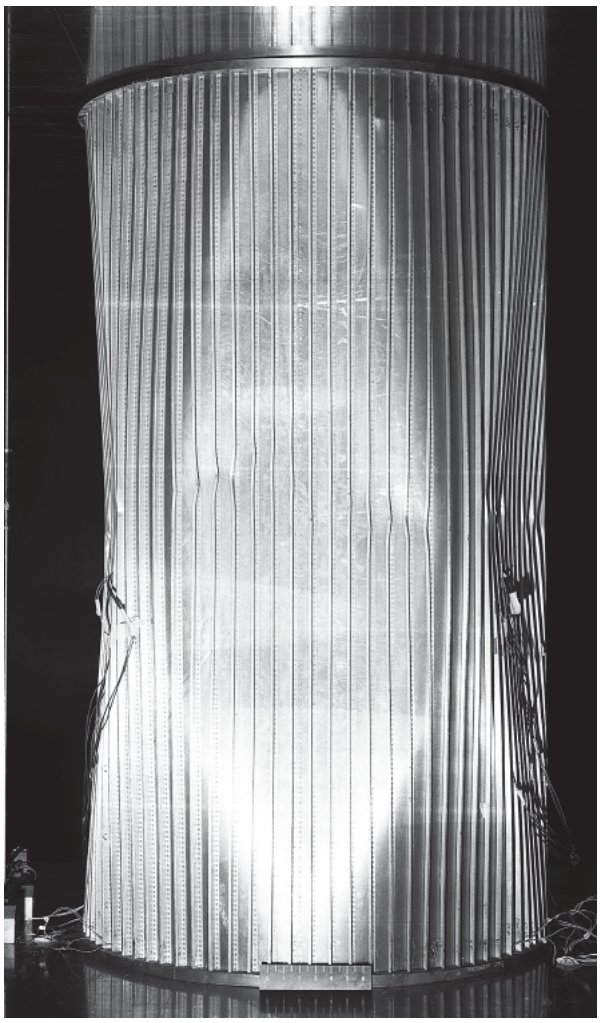

(a) Buckled cylinder

Figure 52. Buckled cylinder with external Z-shaped stringers and stringer details.

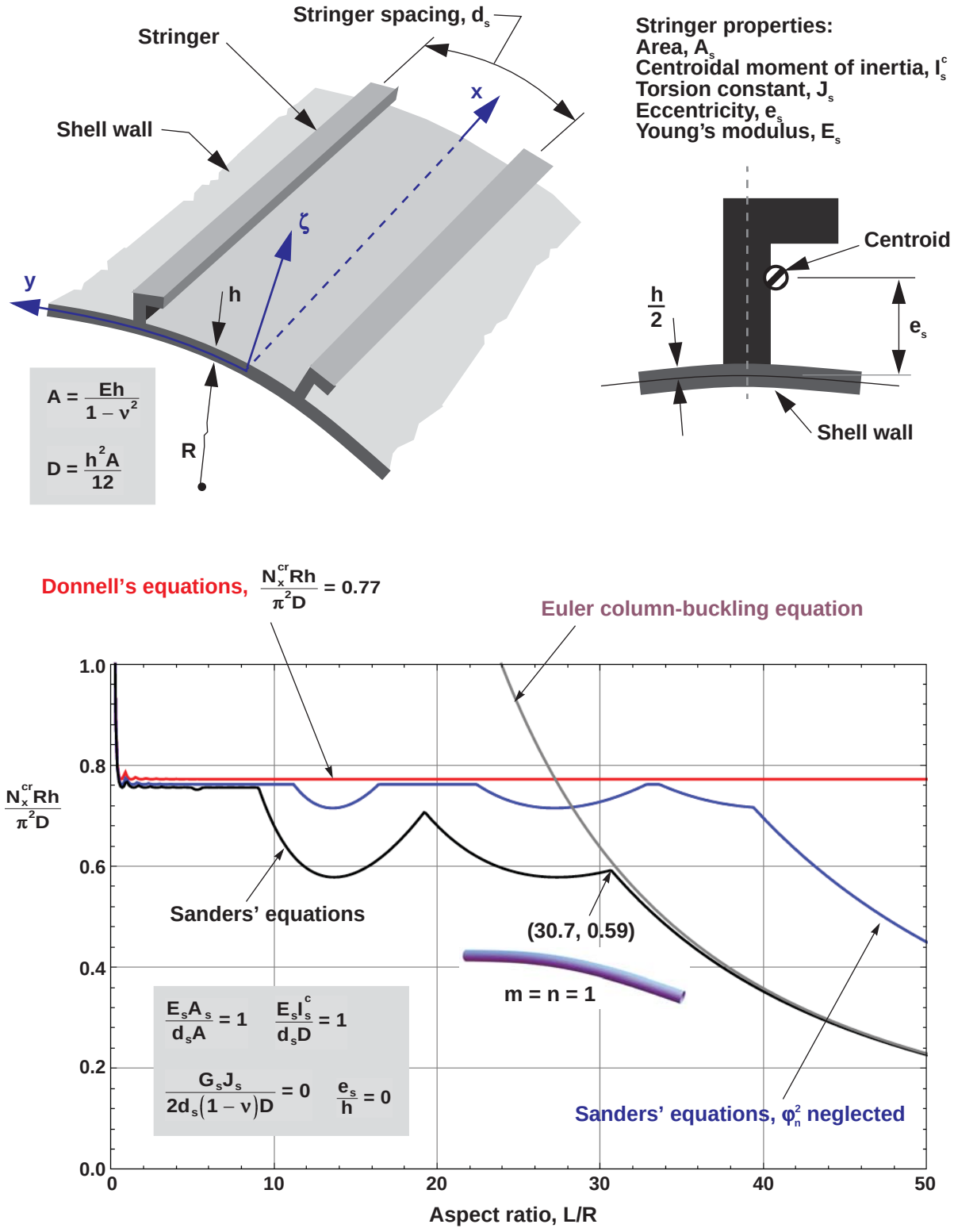

Figure 53. Nondimensional buckling loads for compression-loaded stringer-stiffened isotropic cylinders with simply supported edges for R/h = 50 (ν = 0.3).

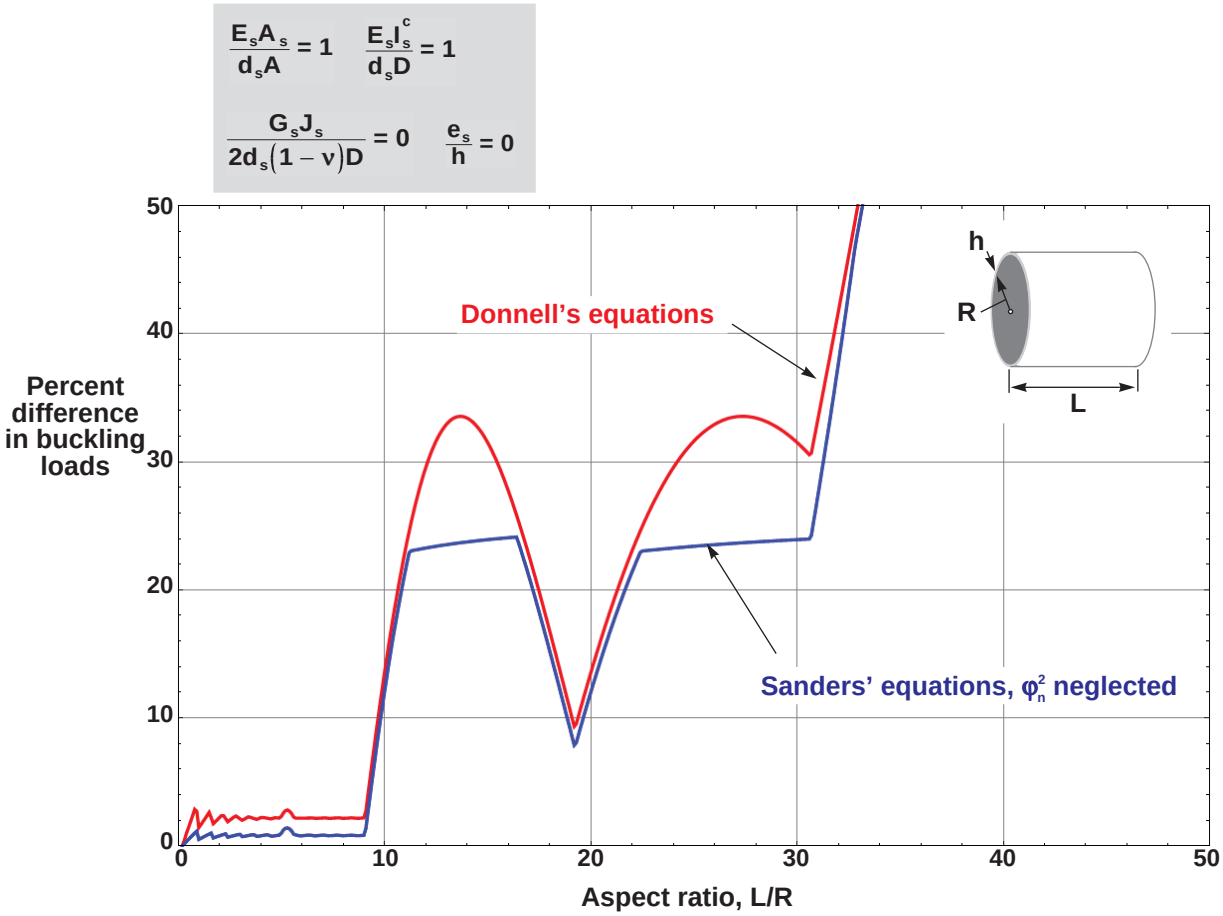

Figure 54. Difference in buckling loads, with respect to results based on Sanders' equations, for compression-loaded stringer-stiffened isotropic cylinders with simply supported edges for R/h = 50 (ν = 0.3).

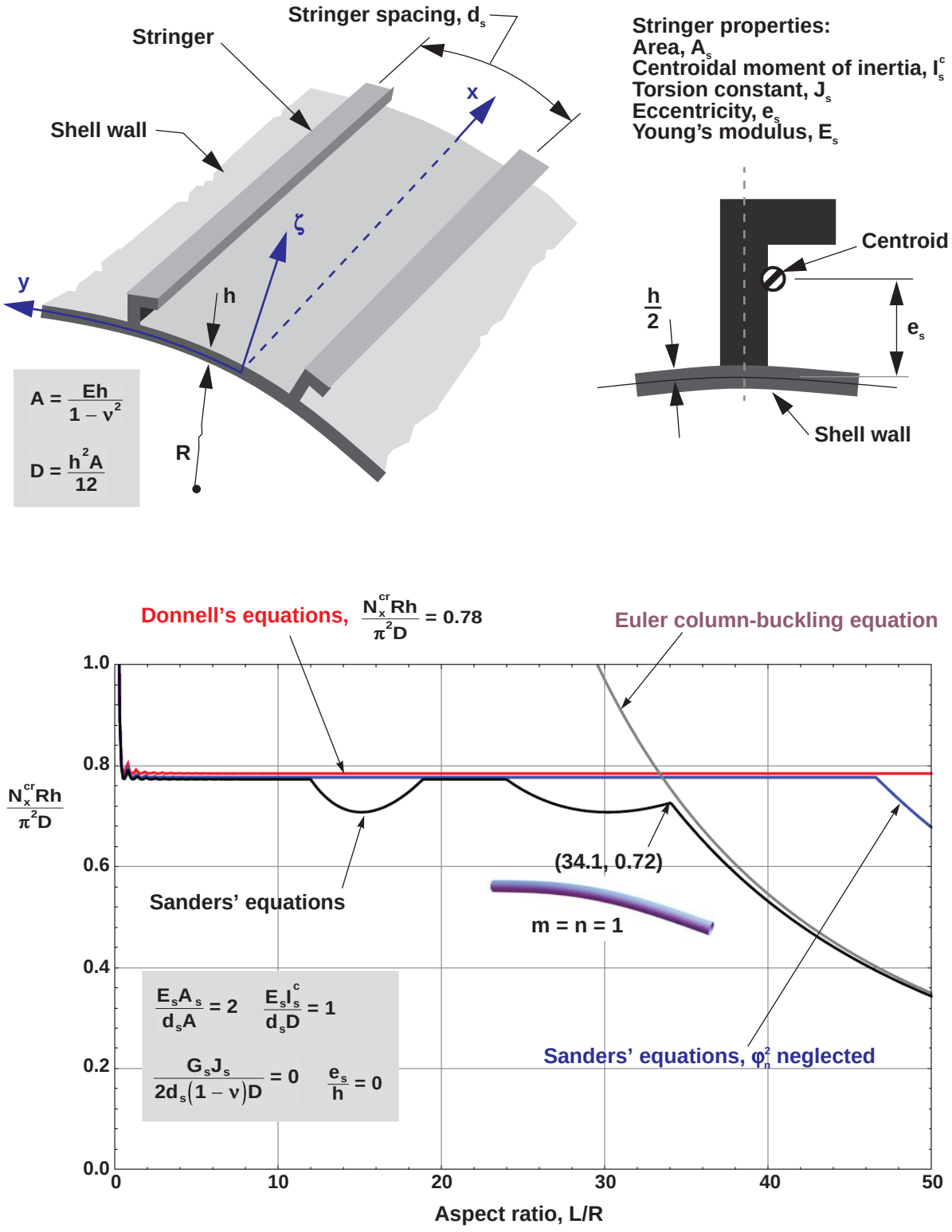

Figure 55. Nondimensional buckling loads for compression-loaded stringer-stiffened isotropic cylinders with simply supported edges for R/h = 50 (ν = 0.3).

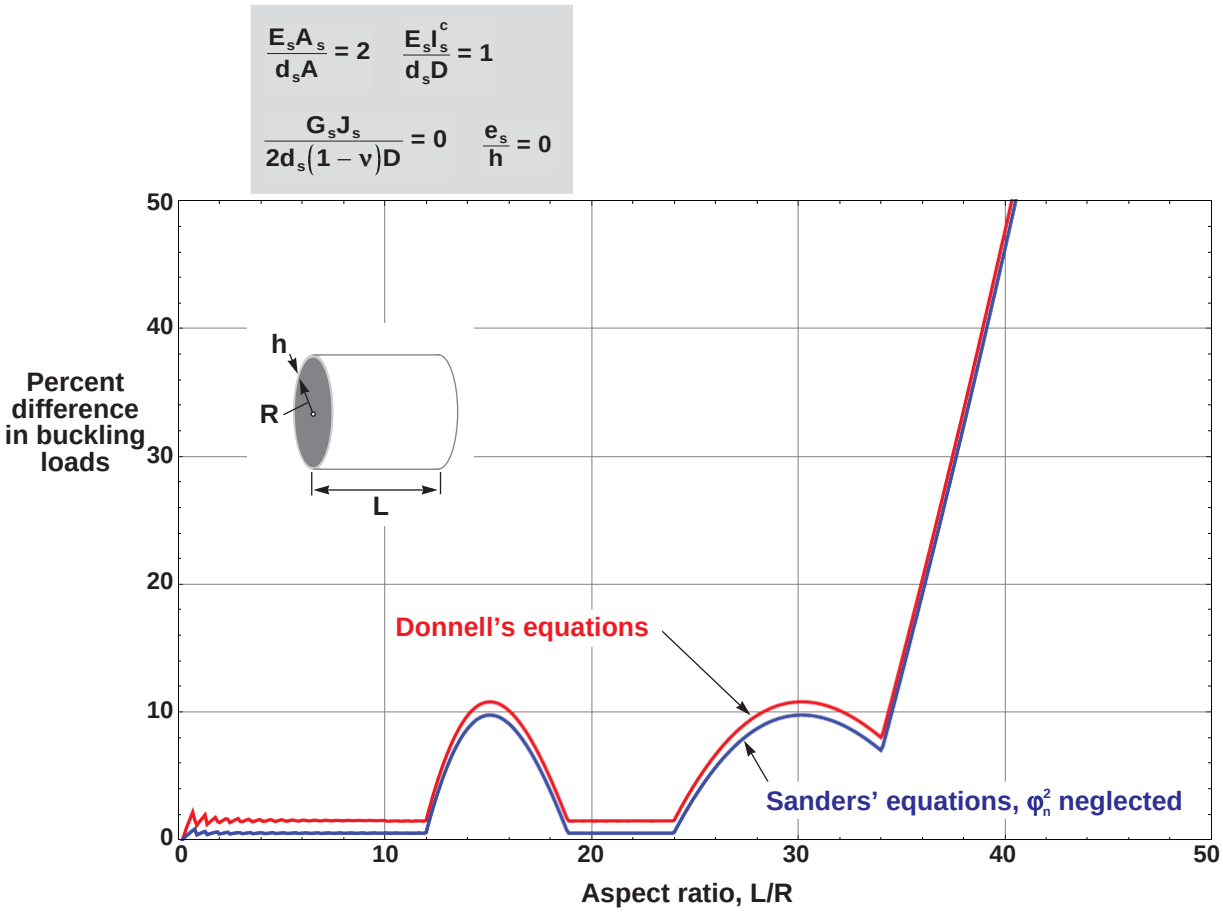

Figure 56. Difference in buckling loads, with respect to results based on Sanders' equations, for compression-loaded stringer-stiffened isotropic cylinders with simply supported edges for R/h = 50 (ν = 0.3).

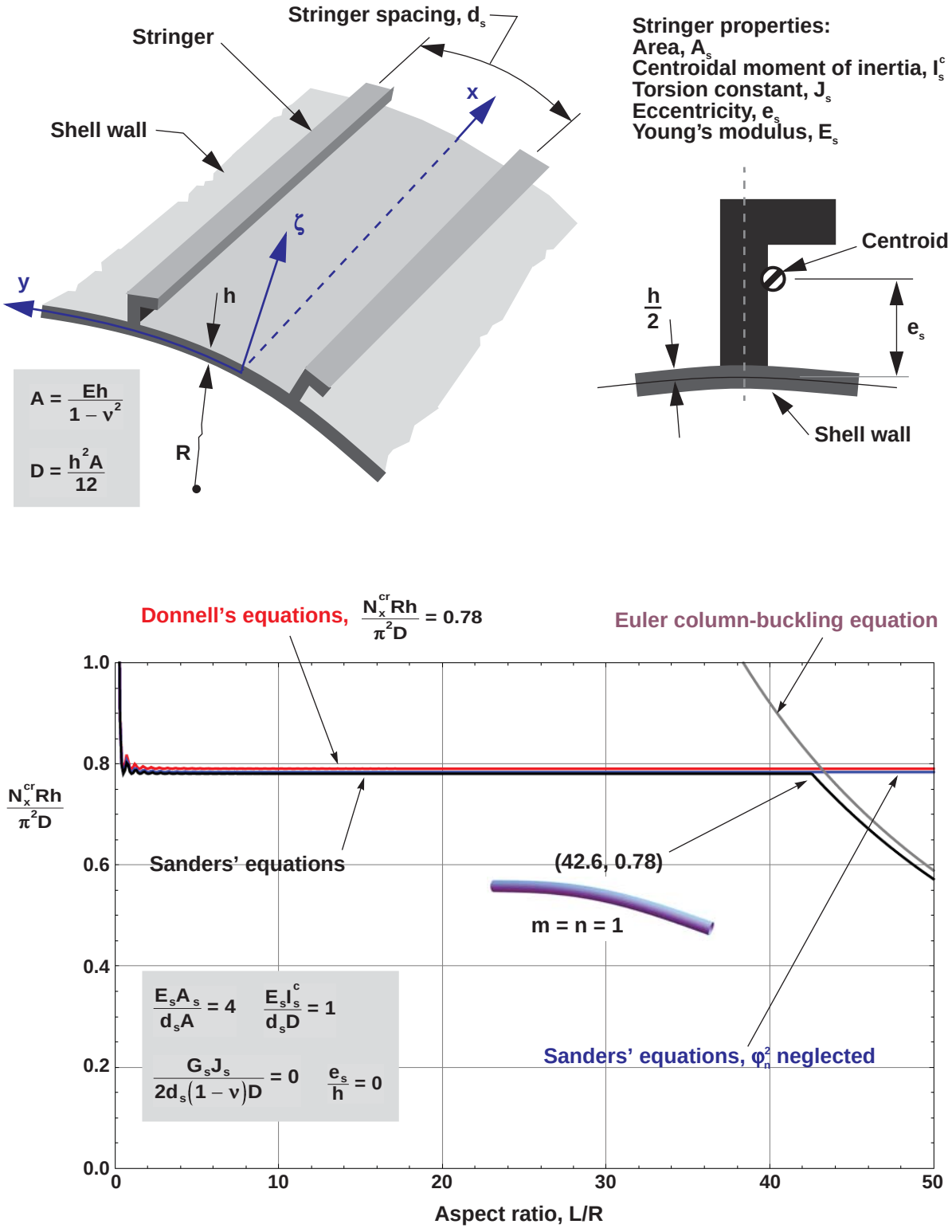

Figure 57. Nondimensional buckling loads for compression-loaded stringer-stiffened isotropic cylinders with simply supported edges for R/h = 50 (ν = 0.3).

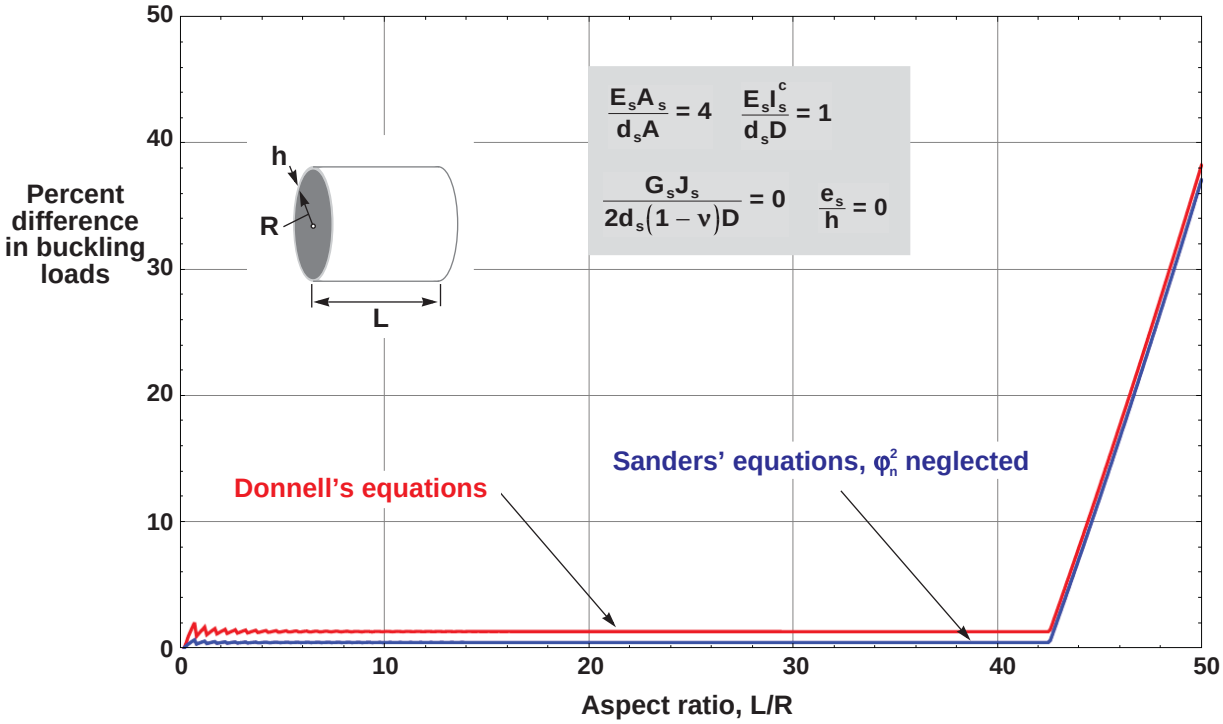

Figure 58. Difference in buckling loads, with respect to results based on Sanders' equations, for compression-loaded stringer-stiffened isotropic cylinders with simply supported edges for R/h = 50 (ν = 0.3).

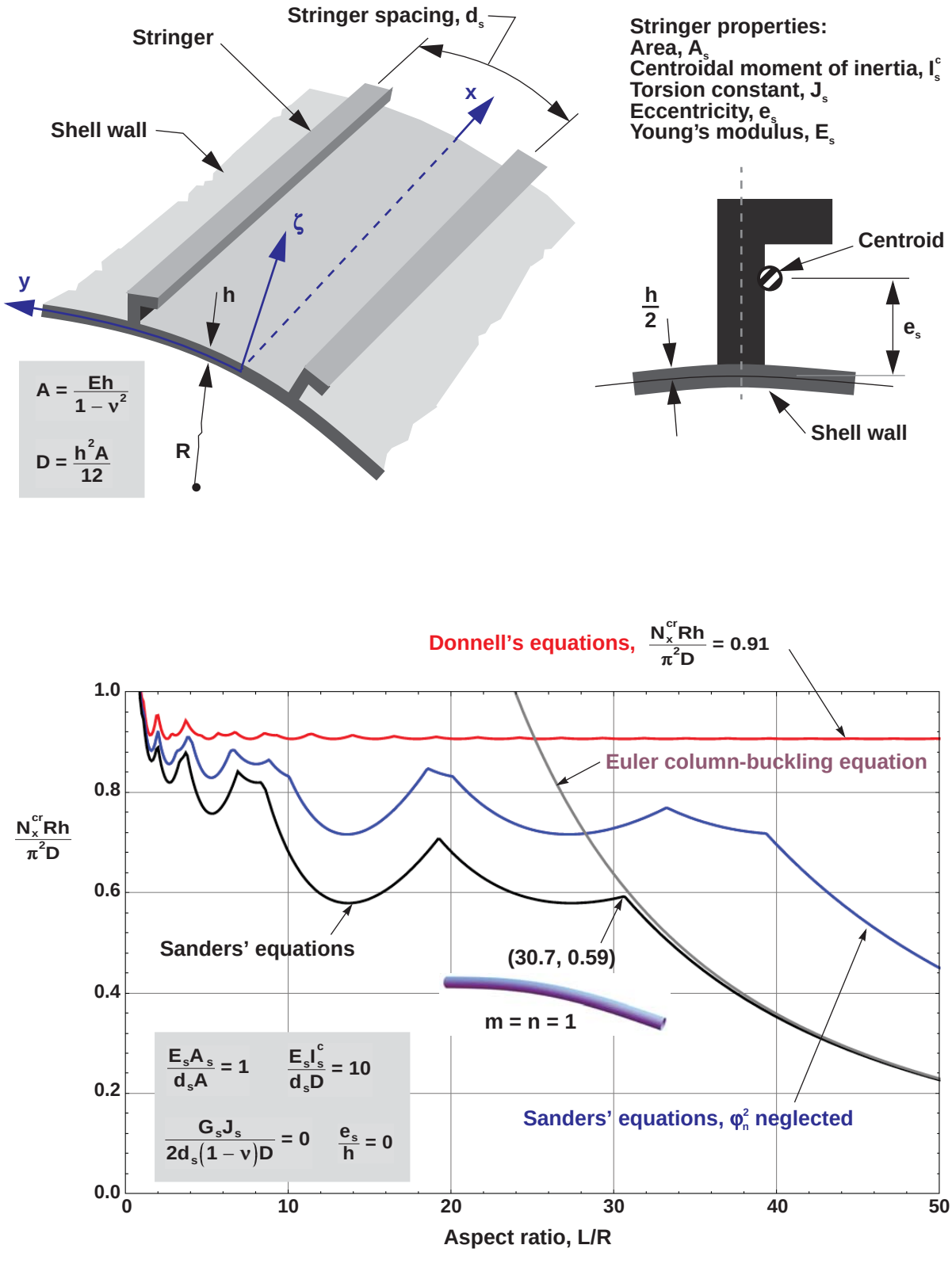

Figure 59. Nondimensional buckling loads for compression-loaded stringer-stiffened isotropic cylinders with simply supported edges for R/h = 50 (ν = 0.3).

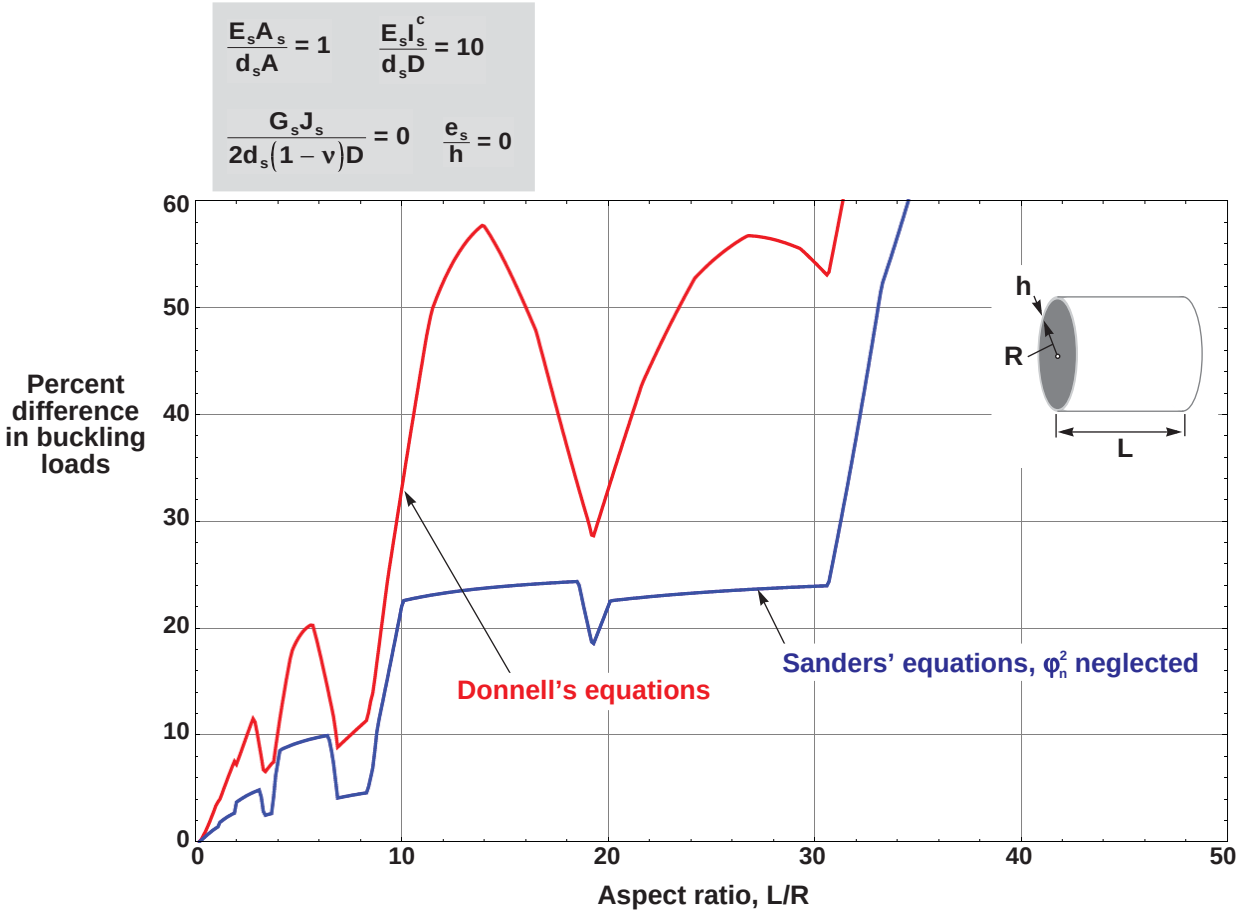

Figure 60. Difference in buckling loads, with respect to results based on Sanders' equations, for compression-loaded stringer-stiffened isotropic cylinders with simply supported edges for R/h = 50 (ν = 0.3).

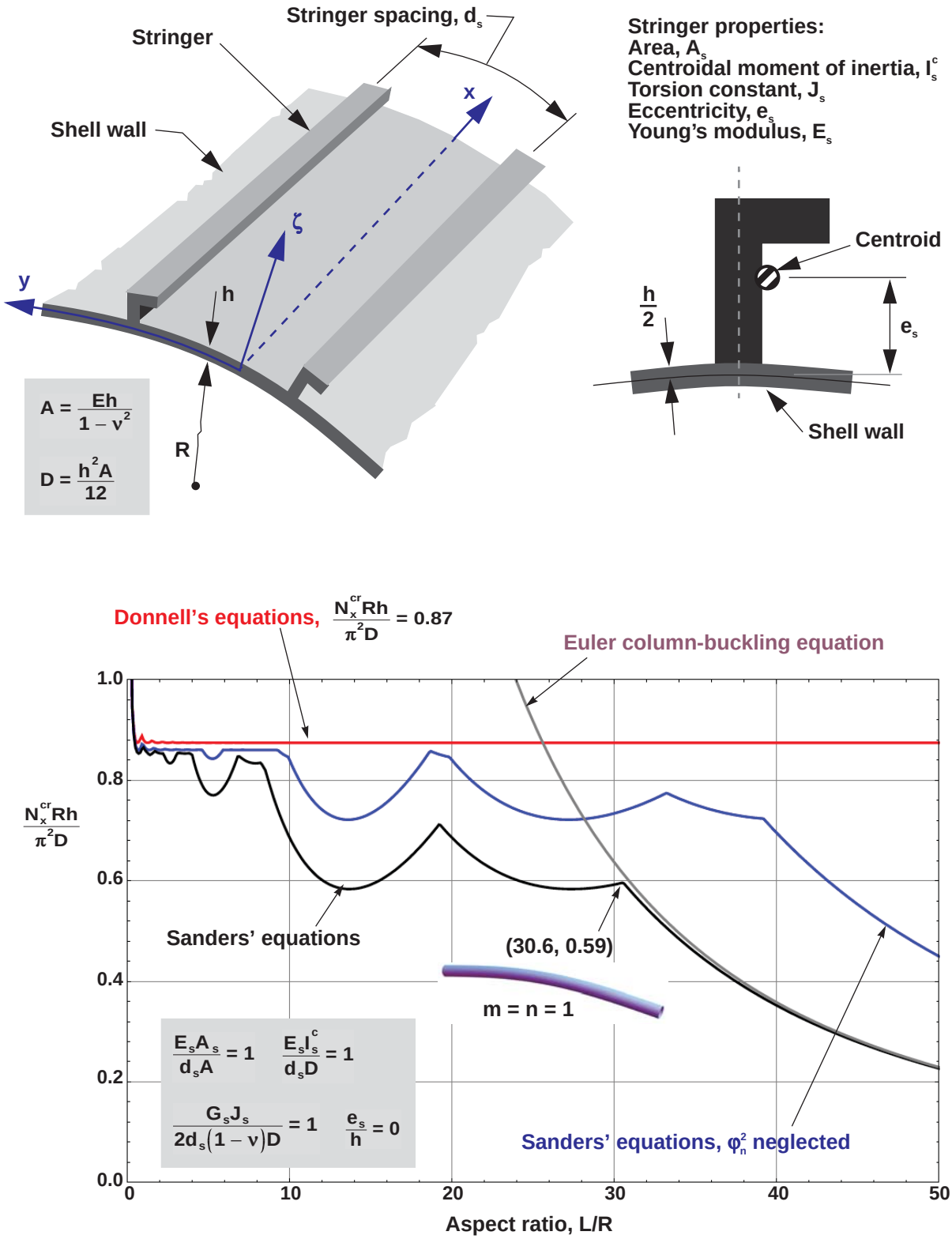

Figure 61. Nondimensional buckling loads for compression-loaded stringer-stiffened isotropic cylinders with simply supported edges for R/h = 50 (ν = 0.3).

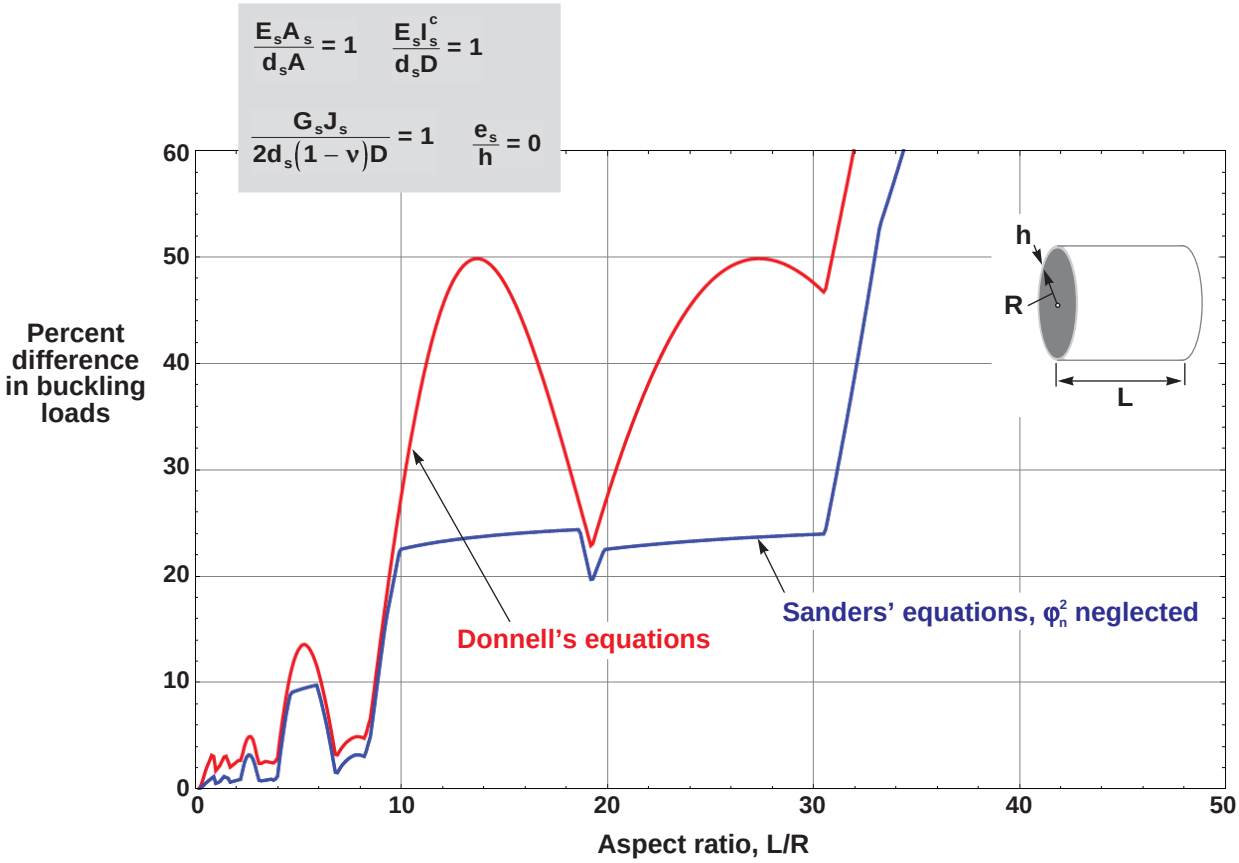

Figure 62. Difference in buckling loads, with respect to results based on Sanders' equations, for compression-loaded stringer-stiffened isotropic cylinders with simply supported edges for R/h = 50 (ν = 0.3).

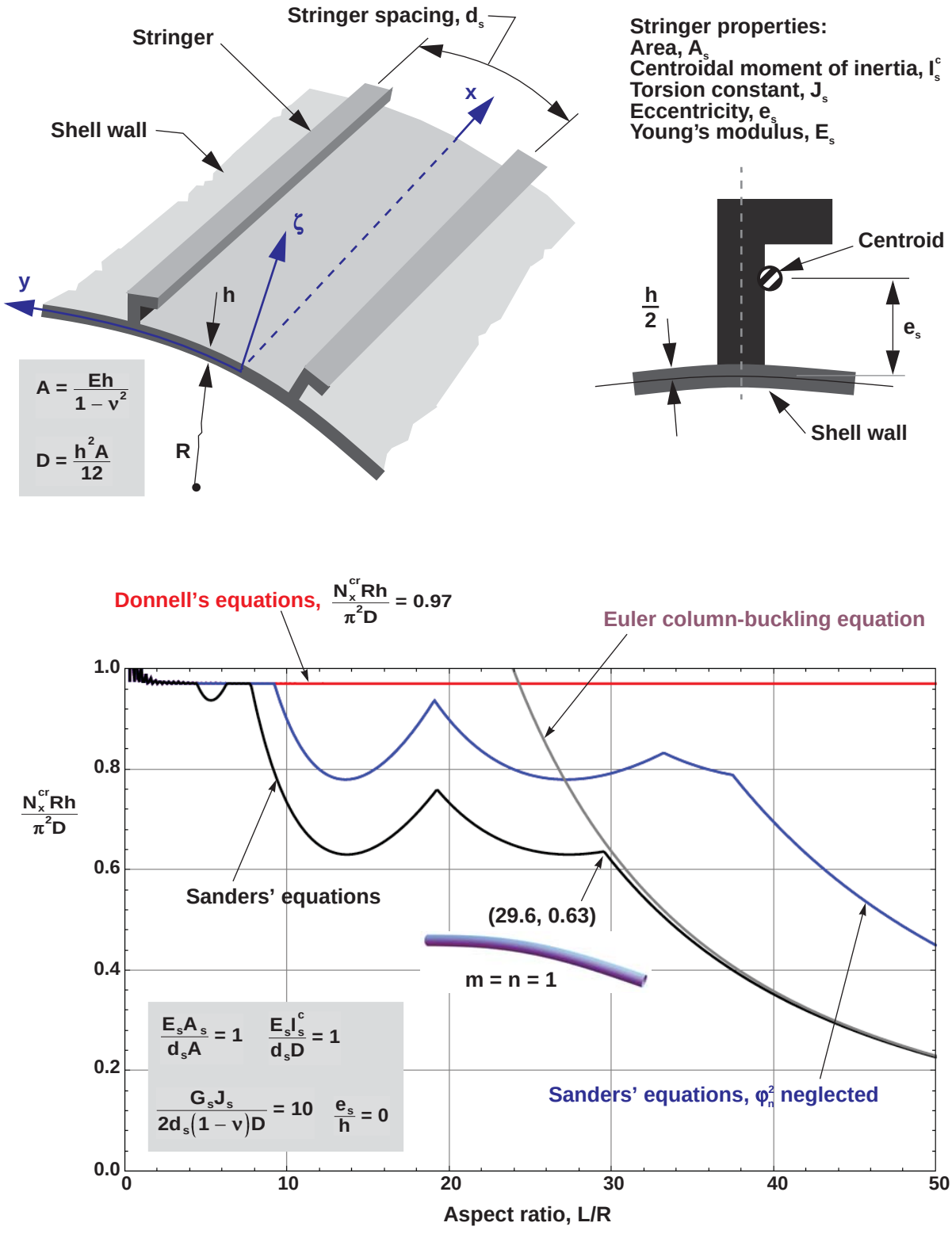

Figure 63. Nondimensional buckling loads for compression-loaded stringer-stiffened isotropic cylinders with simply supported edges for R/h = 50 (ν = 0.3).

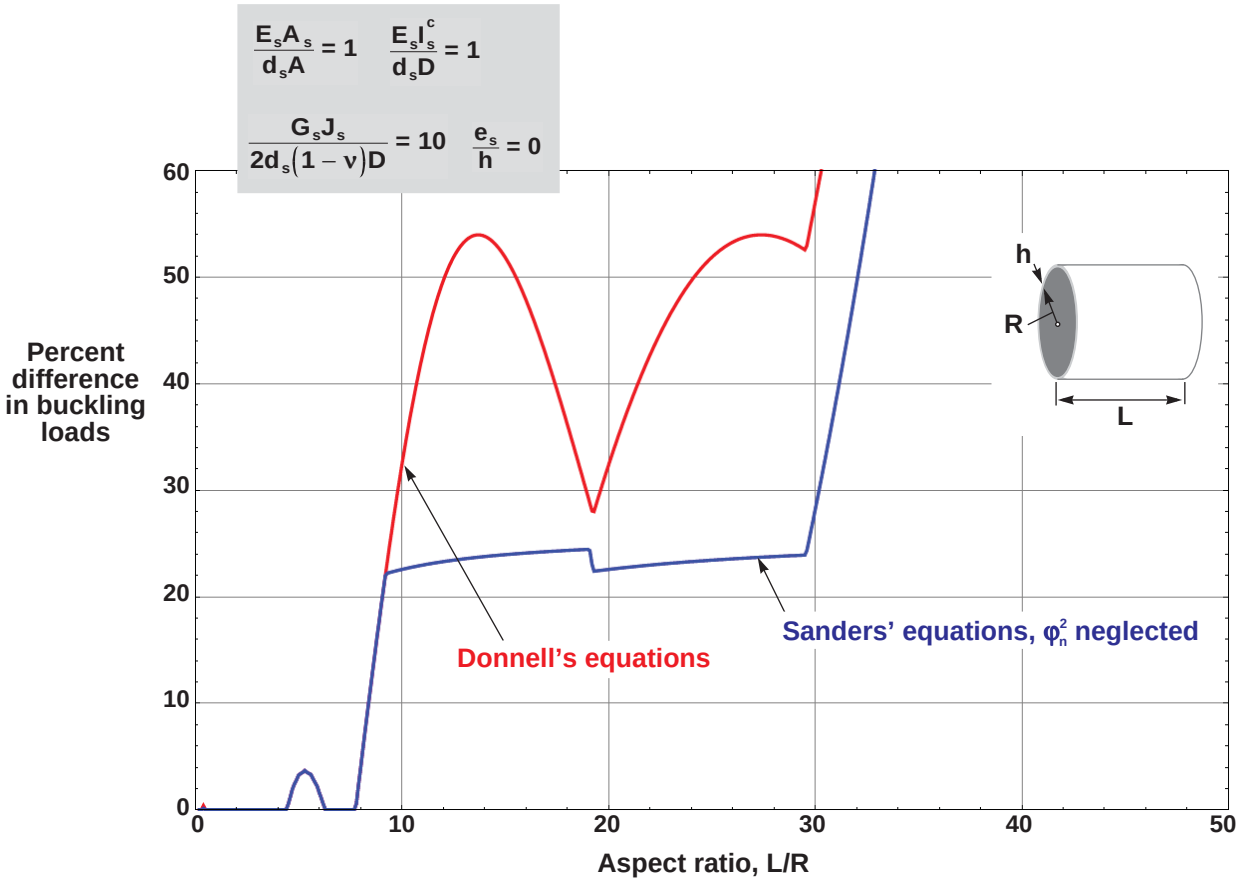

Figure 64. Difference in buckling loads, with respect to results based on Sanders' equations, for compression-loaded stringer-stiffened isotropic cylinders with simply supported edges for R/h = 50 (ν = 0.3).

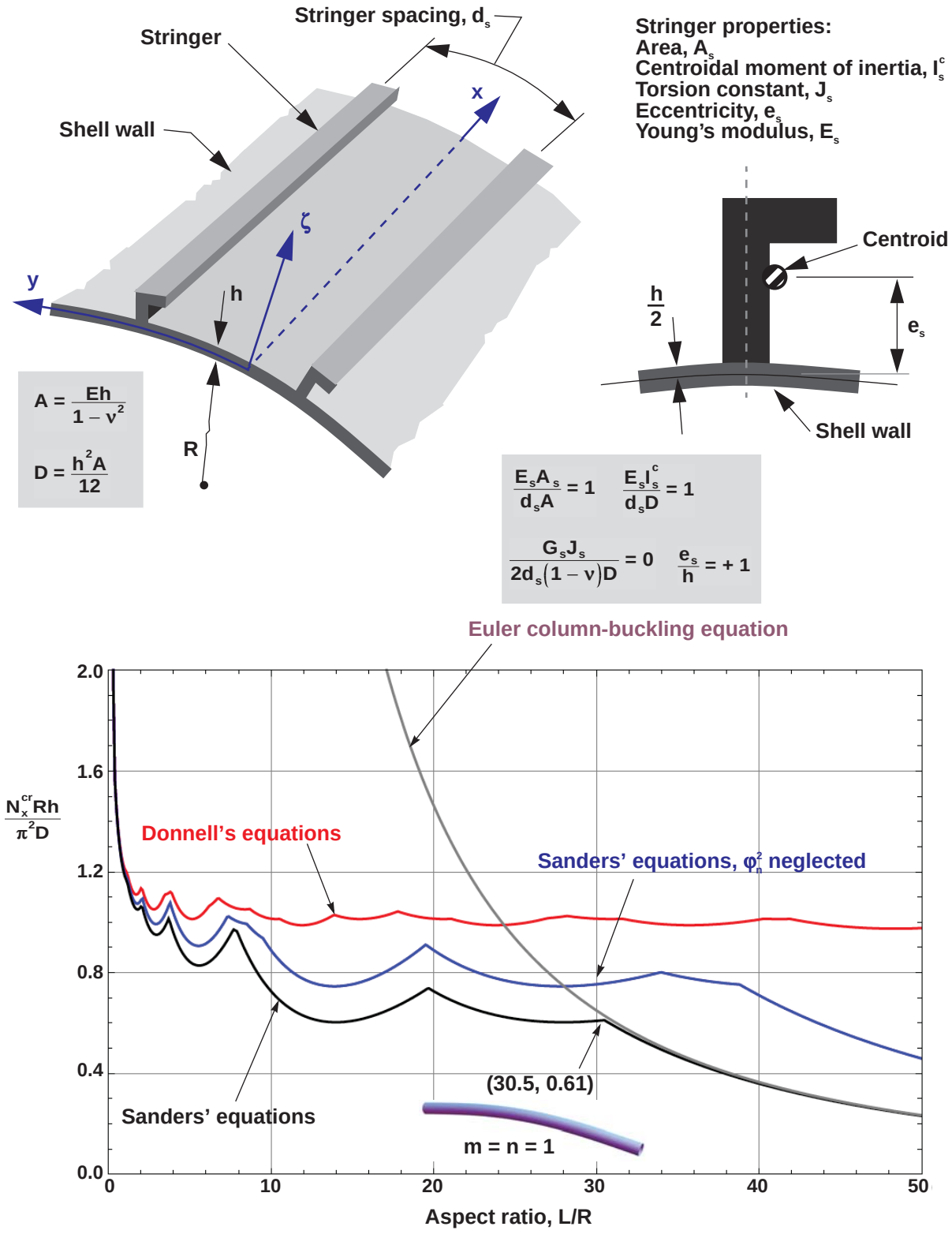

Figure 65. Nondimensional buckling loads for compression-loaded stringer-stiffened isotropic cylinders with simply supported edges for R/h = 50 (ν = 0.3).

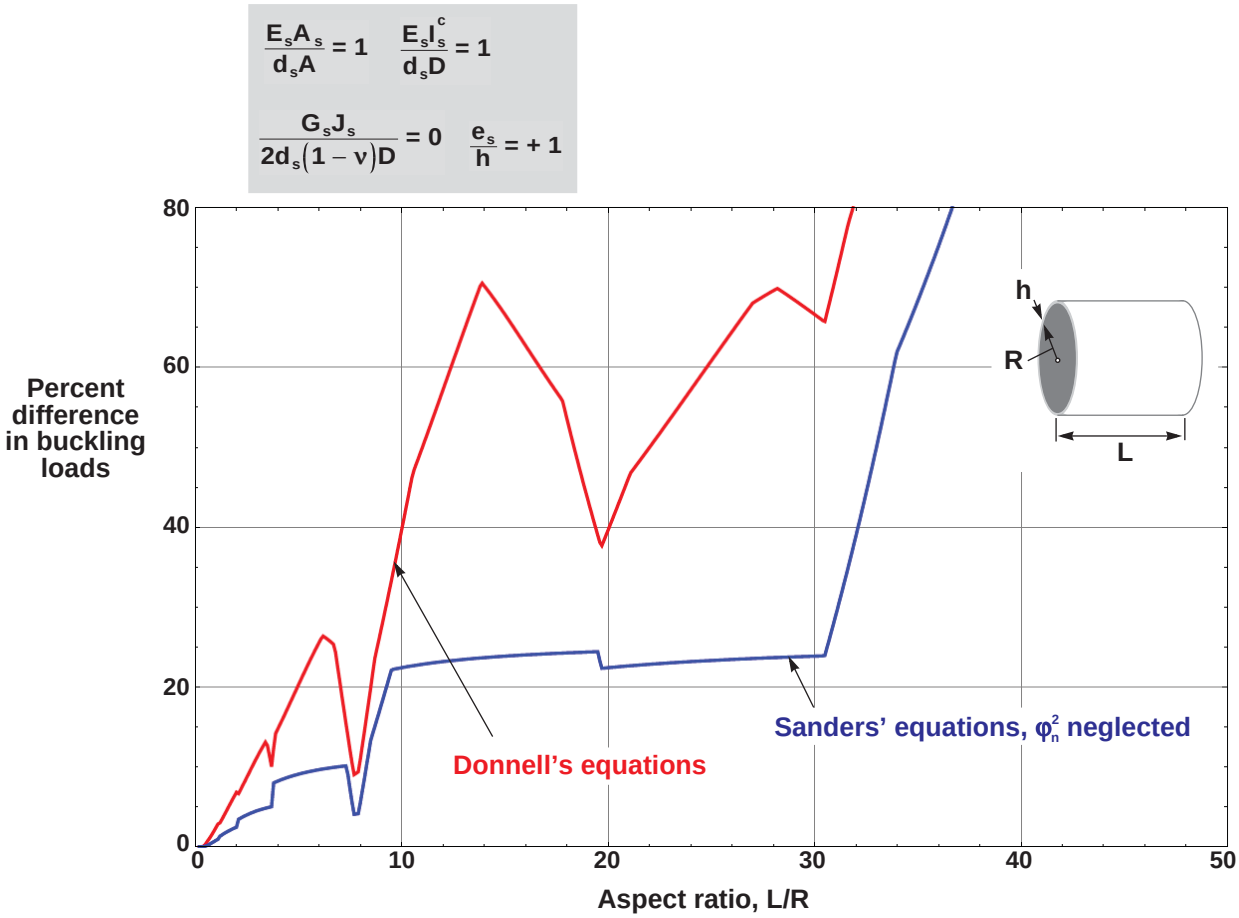

Figure 66. Difference in buckling loads, with respect to results based on Sanders' equations, for compression-loaded stringer-stiffened isotropic cylinders with simply supported edges for R/h = 50 (ν = 0.3).

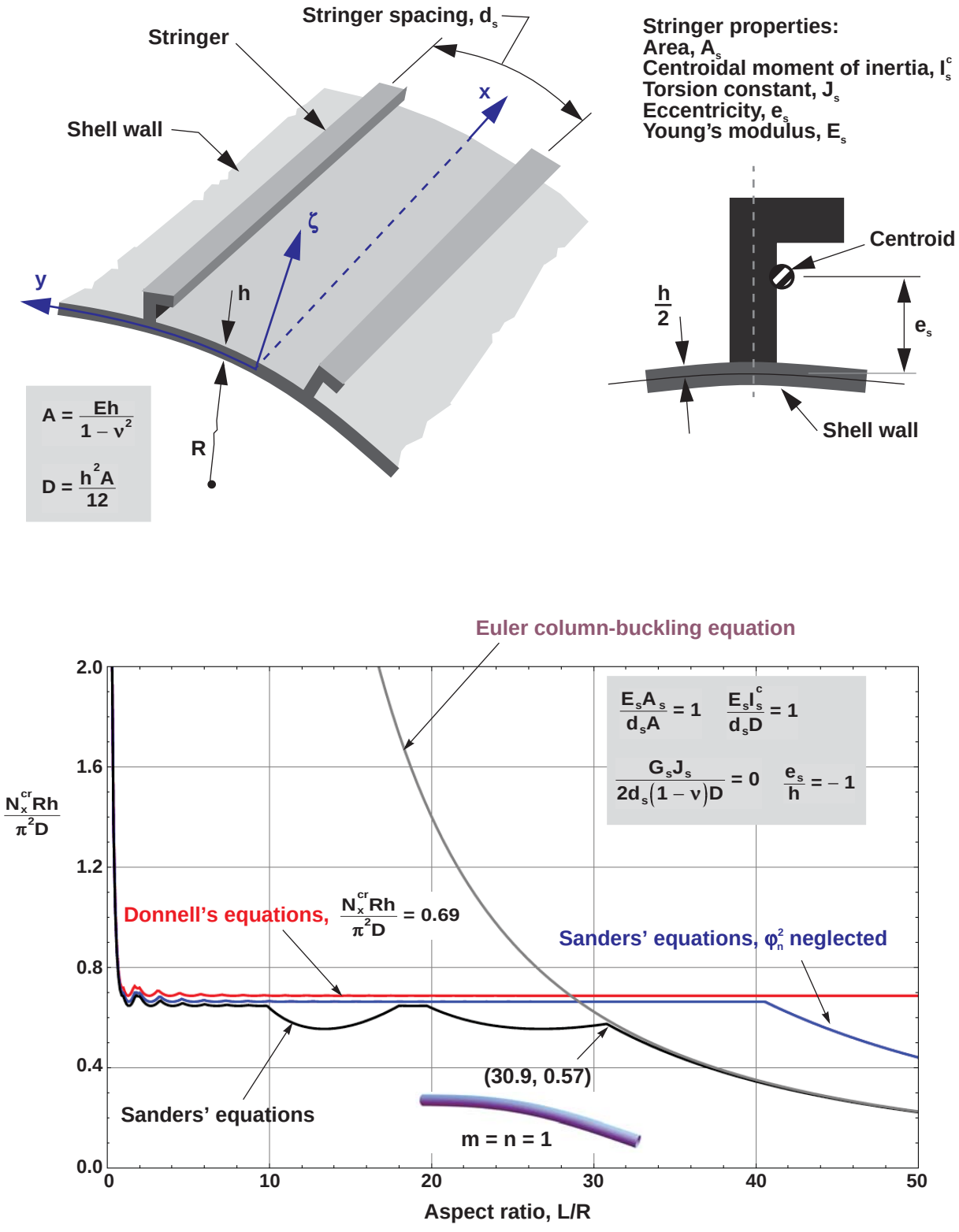

Figure 67. Nondimensional buckling loads for compression-loaded stringer-stiffened isotropic cylinders with simply supported edges for R/h = 50 (ν = 0.3).

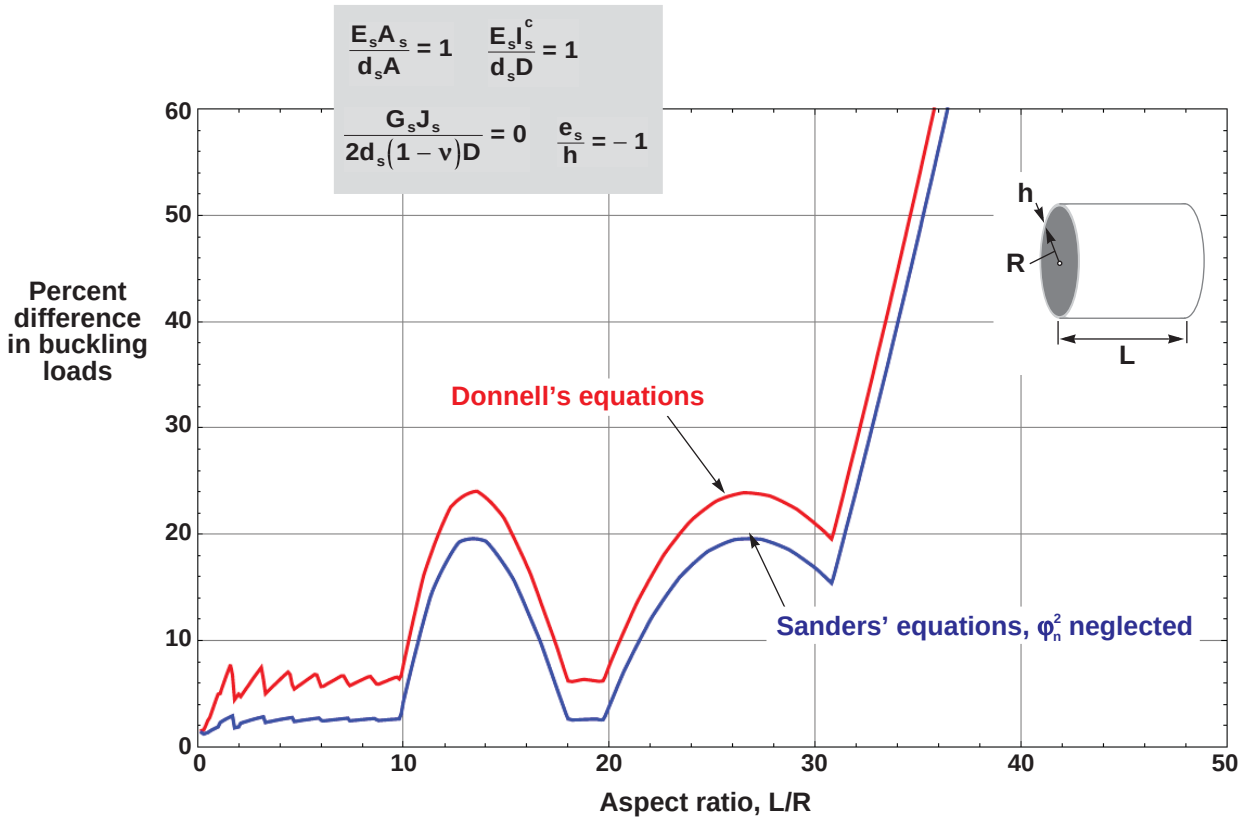

Figure 68. Difference in buckling loads, with respect to results based on Sanders' equations, for compression-loaded stringer-stiffened isotropic cylinders with simply supported edges for R/h = 50 (ν = 0.3).

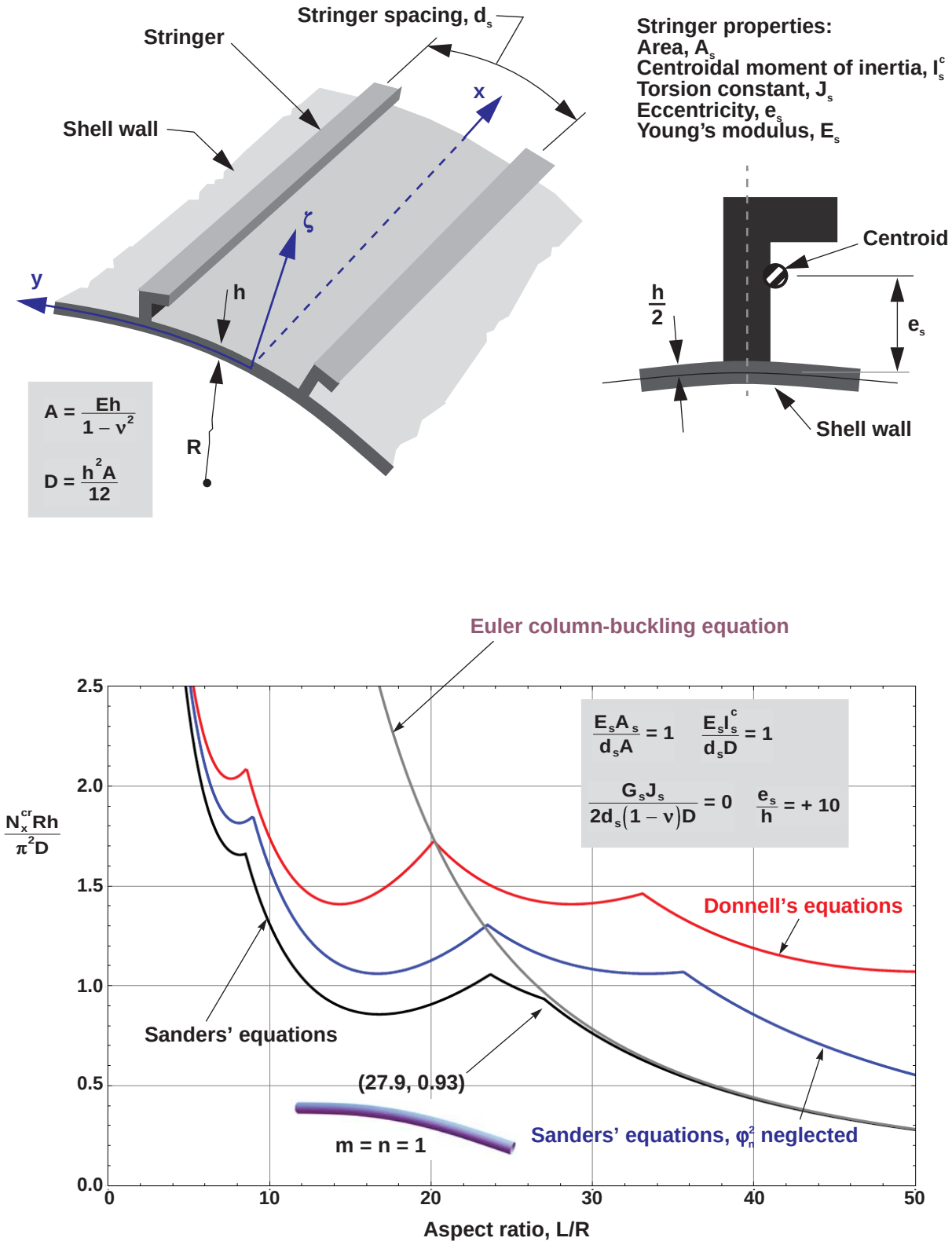

Figure 69. Nondimensional buckling loads for compression-loaded stringer-stiffened isotropic cylinders with simply supported edges for R/h = 50 (ν = 0.3).

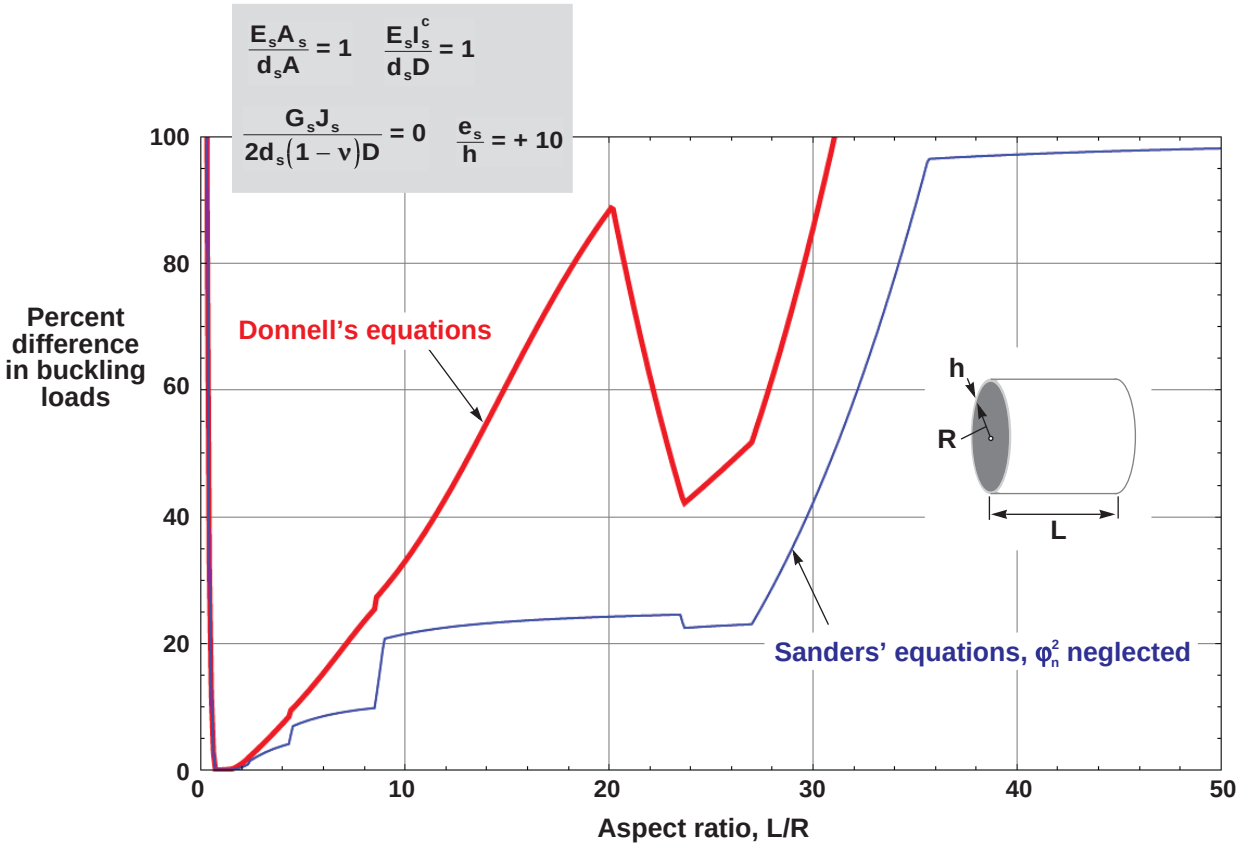

Figure 70. Difference in buckling loads, with respect to results based on Sanders' equations, for compression-loaded stringer-stiffened isotropic cylinders with simply supported edges for R/h = 50 (ν = 0.3).

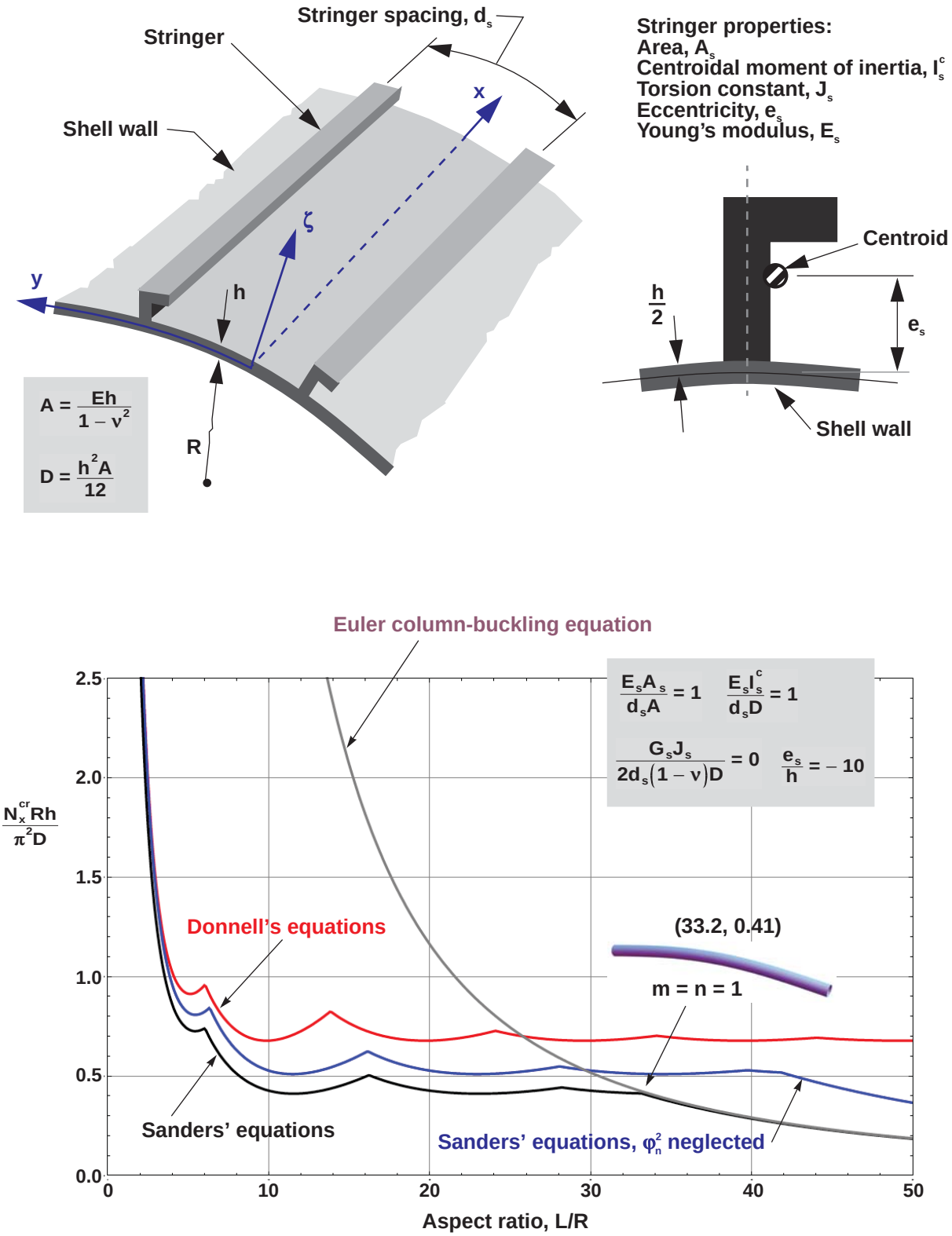

Figure 71. Nondimensional buckling loads for compression-loaded stringer-stiffened isotropic cylinders with simply supported edges for R/h = 50 (ν = 0.3).

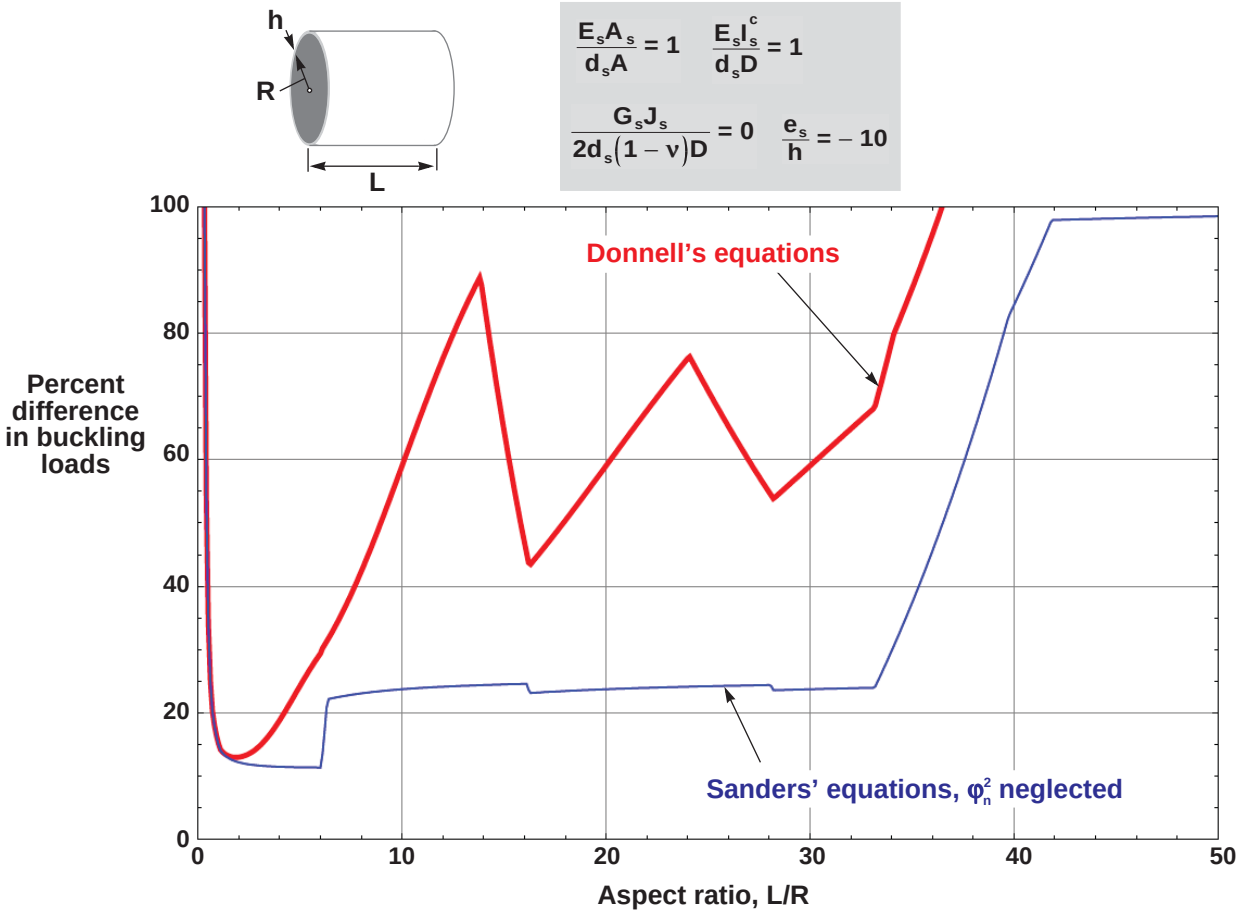

Figure 72. Difference in buckling loads, with respect to results based on Sanders' equations, for compression-loaded stringer-stiffened isotropic cylinders with simply supported edges for R/h = 50 (ν = 0.3).

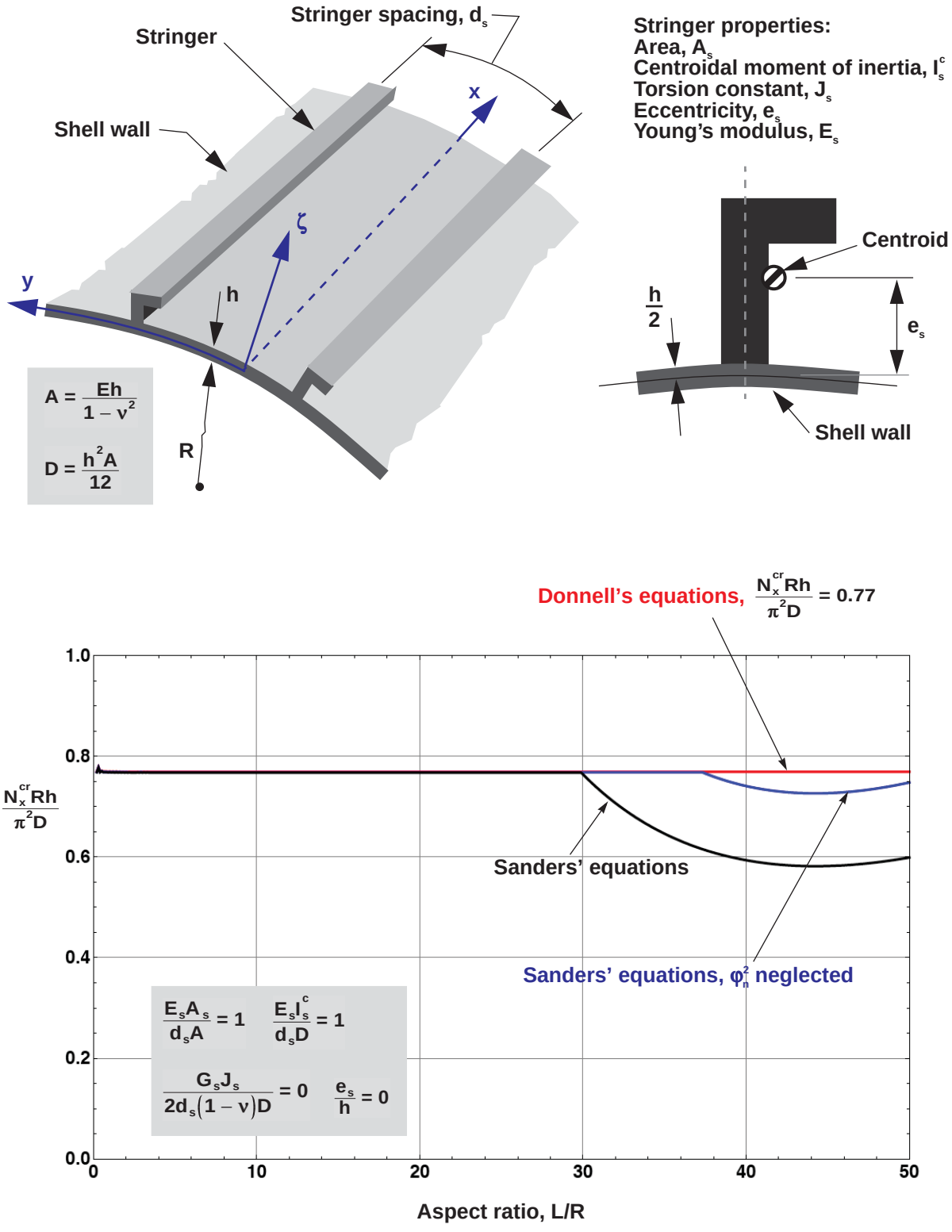

Figure 73. Nondimensional buckling loads for compression-loaded stringer-stiffened isotropic cylinders with simply supported edges for R/h = 500 (ν = 0.3).

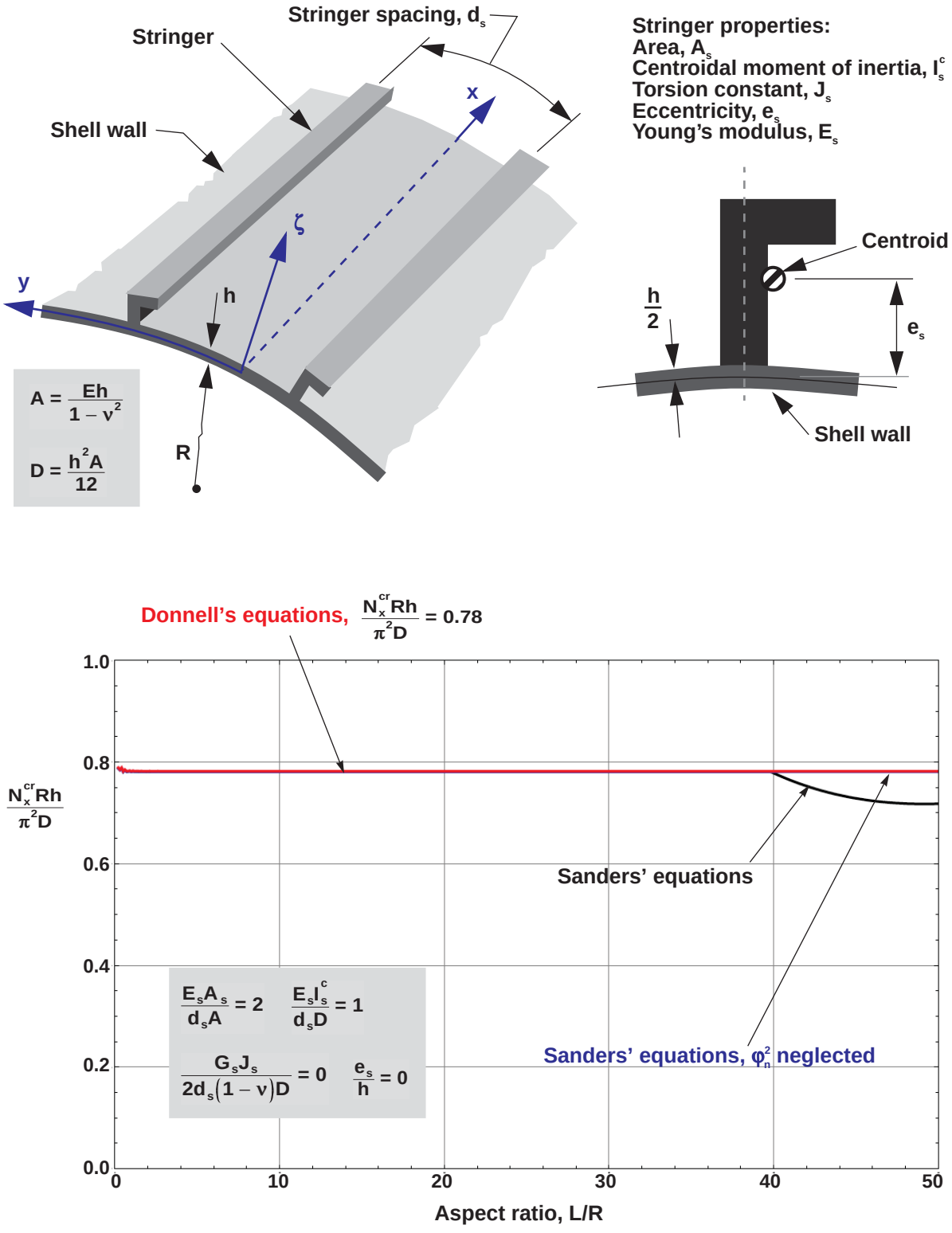

Figure 74. Nondimensional buckling loads for compression-loaded stringer-stiffened isotropic cylinders with simply supported edges for R/h = 500 (ν = 0.3).

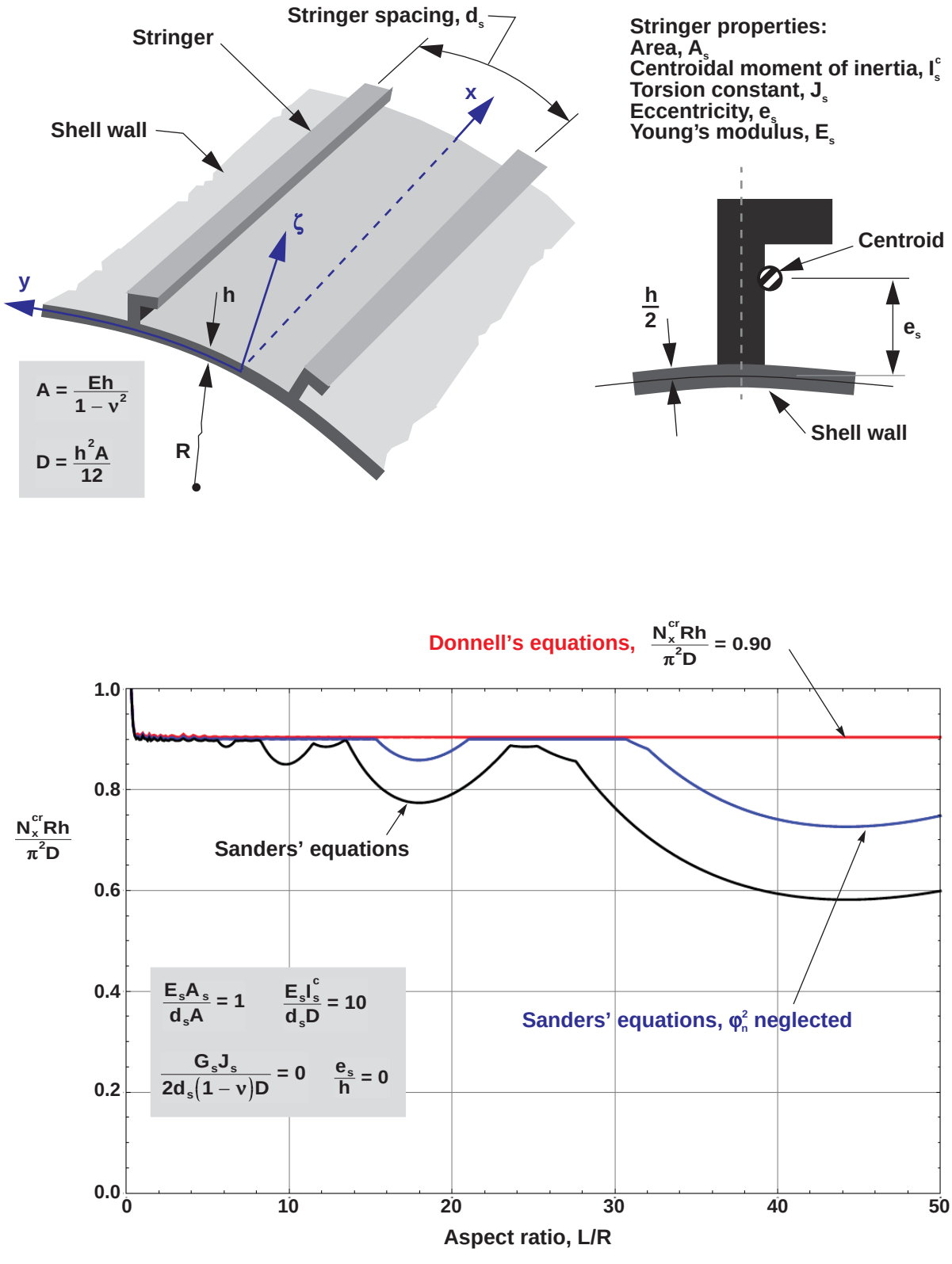

Figure 75. Nondimensional buckling loads for compression-loaded stringer-stiffened isotropic cylinders with simply supported edges for R/h = 500 (ν = 0.3).

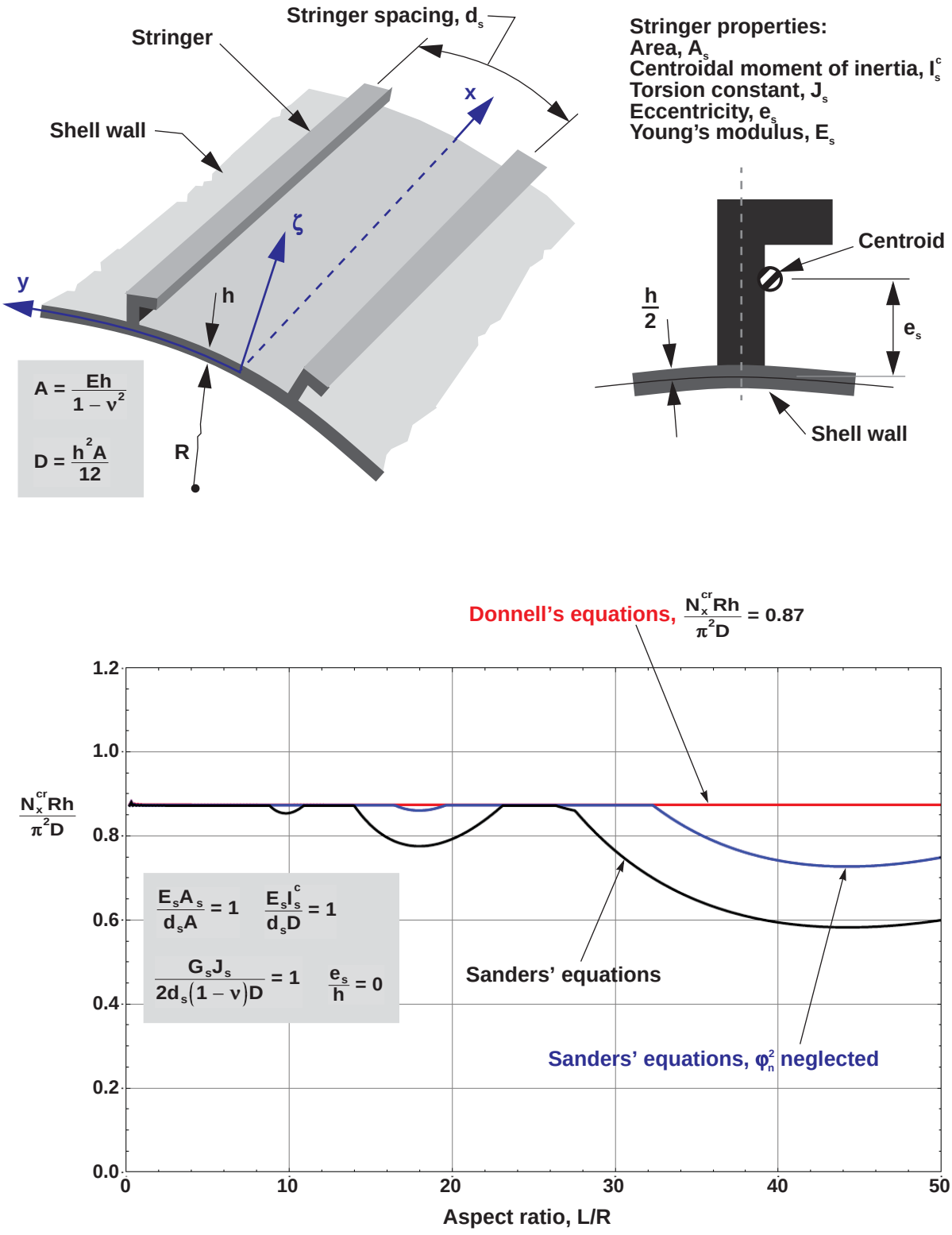

Figure 76. Nondimensional buckling loads for compression-loaded stringer-stiffened isotropic cylinders with simply supported edges for R/h = 500 (ν = 0.3).

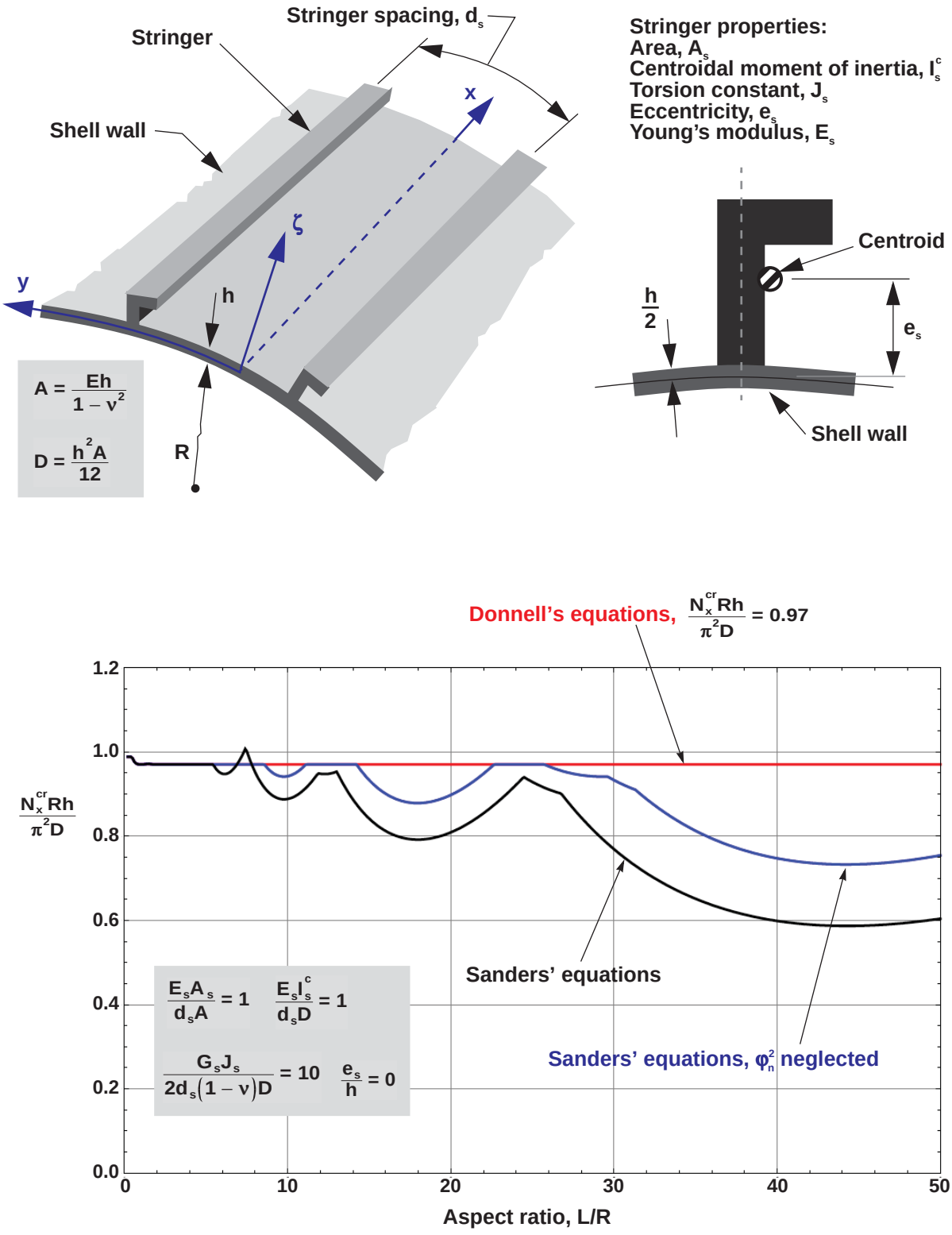

Figure 77. Nondimensional buckling loads for compression-loaded stringer-stiffened isotropic cylinders with simply supported edges for R/h = 500 (ν = 0.3).

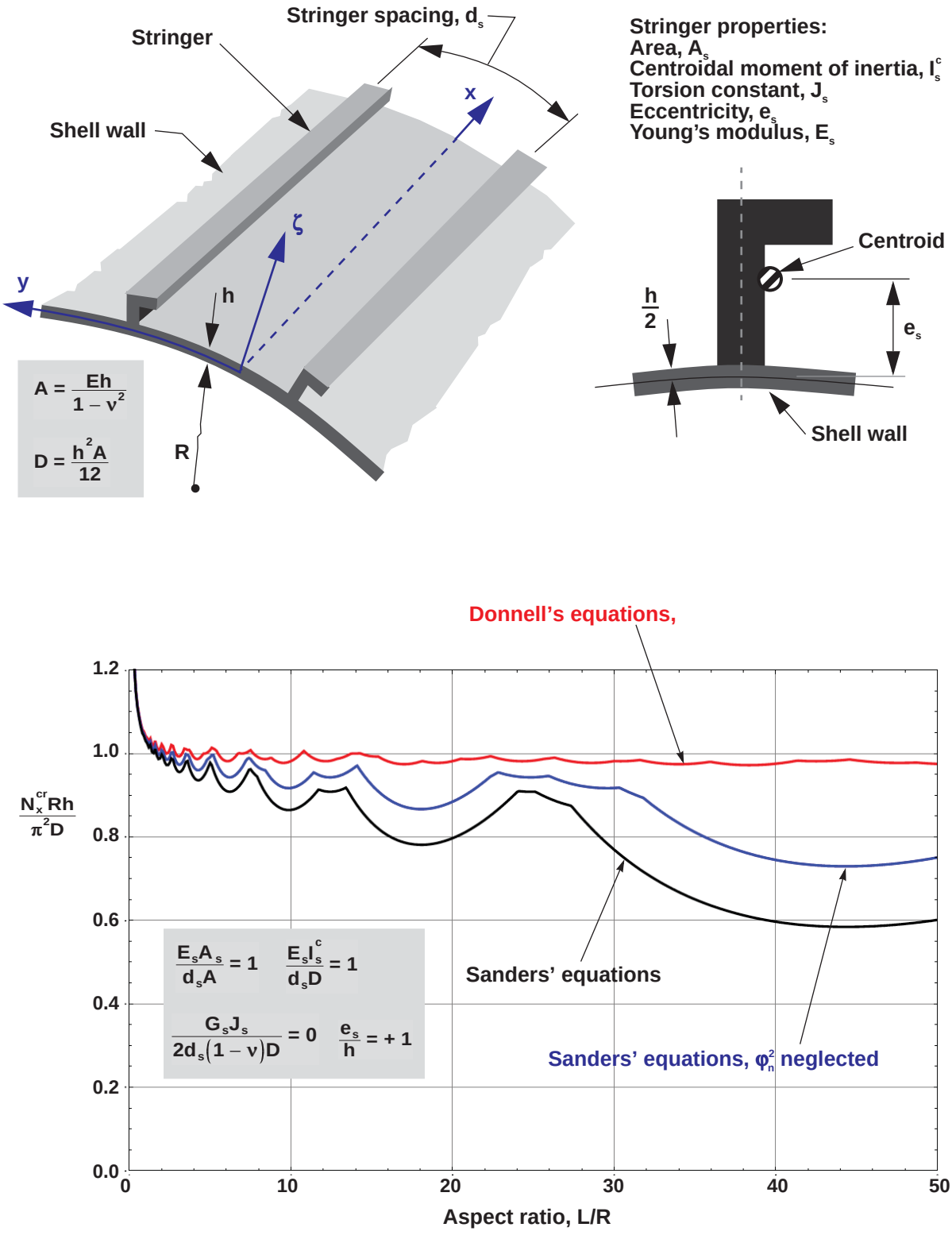

Figure 78. Nondimensional buckling loads for compression-loaded stringer-stiffened isotropic cylinders with simply supported edges for R/h = 500 (ν = 0.3).

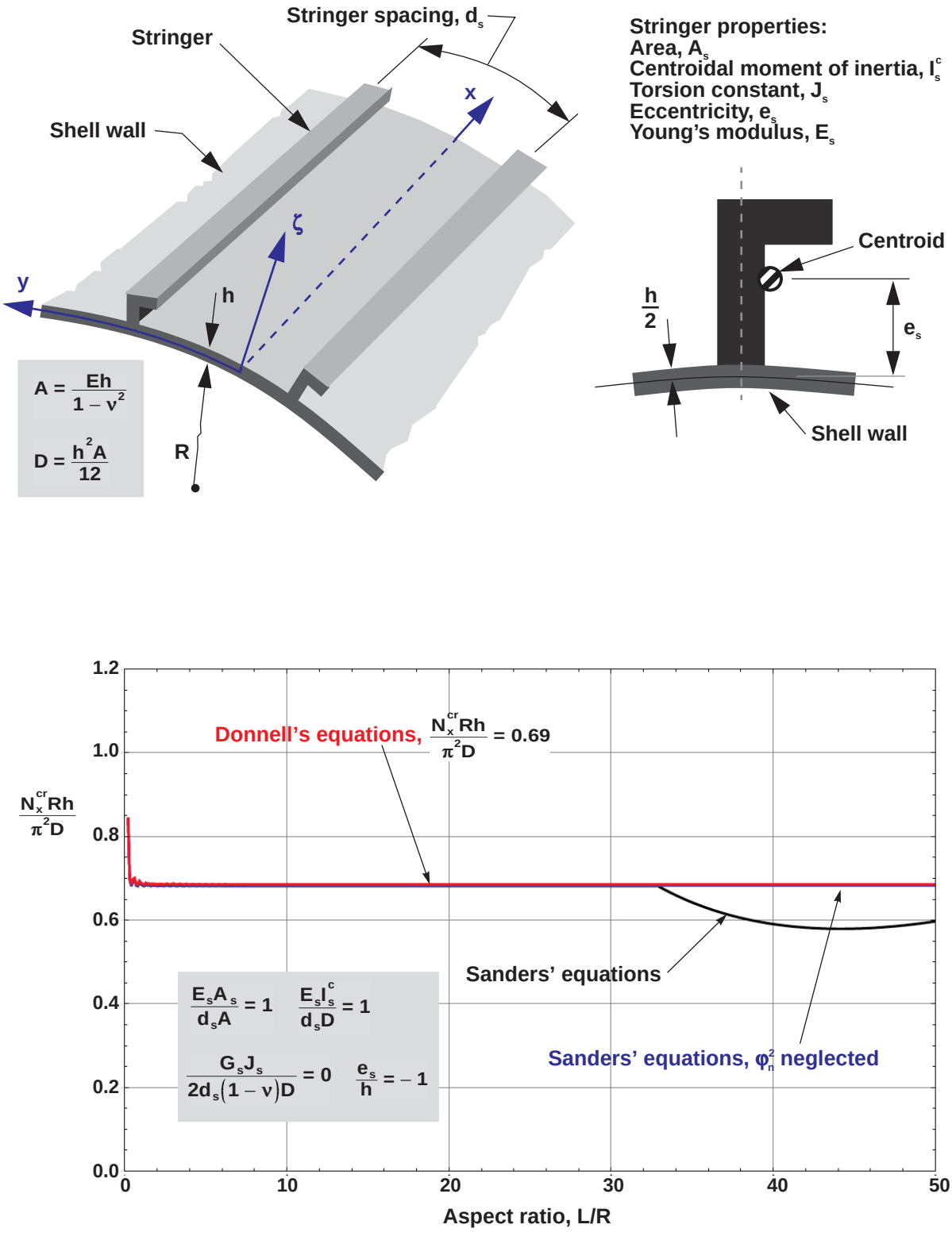

Figure 79. Nondimensional buckling loads for compression-loaded stringer-stiffened isotropic cylinders with simply supported edges for R/h = 500 (ν = 0.3).

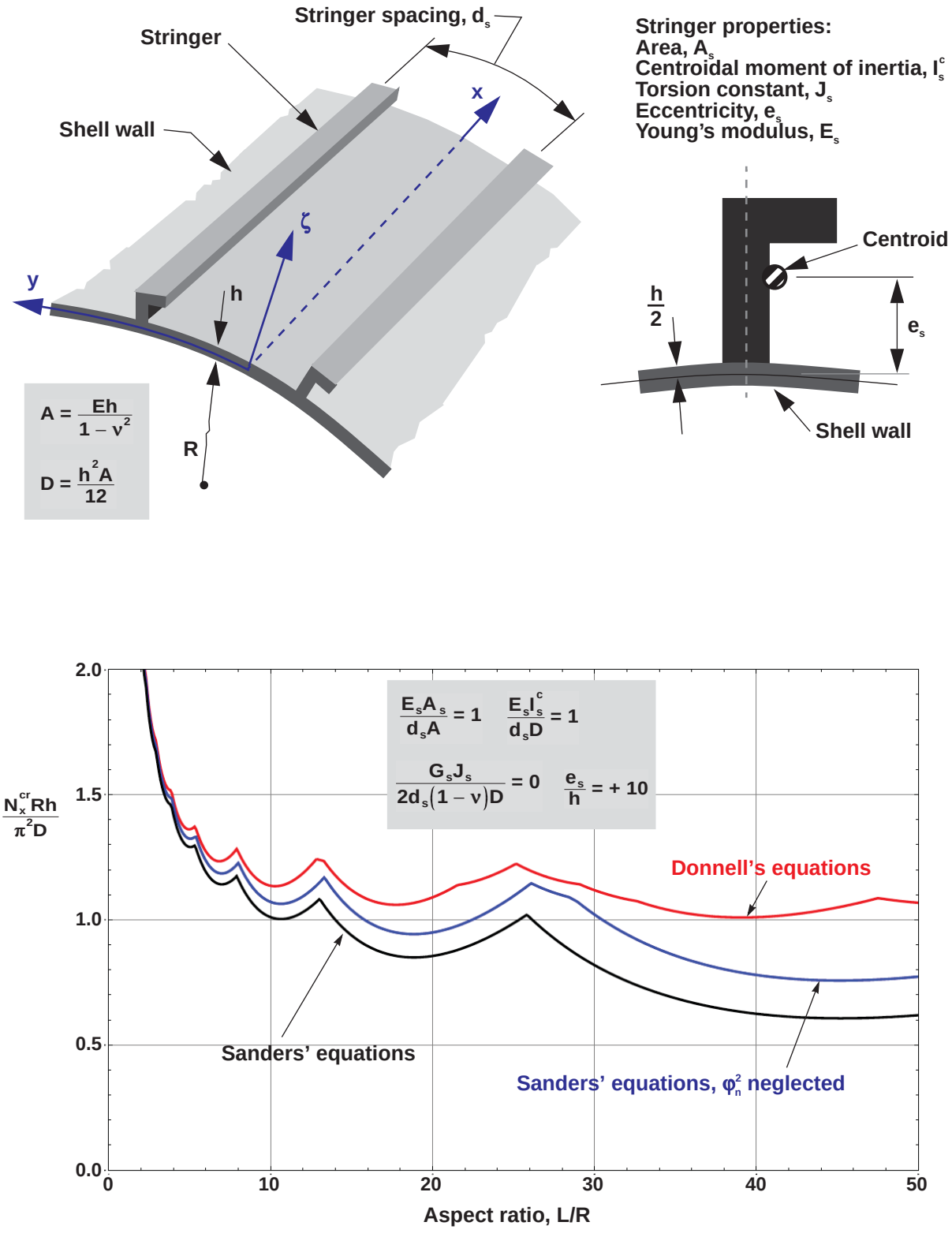

Figure 80. Nondimensional buckling loads for compression-loaded stringer-stiffened isotropic cylinders with simply supported edges for R/h = 500 (ν = 0.3).

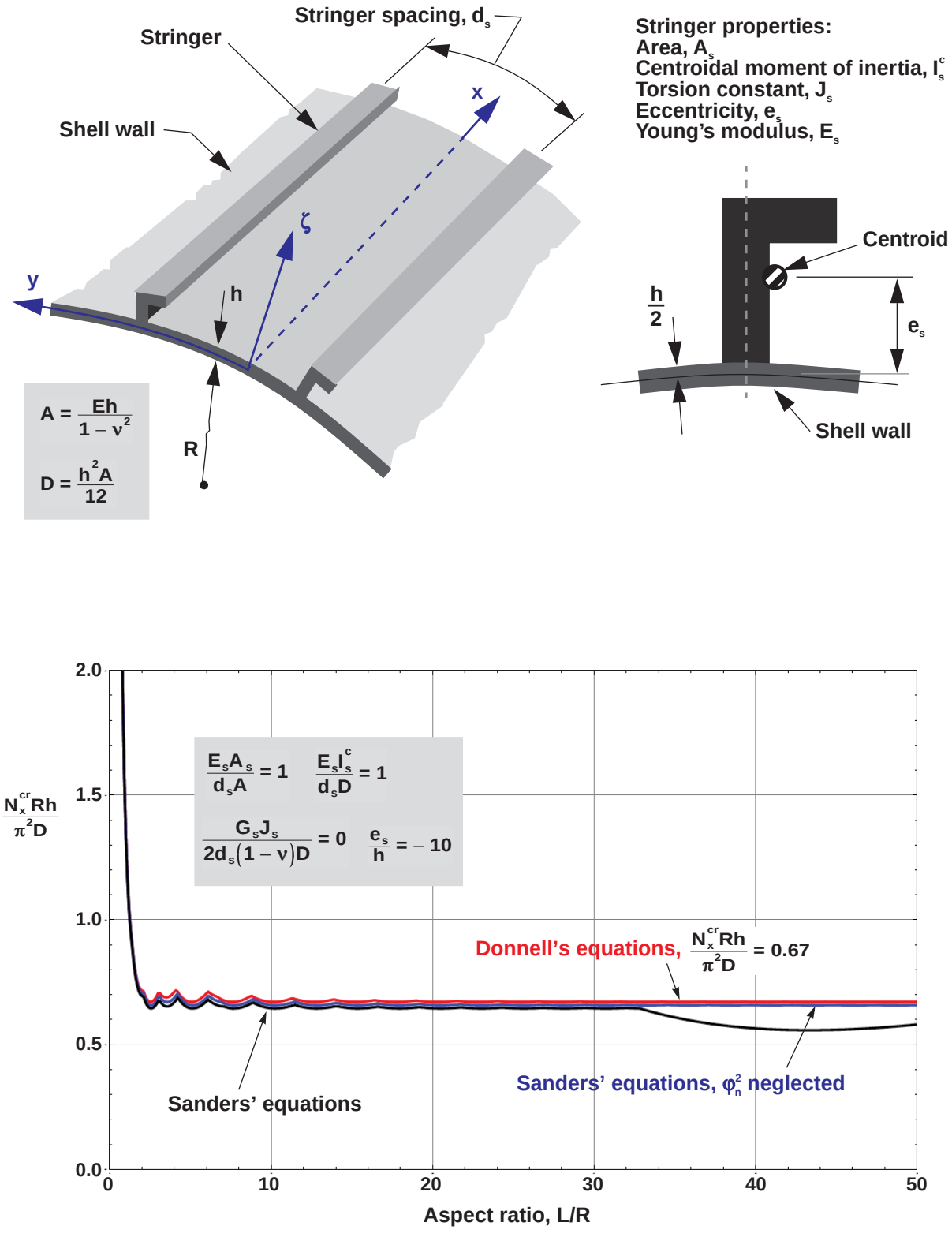

Figure 81. Nondimensional buckling loads for compression-loaded stringer-stiffened isotropic cylinders with simply supported edges for R/h = 500 (ν = 0.3).

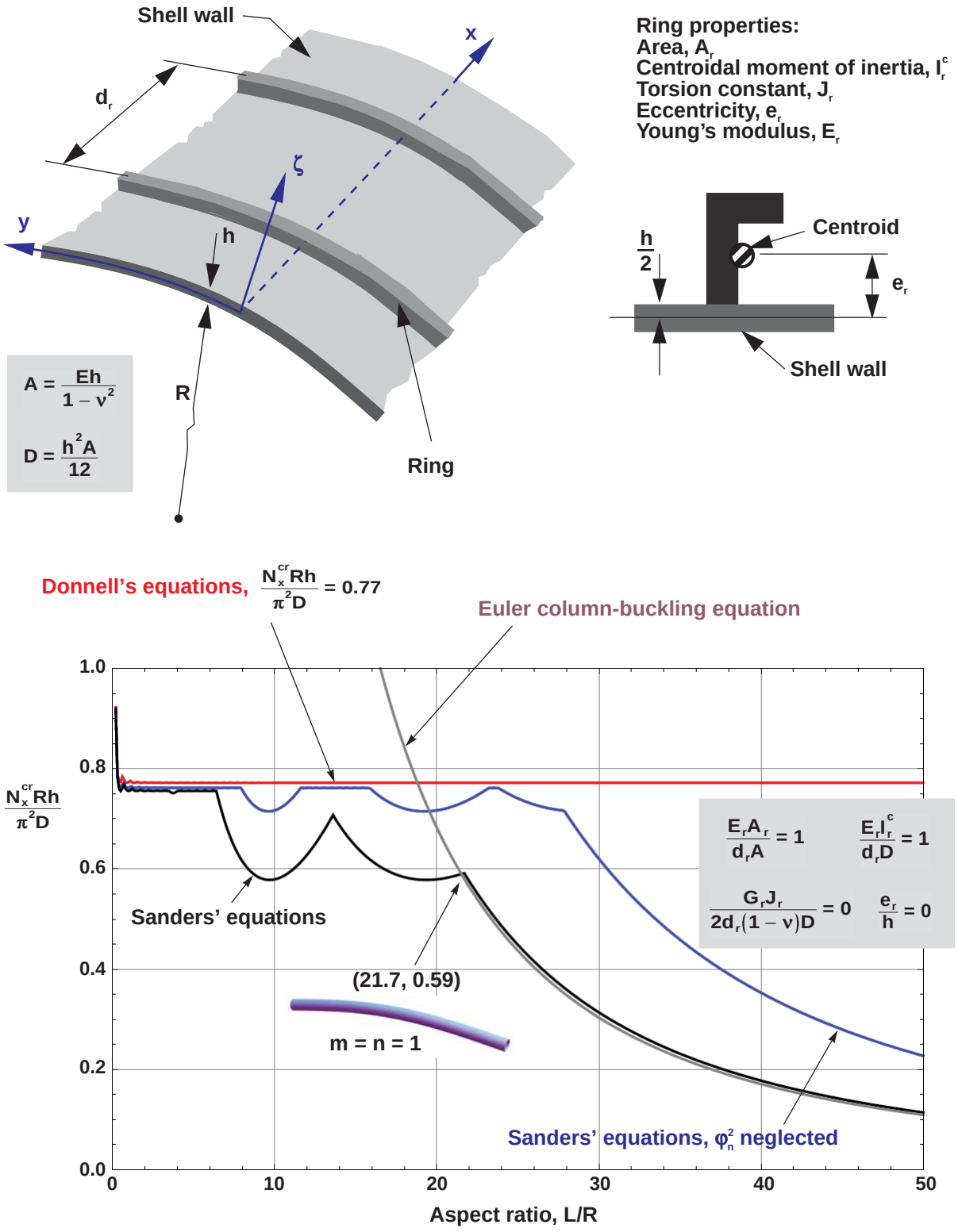

Figure 82. Nondimensional buckling loads for compression-loaded ring-stiffened isotropic cylinders with simply supported edges for R/h = 50 (ν = 0.3).

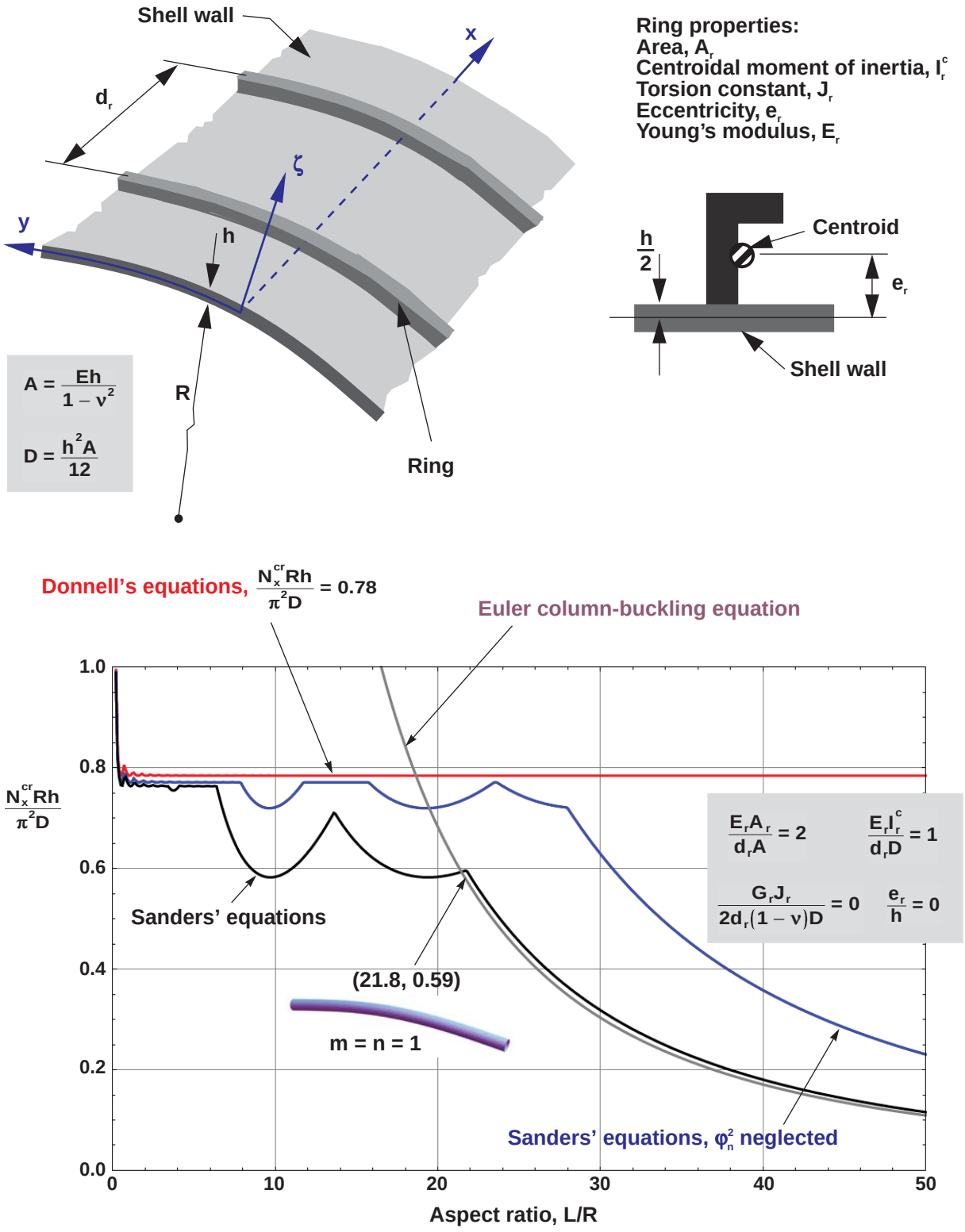

Figure 83. Nondimensional buckling loads for compression-loaded ring-stiffened isotropic cylinders with simply supported edges for R/h = 50 (ν = 0.3).

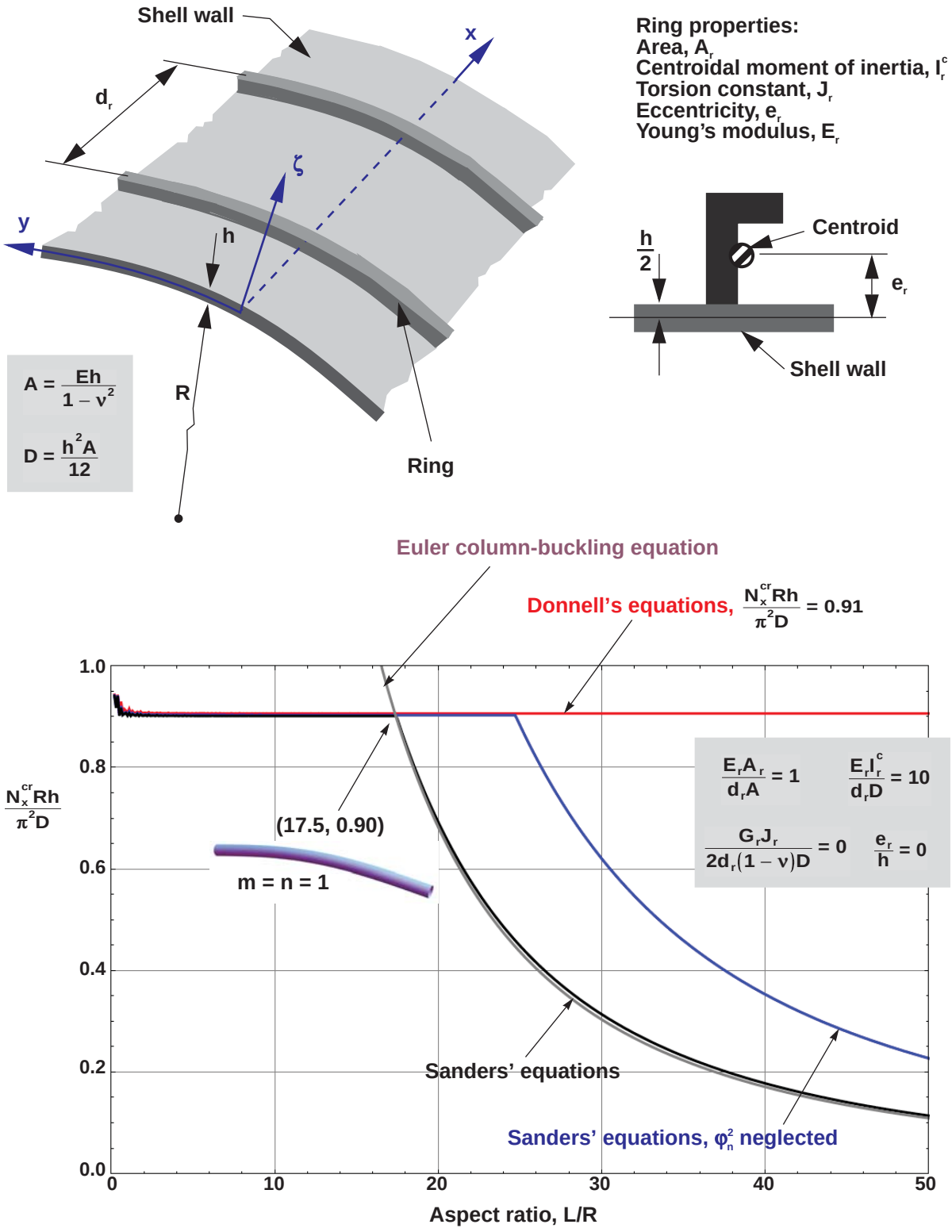

Figure 84. Nondimensional buckling loads for compression-loaded ring-stiffened isotropic cylinders with simply supported edges for R/h = 50 (ν = 0.3).

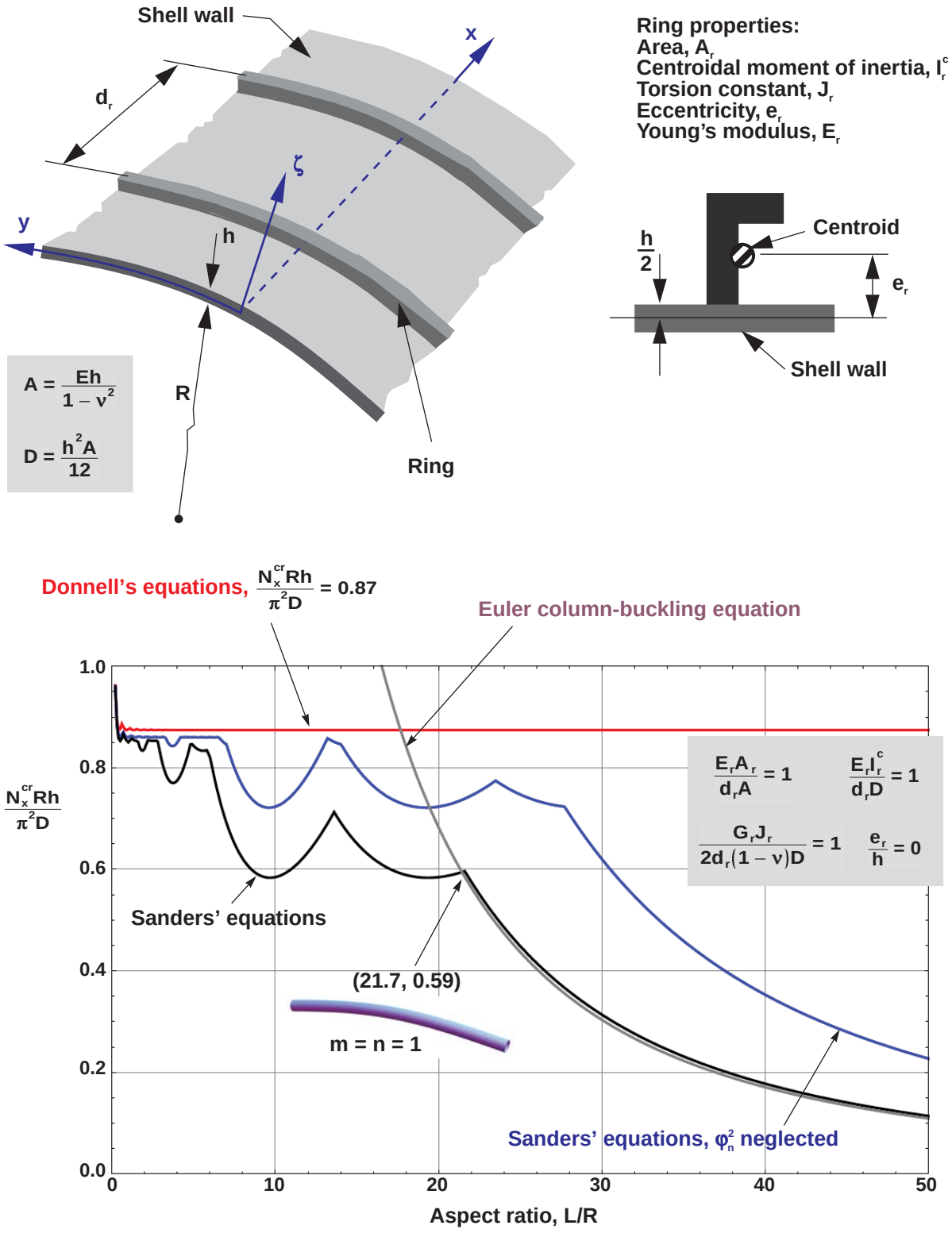

Figure 85. Nondimensional buckling loads for compression-loaded ring-stiffened isotropic cylinders with simply supported edges for R/h = 50 (ν = 0.3).

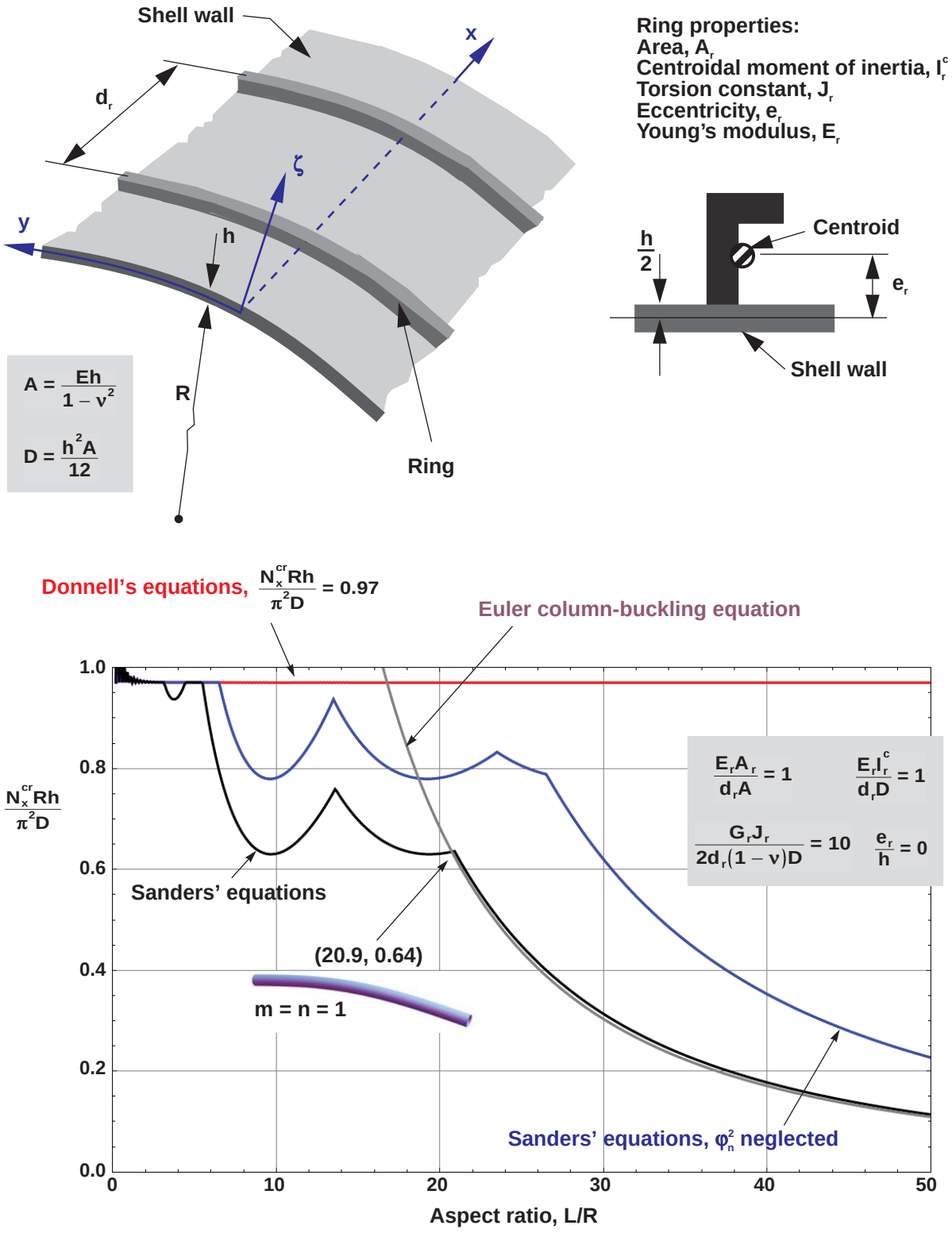

Figure 86. Nondimensional buckling loads for compression-loaded ring-stiffened isotropic cylinders with simply supported edges for R/h = 50 (ν = 0.3).

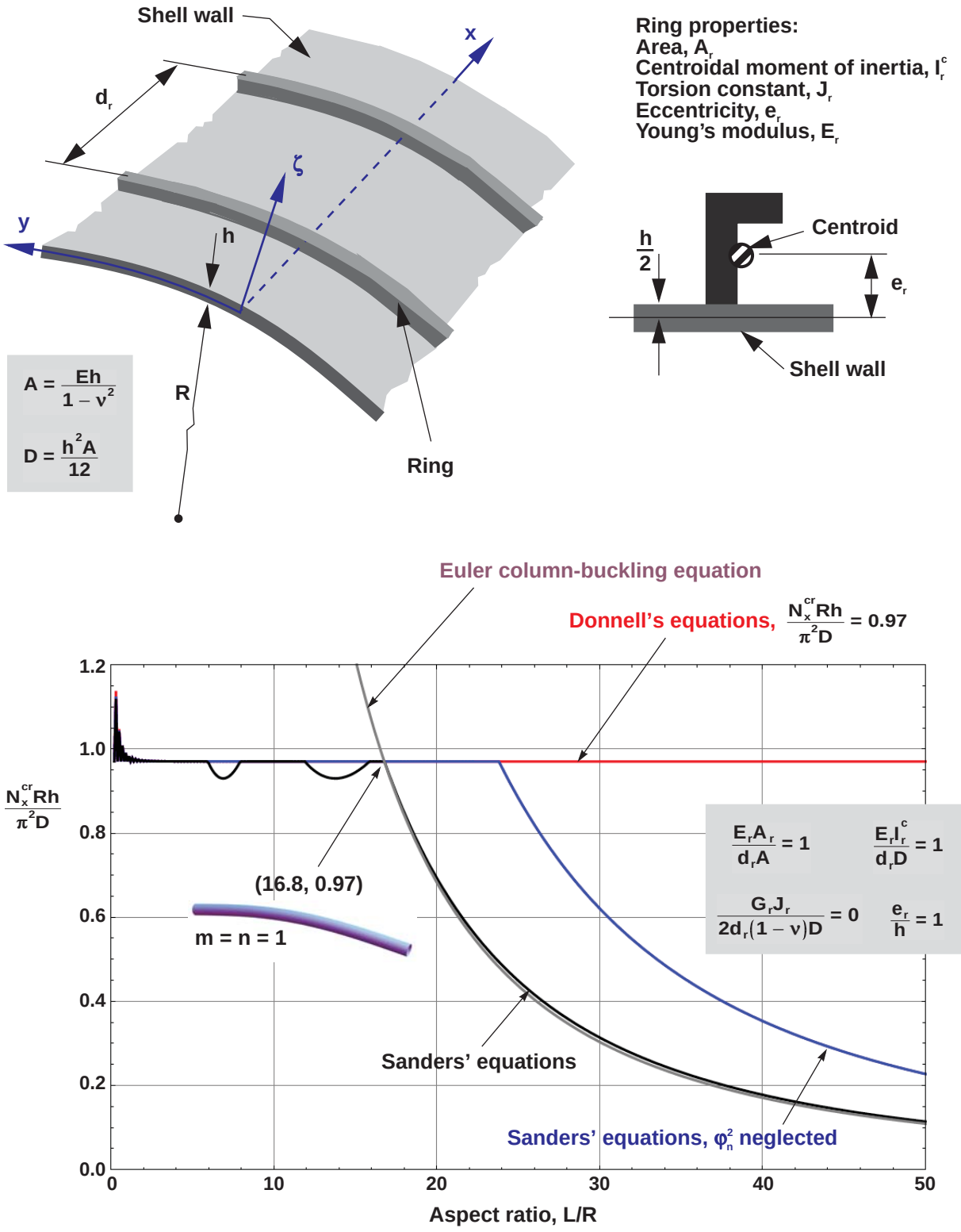

Figure 87. Nondimensional buckling loads for compression-loaded ring-stiffened isotropic cylinders with simply supported edges for R/h = 50 (ν = 0.3).

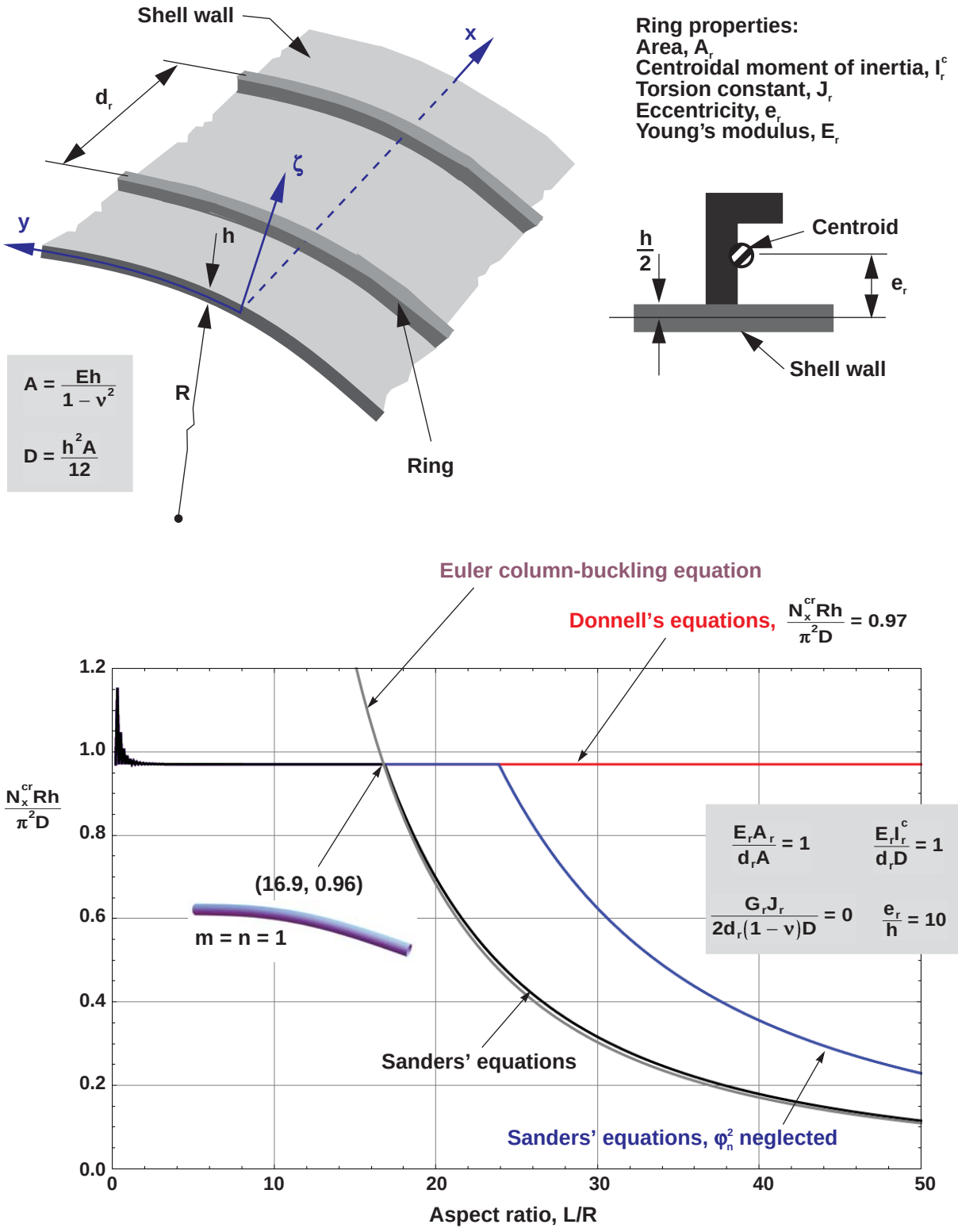

Figure 88. Nondimensional buckling loads for compression-loaded ring-stiffened isotropic cylinders with simply supported edges for R/h = 50 (ν = 0.3).

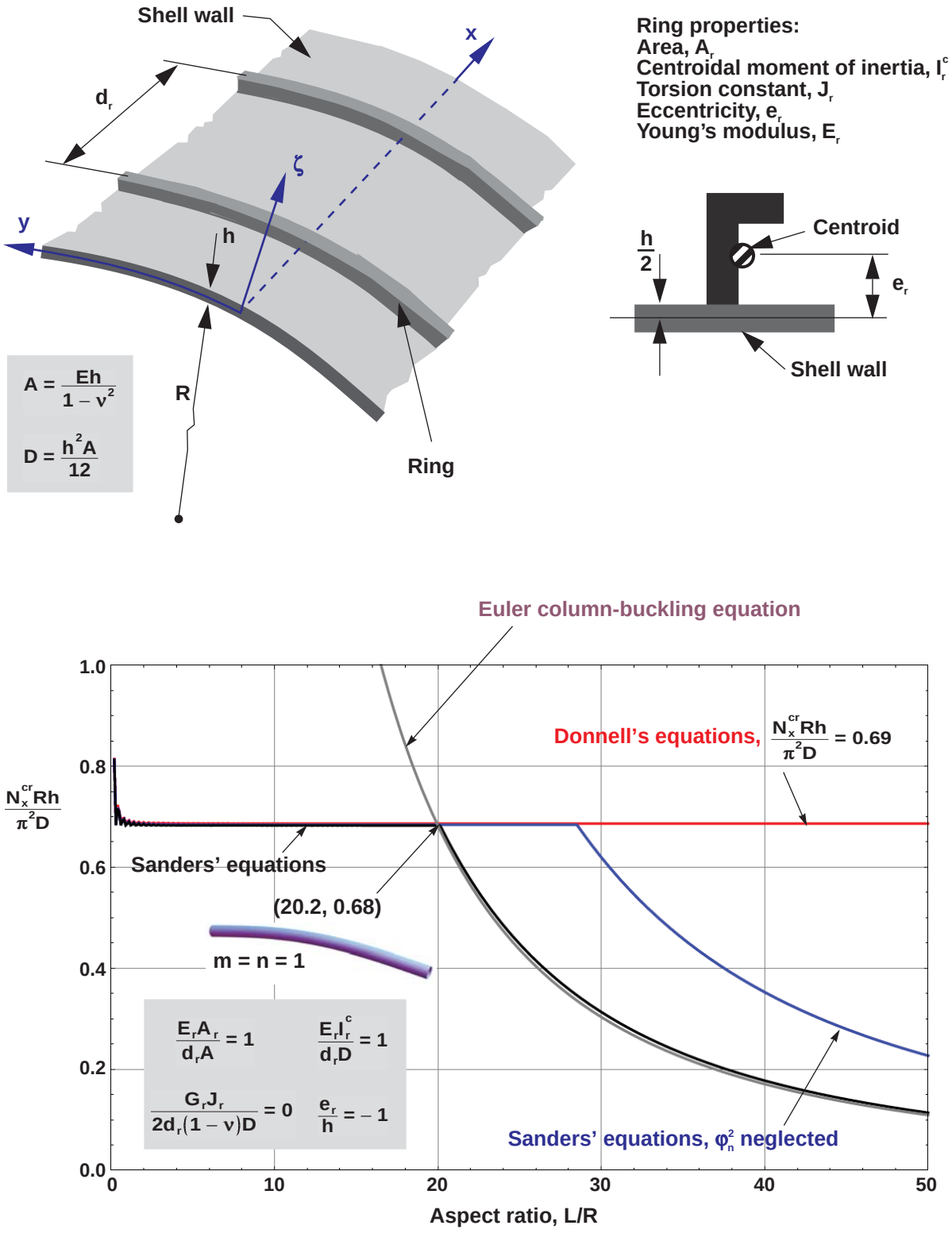

Figure 89. Nondimensional buckling loads for compression-loaded ring-stiffened isotropic cylinders with simply supported edges for R/h = 50 (ν = 0.3).

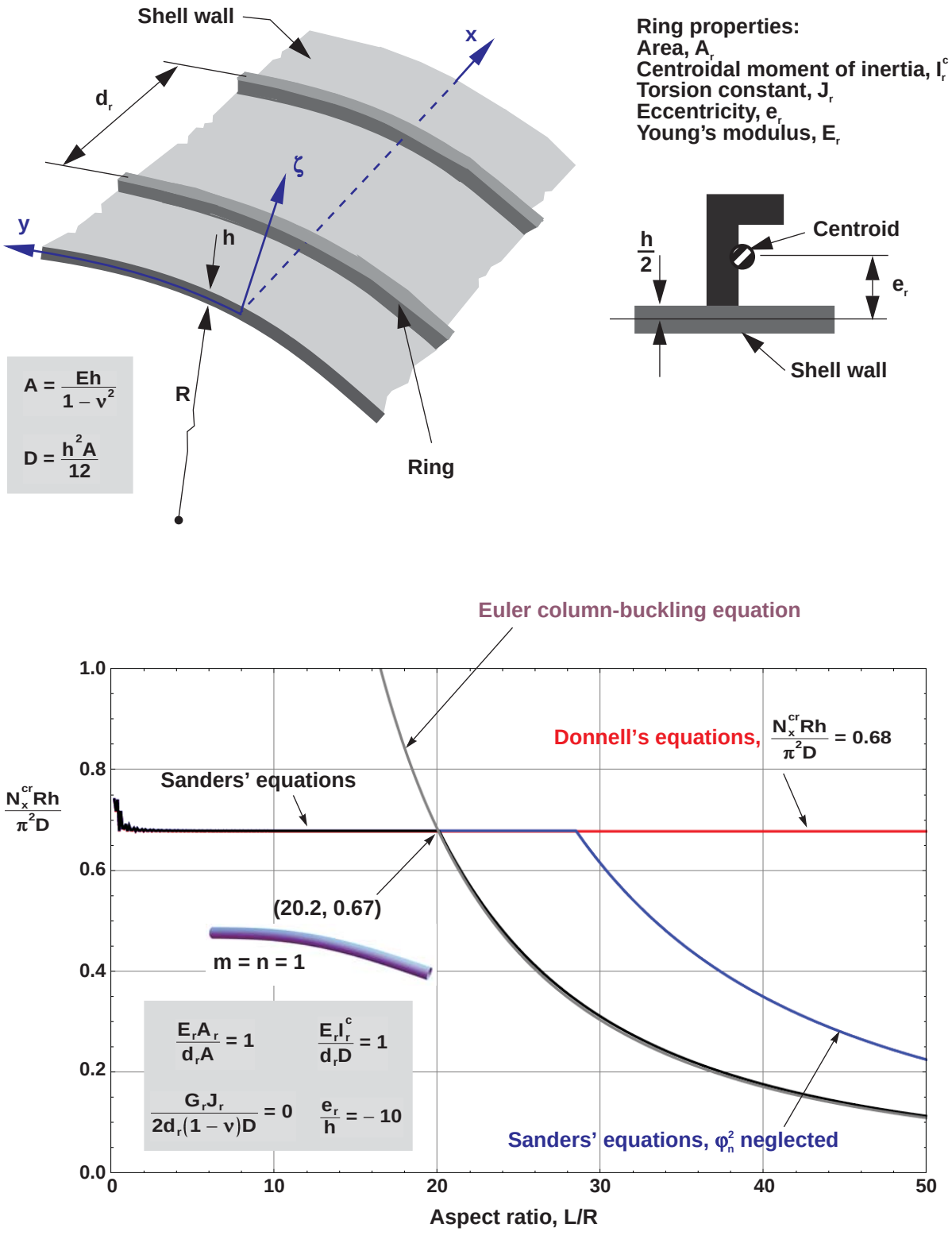

Figure 90. Nondimensional buckling loads for compression-loaded ring-stiffened isotropic cylinders with simply supported edges for R/h = 50 (ν = 0.3).

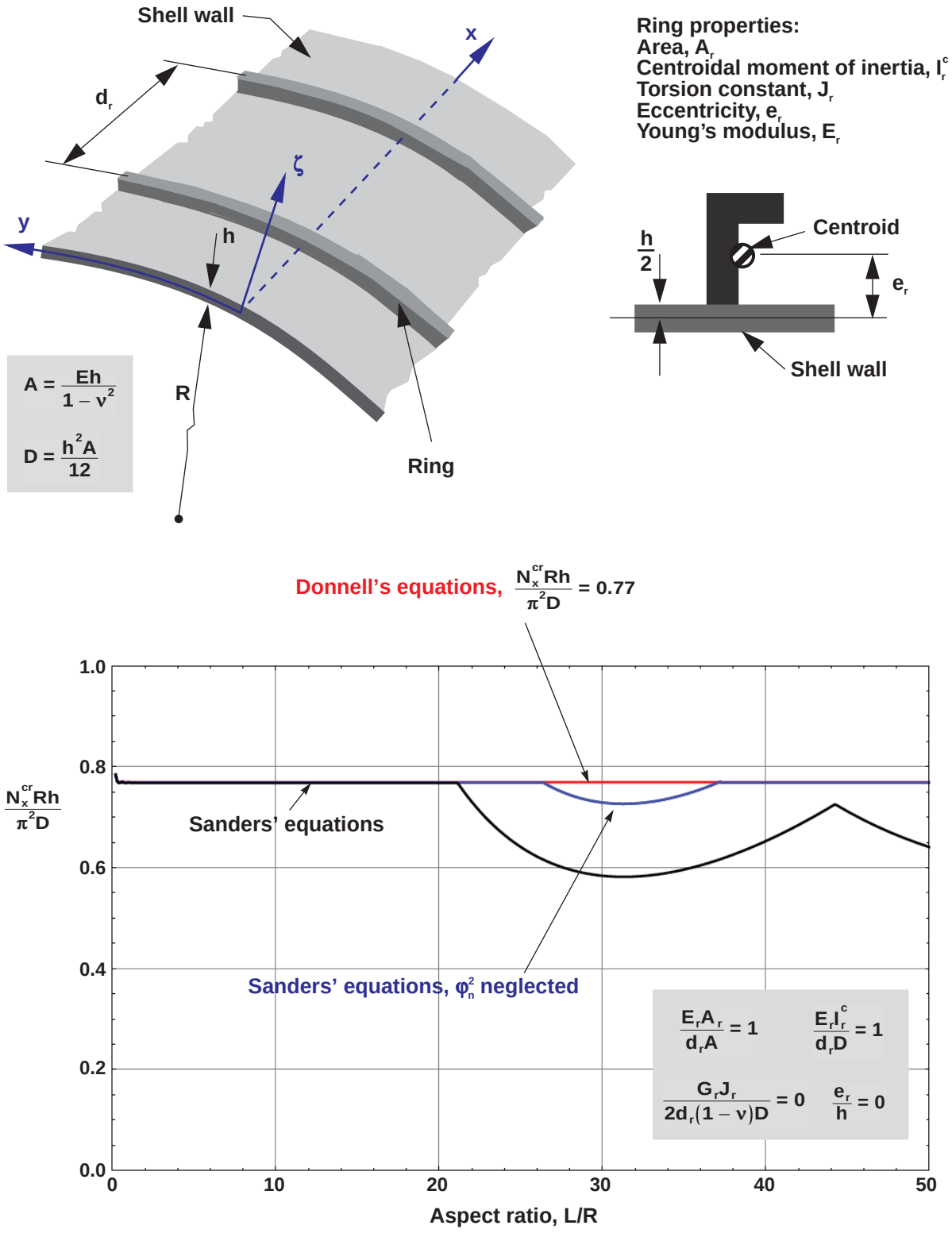

Figure 91. Nondimensional buckling loads for compression-loaded ring-stiffened isotropic cylinders with simply supported edges for R/h = 500 (ν = 0.3).

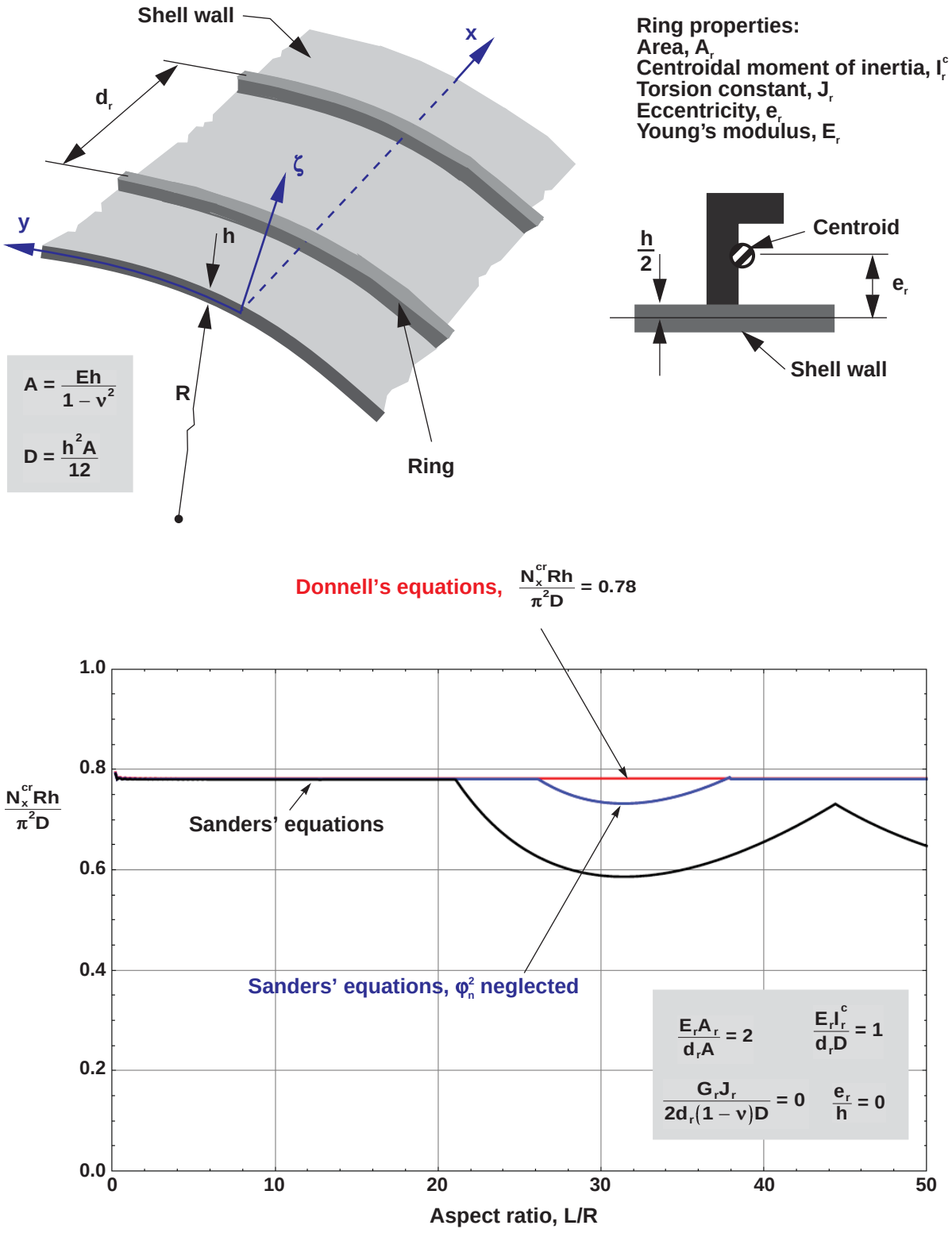

Figure 92. Nondimensional buckling loads for compression-loaded ring-stiffened isotropic cylinders with simply supported edges for R/h = 500 (ν = 0.3).

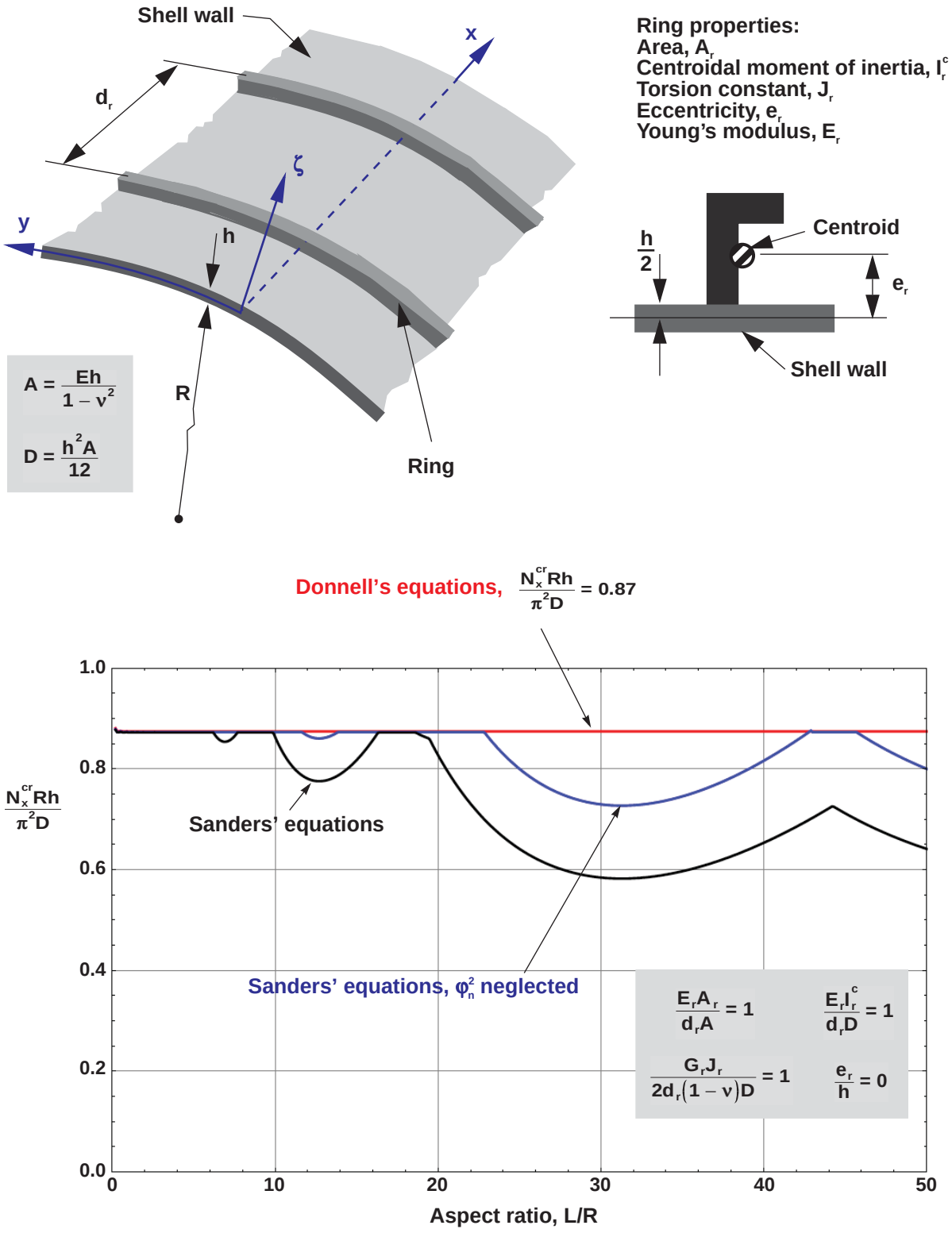

Figure 93. Nondimensional buckling loads for compression-loaded ring-stiffened isotropic cylinders with simply supported edges for R/h = 500 (ν = 0.3).

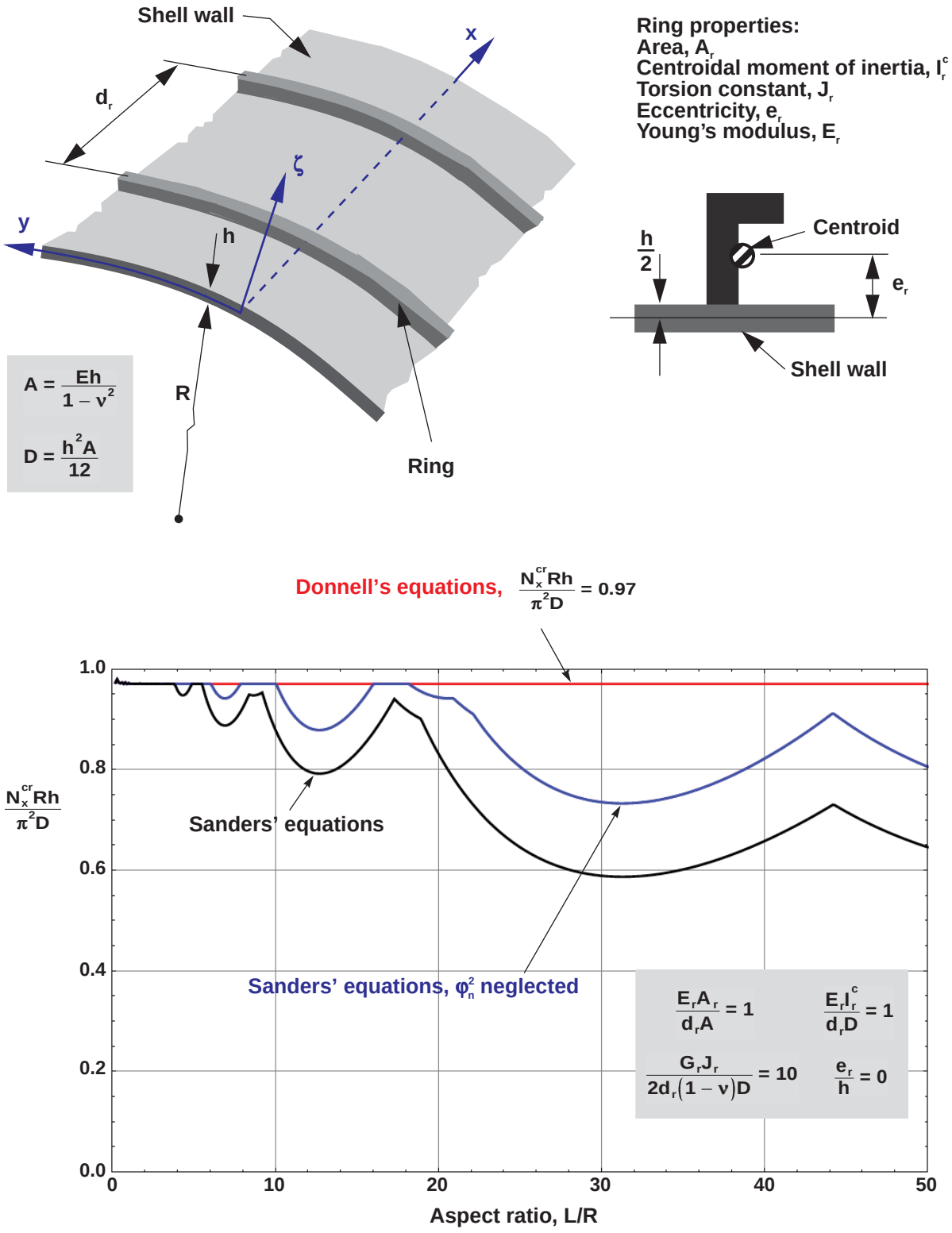

Figure 94. Nondimensional buckling loads for compression-loaded ring-stiffened isotropic cylinders with simply supported edges for R/h = 500 (ν = 0.3).

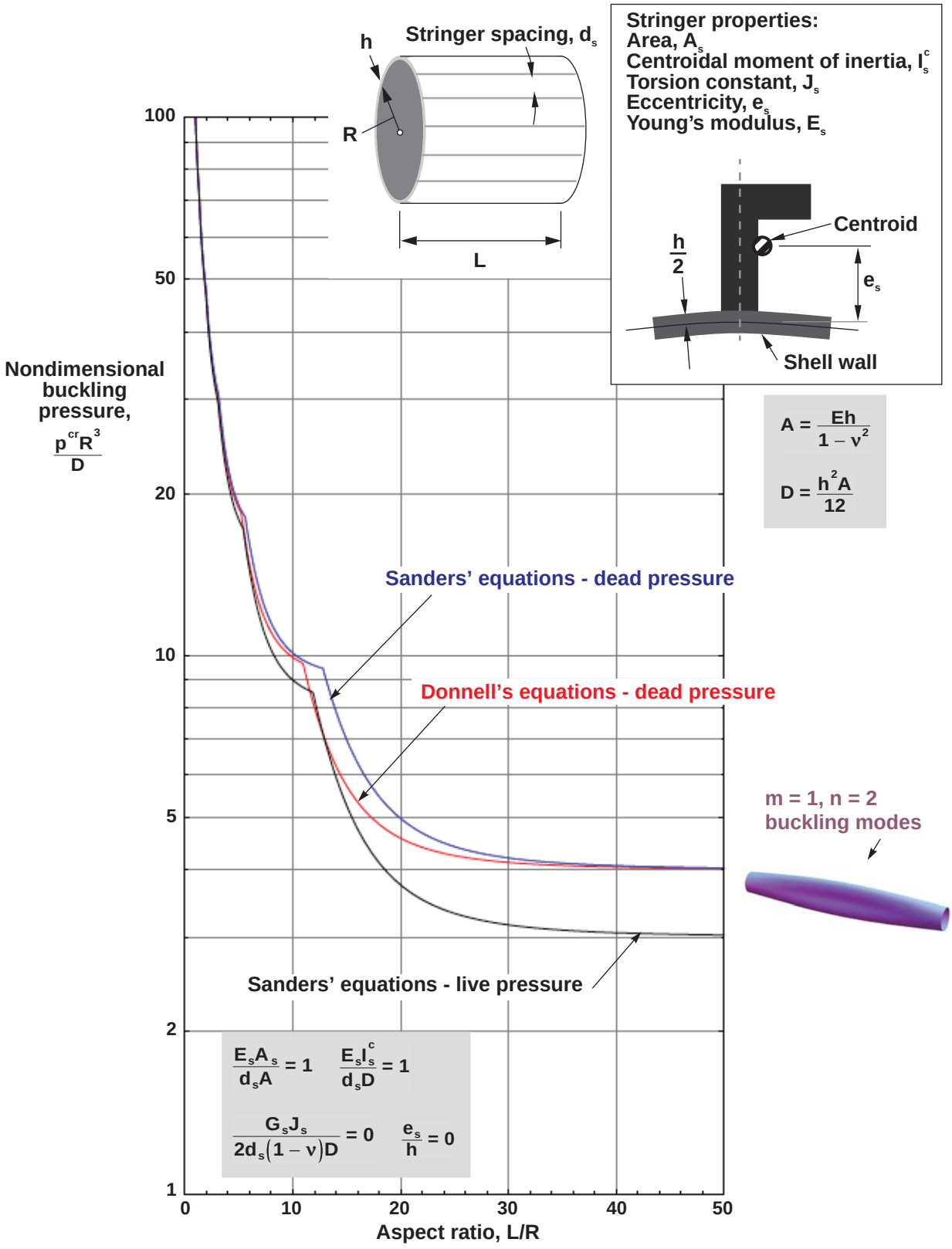

Figure 95. Nondimensional buckling loads for external-pressure-loaded stringer-stiffened isotropic cylinders with simply supported edges for R/h = 50 (ν = 0.3).

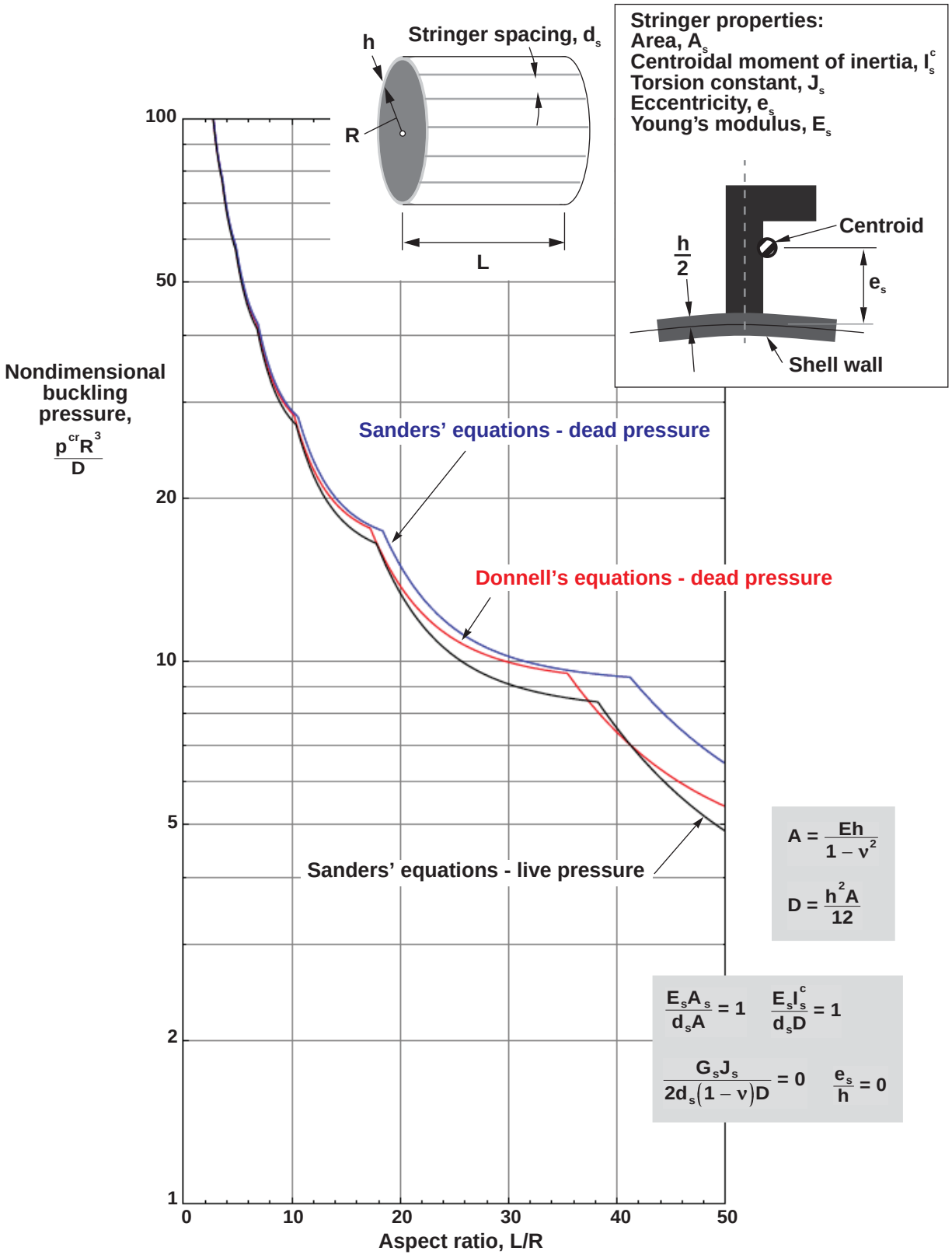

Figure 96. Nondimensional buckling loads for external-pressure-loaded stringer-stiffened isotropic cylinders with simply supported edges for R/h = 500 (ν = 0.3).

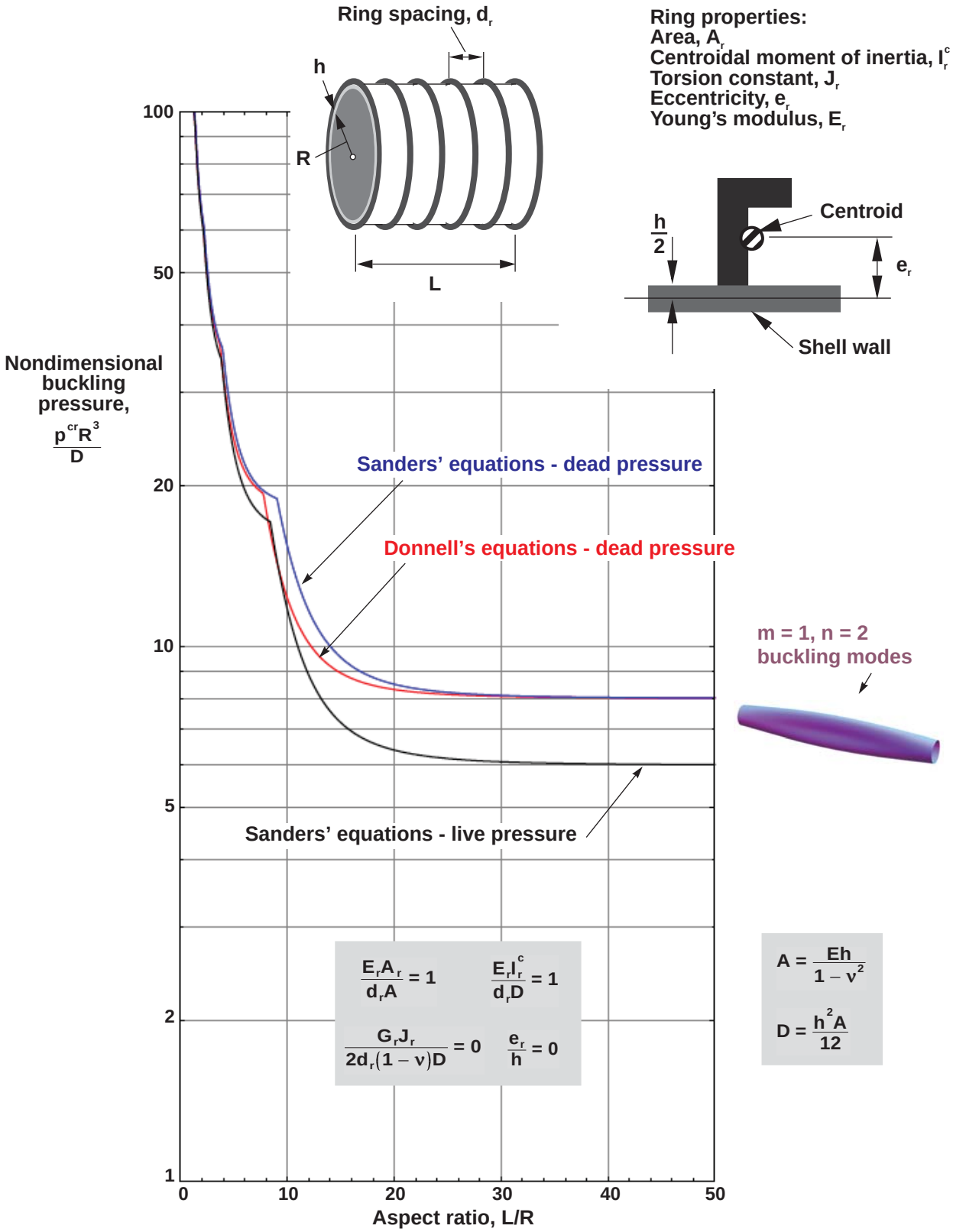

Figure 97. Nondimensional buckling loads for external-pressure-loaded ring-stiffened isotropic cylinders with simply supported edges for R/h = 50 (ν = 0.3).

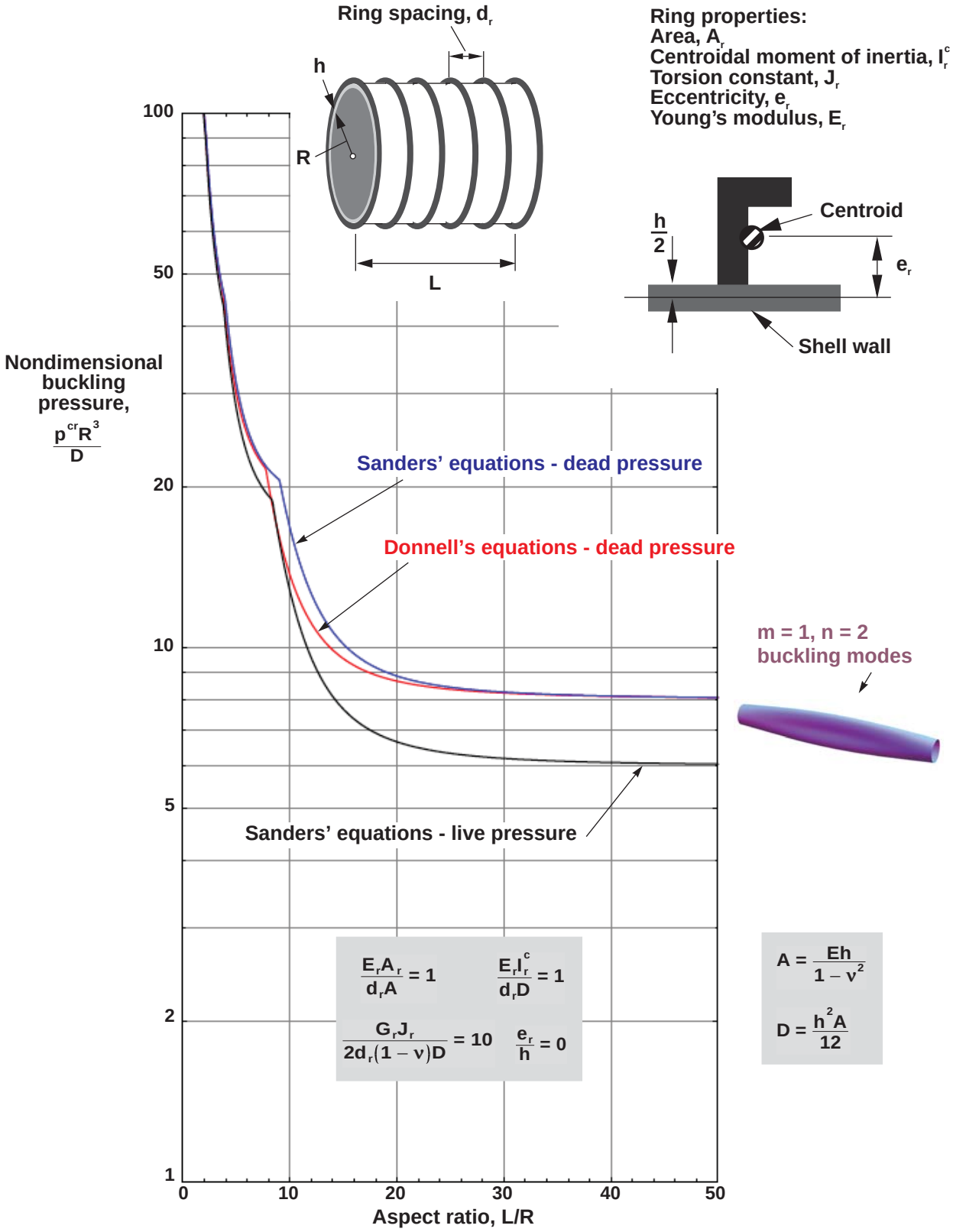

Figure 98. Nondimensional buckling loads for external-pressure-loaded ring-stiffened isotropic cylinders with simply supported edges for R/h = 50 (ν = 0.3).

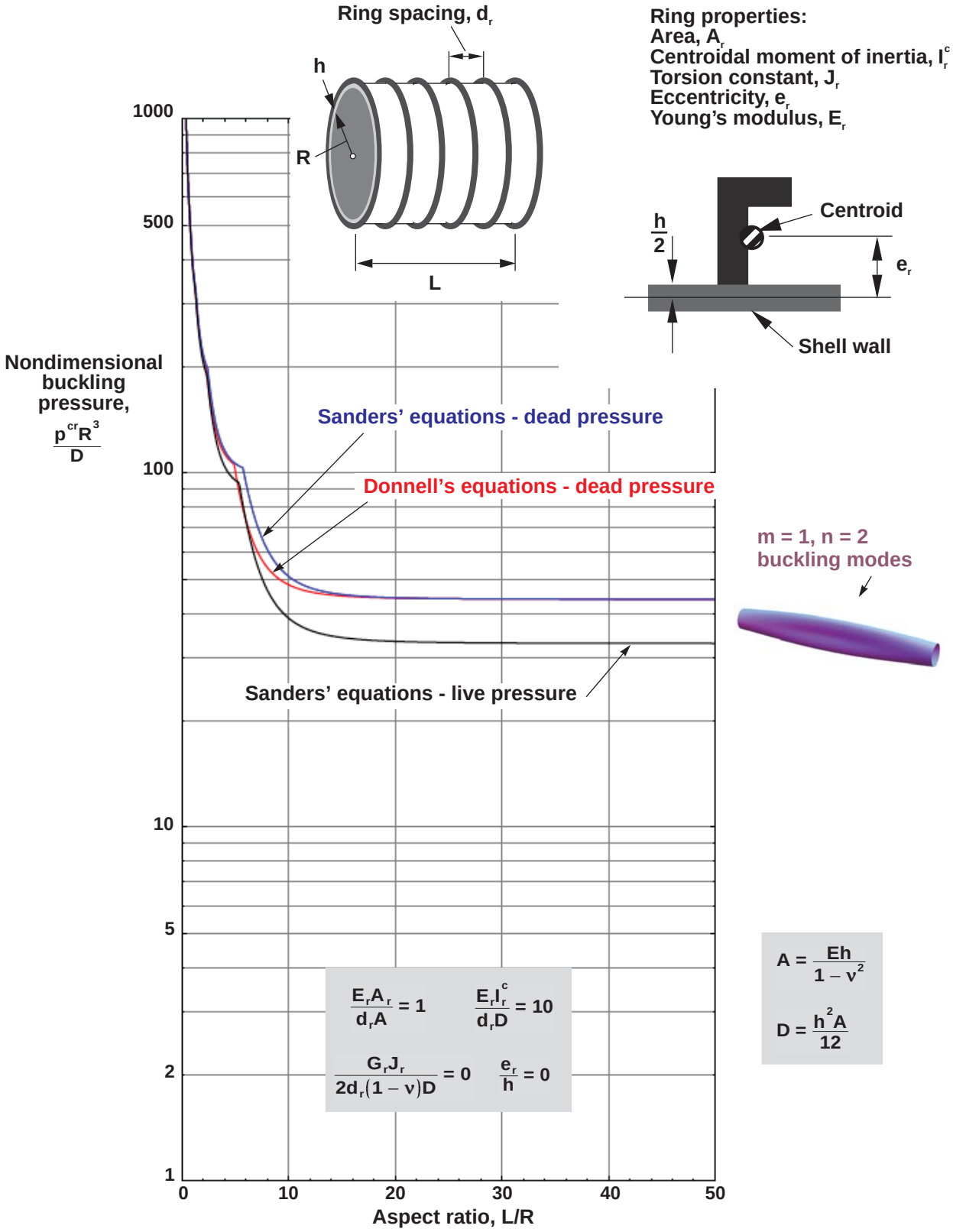

Figure 99. Nondimensional buckling loads for external-pressure-loaded ring-stiffened isotropic cylinders with simply supported edges for R/h = 50 (ν = 0.3).

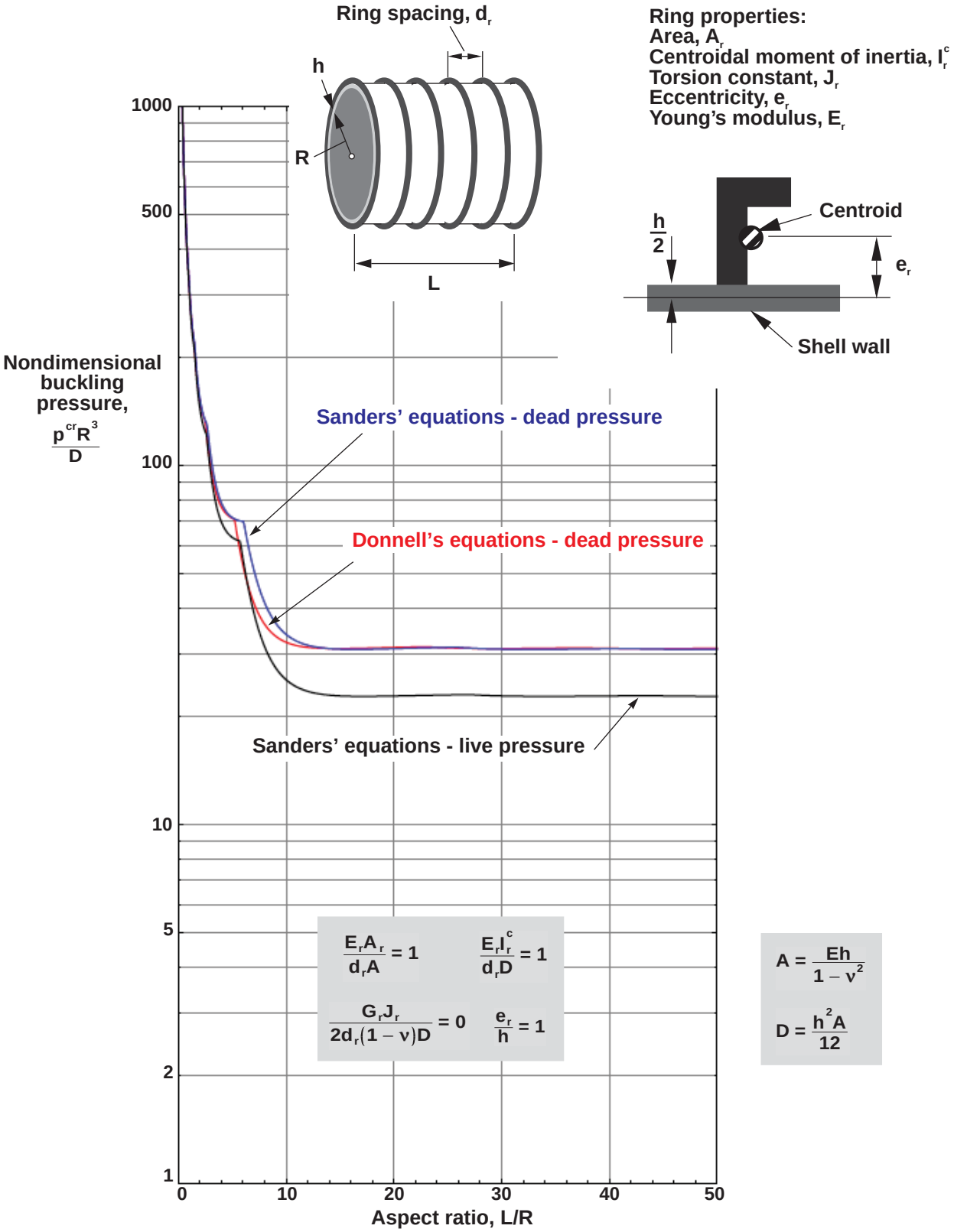

Figure 100. Nondimensional buckling loads for external-pressure-loaded ring-stiffened isotropic cylinders with simply supported edges for R/h = 50 (ν = 0.3).

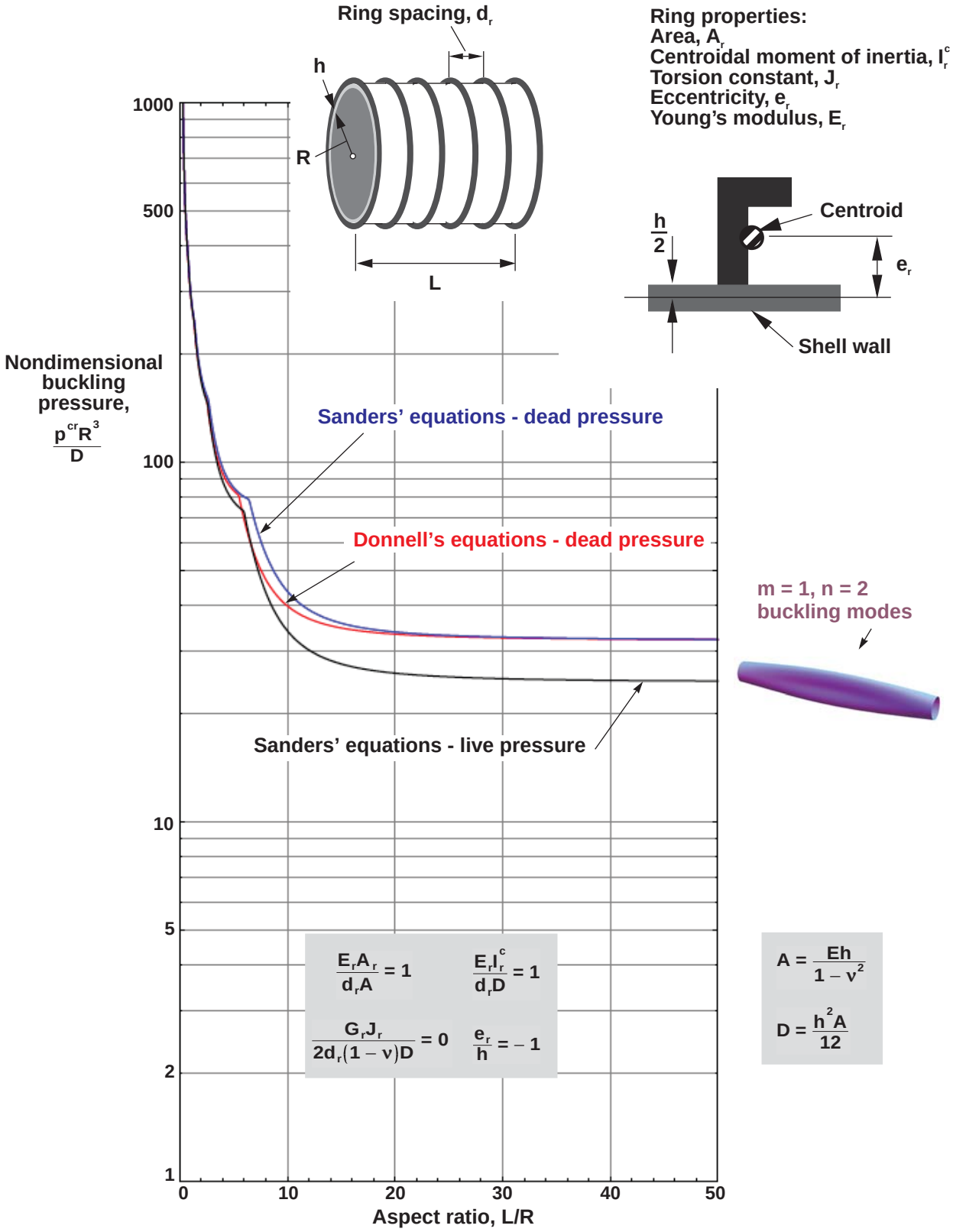

Figure 101. Nondimensional buckling loads for external-pressure-loaded ring-stiffened isotropic cylinders with simply supported edges for R/h = 50 (ν = 0.3).

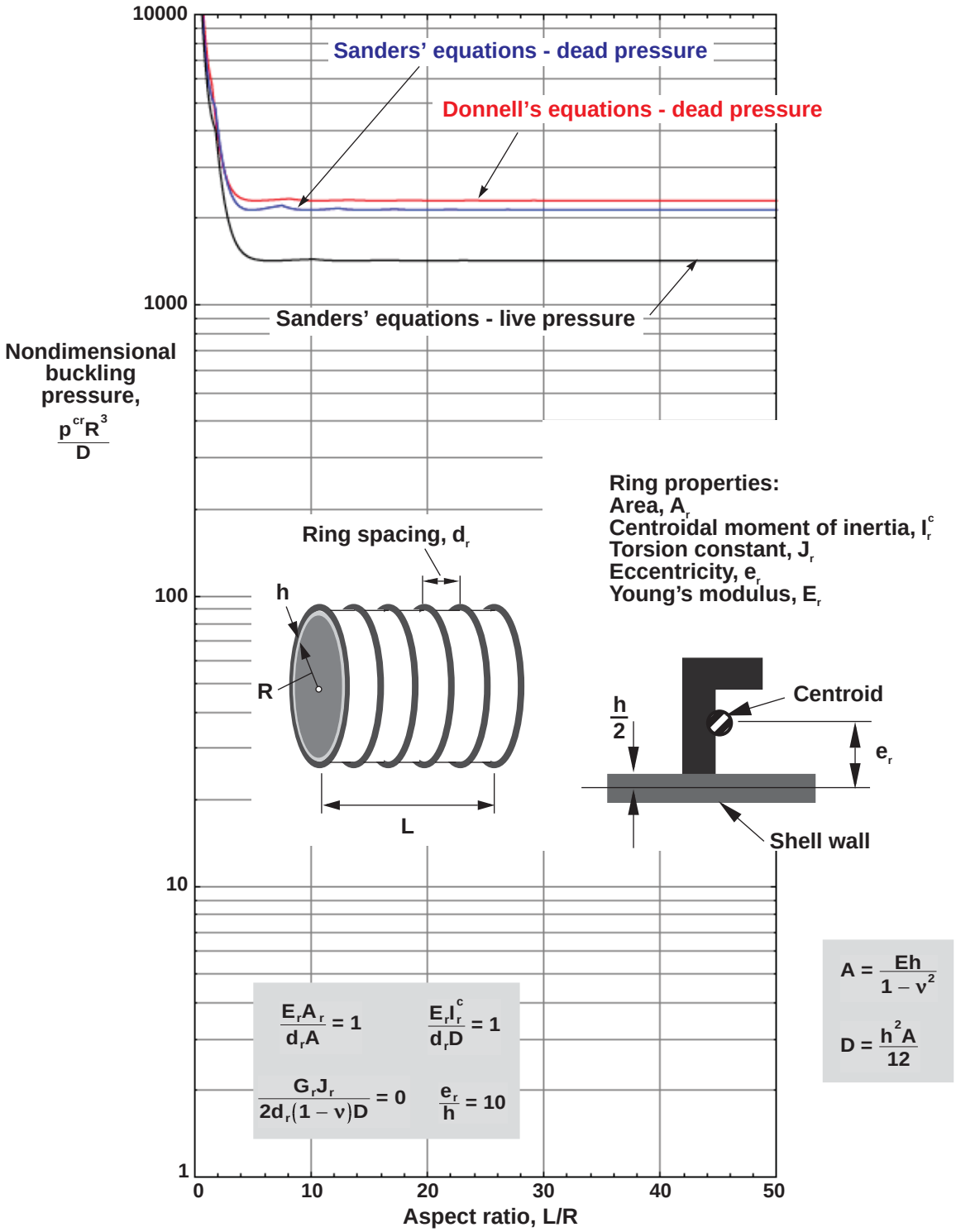

Figure 102. Nondimensional buckling loads for external-pressure-loaded ring-stiffened isotropic cylinders with simply supported edges for R/h = 50 (ν = 0.3).

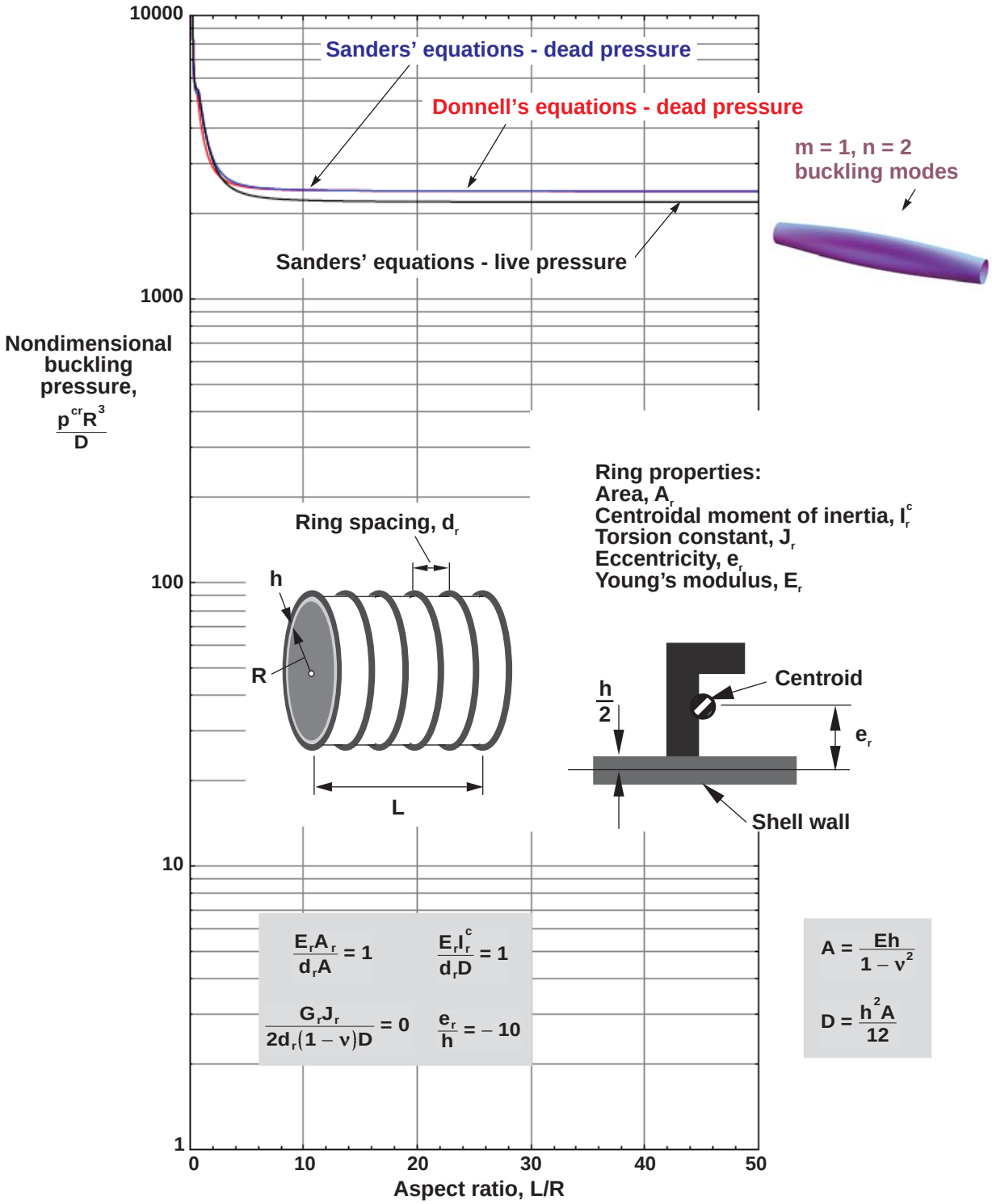

Figure 103. Nondimensional buckling loads for external-pressure-loaded ring-stiffened isotropic cylinders with simply supported edges for R/h = 50 (ν = 0.3).

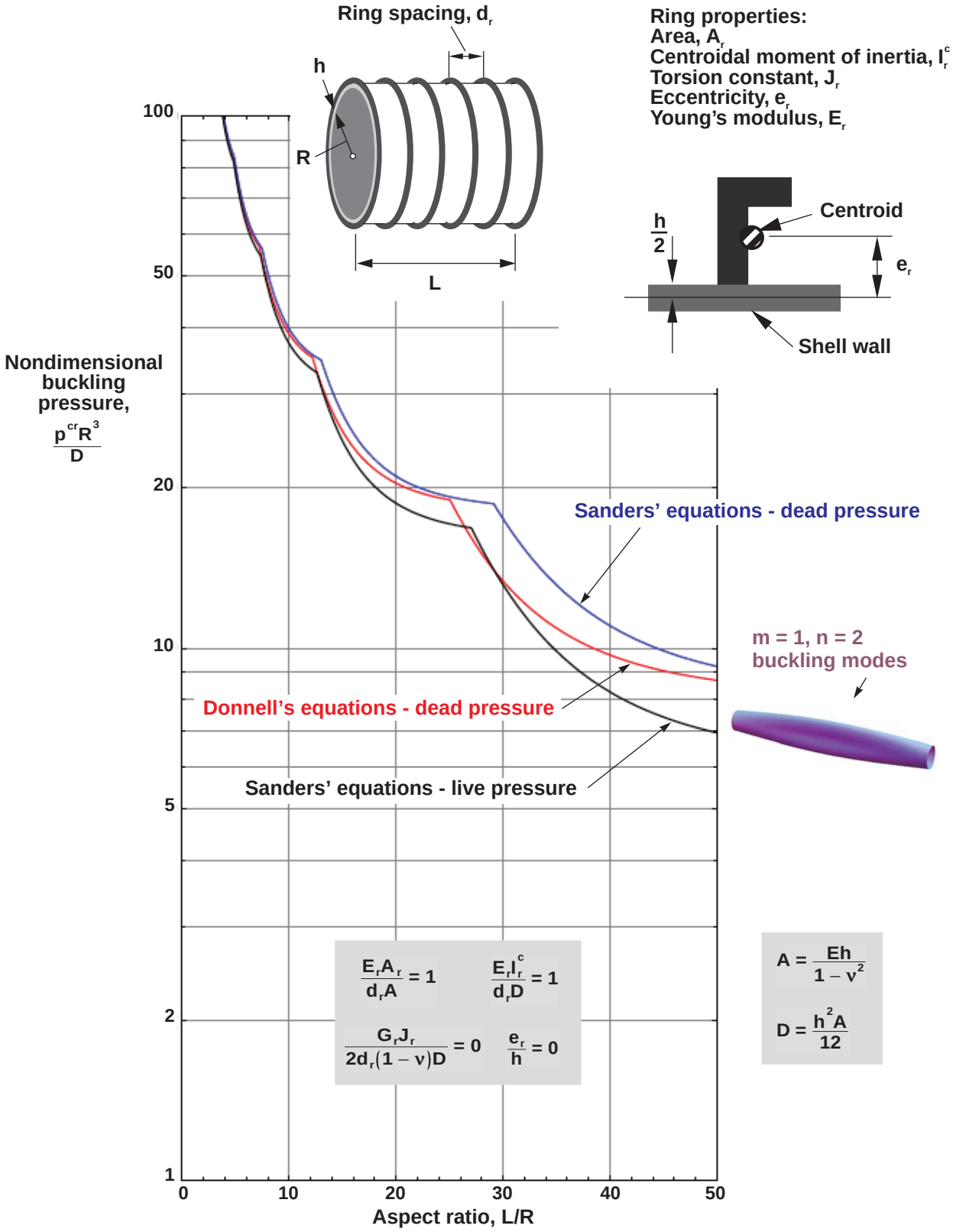

Figure 104. Nondimensional buckling loads for external-pressure-loaded ring-stiffened isotropic cylinders with simply supported edges for R/h = 500 (ν = 0.3).

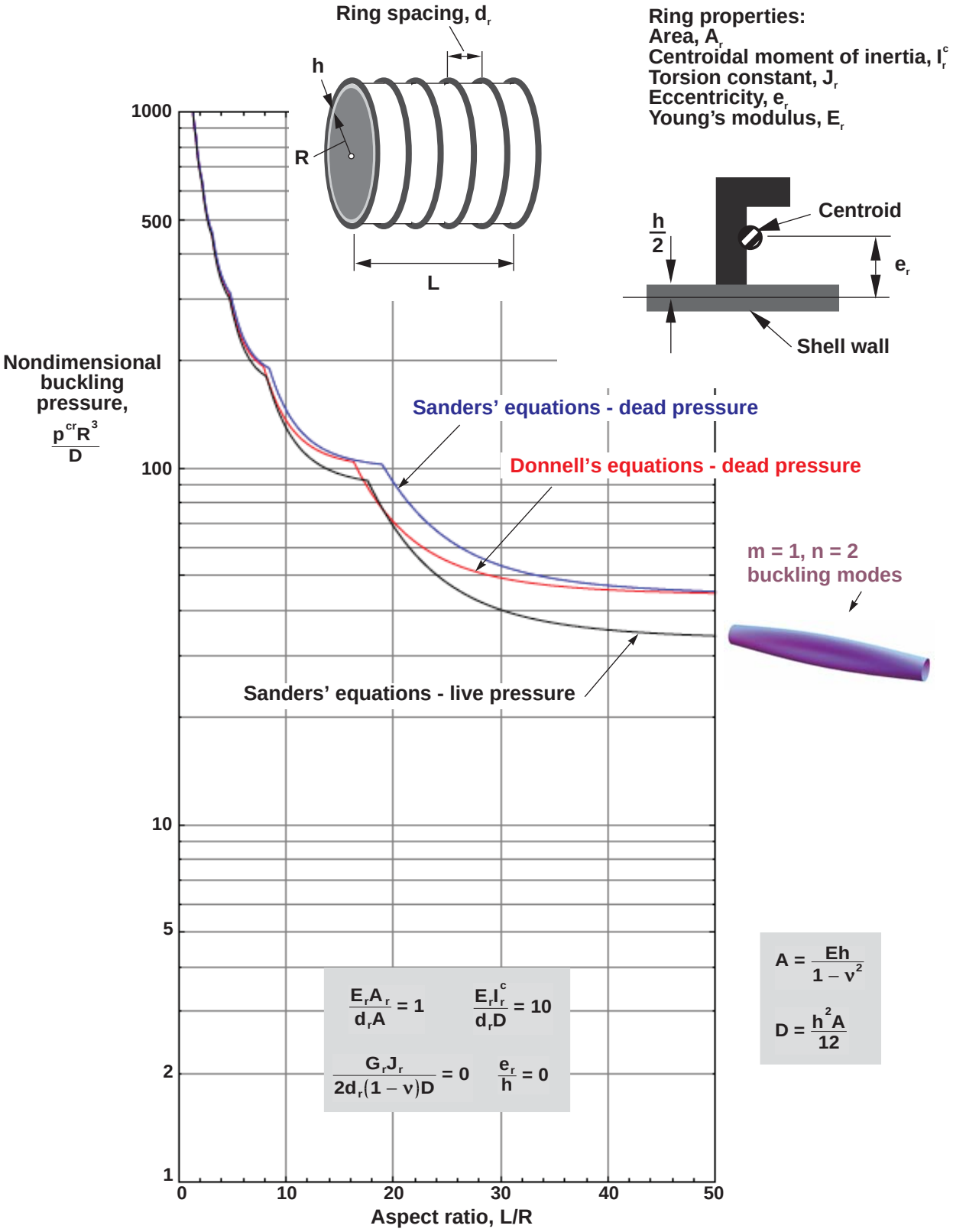

Figure 105. Nondimensional buckling loads for external-pressure-loaded ring-stiffened isotropic cylinders with simply supported edges for R/h = 500 (ν = 0.3).

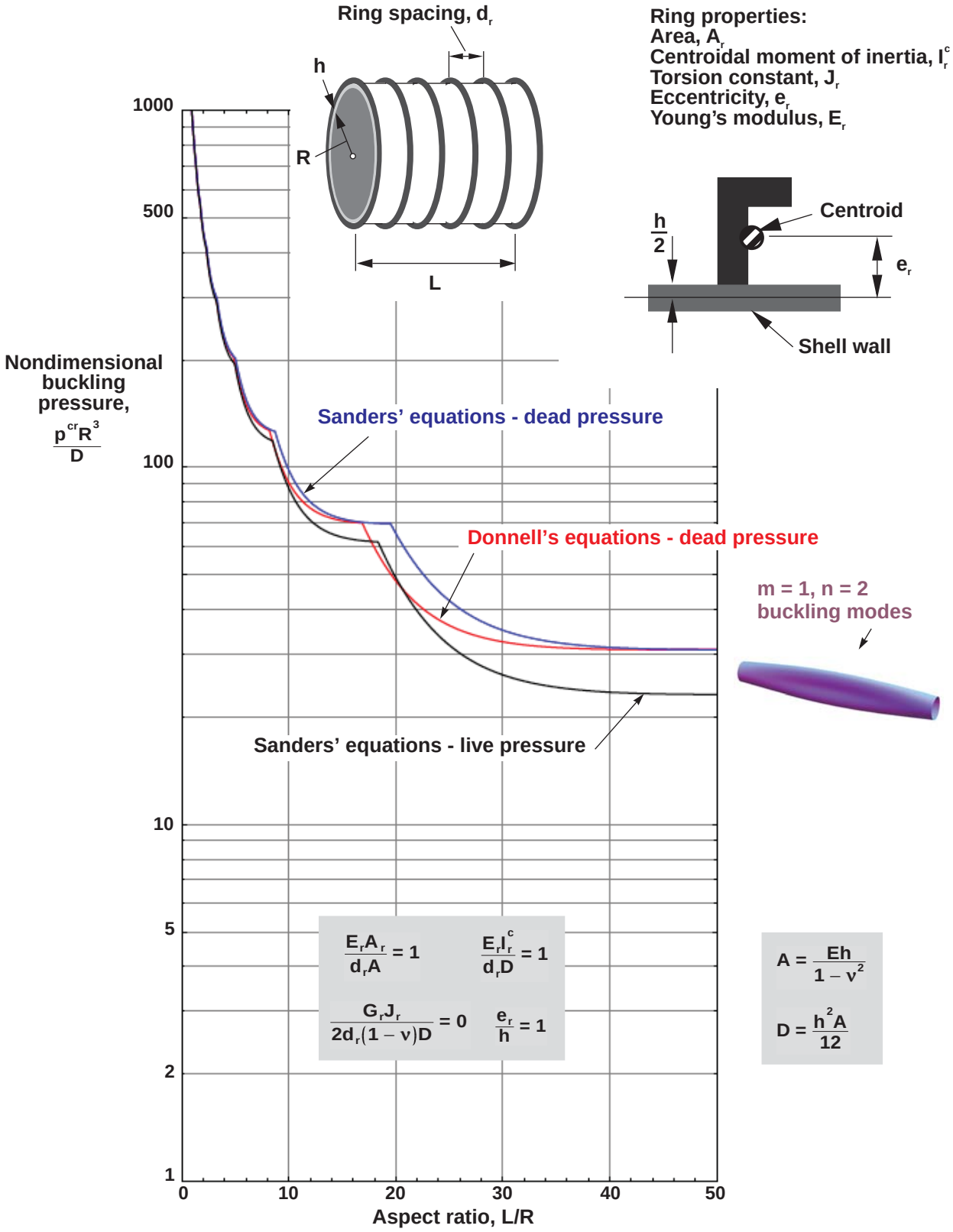

Figure 106. Nondimensional buckling loads for external-pressure-loaded ring-stiffened isotropic cylinders with simply supported edges for R/h = 500 (ν = 0.3).

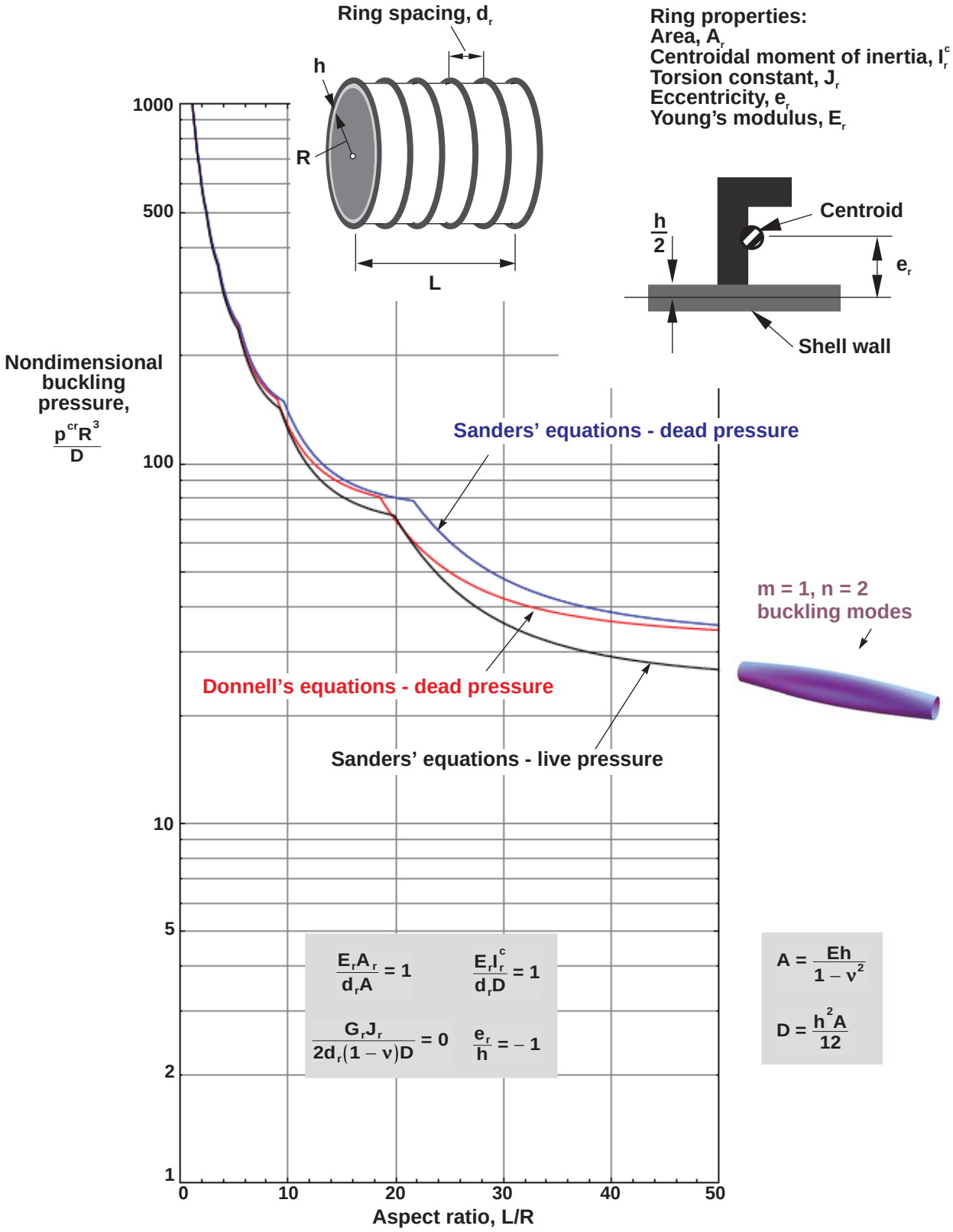

Figure 107. Nondimensional buckling loads for external-pressure-loaded ring-stiffened isotropic cylinders with simply supported edges for R/h = 500 (ν = 0.3).

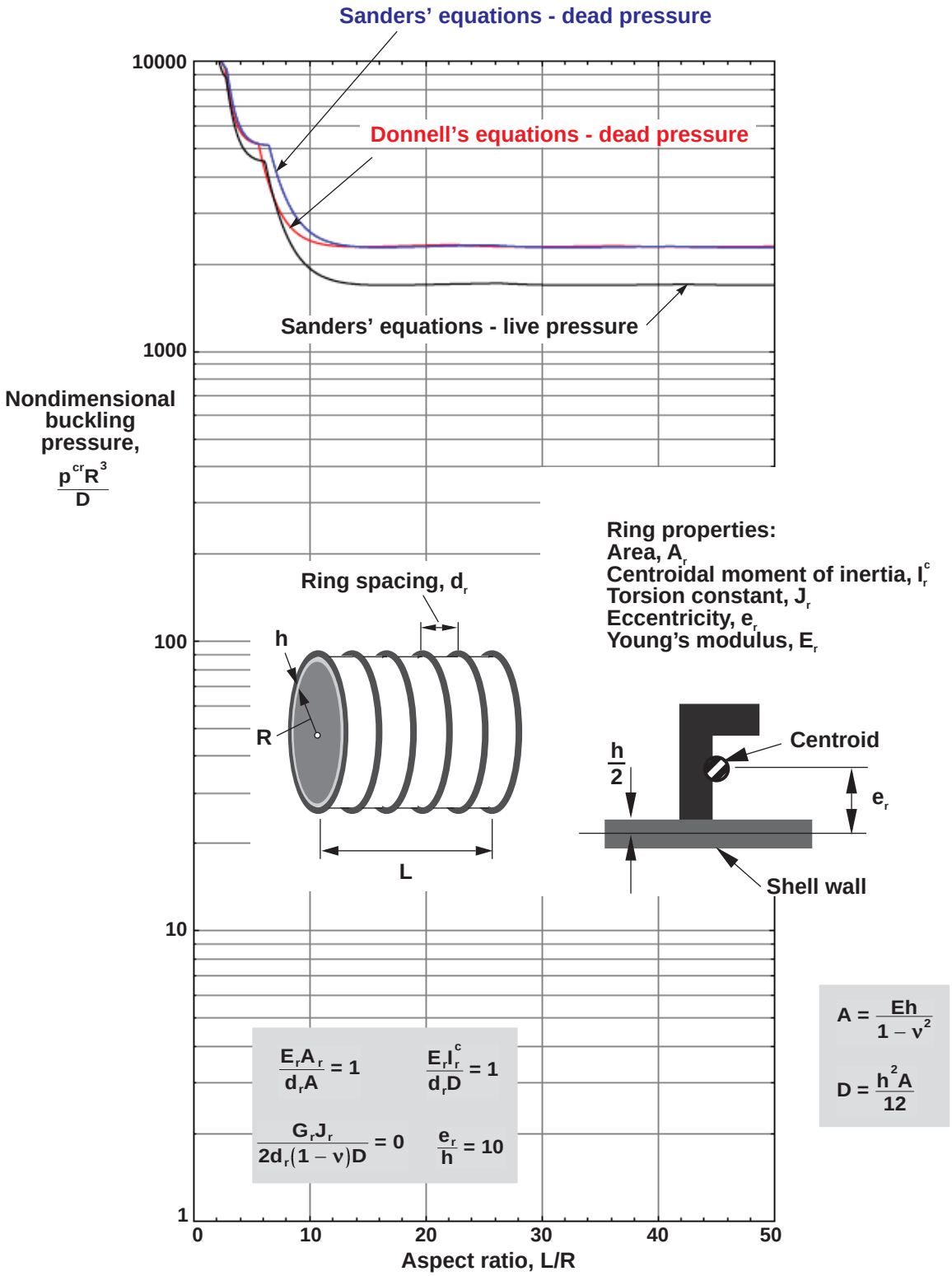

Figure 108. Nondimensional buckling loads for external-pressure-loaded ring-stiffened isotropic cylinders with simply supported edges for R/h = 500 (ν = 0.3).

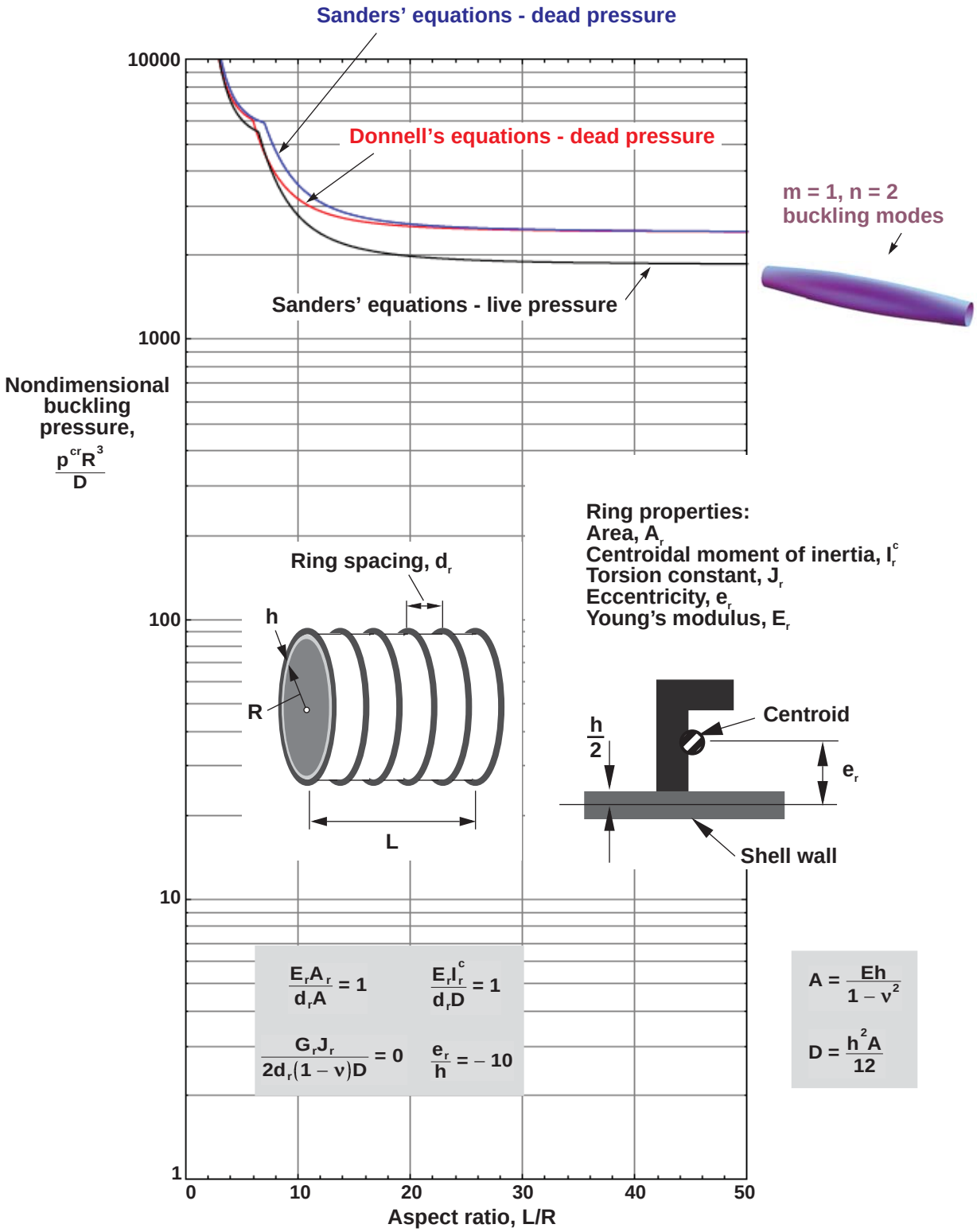

Figure 109. Nondimensional buckling loads for external-pressure-loaded ring-stiffened isotropic cylinders with simply supported edges for R/h = 500 (ν = 0.3).

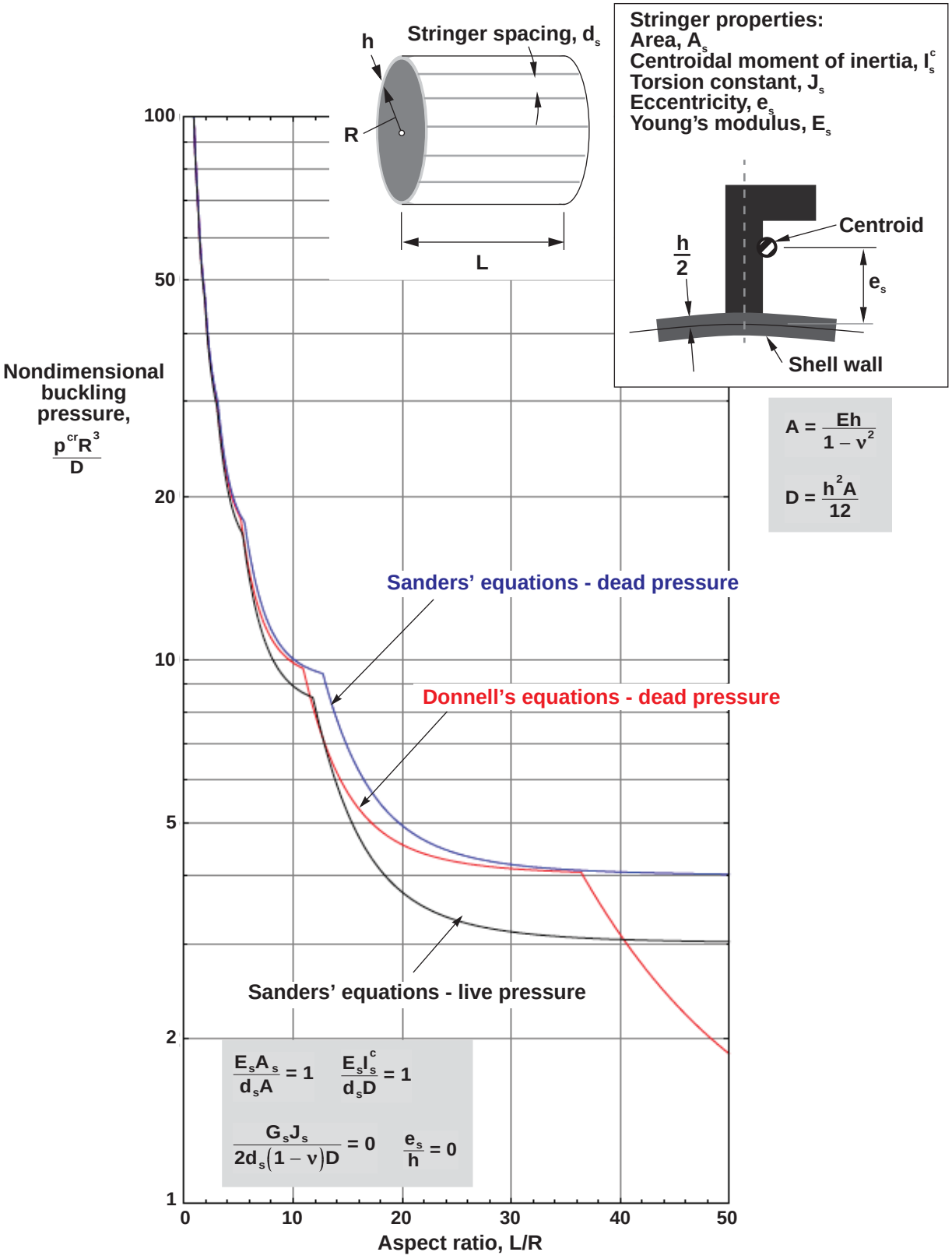

Figure 110. Nondimensional buckling loads for external-hydrostatic-pressure-loaded stringer-stiffened isotropic cylinders with simply supported edges for R/h = 50 (ν = 0.3).

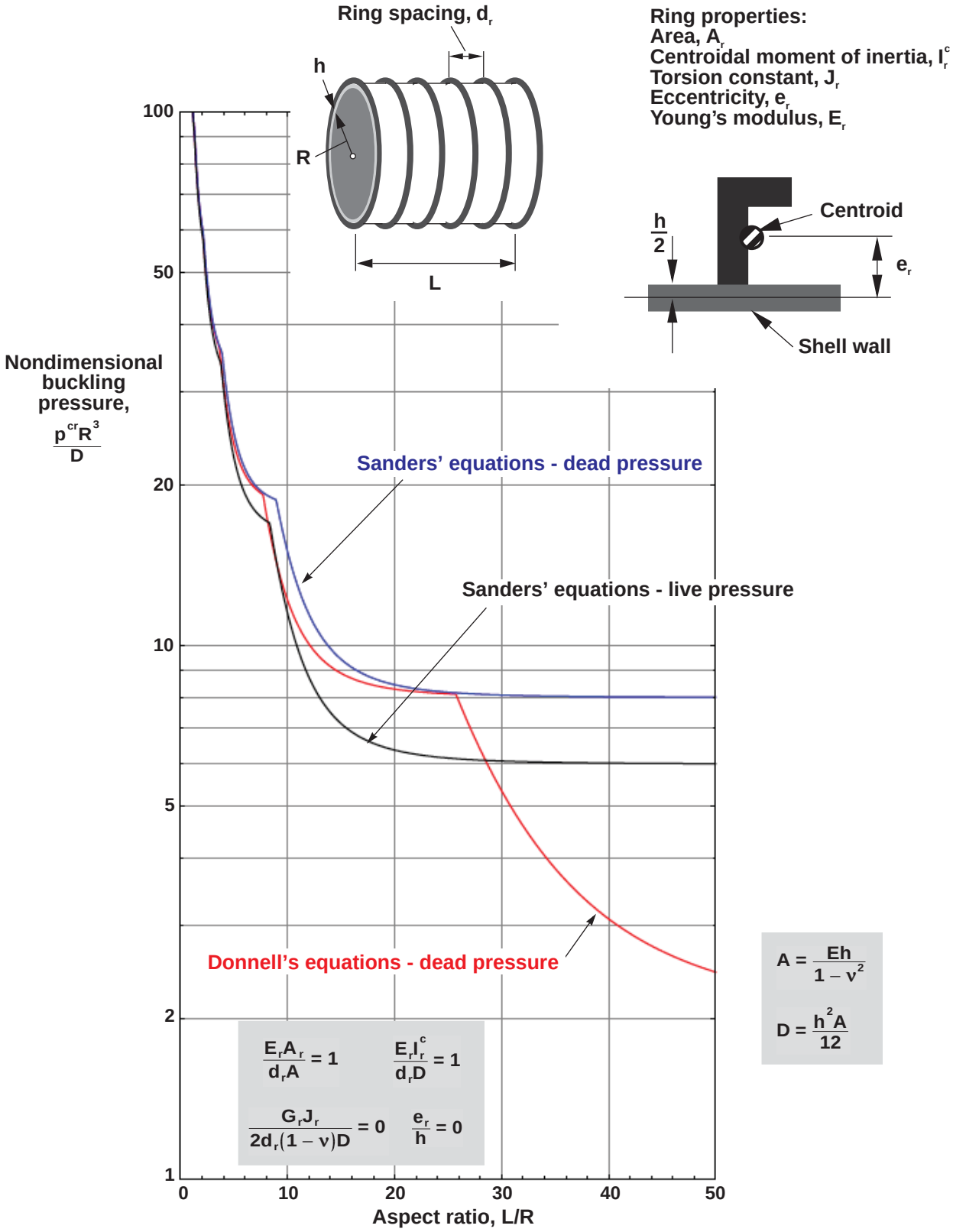

Figure 111. Nondimensional buckling loads for external-hydrostatic-pressure-loaded ring-stiffened isotropic cylinders with simply supported edges for R/h = 50 (ν = 0.3).

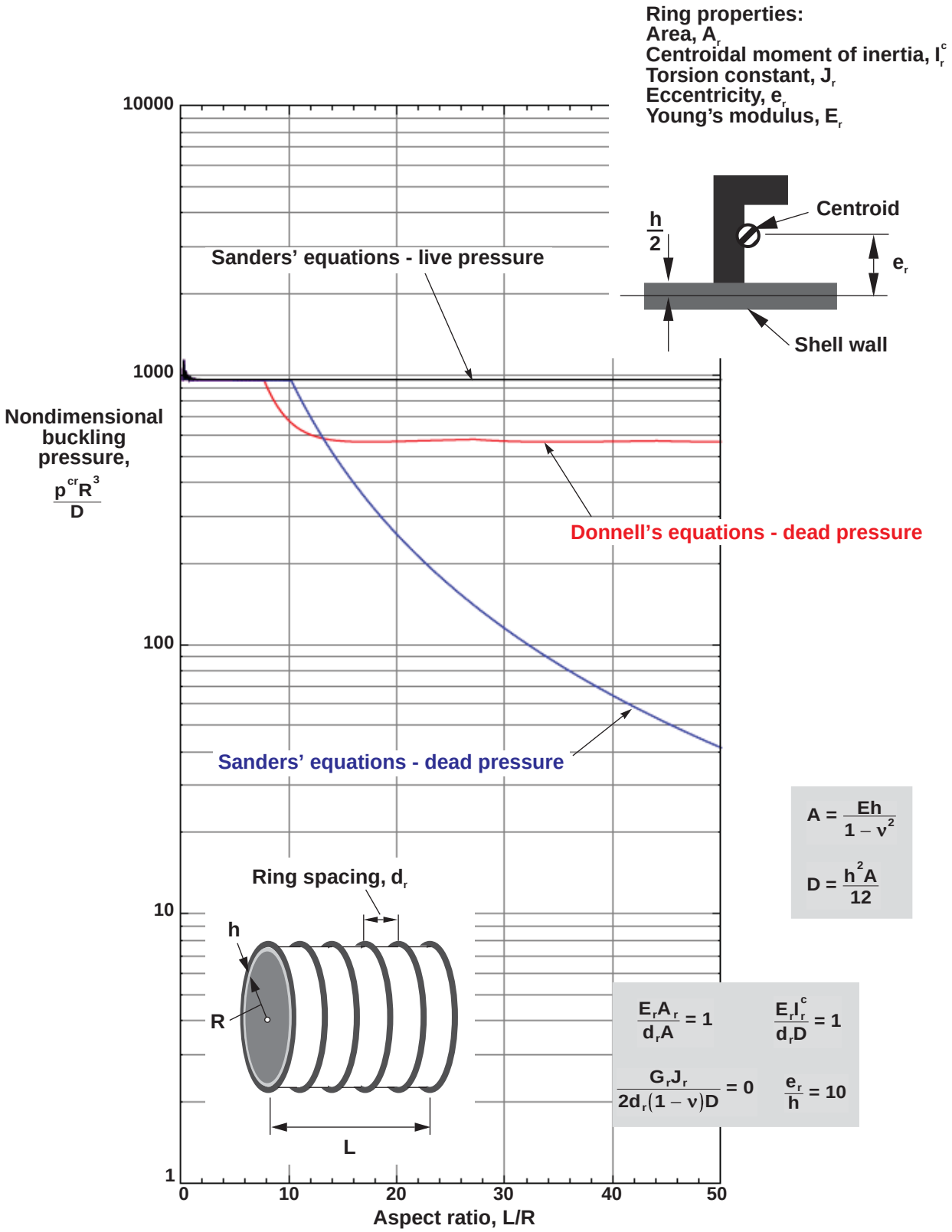

Figure 112. Nondimensional buckling loads for external-hydrostatic-pressure-loaded ring-stiffened isotropic cylinders with simply supported edges for R/h = 50 (ν = 0.3).

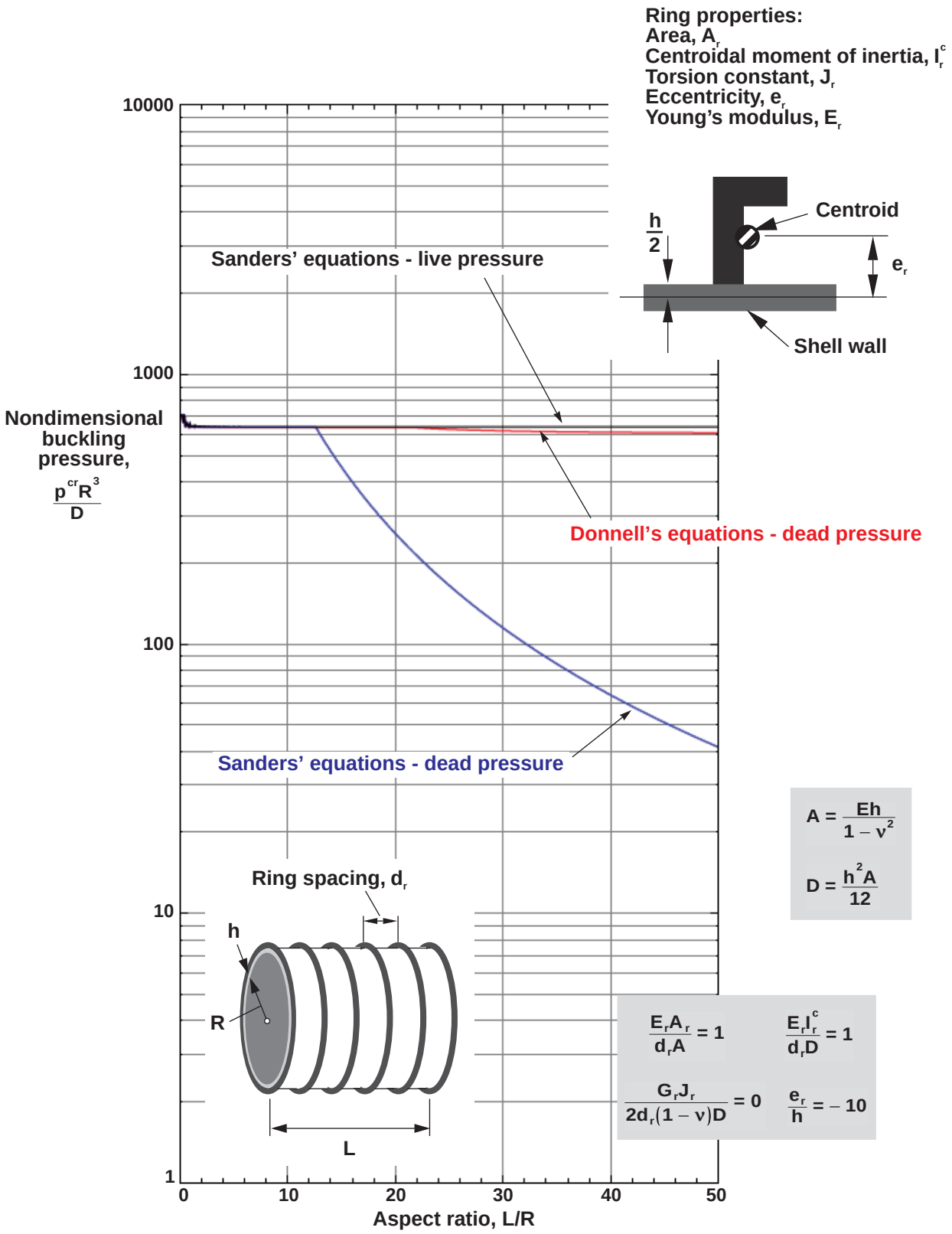

Figure 113. Nondimensional buckling loads for external-hydrostatic-pressure-loaded ring-stiffened isotropic cylinders with simply supported edges for R/h = 50 (ν = 0.3).

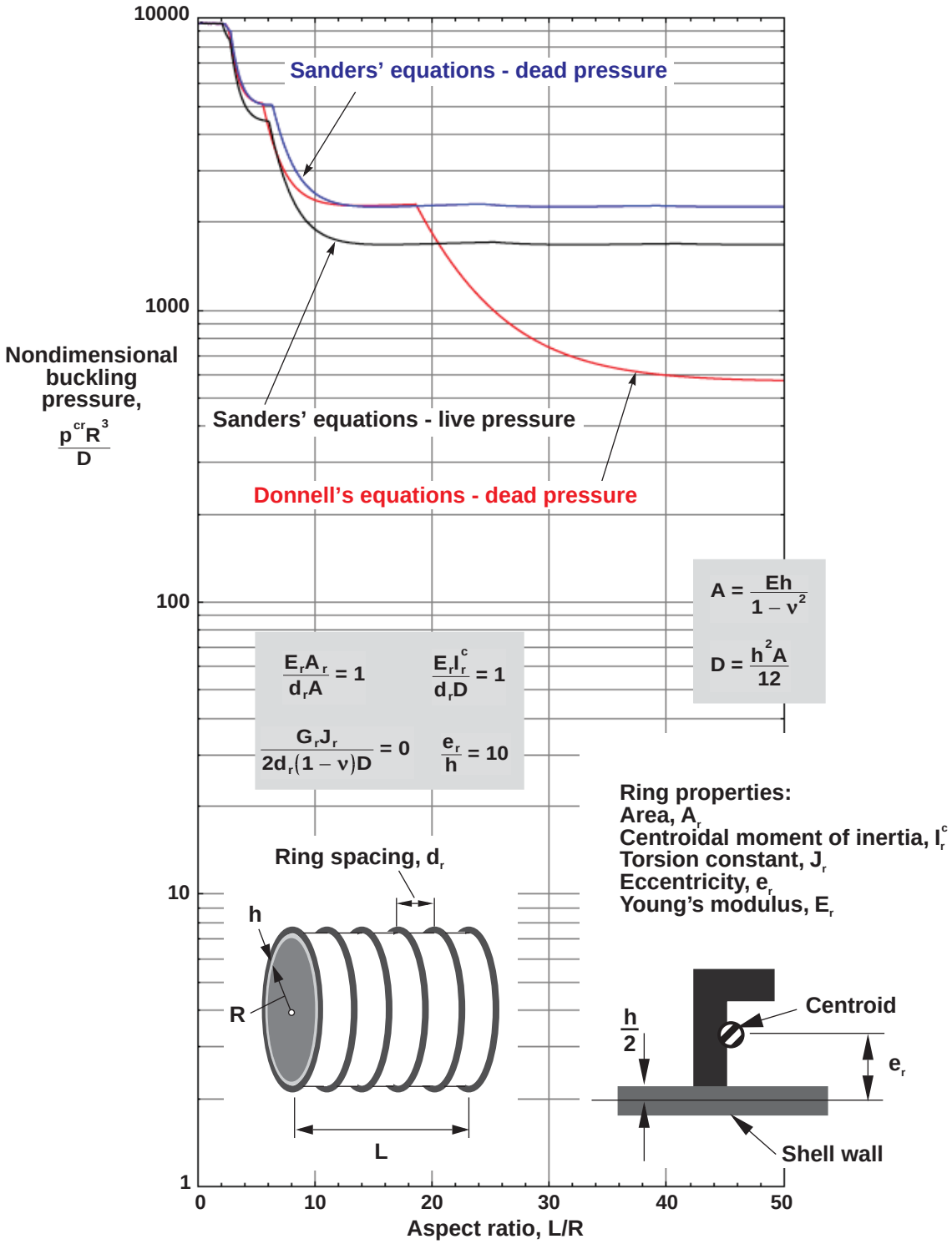

Figure 114. Nondimensional buckling loads for external-hydrostatic-pressure-loaded ring-stiffened isotropic cylinders with simply supported edges for R/h = 500 (ν = 0.3).

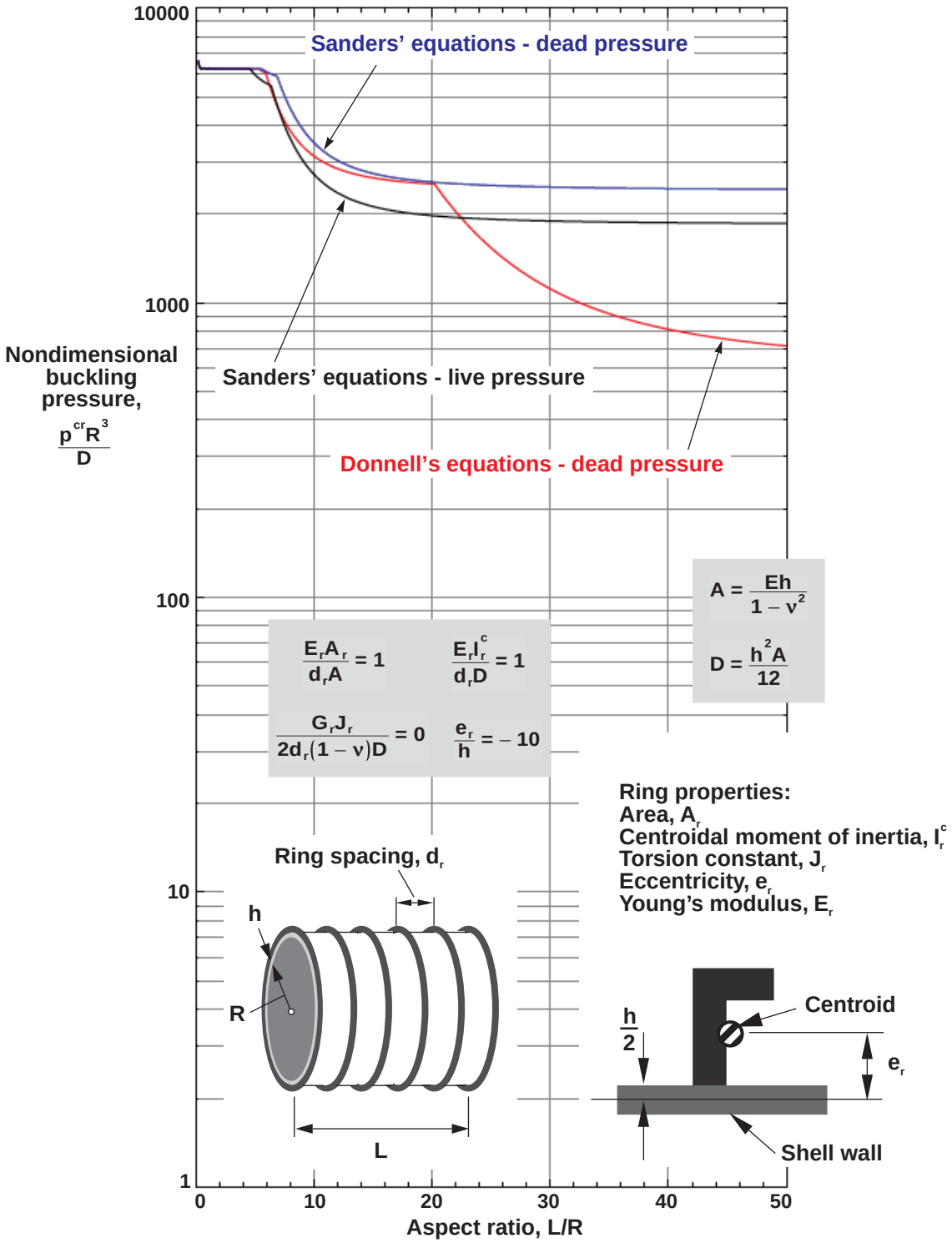

Figure 115. Nondimensional buckling loads for external-hydrostatic-pressure-loaded ring-stiffened isotropic cylinders with simply supported edges for R/h = 500 (ν = 0.3).

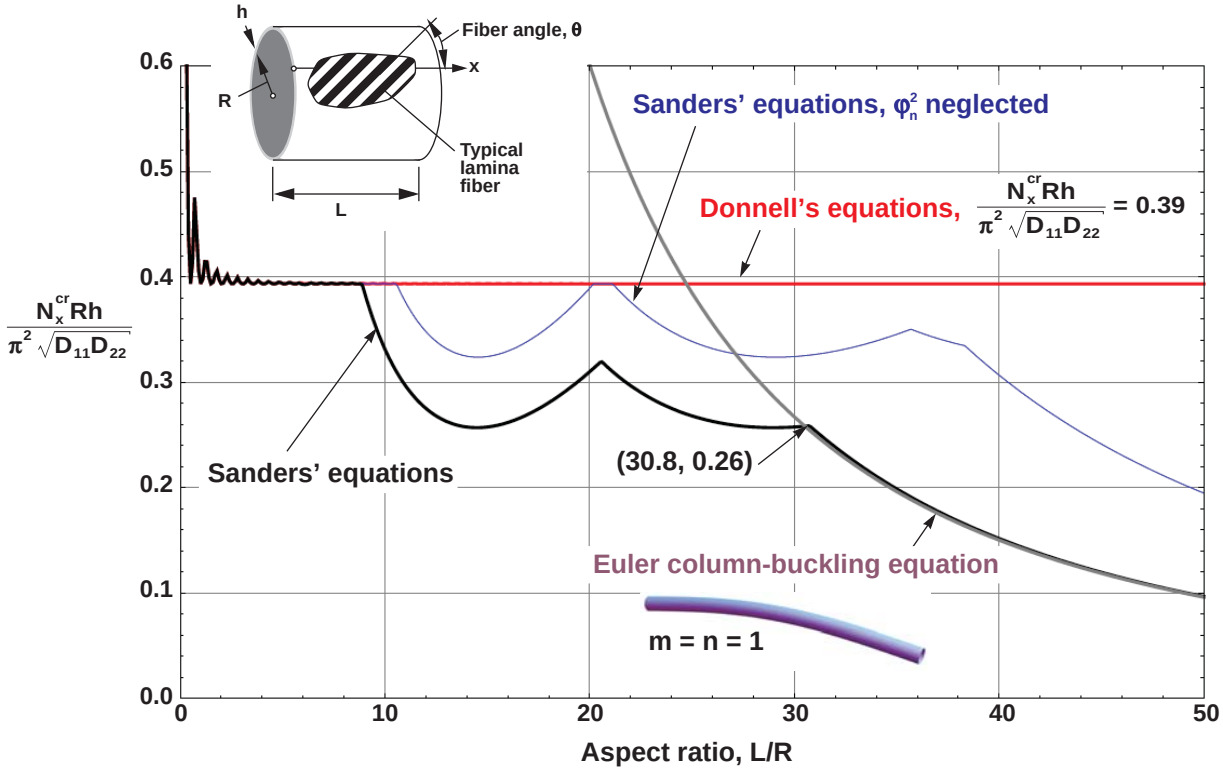

Figure 116. Nondimensional buckling loads for compression-loaded $[(\pm 30)_6]_s$ cylinders with simply supported edges for R/h = 50 and L/R ≤ 50.

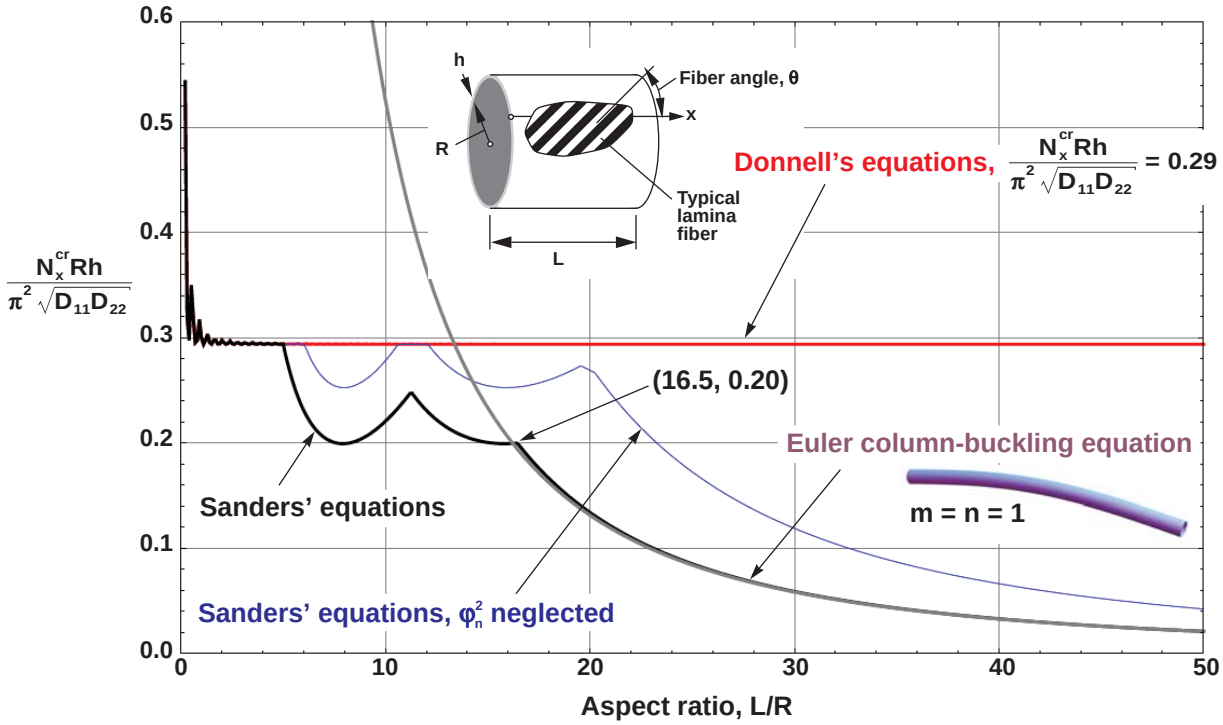

Figure 117. Nondimensional buckling loads for compression-loaded $[(\pm 45)_6]_s$ cylinders with simply supported edges for R/h = 50 and L/R ≤ 50.

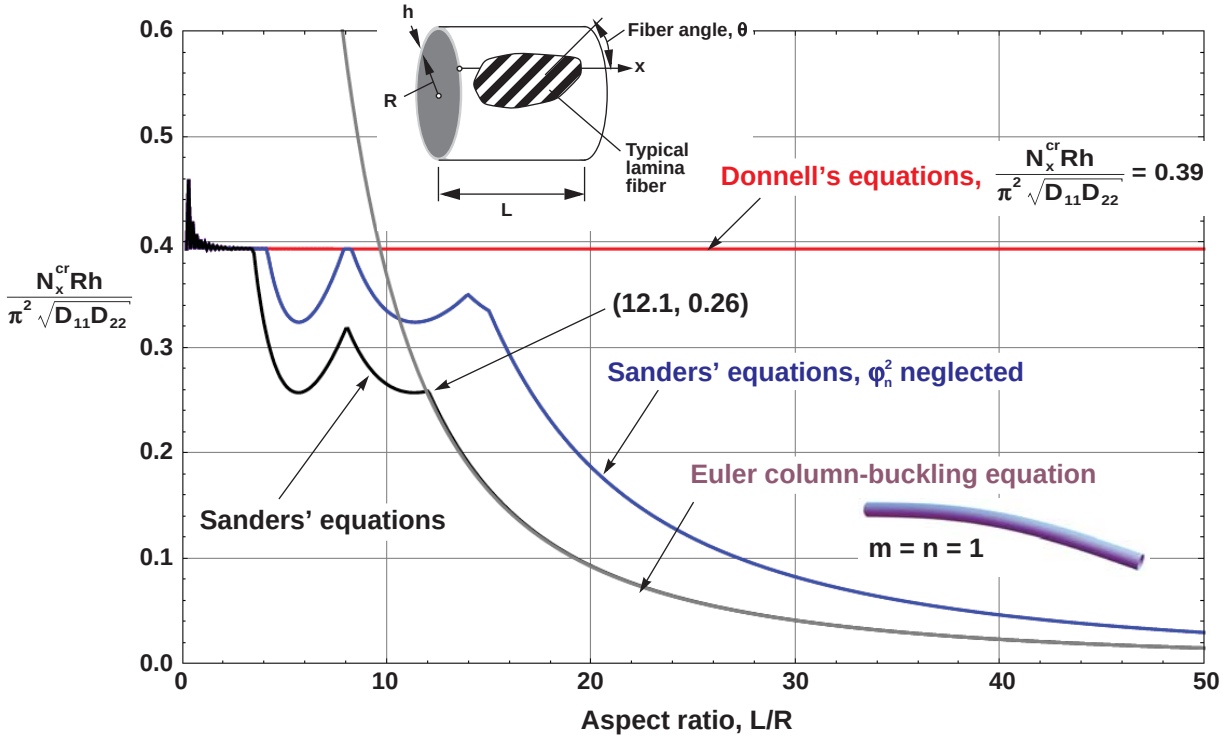

Figure 118. Nondimensional buckling loads for compression-loaded $[(\pm 60)_6]_s$ cylinders with simply supported edges for R/h = 50 and L/R ≤ 50.

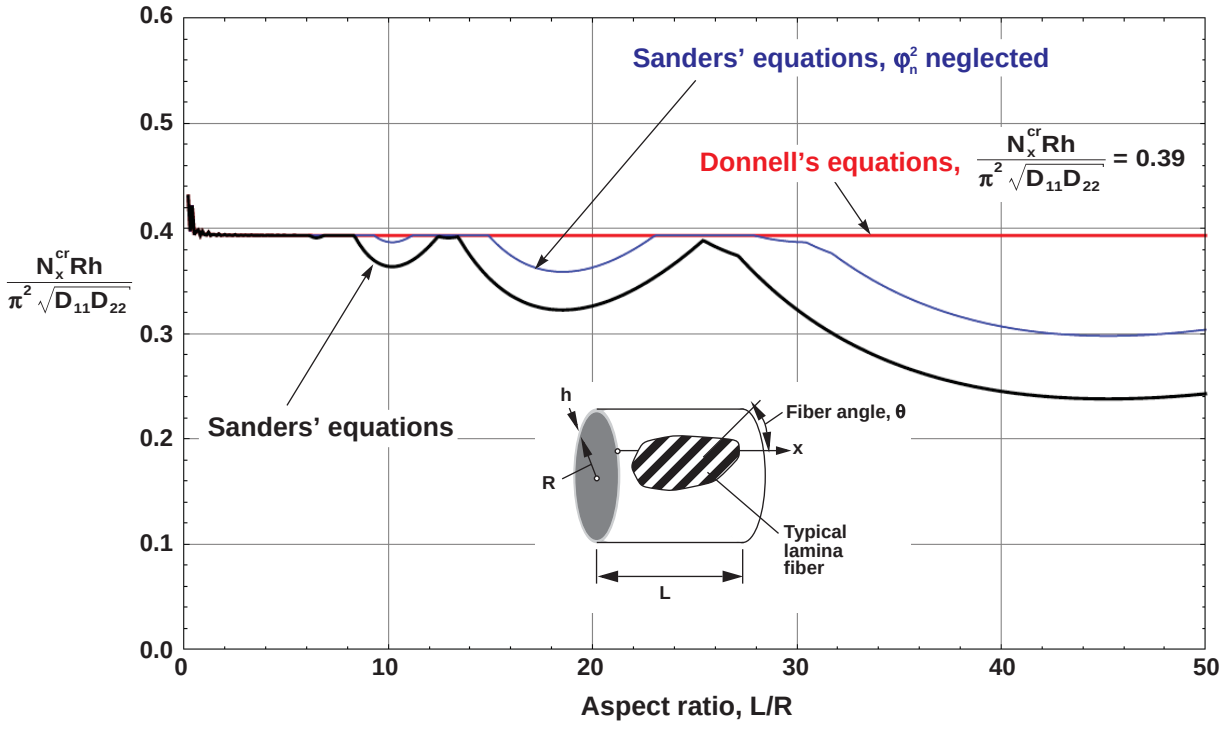

Figure 119. Nondimensional buckling loads for compression-loaded $[(\pm 30)_6]_s$ cylinders with simply supported edges for R/h = 500 and L/R ≤ 50.

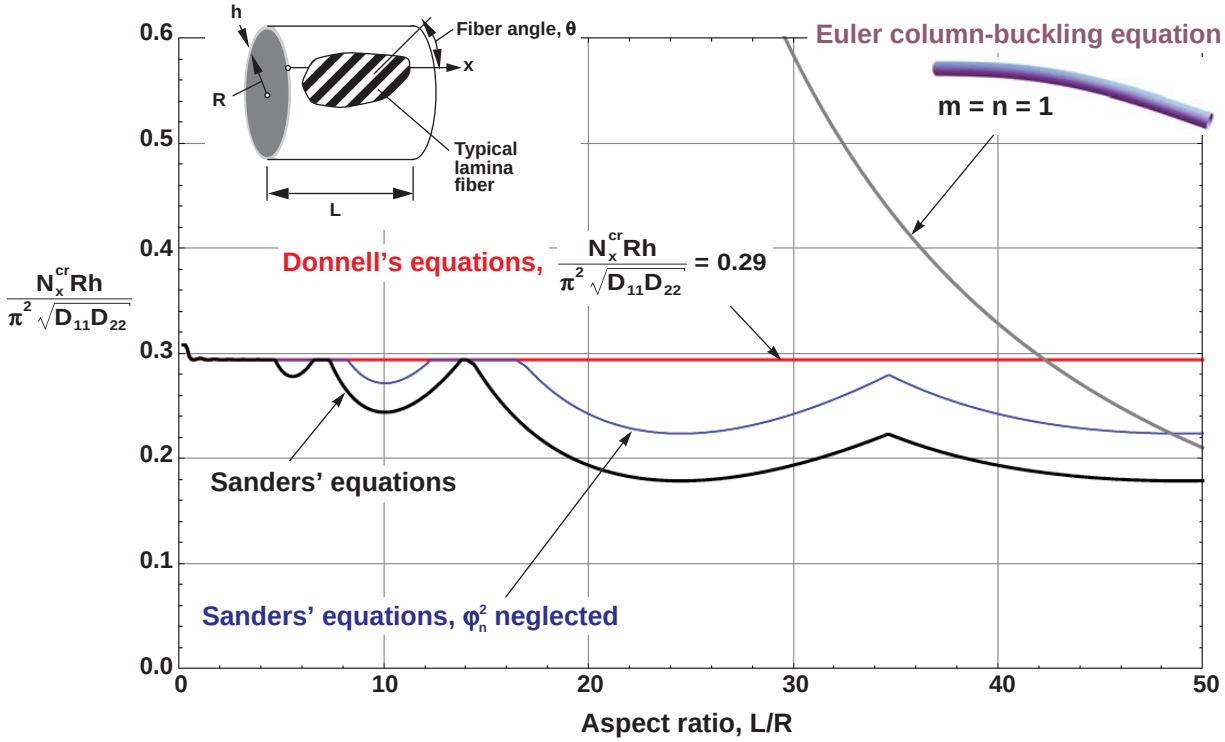

Figure 120. Nondimensional buckling loads for compression-loaded $[(\pm 45)_6]_s$ cylinders with simply supported edges for R/h = 500 and L/R ≤ 50.

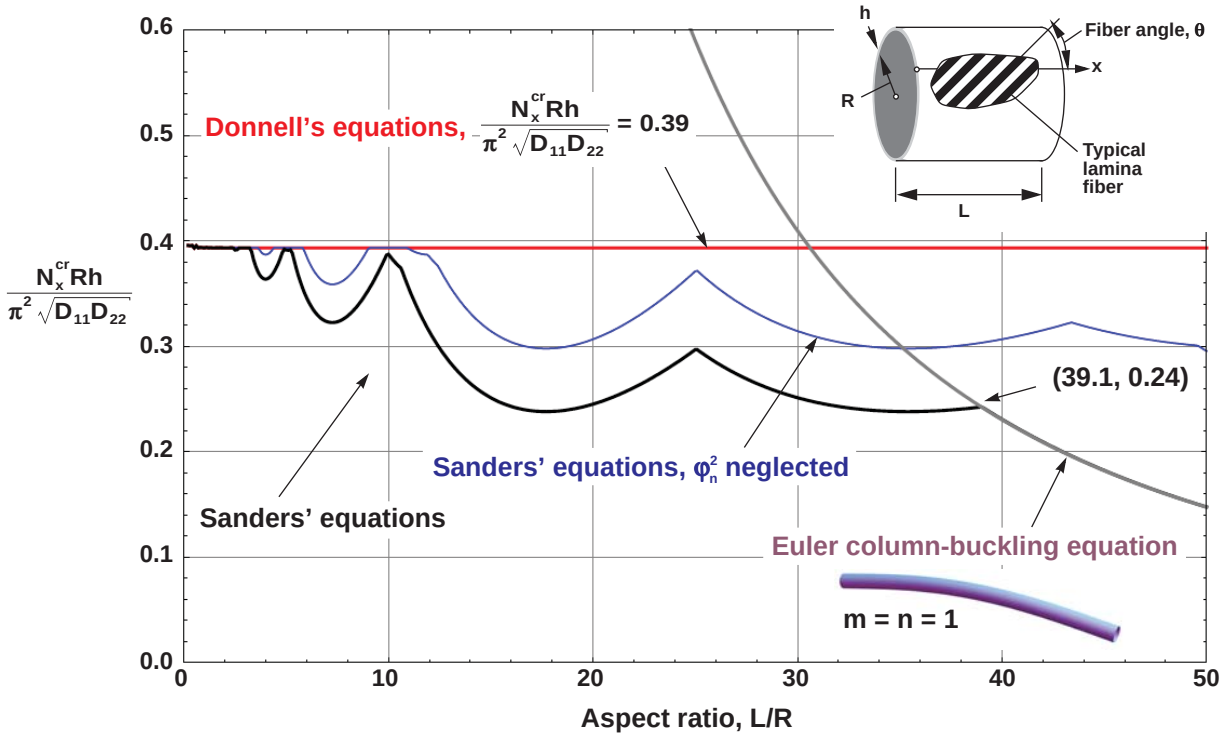

Figure 121. Nondimensional buckling loads for compression-loaded $[(\pm 60)_6]_s$ cylinders with simply supported edges for R/h = 500 and L/R ≤ 50.

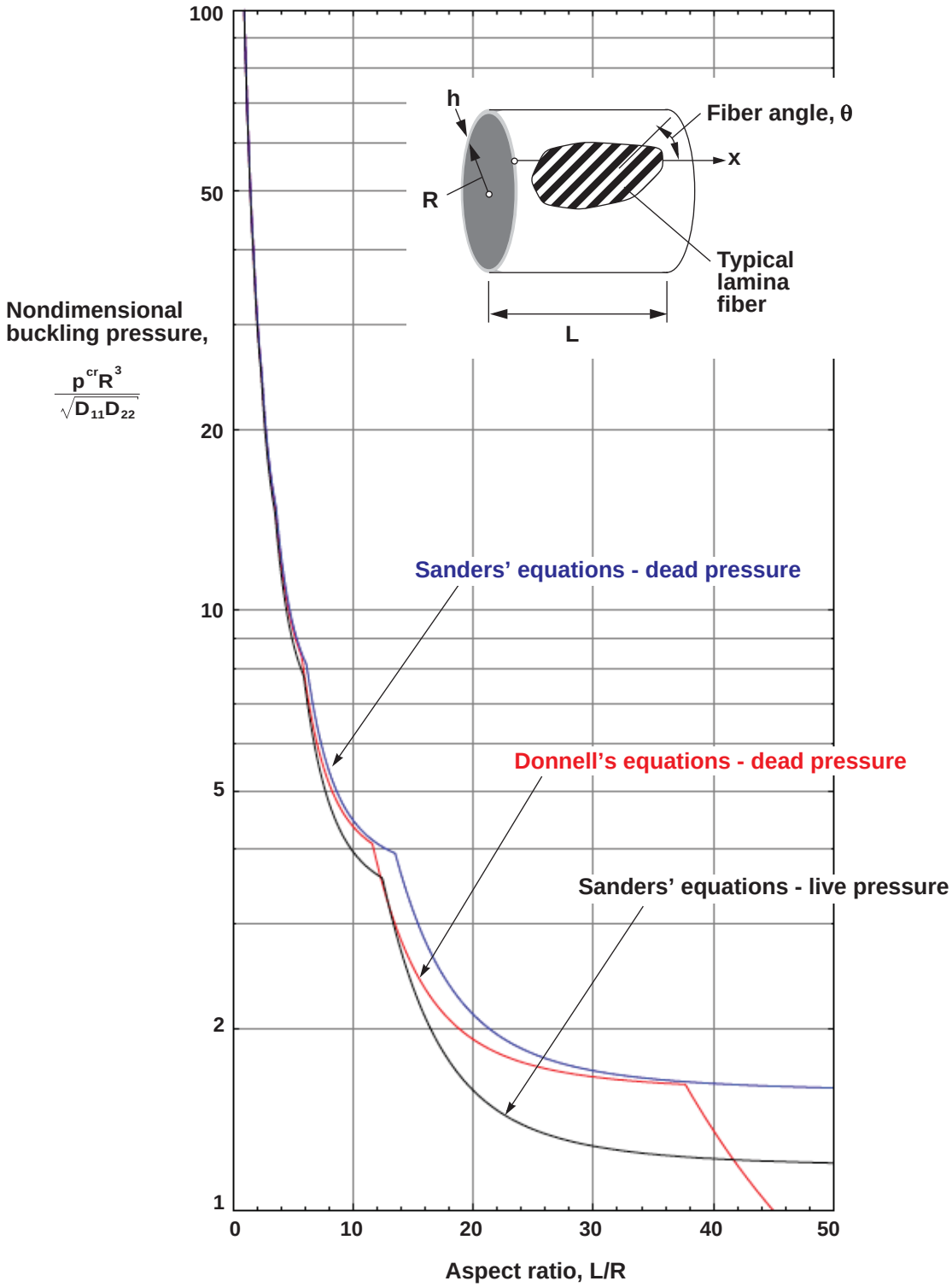

Figure 122. Nondimensional buckling loads for external-pressure-loaded $[(\pm 30)_6]_s$ cylinders with simply supported edges for R/h = 50.

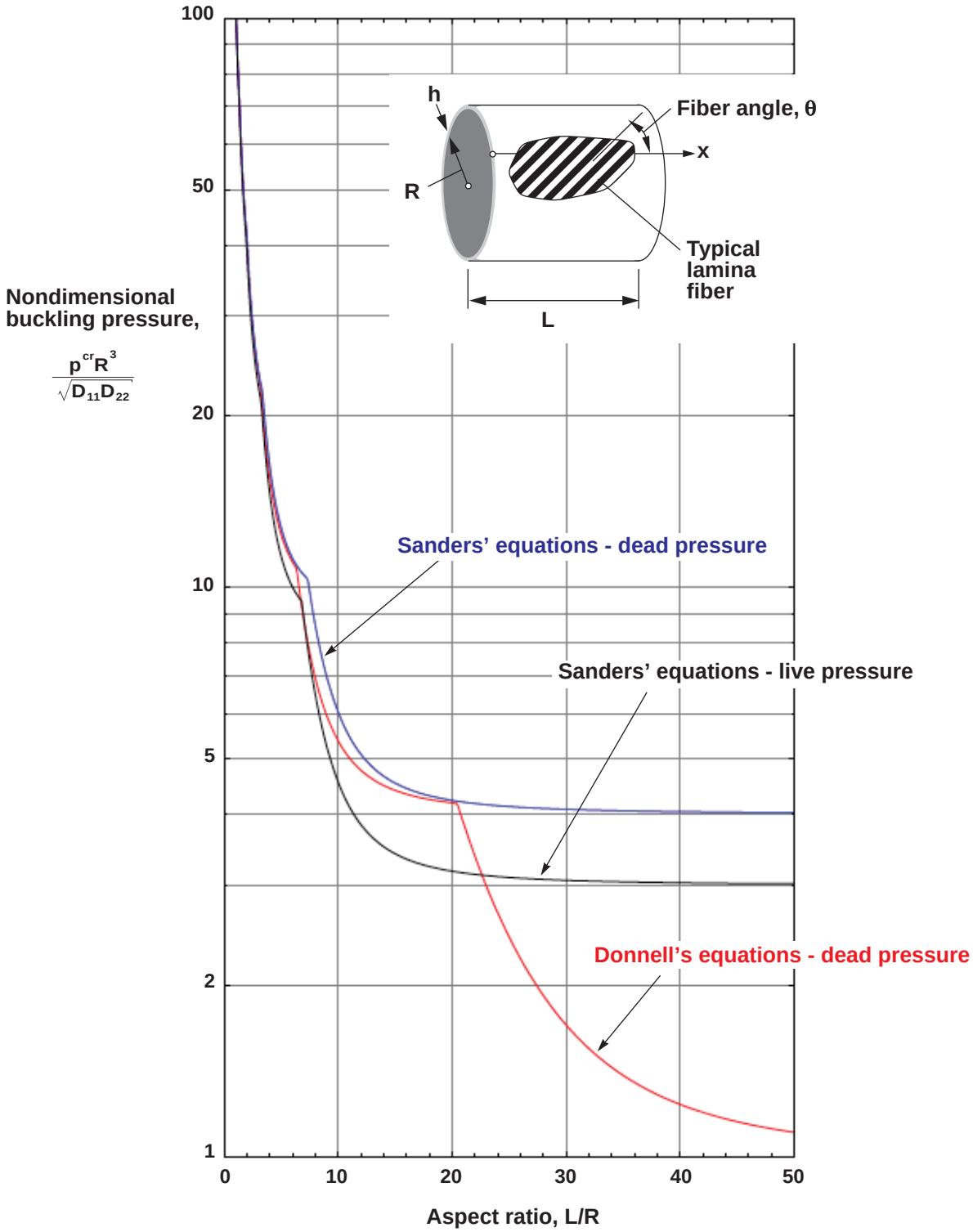

Figure 123. Nondimensional buckling loads for external-pressure-loaded $[(\pm 45)_6]_s$ cylinders with simply supported edges for R/h = 50.

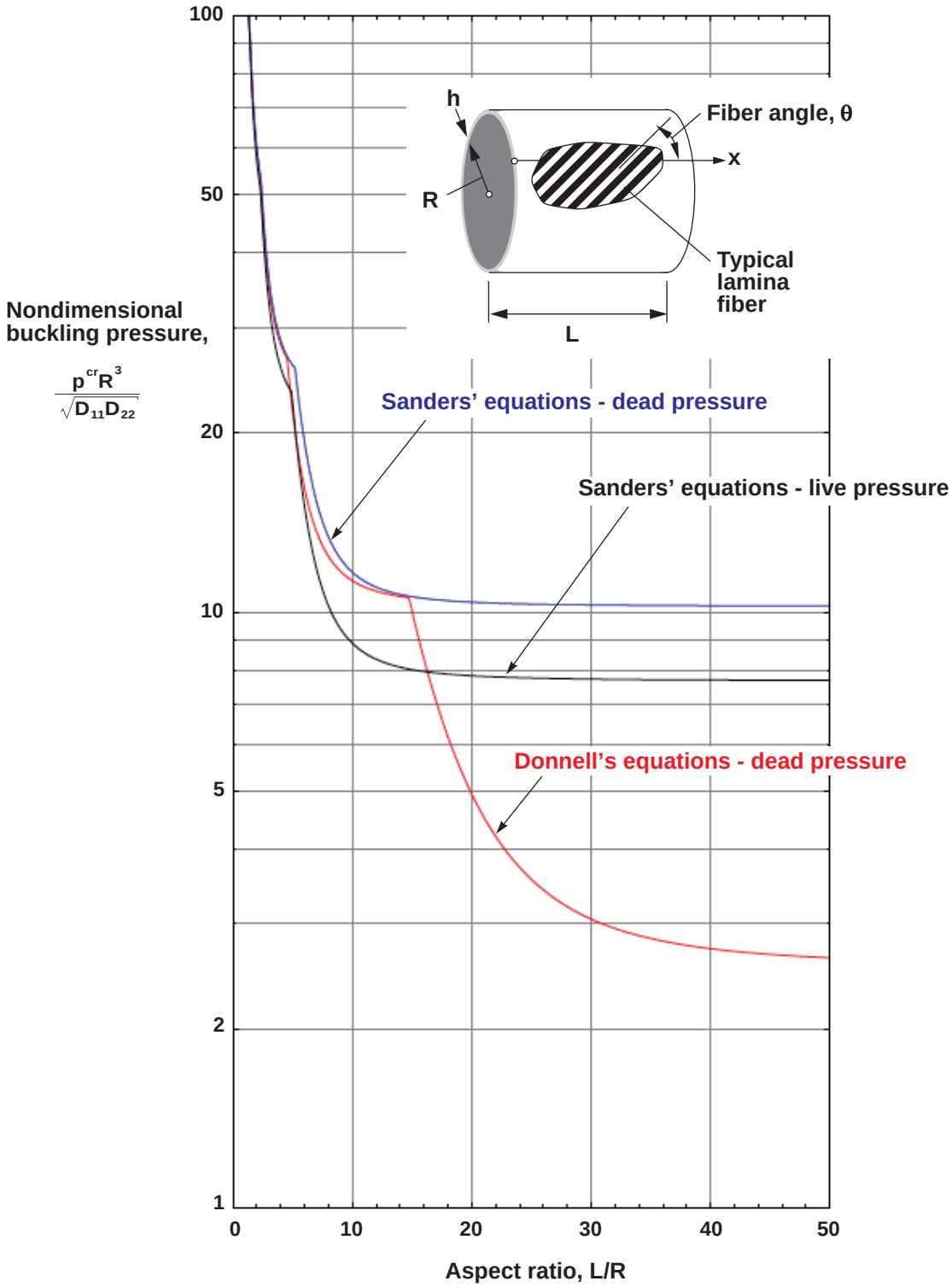

Figure 124. Nondimensional buckling loads for external-pressure-loaded $[(\pm 60)_6]_s$ cylinders with simply supported edges for R/h = 50.

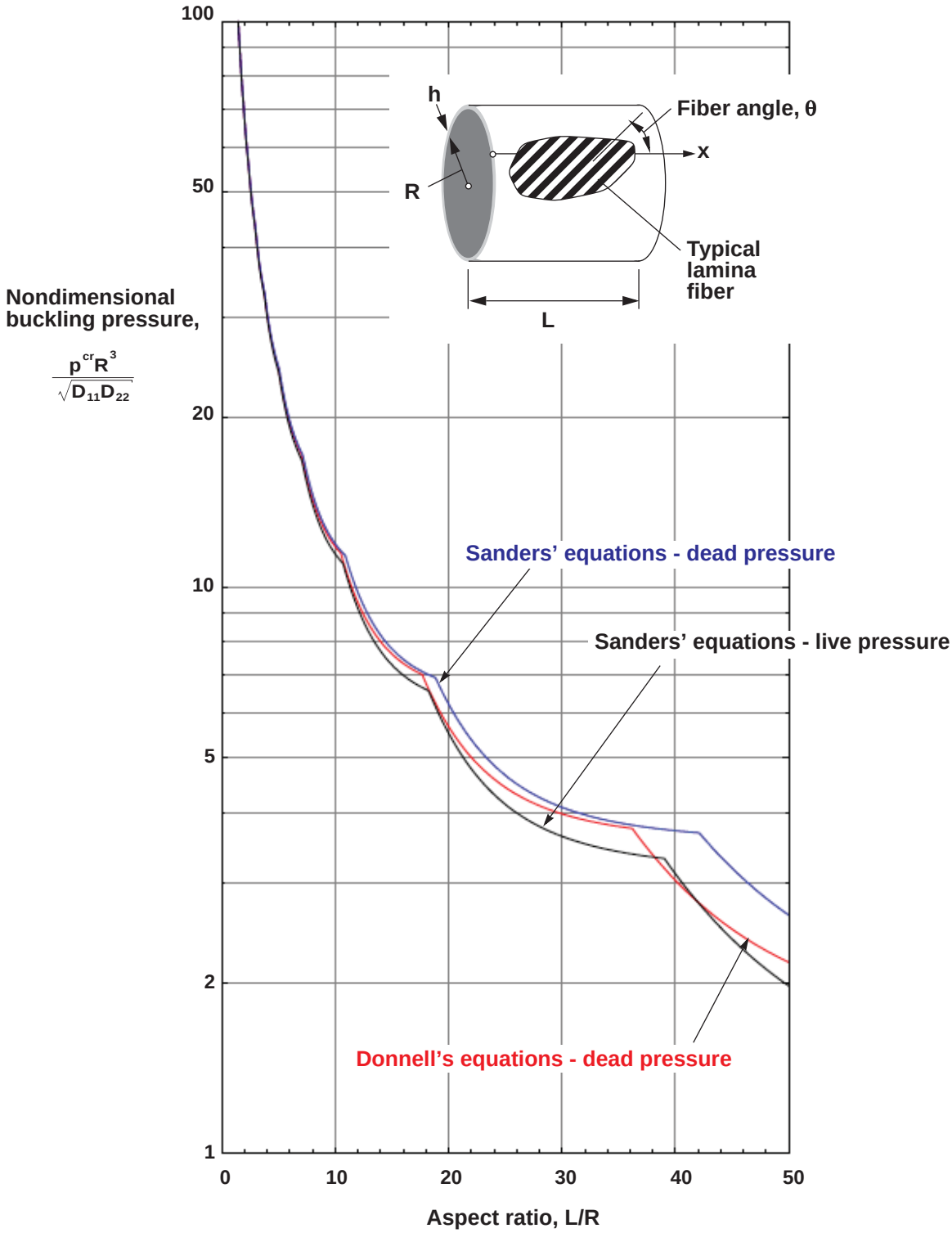

Figure 125. Nondimensional buckling loads for external-pressure-loaded $[(\pm 30)_6]_s$ cylinders with simply supported edges for R/h = 500.

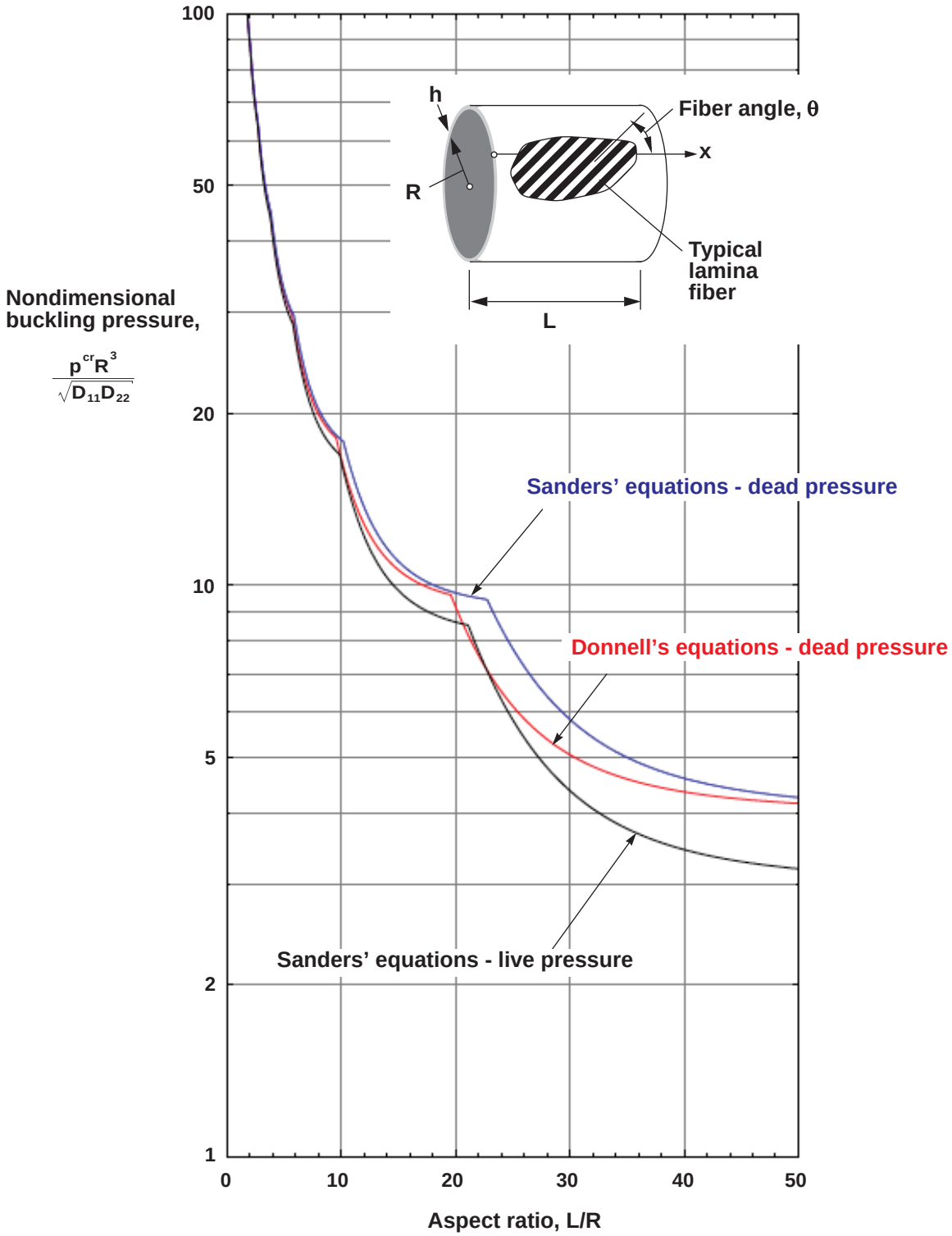

Figure 126. Nondimensional buckling loads for external-pressure-loaded $[(\pm 45)_6]_s$ cylinders with simply supported edges for R/h = 500.

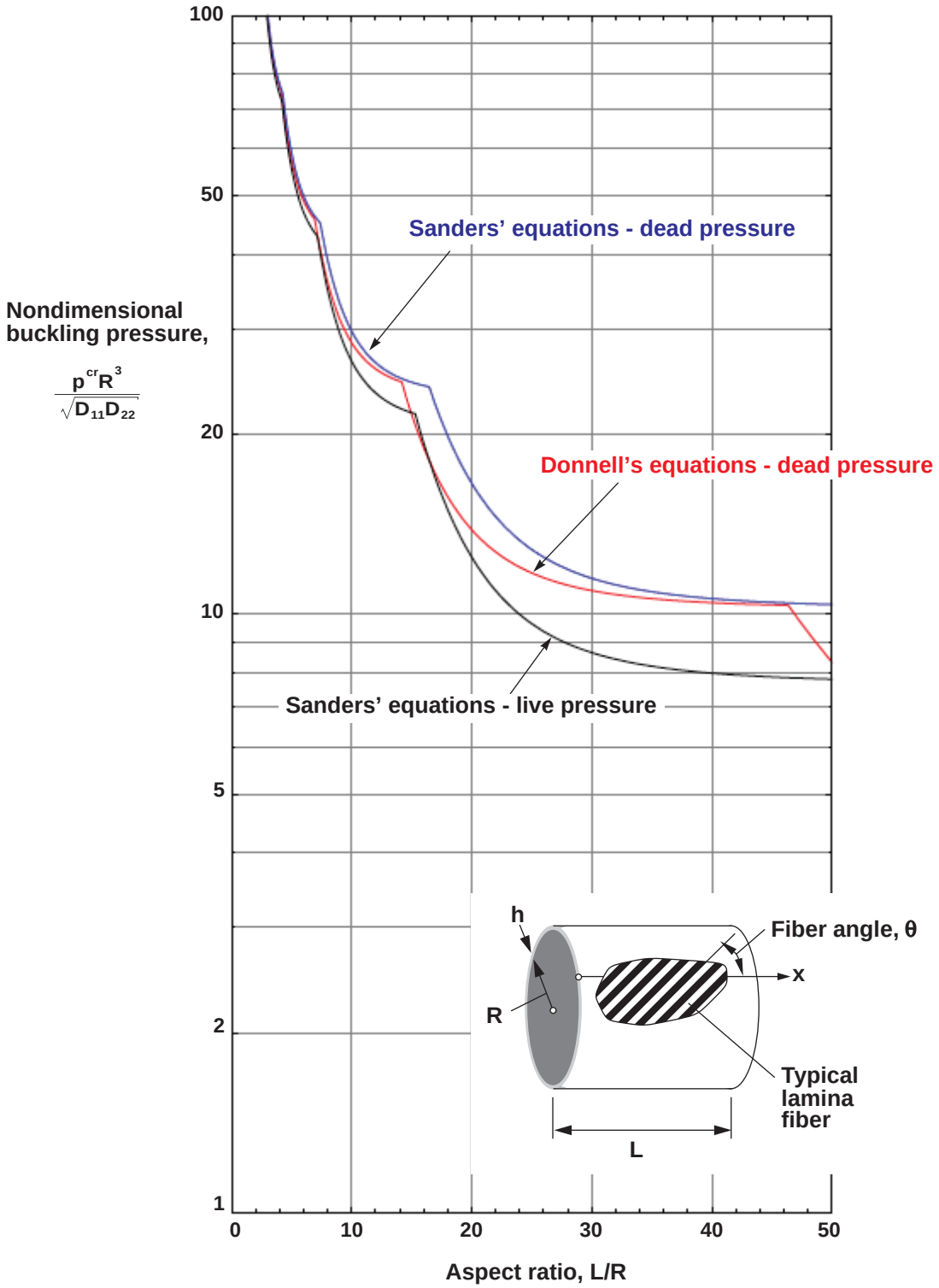

Figure 127. Nondimensional buckling loads for external-pressure-loaded $[(\pm 60)_6]_s$ cylinders with simply supported edges for R/h = 500.

Appendix A
Displacement Formulation of the Buckling Equations

The buckling equations are expressed in a form in which the loading parameter and the displacements $\overset{(1)}{u}_{x(x,y)}$, $\overset{(1)}{u}_{y(x,y)}$, and $\overset{(1)}{w}_{(x,y)}$ are the primary unknowns as follows. First, equations (18b) and (18c) are substituted into equation (21c) to get

$$\overset{(1)}{\mathcal{N}}_{xx} = \mathcal{N}_{11}\left(\overset{(1)}{u}_x\right) + \mathcal{N}_{12}\left(\overset{(1)}{u}_y\right) + \mathcal{N}_{13}\left(\overset{(1)}{w}\right) \tag{A1a}$$

$$\overset{(1)}{\mathcal{N}}_{yy} = \mathcal{N}_{21}\left(\overset{(1)}{u}_x\right) + \mathcal{N}_{22}\left(\overset{(1)}{u}_y\right) + \mathcal{N}_{23}\left(\overset{(1)}{w}\right) \tag{A1b}$$

$$\overset{(1)}{\mathcal{N}}_{xy} = \mathcal{N}_{31}\left(\overset{(1)}{u}_x\right) + \mathcal{N}_{32}\left(\overset{(1)}{u}_y\right) + \mathcal{N}_{33}\left(\overset{(1)}{w}\right) \tag{A1c}$$

where

$$\mathcal{N}_{11}(\ ) = A_{11}\frac{\partial}{\partial x} + \left(A_{16} - B_{16}\frac{c_2}{2R}\right)\frac{\partial}{\partial y} \tag{A2a}$$

$$\mathcal{N}_{12}(\ ) = \left(A_{16} + B_{16}\frac{3c_2}{2R}\right)\frac{\partial}{\partial x} + \left(A_{12} + B_{12}\frac{c_2}{R}\right)\frac{\partial}{\partial y} \tag{A2b}$$

$$\mathcal{N}_{13}(\ ) = \frac{A_{12}}{R}(\ ) - B_{11}\frac{\partial^2}{\partial x^2} - B_{12}\frac{\partial^2}{\partial y^2} - 2B_{16}\frac{\partial^2}{\partial x \partial y} \tag{A2c}$$

$$\mathcal{N}_{21}(\ ) = A_{12}\frac{\partial}{\partial x} + \left(A_{26} - B_{26}\frac{c_2}{2R}\right)\frac{\partial}{\partial y} \tag{A2d}$$

$$\mathcal{N}_{22}(\ ) = \left(A_{26} + B_{26}\frac{3c_2}{2R}\right)\frac{\partial}{\partial x} + \left(A_{22} + B_{22}\frac{c_2}{R}\right)\frac{\partial}{\partial y} \tag{A2e}$$

$$\mathcal{N}_{23}(\ ) = \frac{A_{22}}{R}(\ ) - B_{12}\frac{\partial^2}{\partial x^2} - B_{22}\frac{\partial^2}{\partial y^2} - 2B_{26}\frac{\partial^2}{\partial x \partial y} \tag{A2f}$$

$$\mathcal{N}_{31}(\ ) = A_{16}\frac{\partial}{\partial x} + \left(A_{66} - B_{66}\frac{c_2}{2R}\right)\frac{\partial}{\partial y} \tag{A2g}$$

$$\mathcal{N}_{32}(\ ) = \left(A_{66} + B_{66}\frac{3c_2}{2R}\right)\frac{\partial}{\partial x} + \left(A_{26} + B_{26}\frac{c_2}{R}\right)\frac{\partial}{\partial y} \tag{A2h}$$

$$\mathcal{N}_{33}(\ ) = \frac{A_{26}}{R}(\ ) - B_{16}\frac{\partial^2}{\partial x^2} - B_{26}\frac{\partial^2}{\partial y^2} - 2B_{66}\frac{\partial^2}{\partial x \partial y} \tag{A2i}$$

Similarly, equation (21d) gives

$$\overset{(1)}{\mathcal{M}}_{xx} = \mathcal{M}_{11}\left(\overset{(1)}{u}_x\right) + \mathcal{M}_{12}\left(\overset{(1)}{u}_y\right) + \mathcal{M}_{13}\left(\overset{(1)}{w}\right) \tag{A3a}$$

$$\overset{(1)}{\mathcal{M}}_{yy} = \mathcal{M}_{21}\left(\overset{(1)}{u}_x\right) + \mathcal{M}_{22}\left(\overset{(1)}{u}_y\right) + \mathcal{M}_{23}\left(\overset{(1)}{w}\right) \tag{A3b}$$

$$\overset{(1)}{\mathcal{M}}_{xy} = \mathcal{M}_{31}\left(\overset{(1)}{u}_x\right) + \mathcal{M}_{32}\left(\overset{(1)}{u}_y\right) + \mathcal{M}_{33}\left(\overset{(1)}{w}\right) \tag{A3c}$$

where

$$\mathcal{M}_{11}(\ ) = B_{11}\frac{\partial}{\partial x} + \left(B_{16} - D_{16}\frac{c_2}{2R}\right)\frac{\partial}{\partial y} \tag{A4a}$$

$$\mathcal{M}_{12}(\ ) = \left(B_{16} + D_{16}\frac{3c_2}{2R}\right)\frac{\partial}{\partial x} + \left(B_{12} + D_{12}\frac{c_2}{R}\right)\frac{\partial}{\partial y} \tag{A4b}$$

$$\mathcal{M}_{13}(\ ) = \frac{B_{12}}{R}(\ ) - D_{11}\frac{\partial^2}{\partial x^2} - D_{12}\frac{\partial^2}{\partial y^2} - 2D_{16}\frac{\partial^2}{\partial x \partial y} \tag{A4c}$$

$$\mathcal{M}_{21}(\ ) = B_{12}\frac{\partial}{\partial x} + \left(B_{26} - D_{26}\frac{c_2}{2R}\right)\frac{\partial}{\partial y} \tag{A4d}$$

$$\mathcal{M}_{22}(\ ) = \left(B_{26} + D_{26}\frac{3c_2}{2R}\right)\frac{\partial}{\partial x} + \left(B_{22} + D_{22}\frac{c_2}{R}\right)\frac{\partial}{\partial y} \tag{A4e}$$

$$\mathcal{M}_{23}(\ ) = \frac{B_{22}}{R}(\ ) - D_{12}\frac{\partial^2}{\partial x^2} - D_{22}\frac{\partial^2}{\partial y^2} - 2D_{26}\frac{\partial^2}{\partial x \partial y} \tag{A4f}$$

$$\mathcal{M}_{31}(\ ) = B_{16}\frac{\partial}{\partial x} + \left(B_{66} - D_{66}\frac{c_2}{2R}\right)\frac{\partial}{\partial y} \tag{A4g}$$

$$\mathcal{M}_{32}(\ ) = \left(B_{66} + D_{66}\frac{3c_2}{2R}\right)\frac{\partial}{\partial x} + \left(B_{26} + D_{26}\frac{c_2}{R}\right)\frac{\partial}{\partial y} \tag{A4h}$$

$$\mathcal{M}_{33}(\ ) = \frac{B_{26}}{R}(\ ) - D_{16}\frac{\partial^2}{\partial x^2} - D_{26}\frac{\partial^2}{\partial y^2} - 2D_{66}\frac{\partial^2}{\partial x \partial y} \tag{A4i}$$

Next, equations (A3) and (A4) are substituted into (23c) and (23d) to get

$$\overset{(1)}{Q}_x = q_{11}\left(\overset{(1)}{u}_x\right) + q_{12}\left(\overset{(1)}{u}_y\right) + q_{13}\left(\overset{(1)}{w}\right) \tag{A5a}$$

and

$$\overset{(1)}{Q}_y = q_{21}\left(\overset{(1)}{u}_x\right) + q_{22}\left(\overset{(1)}{u}_y\right) + q_{23}\left(\overset{(1)}{w}\right) \tag{A5b}$$

where

$$\begin{aligned} q_{11}(\ ) &= \frac{\partial}{\partial x}\mathcal{M}_{11}(\ ) + \frac{\partial}{\partial y}\mathcal{M}_{31}(\ ) \\ &= B_{11}\frac{\partial^2}{\partial x^2} + \left(2B_{16} - D_{16}\frac{c_2}{2R}\right)\frac{\partial^2}{\partial x \partial y} + \left(B_{66} - D_{66}\frac{c_2}{2R}\right)\frac{\partial^2}{\partial y^2} \end{aligned} \tag{A6a}$$

$$\begin{aligned} q_{12}(\ ) &= \frac{\partial}{\partial x}\mathcal{M}_{12}(\ ) + \frac{\partial}{\partial y}\mathcal{M}_{32}(\ ) \\ &= \left(B_{16} + D_{16}\frac{3c_2}{2R}\right)\frac{\partial^2}{\partial x^2} + \left(B_{12} + B_{66} + \left[2D_{12} + 3D_{66}\right]\frac{c_2}{2R}\right)\frac{\partial^2}{\partial x \partial y} + \left(B_{26} + D_{26}\frac{c_2}{R}\right)\frac{\partial^2}{\partial y^2} \end{aligned} \tag{A6b}$$

$$\begin{aligned} q_{13}(\ ) &= \frac{\partial}{\partial x}\mathcal{M}_{13}(\ ) + \frac{\partial}{\partial y}\mathcal{M}_{33}(\ ) \\ &= \frac{B_{12}}{R}\frac{\partial}{\partial x} + \frac{B_{26}}{R}\frac{\partial}{\partial y} - D_{11}\frac{\partial^3}{\partial x^3} - \left(D_{12} + 2D_{66}\right)\frac{\partial^3}{\partial x \partial y^2} - 3D_{16}\frac{\partial^3}{\partial x^2 \partial y} - D_{26}\frac{\partial^3}{\partial y^3} \end{aligned} \tag{A6c}$$

$$\begin{aligned} q_{21}(\ ) &= \frac{\partial}{\partial x}\mathcal{M}_{31}(\ ) + \frac{\partial}{\partial y}\mathcal{M}_{21}(\ ) \\ &= B_{16}\frac{\partial^2}{\partial x^2} + \left(B_{66} + B_{12} - D_{66}\frac{c_2}{2R}\right)\frac{\partial^2}{\partial x \partial y} + \left(B_{26} - D_{26}\frac{c_2}{2R}\right)\frac{\partial^2}{\partial y^2} \end{aligned} \tag{A6d}$$

$$q_{22}(\ ) = \frac{\partial}{\partial x}\mathcal{M}_{32}(\ ) + \frac{\partial}{\partial y}\mathcal{M}_{22}(\ )$$
$$= \left(B_{66} + D_{66}\frac{3c_2}{2R}\right)\frac{\partial^2}{\partial x^2} + \left(2B_{26} + D_{26}\frac{5c_2}{2R}\right)\frac{\partial^2}{\partial x\partial y} + \left(B_{22} + D_{22}\frac{c_2}{R}\right)\frac{\partial^2}{\partial y^2} \tag{A6e}$$

$$q_{23}(\ ) = \frac{\partial}{\partial x}\mathcal{M}_{33}(\ ) + \frac{\partial}{\partial y}\mathcal{M}_{23}(\ )$$
$$= \frac{B_{26}}{R}\frac{\partial}{\partial x} + \frac{B_{22}}{R}\frac{\partial}{\partial y} - D_{16}\frac{\partial^3}{\partial x^3} - 3D_{26}\frac{\partial^3}{\partial x\partial y^2} - \left(D_{12} + 2D_{66}\right)\frac{\partial^3}{\partial x^2\partial y} - D_{22}\frac{\partial^3}{\partial y^3} \tag{A6f}$$

Equations (26) and (A1) - (A6) are substituted into equations (23) to get

$$\begin{bmatrix} \mathcal{L}_{11}(\ ) & \mathcal{L}_{12}(\ ) & \mathcal{L}_{13}(\ ) \\ \mathcal{L}_{12}(\ ) & \mathcal{L}_{22}(\ ) & \mathcal{L}_{23}(\ ) \\ \mathcal{L}_{13}(\ ) & \mathcal{L}_{23}(\ ) & \mathcal{L}_{33}(\ ) \end{bmatrix} \begin{Bmatrix} u_x^{(1)} \\ u_y^{(1)} \\ w^{(1)} \end{Bmatrix} = \tilde{p} \begin{bmatrix} \mathcal{G}_{11}(\ ) & \mathcal{G}_{12}(\ ) & \mathcal{G}_{13}(\ ) \\ \mathcal{G}_{21}(\ ) & \mathcal{G}_{22}(\ ) & \mathcal{G}_{23}(\ ) \\ \mathcal{G}_{31}(\ ) & \mathcal{G}_{32}(\ ) & \mathcal{G}_{33}(\ ) \end{bmatrix} \begin{Bmatrix} u_x^{(1)} \\ u_y^{(1)} \\ w^{(1)} \end{Bmatrix} \tag{A7}$$

where

$$\mathcal{L}_{11}(\ ) = A_{11}\frac{\partial^2}{\partial x^2} + \left(2A_{16} - B_{16}\frac{c_2}{R}\right)\frac{\partial^2}{\partial x\partial y} + \left(A_{66} - B_{66}\frac{c_2}{R} + D_{66}\frac{c_2}{4R^2}\right)\frac{\partial^2}{\partial y^2} \tag{A8a}$$

$$\mathcal{L}_{12}(\ ) = \left(A_{16} + B_{16}\frac{3c_2}{2R}\right)\frac{\partial^2}{\partial x^2} + \left(A_{12} + A_{66} + \left[B_{12} + B_{66}\right]\frac{c_2}{R} - D_{66}\frac{3c_2}{4R^2}\right)\frac{\partial^2}{\partial x\partial y} + \left(A_{26} + B_{26}\frac{c_2}{2R} - D_{26}\frac{c_2}{2R^2}\right)\frac{\partial^2}{\partial y^2} \tag{A8b}$$

$$\mathcal{L}_{13}(\ ) = \frac{A_{12}}{R}\frac{\partial}{\partial x} + \frac{1}{R}\left(A_{26} - B_{26}\frac{c_2}{2R}\right)\frac{\partial}{\partial y} - B_{11}\frac{\partial^3}{\partial x^3} - \left(B_{12} + 2B_{66} - D_{66}\frac{c_2}{R}\right)\frac{\partial^3}{\partial x\partial y^2} + \left(D_{16}\frac{c_2}{2R} - 3B_{16}\right)\frac{\partial^3}{\partial x^2\partial y} + \left(D_{26}\frac{c_2}{2R} - B_{26}\right)\frac{\partial^3}{\partial y^3} \tag{A8c}$$

$$\mathcal{L}_{22}(\ ) = \left(A_{66} + 3B_{66}\frac{c_2}{R} + D_{66}\frac{9c_2}{4R^2}\right)\frac{\partial^2}{\partial x^2} + \left(2A_{26} + B_{26}\frac{5c_2}{R} + D_{26}\frac{3c_2}{R^2}\right)\frac{\partial^2}{\partial x\partial y} + \left(A_{22} + 2B_{22}\frac{c_2}{R} + D_{22}\frac{c_2}{R^2}\right)\frac{\partial^2}{\partial y^2} \tag{A8d}$$

$$\mathcal{L}_{23}(\ ) = \frac{1}{R}\left(A_{26} + B_{26}\frac{3c_2}{2R}\right)\frac{\partial}{\partial x} + \frac{1}{R}\left(A_{22} + B_{22}\frac{c_2}{R}\right)\frac{\partial}{\partial y} - \left(B_{16} + D_{16}\frac{3c_2}{2R}\right)\frac{\partial^3}{\partial x^3} - \left(3B_{26} + 7D_{26}\frac{c_2}{2R}\right)\frac{\partial^3}{\partial x\partial y^2} - \left(B_{12} + 2B_{66} + \left[D_{12} + 3D_{66}\right]\frac{c_2}{R}\right)\frac{\partial^3}{\partial x^2\partial y} - \left(B_{22} + D_{22}\frac{c_2}{R}\right)\frac{\partial^3}{\partial y^3} \tag{A8e}$$

$$\mathcal{L}_{33}(\ ) = D_{11}\frac{\partial^4}{\partial x^4} + 4D_{16}\frac{\partial^4}{\partial x^3\partial y} + 2\left(D_{12} + 2D_{66}\right)\frac{\partial^4}{\partial x^2\partial y^2} + 4D_{26}\frac{\partial^4}{\partial x\partial y^3} + D_{22}\frac{\partial^4}{\partial y^4} - \frac{2B_{12}}{R}\frac{\partial^2}{\partial x^2} - \frac{2B_{22}}{R}\frac{\partial^2}{\partial y^2} - \frac{4B_{26}}{R}\frac{\partial^2}{\partial x\partial y} + \frac{A_{22}}{R^2}(\ ) \tag{A8f}$$

and

$$\mathcal{G}_{11}(\ ) = \frac{c_1}{4}\frac{\partial}{\partial y}\left[\left(L_1\overset{(0)}{\varepsilon}_{xx} + L_2\overset{(0)}{\varepsilon}_{yy}\right)\frac{\partial}{\partial y}\right] \tag{A9a}$$

$$\mathcal{G}_{12}(\ ) = -\frac{c_1}{4}\frac{\partial}{\partial y}\left[\left(L_1\overset{(0)}{\varepsilon}_{xx} + L_2\overset{(0)}{\varepsilon}_{yy}\right)\frac{\partial}{\partial x}\right] \tag{A9b}$$

$$\mathcal{G}_{13}(\ ) = c_4\ell_3 q_\zeta\frac{\partial}{\partial x} \tag{A9c}$$

$$\mathcal{G}_{21}(\ ) = -\frac{c_1}{4}\frac{\partial}{\partial x}\left[\left(L_1\overset{(0)}{\varepsilon}_{xx} + L_2\overset{(0)}{\varepsilon}_{yy}\right)\frac{\partial}{\partial y}\right] \tag{A9d}$$

$$\mathcal{G}_{22}(\ ) = -\frac{c_2}{R^2}L_2\overset{(0)}{\varepsilon}_{yy}(\ ) + \frac{c_1}{4}\frac{\partial}{\partial x}\left[\left(L_1\overset{(0)}{\varepsilon}_{xx} + L_2\overset{(0)}{\varepsilon}_{yy}\right)\frac{\partial}{\partial x}\right] - c_4\ell_3\frac{q_\zeta}{R}(\ ) \tag{A9e}$$

$$\mathcal{G}_{23}() = \frac{c_2}{R}\left(L_2\overset{(0)}{\varepsilon}_{yy}\frac{\partial}{\partial y} - L_3\overset{(0)}{\varepsilon}_{xy}\frac{\partial}{\partial x}\right) + c_4\ell_3 q_\zeta\frac{\partial}{\partial y} \tag{A9f}$$

$$\mathcal{G}_{31}(\ ) = c_4\ell_3\left[q_\zeta\frac{\partial}{\partial x} + \frac{\partial q_\zeta}{\partial x}(\ )\right] \tag{A9c}$$

$$\mathcal{G}_{32}(\ ) = -\frac{c_2 L_3}{R}\frac{\partial}{\partial x}\left[\overset{(0)}{\kappa}_{xy}(\ )\right] + \frac{c_2 L_2}{R}\frac{\partial}{\partial y}\left[\overset{(0)}{\kappa}_{yy}(\ )\right] + c_4\ell_3\left[q_\zeta\frac{\partial}{\partial y} + \frac{\partial q_\zeta}{\partial y}(\ )\right] \tag{A9g}$$

$$\mathcal{G}_{33}(\ ) = \frac{\partial}{\partial x}\left(-L_1\overset{(0)}{\kappa}_{xx}\frac{\partial}{\partial x} + L_3\overset{(0)}{\kappa}_{xy}\frac{\partial}{\partial y}\right) + \frac{\partial}{\partial y}\left(L_3\overset{(0)}{\kappa}_{xy}\frac{\partial}{\partial x} - L_2\overset{(0)}{\kappa}_{yy}\frac{\partial}{\partial y}\right) + c_4\ell_3\left[\frac{q_\zeta}{R} + \frac{\partial q_\zeta}{\partial\zeta}\right](\ ) \tag{A9h}$$

The boundary conditions given by equations (25) are expressed as

$$\mathcal{B}_{11}\left(\overset{(1)}{u}_x\right) + \mathcal{B}_{12}\left(\overset{(1)}{u}_y\right) + \mathcal{B}_{13}\left(\overset{(1)}{w}\right) = 0 \quad \text{or} \quad \overset{(1)}{u}_x = 0 \tag{A10a}$$

$$\mathcal{B}_{21}\left(\overset{(1)}{u}_x\right) + \mathcal{B}_{22}\left(\overset{(1)}{u}_y\right) + \mathcal{B}_{23}\left(\overset{(1)}{w}\right) = \tilde{p}\left[\overline{\mathcal{B}}_{21}\left(\overset{(1)}{u}_x\right) + \overline{\mathcal{B}}_{22}\left(\overset{(1)}{u}_y\right)\right] \quad \text{or} \quad \overset{(1)}{u}_y = 0 \tag{A10b}$$

$$\mathcal{B}_{31}\left(\overset{(1)}{u}_x\right) + \mathcal{B}_{32}\left(\overset{(1)}{u}_y\right) + \mathcal{B}_{33}\left(\overset{(1)}{w}\right) = \tilde{p}\left[\overline{\mathcal{B}}_{32}\left(\overset{(1)}{u}_y\right) + \overline{\mathcal{B}}_{33}\left(\overset{(1)}{w}\right)\right] \quad \text{or} \quad \overset{(1)}{w} = 0 \tag{A10c}$$

$$\mathcal{B}_{41}\left(\overset{(1)}{u}_x\right) + \mathcal{B}_{42}\left(\overset{(1)}{u}_y\right) + \mathcal{B}_{43}\left(\overset{(1)}{w}\right) = 0 \quad \text{or} \quad \frac{\partial\overset{(1)}{w}}{\partial x} = 0 \tag{A10d}$$

where

$$\mathcal{B}_{11}(\ ) = A_{11}\frac{\partial}{\partial x} + \left(A_{16} - B_{16}\frac{c_2}{2R}\right)\frac{\partial}{\partial y} \tag{A11a}$$

$$\mathcal{B}_{12}(\ ) = \left(A_{16} + B_{16}\frac{3c_2}{2R}\right)\frac{\partial}{\partial x} + \left(A_{12} + B_{12}\frac{c_2}{R}\right)\frac{\partial}{\partial y} \tag{A11b}$$

$$\mathcal{B}_{13}(\ ) = \frac{A_{12}}{R}(\ ) - B_{11}\frac{\partial^2}{\partial x^2} - B_{12}\frac{\partial^2}{\partial y^2} - 2B_{16}\frac{\partial^2}{\partial x\partial y} \tag{A11c}$$

$$\mathcal{B}_{21}(\ ) = \left(A_{16} + \frac{3c_2}{2R}B_{16}\right)\frac{\partial}{\partial x} + \left(A_{66} + B_{66}\frac{c_2}{R} - D_{66}\frac{3c_2}{4R^2}\right)\frac{\partial}{\partial y} \tag{A11d}$$

$$\overline{\mathcal{B}}_{21}(\ ) = -\frac{c_1 c_2}{4}\left[L_1\overset{(0)}{\kappa}_{xx} + L_2\overset{(0)}{\kappa}_{yy}\right]\frac{\partial}{\partial y} \tag{A11e}$$

$$\mathcal{E}_{22}(\ ) = \left(A_{66} + B_{66}\frac{3c_2}{R} + D_{66}\frac{9c_2}{4R^2}\right)\frac{\partial}{\partial x} + \left(A_{26} + B_{26}\frac{5c_2}{2R} + D_{26}\frac{3c_2}{2R^2}\right)\frac{\partial}{\partial y} \tag{A11d}$$

$$\overline{\mathcal{E}}_{22}(\ ) = \frac{c_1 c_2}{4}\left[L_1 \overset{(0)}{\varepsilon}_{xx} + L_2 \overset{(0)}{\varepsilon}_{yy}\right]\frac{\partial}{\partial x} \tag{A11e}$$

$$\begin{aligned}\mathcal{E}_{23}(\ ) = \frac{1}{R}\left(A_{26} + \frac{3c_2}{2R}B_{26}\right)(\ ) - \left(B_{16} + \frac{3c_2}{2R}D_{16}\right)\frac{\partial^2}{\partial x^2} \\ - \left(B_{26} + \frac{3c_2}{2R}D_{26}\right)\frac{\partial^2}{\partial y^2} - 2\left(B_{66} + \frac{3c_2}{2R}D_{66}\right)\frac{\partial^2}{\partial x \partial y}\end{aligned} \tag{A11f}$$

$$\mathcal{E}_{31}(\ ) = B_{11}\frac{\partial^2}{\partial x^2} + \left(3B_{16} - D_{16}\frac{c_2}{2R}\right)\frac{\partial^2}{\partial x \partial y} + 2\left(B_{66} - D_{66}\frac{c_2}{2R}\right)\frac{\partial^2}{\partial y^2} \tag{A11g}$$

$$\begin{aligned}\mathcal{E}_{32}(\ ) = \left(B_{16} + D_{16}\frac{3c_2}{2R}\right)\frac{\partial^2}{\partial x^2} + \left(B_{12} + 2B_{66} + \left[D_{12} + 3D_{66}\right]\frac{c_2}{R}\right)\frac{\partial^2}{\partial x \partial y} + \\ 2\left(B_{26} + D_{26}\frac{c_2}{R}\right)\frac{\partial^2}{\partial y^2}\end{aligned} \tag{A11h}$$

$$\overline{\mathcal{E}}_{32}(\ ) = -L_3 \overset{(0)}{\varepsilon}_{xy}\frac{c_2}{R}(\ ) \tag{A11h}$$

$$\mathcal{E}_{33}(\ ) = \frac{B_{12}}{R}\frac{\partial}{\partial x} + \frac{2B_{26}}{R}\frac{\partial}{\partial y} - D_{11}\frac{\partial^3}{\partial x^3} - \left(D_{12} + 4D_{66}\right)\frac{\partial^3}{\partial x \partial y^2} - 4D_{16}\frac{\partial^3}{\partial x^2 \partial y} - 2D_{26}\frac{\partial^3}{\partial y^3} \tag{A11i}$$

$$\overline{\mathcal{E}}_{33}(\ ) = -L_1 \overset{(0)}{\varepsilon}_{xx}\frac{\partial}{\partial x} + L_3 \overset{(0)}{\varepsilon}_{xy}\frac{\partial}{\partial y} \tag{A11i}$$

$$\mathcal{E}_{41}(\ ) = B_{11}\frac{\partial}{\partial x} + \left(B_{16} - D_{16}\frac{c_2}{2R}\right)\frac{\partial}{\partial y} \tag{A11j}$$

$$\mathcal{E}_{42}(\ ) = \left(B_{16} + D_{16}\frac{3c_2}{2R}\right)\frac{\partial}{\partial x} + \left(B_{12} + D_{12}\frac{c_2}{R}\right)\frac{\partial}{\partial y} \tag{A11k}$$

$$\mathcal{E}_{43}(\ ) = \frac{B_{12}}{R}(\ ) - D_{11}\frac{\partial^2}{\partial x^2} - D_{12}\frac{\partial^2}{\partial y^2} - 2D_{16}\frac{\partial^2}{\partial x \partial y} \tag{A11l}$$

For the case of passive loads,

$$\left[\begin{bmatrix}\mathcal{L}_{11}(\ )&\mathcal{L}_{12}(\ )&\mathcal{L}_{13}(\ )\\ \mathcal{L}_{12}(\ )&\mathcal{L}_{22}(\ )&\mathcal{L}_{23}(\ )\\ \mathcal{L}_{13}(\ )&\mathcal{L}_{23}(\ )&\mathcal{L}_{33}(\ )\end{bmatrix}-\tilde{\lambda}\begin{bmatrix}\mathcal{G}^{*}_{11}(\ )&\mathcal{G}^{*}_{12}(\ )&\mathcal{G}^{*}_{13}(\ )\\ \mathcal{G}^{*}_{21}(\ )&\mathcal{G}^{*}_{22}(\ )&\mathcal{G}^{*}_{23}(\ )\\ \mathcal{G}^{*}_{31}(\ )&\mathcal{G}^{*}_{32}(\ )&\mathcal{G}^{*}_{33}(\ )\end{bmatrix}\right]\begin{Bmatrix}\overset{(1)}{u}_x\\ \overset{(1)}{u}_y\\ \overset{(1)}{w}\end{Bmatrix}=\tilde{p}\begin{bmatrix}\mathcal{G}_{11}(\ )&\mathcal{G}_{12}(\ )&\mathcal{G}_{13}(\ )\\ \mathcal{G}_{21}(\ )&\mathcal{G}_{22}(\ )&\mathcal{G}_{23}(\ )\\ \mathcal{G}_{31}(\ )&\mathcal{G}_{32}(\ )&\mathcal{G}_{33}(\ )\end{bmatrix}\begin{Bmatrix}\overset{(1)}{u}_x\\ \overset{(1)}{u}_y\\ \overset{(1)}{w}\end{Bmatrix} \tag{A12}$$

where

$$\mathcal{G}^{*}_{11}(\ )=\frac{c_1}{4}\frac{\partial}{\partial y}\left[\left(L^{*}_{1}\overset{*(0)}{\varepsilon}_{xx}+L^{*}_{2}\overset{*(0)}{\varepsilon}_{yy}\right)\frac{\partial}{\partial y}\right] \tag{A13a}$$

$$\mathcal{G}^{*}_{12}(\ )=-\frac{c_1}{4}\frac{\partial}{\partial y}\left[\left(L^{*}_{1}\overset{*(0)}{\varepsilon}_{xx}+L^{*}_{2}\overset{*(0)}{\varepsilon}_{yy}\right)\frac{\partial}{\partial x}\right] \tag{A13b}$$

$$\mathcal{G}^{*}_{13}(\ )=c_4\ell^{*}_{3}q^{*}_{\zeta}\frac{\partial}{\partial x} \tag{A13c}$$

$$\mathcal{G}^{*}_{21}(\ )=-\frac{c_1}{4}\frac{\partial}{\partial x}\left[\left(L^{*}_{1}\overset{*(0)}{\varepsilon}_{xx}+L^{*}_{2}\overset{*(0)}{\varepsilon}_{yy}\right)\frac{\partial}{\partial y}\right] \tag{A13d}$$

$$\mathcal{G}^{*}_{22}(\ )=-\frac{c_2}{R^2}L^{*}_{2}\overset{*(0)}{\varepsilon}_{yy}(\ )+\frac{c_1}{4}\frac{\partial}{\partial x}\left[\left(L^{*}_{1}\overset{*(0)}{\varepsilon}_{xx}+L^{*}_{2}\overset{*(0)}{\varepsilon}_{yy}\right)\frac{\partial}{\partial x}\right]-c_4\ell^{*}_{3}\frac{q^{*}_{\zeta}}{R}(\ ) \tag{A13e}$$

$$\mathcal{G}^{*}_{23}(\ )=\frac{c_2}{R}\left(L^{*}_{2}\overset{*(0)}{\varepsilon}_{yy}\frac{\partial}{\partial y}-L^{*}_{3}\overset{*(0)}{\varepsilon}_{xy}\frac{\partial}{\partial x}\right)+c_4\ell^{*}_{3}q^{*}_{\zeta}\frac{\partial}{\partial y} \tag{A13f}$$

$$\mathcal{G}^{*}_{31}(\ )=c_4\ell^{*}_{3}\left[q^{*}_{\zeta}\frac{\partial}{\partial x}+\frac{\partial q^{*}_{\zeta}}{\partial x}(\ )\right] \tag{A13g}$$

$$\mathcal{G}^{*}_{32}(\ )=-\frac{c_2L^{*}_{3}}{R}\frac{\partial}{\partial x}\left[\overset{(0)*}{\varepsilon}_{xy}(\ )\right]+\frac{c_2L^{*}_{2}}{R}\frac{\partial}{\partial y}\left[\overset{(0)*}{\varepsilon}_{yy}(\ )\right]+c_4\ell^{*}_{3}\left[q^{*}_{\zeta}\frac{\partial}{\partial y}+\frac{\partial q^{*}_{\zeta}}{\partial y}(\ )\right] \tag{A13h}$$

$$\mathcal{G}^{*}_{33}(\ )=\frac{\partial}{\partial x}\left(-L^{*}_{1}\overset{*(0)}{\varepsilon}_{xx}\frac{\partial}{\partial x}+L^{*}_{3}\overset{*(0)}{\varepsilon}_{xy}\frac{\partial}{\partial y}\right)+\frac{\partial}{\partial y}\left(L^{*}_{3}\overset{*(0)}{\varepsilon}_{xy}\frac{\partial}{\partial x}-L^{*}_{2}\overset{*(0)}{\varepsilon}_{yy}\frac{\partial}{\partial y}\right)+c_4\ell^{*}_{3}\frac{q^{*}_{\zeta}}{R}(\ ) \tag{A13i}$$

Likewise, the boundary conditions become

$$\mathcal{B}_{11}\left(\overset{(1)}{u}_x\right) + \mathcal{B}_{12}\left(\overset{(1)}{u}_y\right) + \mathcal{B}_{13}\left(\overset{(1)}{w}\right) = 0 \quad \text{or} \quad \overset{(1)}{u}_x = 0 \tag{A14a}$$

$$\left[\mathcal{B}_{21}(\ ) - \tilde{\lambda}\overline{\mathcal{B}}^{*}_{21}(\ )\right]\overset{(1)}{u}_x + \left[\mathcal{B}_{22}(\ ) - \tilde{\lambda}\overline{\mathcal{B}}^{*}_{22}(\ )\right]\overset{(1)}{u}_y + \mathcal{B}_{23}\left(\overset{(1)}{w}\right) = \tilde{p}\left[\overline{\mathcal{B}}_{21}\left(\overset{(1)}{u}_x\right) + \overline{\mathcal{B}}_{22}\left(\overset{(1)}{u}_y\right)\right]$$

$$\text{or} \quad \overset{(1)}{u}_y = 0 \tag{A14b}$$

$$\mathcal{B}_{31}\left(\overset{(1)}{u}_x\right) + \left[\mathcal{B}_{32}(\ ) - \tilde{\lambda}\overline{\mathcal{B}}^{*}_{32}(\ )\right]\overset{(1)}{u}_y + \left[\mathcal{B}_{33}(\ ) - \tilde{\lambda}\overline{\mathcal{B}}^{*}_{33}(\ )\right]\overset{(1)}{w} = \tilde{p}\left[\overline{\mathcal{B}}_{32}\left(\overset{(1)}{u}_y\right) + \overline{\mathcal{B}}_{33}\left(\overset{(1)}{w}\right)\right]$$

$$\text{or} \quad \overset{(1)}{w} = 0 \tag{A14c}$$

$$\mathcal{B}_{41}\left(\overset{(1)}{u}_x\right) + \mathcal{B}_{42}\left(\overset{(1)}{u}_y\right) + \mathcal{B}_{43}\left(\overset{(1)}{w}\right) = 0 \quad \text{or} \quad \frac{\partial \overset{(1)}{w}}{\partial x} = 0 \tag{A14d}$$

where

$$\overline{\mathcal{B}}^{*}_{21}(\ ) = -\frac{c_1 c_2}{4}\left[L_1 \overset{*(0)*}{\kappa}_{xx} + L_2 \overset{*(0)*}{\kappa}_{yy}\right]\frac{\partial}{\partial y} \tag{A15a}$$

$$\overline{\mathcal{B}}^{*}_{22}(\ ) = \frac{c_1 c_2}{4}\left[L_1 \overset{*(0)*}{\kappa}_{xx} + L_2 \overset{*(0)*}{\kappa}_{yy}\right]\frac{\partial}{\partial x} \tag{A15b}$$

$$\overline{\mathcal{B}}^{*}_{32}(\ ) = -L_3 \overset{*(0)*}{\kappa}_{xy}\frac{c_2}{R}(\ ) \tag{A15c}$$

$$\overline{\mathcal{B}}^{*}_{33}(\ ) = -L_1 \overset{*(0)*}{\kappa}_{xx}\frac{\partial}{\partial x} + L_3 \overset{*(0)*}{\kappa}_{xy}\frac{\partial}{\partial y} \tag{A15d}$$

Appendix B
Coefficients in Equation (112)

The stiffness coefficents in equation (112) are given by

$$k_{11} = A_{11}\int_0^{2\pi R}\int_0^{L}\left(\frac{\partial \ell_{11}}{\partial x}\right)^2 dxdy + \left(A_{66} - B_{66}\frac{c_2}{R} + D_{66}\frac{c_2}{4R^2} - \frac{c_1 L_2^*}{4}\right)\int_0^{2\pi R}\int_0^{L}\left(\frac{\partial \ell_{11}}{\partial y}\right)^2 dxdy +$$
$$\left(2A_{16} - B_{16}\frac{c_2}{R}\right)\int_0^{2\pi R}\int_0^{L}\left(\frac{\partial \ell_{11}}{\partial x}\,\frac{\partial \ell_{11}}{\partial y}\right)dxdy \tag{B1}$$

$$k_{12} = \left(A_{12} + B_{12}\frac{c_2}{R}\right)\int_0^{2\pi R}\int_0^{L}\left(\frac{\partial \ell_{11}}{\partial x}\,\frac{\partial \ell_{22}}{\partial y}\right)dxdy + \left(A_{16} + B_{16}\frac{3c_2}{2R}\right)\int_0^{2\pi R}\int_0^{L}\left(\frac{\partial \ell_{11}}{\partial x}\,\frac{\partial \ell_{22}}{\partial x}\right)dxdy +$$
$$\left(A_{66} + B_{66}\frac{c_2}{R} - D_{66}\frac{3c_2}{4R^2} + \frac{c_1 L_2^*}{4}\right)\int_0^{2\pi R}\int_0^{L}\left(\frac{\partial \ell_{11}}{\partial y}\,\frac{\partial \ell_{22}}{\partial x}\right)dxdy + \tag{B2}$$
$$\left(A_{26} + B_{26}\frac{c_2}{R} - D_{26}\frac{c_2}{2R^2}\right)\int_0^{2\pi R}\int_0^{L}\left(\frac{\partial \ell_{11}}{\partial y}\,\frac{\partial \ell_{22}}{\partial y}\right)dxdy$$

$$k_{22} = \left(A_{22} + B_{22}\frac{2c_2}{R} + D_{22}\frac{c_2}{R^2}\right)\int_0^{2\pi R}\int_0^{L}\left(\frac{\partial \ell_{22}}{\partial y}\right)^2 dxdy +$$
$$\left(A_{66} + B_{66}\frac{3c_2}{R} + D_{66}\frac{9c_2}{4R^2} - \frac{c_1 L_2^*}{4}\right)\int_0^{2\pi R}\int_0^{L}\left(\frac{\partial \ell_{22}}{\partial x}\right)^2 dxdy + \tag{B3}$$
$$\left(2A_{26} + B_{26}\frac{5c_2}{R} + D_{26}\frac{3c_2}{R^2}\right)\int_0^{2\pi R}\int_0^{L}\left(\frac{\partial \ell_{22}}{\partial x}\,\frac{\partial \ell_{22}}{\partial y}\right)dxdy - \frac{(c_2 - c_4)L_2^*}{R^2}\int_0^{2\pi R}\int_0^{L}(\ell_{22})^2 dxdy$$

$$k_{13} = \frac{2A_{12} + c_4 L_2^*}{2R}\int_0^{2\pi R}\int_0^{L}\left(\frac{\partial \ell_{11}}{\partial x}\,\ell_{33}\right)dxdy + \frac{1}{R}\left(A_{26} - B_{26}\frac{c_2}{2R}\right)\int_0^{2\pi R}\int_0^{L}\left(\frac{\partial \ell_{11}}{\partial y}\,\ell_{33}\right)dxdy +$$

$$- B_{11}\int_0^{2\pi R}\int_0^{L}\left(\frac{\partial \ell_{11}}{\partial x}\,\frac{\partial^2 \ell_{33}}{\partial x^2}\right)dxdy - B_{12}\int_0^{2\pi R}\int_0^{L}\left(\frac{\partial \ell_{11}}{\partial x}\,\frac{\partial^2 \ell_{33}}{\partial y^2}\right)dxdy - \frac{c_4 L_2^*}{2R}\int_0^{2\pi R}\int_0^{L}\left(\ell_{11}\,\frac{\partial \ell_{33}}{\partial x}\right)dxdy$$

$$- 2B_{16}\int_0^{2\pi R}\int_0^{L}\left(\frac{\partial \ell_{11}}{\partial x}\,\frac{\partial^2 \ell_{33}}{\partial x \partial y}\right)dxdy + \left(D_{16}\frac{c_2}{2R} - B_{16}\right)\int_0^{2\pi R}\int_0^{L}\left(\frac{\partial \ell_{11}}{\partial y}\,\frac{\partial^2 \ell_{33}}{\partial x^2}\right)dxdy + \tag{B4}$$

$$\left(D_{26}\frac{c_2}{2R} - B_{26}\right)\int_0^{2\pi R}\int_0^{L}\left(\frac{\partial \ell_{11}}{\partial y}\,\frac{\partial^2 \ell_{33}}{\partial y^2}\right)dxdy + \left(D_{66}\frac{c_2}{R} - 2B_{66}\right)\int_0^{2\pi R}\int_0^{L}\left(\frac{\partial \ell_{11}}{\partial y}\,\frac{\partial^2 \ell_{33}}{\partial x \partial y}\right)dxdy$$

$$k_{23} = \frac{1}{R}\left(A_{22} + B_{22}\frac{c_2}{R}\right)\int_0^{2\pi R}\int_0^{L}\left(\frac{\partial \ell_{22}}{\partial y}\,\ell_{33}\right)dxdy + \frac{1}{R}\left(A_{26} + B_{26}\frac{3c_2}{2R}\right)\int_0^{2\pi R}\int_0^{L}\left(\frac{\partial \ell_{22}}{\partial x}\,\ell_{33}\right)dxdy +$$

$$- \left(B_{12} + D_{12}\frac{c_2}{R}\right)\int_0^{2\pi R}\int_0^{L}\left(\frac{\partial \ell_{22}}{\partial y}\,\frac{\partial^2 \ell_{33}}{\partial x^2}\right)dxdy - \left(B_{22} + D_{22}\frac{c_2}{R}\right)\int_0^{2\pi R}\int_0^{L}\left(\frac{\partial \ell_{22}}{\partial y}\,\frac{\partial^2 \ell_{33}}{\partial y^2}\right)dxdy$$

$$- 2\left(B_{26} + D_{26}\frac{c_2}{R}\right)\int_0^{2\pi R}\int_0^{L}\left(\frac{\partial \ell_{22}}{\partial y}\,\frac{\partial^2 \ell_{33}}{\partial x \partial y}\right)dxdy - \left(D_{16}\frac{3c_2}{2R} + B_{16}\right)\int_0^{2\pi R}\int_0^{L}\left(\frac{\partial \ell_{22}}{\partial x}\,\frac{\partial^2 \ell_{33}}{\partial x^2}\right)dxdy +$$

$$- \left(D_{26}\frac{3c_2}{2R} + B_{26}\right)\int_0^{2\pi R}\int_0^{L}\left(\frac{\partial \ell_{22}}{\partial x}\,\frac{\partial^2 \ell_{33}}{\partial y^2}\right)dxdy - \left(D_{66}\frac{3c_2}{R} + 2B_{66}\right)\int_0^{2\pi R}\int_0^{L}\left(\frac{\partial \ell_{22}}{\partial x}\,\frac{\partial^2 \ell_{33}}{\partial x \partial y}\right)dxdy$$

$$- \frac{(c_4 - 2c_2)L_2^*}{2R}\int_0^{2\pi R}\int_0^{L}\left(\frac{\partial \ell_{33}}{\partial y}\,\ell_{22}\right)dxdy - \frac{c_2 L_3^*}{R}\int_0^{2\pi R}\int_0^{L}\left(\frac{\partial \ell_{33}}{\partial x}\,\ell_{22}\right)dxdy + \tag{B5}$$

$$\frac{c_4 L_2^*}{2R}\int_0^{2\pi R}\int_0^{L}\left(\ell_{33}\,\frac{\partial \ell_{22}}{\partial y}\right)dxdy$$

$$k_{33} = \frac{A_{22} + c_4 L_2^*}{R^2}\int_0^{2\pi R}\int_0^{L}\left(\ell_{33}\right)^2 dxdy - \frac{2B_{12}}{R}\int_0^{2\pi R}\int_0^{L}\left(\ell_{33}\frac{\partial^2 \ell_{33}}{\partial x^2}\right)dxdy$$

$$- \frac{4B_{26}}{R}\int_0^{2\pi R}\int_0^{L}\left(\ell_{33}\frac{\partial^2 \ell_{33}}{\partial x \partial y}\right)dxdy - \frac{2B_{22}}{R}\int_0^{2\pi R}\int_0^{L}\left(\ell_{33}\frac{\partial^2 \ell_{33}}{\partial y^2}\right)dxdy +$$

$$D_{11}\int_0^{2\pi R}\int_0^{L}\left(\frac{\partial^2 \ell_{33}}{\partial x^2}\right)^2 dxdy + 4D_{16}\int_0^{2\pi R}\int_0^{L}\left(\frac{\partial^2 \ell_{33}}{\partial x^2}\frac{\partial^2 \ell_{33}}{\partial x \partial y}\right)dxdy +$$

$$2D_{12}\int_0^{2\pi R}\int_0^{L}\left(\frac{\partial^2 \ell_{33}}{\partial x^2}\frac{\partial^2 \ell_{33}}{\partial y^2}\right)dxdy + 4D_{66}\int_0^{2\pi R}\int_0^{L}\left(\frac{\partial^2 \ell_{33}}{\partial x \partial y}\right)^2 dxdy$$

$$+ 4D_{26}\int_0^{2\pi R}\int_0^{L}\left(\frac{\partial^2 \ell_{33}}{\partial y^2}\frac{\partial^2 \ell_{33}}{\partial x \partial y}\right)dxdy + D_{22}\int_0^{2\pi R}\int_0^{L}\left(\frac{\partial^2 \ell_{33}}{\partial y^2}\right)^2 dxdy$$

$$- L_2^*\int_0^{2\pi R}\int_0^{L}\left(\frac{\partial \ell_{33}}{\partial y}\right)^2 dxdy + 2L_3^*\int_0^{2\pi R}\int_0^{L}\left(\frac{\partial \ell_{33}}{\partial x}\frac{\partial \ell_{33}}{\partial y}\right)dxdy \qquad \text{(B6)}$$

$$g_{11} = \frac{c_1}{4}\left(L_1 + L_2\right)\int_0^{2\pi R}\int_0^{L}\left(\frac{\partial \ell_{11}}{\partial y}\right)^2 dxdy \qquad \text{(B7)}$$

$$g_{12} = -\frac{c_1}{4}\left(L_1 + L_2\right)\int_0^{2\pi R}\int_0^{L}\left(\frac{\partial \ell_{11}}{\partial y}\frac{\partial \ell_{22}}{\partial x}\right)dxdy \qquad \text{(B8)}$$

$$g_{13} = \frac{c_4 L_2}{2R}\int_0^{2\pi R}\int_0^{L}\left(\ell_{11}\frac{\partial \ell_{33}}{\partial x} - \ell_{33}\frac{\partial \ell_{11}}{\partial x}\right)dxdy \qquad \text{(B9)}$$

$$g_{22} = \left(c_2 - c_4\right)\frac{L_2}{R^2}\int_0^{2\pi R}\int_0^{L}\left(\ell_{22}\right)^2 dxdy + \frac{c_1}{4}\left(L_1 + L_2\right)\int_0^{2\pi R}\int_0^{L}\left(\frac{\partial \ell_{22}}{\partial x}\right)^2 dxdy \qquad \text{(B10)}$$

$$g_{23} = \frac{(c_4 - 2c_2)L_2}{2R}\int_0^{2\pi R}\int_0^{L}\left(\frac{\partial \ell_{33}}{\partial y}\,\ell_{22}\right)dxdy + \frac{c_2 L_3}{R}\int_0^{2\pi R}\int_0^{L}\left(\frac{\partial \ell_{33}}{\partial x}\,\ell_{22}\right)dxdy - \frac{c_4 L_2}{2R}\int_0^{2\pi R}\int_0^{L}\left(\ell_{33}\,\frac{\partial \ell_{22}}{\partial y}\right)dxdy \tag{B11}$$

$$g_{33} = L_1\int_0^{2\pi R}\int_0^{L}\left(\frac{\partial \ell_{33}}{\partial x}\right)^2 dxdy + L_2\int_0^{2\pi R}\int_0^{L}\left(\frac{\partial \ell_{33}}{\partial y}\right)^2 dxdy - \frac{c_4 L_2}{R^2}\int_0^{2\pi R}\int_0^{L}(\ell_{33})^2 dxdy - 2L_3\int_0^{2\pi R}\int_0^{L}\left(\frac{\partial \ell_{33}}{\partial x}\,\frac{\partial \ell_{33}}{\partial y}\right)dxdy \tag{B12}$$

Using equations (110) gives

$$\int_0^{2\pi R}\int_0^{L}\left(\frac{\partial \ell_{11}}{\partial x}\right)^2 dxdy = \frac{m^2\pi^3 R}{2L}\left[1 + \left(\frac{nL}{m\pi R}\right)^2\tau^2\right] \tag{B13}$$

$$\int_0^{2\pi R}\int_0^{L}\left(\frac{\partial \ell_{11}}{\partial y}\right)^2 dxdy = \frac{m^2\pi^3 R}{2L}\left(\frac{nL}{m\pi R}\right)^2 \tag{B14}$$

$$\int_0^{2\pi R}\int_0^{L}\left(\frac{\partial \ell_{11}}{\partial x}\,\frac{\partial \ell_{11}}{\partial y}\right)dxdy = -\frac{m^2\pi^3 R}{2L}\left(\frac{nL}{m\pi R}\right)^2\tau \tag{B15}$$

$$\int_0^{2\pi R}\int_0^{L}\left(\frac{\partial \ell_{11}}{\partial x}\,\frac{\partial \ell_{22}}{\partial y}\right)dxdy = -\frac{mn\pi^2}{2} \tag{B16}$$

$$\int_0^{2\pi R}\int_0^{L}\left(\frac{\partial \ell_{11}}{\partial y}\,\frac{\partial \ell_{22}}{\partial x}\right)dxdy = -\frac{mn\pi^2}{2} \tag{B17}$$

$$\int_0^{2\pi R}\int_0^{L}\left(\frac{\partial \ell_{11}}{\partial x}\frac{\partial \ell_{22}}{\partial x}\right)dxdy = mn\pi^2\tau \tag{B18}$$

$$\int_0^{2\pi R}\int_0^{L}\left(\frac{\partial \ell_{11}}{\partial y}\frac{\partial \ell_{22}}{\partial y}\right)dxdy = 0 \tag{B19}$$

$$\int_0^{2\pi R}\int_0^{L}\left(\frac{\partial \ell_{11}}{\partial x}\ell_{33}\right)dxdy = -\frac{m\pi^2 R}{2} \tag{B20}$$

$$\int_0^{2\pi R}\int_0^{L}\left(\frac{\partial \ell_{11}}{\partial y}\ell_{33}\right)dxdy = 0 \tag{B21}$$

$$\int_0^{2\pi R}\int_0^{L}\left(\frac{\partial \ell_{11}}{\partial x}\frac{\partial^2 \ell_{33}}{\partial x^2}\right)dxdy = \frac{m^2\pi^3 R}{2L}\left(\frac{m\pi}{L}\right)\left[1+3\left(\frac{nL}{m\pi R}\right)^2\tau^2\right] \tag{B22}$$

$$\int_0^{2\pi R}\int_0^{L}\left(\frac{\partial \ell_{11}}{\partial x}\frac{\partial^2 \ell_{33}}{\partial y^2}\right)dxdy = \frac{mn^2\pi^2}{2R} \tag{B23}$$

$$\int_0^{2\pi R}\int_0^{L}\left(\frac{\partial \ell_{11}}{\partial x}\frac{\partial^2 \ell_{33}}{\partial x\partial y}\right)dxdy = -\frac{mn^2\pi^2}{R}\tau \tag{B24}$$

$$\int_0^{2\pi R}\int_0^{L}\left(\frac{\partial \ell_{11}}{\partial y}\frac{\partial^2 \ell_{33}}{\partial x^2}\right)dxdy = -\frac{mn^2\pi^2}{R}\tau \tag{B25}$$

$$\int_0^{2\pi R}\int_0^{L}\left(\frac{\partial \ell_{11}}{\partial y}\frac{\partial^2 \ell_{33}}{\partial y^2}\right)dxdy = 0 \tag{B26}$$

$$\int_0^{2\pi R}\int_0^{L}\left(\frac{\partial \ell_{11}}{\partial y}\,\frac{\partial^2 \ell_{33}}{\partial x\partial y}\right)dxdy = \frac{mn^2\pi^2}{2R} \tag{B27}$$

$$\int_0^{2\pi R}\int_0^{L}\left(\frac{\partial \ell_{22}}{\partial y}\right)^2 dxdy = \frac{n^2\pi L}{2R} \tag{B28}$$

$$\int_0^{2\pi R}\int_0^{L}\left(\frac{\partial \ell_{22}}{\partial x}\right)^2 dxdy = \frac{m^2\pi^3 R}{2L}\left[1+\left(\frac{nL}{m\pi R}\right)^2\tau^2\right] \tag{B29}$$

$$\int_0^{2\pi R}\int_0^{L}\left(\frac{\partial \ell_{22}}{\partial x}\,\frac{\partial \ell_{22}}{\partial y}\right)dxdy = -\frac{n^2\pi L}{2R}\tau \tag{B30}$$

$$\int_0^{2\pi R}\int_0^{L}\left(\frac{\partial \ell_{22}}{\partial y}\,\ell_{33}\right)dxdy = \frac{n\pi L}{2} \tag{B31}$$

$$\int_0^{2\pi R}\int_0^{L}\left(\frac{\partial \ell_{22}}{\partial x}\,\ell_{33}\right)dxdy = -\frac{n\pi L}{2}\tau \tag{B32}$$

$$\int_0^{2\pi R}\int_0^{L}\left(\frac{\partial \ell_{22}}{\partial y}\,\frac{\partial^2 \ell_{33}}{\partial x^2}\right)dxdy = -\frac{m^2\pi^3 R}{2L}\left(\frac{nL}{m\pi R}\right)\left(\frac{m\pi}{L}\right)\left[1+\left(\frac{nL}{m\pi R}\right)^2\tau^2\right] \tag{B33}$$

$$\int_0^{2\pi R}\int_0^{L}\left(\frac{\partial \ell_{22}}{\partial y}\,\frac{\partial^2 \ell_{33}}{\partial y^2}\right)dxdy = -\frac{n^3\pi L}{2R^2} \tag{B34}$$

$$\int_0^{2\pi R}\int_0^{L}\left(\frac{\partial \ell_{22}}{\partial y}\,\frac{\partial^2 \ell_{33}}{\partial x\partial y}\right)dxdy = \frac{n^3\pi L}{2R^2}\tau \tag{B35}$$

$$\int_0^{2\pi R}\int_0^{L}\left(\frac{\partial \ell_{22}}{\partial x}\frac{\partial^2 \ell_{33}}{\partial x^2}\right)dxdy = \frac{m^2\pi^3 R}{2L}\left(\frac{nL}{m\pi R}\right)\left(\frac{m\pi}{L}\right)\left[3+\left(\frac{nL}{m\pi R}\right)^2\tau^2\right]\tau \qquad \text{(B36)}$$

$$\int_0^{2\pi R}\int_0^{L}\left(\frac{\partial \ell_{22}}{\partial x}\frac{\partial^2 \ell_{33}}{\partial y^2}\right)dxdy = \frac{n^3\pi L}{2R^2}\tau \qquad \text{(B37)}$$

$$\int_0^{2\pi R}\int_0^{L}\left(\frac{\partial \ell_{22}}{\partial x}\frac{\partial^2 \ell_{33}}{\partial x\partial y}\right)dxdy = -\frac{m^2\pi^3 R}{2L}\left(\frac{nL}{m\pi R}\right)\left(\frac{m\pi}{L}\right)\left[1+\left(\frac{nL}{m\pi R}\right)^2\tau^2\right] \qquad \text{(B38)}$$

$$\int_0^{2\pi R}\int_0^{L}\left(\ell_{33}\right)^2 dxdy = \frac{\pi RL}{2} \qquad \text{(B39)}$$

$$\int_0^{2\pi R}\int_0^{L}\left(\ell_{33}\frac{\partial^2 \ell_{33}}{\partial x^2}\right)dxdy = -\frac{m^2\pi^3 R}{2L}\left[1+\left(\frac{nL}{m\pi R}\right)^2\tau^2\right] \qquad \text{(B40)}$$

$$\int_0^{2\pi R}\int_0^{L}\left(\ell_{33}\frac{\partial^2 \ell_{33}}{\partial y^2}\right)dxdy = -\frac{n^2\pi L}{2R} \qquad \text{(B41)}$$

$$\int_0^{2\pi R}\int_0^{L}\left(\ell_{33}\frac{\partial^2 \ell_{33}}{\partial x\partial y}\right)dxdy = \frac{n^2\pi L}{2R}\tau \qquad \text{(B42)}$$

$$\int_0^{2\pi R}\int_0^{L}\left(\frac{\partial^2 \ell_{33}}{\partial x^2}\right)^2 dxdy = \frac{m^2\pi^3 R}{2L}\left(\frac{m\pi}{L}\right)^2\left(1+6\left(\frac{nL}{m\pi R}\right)^2\tau^2+\left(\frac{nL}{m\pi R}\right)^4\tau^4\right) \qquad \text{(B43)}$$

$$\int_0^{2\pi R}\int_0^{L}\left(\frac{\partial^2 \ell_{33}}{\partial x^2}\frac{\partial^2 \ell_{33}}{\partial x\partial y}\right)dxdy = -\frac{m^2\pi^3 R}{2L}\left(\frac{m\pi}{L}\right)^2\left(\frac{nL}{m\pi R}\right)^2\left[3+\left(\frac{nL}{m\pi R}\right)^2\tau^2\right]\tau \qquad \text{(B44)}$$

$$\int_0^{2\pi R}\int_0^{L}\left(\frac{\partial^2 \ell_{33}}{\partial x^2}\,\frac{\partial^2 \ell_{33}}{\partial y^2}\right)dxdy = \frac{m^2\pi^3 R}{2L}\left(\frac{m\pi}{L}\right)^2\left(\frac{nL}{m\pi R}\right)^2\left[1+\left(\frac{nL}{m\pi R}\right)^2\tau^2\right] \tag{B45}$$

$$\int_0^{2\pi R}\int_0^{L}\left(\frac{\partial^2 \ell_{33}}{\partial x\partial y}\right)^2 dxdy = \frac{m^2\pi^3 R}{2L}\left(\frac{m\pi}{L}\right)^2\left(\frac{nL}{m\pi R}\right)^2\left[1+\left(\frac{nL}{m\pi R}\right)^2\tau^2\right] \tag{B46}$$

$$\int_0^{2\pi R}\int_0^{L}\left(\frac{\partial^2 \ell_{33}}{\partial y^2}\,\frac{\partial^2 \ell_{33}}{\partial x\partial y}\right)dxdy = -\frac{m^2\pi^3 R}{2L}\left(\frac{m\pi}{L}\right)^2\left(\frac{nL}{m\pi R}\right)^4\tau \tag{B47}$$

$$\int_0^{2\pi R}\int_0^{L}\left(\frac{\partial^2 \ell_{33}}{\partial y^2}\right)^2 dxdy = \frac{m^2\pi^3 R}{2L}\left(\frac{m\pi}{L}\right)^2\left(\frac{nL}{m\pi R}\right)^4 \tag{B48}$$

$$\int_0^{2\pi R}\int_0^{L}\left(\frac{\partial \ell_{11}}{\partial y}\right)^2 dxdy = \frac{n^2\pi L}{2R} \tag{B49}$$

$$\int_0^{2\pi R}\int_0^{L}\left(\frac{\partial \ell_{11}}{\partial y}\,\frac{\partial \ell_{22}}{\partial x}\right)dxdy = -\frac{mn\pi^2}{2} \tag{B50}$$

$$\int_0^{2\pi R}\int_0^{L}\left(\ell_{22}\right)^2 dxdy = \frac{\pi RL}{2} \tag{B51}$$

$$\int_0^{2\pi R}\int_0^{L}\left(\frac{\partial \ell_{22}}{\partial x}\right)^2 dxdy = \frac{m^2\pi^3 R}{2L}\left[1+\left(\frac{nL}{m\pi R}\right)^2\tau^2\right] \tag{B52}$$

$$\int_0^{2\pi R}\int_0^{L}\left(\frac{\partial \ell_{33}}{\partial y}\,\ell_{22}\right)dxdy = -\frac{1}{2}\,n\pi L \tag{B53}$$

$$\int_0^{2\pi R}\int_0^{L}\left(\frac{\partial \mathscr{l}_{33}}{\partial x}\,\mathscr{l}_{22}\right)dxdy = \frac{1}{2}\,n\pi L\,\tau \tag{B54}$$

$$\int_0^{2\pi R}\int_0^{L}\left(\frac{\partial \mathscr{l}_{33}}{\partial x}\right)^2 dxdy = \frac{m^2\pi^3 R}{2L}\left[1+\left(\frac{nL}{m\pi R}\right)^2\tau^2\right] \tag{B55}$$

$$\int_0^{2\pi R}\int_0^{L}\left(\frac{\partial \mathscr{l}_{33}}{\partial y}\right)^2 dxdy = \frac{n^2\pi L}{2R} \tag{B56}$$

$$\int_0^{2\pi R}\int_0^{L}\left(\frac{\partial \mathscr{l}_{33}}{\partial x}\,\frac{\partial \mathscr{l}_{33}}{\partial y}\right)dxdy = -\frac{n^2\pi L}{2R}\tau \tag{B57}$$

$$\int_0^{2\pi R}\int_0^{L}\left(\frac{\partial \mathscr{l}_{33}}{\partial x}\,\mathscr{l}_{11}\right)dxdy = \frac{m\pi^2 R}{2} \tag{B58}$$

Using these expressions for the integrals, the stiffness coefficients given by equations (B1) through (B6) become

$$k_{11} = \frac{m^2\pi^3 R}{2L}\left\{A_{11}\left[1+\left(\frac{nL}{m\pi R}\right)^2\tau^2\right]+\left[A_{66}-\frac{c_2}{R}B_{66}+\frac{c_2}{4R^2}D_{66}-\left(2A_{16}-\frac{c_2}{R}B_{16}\right)\tau-\frac{c_1 L_2^*}{4}\right]\left(\frac{nL}{m\pi R}\right)^2\right\} \tag{B59}$$

$$k_{12} = -\frac{m^2\pi^3 R}{2L}\left(\frac{nL}{m\pi R}\right)\left[A_{12}+A_{66}+\frac{c_2}{R}\left[B_{12}+B_{66}\right]-\frac{3c_2}{4R^2}D_{66}-\left(2A_{16}+\frac{3c_2}{R}B_{16}\right)\tau+\frac{c_1 L_2^*}{4}\right] \tag{B60}$$

$$\begin{aligned} k_{13} = -\frac{m^2\pi^3 R}{2L}\left(\frac{m\pi}{L}\right)\Bigg[&\left(\frac{A_{12}}{R}+\frac{c_4 L_2^*}{R}\right)\left(\frac{L}{m\pi}\right)^2+B_{11}+ \\ &\left(B_{12}+2B_{66}-\frac{c_2}{R}D_{66}+3B_{11}\tau^2-6B_{16}\tau+\frac{c_2}{R}D_{16}\tau\right)\left(\frac{nL}{m\pi R}\right)^2\Bigg] \end{aligned} \tag{B61}$$

$$k_{22} = \frac{m^2\pi^3 R}{2L}\left\{\left(A_{66} + \frac{3c_2}{R}B_{66} + \frac{9c_2}{4R^2}D_{66} - \frac{c_1 L_2^*}{4}\right)\left[1 + \left(\frac{nL}{m\pi R}\right)^2\tau^2\right] + \right.$$
$$\left(A_{22} + \frac{2c_2}{R}B_{22} + \frac{c_2}{R^2}D_{22}\right)\left(\frac{nL}{m\pi R}\right)^2 - \left(2A_{26} + \frac{5c_2}{R}B_{26} + \frac{3c_2}{R^2}D_{26}\right)\left(\frac{nL}{m\pi R}\right)^2\tau \qquad \text{(B62)}$$
$$\left. - \left(c_2 - c_4\right)\frac{L_2^*}{R^2}\left(\frac{L}{m\pi}\right)^2\right\}$$

$$k_{23} = \frac{m^2\pi^3 R}{2L}\left(\frac{m\pi}{L}\right)\left(\frac{nL}{m\pi R}\right)\left\{\frac{1}{R}\left(A_{22} + \frac{c_2}{R}B_{22} - \left[A_{26} + \frac{3c_2}{2R}B_{26}\right]\tau - c_2 L_3^*\tau + \left(c_4 - c_2\right)L_2^*\right)\left(\frac{L}{m\pi}\right)^2 + \right.$$
$$\left(B_{12} + 2B_{66} + \frac{c_2}{R}\left[D_{12} + 3D_{66}\right]\right)\left(1 + \left(\frac{nL}{m\pi R}\right)^2\tau^2\right) + \qquad \text{(B63)}$$
$$\left. + \left(B_{22} + \frac{c_2}{R}D_{22} - 3\left[B_{26} + \frac{7c_2}{6R}D_{26}\right]\tau\right)\left(\frac{nL}{m\pi R}\right)^2 - \left(B_{16} + \frac{3c_2}{2R}D_{16}\right)\left(3 + \left(\frac{nL}{m\pi R}\right)^2\tau^2\right)\tau\right\}$$

$$k_{33} = \frac{m^2\pi^3 R}{2L}\left(\frac{m\pi}{L}\right)^2\left\{\frac{A_{22} + c_4 L_2^*}{R^2}\left(\frac{L}{m\pi}\right)^4 + \frac{2}{R}\left(\frac{L}{m\pi}\right)^2\left[B_{12} + \left(B_{22} + B_{12}\tau^2 - 2B_{26}\tau\right)\left(\frac{nL}{m\pi R}\right)^2\right] + \right.$$
$$D_{11}\left(1 + 6\left(\frac{nL}{m\pi R}\right)^2\tau^2 + \left(\frac{nL}{m\pi R}\right)^4\tau^4\right) + 2\left(D_{12} + 2D_{66}\right)\left(\frac{nL}{m\pi R}\right)^2\left(1 + \left(\frac{nL}{m\pi R}\right)^2\tau^2\right) + D_{22}\left(\frac{nL}{m\pi R}\right)^4 \qquad \text{(B64)}$$
$$\left. - 4D_{16}\left(\frac{nL}{m\pi R}\right)^2\left(3 + \left(\frac{nL}{m\pi R}\right)^2\tau^2\right)\tau - 4D_{26}\left(\frac{nL}{m\pi R}\right)^4\tau - \left(L_2^* + 2L_3^*\tau\right)\left(\frac{L}{m\pi}\right)^2\left(\frac{nL}{m\pi R}\right)^2\right\}$$

Similarly,

$$g_{11} = \frac{m^2\pi^3 R}{2L}\left\{\frac{c_1}{4}\left(L_1 + L_2\right)\left(\frac{nL}{m\pi R}\right)^2\right\} \qquad \text{(B65)}$$

$$g_{12} = \frac{m^2\pi^3 R}{2L}\left\{\frac{c_1}{4}\left(L_1 + L_2\right)\left(\frac{nL}{m\pi R}\right)\right\} \qquad \text{(B66)}$$

$$g_{13} = \frac{m^2\pi^3 R}{2L}\left\{\frac{c_4 L_2}{R}\left(\frac{L}{m\pi}\right)\right\} \qquad \text{(B67)}$$

$$g_{22} = \frac{m^2\pi^3 R}{2L}\left\{\left(c_2 - c_4\right)\frac{L_2}{R^2}\left(\frac{L}{m\pi}\right)^2 + \frac{c_1}{4}\left(L_1 + L_2\right)\left(1 + \left(\frac{nL}{m\pi R}\right)^2\tau^2\right)\right\} \tag{B68}$$

$$g_{23} = \frac{m^2\pi^3 R}{2L}\left(\frac{m\pi}{L}\right)\left\{\left[\frac{c_2}{R}\left(L_2 + L_3\tau\right) - \frac{c_4 L_2}{R}\right]\left(\frac{L}{m\pi}\right)^2\left(\frac{nL}{m\pi R}\right)\right\} \tag{B69}$$

$$g_{33} = \frac{m^2\pi^3 R}{2L}\left(\frac{m\pi}{L}\right)^2\left\{\left(\frac{L}{m\pi}\right)^2\left[L_1 + \left(L_1\tau^2 + L_2 + 2L_3\tau\right)\left(\frac{nL}{m\pi R}\right)^2 - \frac{c_4 L_2}{R^2}\left(\frac{L}{m\pi}\right)^2\right]\right\} \tag{B70}$$

REPORT DOCUMENTATION PAGE

Form Approved
OMB No. 0704-0188

1. REPORT DATE *(DD-MM-YYYY)*	2. REPORT TYPE	3. DATES COVERED *(From - To)*
01- 03 - 2014	Technical Memorandum	

4. TITLE AND SUBTITLE

Buckling Analysis for Stiffened Anisotropic Circular Cylinders Based on Sanders' Nonlinear Shell Theory

5a. CONTRACT NUMBER

5b. GRANT NUMBER

5c. PROGRAM ELEMENT NUMBER

6. AUTHOR(S)

Nemeth, Michael P.

5d. PROJECT NUMBER

5e. TASK NUMBER

5f. WORK UNIT NUMBER

869021.04.07.01.13

7. PERFORMING ORGANIZATION NAME(S) AND ADDRESS(ES)

NASA Langley Research Center
Hampton, VA 23681-2199

8. PERFORMING ORGANIZATION REPORT NUMBER

L-20320

9. SPONSORING/MONITORING AGENCY NAME(S) AND ADDRESS(ES)

National Aeronautics and Space Administration
Washington, DC 20546-0001

10. SPONSOR/MONITOR'S ACRONYM(S)

NASA

11. SPONSOR/MONITOR'S REPORT NUMBER(S)

NASA/TM-2014-218176

12. DISTRIBUTION/AVAILABILITY STATEMENT

Unclassified - Unlimited
Subject Category 39
Availability: NASA CASI (443) 757-5802

13. SUPPLEMENTARY NOTES

14. ABSTRACT

Nonlinear and bifurcation buckling equations for elastic, stiffened, geometrically perfect, right-circular cylindrical, anisotropic shells subjected to combined loads are presented that are based on Sanders' shell theory. Based on these equations, a three-parameter approximate Rayleigh-Ritz solution and a classical solution to the buckling problem are presented for cylinders with simply supported edges. Extensive comparisons of results obtained from these solutions with published results are also presented for a wide range of cylinder constructions. These comparisons include laminated-composite cylinders with a wide variety of shell-wall orthotropies and anisotropies. Numerous results are also given that show the discrepancies between the results obtained by using Donnell's equations and variants of Sanders' equations. For some cases, nondimensional parameters are identified and "master" curves are presented that facilitate the concise representation of results.

15. SUBJECT TERMS

Anisotropic shells; Buckling; Shell theory; Stiffened cylinders

16. SECURITY CLASSIFICATION OF:			17. LIMITATION OF ABSTRACT	18. NUMBER OF PAGES	19a. NAME OF RESPONSIBLE PERSON
a. REPORT	b. ABSTRACT	c. THIS PAGE			STI Help Desk (email: help@sti.nasa.gov)
					19b. TELEPHONE NUMBER *(Include area code)*
U	U	U	UU	413	(443) 757-5802